

4

Q

1

P5

SER. 7

V. 31

1941

PER

THE
LONDON, EDINBURGH AND DUBLIN
PHILOSOPHICAL MAGAZINE
AND
JOURNAL OF SCIENCE

CONDUCTED BY
SIR LAWRENCE BRAGG, O.B.E., M.A., D.Sc., F.R.S.
PROF. G. P. THOMSON, M.A., D.Sc., F.R.S.
AND
ALLAN FERGUSON, M.A., D.Sc.

"Nec araneorum sane textus ideo melior quia ex se fila gignunt, nec
noster vilior quia ex allenis libamus ut apes."

JUST. LIPS. *Polit. lib. i. cap. l. Not.*

VOL. XXXI.—SEVENTH SERIES

JANUARY—JUNE 1941

LONDON:

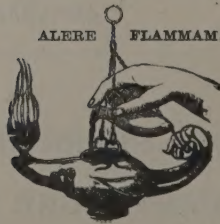
TAYLOR & FRANCIS, LTD., RED LION COURT, FLEET STREET, E.C. 4.

Agents: WM. DAWSON & SONS, LTD., 129 CANNON STREET, E.C. 4.

“Meditationis est perscrutari occulta; contemplationis est admirari perspicua Admiratio generat quæstionem, quæstio investigationem, investigatio inventionem.”—*Hugo de S. Victore.*

— “Cur spirent venti, cur terra dehiscat,
Cur mare turgescat, pelago cur tantus amaror,
Cur caput obscura Phœbus ferrugine condât,
Quid toties diros cogat flagrare cometas,
Quid pariat nubes, veniant cur fulmina cœlo,
Quo micet igne Iris, superos quis conciat orbes
Tam vario motu.”

J. B. Pinelli ad Mazonium.



CONTENTS OF VOL. XXXI. (Nos. 204-209)

(SEVENTH SERIES)

NUMBER 204—JANUARY

	Page
I. Formulæ for the Natural Dispersion of some Organic Liquids. By W. J. GRANVILLE BEYNON, Ph.D., Physics Department, University College, Swansea	1
II. A General Interferential Method. By L. STURKEY and B. P. RAMSAY, University of Kentucky	13
III. Rocket Flight to the Moon. By J. W. CAMPBELL, Ph.D.	24
IV. The Air-Jet with a Velocity exceeding that of Sound. By JUL. HARTMANN and FREIMUT LAZARUS. (Plates I.-V.)	35
V. Factors determining Electrolytic Dissociation.—Part II. The Free Energies of Dissociation of Salt Molecules in Aqueous Solution. By WILLIAM J. C. ORR, Ph.D., Department of Colloid Science, Cambridge ...	51
VI. The Crystal Structures of some Heterocyclic Organic Compounds of Analogous Constitution.—Part I. Thianthren and Selenanthren. By R. G. WOOD, M.Sc., and J. E. CRACKSTON, M.Sc.	62
VII. The Crystal Structures of some Heterocyclic Organic Compounds of Analogous Constitution.—Part II. Phenthiazine, Phenoxthionine, Phenoxselenine, and Phenoxtellurine. By R. G. WOOD, M.Sc., C. H. McCALE, M.Sc., and G. WILLIAMS, M.Sc.	71
VIII. A Heat Conduction Problem introduced by C. J. Tranter. By R. V. CHURCHILL	81
IX. Notices respecting New Books :— Mr. WILLIAM R. SMYTHE's Static and Dynamic Electricity	88

NUMBER 205—FEBRUARY

X. The Wind Tunnel with Open Working-Section. By N. SIMMONS, M.Sc., Ph.D., King's College, London	89
XI. Some Evidence for the Existence of Higher Hydrates of Ferric Oxide as Transition Intermediates. By LARS A. WELO, Tottenville, Staten Island, New York, and OSKAR BAUDISCH, Saratoga Springs Authority, Saratoga Springs, New York	103

	Page
XII. The Crystal Structures of some Heterocyclic Organic Compounds of Analogous Constitution.—Part III. Phenazine and Diphenylene Dioxide. By R. G. WOOD, M.Sc., and G. WILLIAMS, M.Sc.	115
XIII. On Lamé Functions. By A. ERDÉLYI, Mathematical Institute of the University, Edinburgh	123
XIV. Relationships between Lattice Types and Brillouin Zones. By GEOFFREY VINCENT RAYNOR	131
XV. The Brillouin Zone for the Gallium Structure. By GEOFFREY VINCENT RAYNOR	139
XVI. On Turbulent Liquid Motion Outside a Circular Boundary.—II. By MANOHAR RAY, Lahore, India	144
XVII. Latent Energy and Dissociation in Flame Gases. By W. T. DAVID, A. S. LEAH, and B. PUGH.....	156
XVIII. Circuits with Double Linkages. By Dr. ERIC A. WALKER, Tufts College, Medford, Mass., U.S.A.	169

NUMBER 206—MARCH

XIX. Further Development of the Fabric Theory of Protein Structure. By DOROTHY WRINCH, Carlisle Fellow of Somerville College, Oxford	177
XX. A Method for Measuring the Internal Area of Section of a Glass Tube. By D. J. BEHRENS, University of Manchester	199
XXI. The Determination of Green's Function for Line Sources for the Equation of Conduction of Heat in Cylindrical Coordinates by the Laplace Transformation. By H. S. CARSLAW, Emeritus Professor of Mathematics, University of Sydney, and J. C. JAEGER, Lecturer in Mathematics, University of Tasmania	204
XXII. Measurement of Surface Tension by the Ripple Method. By E. TYLER, D.Sc., M.Sc., F.Inst.P., A.F.R.Ae.S., Senior Lecturer in Physics, Science Department, South-East Essex Technical College, Dagenham.....	209
XXIII. On a Hydraulic Problem involving Discharge into Tidal Water.—II. By A. G. WALKER, Ph.D., Department of Pure Mathematics, University of Liverpool, and J. R. DAYMOND, M.Sc., Assoc.M.Inst.C.E., Department of Civil Engineering, University of Liverpool	222
XXIV. On the Raman Spectrum of <i>m</i> -Diphenyl Benzene. By S. K. MUKERJI, M.Sc., Ph.D., Professor of Physics, Agra College, Agra, and S. ABDUL AZIZ, M.Sc., Agra University Research Scholar in Physics. (Plate VI.)	231
XXV. On the Space Attenuation of Impact Sounds in a Brick Building. By A. E. KNOWLER, M.Sc., Physics Department, National Physical Laboratory, Teddington, Middlesex	240

	Page
XXVI. The Latent Heats of Fusion of some Organic Refrigerants. By J. H. AWBERY, B.A., B.Sc., F.Inst.P., Physics Department, National Physical Laboratory	247
XXVII. Some Formulæ for the E-function. By T. M. MACROBERT, Professor of Mathematics, University of Glasgow	254
XXVIII. Notices respecting New Books :—	
Professor L. BAIRSTOW's Applied Aerodynamics	261
Mr. J. C. SLATER's Introduction to Chemical Physics.....	263
Mr. GABRIEL KRON's Tensor Analysis of Networks	264

NUMBER 207—APRIL

XXIX. The Hall Effect and other Physical Properties of the Copper-Tin System of Alloys. By G. G. ANDREWARTHA, M.Sc., and Professor E. J. EVANS, M.Sc. (Physics Department, University College of Swansea)	265
XXX. An Investigation of the Flow of a Viscous Fluid past a Flat Plate, using Elliptic Coordinates. By T. V. DAVIES, B.Sc.	283
XXXI. On the Migration of Atoms in Iron-Nickel Alloys. By Professor E. A. OWEN, M.A., Sc.D., and A. H. SULLY, Ph.D., University College of North Wales, Bangor. (Plate VII.)	314
XXXII. On the Measurement of Particle Size by the X-Ray Method. By A. TAYLOR, Ph.D., F.Inst.P.	339
XXXIII. Notices respecting New Books :—	
Dr. E. A. MOELWYN-HUGHES's Physical Chemistry. An Introduction	348
Mr. A. S. RAMSEY's An Introduction to the Theory of Newtonian Attraction	348

NUMBER 208—MAY

XXXIV. The Excitation of the Hydrogen Molecule by Electron Impact. By R. ROSCOE, Ph.D., Physics Department, King's College, Newcastle- upon-Tyne	349
XXXV. The Effective Separation of Points Discharging Atmospheric Electricity. By J. ALAN CHALMERS, M.A., Ph.D., Lecturer in Physics in the Durham Colleges of the University of Durham.....	363
XXXVI. On the Problem of Wave-motion for the Wedge of an Angle. By Dr. ARNOLD N. LOWAN	373

	Page
XXXVII. The Emission of Secondary Electrons from Nickel. By RAFI MOHAMMAD CHAUDHRI, Ph.D.(Cantab.), M.Sc., Reader in Physics, and ABDUL WAHEED KHAN, M.Sc., Department of Physics, Muslim University, Aligarh	382
XXXVIII. The Reflexion and Refraction of Photons. By E. TAYLOR JONES, D.Sc., Professor of Natural Philosophy in the University of Glasgow.	394
XXXIX. The Electrical Conductivity of Plastic Dielectrics. By ANDREW GEMANT, Department of Electrical Engineering, University of Wisconsin, Madison, Wisconsin	405
XL. Asymptotic Solution of Southwell and Squire; Modification to Oseen's Equations. By J. H. PRESTON, B.Sc., Ph.D., A.F.R.Ae.S., of the Aerodynamics Department, National Physical Laboratory	413
XLI. Crystal Lattice Orientation of Rolled Magnesium. By D. E. THOMAS, M.A., B.Sc., F.Inst.P., Research Department, Woolwich. (Plate VIII.)	425
XLII. Note on a Problem in the Conduction of Heat. By C. J. TRANTER.	432
XLIII. Notices respecting New Books :—	
Professor G. H. HARDY's A Mathematician's Apology	433
Mr. PAUL W. MERRILL's Spectra of Long-Period Variable Stars	434
Culture, Vol. V. No. 2.....	434
The Half-Yearly Journal of the Mysore University.....	434
Table of Powers (British Association Mathematical Tables, Vol. ix.).....	435
Mr. G. WINDRED's Electrical Contacts	435
Professor R. V. SOUTHWELL's Relaxation Methods in Engineering Science	436

NUMBER 209—JUNE

XLIV. The Measurement by Ionization Methods of Real Energy Absorption from an X-ray Beam. By J. R. CLARKSON, Ph.D. (Plate IX.).	437
XLV. Note on the Method of Successive Approximations for the Solution of the Boundary Layer Equations. By J. H. PRESTON, B.Sc., Ph.D., A.F.R.Ae.S., of the Aerodynamics Department, National Physical Laboratory	452
XLVI. Note on the Paper "A new Determination of the Viscosity of Air by the Rotating Cylinder Method" (Phil. Mag. ser. 7, vol. xxiii. p. 313 (1937)). By GUNNAR KELLSTRÖM, D.Sc., Physics Laboratory, University of Uppsala	466

	Page
XLVII. The Steady Flow of Heat from certain Objects buried under Flat Air-cooled Surfaces. By F. H. SCHOFIELD, B.A., D.Sc., Physics Department, National Physical Laboratory, Teddington, Middlesex	471
XLVIII. The Drift of the Selenium Barrier-Layer Photo-cell. By R. A. HOUSTOUN, D.Sc., University of Glasgow	498
XLIX. Notices respecting New Books :—	
Messrs. J. A. SHOHAT, EINAR HILLE, and JOSEPH L. WALSH'S A Bibliography of Orthogonal Polynomials	507
Mr. W. L. FERRAR'S Algebra, a Text-Book of Determinants, Matrices and Algebraic Forms	507
M. LOUIS SAUTY'S La Mécanique Ondulatoire et less Quanta Électromagnétiques	508
Prof. G. H. HARDY'S Ramanujan	508
Mr. B. L. GULATEE'S Gravity Anomalies and the Figure of the Earth	509
Survey of India, Geodetic Report for 1939	509
Mr. THORKELL THORKELSSON'S On Thermal Activity in Iceland and Geyser Action	509
Prof. S. BHAGAVANTAM'S Scattering of Light and the Raman Effect	510
Prof. H. C. PLUMMER'S Four-Figure Tables with Mathematical Formulæ	510
Dr. R. S. BURDON'S Surface Tension and the Spreading of Liquids. (Cambridge Physical Tracts.)	511
Dr. E. G. RICHARDSON'S Physical Science in Art and Industry..	511
Prof. GILBERT DE B. ROBINSON'S The Foundations of Geometry	512
Index	513

PLATES

- I.-V. Illustrative of Messrs. JUL. HARTMANN and FREIMUT LAZARUS's Paper on the Air-Jet with a Velocity exceeding that of Sound.
- VI. Illustrative of Prof. S. K. MUKERJI and Mr. S. A. AZIZ's Paper on the Raman Spectrum of *m*-Diphenyl Benzene.
- VII. Illustrative of Professor E. A. OWEN and Dr. A. H. SULLY's Paper on the Migration of Atoms in Iron-Nickel Alloys.
- VIII. Illustrative of Mr. D. E. THOMAS's Paper on the Crystal Lattice Orientation of Rolled Magnesium
- IX. Illustrative of Dr. J. R. CLARKSON's Paper on The Measurement by Ionization Methods of Real Energy Absorption from an X-ray Beam.
-

THE
LONDON, EDINBURGH & DUBLIN
PHILOSOPHICAL MAGAZINE
AND
JOURNAL OF SCIENCE

[SEVENTH SERIES—VOL. 31]

I. Formulæ for the Natural Dispersion of some Organic Liquids.

By W. J. GRANVILLE BEYNON, Ph.D.,
Physics Department, University College, Swansea *.

[Received November 9, 1939.]

IN two recent publications ^{(1), (2)} the magneto-optical dispersion formulæ for five organic liquids, viz., methyl alcohol, ethyl alcohol, normal propyl alcohol, normal butyl alcohol, and allyl alcohol have been considered. It was shown that the magneto-optical dispersion in the case of each of the liquids could, within experimental error, be represented by formulæ of the type

$$\phi = n\delta\lambda^2 = \sum_r K_r \left[\frac{\lambda^2}{\lambda^2 - \lambda_r^2} \right]^2,$$

where

δ = Verdet's Constant for the wave-length λ ,

n = refractive index for the wave-length λ , and

K_r, λ_r = constants.

* Communicated by Professor E. J. Evans, D.Sc.

The wave-lengths λ_r were identified with the extreme ultra-violet absorption bands of the substance. These ultra-violet bands were photographed for the substances in the vapour state, and in evolving formulæ for the liquids it was assumed that no shift of the bands occurred during the transition from the vapour to the liquid state.

The theory underlying formulæ of the above type assumes that the natural dispersion can be represented by the usual Ketteler-Helmholtz type of formula

$$n^2 - 1 = b_0 + \sum_r \left[\frac{b_r}{\lambda^2 - \lambda_r^2} \right],$$

n being the refractive index for a wave-length λ , b_0 , b_r being constants, and λ_r the wave-lengths of the ultra-violet bands referred to above.

Formulae of this type for the natural dispersion of the five alcohols previously considered, are given in this paper.

The method of measuring the refractive indices at visible and ultra-violet wave-lengths has been described in detail in a paper by Stephens and Evans ⁽³⁾. Briefly it may be noted that measurements in the visible spectrum were made with a large prism spectrometer, and in the ultra-violet by a photographic method involving the use of overlapping spectra.

It is considered that the measurements at ultra-violet wave-lengths are accurate to within two or three in the fourth place of decimals. The measurements at visual wave-lengths are considered accurate to three or four in the fifth place of decimals.

Methyl Alcohol.

The wave-lengths of the extreme ultra-violet absorption bands used in the magneto-optical dispersion formulæ for this liquid were $\cdot 1588 \mu$, $\cdot 1470 \mu$, and $\cdot 0650 \mu$ respectively. The formula now given for the natural dispersion of methyl alcohol in the visible and near ultra-violet spectrum at $16\cdot 4^\circ \text{C.}$ is

$$n^2 - 1 = \cdot 749637 + \frac{\cdot 00504_2}{\lambda^2 - (\cdot 065)^2} + \frac{\cdot 00163_2}{\lambda^2 - (\cdot 1470)^2} + \frac{\cdot 000193_0}{\lambda^2 - (\cdot 1588)^2}. \quad (1)$$

In Table I. values of the refractive indices calculated from formula (1) are compared with the observed values.

It will be observed that there is fairly good agreement between calculated and observed values over the range of wave-lengths $\cdot 67$ to $\cdot 34 \mu$. At wave-lengths less than $\cdot 34 \mu$, however, formula (1) yields values which fall below those observed. In this connexion it may be noted that the presence of an impurity which produced absorption near $\cdot 27 \mu$ was detected by Jones and Evans ⁽⁴⁾ in their experiments on this liquid. The apparent high values of the refractive indices of methyl alcohol at the shorter

wave-lengths may thus possibly be due to a trace of this impurity which was not removed by distillation.

TABLE I.
Methyl Alcohol. Temperature 16.4° C.

Wave-length in microns.	Refractive index calculated from formula (1).	Refractive index observed.
·6678	1.3287 ₁	1.3289
·5893	1.3304 ₁	1.3306
·4922	1.3338 ₀	1.3339
·4713	1.3348 ₉	1.3352 ₅
·4472	1.3363 ₀	1.3363
·4400	1.3367 ₅	1.3366 ₅
·4200	1.3381 ₇	1.3379 ₅
·4000	1.3398 ₈	1.3396
·3800	1.3418 ₃	1.3417
·3600	1.3442 ₀	1.3441 ₅
·3400	1.3470 ₀	1.3471 ₅
·3200	1.3503 ₂	1.3508
·3000	1.3547 ₁	1.3554
·2800	1.3601 ₃	1.3607

Ethyl Alcohol.

The wave-lengths of the absorption bands used in the magneto-optical dispersion formula for ethyl alcohol were ·1618, ·1518, and ·065 μ respectively. The formula now given for the natural dispersion of ethyl alcohol over the range of wave-lengths ·67 to ·28 μ at 18.4° C. is

$$n^2 - 1 = .832610 + \frac{.00540_4}{\lambda^2 - (.065)^2} + \frac{.00227_7}{\lambda^2 - (.1518)^2} + \frac{.000264}{\lambda^2 - (.1618)^2} \quad (2)$$

Values of the refractive index calculated from formula (2) are compared with observed values in Table II.

The agreement between observed and calculated values is very satisfactory over the whole range of wave-lengths.

n-Propyl-Alcohol.

The wave-lengths of the absorption bands used in the magneto-optical dispersion formula for this liquid were ·1565 and ·0650 μ respectively.

TABLE II.

Ethyl Alcohol. Temperature 18.4° C.

Wave-length in microns.	Refractive index calculated from formula (2).	Refractive index observed.
·6678	1.3604 ₈	1.3604
·5893	1.3624 ₃	1.3624
·5015	1.3658 ₉	1.3658
·4713	1.3675 ₅	1.3675
·4472	1.3692 ₀	1.3692
·4300	1.3705 ₁	1.3705
·4200	1.3713 ₂	1.3713
·4000	1.3732 ₈	1.3733
·3800	1.3755 ₈	1.3755
·3600	1.3782 ₇	1.3782
·3400	1.3815 ₆	1.3816
·3200	1.3854 ₅	1.3857
·3000	1.3906 ₀	1.3906
·2800	1.3970 ₂	1.3970

TABLE III.

n-Propyl Alcohol. Temperature 23.6° C.

Wave-length in microns.	Refractive index calculated from formula (3).	Refractive index observed.
·6678	1.3819 ₁	1.3818
·5893	1.3840 ₀	1.3840
·5015	1.3877 ₆	1.3878
·4713	1.3895 ₈	1.3896
·4472	1.3913 ₃	1.3914
·4300	1.3927 ₇	1.3928
·4200	1.3937 ₀	1.3937 ₅
·4000	1.3958	1.3959
·3800	1.3982 ₈	1.3985
·3600	1.4012 ₄	1.4013 ₅
·3400	1.4048 ₁	1.4050
·3200	1.4090 ₉	1.4093
·3000	1.4147 ₂	1.4147
·2800	1.4217 ₀	1.4217

The formula now given for the natural dispersion of *n*-propyl alcohol at 23.6° C. is

$$n^2 - 1 = .889663 + \frac{.00582_4}{\lambda^2 - (.065)^2} + \frac{.00287_5}{\lambda^2 - (.1565)^2} \quad \dots (3)$$

Calculated and observed values are given in Table III.

The agreement between calculated and observed values to within experimental error is clear.

n-Butyl Alcohol.

The wave-lengths of the absorption bands used in the magnetic rotation formula for *n*-butyl alcohol were .1577 and .0650 μ respectively. The

TABLE IV.

n-Butyl Alcohol. Temperature 13° C.

Wave-length in microns.	Refractive index calculated from formula (4).	Refractive index observed.
.6678	1.4001 ₅	1.4002
.5893	1.4023 ₄	1.4024
.5015	1.4062 ₀	1.4062
.4713	1.4080 ₅	1.4082
.4472	1.4098 ₉	1.4099
.4300	1.4114 ₀	1.4114 ₅
.4200	1.4123 ₅	1.4124
.4000	1.4145 ₂	1.4145 ₅
.3800	1.4170 ₆	1.4171
.3600	1.4201 ₅	1.4200 ₅
.3400	1.4238 ₈	1.4237 ₅
.3200	1.4283 ₁	1.4285
.3000	1.4341 ₇	1.4342
.2800	1.4415 ₂	1.4413

formula now given for the natural dispersion of *n*-butyl alcohol over the range of wave-lengths .67 to .28 μ at 13° C. is

$$n^2 - 1 = .939433 + \frac{.00606_4}{\lambda^2 - (.065)^2} + \frac{.00304_4}{\lambda^2 - (.1577)^2} \quad \dots (4)$$

The satisfactory agreement between observed refractive indices and values calculated from this formula is shown in Table IV.

Allyl Alcohol.

A satisfactory magnetic rotation formula for this liquid was obtained using the two absorption wave-lengths $\cdot 1650$ and $\cdot 0750 \mu$. The natural dispersion formula now given for allyl alcohol at 20°C . using these wave-lengths is

$$n^2 - 1 = \cdot 960207 + \frac{\cdot 00576_0}{\lambda^2 - (\cdot 075)^2} + \frac{\cdot 00654_4}{\lambda^2 - (\cdot 1650)^2} \cdot \cdot \cdot \cdot (5)$$

TABLE V.

Allyl Alcohol. Temperature 20°C .

Wave-length in microns.	Refractive index calculated from formula (5).	Refractive index observed.
$\cdot 7065$	$1\cdot 4091_7$	$1\cdot 4092$
$\cdot 6678$	$1\cdot 4102_8$	$1\cdot 4101$
$\cdot 5893$	$1\cdot 4134_2$	$1\cdot 4135$
$\cdot 5015$	$1\cdot 4187_3$	$1\cdot 4187$
$\cdot 4713$	$1\cdot 4214_0$	$1\cdot 4216$
$\cdot 4472$	$1\cdot 4240_0$	$1\cdot 4240$
$\cdot 4400$	$1\cdot 4248_8$	$1\cdot 4248$
$\cdot 4200$	$1\cdot 4275_1$	$1\cdot 4275$
$\cdot 4000$	$1\cdot 4306_5$	$1\cdot 4307$
$\cdot 3800$	$1\cdot 4344_2$	$1\cdot 4344$
$\cdot 3600$	$1\cdot 4389_2$	$1\cdot 4390$
$\cdot 3400$	$1\cdot 4445_1$	$1\cdot 4446$
$\cdot 3200$	$1\cdot 4513_8$	$1\cdot 4515$
$\cdot 3000$	$1\cdot 4604_0$	$1\cdot 4603$
$\cdot 2900$	$1\cdot 4658_2$	$1\cdot 4655$

Values of the refractive index calculated from formula (5) are compared with observed values in Table V.

There is thus satisfactory agreement between calculated and observed values over the range of wave-lengths $\cdot 70$ to $\cdot 29 \mu$.

Application of Formulae to Dispersion in the Infra-red.

It is evident that the formulae given will fit the natural dispersions of the liquids over the range of spectrum from $\cdot 67$ to about $\cdot 30 \mu$. It will be of interest to examine the extent to which they can be applied to longer wave-lengths.

Measurements upon infra-red refractive indices for some organic liquids have been made by Seegert ⁽⁵⁾ and by Ingersoll ⁽⁶⁾. Seegert measured the refractive indices of methyl alcohol, ethyl alcohol, and *n*-propyl alcohol at a series of wave-lengths ranging from .8 to 2.3 μ . Ingersoll gives the refractive indices of methyl alcohol, ethyl alcohol, and *n*-butyl alcohol. The two sets of measurements available for methyl alcohol and ethyl alcohol are not identical, but the discrepancies are comparatively small, and the accuracy of the measurements seems quite sufficient to justify comparison with values calculated from the formulæ already given. A comparison has been made between refractive indices calculated from the preceding formulæ and observed values at the wave-lengths .8, 1.0, 1.5, and 2.0 μ . In all cases it is found that the calculated values at these near infra-red wave-lengths are greater than the corresponding observed values, and that the discrepancies increase with increasing wave-length. It would appear then that over the region of spectrum from .8 to 2.0 μ the dispersion is being influenced by infra-red absorption bands. Organic compounds containing a CH group have strong characteristic absorption bands in the near infra-red. Thus Lecomte ⁽⁷⁾ found that for each of these four alcohols (methyl, ethyl, *n*-propyl, and *n*-butyl) there are two regions of very strong absorption, the one extending from about 3.0 to 3.5 μ and the other from 6.85 to 8.0 μ . The effect of such bands would be to decrease the refractive index as the centre of absorption is approached from the shorter wave-length side, and this probably explains the abnormally rapid decrease in the refractive indices over the region .8 to 2.0 μ . An examination of the discrepancies between calculated and observed values reveals that the differences could be practically eliminated by slightly modifying the constant terms of the existing formulæ, and also adding a small term of the form $-\frac{b\lambda^2}{\lambda_s^2 - \lambda^2}$

b being a constant, λ the wave-length under consideration, and λ_s the wave-length of the infra-red absorption band. It is found that satisfactory agreement is obtained if λ_s is given the value 3.2 μ , corresponding approximately to the centre of the first group of strong infra-red absorption bands. The modified formulæ are given below, and calculated and observed values at infra-red, visible and ultra-violet wave-lengths are given in Table VI.

Methyl alcohol at 16.4° C. :

$$n^2 - 1 = .7502_4 + \frac{.00504_2}{\lambda^2 - (.065)^2} + \frac{.00163_2}{\lambda^2 - (.1470)^2} + \frac{.000193_0}{\lambda^2 - (.1588)^2} - \frac{.0333_6 \lambda^2}{(3.2)^2 - \lambda^2} \dots (1a)$$

TABLE VI.

Wave-length (in microns).	Methyl alcohol (16.4° C.).		Ethyl alcohol (18.4° C.).		<i>n</i> -Propyl alcohol (23.6° C.).		<i>n</i> -Butyl alcohol (13.0° C.).	
	<i>n</i> calc.	<i>n</i> obs.	<i>n</i> calc.	<i>n</i> obs.	<i>n</i> calc.	<i>n</i> obs.	<i>n</i> calc.	<i>n</i> obs.
2.0	1.3152	1.3153	1.3488	1.3485	1.3696	1.3699	1.3904	1.389 ₀ *
1.5	1.3203	1.3200	1.3527	1.3522	1.3736	1.3732	1.3931	1.392 ₆ *
1.0	1.3243	1.3243	1.3559	1.3558	1.3770	1.3765	1.3956	1.396 ₆ *
.8	1.3262	1.3268	1.3580	1.3582	1.3793	1.3792	1.3977	1.398 ₄ *
.6	1.3299	1.3303	1.3625	1.3625	1.3836	1.3837	1.4020	1.4021
.5	1.3335	1.3336	1.3658	1.3658	1.3879	1.3879	1.4063	1.4063
.43	1.3374	1.3372	1.3705	1.3705	1.3928	1.3928	1.4114	1.4114 ₅
.36	1.3442	1.3441 ₅	1.3783	1.3782	1.4013	1.4013 ₅	1.4201	1.4200 ₅
.30	1.3548	1.3554	1.3907	1.3906	1.4219	1.4217	1.4343	1.4342

* These values were deduced from Ingersoll's measurements at 23° C. Owing to the large temperature correction involved, the accuracy of these values is somewhat uncertain.

Ethyl alcohol at 18.4° C. :

$$n^2 - 1 = .8331_1 + \frac{.00540_4}{\lambda^2 - (.065)^2} + \frac{.00227_7}{\lambda^2 - (.1518)^2} + \frac{.000264}{\lambda^2 - (.1618)^2} - \frac{.0244_8 \lambda^2}{(3.2)^2 - \lambda^2} \quad (2a)$$

n-Propyl alcohol at 23.6° C. :

$$n^2 - 1 = .8901_6 + \frac{.00582_4}{\lambda^2 - (.065)^2} + \frac{.00287_5}{\lambda^2 - (.1565)^2} - \frac{.0256_1 \lambda^2}{(3.2)^2 - \lambda^2} \quad (3a)$$

n-Butyl alcohol at 13.0° C. :

$$n^2 - 1 = .9398_3 + \frac{.00606_4}{\lambda^2 - (.065)^2} + \frac{.00304_4}{\lambda^2 - (.1577)^2} - \frac{.0109_3 \lambda^2}{(3.2)^2 - \lambda^2} \quad (4a)$$

The agreement between calculated and observed values is, in general, satisfactory over the whole range of wave-lengths. The measurements at infra-red wave-lengths are probably much less accurate than those at shorter wave-lengths, but even when more accurate data are available for the infra-red region, it would appear that the type of formula considered in this paper will still be applicable.

Calculation of $\frac{e}{m}$ for the Resonators controlling the Dispersions.

Larmor's derivation of the expression $\delta = \frac{e}{2mC^2} \lambda \cdot \frac{dn}{d\lambda}$ involves the assumption that $\frac{e}{m}$ is the same for all the resonators concerned. Combining the above expression with the natural dispersion formula

$$n^2 - 1 = b_0 + \sum_r \frac{b_r}{\lambda^2 - \lambda_r^2},$$

we get

$$\delta = - \frac{e}{2mC^2} \cdot \frac{1}{n\lambda^2} \sum_r b_r \left(\frac{\lambda^2}{\lambda^2 - \lambda_r^2} \right)^2.$$

If we assume that this summation holds good in the above form when different $\left(\frac{e}{m}\right)$'s are involved, then

$$n\delta\lambda^2 = \sum_r K_r \left(\frac{\lambda^2}{\lambda^2 - \lambda_r^2} \right)^2,$$

where

$$K_r = - \left(\frac{e}{m} \right)_r \frac{b_r}{2C^2}.$$

TABLE VII.

Liquid.	Molr. wt.	Temp. °C.	$K_1, b_1.$	$K_2, b_2.$	$K_3, b_3.$	$\left(\frac{e}{m}\right)_1 \cdot \left \left(\frac{e}{m}\right)_2\right \times 10^7 \text{ e.m.u.}$	$\left(\frac{e}{m}\right)_3$
Methyl alcohol ...	32.03	16.4	$\begin{bmatrix} .00317_1 \\ .00304_2 \end{bmatrix}$	$\begin{bmatrix} .000913_2 \\ .00163_2 \end{bmatrix}$	$\begin{bmatrix} .000103_1 \\ .000193 \end{bmatrix}$	1.098	.935
Ethyl alcohol * ...	46.05	18.4	$\begin{bmatrix} .00354_0 \\ .00340_4 \end{bmatrix}$	$\begin{bmatrix} .00133_6 \\ .00227_7 \end{bmatrix}$	$\begin{bmatrix} .000149_9 \\ .000264 \end{bmatrix}$	1.143	.989
n-Propyl alcohol* .	60.06	23.6	$\begin{bmatrix} .00371_1 \\ .00582_4 \end{bmatrix}$	$\begin{bmatrix} .00163_3 \\ .00287_5 \end{bmatrix}$	—	1.112	.991
n-Butyl alcohol ...	74.08	13.0	$\begin{bmatrix} .00389_7 \\ .00606_4 \end{bmatrix}$	$\begin{bmatrix} .00173_9 \\ .00304_4 \end{bmatrix}$	—	1.121	.996
Allyl alcohol *	58.05	20.0	$\begin{bmatrix} .00374_8 \\ .00576_0 \end{bmatrix}$	$\begin{bmatrix} .00349_3 \\ .00654_4 \end{bmatrix}$	—	1.135	.931

* A slight temperature correction has been applied to the K's for these liquids in order to correct them to the temperature of the refractive index measurements.

Formulae of the above type for the magneto-optical and natural dispersions have been calculated for the five liquids considered in this paper, so that $\left(\frac{e}{m}\right)$ for the different resonators can be readily obtained. The constants of the dispersion formulae together with the values of $\left(\frac{e}{m}\right)$ are given in Table VII.

Summary.

(1) The natural dispersions of methyl, ethyl, *n*-propyl, *n*-butyl, and allyl alcohols over the range of spectrum from $\cdot 67$ to $\cdot 30 \mu$ can be represented by formulae of the type

$$n^2 - 1 = b_0 + \sum_r \frac{b_r}{\lambda^2 - \lambda_r^2}, \quad \text{where}$$

n = refractive index for wave-length λ , and

b_0, b_r, λ_r , are constants.

The constants λ_r have been identified with the extreme ultra-violet absorption bands of the substances in the vapour state. The values of the constants b_0, b_r, λ_r for each liquid are tabulated below:—

Liquid.	Temp.°C.	b_0 .	b_1 .	b_2 .	b_3 .	λ_1 .	λ_2 .	λ_3 .
Methyl alcohol ..	16.4	$\cdot 74963_7$	$\cdot 00504_2$	$\cdot 00163_2$	$\cdot 000193_0$	$\cdot 065$	$\cdot 1470$	$\cdot 1588$
Ethyl alcohol ...	18.4	$\cdot 83261_0$	$\cdot 00540_4$	$\cdot 00227_7$	$\cdot 000264$	$\cdot 065$	$\cdot 1518$	$\cdot 1618$
<i>n</i> -Propyl alcohol.	23.6	$\cdot 88966_3$	$\cdot 00582_4$	$\cdot 00287_5$	—	$\cdot 065$	$\cdot 1565$	
<i>n</i> -Butyl alcohol .	13.0	$\cdot 93943_3$	$\cdot 00606_4$	$\cdot 00304_4$	—	$\cdot 065$	$\cdot 1577$	
Allyl alcohol ...	20.0	$\cdot 96020_7$	$\cdot 00576_0$	$\cdot 00654_4$	—	$\cdot 075$	$\cdot 1650$	

(2) For methyl, ethyl, *n*-propyl, and *n*-butyl alcohols, infra-red refractive index measurements have been compared with values calculated from the formulae. At wave-lengths greater than $\cdot 7 \mu$ the formulae yield values in excess of those observed, and it appears that over the range $\cdot 8$ to $2\cdot 0 \mu$ the natural dispersion is being influenced by infra-red absorption bands. The discrepancies can be practically eliminated by slightly modifying the constants b_0 and by the addition of a small term of the form $-\frac{b\lambda^2}{\lambda_s^2 - \lambda^2}$ to each of the formulae. The constant λ_s has been identified with the wave-length of the infra-red absorption band of these liquids centred about $3\cdot 2 \mu$. The modified formulae are then found to be satisfactory at infra-red, visible, and ultra-violet wave-lengths within the limits of experimental error.

(3) From the constants of the natural dispersion formulæ and those of the corresponding magneto-optical dispersion formulæ (given in earlier papers by the author) it has been possible to calculate the values of $\left(\frac{e}{m}\right)$ for the different resonators responsible for the dispersions. The following broad conclusions may be made concerning the ratio of the charge to the mass of the resonators controlling the dispersions of these liquids in the visible and near ultra-violet spectrum.

(a) The values of $\left(\frac{e}{m}\right)$ indicate that the electron is the resonator, but in all cases the calculated values are much lower than the accepted value (1.77×10^7 e.m.u.) for the electron.

(b) In the case of each liquid, $\left(\frac{e}{m}\right)$ for the respective resonators, increases with increasing frequency.

(c) Apart from the values for ethyl alcohol and one of those for allyl alcohol, it appears that the values of $\left(\frac{e}{m}\right)$ increase with increasing molecular weights. It may be noted that the results of previous workers in these laboratories using simpler formulæ also show that the value of $\left(\frac{e}{m}\right)$ for ethyl alcohol appears to be greater than for the other alcohols in the series. With this exception, earlier work done in these laboratories also yielded the result that $\left(\frac{e}{m}\right)$ increases with increasing molecular weight.

References.

- (1) Beynon and Evans, *Phil. Mag.* xxv. pp. 476–488 (March 1938).
- (2) Beynon, *Phil. Mag.* xxv. pp. 443–455 (March 1938).
- (3) Stephens (E.) and Evans, *Phil. Mag.* x. p. 765 (Nov. 1930).
- (4) Jones and Evans, *Phil. Mag.* v. p. 599 (March 1928).
- (5) Seegert, Landolt and Bornstein, 'Tables of Physical Constants,' pp. 968, 969.
- (6) Ingersoll, *Journ. Opt. Soc. Am.* vi. p. 663 (Sept. 1922).
- (7) Lecomte, *Comptes Rendus*, clxxx. p. 185 (1925).

Physics Department,
University College, Swansea.

II. *A General Interferential Method.*

By L. STURKEY and B. P. RAMSAY,
University of Kentucky *.

[Received June 19, 1939.]

Summary.

Although interferometry deals with various instruments, each treated individually, it appears possible to derive a general intensity equation directly applicable to all. In deriving such an equation it is assumed that the number of beams to be considered must be indefinite. For convenience, these beams are grouped into compatible sets, but for perfect generality the number of beams in each set and the number of sets remain undefined. Special cases of the resulting intensity equation are discussed. The process of applying this general intensity function to specific optical problems is defined as *the interferential method*.

1. *Introduction.*

INTERFERENCE may be considered a method for solving a group of related problems in optics. These problems involve finding the intensity produced at a point by a number of rays in cases where the intensity of the combination is not necessarily the sum of the intensities of the individual rays, although each ray obeys the laws of geometrical optics.

In the actual application of the interferential method to experimental measurements, observations are as a rule made of certain effects produced on the form, or change in form, of the intensity pattern of a particular interferometer. In such applications the various interferential devices are usually treated as separate optical problems, and it is not generally evident that the instrument involved is merely a medium for the application of the method of interference to the problem.

If a general intensity equation could be devised which would include the intensity distribution of every interferometer as special cases, much of the lack of direct connexion between the method and its applications would be removed. The construction of this general function will be based upon the following considerations :

First, it is evident that, for the sake of generality, the number of beams to be superposed must be indefinite.

* Communicated by the Authors.

Second, it is possible to group these beams into a number of *compatible* sets. A *compatible* set is defined as consisting of any number of beams whose amplitudes may be arranged in geometric sequence,

$$s, sr, sr^2, \dots sr^{k-1},$$

and whose respective phase differences form an arithmetical sequence in the same order

$$\phi, \phi + \alpha, \phi + 2\alpha, \dots \phi + (k-1)\alpha.$$

Third, by Young's principle of superposition, each *i*th compatible set will have a resultant amplitude of magnitude Z_i and phase γ_i .

Fourth, it appears that adequate generality may be obtained by assuming that resultant vector amplitudes of the various sets may also be arranged into a compatible set. The advisability of such a restriction may be tested only by the applicability of the method.

2. Derivations.

To describe the various compatible sets of beams, the following notation, geometrically represented in fig. 1, will be employed :

For the *i*th set :

Z_i = resultant amplitude.

k_i = number of beams in the set.

$s_i, s_i r_i, s_i r_i^2, \dots s_i r_i^{(k_i-1)}$ = amplitudes of beams in set.

$\phi_i, \phi_i + \alpha_i, \dots \phi_i + (k_i - 1)\alpha_i$ = corresponding phases of beams.

β_i = phase difference between Z_i and s_i .

(a) *Determination of Z_i .*

If Z_x is the *x*-projection of Z_i , and Z_y is the *y*-projection, then

$$Z_i^2 = Z_x^2 + Z_y^2,$$

$$\text{where} \quad Z_x = \sum_0^{k_i-1} s_i r_i^{k_i} \cos k_i \alpha_i, \quad Z_y = \sum_0^{k_i-1} s_i r_i^{k_i} \sin k_i \alpha_i.$$

Z_i^2 may then be found by a well-known procedure ⁽¹⁾. Its value is

$$Z_i^2 = s_i^2 \frac{(1 - r_i^{k_i})^2 + 4r_i^{k_i} \sin \frac{k_i \alpha_i}{2}}{(1 - r_i)^2 + 4r_i \sin \frac{\alpha_i}{2}}.$$

(b) *Determination of β_i .*

The phase angle β_i is determined if its sine and cosine are known. From fig. 1 :

$$\cos \beta_i = \frac{Z_x}{Z_i}, \quad \sin \beta_i = \frac{Z_y}{Z_i},$$

where
$$Z_x = s_i \sum_0^{k_i-1} r_i^{k_i} \cos k_i \alpha_i = \frac{s_i}{2} \left\{ \sum_0^{k_i-1} (r_i e^{j\alpha_i})^{k_i} + \sum_0^{k_i-1} (r_i e^{-j\alpha_i})^{k_i} \right\},$$

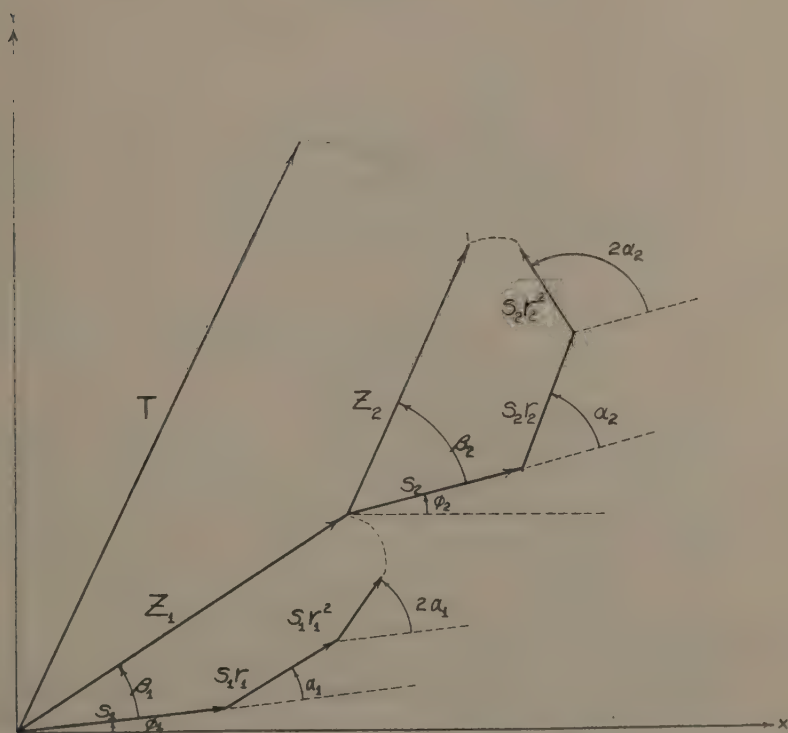
$$Z_y = s_i \sum_0^{k_i-1} r_i^{k_i} \sin k_i \alpha_i = j \frac{s_i}{2} \left\{ \sum_0^{k_i-1} (r_i e^{-j\alpha_i})^{k_i} - \sum_0^{k_i-1} (r_i e^{j\alpha_i})^{k_i} \right\}.$$

Thus

$$Z_x = \frac{s_i}{2} \frac{r_i^{k_i+1} [e^{j(k_i-1)\alpha_i} + e^{-j(k_i-1)\alpha_i}] - r_i^{k_i} [e^{jk_i\alpha_i} + e^{-jk_i\alpha_i}] - r_i [e^{j\alpha_i} + e^{-j\alpha_i}] + 2}{1 + r_i^2 - r_i [e^{j\alpha_i} + e^{-j\alpha_i}]},$$

$$Z_y = j \frac{s_i}{2} \frac{r_i^{k_i+1} [e^{-j(k_i-1)\alpha_i} - e^{j(k_i-1)\alpha_i}] - r_i^{k_i} [e^{-jk_i\alpha_i} - e^{jk_i\alpha_i}] + r_i [e^{-j\alpha_i} - e^{j\alpha_i}]}{1 + r_i^2 - r_i [e^{j\alpha_i} + e^{-j\alpha_i}]}.$$

Fig. 1.



Geometrical representation of the superposition of several groups of beams, where each group is arranged as a compatible set.

(c) The General Intensity Function.

The Z_i 's may be considered vectors whose respective directions are the γ_i 's (see fig. 2). The square of their vector resultant will be the resultant intensity I .

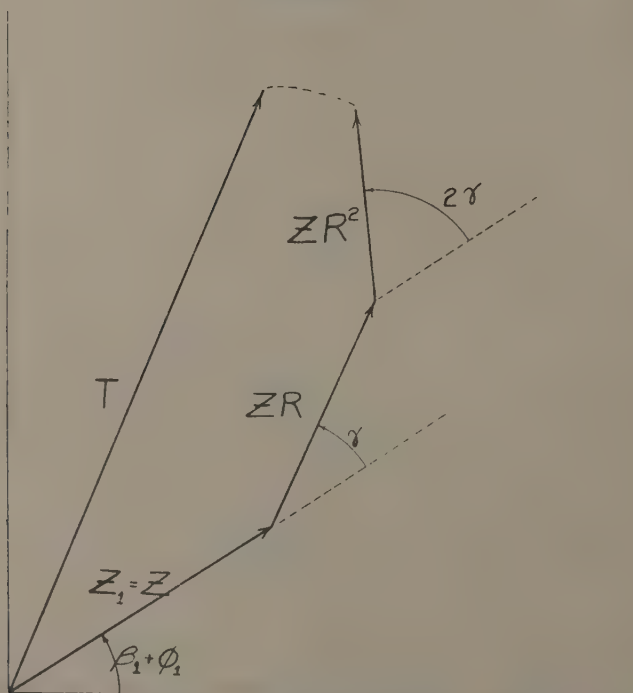
Since it has been assumed that the Z_i 's and the γ_i 's are the amplitudes and phases of a compatible set, the Z_i 's may be arranged in a geometric sequence,

$$Z, ZR, ZR^2, \dots \dots \dots ZR^{K-1},$$

and the γ_i 's in an arithmetical sequence,

$$\beta, \beta + \gamma, \beta + 2\gamma, \dots \dots \dots \beta + (K-1)\gamma.$$

Fig. 2.



Geometrical representation of the superposition of several groups of beams, where the groups themselves are arranged to form a compatible set.

where $Z = Z_1$ and $\beta = \beta_1$. Also

$$\gamma = (\phi_2 - \phi_1) + (\beta_2 - \beta_1).$$

Generally, because of the compatibility assumption, γ may be found from

$$\gamma = (\phi_i - \phi_{i-1}) + (\beta_i - \beta_{i-1}).$$

By the same procedure, used in part (a) of this section, the resultant intensity of the K sets of resultant beams is

$$I = Z^2 \frac{(1 - R^K)^2 + 4R^K \sin^2 \frac{K\gamma}{2}}{(1 - R)^2 + 4R \sin^2 \frac{\gamma}{2}}, \quad \dots \quad (1)$$

where

$$Z = Z_1 \quad \dots \quad (2)$$

$$R = \frac{Z_i}{Z_{i-1}}, \quad \dots \quad (3)$$

$$Z_i^2 = s_i^2 \frac{(1 - r_i^{k_i})^2 + 4r_i^{k_i} \sin^2 \frac{k_i \alpha_i}{2}}{(1 - r_i)^2 + 4r_i \sin^2 \frac{\alpha_i}{2}}, \quad \dots \quad (4)$$

$$\gamma = (\phi_i - \phi_{i-1}) + (\beta_i - \beta_{i-1}), \quad \dots \quad (5)$$

$$\cos \beta_i = \frac{s_i r_i^{k_i+1} \cos (k_i - 1)\alpha_i - r_i^{k_i} \cos k_i \alpha_i - r_i \cos \alpha_i + 1}{Z_i (1 + r_i^2 - 2r_i \cos \alpha_i)}, \quad \dots \quad (6)$$

$$\sin \beta_i = \frac{s_i r_i^{k_i+1} \sin (k_i - 1)\alpha_i - r_i^{k_i} \sin k_i \alpha_i + r_i \sin \alpha_i}{Z_i (1 + r_i^2 - 2r_i \cos \alpha_i)}, \quad \dots \quad (7)$$

The parameters s_i , r_i , k_i , n_i , α_i , ϕ_i are determined by the physical properties of the optical arrangement.

3. Generic Distribution.

The interference equation (1) is more than a general formula from which intensity functions applicable to particular instruments may be conveniently derived. For the general form of the equation describes certain characteristics which are generic to all distribution patterns, and some properties which are not apparent in any one of them.

(a) The Z-constant Distribution.

If Z is considered constant, it is possible to show that principal maxima of (1) occur when $\gamma/2 = m'\pi$. The intensities of the primary maxima have a constant value, except as they may be affected by variations in Z. These maxima coincide with the minimum values of the denominator. The numerator does not have maximum values at these points. The maximum values of the rapidly varying numerator give rise to secondary maxima in the distribution.

The secondary maxima I'' occur when

$$\frac{K\gamma}{2} = (2m'' + 1)\frac{\pi}{2}.$$

Since I'' decreases as the denominator increases, the secondary maxima vary in intensity value, although they are evenly spaced. The largest values are those adjacent to the principal maxima. The smallest values lie midway between the primary maxima.

Between maximum values of I , minima occur at positions for which

$$K\gamma/2 = m'''\pi, \gamma/2 \neq m'''\pi.$$

The angular width of the secondary maxima is $2\pi/K$. The ratio of this width to the angular separation between maxima is $1/K$. The angular width of the principal maxima is twice that of the secondary maxima.

It is a matter of interest that zero values of the intensity can occur when the numerator is zero, Z being still considered constant. That is

$$(1-R^K)^2 + 4R^K \sin^2 \frac{K\gamma}{2} = 0,$$

which is possible only when $R=1$. Moreover, it can be seen that as K becomes indefinitely large, the numerator approaches a constant value. In this way the secondary maxima become non-existent. Although the secondary maxima are not frequently visible, they necessitate troublesome approximating corrections when present. It is also desirable that the minima be zero in order that the visibility be as high as possible.

(b) *The Significance of a Variable Z.*

The true generic distribution is the Z -constant distribution modified by the functional variation of Z . This generic distribution is then the product of formally similar distribution factors; for Z^2 , as given by (4), has the same form as (1). Although this circumstance is frequently noted for slit systems, it may now be observed to be a common property of all interference systems. It may be noted, as in the case of the double slit, that the number, position, and values of the critical points for one of the factors may be altered by the other. Special cases will be observed below.

(c) *Methods of Grouping.*

The resulting intensity equation obtained by this method is apparently somewhat arbitrary, depending upon the chosen grouping of the various terms. For example, the double slit may be considered as the sum of two sets of beams having an infinite number of beams in each set, or as the sum of a large number of sets having two beams per set. Either mathematical convenience or ease of interpretation may determine the method of grouping chosen. The treatments of the special cases discussed below are therefore not unique.

4. Special Cases.

(a) Two-beam Interferometers.

For experimental reasons, the case of (1) where $K=2$ is particularly important. For this case

$$\begin{aligned} \text{or} \quad & \left. \begin{aligned} I &= Z^2 + (RZ)^2 + 2Z(RZ) \cos \gamma, & (a) \\ I &= Z_1^2 + Z_2^2 + 2Z_1Z_2 \cos [\phi_2 - \phi_1 + \beta_2 - \beta_1], & (b) \end{aligned} \right\} \dots (8) \\ \text{If } R=1 \quad & I = 4Z^2 \cos^2 \frac{\gamma}{2}. \dots (c) \end{aligned}$$

(b) Single Slit.

Let $R=1$ and let K become very large. Then

$$I = Z^2 \frac{(1-1^K)^2 + 4 \sin^2 \left(\frac{K\gamma}{2} \right)}{(1-1)^2 + 4 \sin^2 \left(\frac{\gamma}{2} \right)} = Z^2 \frac{\sin^2 \left(\frac{K\gamma}{2} \right)}{\sin^2 \frac{\gamma}{2}}.$$

Since K is very large, $\gamma/2$ is very small and

$$I = \left[(KZ) \frac{\sin \frac{K\gamma}{2}}{\frac{K\gamma}{2}} \right]^2, \dots (9)$$

where $K\gamma$ is the phase difference between the two beams from opposite sides of the slit.

(c) Double Slit.

Let $K=2$ and $R=1$. In this case each of the two sets consists of all the beams from one slit, for which $r=1$ and k is very large. Then

$$\begin{aligned} I &= s^2 \left[\frac{(1-1^k)^2 + 4 \sin^2 \left(\frac{k\alpha}{2} \right)}{(1-1)^2 + 4 \sin^2 \frac{\alpha}{2}} \right] \times \left[\frac{(1-1^2)^2 + 4 \sin^2 \frac{\gamma}{2}}{(1-1)^2 + 4 \sin^2 \left(\frac{\gamma}{2} \right)} \right]. \\ \therefore \quad I &= I_0 \frac{\sin^2 \beta}{\beta^2} \cos^2 \left(\frac{\gamma}{2} \right). \dots (10) \end{aligned}$$

Here a is the width of each slit and b is the distance between slits. Thus

$$\begin{aligned} \beta &= \frac{k\alpha}{2} = \frac{\pi\alpha}{\lambda} (\sin i + \sin i'), \\ \gamma &= \frac{2\pi}{\lambda} (a+b)(\sin i + \sin i'). \end{aligned}$$

(d) *Grating.*

Here the conditions are the same as for the double slit except that $K=N$, the number of rulings on the grating

$$I=I_0 \frac{\sin^2 \beta}{\beta^2} \times \frac{\sin^2 \left(\frac{N\gamma}{2} \right)}{\sin^2 \left(\frac{\gamma}{2} \right)} (11)$$

(e) *Grating Interferometer* ⁽²⁾.

In this case $K=2$, $r=1$, and k_1 and k_2 are determined by the number of rulings on the two gratings

$$I=s_1^2 \left[\frac{\sin \frac{k_1 \alpha_1}{2}}{\sin \frac{\alpha_1}{2}} \right]^2 + s_2^2 \left[\frac{\sin \frac{k_2 \alpha_2}{2}}{\sin \frac{\alpha_2}{2}} \right]^2 + 2s_1 s_2 \cos \left[\phi + \frac{(k_2-1)\alpha_2 - (k_1-1)\alpha_1}{2} \right] . . . (12)$$

(f) *Lummer-Gehrcke Plate.*

For this instrument the intensity pattern is described directly by the Z-constant distribution. The same intensity equation is used by the ruled interferometer of Machler and Fisher ⁽³⁾.

(g) *Fabry-Perot Interferometer.*

If Z is constant, R less than unity, and K very large, equation (1) becomes the intensity equation of the finesse distribution

$$I = \frac{Z^2}{1+R^2-2R \cos \gamma} = \frac{I_{\max}}{1+F \sin^2 \left(\frac{\gamma}{2} \right)} , (13)$$

where $F=4R/(1-R)^2$, which Fabry has named the *coefficient de finesse*.

(h) *Reflexion from a Parallel Plate.*

The various beams reflected from a parallel plate when a beam of amplitude A_0 is incident upon it may be divided into two sets, the first set consisting of a single beam $A_0 a$ and the other of a compatible series having amplitudes

$$\underline{A_0 b d c}, \quad \underline{c^2 A_0 b d c}, \quad \underline{c^4 A_0 b d c}, \quad \dots$$

and phases $0, \quad \epsilon, \quad 2\epsilon, \quad \dots$

Let β be the phase difference introduced between the first beam of the above set and the single beam due to the different numbers and types of reflexions which the two beams have experienced. Here Stokes's

relations ⁽⁴⁾ between a , b , c , and d —the amplitude coefficients of reflexion and transmission—are not assumed. Therefore

$$\begin{array}{lll} s_1 = A_0 a. & s_2 = A_0 b \, dc. & r_2 = r = c^2. \\ k_1 = 1. & k_2 = \infty. & \\ \phi_1 = -(\beta - \epsilon). & \phi_2 = 0. & \\ K = 2. & \alpha_2 = \epsilon. & \end{array}$$

Then
$$I = S_1^2 + \frac{s_2^2}{1 + r^2 - 2r \cos \epsilon},$$

$$+ 2 \times \frac{s_1 s_2}{1 + r^2 - 2r \cos \epsilon} [\cos (\beta - \epsilon) - r \cos \beta]. \quad \dots \quad (14)$$

This equation is that given by Anderson ⁽⁵⁾. It reduces to the equations given by Gilchrist ⁽⁶⁾ and by Airy ⁽⁷⁾ under conditions which have been discussed by Anderson.

(i) *Houston's Compound Interferometer.*

In Houston's arrangement ⁽⁸⁾ the beams may be grouped into an infinite number of sets, each set containing an infinite number of beams,

$$\begin{array}{lll} s_1 = A_0 b^4. & s_2 = a^2 A_0 b^4. & s_3 = a^4 A_0 b^4. \\ \alpha_1 = \beta_2. & \alpha_2 = \beta_2. & \alpha_3 = \beta_2. \\ r_1 = a^2 = r. & r_2 = a^2 = r. & r_3 = a^2 = r. \\ k_1 = \infty. & k_2 = \infty. & k_3 = \infty. \\ \phi_1 = 0. & \phi_2 = \beta_1. & \phi_3 = 2\beta_1. \text{ etc.} \end{array}$$

Then
$$\begin{array}{l} R = a^2 = r, \\ K = \infty, \\ \gamma = \beta_1, \end{array}$$

where β_1 is the phase difference introduced by one reflexion between the first pair of reflecting surfaces, and β_2 is that introduced for the second pair. Consequently,

$$I = \frac{(A_0 b^4)^2}{(1 + r^2 - 2r \cos \beta_1)(1 + r^2 - 2r \cos \beta_2)} \dots \dots \dots (15)$$

5. *Further Possibilities.*

The number of special cases which may be derived from the general equations could be extended indefinitely. However, the cases described in the preceding section are the more familiar ones and serve to illustrate the method. Obvious cases which have not been treated are Brewster's fringes, the pile of plates, and the absorbing prism ⁽⁹⁾ *. In such cases, s_i^2 may

* For the absorbing prism, R would have an exponential character, of the form $e^{-\mu x}$.

play the same sort of rôle in the Z_i^2 factor (4) as Z^2 does in the generic distribution (1). That is, for such cases, we have to set

$$s_i^2 = \sigma_i^2 \frac{(1 - \rho_i^2)^2 + 4\rho_i^2 \sin^2\left(\frac{\xi_i \delta_i}{2}\right)}{(1 - \rho_i^2)^2 + 4\rho_i^2 \sin^2\left(\frac{\delta_i}{2}\right)} \dots \dots \dots (16)$$

This process may be repeated for σ_i , and continued indefinitely. In every case I becomes a product of similar factors. The complexity of an interference pattern probably increases as the number of factors required in the product increases, since each factor, in general, gives rise to its own secondary maxima. It is the simplicity of the relation between the beams in an interferential device, and not the number of beams, which determines the complexity of the intensity pattern produced. For example, in the Houston arrangement the intensity pattern is useful only when β_2 is some integral multiple of β_1 .

Interferential instruments may be classified according as the optical elements are placed in a series or parallel arrangement. In a series arrangement, each optical element would, in general, have its own distribution factor. In a parallel arrangement of similar elements, there would be one factor to describe the element and another to describe the arrangement of the elements. This latter result has been derived by diffraction theory⁽¹⁰⁾. In a series arrangement it is evident that R in (1) could not be unity, although it might for a parallel arrangement, and hence zero minima could occur only for parallel devices. This fact could be used as a criterion for classifying interferential systems.

6. Conclusion.

There are other methods for deriving the results obtained in this paper. For example, the method of diffraction has been applied to many of them. The fact that the properties of a large number of optical arrangements may be described by a single equation suggests that the process of obtaining the intensity pattern in this way be recognized as a distinct method for solving a certain class of optical problems. It is proposed that this procedure be known as *the interferential method*. The possibilities of the method do not consist solely of obtaining the intensity equation, because analytical expressions for the resolving power, dispersion, spectral range, etc., can be obtained from information deduced from the intensity equation.

Although there may be cases in which it would be awkward to apply this general interferential method, every important interferential problem seems to be included. Therefore, equation (1) has the same sort of

significance in the method of interference as the Kirchhoff equation in the method of diffraction.

References.

- (1) 'Handbuch der Physik,' xx. Springer, Berlin (1928), pp. 12, 13.
- (2) B. P. Ramsay, J. O. S. A. xxiv. pp. 253-258 (1934).
- (3) R. C. Machler and R. A. Fisher, J. O. S. A. xxv. pp. 315-319 (1935).
- (4) T. Preston, 'Theory of Light,' Macmillan and Co., New York (1928), pp. 205-206.
- (5) W. E. Anderson, J. O. S. A. xxvii. pp. 300-302 (1937)
- (6) L. Gilchrist, Phys. Rev. xxvii. pp. 596-605 (1926).
- (7) G. B. Airy, Phil. Mag. ii. p. 20 (1833); and *Pogg. Ann.* xli. p. 512 (1837),
q. v.; Born, *Optik*, Springer, Berlin (1933), p. 123.
- (8) W. V. Houston, Phys. Rev. xxix. pp. 478-484 (1927).
- (9) C. M. Sparrow, *Astrophys. J.* xliv. pp. 76-86 (1916).
- (10) P. Drude, 'Theory of Optics,' Longmans, Green and Co., New York (1917), pp. 219-220.

III. *Rocket Flight to the Moon.*

By J. W. CAMPBELL, Ph.D.*

[Received August 18, 1939.]

IN an Edmonton paper in August 1938 there appeared an editorial captioned "Flying to the Moon."

The writer of the editorial quoted an astronomer as having said that "the possibility of travelling to the earth's satellite in a rocket does not seem so remote now as the realization of the television dream did less than a century ago," and in view of the achievements in television the editor painted a rather fascinating picture of the possibilities of space travel. He further stated that the astronomer, while not predicting positively that people from the earth ever will be able to visit the moon, had said he did not consider flight to the moon impossible at some time in the future, considering the scientific principles involved.

But while flight to the moon may be conceded as theoretically possible it is doubtful if some of the difficulties, from a practical standpoint, are fully realized. It is the purpose of this article to discuss some aspects of the problem and to present some numerical calculations regarding mass requirements.

To begin with there are two kinds of rocket flight. A rocket is of the nature of a projectile, and when a projectile is fired there are two motions produced, viz., the forward motion of the projectile and the motion in the opposite direction of the gun. Where, as is usual, the gun when fired is resting on the earth, then the earth takes up some of the recoil from the firing. But if a gun were flying through space and a projectile were fired from it, then the projectile and the gun would receive all the momentum resulting from firing, the change in the velocity of the projectile being greater than the change in the velocity of the gun due to its mass being much smaller.

It is clear, then, that to have an observer travel by the rocket principle he may be thought of as travelling in the rocket, or as travelling in the more massive body from which the rocket is fired.

1. *Travelling in the Rocket.*

For travelling by this method it is necessary to have a system of rockets within rockets. Thus the original rocket might be fired from the earth,

* Communicated by the Author.

and if it could be fired with a velocity of seven miles per second, and if there were no atmosphere to resist, it would soar off and eventually reach the moon, if fired in the right direction. But the highest muzzle velocity yet attained is under one mile per second, and, moreover, the atmospheric resistance is large at high velocities.

To overcome this situation, where the speed has been reduced after reaching a certain height, or rather distance from the earth, an inner rocket is fired and the outer one performs the function of the gun in taking up the recoil. Later on another inner rocket is released, and again the then outer shell takes up the recoil. And so on.

Now in order to get much increase of speed imparted to the fired rocket it would be necessary to have the shell which was discarded at each firing much more massive than the rocket being fired. The series of masses remaining after successive firings would decrease according to the exponential law, and so it is obvious that the original rocket would have to be many times as massive as the innermost rocket of all. Hence if the latter is to provide living accommodation for at least one observer, the original rocket would have to be enormous.

But mass requirement is not the only difficulty for an observer travelling in such a rocket system. An abrupt change of velocity is equally fatal to an observer, irrespective of how it occurs. The sudden stop when an aeroplane falls and hits the ground is usually fatal to the pilot, and the sudden start when the inner core of rockets was fired from the outer shell would be equally fatal to an occupant of the inner rocket.

For this latter reason the possibility of an observer flying to the moon by travelling in the rocket may be rejected as impracticable, and we shall consider the problem of the other type of flight.

2. Travelling in the more Massive Body.

A complete solution of this type of flight will not be attempted, but the problem will be considered from the point of view of minimum mass requirement.

When a mass m , moving at velocity v , is augmented by an increment Δm travelling in the same direction with velocity v' , then by the conservation of linear momentum

$$(v' - v)\Delta m = m\Delta v,$$

whence

$$(v' - v)\frac{dm}{dt} = m\frac{dv}{dt}, \quad . \quad . \quad . \quad . \quad . \quad . \quad (1)$$

if the increments are maintained steadily.

It is clear that this equation will also apply to the case where acceleration is produced by decreasing mass. For in that case, if dv/dt is positive,

then dm/dt is negative if $v'-v$ is negative; that is, if the matter is fired backward. Similarly for negative acceleration by firing matter forward.

Suppose now that there is a mass M_1 , of radius R_1 , at O , the origin, and a mass M_2 , of radius R_2 , at position a , and that the mass m at position x is moving under the gravitational attractions of M_1 and M_2 and under the influence of "rocket propulsion."

Then we have

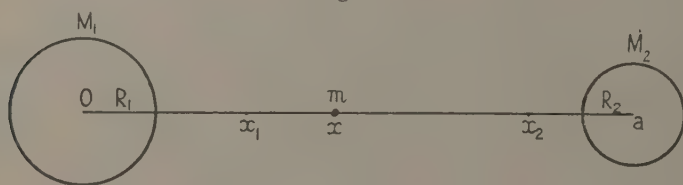
$$m \frac{dv}{dt} = (v'-v) \frac{dm}{dt} - k_1 \frac{m}{x^2} + k_2 \frac{m}{(x-a)^2}, \quad \dots \dots (2)$$

where

$$k_1 = kM_1, \quad k_2 = kM_2. \quad \dots \dots (3)$$

Now for dm/dt negative, $v'-v$ is the velocity of separation, and we shall consider the case where this quantity is constant, A say. This is permissible when the quantity of matter in the process of being fired at any instant is small relative to the whole mass.

Fig. 1.



Then we can write

$$m \frac{d}{dx} \frac{v^2}{2} = Av \frac{dm}{dx} - k_1 \frac{m}{x^2} + k_2 \frac{m}{(x-a)^2}, \quad \dots \dots (4)$$

or

$$Av \frac{dm}{m} = \frac{d}{dx} \frac{v^2}{2} dx + \frac{k_1}{x^2} dx - \frac{k_2}{(x-a)^2} dx. \quad \dots \dots (5)$$

We shall now consider a hypothetical journey of m from M_1 to M_2 , and we shall apply it to the case where m is a "rocket ship" in which an observer is making a trip from the earth to the moon.

In making such a trip either a straight or a curved path might be followed. In the case of a curved path regulation of direction could only be effected by shooting off material in a suitable direction, and speed could only be controlled by shooting off material in the line of motion, either forward or back.

It is clear, then, that the minimum requirements of expenditure of mass in controlling motion will occur if none has to be expended in controlling direction, and so, in order to get an idea of the minimum mass requirements, we shall disregard the orbital motion of the moon about the earth

and consider the path of m as along the straight line connecting the centres of M_1 and M_2 .

Atmospheric resistance will be neglected. For while the earth's atmosphere would form a cushion for landing, and thus save some mass expenditure in controlling speed, it would form an impediment on leaving and hence require an additional mass expenditure to overcome this impediment. Moreover, if air resistance were allowed for, there would be greater mass expenditure on leaving, since the mass to be propelled would then be larger and the resistance greater, than would be saved when returning, at which time the mass to be accelerated would be smaller. Hence neglect of air resistance is consistent with the finding of a *minimum mass requirement*.

Again, in making a direct trip one might proceed by various velocity laws. Thus he might get up speed to some value c' , maintain this speed constant until within a short distance of the moon, and then decelerate to land. But any "control" of speed to maintain it constant would require mass expenditure. Hence a minimum of mass requirement will occur when constancy of speed is not maintained over any section of the trip. It appears, therefore, that a minimum of mass requirement will occur when there is sufficient speed produced at the beginning, so that the traveller may "coast" until within a suitable distance of the moon, and slow down by further mass expenditure.

Let us then consider a hypothetical trip to the moon under the following conditions :—

Using the notation of fig. 1 we shall suppose that m moves from position R_1 (the surface of M_1 , the earth) to position x_1 under an imposed acceleration by rocket propulsion which is constant; that the speed attained at x_1 is sufficient so that m can "coast" under the gravitational attractions of M_1 and M_2 and pass the position of zero potential; that from some position x_2 it moves to $(a-R_2)$ (the surface of M_2 , the moon) under an imposed retardation which again is constant; and that initial and final velocities are zero.

By equation (5) the imposed acceleration due to rocket propulsion is $(Av/m)(dm/dx)$. Hence we take

$$Av \frac{dm}{m} = K dx, \quad R_1 \leq x \leq x_1, \quad (6)$$

where K is constant.

Then by equation (5)

$$\frac{d}{dx} \frac{v^2}{2} dx + \frac{k_1}{x^2} dx - \frac{k_2}{(x-a)^2} dx = K dx, \quad R_1 \leq x \leq x_1, \quad . . . (7)$$

and hence
$$\frac{v^2}{2} - \frac{k_1}{x} + \frac{k_2}{x-a} = Kx + C_1, \quad R_1 \leq x \leq x_1. \quad (8)$$

Then
$$dt = \frac{dx}{\left\{ \frac{2k_1}{x} - \frac{2k_2}{x-a} + 2Kx + 2C_1 \right\}^{\frac{1}{2}}}, \quad R_1 \leq x \leq x_1. \quad \dots \dots (9)$$

Now in the retardation from x_2 to $a - R_2$ equation (6) again will apply, if we assume an imposed acceleration over $R_1 \leq x \leq x_1$ and the imposed deceleration over $x_2 \leq x \leq a - R_2$ to be obtained from rocket propulsions which are numerically equal. For to produce a deceleration, the matter would be shot forward instead of backward, and so the signs on both sides of equation (6) would be reversed. This, of course, would leave it unaltered, and therefore we have

$$Av \frac{dm}{m} = K dx, \quad x_2 \leq x \leq a - R_2. \quad \dots \dots (10)$$

Then
$$\frac{d}{dx} \frac{v^2}{2} dx + \frac{k_1}{x^2} dx - \frac{k_2}{(x-a)^2} dx = -K dx, \quad x_2 \leq x \leq a - R_2, \quad \dots (11)$$

and therefore

$$\frac{v^2}{2} - \frac{k_1}{x} + \frac{k_2}{x-a} = -Kx + C_2, \quad x_2 \leq x \leq a - R_2. \quad \dots \dots (12)$$

Hence
$$dt = \frac{dx}{\left\{ \frac{2k_1}{x} - \frac{2k_2}{x-a} - 2Kx + 2C_2 \right\}^{\frac{1}{2}}}, \quad x_2 \leq x \leq a - R_2. \quad \dots (13)$$

Now with gravitational control only we have

$$m \frac{d}{dx} \frac{v^2}{2} = -k_1 \frac{m}{x^2} + k_2 \frac{m}{(x-a)^2}, \quad \dots \dots (14)$$

whence

$$\frac{v^2}{2} = \frac{k_1}{x} - \frac{k_2}{x-a} + C. \quad \dots \dots (15)$$

Let $v=0$ where the gravitational potential is zero; that is, where

$$-k_1 \frac{m}{x^2} + k_2 \frac{m}{(x-a)^2} = 0.$$

Then

$$-\frac{M_1}{x^2} + \frac{M_2}{(x-a)^2} = 0,$$

and thence we obtain

$$x = \frac{a}{1 + \sqrt{M_2/M_1}}, \quad x-a = \frac{-a\sqrt{M_2/M_1}}{1 + \sqrt{M_2/M_1}}.$$

Therefore

$$C = -\frac{k}{a} (\sqrt{M_1} + \sqrt{M_2})^2 = -\frac{k_1 + k_2 + \sqrt{k_1 k_2}}{a}.$$

Hence (15) becomes

$$\frac{v^2}{2} = \frac{k_1}{x} - \frac{k_2}{x-a} - \frac{k_1 + k_2 + \sqrt{k_1 k_2}}{a}. \quad \dots \dots (16)$$

Then by (8), (12), and (16) we have

$$\left. \begin{aligned} \frac{k_1}{x_1} - \frac{k_2}{x_1 - a} + Kx_1 + C_1 &= \frac{k_1}{x_1} - \frac{k_2}{x_1 - a} - \frac{k_1 + k_2 + \sqrt{k_1 k_2}}{a}, \\ \frac{k_1}{x_2} - \frac{k_2}{x_2 - a} - Kx_2 + C_2 &= \frac{k_1}{x_2} - \frac{k_2}{x_2 - a} - \frac{k_1 + k_2 + \sqrt{k_1 k_2}}{a}. \end{aligned} \right\} \quad (17)$$

Therefore

$$\left. \begin{aligned} x_1 &= -\frac{1}{K} \left\{ C_1 + \frac{k_1 + k_2 + \sqrt{k_1 k_2}}{a} \right\}, \\ x_2 &= +\frac{1}{K} \left\{ C_2 + \frac{k_1 + k_2 + \sqrt{k_1 k_2}}{a} \right\}. \end{aligned} \right\} \quad \dots \dots \dots (18)$$

Again, $v=0$ at $x=R_1$, and at $x=a-R_2$.

Therefore, by (8) and (12),

$$\left. \begin{aligned} C_1 &= -KR_1 - \frac{k_1}{R_1} - \frac{k_2}{a-R_1}, \\ C_2 &= +K(a-R_2) - \frac{k_1}{a-R_2} - \frac{k_2}{R_2}. \end{aligned} \right\} \quad \dots \dots \dots (19)$$

Now equations (6) and (10) may be written

$$A \frac{dm}{m} = K dt, \quad \dots \dots \dots (20)$$

and the solution of this equation is

$$A \log m = Kt + \text{constant}. \quad \dots \dots \dots (21)$$

The mass requirements for rocket propulsion can therefore be found by integrating (9) and (13) to find the intervals of time to go from R_1 to x_1 and again from x_2 to $a-R_2$, and then using (21) to find the ratio of the initial and final masses.

Equations (9) and (13), however, give rise to improper definite integrals when the initial and terminal velocities are zero. Hence they require some special device for integrating.

3. Numerical Solutions.

The following values apply to all earth-moon cases :

$$\left. \begin{aligned} \frac{k_1}{R_1^2} &= 32.2 \frac{\text{ft.}}{\text{sec.}^2}, & R_1 &= 3960 \text{ mi.}, \\ \frac{M_1}{M_2} &= 81.56, & a &= 240,000 \text{ mi.}, \\ R_2 &= 1080 \text{ mi.} \end{aligned} \right\} \quad \dots \dots \dots (22)$$

Thus

$$\left. \begin{aligned} k_1 &= 95,600 \frac{\text{mi.}^3}{\text{sec.}^2}, & k_2 &= 1172 \frac{\text{mi.}^3}{\text{sec.}^2}, \\ \frac{k_1 + k_2 + \sqrt{k_1 k_2}}{a} &= 0.446 \frac{\text{mi.}^2}{\text{sec.}^2}. \end{aligned} \right\} \dots \dots \dots (23)$$

In order to integrate (9) in the vicinity of R_1 and (13) in the vicinity of $a - R_2$, let

$$\left. \begin{aligned} x &= R_1 + y, & R_1 &\leq x \leq x_1, \\ x &= a - R_2 - z, & x_2 &\leq x \leq a - R_2. \end{aligned} \right\} \dots \dots \dots (24)$$

Then in the denominator of (8)

$$\left. \begin{aligned} &\frac{k_1}{x} - \frac{k_2}{x-a} + Kx + C_1 \\ &= \frac{k_1}{R_1 + y} - \frac{k_2}{R_1 + y - a} + K(R_1 + y) - KR_1 - \frac{k_1}{R_1} - \frac{k_2}{a - R_1} \\ &= y \left\{ K - \frac{k_1}{R_1^2} - \frac{k_2}{(a - R_1)^2} \right\} + y^2 \left\{ \frac{k_1}{R_1^3} - \frac{k_2}{(a - R_1)^3} \right\} + \dots \end{aligned} \right\} \dots (25)$$

and in the denominator of (13)

$$\left. \begin{aligned} &\frac{k_1}{x} - \frac{k_2}{x-a} - Kx + C_2 \\ &= \frac{k_1}{a - R_2 - z} + \frac{k_2}{R_2 + z} - K(a - R_2 - z) + K(a - R_2) - \frac{k_1}{a - R_2} - \frac{k_2}{R_2} \\ &= z \left\{ K - \frac{k_1}{(a - R_2)^2} - \frac{k_2}{R_2^2} \right\} + z^2 \left\{ \frac{k_2}{R_2^3} - \frac{k_1}{(a - R_2)^3} \right\} + \dots \end{aligned} \right\} \dots \dots \dots (26)$$

We shall now consider the case where

$$K = 64.4 \frac{\text{ft.}}{\text{sec.}^2} = 0.01220 \frac{\text{mi.}}{\text{sec.}^2} \dots \dots \dots (27)$$

Then by (22), (23), (25), (26), and (27) equations (9) and (13) become, for y and z small,

$$dt = \frac{dy}{\sqrt{p_1(2p_2y + y^2)}}, \dots \dots \dots (9')$$

$$dz = - \frac{dz}{\sqrt{q_1(2q_2z + z^2)}}, \dots \dots \dots (13')$$

where

$$\left. \begin{aligned} p_1 &= 0.00000308 \text{ sec.}^{-2}, \\ p_2 &= 1980 \text{ mi.}, \\ q_1 &= 0.000001862 \text{ sec.}^{-2}, \\ q_2 &= 6000 \text{ mi.} \end{aligned} \right\} \dots \dots \dots (28)$$

Also, from (18) and (19) we obtain

$$x_1 = 5900 \text{ mi.}, \quad a - x_2 = 1165 \text{ mi.} \quad (29)$$

The integrals of (9') and (13') are

$$\left. \begin{aligned} t &= \frac{1}{\sqrt{p_1}} \cosh^{-1} \frac{p_2 + y}{p_2} + C_3, \\ t &= -\frac{1}{\sqrt{q_1}} \cosh^{-1} \frac{q_2 + z}{q_2} + C_4, \end{aligned} \right\} (30)$$

respectively.

We shall use (30) to get the time to go the first 140 miles from the earth's surface and the last 25 miles to the surface of the moon.

The times to go from $x=4100$ mi. to $x=5900$ mi., and from 85 mi. above the moon's surface to 25 mi. above it, we shall get by integrating (9) and (13) by Simpson's Rule.

By virtue of (24) equations (9) and (13) become

$$dt = \frac{dy}{\sqrt{2 \left\{ \frac{k_1}{R_1 + y} + \frac{k_2}{a - R_1 - y} + Ky - \frac{k_1}{R_1} - \frac{k_2}{a - R_1} \right\}}}, \quad . \quad (9'')$$

$$dt = \frac{-dz}{\sqrt{2 \left\{ \frac{k_2}{R_2 + z} + \frac{k_1}{a - R_2 - z} + Kz - \frac{k_2}{R_2} - \frac{k_1}{a - R_2} \right\}}}, \quad . \quad (13'')$$

and for convenience in carrying out numerical work these equations may be written, on discarding inappreciable terms,

$$dt = \frac{dy}{\sqrt{2 \left\{ \frac{k_1}{R_1 + y} + K(R_1 + y) + D_1 \right\}}}, \quad (9''')$$

$$dt = \frac{-dz}{\sqrt{2 \left\{ \frac{k_2}{R_2 + z} + K(R_2 + z) + D_2 \right\}}}, \quad (13''')$$

where

$$D_1 = -72.45 \frac{\text{mi.}^2}{\text{sec.}^2}, \quad D_2 = -14.26 \frac{\text{mi.}^2}{\text{sec.}^2}. \quad (3i)$$

On using (30), and the solutions of (9''') and (13''') by Simpson's Rule, we obtain the times for the various intervals as follows:

First 140 mi. from R_1	213 sec.
Next 1800 mi. to x_1	539 sec.
First 60 mi. after x_2	56 sec.
Last 25 mi. to $a - R_2$	68 sec.
	<hr/> 876 sec.

The total time of mass expenditure for rocket propulsion is therefore 876 sec.

Then if m_0 is the initial value of m and m_1 its value on reaching the moon, we have, by (21) and (27),

$$A \log \frac{m_0}{m_1} = -10.7 \frac{\text{mi.}}{\text{sec.}} \dots \dots \dots (32)$$

Again, all of the results will apply equally well to the return trip it is quite obvious, and therefore if m_2 is the value of m on returning to the earth then

$$A \log \frac{m_0}{m_2} = -21.4 \frac{\text{mi.}}{\text{sec.}} \dots \dots \dots (33)$$

Hence if we take $A = -1 \text{ mi./sec.}$, then

$$\log \frac{m_0}{m_2} = 2.14,$$

and

$$m_0 = 2.0 \times 10^9 m_2.$$

This means that for every pound of matter returning a million tons would have to start out, and if we specify

$$m_2 = 10^6 \text{ lb.} = 500 \text{ tons,}$$

then

$$m_0 = 2.0 \times 10^{15} \text{ lb.}$$

The mass of the earth is

$$E = 10^{24} \text{ lb., about.}$$

Therefore we would have

$$\frac{m_0}{E} = 2.0 \times 10^{-9}.$$

Hence, if m_0 were distributed as a homogeneous sphere of material of density about that of surface rock (3.3), then the radius of the sphere would be about

$$3.96 \sqrt[3]{2.0 \times \frac{5}{3}} = 2.74 \text{ mi.}$$

It would thus be over five miles in diameter and so would be almost as massive as Mt. Everest!

4. Summary and Comments.

Two schemes of rocket flight have been considered, viz., where the observer travels in the fired rocket, and, second, where the observer travels in the main body whose motion is controlled by the firing off from it of rockets.

For the first there is necessary a system of rockets within rockets, and each time a firing takes place the inner system is propelled by discarding the outer shell. The disastrous effect to occupants of firing in this type of flight has been pointed out. No calculation of initial mass requirement has been made for this case, but it is obvious that even if a straight line path were assumed so that no matter was used in direction control, the initial mass requirement would be very large. But, of course, in an actual flight there would have to be some expenditure of mass for control of direction, or at any rate there would have to be ability to control direction. It is on this point also that the first scheme offers difficulty. For it would seem that a system of rockets within rockets would of necessity be internally fixed in arrangement, and when out in empty space this would make it impossible to alter the orientation of the system by an internal motion. Under such circumstances it would be impossible to control the direction in which the outer shell should be discarded, and so impossible to control the direction of flight of the inner system of rockets.

In the second type of flight there is not this latter kind of difficulty, for there could be facilities in all directions for firing rockets. It is also true that the internal arrangement of the material in this case would not necessarily be fixed, and therefore it would be theoretically possible to change the orientation of the body by a change of internal arrangement. It would be possible, therefore, to fire rockets in the proper direction to effect any desired change of direction.

But the problem of the second mode of flight has been considered chiefly from the point of view of minimum initial mass requirement. The present muzzle velocity of artillery shells is around 2500 ft. per sec., and in taking the velocity of rocket projection, A, numerically more than double this amount, and assuming a rate of firing which would give an initial upward acceleration as great as that of the earth's surface gravity, the enormous mass obtained above is required. With rockets fired at 2500 ft. per sec. the requirements would be much greater, and even if rockets could be fired at 10 mi. per sec. and the same initial acceleration were experienced, the initial mass would need to be at least ten times the returning mass.

No allowance has been made for possible mass requirement for control of direction of flight, and none has been made for the mass of the explosives which would be needed for firing the rockets. Allowance for them, therefore, would increase the initial mass requirement.

And what of projecting a body to the moon unaccompanied by an observer? Under such circumstances there would be no objection to sudden changes of velocity, and so a system of rockets within rockets could be used and a large initial velocity could be imparted on leaving

the earth. On the other hand, the subsequent successive firings would have to be automatically in the right direction. Aside from the difficulty of attaining this, there would be the further difficulty of ascertaining whether a fired rocket actually hit the moon.

The problem of rocket flight to the moon is not entirely one of having sufficient mass for rocket propulsion. There are many other practical problems, and while it is always dangerous to make a negative prediction, it would appear that the statement that rocket flying to the moon does not seem so remote now as television did less than one hundred years ago is over-optimistic.

University of Alberta.

August 1939.

IV. *The Air-Jet with a Velocity exceeding that of Sound.*

By JUL. HARTMANN and FREIMUT LAZARUS *.

[Plates I.-V.]

[Received February 28, 1939.]

Structure of the Jet.

As is well known, the air-jet with a velocity exceeding that of sound exhibits a periodic structure which may be rendered visible by means of the method of striæ. Fig. 1 (Pl. I.) is a photograph produced by this method. It is clearly seen that the jet consists of a series of nearly equal sections. For the length of the section Prandtl †, on the basis of theoretical considerations, derived the formula

$$\Delta = 1.2 d_0 \sqrt{p - 0.9}, \quad (1^\circ)$$

d_0 being the diameter of the jet aperture, p the excess-pressure measured in atm. in the container from which the jet is discharged. It follows from the formula that the condition for the production of a jet of periodic structure, i. e., of a velocity exceeding that of sound, is that the excess-pressure is higher than 0.9 atm. Emden ‡ found from experiments

$$\Delta = 0.89 d_0 \sqrt{p - 0.9}, \quad (2^\circ)$$

In connexion with the study of the acoustic air-jet generator a great number of photographs of the type in fig. 1 (Pl. I.) was taken, and from these photographs the following formulæ were derived :

$$\Delta_0 = 1.12 d_0 \sqrt{p - 0.9} \quad (3^\circ)$$

and

$$\Delta = 1.035 d_0 \sqrt{p - 0.9}, \quad (4^\circ)$$

the former expression representing the first section, the latter all the following sections. As in this test of the Prandtl formula the values of d_0 only were varied, while p was kept constant at 3.50 atm., two new series of photographs were taken corresponding to the values 4 and 6 mm. of d_0 and otherwise to different values of p between 2.5 and 6.5 kg./cm.² The

* Communicated by the Authors.

† L. Prandtl, *Phys. Zeits.* v. p. 599 (1904).

‡ R. Emden, *Wied. Ann.* lxi. pp. 264 and 426 (1899).

curves in fig. 2 were drawn from the observations. They correspond to the formulæ

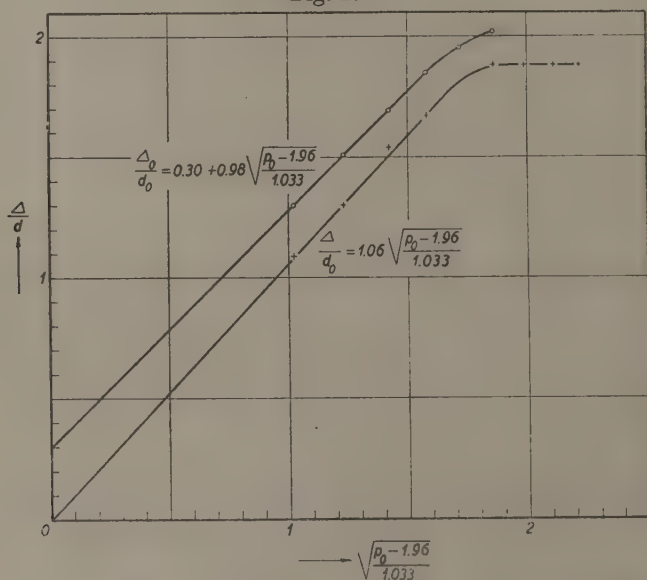
$$\frac{\Delta_0}{d_0} = 0.30 + 0.98 \sqrt{\frac{p_0 - 1.96}{1.033}} \quad (5^\circ)$$

and

$$\frac{\Delta}{d} = 1.06 \sqrt{\frac{p_0 - 1.96}{1.033}} \quad (6^\circ)$$

where p_0 is the absolute pressure in the container measured in kg./cm.² The numerical factors in (4°) and (6°) ought to agree. They differ by

Fig. 2.



Variation of the length of the jet sections with $\sqrt{\frac{p_0 - 1.96}{1.033}}$.

Δ_0 the first jet section, Δ the remainder.

about 2.5 per cent. This may probably be accounted for by the fact that the excess-pressure $p = 3.5$ atm. at which the jet-photographs behind formula (4°) were taken is a little beyond the limit of the pressure interval within which Δ is proportional to $\sqrt{p - 0.9}$ or, which is the same, to

$$\sqrt{\frac{p_0 - 1.96}{1.033}};$$

i. e., the straight part of the lower curve in fig. 2. What causes the proportionality to break down will now be explained.

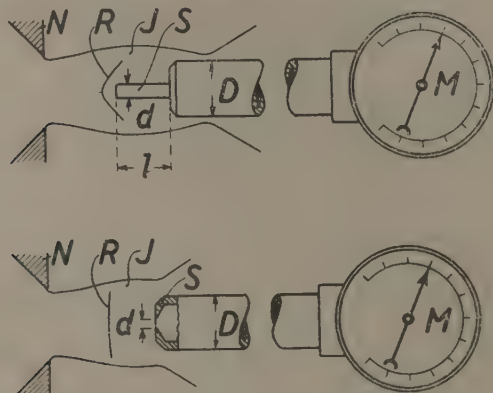
Figs. 3 *a*–3 *i* (Pl. II.) show photographs of an air-jet of 6 mm. diameter at 9 values of p_0 . It will be noted that from about $p_0=4.5$ kg./cm.² a curious change in the aspect of the jet occurs. Below this pressure two oblique lines cutting each other at the axis of the jet are seen just in front of the rear boundary of the section Δ_0 . These lines picture the front of a conical wave or what is in German called a “*schiefer Verdichtungsstoss*.” Above the pressure referred to the apex of this wave disappears and is replaced by a wave-front perpendicular to the axis of the jet, a Riemann wave or “*gerader Verdichtungsstoss*.” In the following we shall occupy ourselves a good deal with this Riemann wave. Here the attention should merely be drawn to the fact that in the front of such a wave the velocity of the flow, which ahead of the wave front, *i. e.*, closer to the jet aperture, exceeds that of sound, is reduced to a value below the velocity of sound. So behind this wave front, *i. e.*, downstream with regard to it, we shall have a jet with a velocity smaller than that of sound embedded in the main jet. This secondary jet is clearly seen in the photographs. Quite obviously it is the production of the Riemann wave which sets the limit to the straight part of the two curves in fig. 2. For when this wave appears, the increase with p_0 of the length of the first jet-section, and of the following sections too, very soon comes to an end. That this is true for the first jet-section is directly observable from figs. 3 *g*–3 *i* (Pl. II.). If the breadth s of the Riemann wave is plotted against the pressure p_0 , one may readily find the pressure p_0 corresponding to $s=0$. The pressure is found to be 4.3 kg./cm.². The limit of proportionality in fig. 2 is nearly at the abscissa 1.6 to which corresponds $p_0=4.6$ kg./cm.². Finally, the excess-pressure 3.5 atm. above corresponds to $p_0=4.65$ kg./cm.², *i. e.*, to a value just at or a little above the limit of proportionality.

The Pitot Curve.

The chief means for studying the conditions within an air-jet of a velocity exceeding that of sound is a Pitot apparatus. Two types of this apparatus are shown in figs. 4 *a* & 4 *b*, one with a narrow sound S, the other with a bore in a plane wall. The sound and the member with the bore are both connected to a manometer M. On this the Pitot pressure is read. If the sound or the member with the bore are moved step by step out along the axis of the jet and the manometer readings corresponding to the steps are plotted against the distance from the nozzle of the sound or bore, a periodic curve is obtained, a so-called Pitot curve. The Pitot curve found with the two types of Pitot apparatus are, however, not identical; the curve depends to some degree on the Pitot apparatus. This is clearly seen in fig. 5, showing a great number of curves taken with various Pitot apparatus characterized in the legend to the right.

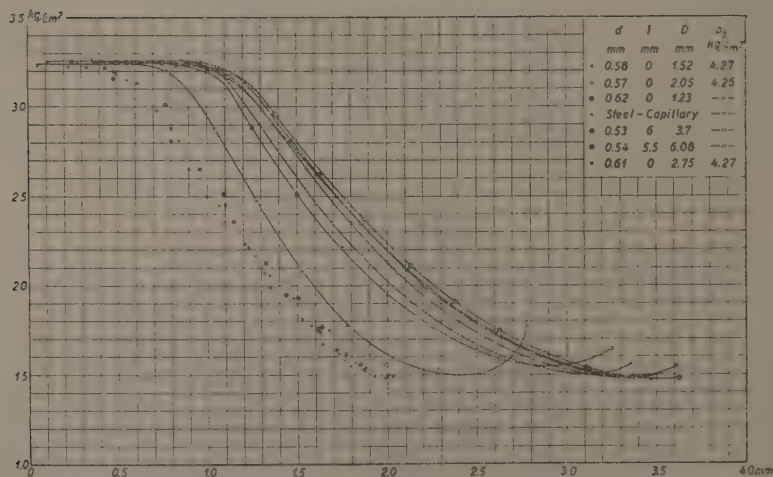
In spite of these differences one may speak of the Pitot curve of a jet, *i. e.*, a curve independent of the Pitot apparatus used for its production and dependent only on the jet proper. This will now be explained.

Figs. 4 a & 4 b.



Two types of Pitot apparatus.

Fig. 5.



Pitot curves produced with various forms of the Pitot apparatus.

In front of the sound S, fig. 4 a, or the member with the bore, fig. 4 b, a stationary wave R of the same character as that considered above is formed. In the case of a narrow sound the wave is conical with rounded

apex lying close to the end of the sound. With the bore in a plane wall the wave is almost plane and situated at a rather great distance from the wall. The actual aspect of the waves in the two cases is shown in figs. 6*a* & 6*b* (Pl. III.). Now it turns out that if the reading on the manometer is plotted against the position of the front of the stationary wave, the axial Pitot curve is always the same, quite independent of the character of the Pitot apparatus. This will be seen from fig. 5, where the clustering points to the left are the readings from the curves to the right plotted against the position of the wave instead of against the position of the sound or bore. The points obviously determine one and the same curve, a curve which may be termed the normal Pitot curve.

It would seem of interest to see how the normal Pitot curve is situated in relation to the structure of the jet as disclosed by the photographs in fig. 3 (Pl. II.). This question is answered in figs. 7*a*–7*d*. In the cases illustrated in figs. 7*a* & 7*b* the absolute pressure p_0 in the container was still below the limit 4.3 kg./cm.² at which the apex of the conical wave is flattened out. Here the Pitot curve exhibits a marked minimum a little in front of the top of the conical wave. Behind the top the Pitot pressure increases rapidly and then becomes constant within a certain interval on both sides of the borderline between the first and the second jet section. This means that the velocity of the jet is here just equal to the velocity of sound. Figs. 7*c* & 7*d* show how the Pitot curve is influenced by the replacement of the apex of the conical wave by a plane stationary wave perpendicular to the axis, *i. e.*, a Riemann wave. Behind this wave the velocity is reduced to a value smaller than that of sound, which means that the Pitot pressure becomes constant, for with a flow of such velocity the Pitot pressure is independent of the velocity. This is particularly evident in fig. 7*d*, while fig. 7*c* represents an intermediate phase.

Theory of the Pitot Curve.

We shall now show how all the qualities characterizing the state in any axial point of a jet with a velocity exceeding that of sound can be derived from the Pitot curve of the jet.

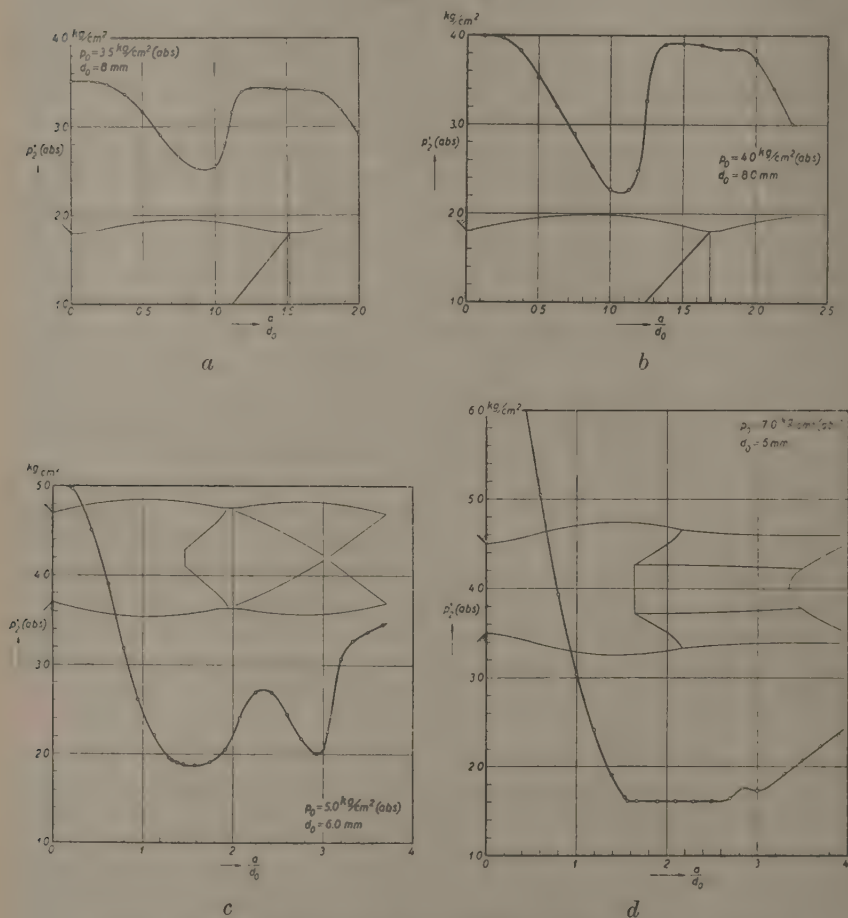
In a jet with a velocity smaller than that of sound the flow of air from the container up to a Pitot sound may be described completely by the equations of a steady, adiabatic, and irrotational flow of a frictionless gas. These equations may be written

$$\frac{T}{T_0} = \left(\frac{\rho}{\rho_0}\right)^{\kappa-1} = \left(\frac{p}{p_0}\right)^{\frac{\kappa-1}{\kappa}} = 1 - \frac{\kappa-1}{2} \cdot \frac{u^2}{\kappa RT_0}, \quad (1^{\circ}-3^{\circ})$$

where T means the temperature, ρ the density, p the pressure, u the velocity at an arbitrary point of the jet, while T_0 , ρ_0 , p_0 , $u_0=0$ stand for the same qualities in the container. Further, κ is the ratio c_p/c_v of the

two specific heats and R is the constant of Boyle's law. Just in front of the Pitot aperture the velocity is reduced to zero and so the pressure, *i. e.*, the Pitot pressure must here be identical with p_0 —as it is actually

Figs. 7a-7d.



Normal Pitot curves drawn in true positions relatively to pictures of the structure of the corresponding jets.

found to be with a jet of a velocity smaller than that of sound. It is otherwise with a jet of a velocity exceeding that of sound.

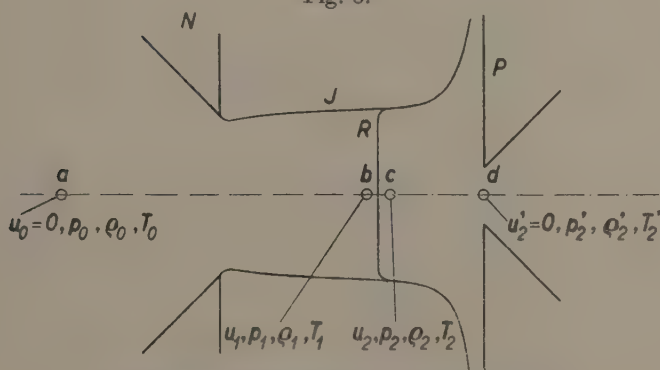
Here a stationary wave, a Riemann wave, is formed in front of the Pitot sound or bore. In fig. 8 R is the front of this wave. We consider the flow of air from a point a well behind the nozzle, where the velocity

is practically zero up to a point d in the aperture of the Pitot apparatus, where the velocity is again zero. Our aim is to develop a formula for the pressure p_2' at d , i. e., the Pitot pressure. In so doing we shall divide the stretch $a-d$ into three parts: (1°) the distance from a up to the point b immediately to the left of the front of the stationary wave, (2°) the passage through this front from b to c , (3°) the stretch from c to d . Now the flows from a to b and from c to d are adiabatic, steady, and irrotational flows, just as with a jet of a velocity smaller than that of sound. This means that the following relations obtain between the qualities written in fig. 8:—

$$\frac{T_1}{T_0} = \left(\frac{\rho_1}{\rho_0}\right)^{\kappa-1} = \left(\frac{p_1}{p_0}\right)^{\frac{\kappa-1}{\kappa}} = 1 - \frac{\kappa-1}{2} \cdot \frac{u_1^2}{\kappa RT_0}, \quad . \quad . \quad (4^\circ-6^\circ)$$

$$\frac{T_2'}{T_2} = \left(\frac{\rho_2'}{\rho_2}\right)^{\kappa-1} = \left(\frac{p_2'}{p_2}\right)^{\frac{\kappa-1}{\kappa}} = 1 + \frac{\kappa-1}{2} \frac{u_2^2}{\kappa RT_2} \quad . \quad . \quad (7^\circ-9^\circ)$$

Fig. 8.



To illustrate the theory of the Pitot curve.

Then, there are the changes which occur in the very front R of the stationary wave. On the assumption that the flow through the front takes place without change of mass, momentum or energy, the following expression may be derived:

$$\frac{p_2}{p_1} = \frac{4}{(\kappa+1)(\kappa-1)} \left[\kappa \left(\frac{p_0}{p_1}\right)^{\frac{\kappa-1}{\kappa}} - \left(\frac{\kappa+1}{2}\right)^2 \right], \quad . \quad . \quad (10^\circ)$$

$$\frac{\rho_2}{\rho_1} = \frac{\kappa+1}{\kappa-1} \frac{\left(\frac{p_0}{p_1}\right)^{\frac{\kappa-1}{\kappa}} - 1}{\left(\frac{p_0}{p_1}\right)^{\frac{\kappa-1}{\kappa}}} = \frac{u_1}{u_2}, \quad . \quad . \quad . \quad (11^\circ)$$

$$\frac{T_2}{T_1} = \left(\frac{\kappa+1}{2}\right)^2 \cdot \left(\frac{p_0}{p_1}\right)^{\frac{\kappa-1}{\kappa}} \cdot \frac{\left(\frac{p_0}{p_1}\right)^{\frac{\kappa-1}{\kappa}} - \left(\frac{\kappa+1}{2}\right)}{\left(\frac{p_0}{p_1}\right)^{\frac{\kappa-1}{\kappa}} - 1} \quad (12^{\circ})$$

From equations (4°) to (12°) the following formula,

$$\frac{p_2'}{p_0} = \left(\frac{\kappa+1}{\kappa-1}\right)^{\frac{\kappa+1}{\kappa-1}} \cdot \frac{\left(\frac{p_0}{p_1}\right)^{\frac{\kappa-1}{\kappa}} - 1}{\frac{p_0}{p_1} \left[\frac{4\kappa}{(\kappa-1)^2} - \frac{1}{\left(\frac{p_0}{p_1}\right)^{\frac{\kappa-1}{\kappa}} - 1} \right]^{\frac{1}{\kappa-1}}} \quad (13^{\circ})$$

is finally derived.

From this expression it is clearly seen that the Pitot pressure p_2' with a given jet is solely a function of the static pressure p_1 just ahead of the front of the stationary wave formed before the Pitot sound or aperture. So if with two Pitot tubes the tubes are adjusted so as to ensure the same position of the front of the stationary wave, the readings of the two tubes must be the same, or all Pitot tubes must give the same Pitot curve if the Pitot pressure is plotted against the position of the front of the stationary wave.

One may be interested in knowing the actual values of one or more of the qualities u , p , ρ , T , in an arbitrary point of a jet with a velocity exceeding that of sound. It would seem difficult, or perhaps almost impossible, to measure directly any of these qualities. On the other hand, it is an easy matter to measure the Pitot pressure p_2' and also the pressure p_0 in the container. This is a fact of great practical moment. For it follows from the expression (13°) that if p_2' and p_0 are known then we also know the static pressure p_1 in that point of the jet where the front of the stationary wave in front of the sound of the Pitot apparatus is situated. So it must be possible to derive from the normal Pitot curve, *i. e.*, the curve with the Pitot pressure plotted against the position of the said stationary wave, curves for all the characteristics of the jet, thus curves for the static pressure p_1 , the temperature T_1 , the density δ_1 , and the velocity u_1 . We now proceed to show how these curves are obtained.

The first step is to produce a curve picturing formula (13°), which with $\kappa=1.41$ may be written

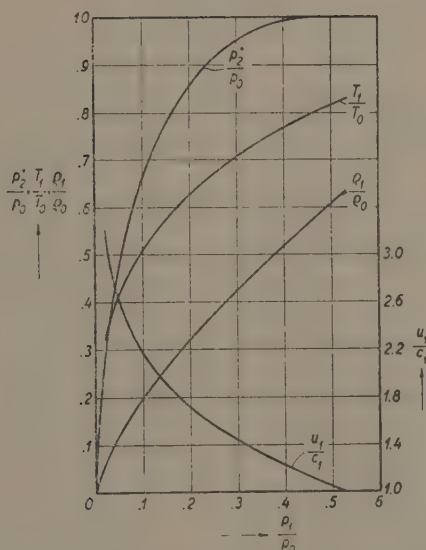
$$\frac{p_2'}{p_0} = 33240 \cdot \frac{\left(\frac{p_0}{p_1}\right)^{0.291} - 1}{\frac{p_0}{p_1} \left[33.55 - \frac{1}{\left(\frac{p_0}{p_1}\right)^{0.291} - 1} \right]^{2.44}} \quad (14^{\circ})$$

Fig. 9 shows the curve, the abscissa being, however, $\frac{p_1}{p_0}$. In addition, curves for $\frac{T_1}{T_0}$, $\frac{\rho_1}{\rho_0}$, and $\frac{u_1}{c_1}$ are plotted. They picture the formulæ

$$\frac{T_1}{T_0} = \left(\frac{p_1}{p_0}\right)^{0.291}, \quad \frac{\rho_1}{\rho_0} = \left(\frac{p_1}{p_0}\right)^{0.710}, \quad \text{and} \quad \frac{u_1}{c_1} = \sqrt{4.88 \left[\left(\frac{p_0}{p_1}\right)^{0.291} - 1 \right]}$$

. (15°-17°)

Fig. 9.

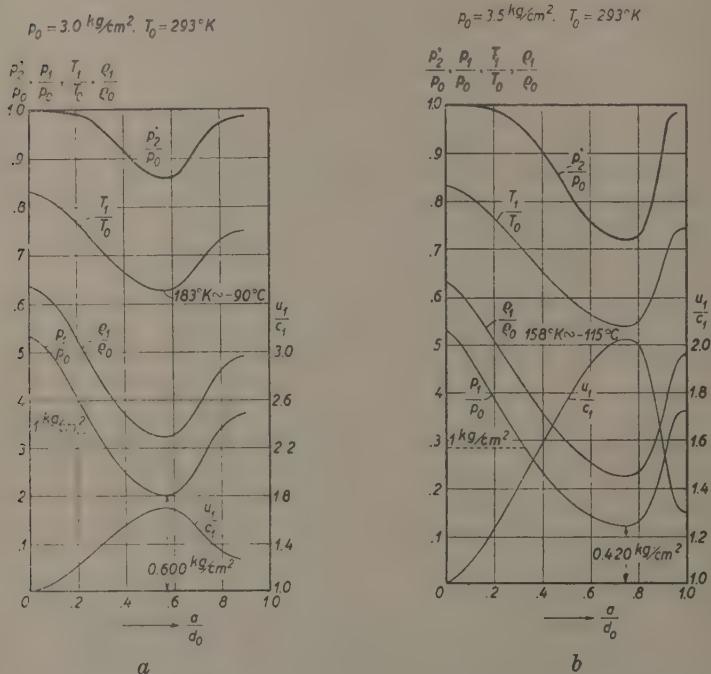


Determination of the characteristics of a jet: p_1 , ρ_1 , T_1 , and u_1 on the basis of the Pitot pressure p_2 .

which formulæ are derivable from the equations (4°)-(6°), it being noted that the velocity of sound $c_1 = \sqrt{\kappa R T_1}$. The application of these curves is illustrated in figs. 10a-10c. The diagrams correspond to a jet of 8 mm. at the three values of p_0 : 3.0, 3.5, and 4.0 kg./cm.² respectively. (Note that p_0 is the absolute pressure in the container.) The uppermost curve in the diagrams is the Pitot curve, or rather the $\frac{p_2'}{p_0}$ -curve plotted against the position of the stationary wave in front of the Pitot sound, the latter position being characterized by the distance a from the nozzle measured with the jet diameter d_0 as unit. By means of fig. 9 the $\frac{p_1}{p_0}$ -curves are

derived from the Pitot curves and then again from the p^1 -curves and fig. 9 the curves for $\frac{T_1}{T_0}$, $\frac{\rho_1}{\rho_0}$, and $\frac{u_1}{c_1}$ are determined. It will be seen that pressure, density, and temperature exhibit very pronounced minima at the same place where the Pitot pressure has a minimum. At this place

Figs. 10 a & 10 b.



Characteristic curves of jets of 8 mm. derived from the Pitot curves, $p=3.0, 3.5$, and 4.0 kg./cm.^2

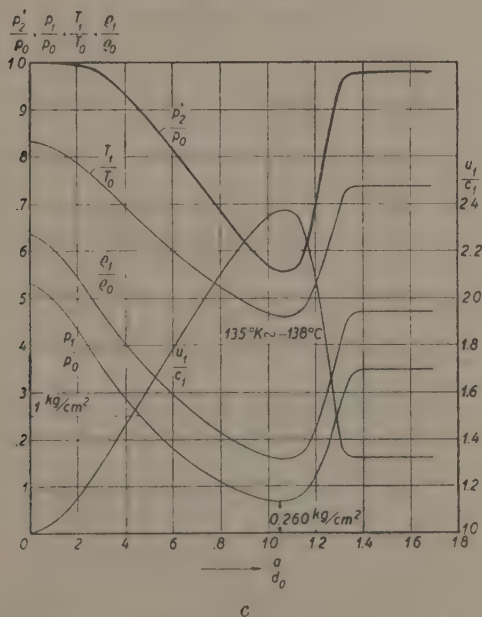
the velocity ratio $\frac{u_1}{c_1}$ has a maximum. In Table I. a the minimum and maximum values of the characteristics of the jets are entered. It will be noted that the static pressure sinks well below the external pressure and that the minimum temperature may be as low as -138°C . or lower still.

The curves in figs. 10 a-10 c yield a clear insight into the structure of the jet. It may in some cases be of interest to know the changes of the

characteristics of the jet in the front of a stationary Riemann wave in some point of the jet. With a view to facilitating the determination of these changes, the values of $\frac{p_2}{p_1}$, $\frac{\rho_2}{\rho_1}$, and $\frac{T_2}{T_1}$ were plotted against $\frac{p_1}{p_0}$ in fig. 11, formulæ (10°-12°) being used for the calculation of the curves. Some values of the changes corresponding to the minimum values of $\frac{p_1}{p_0}$ in the jets of figs. 10 a-10 c are stated in Tables I. a & I. b.

Fig. 10 c.

$$p_0 = 4.0 \text{ kg/cm}^2, \quad T_0 = 293^\circ \text{K}$$



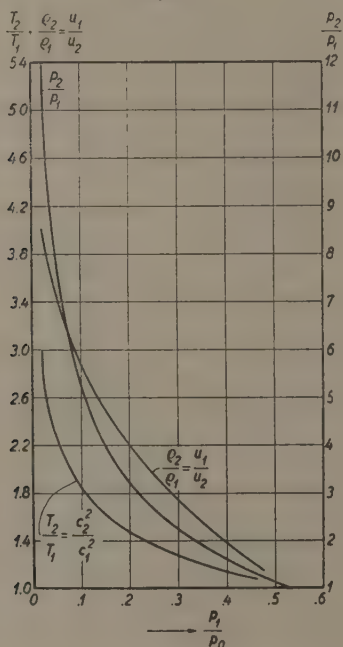
Characteristic curves of jets of 8 mm. derived from the Pitot curves, $p_0 = 3.0, 3.5, \text{ and } 4.0 \text{ kg./cm}^2$

Test of the Theory of the Pitot Curve.

A test of the theory of the Pitot curve would quite obviously be of very great interest. Figs. 12 a-12 c are to illustrate three possibilities. One might attempt to determine a curve for the variation of the static pressure along the axis of the jet by means of a static pressure sound like that indicated in fig. 12 a. If, then, the normal Pitot curve were found for the same jet and the static pressure curve were derived from the

Pitot curve by the theory given above, a direct comparison of theory and observation could be carried out. The value of this test is, however, rather doubtful. For, as indicated in fig. 12 a, a stationary wave of conical shape (compare fig. 4 a) is formed in front of the static pressure sound. Behind such a wave the conditions are more or less changed from what they are in the jet without the sound. So the pressure read on the manometer of the static pressure sound is not likely to be what is looked for, *i. e.*, the static pressure in the undisturbed jet. Stodola *

Fig. 11.



Curves for the changes of the characteristics of the jet in the front of the stationary Riemann wave.

modified the method by extending the sound into the container (fig. 12 b). In this case no conical wave is formed, but obviously the normal structure of the jet is, nevertheless, disturbed. So it is also in this case impossible to foretell what error may accrue from the introduction of the sound.

Quite another test is indicated in fig. 12 c. If a pin P is introduced into the jet here considered with the point turned against the flow, a

* A. Stodola, 'Die Dampfturbinen,' iv. Aufl. Berlin (1910).

conical stationary wave is formed, as in the case of fig. 12*a*. Now, however, we shall use this wave to measure the velocity u_1 of the flow in the neighbourhood of the pin point. This velocity is assumed to be determined by the expression

$$\sin \theta = \frac{c_1}{u_1}, \dots \dots \dots (1^\circ)$$

TABLE I. *a.*

Minimum and Maximum Values of the Characteristics of the Jet.

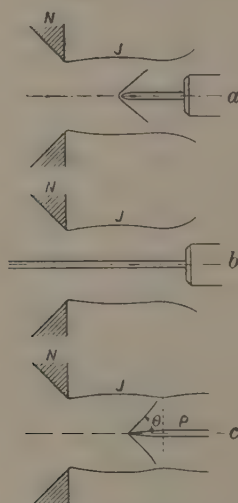
$\frac{p_0}{\text{kg./cm.}^2}$	$\frac{\frac{p^2}{p_0}}{\text{Min.}}$	$\frac{\frac{p_1}{p_0}}{\text{Min.}}$	$\frac{\frac{\rho_1}{\rho_0}}{\text{Min.}}$	$\frac{\frac{T_1}{T_0}}{\text{Min.}}$	$\frac{\frac{u_1}{c_1}}{\text{Max.}}$	$\frac{p_1}{\text{kg./cm.}^2}$	$\frac{T_1}{^\circ\text{C.}}$
3.0	0.860	0.200	0.320	0.625	1.69	0.600	— 90°
3.5	0.720	0.120	0.225	0.540	2.02	0.420	— 115°
4.0	0.555	0.067	0.155	0.460	2.37	0.260	— 138°

TABLE I. *b.*

p_0 kg./m. ²	p_1 p_0 Min.	p_2 p_1	$\rho_2 = \frac{u_1}{u_2}$	$\frac{T_2}{T_1}$	p_2 kg./cm. ²
3.0	0.200	4.0	2.2	1.5	2.40
3.5	0.120	5.3	2.7	1.7	2.23
4.0	0.067	6.8	3.2	2.1	1.77

where θ , or the Mach-angle, is half of the apex-angle of the conical wave. Thus, actually, it is the ratio of u_1 and the velocity of sound c_1 at the point in question which is found. Again, however, it would undoubtedly be too rash to assert *a priori* that the ratio so measured is identical with that which obtains in the undisturbed jet. The only thing we can do is to determine a value of $\frac{c_1}{u_1}$ by means of 1° and then compare it with the value derived from the Pitot curve by means of the theory.

Now, in figs. 13 *a* & 13 *b* two experimentally determined curves for the static pressure are compared to the corresponding curves calculated from the Pitot curves. In both cases both of the two forms of the static pressure sounds have been employed. It will be noted that the agreement is only tolerably good with the lowest value of the absolute pressure in the container: $p_0 = 3 \text{ kg./cm.}^2$. At $p_0 = 4 \text{ kg./cm.}^2$ there is still a rough agreement between the theoretical and the experimental curve found by means of the short sound (fig. 12 *a*), while the curve found by the long sound is completely at variance with the curve derived from the Pitot curve. (Finally, at $p_0 = 5 \text{ kg./cm.}^2$ —and with still higher pressures—

Figs. 12 *a*–12 *c*.

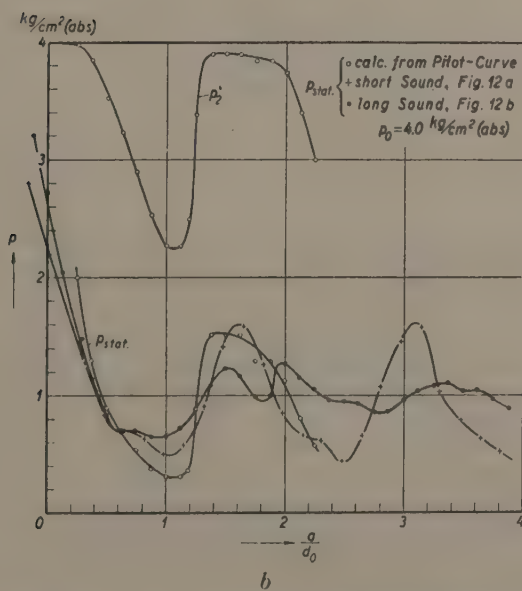
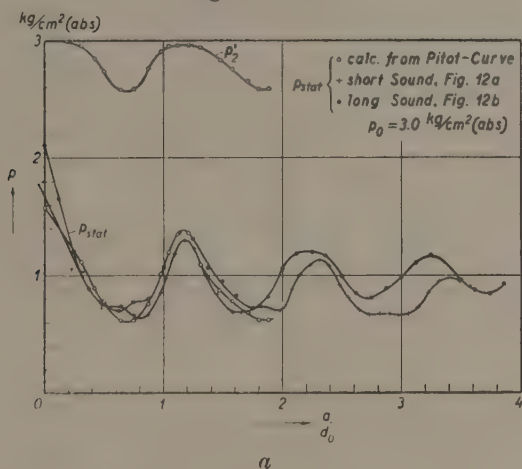
Propositions for experimental tests of the theory of the Pitot curve.

the experimental and the theoretical curves differ totally.) This is not to be wondered at; on the contrary, the relatively good agreement at low pressures is rather more than might be expected.

We now proceed to give the results of the comparison of the values of the velocity ratio $\frac{u_1}{c_1}$ as found by measurement of the Mach-angle θ and from the Pitot curve. Firstly, a series of photographs produced by the method of striæ may be presented. Figs. 14 *a*–14 *i* show pictures from a 6 mm. jet at an absolute pressure $p_0 = 3.5 \text{ kg./cm.}^2$ in the container. It is clearly seen how the velocity ratio $\frac{u_1}{c_1}$ increases when the needle is removed from

the nozzle within the first jet section. It is also seen how it drops to about 1 at the passage of the rear border line of the first jet section,

Figs. 13a & 13b.



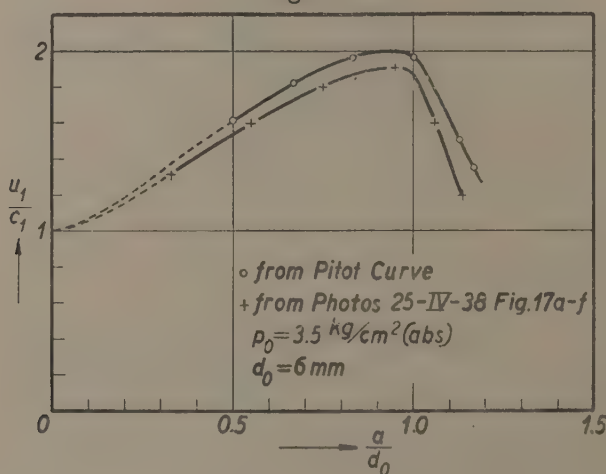
Experimentally determined curves for the static pressure compared with the curve derived from the Pitot curve.

increasing anew when the needle is carried farther into the second jet section. Fig. 15 shows curves for the variation of $\frac{u_1}{c_1}$ out along the axis

of a 6 mm. jet. As will be seen, they agree remarkably well, the Mach-angle value being generally only a few per cent. smaller than the theoretical value. It should, however, be noted that the comparison has been made at a relatively low value of p_0 and that it covers only the first jet section.

It was found of interest to examine also the influence of introducing a needle in a jet emitted under a higher pressure p_0 . Figs. 16 a-16 i (Pl. V.)

Fig. 15.



Comparison of curves for the velocity-ratio $\frac{u_1}{c_1}$ derived from Pitot curve and from Mach-angle measurement.

originate from a jet of 4 mm. at a pressure $p_0 = 7 \text{ kg./cm.}^2 \text{ abs.}$ At this high pressure a Riemann wave (gerade Verdichtungsstoss) is formed in the jet. The photos serve to illustrate what happens when the needle point is carried through this wave.

The authors are indebted to the Trustees of the Carlsberg Foundation, the Rask-Örsted Fund, and the Otto Mönsted Fund for financial aid in connexion with the research work reviewed above.

The Laboratory of Technical Physics,
 The Royal Technical College,
 Copenhagen.

V. *Factors determining Electrolytic Dissociation.*—Part II. *The Free Energies of Dissociation of Salt Molecules in Aqueous Solution.*

By WILLIAM J. C. ORR, Ph.D., Department of Colloid Science, Cambridge *.

[Received October 24, 1939.]

In a previous paper ⁽¹⁾ (hereafter referred to as Paper I.) calculations were made of the energies of dissociation of a number of diatomic salt molecules in the gas phase which agreed well with the experimental values when suitable constants in the repulsive potential, characterizing the ions

TABLE I.

	r_e (expt.).	r_e (calc.).		r_e (expt.).	r_e (calc.).		$\mu \times 10^{18}$ (expt.).	μ (calc.).
NaCl.	2.51	2.45	RbCl.	2.89	2.85	KCl.	9.5	9.9
NaBr.	2.64	2.61	RbBr.	3.06	3.01	KBr.	10.8–10.9	10.6
NaI .	2.90	2.89	RbI .	3.26	3.31	KI .	11.0–11.1	11.0
KCl .	2.79	2.70	CsCl .	3.06	3.10			
KBr .	2.94	2.89	CsBr .	3.14	3.27	CSI .	12.1	13.8
KI . .	3.23	3.13	CsI . .	3.41	3.63			

involved, had been determined. These calculations allowed one to draw conclusions about the degree of homopolar binding involved in certain of the transition metal halides. A proper test of the validity of the calculations could not be made at the time for lack of suitable data. Since then, however, measurements have been made of both the equilibrium distances ⁽²⁾ and the dipole moments ⁽³⁾ of a number of the alkali halides. The figures calculated are compared with these experimental values in Table I., from which it is evident that fairly satisfactory agreement is obtained.

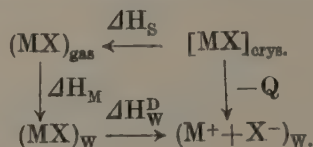
A further point that might be criticized in the calculations of the previous paper is the fact that Sherman's ⁽⁴⁾ calculated values of the lattice energies were used. Indirect experimental confirmation of these calculations

* Communicated by Professor E. K. Rideal.

was obtained by Sherman, who showed that values of the electron affinities of the halides calculated from these data using a Born cycle were constant and independent of the salt considered. Since then, however, direct measurements of both lattice energies⁽⁵⁾ and electron affinities⁽⁶⁾ have been made, and the results show that the Sherman lattice energies agree to within 3 per cent. with experiment.

However, in order to obtain a quantitative measure of the tendency of a salt to ionize in a solvent medium the free energy of dissociation must be calculated. In this paper we make calculations of the free energies of dissociation of a number of alkali halide and transition metal diatomic halides and the triatomic halides of Zn^{++} , Cu^{++} , and Hg^{++} in water, calculating first the total energy change, then the entropy change, and thus, by the Gibbs-Helmholtz relation, the free energy.

(1) *The Total Energy of Dissociation of Salt Molecules in Water.*



From the above cycle we have

$$-\Delta H_W^D = \Delta H_M + \Delta H_S + Q, \quad \dots \quad (1)$$

where ΔH_S is the energy of sublimation of the crystal and Q the heat of solution of the crystal in water at infinite dilution, both of which quantities are known experimentally. ΔH_M , the energy of hydration of the undissociated molecule, must now be calculated.

We shall calculate first the energy of applying one water molecule to an ion-pair in the configuration shown in fig. 1 (a).

The following trigonometrical relations hold between the various dimensions shown in the figures:—

$$\begin{aligned}
 S^2 &= R^2 + a^2 - 2aR \cos \chi, \\
 \sin \psi &= \frac{a}{S} \sin \chi.
 \end{aligned}$$

The hydration energy is

$$\phi = -\frac{e_1(\mu + \mu_i) \cos \theta}{R^2} + \frac{e_2(\mu + \mu_i) \cos(\theta + \psi)}{S^2} + \frac{\mu_i^2}{2\alpha} - \frac{A}{R^6} + \frac{B}{R^{m_0}},$$

where μ_i is the moment induced in the water molecule whose permanent dipole is $\mu = 1.87 \times 10^{-18}$ e.s.u. and polarizability is $\alpha = 1.575 \times 10^{-24}$ c.c. and where A is the constant of the van der Waals energy.

Now, since $\frac{\partial \phi}{\partial \mu_i} = 0$, we have

$$\mu_i = \left[\frac{e_1 \cos \theta}{R^2} - \frac{e_2 \cos (\theta + \psi)}{S^2} \right]. \quad \dots \quad (2)$$

Fig. 1 (a).

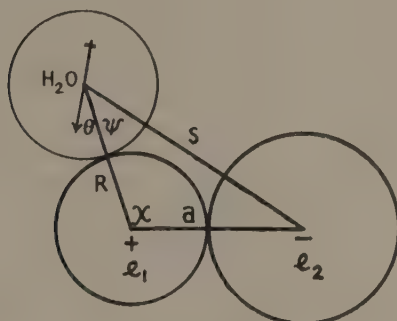
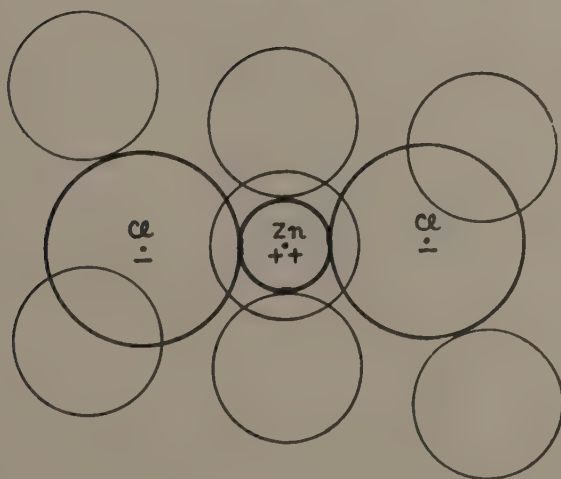


Fig. 1 (b).



Thus
$$\phi = -\frac{1}{\alpha} [\mu \mu_i + \frac{1}{2} \mu_i^2] - \frac{A}{R^6} + \frac{B}{R^m}.$$

Further, for equilibrium,
$$\frac{\partial \phi}{\partial R} = 0.$$

Thus
$$\frac{B}{R^m} = \frac{R}{\alpha m_0} [\mu + \mu_i] \frac{\partial \mu_i}{\partial R}.$$

Hence

$$\phi_{\text{hydr.}} = -\frac{\mu_i}{\alpha}(\mu + \frac{1}{2}\mu_i) + \frac{2(\mu + \mu_i)}{m_0\alpha} \left[\mu_i + \frac{e_2\alpha \cos(\theta + \psi)}{S^2} \left\{ 1 - \frac{R(R - a \cos \chi)}{S^2} \right\} \right]. \quad (3)$$

This formula will be of general applicability for the cases of both diatomic and triatomic molecules.

Secondly, we shall adopt the dimensions and structure proposed by Bernal and Fowler ⁽⁷⁾ for liquid water in calculating the energy of making cavities in the liquid. The energy required to evaporate n molecules into the gas phase leaving a n -molecular cavity is $(3n+1)\frac{U}{2}$ for a tetrahedral structure where U , the internal latent heat of water at 25° C., is equal to 9.88 k. cal. per mol. ⁽⁸⁾. If these n molecules are re-condensed elsewhere in the liquid we obtain nU k. cal., so that the energy of forming a n -molecular cavity in the liquid is $(n+1)\frac{U}{2}$. For large values of n this tends to $\frac{U}{2}$ k. cal. per mol. To calculate the energy involved in expanding or contracting a cavity where the change in volume (ΔV) is not large enough to alter the configuration of the water molecules surrounding the cavity we assume that the work done will be shared equally among a large number of molecules in the neighbourhood of the cavity, and will thus be $\left(\frac{\Delta V}{\bar{V}}\right)\frac{U}{2}$, where \bar{V} is the molecular volume of a single water molecule. Thus summing the two effects, the energy of forming an n -molecular hole and expanding it to fit a tetrahedral structure, the components of which have radii $r_1, r_2 \dots r_n$ instead of r_0 (the radius of the water molecules originally present), is

$$\begin{aligned} \Delta H_{\text{cav.}} &= (n+1)\frac{U}{2} + \left[\left(\frac{1}{r_0^3} \sum_{1,2,3}^n r_n^3 \right) - n \right] \frac{U}{2} \\ &= \left[1 + \frac{1}{r_0^3} \sum_n r_n^3 \right] \frac{U}{2} \\ &= 4.94(1 + 0.38 \sum_n r_n^3) \text{ k. cal./gram. mol.} \quad (4) \end{aligned}$$

There is, thirdly, the energy obtained since a dipole is transferred from a vacuum into a dielectric medium. The expression for this, which has been derived by Bell ⁽⁹⁾, is as follows:—

$$\Delta H_{\text{dip}} = -\frac{\mu_s^2}{3(S+r_0)^3} \left[\frac{(D+1)}{(2D+1)} - \frac{3T}{(2D+1)^2} \right] \times 14.49 \times 10^{12} \text{ k. cal./gram. mol.}, \quad (5)$$

where μ_s , the dipole moments of the salt molecules are taken from paper I

and S is assumed equal to $\frac{1}{2}(S_+ + S_-)$. The values of D and $\frac{\partial D}{\partial T}$ are taken from the Int. Crit. Tab.

We may now calculate ΔH_M for a diatomic molecule. It will be evident from the geometry of the water configuration that, if we introduce an ion-pair in the cavity left by removing two adjacent water molecules and suitably adjust the volume to fit, there are two possible configurations of the water dipole with respect to the dissolved molecule. Either each ion has two waters orientated to give electrostatic attraction ϕ_A and a third repelling ϕ_R , or else two repelling and a third attracting. As the molecule moves in the water each configuration is equally probable, so that an average value of the electrostatic energy must be taken, viz.,

$$\Delta H_{\text{hydr.}} = \frac{3}{2}(\phi_A^+ + \phi_R^+ + \phi_A^- + \phi_R^-) \times 14.49 \times 10^{12} \text{ k. cal./gram. mol.},$$

where the $+$ and $-$ signs distinguish energies round the two oppositely charged ions, ϕ being given by formula (3). For this case $\chi = 109.54^\circ$, while $\theta = 35.27^\circ$ for ϕ_A^+ and ϕ_R^- and 54.73° for ϕ_R^+ and ϕ_A^- . Further, ψ is positive in sign for ϕ_A and negative for ϕ_R . Thus we have finally

$$\Delta H_M = \Delta H_{\text{cav.}} + \Delta H_{\text{dip}} + \Delta H_{\text{hydr}}$$

Goldschmidt's ⁽¹⁰⁾ radii are used for r_+ and r_- and the Bernal and Fowler's ⁽⁷⁾ value $r_0 = 1.38$ in formulæ (3), (4), and (5). The van der Waals energy is evaluated as in paper I. The constant m_0 of the repulsive potential for any water-ion interaction is obtained using Slater's ⁽¹¹⁾ assumption that $m_0 = \frac{1}{2}(m_{\pm} + m_{\text{H}_2\text{O}})$, where $m_{\text{H}_2\text{O}} = 12$ and the values of m_{\pm} are given by Sherman ⁽⁴⁾.

The calculated results are collected in Table II.

In the case of the triatomic Zn^{++} , Cd^{++} , and Hg^{++} halides, which Raman spectra investigations ⁽¹²⁾ have shown to have linear structures, the problem is much more complicated than in the previous case because the three ions can no longer be fitted directly into the water structure. In the gas phase it is evidently geometrically possible to arrange three water molecules tetrahedrally around each of the negative ions and four others in a plane around the central positive ion (see fig. 1(b)). In this configuration, due to the fact that the central ions are small and doubly charged, the four central water molecules are extraordinarily energetically attracted to the salt molecule (see Table II. column 2). Further, since these four water molecules are already approximately 3-coordinated in the hydrated complex, the coordination between these and the surrounding liquid of the cavity will be below normal, so that they will tend to be permanently attracted and orientated to the molecule. The waters coordinated to the halogen ions will, as in the diatomic case, exchange freely with the rest of the liquid. ΔH_M may now be calculated

in the following stages. (1) Evaporate ten water molecules into the gas phase, leaving a cavity in the liquid. (2) Apply these molecules to the salt molecule in the way described above. In calculating $\phi_{\text{hydr.}}$ in this case extra terms must be introduced in equations (2) and (3) for the mutual electrostatic repulsion of the coordinated waters and for their van der Waals interactions with the negative ions on either side. In $\Sigma\phi^{++}$, $\chi=90^\circ$ and $\theta=0^\circ$. The $\Sigma\phi^-$ are averaged as in the diatomic case. (3) We now assume that a spherical volume $V=\frac{4}{3}\pi\sigma^3$ will be a fair estimate of the volume of the cavity required, where $\sigma=\frac{1}{2}(r_++r_-)+2r_0$.

TABLE II.
Energies in k. cal. per. grm. mol.

	$-\Delta H_{\text{electrostatic.}}$	$-\Delta H_{\text{v.d.W.}}$	$-\Delta H_{\text{hydr.}}$	$\Delta H_{\text{cav.}}$	$-\Delta H_{\text{dip.}}$	$\Delta H_{\text{M.}}$
KF. . . .	17.30	2.89	20.19	13.78	0.94	-7.3
KCl . . .	14.40	3.21	17.61	20.51	0.93	+2.0
KBr . .	14.13	3.21	17.33	23.51	1.01	+5.2
KI	13.38	3.28	16.60	29.38	0.92	+11.9
LiCl . .	19.21	1.68	20.89	16.98	0.36	-4.3
NaCl . .	19.68	2.18	21.86	17.86	0.86	-4.9
KCl . . .	14.40	3.21	17.61	20.51	0.93	+2.0
RbCl . .	12.85	3.53	16.38	22.35	1.00	+5.0
CsCl . .	11.97	4.51	16.48	24.53	1.08	+6.9
AgCl . .	16.83	7.21	24.04	18.49	0.47	-6.0
TlCl . .	18.61	16.92	35.55	18.31	0.21	-17.4
ZnCl ₂ . .	110.0	8.2	118.2	40.7	0	-77.5
CdCl ₂ . .	101.9	11.1	113.0	44.7	0	-68.3
HgCl ₂ . .	106.4	10.8	117.2	47.1	0	-60.1

In the normal liquid this volume would contain $n_r = \frac{6.064 V}{18.06 \times 10}$ water molecules, where 18.06 is the molecular volume of water at 25° C. (For the Zn¹¹, Cd¹¹, and Hg¹¹ chlorides $n_r=9.24$, 10.05, and 10.53 respectively.) Expand the cavity to the volume V. (4) Introduce the hydrated complex into the cavity. Since, in this case, the molecule has no permanent dipole moment, $\Delta H_{\text{dip.}}$ is zero. The sum of the energies involved is thus

$$\begin{aligned}
 -\Delta H_{\text{M}} &= 31 \frac{U}{2} - (n_r - 10) \frac{U}{2} - \Delta H_{\text{hydr.}} + (18 + 4) \frac{U}{2} \\
 &= -\Delta H_{\text{hydr.}} - (n_r - 1) \frac{U}{2}.
 \end{aligned}$$

The values of ΔH_M calculated are given in Table II. The ionization potentials required in evaluating the van der Waals energies for Zn^{++} and Cu^{++} are 63.7 and 55.7⁽¹³⁾, while for Hg^{++} a value of 56×10^{-12} ergs/mol. has been assumed. This uncertainty, however, does not introduce any large error, since the van der Waals energies in this case are only about 10 per cent. of the electrostatic.

In Table III. are collected the best experimental values of ΔH_g and Q (taken from Landolt-Bornstein Tabellen) and the calculated values of ΔH_M from Table II. The total heats of dissociation of the salt molecules in water ΔH_W^D , given in column 5, are then obtained, using equation (1).

TABLE III.

Energies in k. cals./gram. mol.

	ΔH_g	Q	ΔH_M	ΔH_W^D		ΔH_g	Q	ΔH_M	$-\Delta H_W^D$
KF ..	59	3.9	-7.3	55.6	AgCl TlCl	53.6 32.3	-16.0 -10.1	-6.0 -17.4	31.6 4.8
KCl ..	52	4.2	2.0	49.8					
KBr ..	50	4.9	5.2	50.3					
KI ..	47	4.9	11.9	54.0					
LiCl ..	47	+8.8	-4.3	51.5	ZnCl ₂ CdCl ₂ HgCl ₂	40 44 19.9	15.6 3.0 -3.3	-77.5 -68.3 -70.1	-21.9 -21.3 -53.5
NaCl ..	54	-1.0	-4.9	48.1					
KCl ..	52	-4.2	2.0	49.8					
RbCl ..	51	-4.5	5.0	51.5					

(2) The Entropy of Dissociation of Salt Molecules in Water.

We may express the entropy difference between that of a dissolved undissociated molecule in water, S_W^M , and the entropies of the dissolved ions, S_W^I (namely, ΔS_W^D), introducing the entropy of the gas molecule, S_g^M , as follows:—

$$-\Delta S_W^D = (S_g^M - S_W^I) - (S_g^M - S_W^M). \quad (6)$$

The statistical formula for the entropy of a linear molecule in the gas phase, with moment of inertia, $I = (\text{reduced-mass} \times r_e^2)$, frequency ν , and symmetry number σ , is⁽¹⁴⁾

$$S_g^M = R \left[0.245 + \frac{7}{2} \log_e T + \log_e M + \log \frac{I}{\sigma} + \sum_{\nu} \left\{ \frac{h\nu/kT}{(e^{h\nu/kT} - 1)} - \log_e (1 - e^{-h\nu/kT}) \right\} \right],$$

where M is in grms. and I in 10^{-38} c.g.s. units. In the case of the alkali halides the values of ν ⁽¹⁵⁾ and r_e ⁽²⁾ required have been taken from

experimental data where available, and calculated values are used where these are lacking. In the case of the Zn^{++} , Cd^{++} , and Hg^{++} halides the frequencies of certain of the salts have been measured in Raman spectra ⁽¹⁶⁾; where these are lacking estimated values are used. The equilibrium distances for the Hg^{++} halides have been measured by Braune and Knoke ⁽¹⁷⁾ and for the Zn^{++} and Cd^{++} iodides by Hassel and Strome ⁽¹⁸⁾. The ionic radii of Zn^{++} and Cd^{++} found in the iodides are used to calculate the equilibrium distances here employed for the chlorides. The values of S_g^M calculated are given in Table IV., column 2. The entropies of the ions at infinite dilution in water have been calculated from experimental data by Latimer ⁽¹⁹⁾ and are given in column 3.

The difference ($S_g^M - S_W^M$) must now be calculated. The part of this difference due to change in translational entropy, namely ($S_g^t - S_W^t$),

TABLE IV.
Entropies in cal./° K.

	S_g^M .	S_W^L .	$(S_g^M - S_W^M)$.	$-\Delta S_W^D$.		S_g^M .	S_W^L .	$(S_g^M - S_W^M)$.	$-\Delta S_W^D$.
KF ..	52.9	19.6	8.3	25.0	AgCl . TlCl .	55.3 58.4	31.9 42.1	8.3	15.1 8.0
KCl ..	55.9	38.1		9.5					
KBr ..	58.5	44.0		6.2					
KI ..	60.2	50.3		1.6					
LiCl .	49.4	15.3	8.3	25.8	ZnCl ₂ . CdCl ₂ . HgCl ₂ .	63.7 64.7 65.9	- 0.2 14.3 20.5	29.0 29.3 29.6	34.9 21.1 15.8
NaCl .	53.8	28.2		17.3					
KCl ..	55.9	38.1		9.5					
RbCl .	58.6	36.3		14.0					

is obtained from the relations $S_g^t = \frac{3}{2}R \log_e M + 26.03$ and $S_W^t = \frac{3}{2}R \log_e M_i + 17.67$, the latter relation being that derived by Eley and Evans ⁽²⁰⁾ for the translational entropy of an ion in water, M_i being the reduced mass of the ion and the water molecules permanently coordinated to it. It seems probable that the process of solution will result in some loss of rotational entropy possibly, as a maximum, about three entropy units. However, since it is not possible to calculate this effect precisely, and in view of the fact that it makes a contribution of less than 1 k. cal. to the final values of ΔF_W^D , for the purpose of the present calculation, this effect may be neglected. Further, the change in vibrational entropy on solution is entirely negligible. Thus in the case of the diatomic salts, where, as has already been pointed out, the restrictive influence of the two ions of the salt molecule on the surrounding water molecules must be very little different from the normal restrictive influence of the pair of water mole-

cules they may be considered replacing, we may take $(S_g^M - S_W^M) \equiv (S_g^t - S_W^t)$. In the case of the triatomic salts, however, allowance must be made for the entropy change due to the coordination of the four water molecules round the central positive ion. These molecules can be considered as frozen out of the liquid and to have a vibrational and rotational motion comparable to that of a water molecule in ice. Since their translational motion is already included in the above expression for S_W^t , we hence obtain in this case an extra decrease in entropy of $4S_M = 22.04$ cal./degree, where S_M is the entropy of melting of ice. The values of $(S_g^M - S_W^M)$ so calculated are given in Table IV., column 4. Finally, the values of ΔS_W^D calculated using equation (6) are given in column 5.

(3) *The Free Energy of Dissociation of Salt Molecules in Water.*

The values of the free energies of dissociation of salt molecules in water, given by $\Delta G_W^D = \Delta H_W^D - T\Delta S_W^D$, are collected in Table V.

TABLE V.
Energies in k. cal./grm. mol.

	$-\Delta H_W^D$	$-T\Delta S_W^D$	$-\Delta G_W^D$		$-\Delta H_W^D$	$-T\Delta S_W^D$	$-\Delta G_W^D$
KF ...	55.6	7.5	48.1	AgCl ..	31.6	4.5	27.1
KCl ...	49.8	2.8	47.0	TlCl ...	4.8	2.4	2.4
KBr ...	50.3	1.9	48.4				
KI	54.0	0.5	53.5				
LiCl ...	51.5	7.7	43.8	ZnCl ₂ .	-21.9	10.4	-32.3
NaCl...	48.1	5.2	42.9	CdCl ₂ .	-21.3	6.3	-27.6
KCl ...	49.8	2.8	47.0	HgCl ₂ .	-53.5	4.7	-58.2
RbCl ..	51.5	4.2	47.3				

In the case of the diatomic salts the values of ΔH_W^D are possibly accurate to ± 3 k. cal. and those of the entropies to ± 5 entropy units, leading to a possible error of ± 5 k. cal. in ΔG_W^D . In the case of the Zn^{++} , Cd^{++} , and Hg^{++} halides the values of (ΔH_W^D) are to be regarded as maximum estimates, since these salts are certainly not completely ionic in character, and thus the true ΔG_W^D values will probably be somewhat less positive than those here calculated.

It is of interest to note from Table V. that the values of ΔS_W^D do not alter markedly from one type of salt to another, but that the changes in ΔG_W^D are determined by changes occurring in ΔH_W^D . Further, the calculations exhibit clearly the very large quantitative differences in

ionizing capacity which exist between the alkali, the univalent transition, and the bivalent transition metal halides.

Although the calculations refer to concentrations at which interionic effects are negligible, the alterations in Q , ΔH_M , and the entropy terms involved on increasing the concentrations even to saturation introduce only a few k. cal. correction to the above figures. Thus, using the relation $[MX] = [M^+][X^-] \exp. (\Delta G_W^D/RT)$, it follows that the concentration of undissociated salt in the alkali metal and silver halide solutions will be vanishingly small at all concentrations. Since thallous chloride is saturated at approximately 10^{-2} mol./litre, it is evident that in this case also, taking account of the possible error, the concentration of undissociated salt will probably always be less than 2 per cent. On the basis of the present calculations the bivalent transition metal halides would be almost non-electrolytes in aqueous solution, as is the case experimentally for these salts in such solvents as alcohol and acetone⁽²¹⁾. In aqueous solutions, however, special features may intervene which we have so far not considered, but which might lead to an abnormal increase in dissociation in water compared with organic solvents. These small doubly charged transition metal cations have the capacity to utilize the d -orbitals from an inner electron shell to give coordination links. This leads to the formation of complex anions or cations involving bonded water molecules, and at the same time to a change in the character of the anion-cation bond, possibly in the direction of making it more ionic.

Summary.

Calculations are made of the total heats, the entropies, and the free energies of dissociation of various types of salt molecules in water which permit quantitative estimates to be made of the degree of dissociation of these salts in aqueous solution.

The author wishes to express his gratitude to Professor E. K. Rideal, F.R.S., for his interest and encouragement, and gratefully acknowledges his indebtedness to the Carnegie Trust and to the Commissioners for the Exhibition of 1851 for Fellowships held during the course of this work.

References.

- (1) Orr and Butler, *Phil. Mag.* ser. 7, xviii. p. 778 (1934).
- (2) Maxwell, Hendricks, and Moseley, *Phys. Rev.* lii. p. 968 (1937).
- (3) Rodebush, *J. Chem. Physics*, iv. p. 372 (1936).
- (4) Sherman, *Chem. Rev.* xi. p. 93 (1932).
- (5) Helmholtz and Mayer, *J. Chem. Physics*, ii. p. 245 (1934).
- (6) Sutton and Mayer, *J. Chem. Physics*, iii. p. 20 (1935); Glockler and Calvin, *J. Chem. Physics*, iv. p. 492 (1936); Blewett, *Phys. Rev.* xlix. p. 900 (1936).

- (7) Bernal and Fowler, *J. Chem. Physics*, i. p. 515 (1933).
- (8) Lange and Martin, *Z. f. phys. Chem. A*, clxxviii. p. 214 (1937); *ibid.*, clxxx. p. 233 (1937).
- (9) Bell, *Trans. Far. Soc.* xxvii. p. 797 (1931); *J. Chem. Soc.* p. 2905 (1932).
- (10) Goldschmidt, *Berichte*, cx. p. 1263 (1927).
- (11) Slater, *Phys. Rev.* xxiii. p. 488 (1934).
- (12) Venkateswaran, *Proc. Ind. Acad. Sci. i. sect. A*, p. 850 (1938).
- (13) van Arkel and de Boer, 'La Valence et l'Electrostatique,' p. 63 (1936).
- (14) Born and Mayer, *Z. f. Physik*, lxxv. p. 11 (1932).
- (15) Sommermeyer, *Z. f. Physik*, lvi. p. 548 (1929).
- (16) Krishnamurti, *Ind. J. Physics*, v. p. 183 (1930); Braune and Engelbrecht, *Z. f. phys. Chem. B*, xix. p. 303 (1932).
- (17) Braune and Knoke, *Z. f. phys. Chem. B*, xxiii. p. 163 (1933).
- (18) Hassel and Stromme, *Z. f. Phys. Chem. B*, xxxviii. p. 466 (1938).
- (19) Latimer, Schutz, and Hicks, *J. Chem. Physics*, ii. p. 82 (1934).
- (20) Eley and Evans, *Trans. Far. Soc.* xxxiv. p. 1093 (1938).
- (21) Jones, *Publ. Carnegie Inst.* lxxx. p. 1 (1907); Connell, Hamilton, and Butler, *Proc. Roy. Soc. A*, cxlvii. p. 418 (1934).

VI. *The Crystal Structures of some Heterocyclic Organic Compounds of Analogous Constitution.*—Part I. *Thianthren and Selenanthren.*

By R. G. WOOD, M.Sc., and J. E. CRACKSTON, M.Sc.*

[Received March 4, 1940.]

1. *Introduction.*

The three papers included under the above general title contain a report on a preliminary structural analysis by X-ray, crystallographic and optical methods of a number of organic compounds of analogous constitution: thianthren and selenanthren (Part I.); phenthiazine, phenoxthionine, phenoxselenine, and phenoxtellurine (Part II.); and phenazine and diphenylene dioxide (Part III.). The detailed structural analysis of the substances, involving the determination of the relative positions of the atoms in the molecule, is as yet only in its preliminary stages, but the results obtained up to the present have enabled us to arrive at certain conclusions which are set out below.

The structures with which we are concerned have already received some attention: Cullinane and his co-workers, for example, have investigated the isomorphous relationships of several of the substances, taking as a criterion for isomorphism the ability of binary mixtures to form a continuous series of solid solutions; and determinations of dipole moments by other investigators have shown that the molecules of some of the compounds are plane whereas those of others must be folded. It will be interesting to see to what extent the conclusions reached by chemical and other methods are borne out by the results obtained by X-ray methods.

It is hoped that the detailed analysis of selenanthren, which is at present well under way, will lead to an exact determination of the structure of that substance.

2. *Crystallography.*

Thianthren (diphenylene disulphide, I.) and selenanthren (diphenylene diselenide, II.) crystallize from acetone in colourless plates with well-

* Communicated by Professor R. T. Dunbar,

formed faces. The crystals of selenanthren closely resemble those of thianthren, though fewer faces are developed.



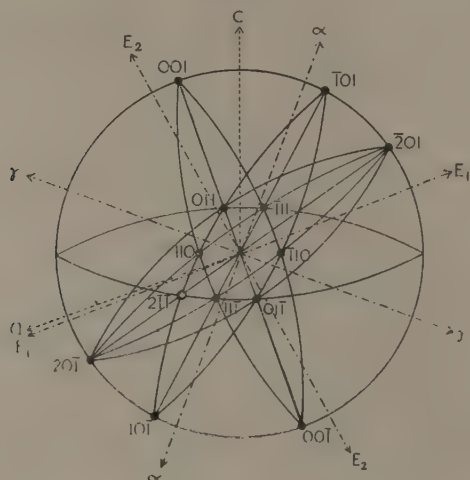
TABLE I.

	Thianthren.		Selenanthren.	
	Observed.	Calculated.	Observed.	Calculated.
001 : 201	74° 18' *	—	74° 57' *	—
001 : 110	98° 6' *	—	98° 14' *	—
201 : 110	70° 36' *	—	70° 21' *	—
201 : 111	63° 37'	63° 41'	63° 25'	63° 44'
110 : 111	27° 58'	27° 56'	28° 8'	27° 46'
001 : 101	47° 17'	47° 8'	—	—
111 : 101	60° 8'	60° 6'	—	—
001 : 011	61° 17'	61° 24'	61° 11'	61° 31'
101 : 011	70° 52'	71° 0'	—	—
101 : 110	79° 11'	79° 16'	—	—
201 : 011	82° 25'	82° 33'	82° 32'	82° 53'
101 : 211	53° 55'	54° 8'	—	—
201 : 211	48° 37'	48° 48'	—	—
001 : 211	79° 38'	79° 44'	—	—
110 : 211	62° 32'	62° 7'	—	—
001 : 111	22° 48'	22° 34'	22° 29'	22° 48'
111 : 211	19° 12'	19° 11'	—	—
111 : 211	69° 40'	68° 53'	—	—
110 : 110	48° 37'	48° 20'	48° 43'	48° 42'
111 : 111	—	—	60° 5'	59° 39'
110 : 011	—	—	43° 9'	42° 56'
011 : 111	—	—	20° 29'	20° 13'

The first crystallographic examination of thianthren was made by Friedel and Crafts ⁽¹⁾, whose measurements are recorded by Groth ⁽²⁾, and more recently measurements have been made by Prasad, Shanker

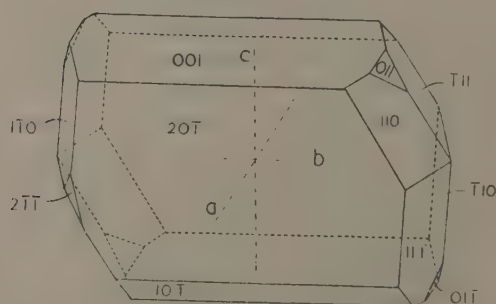
and Peermohamed⁽³⁾ and by Cox *. No previous crystallographic examination of selenanthren has been published. The observed interfacial angles for thianthren and selenanthren are tabulated in Table I.;

Fig. 1.



Stereographic projection of thianthren.

Fig. 2.



Typical crystal of thianthren.

the crystals are represented in stereographic projection in figs. 1 and 3, and typical specimens are drawn in figs. 2 and 4. Both crystals belong to the monoclinic holohedral class. The axial ratios and angle (β)

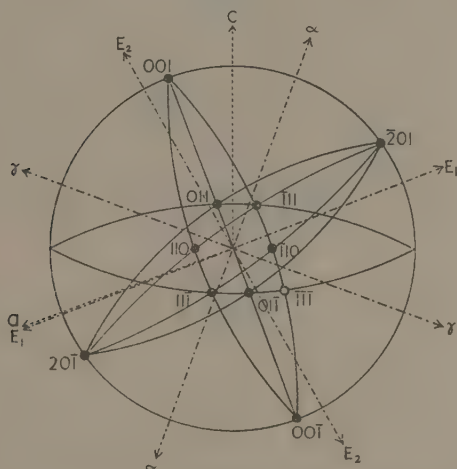
* We are indebted to Dr. E. G. Cox for communicating to us privately his preliminary crystallographic, optical and X-ray measurements on thianthren.

calculated from the three most accurately known angles (marked with an asterisk in Table I.) are as follows, the angle β being given to the nearest $10'$:—

Thianthren $a : b : c = 2.37 : 1 : 1.95$, $\beta = 110^\circ 0'$.

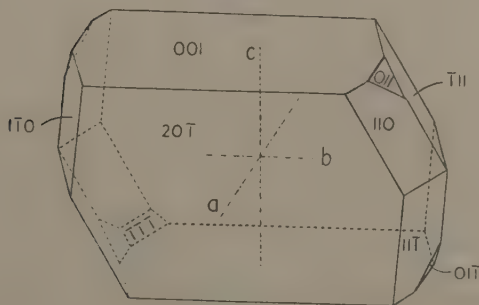
Selenanthren $a : b : c = 2.36 : 1 : 1.97$, $\beta = 110^\circ 20'$.

Fig. 3.



Stereographic projection of selenanthren.

Fig. 4.



Typical crystal of selenanthren.

These results have already been reported⁽⁴⁾, and preliminary values referring to a different set of axes were included in a paper by Cullinane and Plummer⁽⁵⁾.

Table I. also gives the value of the angle corresponding to each observed angle as calculated from the three fundamental angles for each crystal. It will be seen that there is a close similarity between the observed angles for the two crystals and that the axial ratios and angles are almost identical. This shows that thianthren and selenanthren are isomorphous, a result which confirms the same conclusion reached by Cullinane and Plummer ⁽⁵⁾ from the observation that thianthren and selenanthren form a continuous series of solid solutions.

3. X-ray Measurements.

Rotation photographs have been taken of each crystal rotating about the axes a , b , and c , using copper radiation. The values deduced for the dimensions of the unit cells are given in Table II. The densities of the crystals were determined by flotation in an aqueous solution of zinc chloride, and the observed densities are given in the table together with

TABLE II.

	a .	b .	c .	β .	Density gm./ml.		Mols. per unit cell.
					Obs.	Calc.	
Thianthren	14.4 Å.	6.11 Å.	11.9 Å.	110° 0'	1.45	1.47	4
Selenanthren.	14.5	6.24	12.1	110° 20'	1.95	2.01	4

densities calculated on the assumption that there are four molecules in the unit cell.

An X-ray examination of thianthren has been reported by Prasad, Shanker, and Peermohamed ⁽³⁾. Cox ⁽⁶⁾, however, has pointed out that the unit cell chosen by them is not primitive, but is centred in the basal plane, and that the explanation given by them for the existence of eight molecules in their unit cell is therefore unnecessary. Fig 5 shows the relationship between the unit cell of Prasad *et al.* (denoted by a' , c' , and β') and the unit cell adopted in the present work. Prasad's axes and angle have the values $a'=23.3$ Å., $b' \leq 6.14$ Å., $c'=14.52$ Å., $\beta'=105^\circ 51'$ respectively, the b -axes having the same direction in the two cells. The axes given by Groth correspond to a cell a' , $\frac{1}{2}c'$, β' , which is not a true unit cell.

In order to determine the space-group a series of oscillation photographs was taken for each crystal rotating about the axes a and b . These were

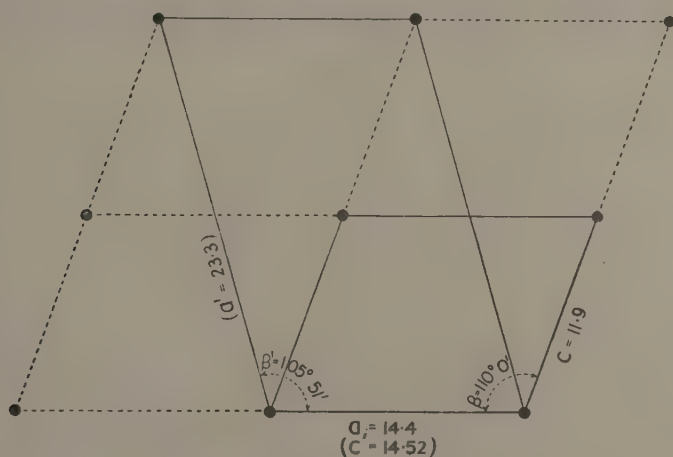
indexed graphically by Bernal's method ⁽⁷⁾. Indices of all general types (hkl) appear, showing that the lattices are primitive and of type Γ_{7n} . The following features of special indices were found for both crystals :—

($h0l$) absent when h is odd,

($0k0$) absent when k is odd.

These extinctions characterize the space-group $P2_1/a$ (C_{2h}^5), in agreement with Prasad, Shanker, and Peermohamed, who found the same space-group for thianthren. The assignment of this space-group has also been confirmed by Weissenberg photographs taken by one of the authors (R. G. W.)

Fig. 5.



Unit cells of thianthren.

in the Crystallographic Laboratory, University of Cambridge, by kind permission of Dr. W. A. Wooster.

4. Optical Measurements.

The refractive indices of the crystals for sodium light were measured by the immersion method described by Wood and Ayliffe ⁽⁸⁾. It is found that the β -axis of the indicatrix coincides with the crystallographic b -axis. The α - and γ -axes are indicated on the stereographic projections, figs. 1 and 3, which also show the positions of the optic axes. One of the optic axes in each case makes a very small angle with the crystallographic axis a (about $1\frac{1}{4}^\circ$ in thianthren and about $\frac{1}{4}^\circ$ in selenanthren). The axis γ is the acute bisectrix in each crystal, so that the birefringence is positive.

The values of the refractive indices, the optic axial angles ($2V$), and the angles made by the γ -axis of the indicatrix with the crystallographic c -axis are tabulated in Table III. (angles to nearest $10'$).

5. Structure.

The space-group $P2_1/a$ possesses two-fold screw axes perpendicular to the plane (010) and glide-planes parallel to (010). It requires four asymmetric elements per unit cell for its description, and since the unit cells of thianthren and selenanthren contain four molecules it follows that these molecules may be asymmetric. The existence of a finite dipole moment (see below) in thianthren and selenanthren has been interpreted as indicating in each case that the molecule is folded, most probably along the lines joining the two sulphur and the two selenium atoms respectively. The dipole moment of thianthren was first measured by Bergmann and Tschudnowsky⁽⁹⁾, who suggested the folding of the

TABLE III.

	α .	β .	γ .	$2V$.	Sign.	Angle γc .
Thianthren	1.646	1.759	1.950	$82^\circ 10'$	+	$70^\circ 10'$
Selenanthren	1.686	1.790	1.964	$82^\circ 0'$	+	$69^\circ 30'$

molecule, a hypothesis which was further discussed by Bennett and Glasstone⁽¹⁰⁾. Measurements on thianthren have also been made by Walls and Smyth⁽¹¹⁾, and on thianthren and selenanthren by Campbell, Le Fèvre, Le Fèvre, and Turner⁽¹²⁾. The folded configuration of the thianthren molecule leads to the expectation of the existence of certain isomeric derivatives which would not occur with a plane molecule. Attempts to find these by Baw, Bennett, and Dearn⁽¹³⁾ have failed. Unsuccessful attempts have also been made to accomplish the optical resolution of thianthren derivatives⁽¹⁴⁾. It has been suggested that these failures are due to insufficient rigidity of the thianthren molecule, which may be flexible about the line of folding.

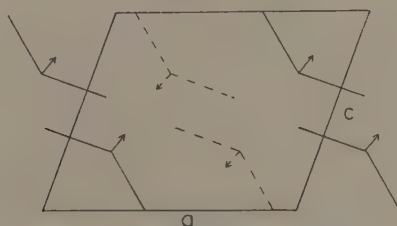
By assuming reasonable values for the valency angles of carbon, sulphur, and selenium, and making use of the known radii of these atoms, it has been shown that the angle of fold for thianthren and selenanthren (*i. e.*, the angle between the planes of the benzene nuclei) is in the neighbourhood of 140° ⁽¹²⁾. This value will be assumed until a more accurate determination is obtained.

As a starting-point in suggesting a possible structure use is made of the optical and magnetic properties of the crystals. It is assumed that the

vibration direction of the slow ray (γ) will correspond approximately to the longest dimension of the molecule. This direction makes an angle of approximately 40° with the crystallographic axis a in the obtuse angle β in both crystals (see figs. 1 and 3). The same molecular orientation is indicated by the magnetic measurements of Banerjee⁽¹⁵⁾ on thianthren, which have been confirmed in a private communication from Dr. Lonsdale. The direction of minimum (numerical) diamagnetic susceptibility χ_1 is found by Banerjee to make an angle of 40° with the axis c' on the side of c' opposite to the obtuse angle β' . (Banerjee refers his results to the axes of Prasad, Shanker and Peermohamed.) In terms of the axes adopted in the present work this means that χ_1 makes an angle of 40° with a in the obtuse angle β , so that χ_1 is practically coincident with γ .

If the molecules are arranged with their lengths in the direction thus suggested it is found that they can be accommodated in the unit cell provided they are inclined at an angle of about 30° to the b -axis. An

Fig. 6.



Suggested structure for thianthren and selenanthren.

arrangement consistent with the symmetry requirements of the space-group is shown diagrammatically in fig. 6, which represents a projection on the (010) face of the unit cell. The direction of tilt of each molecule to the b -axis is indicated by a small arrow at the centre of its projection. (The effect of the tilt on the apparent angle of fold in the projection has not been taken into account, since the diagram is intended as a qualitative representation only.) Broken lines represent molecules which are translated $b/2$ parallel to b relative to the molecules in full line. The coordinates of the centres of the molecules are not yet determined, but preliminary intensity measurements in the case of selenanthren have shown that their projections are probably near the points indicated in the figure.

6. Summary.

An account is given of crystallographic, X-ray and optical measurements on thianthren and selenanthren. A preliminary structure is

suggested which is in general agreement with the optical and magnetic properties and in which the molecule is non-planar.

Our thanks are due to Dr. N. M. Cullinane, of the Chemistry Department of this College, who prepared the crystals used in this investigation, and to Dr. Kathleen Lonsdale for the magnetic measurements. Mr. C. H. McCale and Mr. Gordon Williams also rendered valuable assistance with the optical work.

[It is with deep regret that I have to record the death of Mr. J. E. Crackston in August 1939 during the preparation of this work for publication.—R. G. W.]

References.

- (1) Friedel and Crafts, *Ann. Chim. (Phys.)* (6) xiv. p. 439 (1888).
- (2) Groth, *Chem. Kryst.* v. p. 34 (1919).
- (3) Prasad, Shanker, and Peermohamed, *J. Ind. Chem. Soc.* xiv. p. 177 (1937).
- (4) Crackston and Wood, 'Nature,' cxlii. p. 257 (1938).
- (5) Cullinane and Plummer, *J. Chem. Soc.* p. 63 (1938).
- (6) Cox, *Chem. Soc. Ann. Rep.* p. 189 (1937).
- (7) Bernal, *Proc. Roy. Soc. A*, cxiii. p. 117 (1926).
- (8) Wood and Ayliffe, *Phil. Mag.* (7) xxi. p. 321 (1936).
- (9) Bergmann and Tschudnowsky, *Ber. dtsh. chem. Ges.* lxv. p. 457 (1932).
- (10) Bennett and Glasstone, *J. Chem. Soc.* p. 128 (1934).
- (11) Walls and Smyth, *J. Chem. Phys.* i. p. 337 (1933).
- (12) Campbell, Le Fèvre, Le Fèvre, and Turner, *J. Chem. Soc.* p. 404 (1938).
- (13) Baw, Bennett, and Dearn, *J. Chem. Soc.* p. 680 (1934).
- (14) Bennett, Lesslie, and Turner, *J. Chem. Soc.* p. 444 (1937).
- (15) Banerjee, *Z. Kristallogr. c.* p. 316 (1938).

University College, Cardiff.
March 2, 1940.

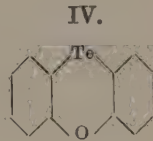
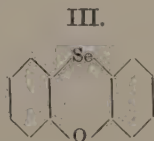
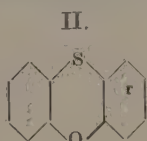
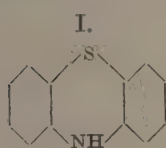
VII. *The Crystal Structures of some Heterocyclic Organic Compounds of Analogous Constitution.*—Part II. *Phenthiazine, Phenoxthionine, Phenoxselenine, and Phenotellurine.*

By R. G. WOOD, M.Sc., C. H. McCALÉ, M.Sc., and G. WILLIAMS, M.Sc.*

[Received March 4, 1940.]

1. *Introduction.*

THIS paper describes a crystallographic, optical and X-ray examination of phenthiazine (thiodiphenylamine, I.), phenoxthionine (II.), phenoxselenine (III.), and phenotellurine (IV.).



2. *Crystallography.*

(a) *Phenthiazine.*

Phenthiazine crystallizes from alcohol in the form of diamond-shaped plates which are colourless but turn brown on exposure. The observed interfacial angles are as follows :—

001 : 111	77° 19',
111 : 111	76° 56',
111 : 111	71° 6'.

A stereographic projection of the crystal is given in fig. 1 and a drawing in fig. 2. As far as the external symmetry is concerned the crystal belongs to the orthorhombic holohedral class. The axial ratios calculated from the above angles are

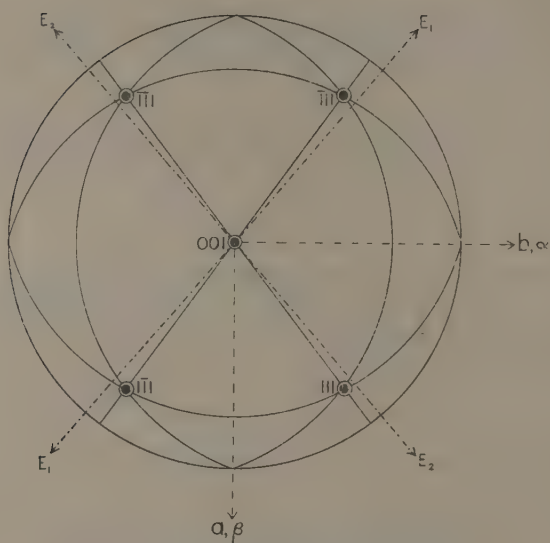
$$a : b : c = 0.742 : 1 : 2.65.$$

(b) *Phenoxthionine.*

Using alcohol as a solvent, well-formed, long, colourless needle-like crystals of phenoxthionine were obtained. The observed interfacial angles

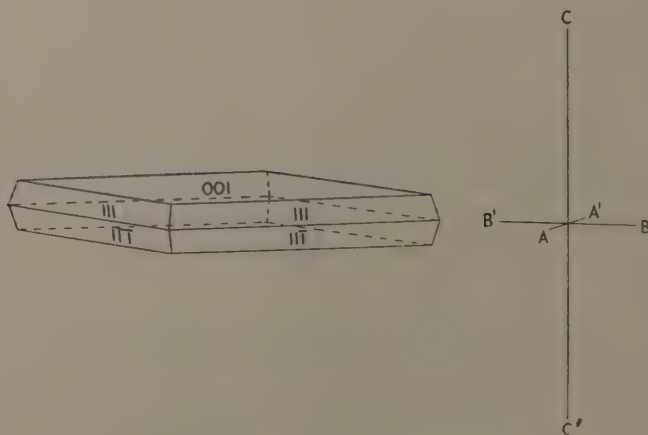
* Communicated by Professor R. T. Dunbar.

Fig. 1.



Stereographic projection of phenthiazine.

Fig. 2.



Typical crystal of phenthiazine.

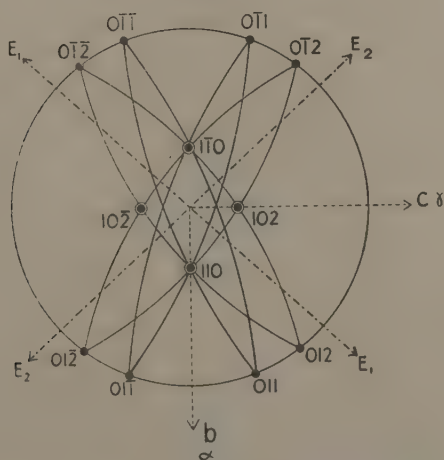
will be found in Table I., together with the angles calculated from those taken as fundamental (marked with an asterisk). The crystal is repre-

TABLE I.

Interfacial angles of phenoxthionine and phenoxselenine.

	Phenoxthionine.		Phenoxselenine.
	Observed.	Calculated.	Observed.
012 : 0 $\bar{1}$ 2	105° 39'	105° 20'	105° 7'
012 : 011	16° 9'*	—	16° 17'
011 : 01 $\bar{1}$	42° 7'	42° 22'	42° 23'
012 : 110	61° 19'*	—	—
110 : 102	46° 20'*	—	—
011 : 110	55° 30'	55° 45'	—

Fig. 3.



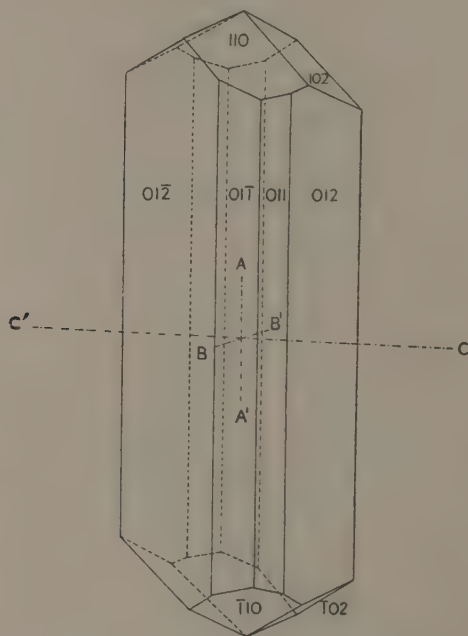
Stereographic projection of phenoxthionine.

sented in stereographic projection in fig. 3 and is drawn in fig. 4. It appears to belong to the orthorhombic holohedral class, though it will be seen later that the X-ray results show it to be actually enantiomorphic.

The axial ratios calculated from the three fundamental angles are

$a : b : c = 0.757 : 1 : 2.58$. These are very close to the ratios found for phenthiazine, indicating that the crystals are isomorphous. The external appearances of the two crystals, however, are quite different, since the only faces which occur in phenthiazine belong to the pinacoidal form [001] and the pyramidal form [111], forms which do not occur at all in phenoxthionine.

Fig. 4.



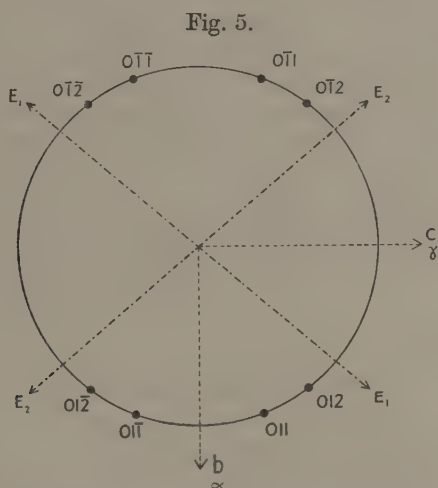
Typical crystal of phenoxthionine.

(c) *Phenoxselenine*.

Colourless crystals were obtained from alcohol and from acetic acid, but they were small and needle-like. The end faces were too badly formed to be measurable, so that only the principal zone parallel to the a -axis could be measured. The angles in this zone are given in Table I, and the crystal is represented in stereographic projection in fig. 5. The observed data are insufficient for calculating the axial ratios, but from the close similarity of the angles in the principal zone it appears probable that phenoxthionine and phenoxselenine are isomorphous, a conclusion which is confirmed by the X-ray observations.

(d) *Phenoxtellurine*.

Long yellow needle-like crystals were obtained from alcohol, but it was impossible to make any goniometric measurements as the faces were too imperfect.



Stereographic projection of phenoxselenine.

TABLE II.

	a .	b .	c .	$a : b : c$.	Density gm./ml.		Number of molecules per unit cell.
					Obs.	Calc.	
Phenthiazine...	5.91 Å.	7.90 Å.	21.0 Å.	0.748 : 1 : 2.66	1.34	1.35	4
Phenoxthionine.	5.94	7.76	20.5	0.765 : 1 : 2.64	1.38	1.41	4
Phenoxselenine.	5.93	7.85	20.5	0.755 : 1 : 2.61	1.70	1.72	4
Phenoxtellurine.	5.97	8.16	20.5	0.732 : 1 : 2.51	1.97	1.97	4

3. *X-ray Measurements.*

Complete rotation photographs taken around the a , b , and c axes of each crystal using copper radiation gave the spacings and axial ratios tabulated in Table II. The spacings are very nearly equal for all four

crystals, showing that they are isomorphous. This conclusion has already been suggested by the crystallographic measurements and is in agreement with other observations. Thus Drew ⁽¹⁾ has shown that phenoxthionine, phenoxselenine, and phenoxtellurine taken in pairs form mixed crystals. Again, Cullinane and Rees ⁽²⁾ have found that phenthiazine and phenoxthionine give a continuous series of solid solutions.

The densities of the crystals were determined by flotation in an aqueous solution of zinc chloride, and comparison of the observed densities with the calculated densities shows that there are four molecules in the unit cell in each case. The observed and calculated densities are included in Table II.

Oscillation photographs were taken about the *a* and *c* axes of phenthiazine and about the *b* and *c* axes of the other crystals. All general (*hkl*) spectra were present in each case, showing that the unit cells chosen are primitive.

(a) *Phenthiazine*.

Special indices showed the following features :—

(*h*0*l*) absent when *h*+*l* is odd,

(0*k**l*) absent when *k* is odd.

The lattice is therefore Γ_0 and the most probable space-groups are *Pbn* (C_{2v}^9) or *Pbnm* (D_{2h}^{16}). These two space-groups differ only in that the latter possesses a centre of symmetry. In order to decide between these alternatives the crystal was cooled down to liquid-air temperature to see if a pyroelectric effect could be detected ⁽³⁾. A very slight effect was in fact observed, which, if genuine, would indicate the absence of a centre of symmetry. The effect observed, however, was only of the order of one that observed with symmetrical triphenyl-benzene which is known to seventh of exhibit a very small pyro-electric effect ⁽³⁾, and it may therefore be spurious. The correct allocation of the space-group cannot be decided with certainty from this.

(b) *Phenoxthionine, Phenoxselenine, Phenoxtellurine*.

Special indices showed the following features :—

(*h*00) absent when *h* is odd,

(0*k*0) absent when *k* is odd,

(00*l*) absent when *l* is odd.

The lattice is therefore Γ_0 and the space-group $P2_12_12_1$ (D_2^4). This is the only orthorhombic space-group satisfying the observed extinctions, and since it is enantiomorphic the crystals are not holohedral, as was

indicated by the external symmetry. In this space-group there is no centre of symmetry, so further confirmation of its correctness was sought by examining the crystals for a pyro-electric effect. As already mentioned, the presence of such an effect indicates the absence of a centre of symmetry, but the converse is not true. In the present case no pyro-electric effect was found with any of these three crystals, so that no definite conclusion can be drawn.

4. Optical Measurements.

The optical properties of the crystals in sodium light have been investigated by the method of Wood and Ayliffe ⁽⁴⁾, using solutions of potassium mercuric iodide as the immersion liquid. Other liquids of sufficiently high refractive index were found to attack the crystals rapidly.

The refractive index β of phenoxthionine is slightly greater than that of a concentrated solution of potassium mercuric iodide, so that the optic

TABLE III.

	α .	β .	γ .	2V.	α .	β .	γ .	Sign.
Phenthiazine	1.61	1.73	1.95	81°	<i>b</i>	<i>a</i>	<i>c</i>	+
Phenoxthionine ...	1.62	1.72	1.86	85°	<i>b</i>	<i>a</i>	<i>c</i>	+
Phenoxselenine	1.66	1.74	1.87	81°	<i>b</i>	<i>a</i>	<i>c</i>	+
Phenoxtellurine ...	>1.73	—	—	—	<i>b</i>	<i>a</i>	<i>c</i>	+

axial angle could not be measured quite accurately. The same difficulty was still more marked in the cases of phenthiazine and phenoxselenine, in which β is larger. The angles given below are probably correct to 1°. In the case of phenoxtellurine the refractive index α was greater than that of any suitable immersion liquid, and only a lower limit can be recorded. Table III. gives the values of the principal refractive indices, the optic axial angle, and the orientation of the indicatrix. The orientations of the optic axes and the directions of α and γ are indicated in the stereographic projections, figs. 1, 3, and 5. The refractive indices in Table III. are rounded-off values correct to ± 0.01 , so that the figures are not quite self-consistent.

5. Structure.

(a) Phenoxthionine, Phenoxselenine, Phenoxtellurine.

These three compounds are so similar that it is convenient to deal with them together before considering phenthiazine. By making reasonable assumptions about the valency angles and using the known atomic radii

of the elements concerned it can be shown that the molecules of these compounds are folded about the line joining the heterocyclic atoms. Suggested angles of fold are included in Table IV. Attempts have been made by Turner and his co-workers to demonstrate the presence of this folding by isolating optically active derivatives ^{(5), (6), (7)}. As in the case of thianthren the efforts have been unsuccessful. Evidence for the folding based on the melting-points of mixtures is also inconclusive. Thus Cullinane and Rees ⁽²⁾ have found that whilst phenoxthionine gives no solid solution formation with diphenylene dioxide (which has a flat molecule), it also gives no solid solution formation with thianthren (which has a folded molecule). A possible reason for this behaviour is that the angle of fold for phenoxthionine may be appreciably different from that for thianthren (140°), as suggested in Table IV. It would be of interest to test this explanation by phase rule investigations of the systems thianthren-phenoxselenine and thianthren-phenoxtellurine.

TABLE IV.

	Suggested angle of fold.	$\beta-a.$	$\gamma-\beta.$	$\chi_a-\chi_b.$	$\chi_a-\chi_c.$
Phenthiazine	$160^\circ-170^\circ$ ⁽²⁾	0.12	0.22	47.1	{ too small to measure. 8.3
Phenoxthionine . . .	$150^\circ-160^\circ$	0.10	0.14	42.0	
Phenoxselenine . . .	$140^\circ-150^\circ$ ⁽⁶⁾	0.08	0.13	—	—
Phenoxtellurine . . .	$135^\circ-145^\circ$ ⁽⁷⁾	—	—	37.6	10.4

The optical observations given in § 4 show that the direction of the γ -axis of the indicatrix is parallel to the longest edge of the unit cell c . It may therefore be assumed that the length of the molecule in the crystal is approximately parallel to c . Magnetic measurements by Dr. Lonsdale on phenoxthionine and phenoxtellurine are consistent with this conclusion and indicate that the planes of the molecules lie near the (010) plane.

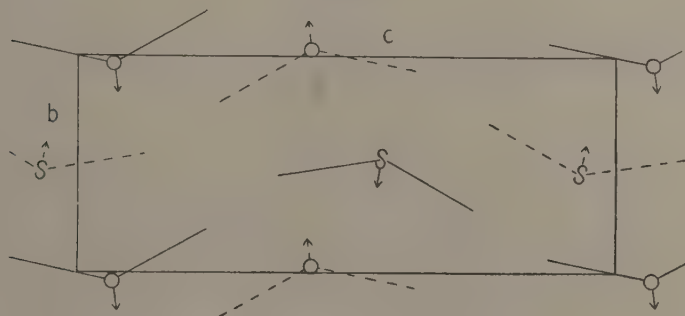
One possible structure which does not overcrowd the cell is illustrated in fig. 6, which represents a projection on the (100) plane. In this diagram a representative molecule has been placed in a general position near the origin and its projection has been rotated through 10° about the a -axis in order to obtain approximately uniform packing. The other molecules in the figure are obtained by the operations of the space-group $P2_12_12_1$. The molecules are supposed to be folded along the line joining the heterocyclic atoms, the upper atom being indicated by the symbol O or S. Molecules in the plane of the diagram are drawn in full line, those $a/2$

beneath are drawn in broken line. In order that the molecules may fit into the unit cell the line joining the heterocyclic atoms must be inclined to the a -axis at an angle of about 30° , the direction of inclination for each molecule being indicated in the diagram by a small arrow.

(b) *Phenthiazine*.

This crystal is considered separately from the other three, since, although isomorphous with them, it exhibits certain interesting differences. Besides crystallizing in a different habit (§ 2), additional extinctions are observed (§ 3) which indicate either $Pbnm$ or Pbn as the most probable space-group. The data at present available are somewhat conflicting, and do not allow of a final conclusion being reached concerning the special features of phenthiazine which give rise to the extra extinctions.

Fig. 6.



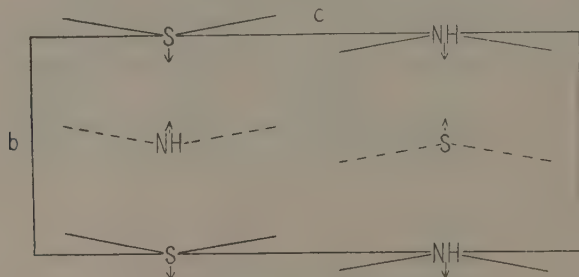
Possible structure for phenoxthionine.

The isomorphism of phenthiazine and phenoxthionine suggests that the space-group of phenthiazine is not Pbn , since this does not possess $P2_12_12_1$ as a subgroup. This objection does not apply to $Pbnm$, but in this case, since there are only four molecules in the unit cell, each molecule must possess a plane of symmetry and must lie on a plane of symmetry in the unit cell. There is no structural difficulty about this, and one possible arrangement is illustrated in fig. 7. This structure is consistent with the optical and magnetic properties of the crystal. It will be seen from Table IV. that these properties change progressively in passing from phenthiazine to phenoxtellurine, and that the largest change takes place between phenthiazine and phenoxthionine. It appears that phenthiazine is a kind of limiting case in the series, and it is possible that it may even possess a plane molecule. The birefringence of phenthiazine is much greater than that of the other crystals, and almost the whole of the increase is due to increase in γ . This suggests that, on the average,

there is a larger component of the length of the molecule parallel to *c*. The only observation contrary to the assignment of the space-group *Pbnm* to phenthiazine is the apparent existence of a pyro-electric effect, but as already stated in § 3 this effect may be spurious.

It is hoped to make intensity measurements shortly in order to determine the exact structures of the crystals discussed in this paper.

Fig. 7.



Possible structure for phenthiazine.

6. Summary.

An account is given of crystallographic, optical, and X-ray measurements on phenthiazine, phenoxthionine, phenoxselenine, and phenoxtellurine, with a preliminary discussion of possible crystal structures.

Our thanks are due to Dr. N. M. Cullinane, of the Chemistry Department of this College, for specimens of phenoxthionine and phenthiazine; to Dr. H. D. K. Drew for specimens of phenoxselenine and phenoxtellurine; and to Dr. E. E. Turner for specimens of phenoxtellurine.

We are also indebted to Dr. Kathleen Lonsdale for permission to include her measurements of diamagnetic susceptibilities which appear in Table IV.

References.

- (1) Drew, J. Chem. Soc. p. 511 (1928).
- (2) Cullinane and Rees, Trans. Faraday Soc. xxxvi. p. 507 (1940).
- (3) Orelkin and Lonsdale, Proc. Roy. Soc. A, cxliv. p. 630 (1934).
- (4) Wood and Ayliffe, Phil. Mag. (7) xxi. p. 321 (1936).
- (5) Bennett, Lesslie, and Turner, J. Chem. Soc. p. 444 (1937).
- (6) Thompson and Turner, J. Chem. Soc. p. 29 (1938).
- (7) Campbell and Turner, J. Chem. Soc. p. 37 (1938).
- (8) Wood and McCale, J. Sci. Inst. xvii. p. 225 (1940).

University College, Cardiff.
March 2, 1940.

VIII. *A Heat Conduction Problem introduced by C. J. Tranter.*

By R. V. CHURCHILL *.

[Received May 7, 1940.]

1. *Introduction.*

In an earlier issue of this Magazine † contour integrals were used to write a formal solution of a problem which can be stated as follows :—Find the temperatures in a semi-infinite solid $x > 0$ composed of a layer $0 < x < a$ of one material initially at the uniform temperature A in contact with a semi-infinite solid $x > a$ of another material initially at temperature zero, when the face $x = 0$ is kept insulated.

It is the first objective of the present paper to obtain the correct solution of this problem ; the result given by Mr. Tranter does not satisfy the required conditions at the surface of separation $x = a$ of the two media. The temperature formulæ will be given here in the form of series which are quite practical to use. In addition the result will be completely established as a solution, and the boundary problem will be stated completely so that just one solution exists. Both the solution and its uniqueness will be obtained by the Laplace transformation ; and it is the final objective of this paper to furnish another illustration of the direct character of this method ‡. This transformation method is the reliable form of the operational calculus ; it has obvious advantages over the contour integration process.

The boundary problem in the temperatures $V_i(x, t)$, ($i = 1, 2$) is the following.

$$\frac{\partial V_i}{\partial t} = k_i \frac{\partial^2 V_i}{\partial x^2}, \quad (t > 0, \quad 0 < x < a \text{ for } i = 1; \quad x > a \text{ for } i = 2) \quad . \quad . \quad (1)$$

$$V_1(x, +0) = A, \quad (0 < x < a); \quad V_2(x, +0) = 0, \quad (x > a) \quad . \quad . \quad (2)$$

* Communicated by the Author.

† C. J. Tranter, *Phil. Mag.* xxviii. pp. 579–583 (1939). The problem under consideration is his Example II., p. 582. I have used V_1 , V_2 , A and λ for Mr. Tranter's v_1 , v_2 , Φ , and y respectively ; the rest of the notation is the same as his.

‡ For other examples, some of which are more elementary than the present one, the reader is referred to papers by Carslaw, *Math. Gazette*, xxii. pp. 264–280 (1938) ; Carslaw and Jaeger, *Phil. Mag.* (7) xxvi. pp. 473–495 (1938) ; and Jaeger, *Math. Gazette*, xxiii. pp. 62–67 (1939), and xxiv. pp. 42–50 (1940).

$$V_1(a-0, t) = V_2(a+0, t); \quad K_1 \frac{\partial}{\partial x} V_1(a-0, t) = K_2 \frac{\partial}{\partial x} V_2(a+0, t); \quad (t > 0). \quad (3)$$

$$\frac{\partial}{\partial x} V_1(+0, t) = 0, \quad (t > 0); \quad |V_2(x, t)| < M, \quad (x \geq a, t \geq 0), \quad . \quad . \quad (4)$$

where M is some constant.

2. The Formal Solution of the Problem.

Let $v_i(x, s)$ be the Laplace transform of $V_i(x, t)$,

$$v_i(x, s) = L\{V_i\} = \int_0^\infty e^{-st} V_i(x, t) dt,$$

where the variable s can be taken as real and positive throughout this paper. To obtain a formal solution, which will be verified later, we apply the transformation to the members of (1) and use the conditions (2) in the well-known formula for the transform of the derivative,

$$L\left\{\frac{\partial V_i}{\partial t}\right\} = sL\{V_i\} - V_i(x, +0).$$

Applying L formally to the conditions (3) and (4) as well, we obtain the following boundary problem in $v_i(x, s)$.

$$sv_1 - A = k_1 \frac{d^2 v_1}{dx^2}, \quad (0 < x < a); \quad sv_2 = k_2 \frac{d^2 v_2}{dx^2}, \quad (x > a) \quad . \quad . \quad . \quad (5)$$

$$v_1(a, s) = v_2(a, s); \quad K_1 \frac{d}{dx} v_1(a, s) = K_2 \frac{d}{dx} v_2(a, s), \quad . \quad . \quad . \quad (6)$$

$$\frac{d}{dx} v_1(0, s) = 0; \quad |v_2(x, s)| < \frac{M}{s} \quad . \quad . \quad . \quad . \quad . \quad . \quad (7)$$

The solution of this simple problem in ordinary differential equations containing s as a parameter can be written

$$v_1(x, s) = \frac{A}{s} \left[1 - \frac{1 - \lambda e^{-\alpha(a-x)} + e^{-\alpha(a+x)}}{1 - \lambda e^{-2\alpha a}} \right], \quad (0 < x < a). \quad . \quad . \quad . \quad (8)$$

$$v_2(x, s) = \frac{A}{s} \frac{1 + \lambda e^{-\alpha\mu(x-a)} - e^{-\alpha[2a+\mu(x-a)]}}{1 - \lambda e^{-2\alpha a}}, \quad (x > a), \quad . \quad . \quad . \quad (9)$$

where we have put

$$\alpha = \sqrt{\frac{s}{k_1}}, \quad \mu = \sqrt{\frac{k_1}{k_2}}, \quad \lambda = \frac{K_1 \sqrt{k_2} - K_2 \sqrt{k_1}}{K_1 \sqrt{k_2} + K_2 \sqrt{k_1}},$$

so that $|\lambda| < 1$ and $\alpha\mu = \sqrt{s/k_2}$.

To find the inverse transforms of the functions defined by (8) and (9) we may put

$$(1 - \lambda e^{-2\alpha a})^{-1} = \sum_{n=0}^{\infty} \lambda^n e^{-2n\alpha a}.$$

Then

$$v_1 = \frac{A}{s} - A \frac{1-\lambda}{2} \sum_0^{\infty} \frac{\lambda^n}{s} \{e^{-\alpha[(2n+1)a-x]} + e^{-\alpha[(2n+1)a+x]}\} \quad (10)$$

$$v_2 = A \frac{1+\lambda}{2} \sum_0^{\infty} \frac{\lambda^n}{s} \{e^{-\alpha[2na+\mu(x-a)]} - e^{-\alpha[(2n+2)a+\mu(x-a)]}\}, \quad (11)$$

But the inverse transform of each term here is known * since, for any constant $b \geq 0$,

$$L^{-1}\left\{\frac{e^{-b\sqrt{s}}}{s}\right\} = P\left(\frac{b}{2\sqrt{t}}\right), \quad (12)$$

where

$$P(u) = \frac{2}{\sqrt{\pi}} \int_u^{\infty} e^{-\eta^2} d\eta.$$

Recalling that $\alpha = \sqrt{s}/\sqrt{k_1}$ and applying the inverse transformation L^{-1} termwise to (10) and (11), we find

$$V_1(x, t) = A - A \frac{1-\lambda}{2} \sum_0^{\infty} \lambda^n \left\{ P\left[\frac{(2n+1)a-x}{2\sqrt{k_1 t}}\right] + P\left[\frac{(2n+1)a+x}{2\sqrt{k_1 t}}\right] \right\}, \quad (0 < x < a). \quad (13)$$

$$V_2(x, t) = A \frac{1+\lambda}{2} \sum_0^{\infty} \lambda^n \left\{ P\left[\frac{2na+\mu(x-a)}{2\sqrt{k_1 t}}\right] - P\left[\frac{(2n+2)a+\mu(x-a)}{2\sqrt{k_1 t}}\right] \right\}, \quad (x > a). \quad (14)$$

This is the formal solution of the problem. Since the value of the positive function P here diminishes rapidly as n increases in general, the convergence of the series is rapid, especially for small t . Moreover, $P = 1 - \Theta$ where Θ is the tabulated probability integral, so the series is well adapted to computation †.

3. The Verification of the Solution.

We shall now show that the functions defined by (13) and (14) satisfy all the conditions of the problem (1)–(4).

Consider first the series in (13). We assign the value zero to the function P when its argument becomes infinite. For each fixed x , ($0 \leq x \leq a$) and t , ($t \geq 0$) the coefficients of λ^n are clearly monotone non-increasing functions of n , except for $t = x - a = 0$ when the argument of the first P function with $n = 0$ becomes meaningless. The coefficients of λ^n are

* See, for instance, Churchill, *Math. Annalen*, cxv. p. 726 (1938).

† The above formula for V_1 agrees with Mr. Tranter's; but his series is written in terms of the function Θ in such a manner that the convergence is slower. The formula for V_2 above does not agree with his formula.

bounded ; in fact, their values always lie between zero and 2. Since the series $\sum \lambda^n$ converges it follows from a theorem due to Abel * that our series converges uniformly with respect to x , ($0 \leq x \leq a$) for each $t > 0$ and with respect to $t \geq 0$ for each x , ($0 \leq x < a$). The convergence is also uniform with respect to x and t together for $t \geq t_0 > 0$. Since the terms are continuous the series converges to a continuous function of x and t in the intervals indicated. The same argument applies to the series in (14), for $x \geq a$. Hence the functions defined by (13) and (14) satisfy the conditions

$$V_1(x, +0) = V_1(x, 0) = A, \quad (0 \leq x < a),$$

$$V_2(x, +0) = V_2(x, 0) = 0, \quad (x > a).$$

That is, they satisfy the initial conditions (2).

For all x and t , it is clear that $0 \leq P \leq 1$; also the series $\sum |\lambda|^n$ converges. Hence V_1 and V_2 are uniformly bounded for all $t \geq 0$ and $x \geq 0$, so the second of conditions (4) is satisfied.

Writing $P(n)$ for $P[2na/\sqrt{4k_1t}]$ we also have from (13) and (14), for $t > 0$,

$$\begin{aligned} V_1(a-0, t) - V_2(a+0, t) &= V_1(a, t) - V_2(a, t) \\ &= A \left[1 - \sum_0^{\infty} \lambda^n P(n) + \lambda \sum_0^{\infty} \lambda^n P(n+1) \right] \\ &= A \left[- \sum_1^{\infty} \lambda^n P(n) + \lambda \sum_0^{\infty} \lambda^n P(n+1) \right] = 0. \end{aligned}$$

So the first of conditions (3) is satisfied by our functions.

The arguments of each of the P functions in our series are of one of the types $(c \pm x)/\sqrt{4k_i t}$ where c is an increasing function of n . It is easily verified that the function P with these arguments satisfies the corresponding heat equation (1). Furthermore, the function

$$\frac{\partial}{\partial t} P \left[\frac{c \pm x}{2\sqrt{k_i t}} \right] = \frac{2}{\sqrt{\pi}} \frac{c \pm x}{4\sqrt{k_i t^3}} \exp \left[- \frac{(c \pm x)^2}{4k_i t} \right] \quad \dots \quad (15)$$

is monotone decreasing in n for each fixed x and t confined to any finite closed intervals with $t > 0$, for all $n > n_0$ where n_0 may depend upon the intervals. This function is also uniformly bounded in those intervals. Likewise for the derivatives with respect to x . According to Abel's theorem then the series obtained by differentiating our series termwise, once with respect to t , or once or twice with respect to x , converge uniformly and so termwise differentiation is permissible for each $t > 0$. Since the terms satisfy the heat equation (1) our functions satisfy (1).

* See, for instance, Carslaw, 'Fourier Series and Integrals,' 1930, p. 149.

Moreover, their derivatives are continuous functions of x and t for $t > 0$, and so

$$K_1 \frac{\partial}{\partial x} V_1(a-0, t) - K_2 \frac{\partial}{\partial x} V_2(a+0, t) = \frac{A}{4\sqrt{t}} \left[\frac{K_1}{\sqrt{k_1}} (1-\lambda) - \frac{K_2}{\sqrt{k_2}} (1+\lambda) \right] \\ \times \sum_0^{\infty} \lambda^n \left\{ -\exp \left[-\frac{n^2 a^2}{k_1 t} \right] + \exp \left[-\frac{(n+1)^2 a^2}{k_1 t} \right] \right\}.$$

The factor in the brackets vanishes according to the definition of λ , so the second of conditions (3) is satisfied.

The satisfaction of the first of conditions (4) is also evident now, so our functions (13) and (14) are completely established as a solution of the problem (1)–(4).

4. The Complete Boundary Problem. Uniqueness of the Solution.

The conditions (1)–(4) are not sufficient to insure just one solution. Let the functions $V_i(x, t)$ be required to satisfy these additional conditions:—

(a) they are continuous in x and t , together with their first derivatives with respect to these variables, for each $t > 0$, ($0 < x < a$, when $i=1$; $x > a$, when $i=2$);

(b) they are uniformly bounded for all x and $t > 0$, while $\partial V_i / \partial x$ and $\partial V_i / \partial t$ are uniformly bounded for all $t \geq 0$ and all x in each finite closed interval not containing $x=a$;

$$(c) \quad \lim_{t_0 \rightarrow 0} \int_0^{t_0} \left| \frac{\partial V_i}{\partial x} \right| dt = 0,$$

uniformly for all x in a neighbourhood of $x=a$.

Physically the chief purpose of these conditions is to prevent the presence of instantaneous sources of heat.

Suppose there are two solutions of the problem (1)–(4) satisfying the conditions (a)–(c). Their difference $W_i(x, t)$ will satisfy (1), (3) and (4) and, in place of (2), the condition

$$W_i(x, +0) = 0, \quad (i=1, 2).$$

Of course W_i will satisfy the conditions (a)–(c), and so $L\{W_i\}$ converges for each $s > 0$ and the transform $w_i(x, s)$ is continuous in x and bounded for all x . The integral $L\{\partial W_i / \partial x\}$ converges uniformly in x since

$$\left| L \left\{ \frac{\partial W_i}{\partial x} \right\} \right| < \int_0^{t_0} \left| \frac{\partial W_i}{\partial x} \right| dt + \int_{t_0}^{\infty} \left| e^{-st} \frac{\partial W_i}{\partial x} \right| dt,$$

and the first integral on the right approaches zero as $t_0 \rightarrow 0$, uniformly for all x in each finite interval. Therefore

$$L\left\{\frac{\partial W_i}{\partial x}\right\} = \frac{d}{dx} L\{W_i\} = \frac{d}{dx} w_i(x, s),$$

and this is a continuous function of x .

Also $\partial W_i / \partial t$ is continuous in t for each $t > 0$ and bounded for $t \geq 0$ when $x \neq a$, so it has a transform for $s > 0$, and since $W_i(x, +0) = 0$ it is known* that

$$L\left\{\frac{\partial W_i}{\partial t}\right\} = s w_i(x, s), \quad (x \neq a, s > 0).$$

Since W_i satisfies the heat equation its second derivative with respect to x satisfies the conditions imposed upon $\partial W_i / \partial t$, and it follows that

$$L\left\{\frac{\partial^2 W_i}{\partial x^2}\right\} = \frac{d^2 w_i}{dx^2}, \quad (x \neq a).$$

So when L is applied to the members of (1), (3), and (4) with V_i replaced by W_i it follows that $w_i(x, s)$ must satisfy the conditions

$$s w_i = k_i \frac{d^2 w_i}{dx^2}, \quad (16)$$

$$w_i(a, s) = w_2(a, s); \quad K_1 \frac{d}{dx} w_1(a, s) = K_2 \frac{d}{dx} w_2(a, s). \quad . . . (17)$$

$$\frac{d}{dx} w_1(0, s) = 0, \quad |w_2(x, s)| < M', \quad (18)$$

for each $s > 0$, where M' is a constant and w_i and dw_i/dx are continuous in x .

But for $s > 0$ the homogeneous problem (16)–(18) in ordinary differential equations is easily seen to have as its only solution

$$w_i(x, s) \equiv 0;$$

that is, the transform of W_i vanishes. Now W_i is continuous in t and, according to Lerch's theorem†, there is just one continuous function whose transform is zero for all $s > 0$. Since

$$W_i(x, t) \equiv 0$$

is such a function, the difference of the two solutions vanishes for all x and t .

Thus we have shown that not more than one solution can exist.

* Doetsch, 'Theorie u. Anwendung der Laplace-Transformation,' p. 152.

† Doetsch, *l. c.* p. 35.

We saw in Section 3 that our functions (13) and (14) satisfy the conditions (a) and the first of conditions (b). Setting

$$y = \frac{c \pm x}{2\sqrt{k_1 t}}$$

it follows from (15) that

$$\frac{\partial}{\partial t} P(y) = -\frac{4k_1}{\sqrt{\pi}(c \pm x)^2} y^3 e^{-y^2} \leq \frac{4Nk_1}{\sqrt{\pi}} y^3 e^{-y^2},$$

where N is the maximum value of $(c \pm x)^{-2}$ for all x in any closed interval not containing $x=a$. In such an interval $(c \pm x)$ has a positive lower bound for all n . Since $y^3 e^{-y^2}$ is bounded for all y , the first derivative with respect to t of all the P functions in our series are bounded uniformly in n , x , and t for $t \geq 0$ and x in any closed interval not containing $x=a$. From the convergence of $\sum |\lambda|^n$ we therefore conclude that $\partial V_i / \partial t$ is bounded. Likewise for $\partial V_i / \partial x$. Hence our functions satisfy the remaining conditions in (b).

For each $t > 0$, according to (13),

$$\frac{\partial V_1}{\partial x} = -\frac{A(1-\lambda)}{2\sqrt{\pi k_1}} \frac{1}{\sqrt{t}} \sum_0^\infty \lambda^n \{e^{-x_n^2} - e^{-a^2}\}, \quad \dots \quad (19)$$

where

$$p_n = \frac{(2n+1)a-x}{2\sqrt{k_1 t}}, \quad q_n = \frac{(2n+1)a+x}{2\sqrt{k_1 t}}.$$

Similarly for $\partial V_2 / \partial x$, so for all x and all $t > 0$,

$$\left| \frac{\partial V_i}{\partial x} \right| < \frac{N'}{\sqrt{t}},$$

where N' is a constant independent of x and t . It follows at once that condition (c) is satisfied, and so we have established the

THEOREM.—*The boundary problem consisting of the conditions (1)–(4) and (a)–(c) has one and only one solution; this solution is given by the formulæ (13) and (14).*

When $x=a$, $p_0=0$ in (19) so, separating the first term there,

$$\frac{\partial}{\partial x} V_1(a, t) = -\frac{A(1-\lambda)}{2\sqrt{\pi k_1}} \frac{1}{\sqrt{t}} + T_1(a, t),$$

where the function $T_1(a, t)$ approaches zero as $t \rightarrow 0$. Thus the flux of heat across the surface of separation is infinite at $t=0$ and of order $t^{-1/2}$. This same behaviour at a point of discontinuity of the initial temperature has been noted in a problem of quite general character*.

University of Michigan,
Ann Arbor.

* Churchill, "On the Problem of Temperatures in a Non-homogeneous Bar with Discontinuous Initial Temperatures," *Am. J. Math.* lxi. pp. 651–664 (1939).

IX. *Notices respecting New Books.*

Static and Dynamic Electricity. By WILLIAM R. SMYTHE. [Pp. xviii+560.]
(London: McGraw-Hill, 1939. Price 40s.)

ALTHOUGH it is stated that "this book is written for the experimental research physicist and engineer rather than for the theoretical man," it is essentially a treatise on the mathematical theory of electricity and magnetism, based on the macroscopic experimental facts. It is a book dealing with the same general field as that of Jeans, and at a similar level. A more extensive treatment is, however, given of many topics, and full use is made of vector methods, familiarity with which is assumed.

The first five of the fifteen chapters deal with electrostatics. The mathematical technique of potential theory, as applied to two- and three-dimensional distributions, is fully developed, and a large number of standard problems are worked out. Special attention is devoted to Bessel function methods. Under electric current, the mathematical treatment of general networks and of three-dimensional current flow is considered. Magnetic interaction of currents and electromagnetic induction are then taken up. Magnetic vector potential is introduced as early as possible and used extensively, a procedure which has many advantages. A short chapter deals with transient phenomena in networks, after which consideration is given to alternating currents—there are very useful sections on filter circuits—and eddy currents. The chapter on magnetism seems somewhat academic, largely because the idealized problems to which the elegant mathematical technique can be applied are so remote from the problems occurring in practice. By contrast, in the treatment of electromagnetic waves, the classical mathematical theory is at its happiest. The motion of charged particles is treated on the basis of special relativity theory, and the now unnecessary confusions and contradictions are entirely avoided. A final chapter, on the static electrical properties of matter, gives a brief survey of the modern atomic theory. This chapter is hardly necessary, as many such accounts are available, and a treatment on the same level as that of the classical macroscopic theory would have required another volume.

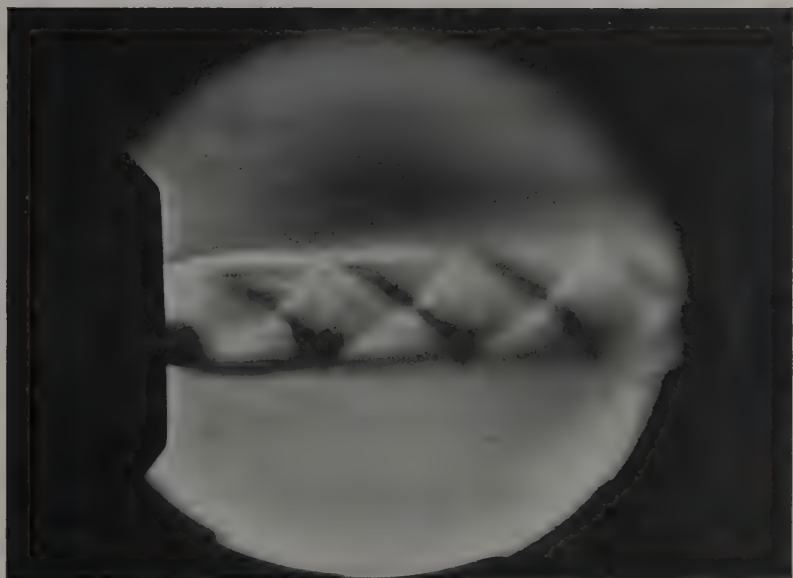
At the end of each chapter there are a number of problems, making a valuable collection of over five hundred, all of which, the author states, the best students can work, though the average student cannot.

Any "theoretical man" who is really familiar with the range of theory developed in this book is well worthy of the title. That the author deems it adapted to the needs of the engineer is perhaps evidence of the high level of mathematical attainment in the New World. More probably he is under-rating his own performance. He has produced a most detailed, comprehensive, and well-proportioned treatise on the mathematical theory of electricity and magnetism, and it will at once take a high place in the literature on that theme.

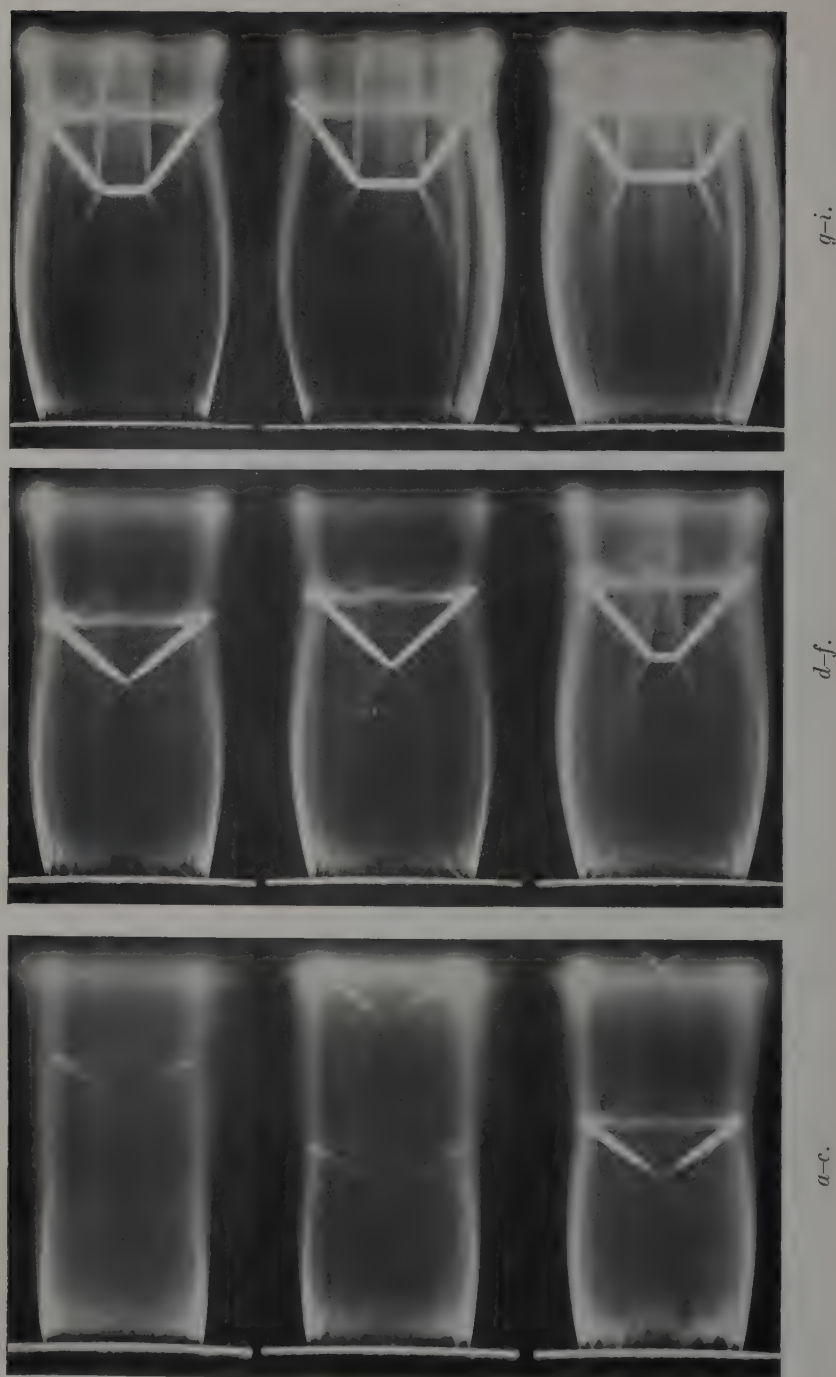
E. C. S.

[*The Editors do not hold themselves responsible for the views
expressed by their correspondents.*]

FIG. 1.

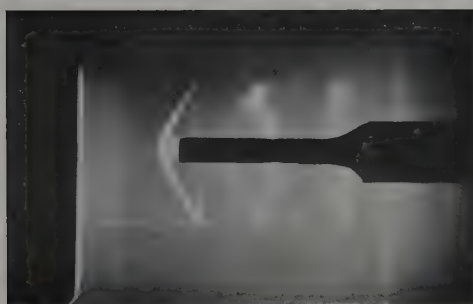


Photograph of an air-jet with a velocity
exceeding that of sound.

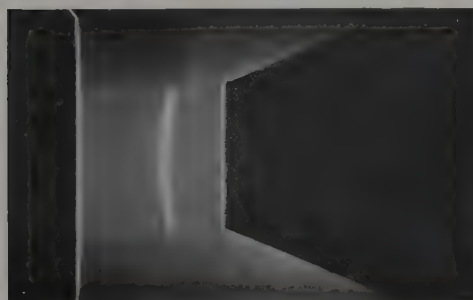
FIGS. 3 *a-i*.

Photographs of an air-jet of 6 mm. diameter with a velocity exceeding that of sound at various values of the absolute pressure p_0 in the container. Values of p_0 : *a*, 3.03; *b*, 3.53; *c*, 4.03; *d*, 4.53; *e*, 5.03; *f*, 5.53; *g*, 6.03; *h*, 6.53; *i*, 7.03 kg./cm.².

FIGS. 6 *a* & 6 *b*.

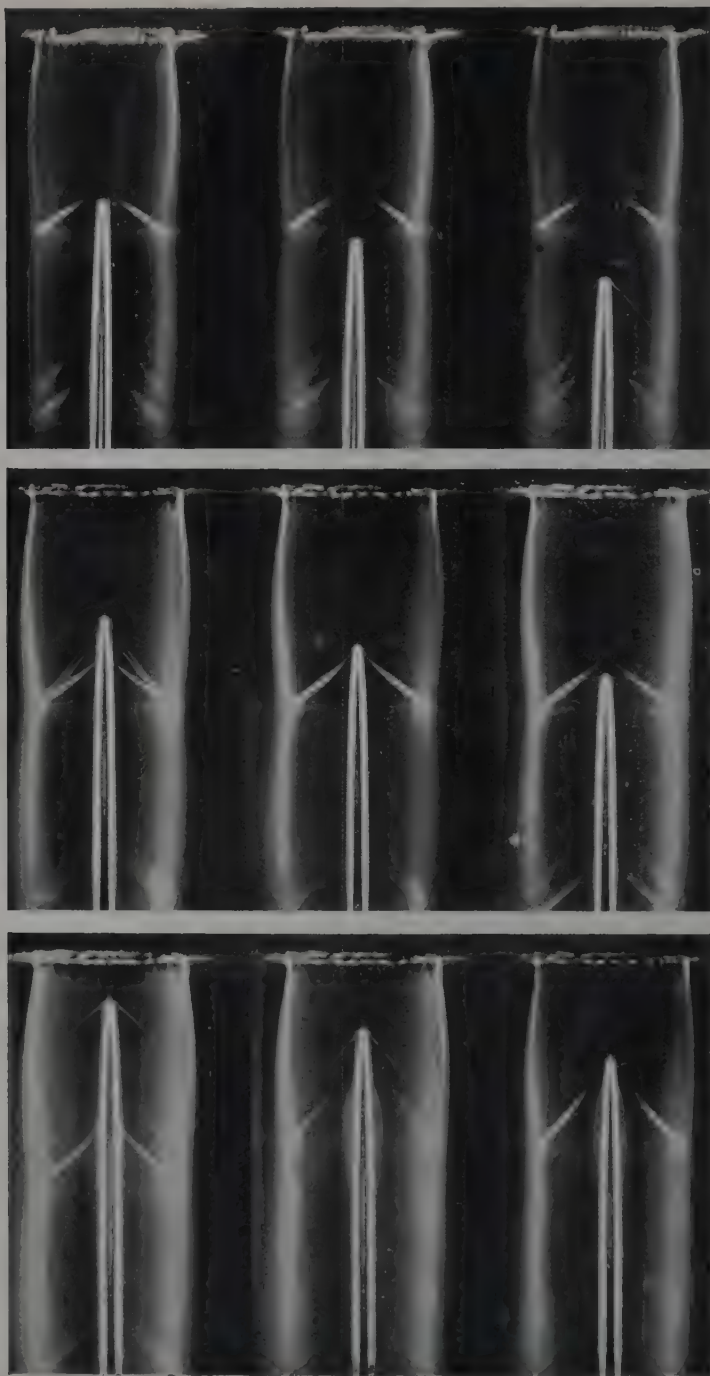


a

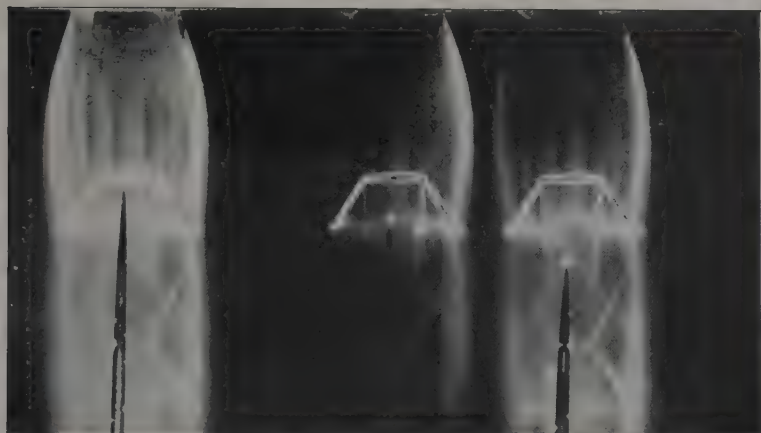
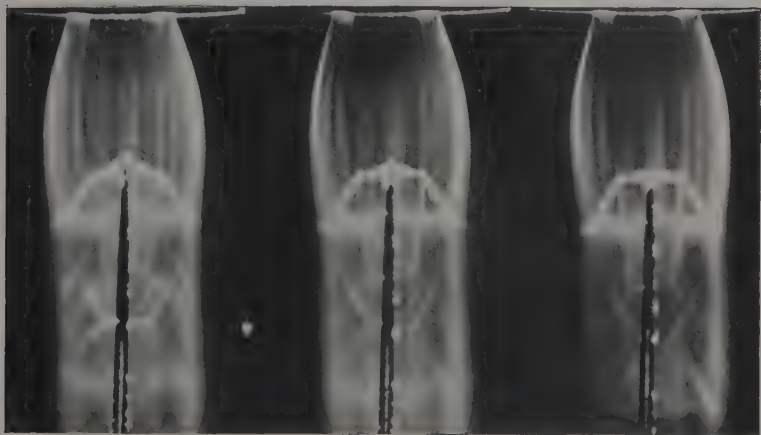


b

Stationary waves in front of a narrow sound and
a plane surface of larger extension.

FIGS. 14 *a*-14 *i*.

Photos used in the determination of the velocity-ratio $\frac{u_1}{c_1}$ from the Mach-angle, $p_0=3.5$ kg./cm.² abs., $d_0=6$ mm.

*g-i.**d-f.**a-c.*

Photos of 4 mm. air-jet at an absolute pressure 7 kg./cm.² with needle in various positions relatively to the Riemann wave.

X. *The Wind Tunnel with Open Working-Section.*

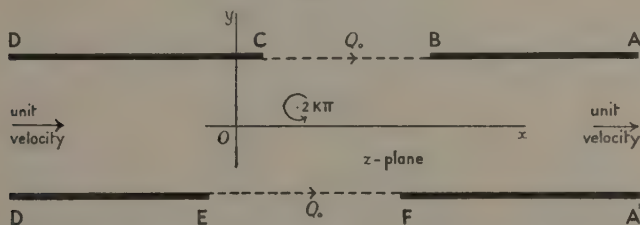
By N. SIMMONS, M.Sc., Ph.D., King's College, London *.

[Received August 14, 1939.]

1. *Introduction.*

THE solution of the problem of a weak vortex in a two-dimensional jet issuing from a channel has been taken as a basis in calculating corrections for an aerofoil placed in a wind tunnel stream ⁽³⁾. The physical reality of a tunnel with open working-section, is, however, more closely approached if we take as our starting-point a stream which, after having left the

Fig. 1.



channel and met the vortex, passes into a collecting channel of similar form. It is the purpose of the present enquiry to discover whether the introduction of such a collector leads to any modifications of the formulae given in ⁽³⁾, and, if so, to determine them.

The hydrodynamical problem is treated first, in §§2-6, the assumption, valid in the practical application, that the vortex is weak, being introduced at the outset in order to render the analysis tractable. The aerodynamical sequel is considered, and the results discussed in § 7.

2. *Preliminaries.*

Fluid issues as a two-dimensional jet from the channel CDD'E, and is collected in the channel BAA'F, CB and EF being free stream-lines (fig. 1): the points A, D, D', A' are all at infinity. The channels are taken to be of equal width. It is assumed that there is no entrainment or loss of working fluid, so that the whole of the issuing fluid passes into

* Communicated by R. C. Knight, M.Sc., Ph.D.

the right-hand channel, and only fluid which has come from the left-hand channel is collected. This requires the collector to be inclined to the first channel at a small angle. Then the velocity at A is the same as that at D. There is a bound vortex in the stream as shown. At the outset, it will be necessary to allow for overlap of the walls of each channel, although ultimately the solution will be obtained for the case of zero overlap.

For convenience, we take the width of the channels as π units, and the velocity of the stream at D or A as unit velocity. This is tantamount to choosing special units of length and time, and so causes no real loss of generality. Take $2d_1$, $2d_2$ as the overlaps of the left- and right-hand channels respectively, and $2l$ as the mean gap $\frac{1}{2}(CB+EF)$. Let the strength of the vortex be $2\kappa\pi$, and the free stream-line velocity Q_0 .

Take for origin O the midpoint of CE, with Ox in the direction of the general stream, and Oy perpendicular. Let z denote the complex variable in this plane. C, E are the points $\pm(d_1 + \frac{1}{2}i\pi)$; B, F are the points $2l \pm (d_2 + \frac{1}{2}i\pi)$. The collector is inclined at angle δ to Ox .

Let Q denote the magnitude of the fluid velocity at any point, and α its inclination to Ox . Let w represent the complex potential, on that convention in which

$$Qe^{-i\alpha} = \frac{dw}{dz} = U - iV. \quad (2.1)$$

Clearly a first approximation to the solution (*i. e.*, when $\kappa=0$) is given by $w=z$, $dw/dz=1$, with the velocities at the vortex $U_1=1$, $V_1=0$. We require a second approximation when κ is small (*i. e.*, including terms of order κ).

First we seek a conformal transformation $u=u(z)$ which shall represent the area of motion in the z -plane on the upper half u -plane, the boundary ABCDD'EFA' transforming into the real axis. In the u -plane B, C, E, F will occur on the real axis in that order. Thus the pairs of points C, E and B, F do not interlace, and so possess real common harmonic conjugates. Choosing the transformation so that the exterior common harmonic conjugate is at infinity and the points C, E are ∓ 1 respectively, the points B, F are seen to be $\mp 1/k$, where $0 < k < 1$. In this transformation, let $u=\gamma_1$, γ_2 denote respectively the points D (D') and A (A'). Let u_1 denote the vortex point.

Following the method of ⁽²⁾, consideration of the motion in the u -plane shows that

$$\begin{aligned} \frac{dw}{du} &= \frac{1}{u-\gamma_1} - \frac{1}{u-\gamma_2} - i\kappa \left[\frac{1}{u-u_1} - \frac{1}{u-\bar{u}_1} \right] \\ &= \frac{\text{quadratic}}{(u-\gamma_1)(u-\gamma_2)(u-u_1)(u-\bar{u}_1)}. \quad (2.2) \end{aligned}$$

The quadratic has real coefficients, and so its zeros are either conjugate complex numbers, or both real, the motion being of the first or second type accordingly. A zero corresponds to a stagnation point if it falls in the upper half-plane. Now the vortex, being weak, must have its stagnation point(s) close to it, so that, for a motion of the second type, the vortex must be very near a boundary. This case we shall exclude. The motion will then be of the first type, the zeros of the quadratic being, say, u_1' , \bar{u}_1' , the first lying in the upper half-plane. The motion has one stagnation point, represented by u_1' . Then

$$\frac{dw}{du} = \frac{\beta(u-u_1')(u-\bar{u}_1')}{(u-\gamma_1)(u-\gamma_2)(u-u_1)(u-\bar{u}_1)}, \quad \dots \quad (2.3)$$

where
and is real.

$$\beta = \gamma_1 - \gamma_2 - i\kappa(u_1 - \bar{u}_1),$$

3. Development of the Method.

Next we define the function Ω by the relation

$$\Omega = -\log \frac{dw}{dz} = -\log Q + i\alpha, \quad \dots \quad (3.1)$$

and by considering, as in ⁽²⁾, the conditions which this function must satisfy, find that

$$\frac{d\Omega}{du} = \frac{1}{\sqrt{\{(1-k^2u^2)(1-u^2)\}}} \left[\frac{\sqrt{\{(1-k^2u_1^2)(1-u_1^2)\}}}{u-u_1} + \frac{\sqrt{\{(1-k^2\bar{u}_1^2)(1-\bar{u}_1^2)\}}}{u-\bar{u}_1} \right. \\ \left. - \frac{\sqrt{\{(1-k^2u_1'^2)(1-u_1'^2)\}}}{u-u_1'} - \frac{\sqrt{\{(1-k^2\bar{u}_1'^2)(1-\bar{u}_1'^2)\}}}{u-\bar{u}_1'} + A_1 \right], \quad (3.2)$$

where A_1 is constant. Now by the Schwarz-Christoffel theorem, the upper half u -plane can be represented on a rectangle in the v -plane by means of the relation

$$v = \int_0^u \frac{du}{\sqrt{\{(1-k^2u^2)(1-u^2)\}}}, \quad \dots \quad (3.3)$$

$$u = \operatorname{sn} v.$$

that is

The points C, E, F, B transform into the vertices of the rectangle, and correspond to $u = -K, K, K+iK', -K+iK'$ respectively (fig. 2). Equation (3.2) now becomes

$$\frac{d\Omega}{dv} = \frac{\operatorname{cn} v_1 \operatorname{dn} v_1}{\operatorname{sn} v - \operatorname{sn} v_1} + \frac{\operatorname{cn} \bar{v}_1 \operatorname{dn} \bar{v}_1}{\operatorname{sn} v - \operatorname{sn} \bar{v}_1} - \frac{\operatorname{cn} v_1' \operatorname{dn} v_1'}{\operatorname{sn} v - \operatorname{sn} v_1'} - \frac{\operatorname{cn} \bar{v}_1' \operatorname{dn} \bar{v}_1'}{\operatorname{sn} v - \operatorname{sn} \bar{v}_1'} + A_1. \quad (3.4)$$

At this stage we restrict consideration to the case for which γ_1 is small, so that $\gamma_1 = O(\kappa)$, and γ_2 is large, so that $\gamma_2^{-1} = O(\kappa)$, in order to obtain

non-overlapping boundaries *. From (2.2) and (2.3) we can now deduce that

$$\frac{\beta}{\gamma_2} = -1 + O(\kappa^2), \quad . \quad . \quad . \quad . \quad . \quad (3.5)$$

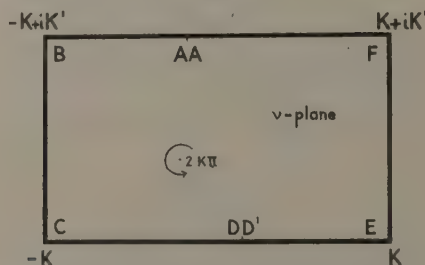
and $u_1' - u_1 = i\kappa u_1$ to a first approximation. The latter easily leads to

$$v_1' - v_1 = \frac{i\kappa \operatorname{sn} v_1}{\operatorname{cn} v_1 \operatorname{dn} v_1} \cdot . \quad . \quad . \quad . \quad . \quad (3.6)$$

Introducing the contracted notation s for $\operatorname{sn} v$, c for $\operatorname{cn} v$, d for $\operatorname{dn} v$, etc., we have, provided that v is not near v_1 ,

$$\frac{1}{v_1 - v_1'} \left[\frac{c_1 d_1}{s - s_1} - \frac{c_1' d_1'}{s - s_1'} \right] = \frac{\partial}{\partial v_1} \left[\frac{c_1 d_1}{s - s_1} \right],$$

Fig. 2.



to a sufficient order of accuracy. A little reduction leads to the form

$$\frac{1}{v_1 - v_1'} \left[\frac{c_1 d_1}{s - s_1} - \frac{c_1' d_1'}{s - s_1'} \right] = d_1^2 - d^2 - \frac{d}{dv} \left[\frac{cd}{s - s_1} \right],$$

so that

$$\frac{c_1 d_1}{s - s_1} - \frac{c_1' d_1'}{s - s_1'} = \frac{i\kappa s_1}{c_1 d_1} \left[\frac{d}{dv} \left\{ Z(v) + \frac{cd}{s - s_1} \right\} + \left(\frac{E}{K} - d_1^2 \right) \right], \quad . \quad (3.7)$$

making use of Jacobi's Z -function. Substituting this and the conjugate equation in (3.4) we have the integrable form

$$\frac{d\Omega}{dv} = \frac{i\kappa s_1}{c_1 d_1} \frac{d}{dv} \left\{ Z(v) + \frac{cd}{s - s_1} \right\} - \frac{i\kappa \bar{s}_1}{\bar{c}_1 \bar{d}_1} \frac{d}{dv} \left\{ Z(v) + \frac{cd}{s - \bar{s}_1} \right\} + A_2, \quad . \quad (3.8)$$

where A_2 is constant. Integrating this, and determining the constants by reference to the vertices of the rectangle, we obtain

$$\Omega = \frac{i\kappa s_1}{c_1 d_1} \left\{ Z(v) + \frac{cd}{s - s_1} \right\} - \frac{i\kappa \bar{s}_1}{\bar{c}_1 \bar{d}_1} \left\{ Z(v) + \frac{cd}{s - \bar{s}_1} \right\} - \log Q_0. \quad . \quad (3.9)$$

* Cf. (3) § 4.

Again, referring to D, where $\Omega=0$ and $v=O(\kappa)$ and to F, we find that

$$Q_0 = \exp\left(-\frac{i\kappa}{c_1 d_1} + \frac{i\kappa}{\bar{c}_1 \bar{d}_1}\right) = 1 - \frac{i\kappa}{c_1 d_1} + \frac{i\kappa}{\bar{c}_1 \bar{d}_1} \dots \quad (3.10)$$

$$\delta = \frac{\kappa\pi}{K} \mathbf{I} \left\{ \frac{s_1}{c_1 d_1} \right\}.$$

Now writing for convenience

$$f(v) \equiv Z(v) + \frac{cd - c_1 d_1}{s - s_1} + \frac{1}{s_1}, \quad g(v) \equiv Z(v) + \frac{cd - \bar{c}_1 \bar{d}_1}{s - \bar{s}_1} + \frac{1}{\bar{s}_1}, \quad (3.11)$$

both of which functions are regular throughout the interior of the rectangle in the v -plane, we have

$$\Omega = \frac{i\kappa s_1}{c_1 d_1} \left[f(v) + \frac{c_1 d_1}{s - s_1} \right] - \frac{i\kappa \bar{s}_1}{\bar{c}_1 \bar{d}_1} \left[g(v) + \frac{\bar{c}_1 \bar{d}_1}{s - \bar{s}_1} \right], \quad (3.12)$$

and

$$\frac{dz}{dw} = 1 + \frac{i\kappa s_1}{c_1 d_1} \left[f(v) + \frac{c_1 d_1}{s - s_1} \right] - \frac{i\kappa \bar{s}_1}{\bar{c}_1 \bar{d}_1} \left[g(v) + \frac{\bar{c}_1 \bar{d}_1}{s - \bar{s}_1} \right].$$

Also, approximation to (2.3) with the aid of (3.5) yields the result

$$\frac{dw}{dv} = \frac{cd}{s} \left[1 + \frac{\gamma_1}{s} + \frac{s}{\gamma_2} - \frac{i\kappa s_1}{s - s_1} + \frac{i\kappa \bar{s}_1}{s - \bar{s}_1} \right]. \quad (3.13)$$

Hence, by multiplication of (3.12) and (3.13),

$$\frac{dz}{dv} = \frac{cd}{s} \left[1 + \frac{\gamma_1}{s} + \frac{s}{\gamma_2} + \frac{i\kappa s_1}{c_1 d_1} f(v) - \frac{i\kappa \bar{s}_1}{\bar{c}_1 \bar{d}_1} g(v) \right], \quad (3.14)$$

providing the relation between z and v . This equation has been established on the supposition that v does not lie in the neighbourhood of v_1 . The condition may now, however, be relaxed since all the functions appearing in (3.14) are regular at v_1 , and so may be analytically continued into its neighbourhood. The equation holds therefore throughout the interior of the rectangle. The condition can also be relaxed for (3.12) and (3.13).

Now putting

$$I_1 = \frac{is_1}{2c_1 d_1} \int_K^{-K} f(v) \frac{cd}{s} dv, \quad I_2 = \frac{i\bar{s}_1}{2\bar{c}_1 \bar{d}_1} \int_K^{-K} g(v) \frac{cd}{s} dv, \quad (3.15)$$

and integrating (3.14) between E and C, we deduce that

$$d_1 = \gamma_1 - \gamma_2^{-1} + \kappa(I_1 - I_2). \quad (3.16)$$

Similarly, putting

$$I_3 = \frac{is_1}{2c_1 d_1} \int_{K+iK'}^{-K+iK'} f(v) \frac{cd}{s} dv, \quad I_4 = \frac{i\bar{s}_1}{2\bar{c}_1 \bar{d}_1} \int_{K+iK'}^{-K+iK'} g(v) \frac{cd}{s} dv, \quad (3.17)$$

we deduce that

$$d_2 = \kappa \gamma_1 - (\kappa \gamma_2)^{-1} + \kappa(I_3 - I_4). \quad (3.18)$$

It follows that the restrictions imposed above on the magnitudes of γ_1 and γ_2 do lead to values of d_1, d_2 which are of order κ . And, by choosing

$$\gamma_1 = \frac{\kappa}{k'^2} [(I_2 - I_1) - k(I_4 - I_3)], \quad \gamma_2^{-1} = \frac{\kappa}{k'^2} [k^2(I_2 - I_1) - k(I_4 - I_3)], \quad (3.19)$$

where, as usual, $k'^2 = 1 - k^2$, we obtain the practically important case $d_1 = d_2 = 0$, i. e., non-overlapping channels. The points C, E are now $\pm \frac{1}{2}i\pi$, and the points B, F are $2l \pm \frac{1}{2}i\pi$.

Further, integrating (3.14) and keeping only the first approximation, we have

$$z + \frac{1}{2}i\pi = \log u = \log \operatorname{sn} v, \quad (3.20)$$

where the logarithm takes its principal value, and the constant of integration has been determined from E. Alternatively, the required relation between u and z , has the form

$$u = ie^z. \quad (3.21)$$

Substitution for the point F in this yields

$$k = e^{-2l}, \quad (3.22)$$

showing that a close relation exists between the width of the gap and the modulus of the elliptic functions.

4. Determination of Constants associated with the Vortex.

The position of the vortex is obtainable immediately, for we have, substituting in (3.20) and (3.21),

$$z_1 + \frac{1}{2}i\pi = \log u_1, \quad u_1 = ie^{z_1}. \quad (4.1)$$

Further, if w_∞ denote the potential due to the vortex in infinite fluid, and w_c the complementary potential $w - w_\infty$, the velocities U_1, V_1 , of the fluid relative to the vortex, and the radius of curvature R_1 , of the stream at the vortex are given by

$$U_1 - iV_1 = Q_1 e^{-iz_1} = \left(\frac{dw_c}{dz} \right)_1, \quad (4.2)$$

$$\frac{1}{R_1} = -\frac{1}{Q_1} \mathbf{I} \left\{ e^{2iz} \frac{d^2 w_c}{dz^2} \right\}_1.$$

But $w_\infty = -i\kappa \log(z - z_1)$, and development in the neighbourhood of the vortex shows that, neglecting terms of order κ^2 ,

$$\frac{dw_\infty}{dz} = -i\kappa \left[\frac{s_1}{s - s_1} + \frac{1}{2} - \frac{1}{12} \frac{s - s_1}{s_1} + \dots \text{higher powers of } \frac{s - s_1}{s_1} \right], \quad (4.3)$$

which, with (3.12), leads to

$$\frac{dw_c}{dz} = 1 - \frac{i\kappa s_1}{c_1 d_1} f(v) + \frac{i\kappa \bar{s}_1}{\bar{c}_1 \bar{d}_1} g(v) + i\kappa \left[\frac{\bar{s}_1}{s - \bar{s}_1} + \frac{1}{2} - \frac{1}{12} \frac{s - s_1}{s_1} \right] + \dots \quad (4.4)$$

We deduce that

$$U_1 - iV_1 = 1 - \frac{i\kappa s_1}{c_1 d_1} f(v_1) + \frac{i\kappa \bar{s}_1}{\bar{c}_1 \bar{d}_1} g(v_1) + \frac{i\kappa(s_1 + \bar{s}_1)}{2(s_1 - \bar{s}_1)}, \quad (4.5)$$

and

$$\frac{1}{R_1} = \kappa \left[\frac{1}{12} + \frac{s_1 \bar{s}_1}{(s_1 - \bar{s}_1)^2} + \mathbf{R} \left\{ \frac{s_1^2}{c_1^2 d_1^2} f'(v_1) \right\} - \left| \frac{s_1^2}{c_1^2 d_1^2} \right| \mathbf{R} \{g'(v_1)\} \right].$$

In using these formulae we require the following expressions, the values of which follow after a little reduction :

$$f(v_1) = Z(v_1) - \frac{s_1}{c_1 d_1} (d_1^2 + k^2 c_1^2) + \frac{1}{s_1}, \quad (4.6)$$

$$g(v_1) = Z(v_1) + \frac{c_1 d_1 - \bar{c}_1 \bar{d}_1}{s_1 - \bar{s}_1} + \frac{1}{\bar{s}_1},$$

$$\mathbf{R} \left\{ \frac{s_1^2}{c_1^2 d_1^2} f'(v_1) \right\} = \left(\frac{k'^2}{2} - \frac{E}{K} \right) \mathbf{R} \left\{ \frac{s_1^2}{c_1^2 d_1^2} \right\} - \frac{k'^4}{2} \mathbf{R} \left\{ \frac{s_1^4}{c_1^4 d_1^4} \right\},$$

$$\mathbf{R} \{g'(v_1)\} = \left(\frac{k'^2}{2} - \frac{E}{K} \right) + \frac{k^2}{2} (s_1 + \bar{s}_1)^2 - \frac{1}{2} \left(\frac{c_1 d_1 - \bar{c}_1 \bar{d}_1}{s_1 - \bar{s}_1} \right)^2.$$

It will be convenient to put

$$U_1 = 1 + \Delta U, \quad V_1 = \Delta V. \quad (4.7)$$

Then ΔU , ΔV are both of order κ .

Again, if we imagine the vortex replaced by a small two-dimensional body, *e. g.*, an aerofoil, round which the circulation is $2\kappa\pi$, there will be a force on the body, say of magnitude F_1 at angle β_1 to *Ox*. This is given by the Kutta-Joukowski law

$$F_1 e^{i\beta_1} = -i2\kappa\pi Q_1 e^{i\alpha_1} = -2\kappa\pi(i - \Delta V), \quad (4.8)$$

so that

$$F_1 = -2\kappa\pi, \quad \beta_1 = \frac{1}{2}\pi + \Delta V, \quad (4.9)$$

if the unit of density is taken to be that of the fluid. We note that the lift force is of order κ , and the drag force of order κ^2 .

In any practical case, the given quantities are l , x_1 , y_1 , κ , and it is necessary to express ΔU , ΔV , R_1 , F_1 , β_1 in terms of these. To assist in the transformation, we have the equation (3.22) and

$$s_1 = ie^{2s_1}, \quad c_1^2 = 1 + e^{2s_1}, \quad d_1^2 = 1 + e^{2s_1 - 4i}. \quad (4.10)$$

Using these, it is possible to reduce the above expressions to the desired form, but in the general case, the results are too complicated to be of

practical value. We therefore confine our attention to the three most important special cases, namely,

- (i.) when the vortex lies on the horizontal axis ($y_1=0$);
- (ii.) when the vortex lies on the vertical axis ($x_1=l$);
- (iii.) when the vortex lies in the central position ($x_1=l, y_1=0$).

It is easily verified that in all these cases, ic_1d_1/s_1 is real. Further, the real part of icd/s is positive throughout the rectangle in the v -plane. Hence we may put

$$\frac{ic_1d_1e^l}{2s_1} = \sigma, \quad (4.11)$$

where σ is real and positive. It follows that

$$\sigma = \sqrt{\cosh z_1 \cosh (2l - z_1)} = \sqrt{\frac{1}{2} \cosh 2l + \frac{1}{2} \cosh 2(l - z_1)}, \quad . (4.12)$$

and

$$c_1d_1 = 2\sigma e^{x_1-l}, \quad (4.13)$$

while (4.5) and (4.6) take the simpler forms

$$\left. \begin{aligned} \Delta U - i \Delta V &= \frac{\kappa e^l}{2\sigma} \{f(v_1) + g(v_1)\} - \frac{\kappa}{2} \tan y_1, \\ \frac{1}{R_1} &= \kappa \left[\frac{1}{12} - \frac{1}{4} \sec^2 y_1 + \mathbf{R} \left\{ \frac{s_1^2}{c_1^2 d_1^2} f'(v_1) \right\} - \frac{e^{2l}}{4\sigma^2} \mathbf{R} \{g'(v_1)\} \right], \\ f(v_1) &= Z(v_1) - \frac{ie^{-l}}{\sigma} (\cosh 2l + e^{2x_1-2l}) - ie^{-x_1-iy_1}, \\ g(v_1) &= Z(v_1) + 2\sigma e^{-l} \tan y + ie^{-x_1+iy}, \\ \mathbf{R} \left\{ \frac{s_1^2}{c_1^2 d_1^2} f'(v_1) \right\} &= \frac{E}{K} \frac{e^{2l}}{4\sigma^2} - \frac{\sinh 2l}{4\sigma^2} - \frac{\sinh^2 2l}{8\sigma^4}, \\ \mathbf{R} \{g'(v_1)\} &= e^{-2l} \sinh 2l - \frac{E}{K} + 2e^{2x_1-4l} \sin^2 y_1 - 2\sigma^2 e^{-2l} \tan^2 y_1. \end{aligned} \right\} . \quad (4.14)$$

Also
$$\delta = \frac{\kappa \pi e^l}{2\sigma \kappa}.$$

In all cases an equation must be found to give v_1 in terms of the physical constants.

We consider these three cases separately in the next section.

5. Special Cases.

(i.) When the vortex lies on the horizontal axis.

Here we have

$$y_1=0, \quad s_1=ie^{x_1}, \quad c_1d_1=2\sigma e^{x_1-l}, \quad \sigma = \sqrt{\cosh x_1 \cosh (2l - x_1)}. \quad (5.1)$$

To determine v_1 , we first note that

$$\operatorname{sn}(v_1 + \bar{v}_1) = \frac{s_1 \bar{c}_1 \bar{d}_1 + \bar{s}_1 c_1 d_1}{1 - k^2 s_1^2 \bar{s}_1^2} = 0, \quad \dots \quad (5.2)$$

and

$$\operatorname{cn}(v_1 - \bar{v}_1) = \frac{c_1 \bar{c}_1 + s_1 \bar{s}_1 d_1 \bar{d}_1}{1 - k^2 s_1^2 \bar{s}_1^2} = \frac{1 + 2e^{2x_1} + e^{4x_1 + 4l}}{1 - e^{4x_1 - 4l}}.$$

From the first, $\mathbf{R}\{v_1\} = 0$. If we put $\mathbf{I}\{v_1\} = \nu$ and apply Jacobi's imaginary transformation ^{(1) p. 69}, the second becomes

$$\operatorname{cn}(2\nu, k') = \frac{1 - e^{4x_1 - 4l}}{1 + 2e^{2x_1} + e^{4x_1 - 4l}}. \quad \dots \quad (5.3)$$

If $x_1 < l$, this expression is positive, so that $0 < 2\nu < K'$ and ν can be found directly from tables. If $x_1 > l$, the expression is negative, so that $K' < 2\nu < 2K'$, and ν can easily be found by making use of the relation

$$\operatorname{cn}(2K' - 2\nu, k') = -\operatorname{cn}(2\nu, k'). \quad \dots \quad (5.4)$$

In either case, $v_1 = i\nu$ and is determined.

We next reduce (4.14) by means of (5.1), and are led to the results :

$$\Delta U = 0, \quad \Delta V = \frac{\kappa}{\sigma} \left[e^l \left\{ E(\nu, k') - \nu \left(1 - \frac{E}{K} \right) \right\} - \frac{\sinh 2l}{2\sigma} \right], \quad \dots \quad (5.5)$$

$$\frac{1}{R_1} = -\kappa \left[\frac{1}{6} - \frac{E}{K} \frac{e^{2l}}{2\sigma^2} + \frac{\sinh 2l}{2\sigma^2} + \frac{\sinh^2 2l}{8\sigma^4} \right].$$

Also, from (3.10),

$$Q_0 = 1. \quad \dots \quad (5.6)$$

(ii.) When the vortex lies on the vertical axis.

In this case,

$$x_1 = l, \quad s_1 = ie^{l+4y_1}, \quad c_1 d_1 = 2\sigma e^{4y_1}, \quad \dots \quad (5.7)$$

$$\sigma = \sqrt{\left\{ \frac{1}{2} \cosh 2l + \frac{1}{2} \cos 2y_1 \right\}} = \sqrt{(\cosh^2 l - \sin^2 y_1)} = \sqrt{(\sinh^2 l + \cos^2 y_1)}.$$

To determine v_1 , we first note that

$$\operatorname{cn}(v_1 - \bar{v}_1) = \frac{c_1 \bar{c}_1 + s_1 \bar{s}_1 d_1 \bar{d}_1}{1 - k^2 |s_1|^4} = \infty, \quad \dots \quad (5.8)$$

so that $\mathbf{I}\{v_1\} = \frac{1}{2}K'$. Put $\mathbf{R}\{v_1\} = \mu$. Then

$$\operatorname{sn} \mu = \operatorname{sn}(v_1 - \frac{1}{2}iK') = \frac{s_1 \operatorname{cn} \frac{1}{2}iK' \operatorname{dn} \frac{1}{2}iK' - \operatorname{sn} \frac{1}{2}iK' c_1 d_1}{1 - k^2 \operatorname{sn}^2 \frac{1}{2}iK' s_1^2},$$

whence, by making use of standard formulæ for sn , cn , dn , $\frac{1}{2}iK'$ ^{(1) p. 74}, and after some reduction,

$$\operatorname{sn} \mu = -\frac{e^l \sin y_1}{\cosh l + \sigma}. \quad \dots \quad (5.9)$$

If $y_1 < 0$, this expression is positive, so that $0 < \mu < K$ and μ can be found directly from the tables. If $y_1 > 0$, the expression is negative, so that

$-K < \mu < 0$, and μ is again easily determined by making use of the fact that $\sin \mu$ is an odd function. In either case, $v_1 = \mu + \frac{1}{2}iK'$.

The addition formula for the Z-function (⁽¹⁾ p. 145) is found to lead to

$$Z(v_1) = Z(\mu) - \frac{i\pi}{4K} + ie^{-l} \cosh l - \frac{e^{-l} \sin y_1 e^{i\psi_1}}{\cosh l + \sigma}, \quad (5.10)$$

and, using this result in the reduction of (4.14), we find that

$$\begin{aligned} \Delta U &= \frac{\kappa}{\sigma} \left[e^l Z(\mu) + \frac{\sin 2y_1 \cosh l}{2\sigma(\cosh l + \sigma)} + \frac{\sigma}{2} \tan y_1 - \sin y_1 \right], \\ \Delta V &= \frac{\kappa\pi e}{4\sigma K}, \\ \frac{1}{R_1} &= -\kappa \left[\frac{1}{6} - \frac{E}{K} \frac{e^{2l}}{2\sigma^2} + \frac{\sinh 2l}{2\sigma^2} + \frac{\sinh^2 2l}{8\sigma^4} + \frac{1}{4} \tan^2 y_1 \left(1 - \frac{2 \sinh^2 l}{\sigma^2} \right) \right], \end{aligned} \quad (5.11)$$

and

$$Q_0 = 1 - \frac{\kappa}{\sigma} \sin y_1.$$

(iii.) When the vortex lies in the central position.

In this case the results take a simpler form. Deduced from either of the previous cases, they are

$$\left. \begin{aligned} v_1 &= \frac{1}{2}iK', \quad \sigma = \cosh l, \\ \Delta U &= 0, \quad \Delta V = \frac{\kappa\pi}{4K} (1 + \tanh l), \\ \frac{1}{R_1} &= \kappa \left[\frac{1}{3} + \frac{1}{2} (1 + \tanh l)^2 \left(\frac{E}{K} - 1 \right) \right], \\ \delta &= \frac{\kappa\pi}{2K} (1 + \tanh l), \quad Q_0 = 1. \end{aligned} \right\} \quad (5.12)$$

6. Summary of Results with Full Dimensions.

In the preceding sections we have for convenience taken the width of the channel as π units, the general velocity and the fluid density as unity. We now restore the dimensions. Let the width of the channels be h and the length of the gap rh (fig. 3), so that the ratio

$$\frac{\text{gap}}{\text{width of channel}} = r. \quad (6.1)$$

Let the general velocity be U_0 , the circulation round the vortex $2\kappa\pi$, and the fluid density ρ . We obtain the generalized results by putting πr for $2l$, $\pi x_1/h$ for x_1 , $\pi y_1/h$ for y_1 , $\kappa\pi/U_0 h$ for κ , $\Delta U/U_0$ for ΔU , $\Delta V/U_0$ for ΔV , $\pi F_1/\rho U_0^2 h$ for F_1 , and so on. The formulæ which apply to all three cases, deduced from (3.22) and (4.9), are

$$k = e^{-\pi r}, \quad F_1 = -\rho 2\kappa\pi U_0, \quad \beta_1 = \frac{1}{2}\pi + \Delta V/U_0. \quad (6.2)$$

The special formulæ for the three cases take the following generalized forms.

(i.) When the vortex lies on the horizontal axis,

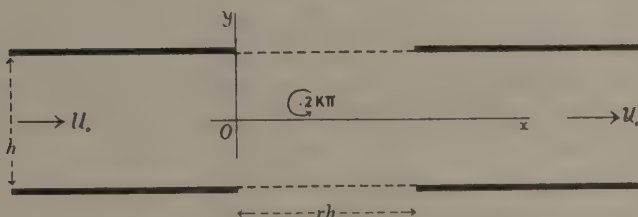
$$\sigma = \sqrt{\left\{ \cosh \frac{\pi x_1}{h} \cosh \frac{\pi}{h} (rh - x_1) \right\}}, \quad \text{cn}(2\nu, k') = \frac{1 - e^{\frac{2\pi}{h}(2x_1 - rh)}}{1 + 2e^{\frac{2\pi x_1}{h}} + e^{\frac{2\pi}{h}(2x_1 - rh)}}. \quad (6.3)$$

$$\Delta U = 0, \quad \Delta V = \frac{\kappa\pi}{h\sigma} \left[e^{\frac{1}{2}\pi r} \left\{ E(\nu, k') - \nu \left(1 - \frac{E}{K} \right) \right\} - \frac{\sinh \pi r}{2\sigma} \right],$$

$$\frac{1}{R_1} = -\frac{\kappa\pi^2}{U_0 h^2} \left[\frac{1}{6} - \frac{E}{K} \frac{e^{\pi r}}{2\sigma^2} + \frac{\sinh \pi r}{2\sigma^2} + \frac{\sinh^2 \pi r}{8\sigma^4} \right],$$

$$\delta = \frac{\kappa\pi^2 e^{\frac{1}{2}\pi r}}{2U_0 n\sigma K}, \quad Q_0 = U_0.$$

Fig. 3.



Here the formulæ for ΔU , ΔV , R_1 , Q_0 , δ must be true to a second approximation, since physical considerations show that ΔU and Q_0 must be even functions of κ , and ΔV , R_1 , δ must be odd functions.

(ii.) When the vortex lies on the vertical axis,

$$\left. \begin{aligned} \sigma &= \sqrt{\left\{ \frac{1}{2} \cosh \pi r + \frac{1}{2} \cos \frac{2\pi y_1}{h} \right\}}, \quad \text{sn } \mu = -\frac{e^{\frac{1}{2}\pi r} \sin \frac{\pi y_1}{h}}{\cosh \frac{1}{2}\pi r + \sigma} \\ \Delta U &= \frac{\kappa\pi}{h\sigma} \left[e^{\frac{1}{2}\pi r} Z(\mu) + \frac{\sin \frac{2\pi y_1}{h} \cosh \frac{1}{2}\pi r}{2\sigma (\cosh \frac{1}{2}\pi r + \sigma)} + \frac{\sigma}{2} \tan \frac{\pi y_1}{h} - \sin \frac{\pi y_1}{h} \right], \\ \Delta V &= \frac{\kappa\pi^2}{4h\sigma} \cdot \frac{e^{\frac{1}{2}\pi r}}{K}, \quad Q_0 = U_0 - \frac{\kappa\pi}{h\sigma} \sin \frac{\pi y_1}{h}, \quad \delta = \frac{\kappa\pi^2 e^{\frac{1}{2}\pi r}}{2U_0 h\sigma K}, \\ \frac{1}{R_1} &= -\frac{\kappa\pi^2}{U_0 h^2} \left[\frac{1}{6} - \frac{E}{K} \frac{e^{\pi r}}{2\sigma^2} + \frac{\sinh \pi r}{2\sigma^2} + \frac{\sinh^2 \pi r}{8\sigma^4} \right. \\ &\quad \left. + \frac{1}{4} \tan^2 \frac{\pi y_1}{h} \left(1 - \frac{2 \sinh^2 \frac{1}{2}\pi r}{\sigma^2} \right) \right]. \end{aligned} \right\} \quad (6.4)$$

(iii.) When the vortex lies in the central position,

$$\left. \begin{aligned} \sigma &= \cosh \frac{1}{2} \pi r, \\ \Delta U &= 0, \quad \Delta V = \frac{\kappa \pi^2}{4hK} (1 + \tanh \frac{1}{2} \pi r), \\ \frac{1}{R_1} &= \frac{\kappa \pi^2}{U_0 h^2} \left[\frac{1}{3} + \frac{1}{2} (1 + \tanh \frac{1}{2} \pi r)^2 \left(\frac{E}{K} - 1 \right) \right], \\ \delta &= \frac{\kappa \pi^2}{2U_0 hK} (1 + \tanh \frac{1}{2} \pi r), \quad Q_0 = U_0. \end{aligned} \right\} \quad (6.5)$$

7. Application to Wind Tunnel Theory.

We can now apply these results to the determination of corrections for a two-dimensional aerofoil placed in the stream of a wind tunnel with open working section, since in all practical cases $\kappa \pi / U_0 h$ is a small quantity.

As usually constructed, such wind tunnels have the ratio r of the order 1 to 1.5. For three typical tunnels, the values are $r = 0.93, 1.33, 1.75$. Now when $r \geq 0.75$ we find that $k \leq 0.095$, and we may safely neglect k^2 . We shall therefore approximate to the formulæ of §6, rejecting powers of k higher than the first. To this order,

$$\left. \begin{aligned} \frac{E}{K} &= 1, \quad \frac{E}{K} e^{\pi r} - \sinh \pi r = \frac{1}{2} e^{\pi r}, \\ \frac{\pi}{2K} &= 1, \quad E(\nu, k') - \nu \left(1 - \frac{E}{K} \right) = \tanh \nu. \end{aligned} \right\} \quad (7.1)$$

Putting at the same time Γ' for the circulation in the clockwise sense, so that

$$\Gamma' = -2\kappa \pi, \quad (7.2)$$

we find the following results for the three cases :

(i.) When the aerofoil lies on the horizontal axis upstream from the central position,

$$\left. \begin{aligned} \sigma &= \frac{e^{\frac{1}{2} \pi r}}{2} \left(\frac{1}{2} + \frac{1}{2} \tanh \frac{\pi x_1}{h} \right)^{-\frac{1}{2}}, \quad \tanh \nu = \left(\frac{1}{2} + \frac{1}{2} \tanh \frac{\pi x_1}{h} \right)^{\frac{1}{2}}, \\ \Delta U &= 0, \quad \Delta V = -\frac{\Gamma'}{4h} \left(1 + \tanh \frac{\pi x_1}{h} \right), \\ \frac{1}{R_1} &= -\frac{\Gamma' \pi}{2U_0 h^2} \left[\frac{1}{3} - \frac{1}{8} \left(1 - \tanh \frac{\pi x_1}{h} \right)^2 \right]. \end{aligned} \right\} \quad (7.3)$$

(ii.) When the aerofoil lies on the vertical axis,

$$\begin{aligned} \sigma &= \frac{e^{k\pi r}}{2} \left(1 + e^{-\pi r} \cos \frac{2\pi y_1}{h} \right), \\ \Delta U &= O(\Gamma'), \quad \Delta V = -\frac{\Gamma'}{2h} \left(1 - e^{-\pi r} \cos \frac{2\pi y_1}{h} \right), \\ \frac{1}{R_1} &= -\frac{\Gamma' \pi}{2U_0 h^2} \left[\frac{1}{2} + \frac{1}{4} \tan^2 \frac{\pi y_1}{h} \right]. \end{aligned} \quad (7.4)$$

In the simplification of the formula for R_1 , k has been neglected, as the contribution of this expression to the final result is small. Only the order of ΔU has been given as its exact value does not enter into the result.

(ii.) When the aerofoil lies in the central position,

$$\Delta U = 0, \quad \Delta V = -\frac{\Gamma'}{2h} (1 - e^{-\pi r}), \quad \frac{1}{R_1} = \frac{\Gamma' \pi}{2U_0 h^2} \cdot \frac{1}{3}. \quad (7.5)$$

In all cases we have

$$F_1 = \rho \Gamma' U_0, \quad \beta_1 = \frac{1}{2} \pi + \Delta V / U_0. \quad (7.6)$$

Now following the argument of ⁽³⁾, the true lift and drag coefficients, C_L and C_D , are given in terms of the apparent coefficients C_L' , C_D' by the relations

$$\begin{aligned} \frac{C_L}{C_L'} &= 1 + \frac{c}{2h} A, \\ C_D' - C_D &= \frac{C_L'^2 c}{4h} B, \end{aligned} \quad (7.7)$$

where c is the chord of the aerofoil, $\frac{c}{2h}$ is a constant which for most aerofoils takes a value about 3.45, and A , B are defined by

$$A = -\frac{4h}{C_L' c} \left(\frac{\Delta V}{U_0} + \frac{c}{4R_1} \right), \quad B = -\frac{4h}{C_L' c} \cdot \frac{\Delta V}{U_0}. \quad (7.8)$$

The values of A and B in these three cases are easily found to be

$$\begin{aligned} \text{(i.) } A &= \frac{1}{2} \left(1 + \tanh \frac{\pi x_1}{h} \right) + \frac{\pi c}{12h} \left[1 - \frac{3}{8} \left(1 - \tanh \frac{\pi x_1}{h} \right)^2 \right], \\ B &= \frac{1}{2} \left(1 + \tanh \frac{\pi x_1}{h} \right); \\ \text{(ii.) } A &= 1 - e^{-\pi r} \cos \frac{2\pi y_1}{h} + \frac{\pi c}{12h} \left[1 + \frac{3}{4} \tan^2 \frac{\pi y_1}{h} \right], \\ B &= 1 - e^{-\pi r} \cos \frac{2\pi y_1}{h}; \\ \text{(iii.) } A &= 1 - e^{-\pi r} + \frac{\pi c}{12h}, \\ B &= 1 - e^{-\pi r}. \end{aligned} \quad (7.9)$$

Now the results of ⁽³⁾, in the present notation, are as follows :-
Symmetrical case (aerofoil on x -axis),

$$A = \frac{1}{2} \left(1 + \tanh \frac{\pi x_1}{h} \right) + \frac{\pi c}{12h} \left[1 - \frac{3}{8} \left(1 - \tanh \frac{\pi x_1}{h} \right)^2 \right], \quad B = \frac{1}{2} \left(1 + \tanh \frac{\pi x_1}{h} \right).$$

Aerofoil appreciably downstream (or in a free stream),

$$A = 1 + \frac{\pi c}{12h} \left[1 + \frac{3}{4} \tanh^2 \frac{\pi y_1}{h} \right], \quad B = 1.$$

We see that (i.) reproduces the results of the symmetrical case of ⁽³⁾, so that the influence of the collector channel is represented by terms which are of the negligible order $e^{-2\pi r}$. Case (ii.) corresponds with the downstream case of ⁽³⁾, the results being modified by terms of magnitude $e^{-\pi r}$. We may say that the corrections given in ⁽³⁾ ^(b) apply here if diminished by the factor $\left(1 - e^{-\pi r} \cos \frac{2\pi y_1}{h} \right)$, where h is the height of the channels, and y_1 denotes the distance of the aerofoil from the midline. A similar result follows in case (iii.), except that the factor here is $(1 - e^{-\pi r})$.

As on previous occasions, the writer is under an obligation to Dr. R. C. Knight in respect of supervision of this work, which, in conclusion, it is a pleasure to acknowledge.

References.

- (1) A. Cayley, 'Elliptic Functions,' 2nd Edition, London, 1895.
- (2) N. Simmons, "Free Stream-line Flow past a Vortex," Quart. J. of Math., Oxford. (Dec. 1939.)
- (3) N. Simmons, "Free Stream-line Flow past Vortices and Aerofoils," Quart. J. of Math., Oxford. (Dec. 1939.)

XI. *Some Evidence for the Existence of Higher Hydrates of Ferric Oxide as Transition Intermediates.*

By LARS A. WELO, Tottenville, Staten Island, New York, and
OSKAR BAUDISCH, Saratoga Springs Authority,
Saratoga Springs, New York *.

[Received August 18, 1939.]

SOME time ago we † described the behaviour of ferromagnetic gamma ferric oxide ($\gamma\text{-Fe}_2\text{O}_3$) when it is heated along with water in sealed tubes. We showed that it could be nearly completely transformed to a non-ferromagnetic ferric oxide in one hour at as low a temperature as 136°C . The temperature necessary for near completion of the same overall transformation during one hour in open tubes was $375\text{--}380^\circ\text{C}$.

In the present paper we shall describe the unexpected and, we believe, significant results that have been obtained in similar studies conducted at still lower temperatures and extended over much longer times.

The Observations.

The way in which ferromagnetic $\gamma\text{-Fe}_2\text{O}_3$ transforms to a non-ferromagnetic isomeric form when heated along with water in sealed tubes at various thermostatically controlled temperatures is shown in fig. 1. The deflexions are proportional to the magnetic susceptibilities which, in turn, are proportional to the concentrations of untransformed $\gamma\text{-Fe}_2\text{O}_3$. These concentrations are the ratios of the ordinates, at any times, to the intercepts on the deflexion axis of the corresponding extrapolated initial line segments. The method of measurement was simple. A tube was suspended from a string 205 cm. long. The oxide column in the tube was caught near the middle with a small electro-magnet which was pulled aside by hand, in front of a board ruled with vertical lines, until the tube dropped from the magnet's gap. Obviously the displacement from the vertical, measured in a horizontal direction, is accurately proportional to the tangential gravity component and to the force on the oxide when the tube drops off.

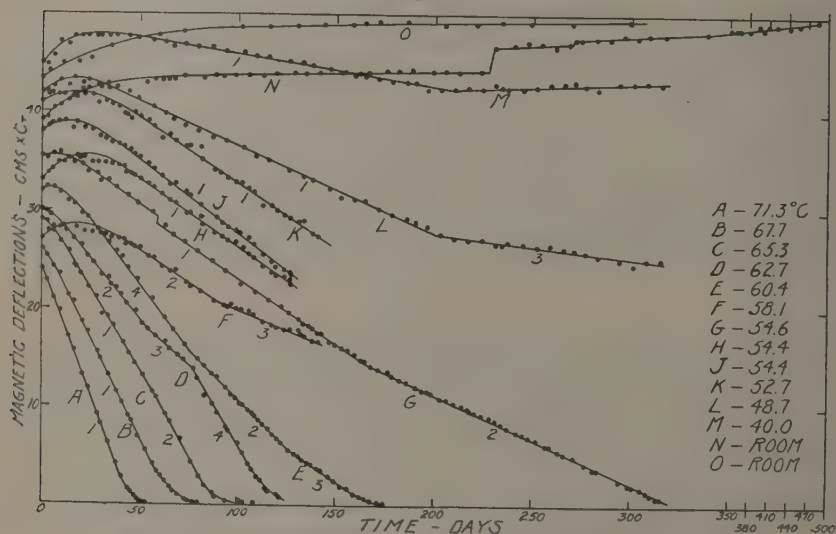
The fact that the oxide containers were cylindrical with axes perpendicular to the field direction necessitates consideration of a possible influence

* Communicated by the Authors.

† L. A. Welo and O. Baudisch, *Phil. Mag.* [7] xxiv. p. 80 (1937).

of the demagnetizing force on the forms of the curves of fig. 1. This influence proves to be quite negligible. The mean value of the field of the magnet, over a circular area 1.5 times the diameter of the 0.63 cm. pole faces, was 2680 oersteds. In a previous paper * we showed that the permeability of $\gamma\text{-Fe}_2\text{O}_3$, derived by the dehydration of synthetic $\gamma\text{-FeOOH}$, when of full magnetic strength and packed to a density of 0.31 g./cm.^3 was 1.25 at 600 oersteds. Accurate extrapolation to 2680 oersteds is not possible, but the permeability at that field should not exceed 1.1. In the present experiments the oxide settled, in water, to densities of about 0.11 g./cm.^3 . Permeabilities at 2680 oersteds would then be of the order

Fig. 1.

Transformations of $\gamma\text{-Fe}_2\text{O}_3$ in sealed tubes along with water.

of 1.03. Even with less favourable spherical instead of cylindrical containers, the ratio of the internal, effective field to the external, applied field would have been, according to the Poisson relation,

$$\frac{H_i}{H_e} = \frac{3\mu_1}{2\mu_1 + \mu_2} = \frac{3}{2 + 1.03} = 0.99.$$

Even at the beginning of a transformation, when the oxide is of full magnetic strength, the effective magnetizing field differs from the applied field by less than one per cent., so that the demagnetizing forces cannot have affected perceptibly the curves of fig. 1.

* L. A. Welo and O. Baudisch, *Phil. Mag.* [7] xvii. p. 753 (1934).

Because of manual operation of the magnet, the deflexion readings scattered over a range of about 5 per cent. Each point plotted in fig. 1 is the mean of from six to a dozen readings.

One of us * has already described the preparation of gamma ferric oxide monohydrate ($\gamma\text{-FeOOH}$) from which $\gamma\text{-Fe}_2\text{O}_3$ is obtainable by dehydration. Our regular dehydration procedure is to heat for one hour at 260–265° C. The particular hydrate used throughout the present study yielded an oxide rather more stable than usual. Instead of being convertible to non-ferromagnetic Fe_2O_3 by heating with water in a sealed tube for one hour at 136° C., more than one hour was required at 146° C. The containers used during the heating were glass tubes of 3 mm. internal and 5 mm. external diameter, which were suitable also for the magnetic measurements. The oxide columns, of lengths 2.5 to 3.0 cm., were completely immersed in water. Each tube contained from 18 to 22 milligrams of oxide.

In two curves of fig. 1, G and N, discontinuities other than those of slope appear. They are due to movement of entrained air bubbles and resultant redistribution of oxide, although care was taken to remove air, while preparing the tubes, by moving the oxide about in the water by means of the magnet. The discontinuities do not appear in curves J and H which repeat curve G, nor in O which repeats curve N.

In every curve of fig. 1 there is an apparent induction period before the transformation becomes linear with respect to time. At the lower temperatures the magnetic deflexions even increase. This induction period is probably fictitious as far as any transformation of $\gamma\text{-Fe}_2\text{O}_3$ to a more magnetic oxide is concerned, or as far as it concerns any change in the true magnetic constants of $\gamma\text{-Fe}_2\text{O}_3$. The apparent induction period denotes rather that some other structural change occurs which allows the oxide to move more freely in the water and to pack more densely under the influence of the magnetic field gradient. A tube was arranged for ballistic measurements, not involving the presence of a field gradient. It was maintained at room temperature and observed from time to time over a period of ninety days. Various field strengths within the range 10 to 500 oersteds were used. According to curves N and O of fig. 1, the susceptibilities should have increased about 10 per cent. during this time. Instead, by plotting the susceptibilities against time, a straight horizontal line was obtained for each value of the magnetic field.

It should be explained that the initial magnetic deflexions were more nearly alike than they would seem to have been from a first glance at the figure. Among the different tubes the initial total deflexions ranged

* O. Baudisch, *Svensk Kemisk Tidskrift*, xlvii. p. 115 (1935).

between 45 and 55 cm. The deflexions were multiplied by the factors C_T , constant for each temperature, in order that all the curves could be placed on one figure without too much overlapping and confusion.

Grouping of the Transformation Rates.

In a previous paper* we wrote as follows regarding the paths of the low temperature transformation of both $\gamma\text{-Fe}_2\text{O}_3$ and $\gamma\text{-FeOOH}$ to non-ferromagnetic oxide when confined with water in sealed tubes:—

“The first step in the transformation of $\gamma\text{-FeOOH}$ in closed tubes with water is then to be regarded as an irreversible transition, $\gamma\text{-FeOOH} \rightarrow \alpha\text{-FeOOH}$. This is a natural property of $\gamma\text{-FeOOH}$ just as the irreversible transition $\gamma\text{-Fe}_2\text{O}_3 \rightarrow \alpha\text{-Fe}_2\text{O}_3$ is a natural property of $\gamma\text{-Fe}_2\text{O}_3$. The rest of the transformation of $\gamma\text{-FeOOH}$ to $\alpha\text{-Fe}_2\text{O}_3$ consists of the shedding of $\alpha\text{-Fe}_2\text{O}_3$ to satisfy the equilibrium requirements of the system $\alpha\text{-FeOOH}$, $\alpha\text{-Fe}_2\text{O}_3$ and water.

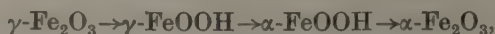
“If we start with $\gamma\text{-Fe}_2\text{O}_3$ instead of $\gamma\text{-FeOOH}$, the transition $\gamma\text{-FeOOH} \rightarrow \alpha\text{-FeOOH}$ is preceded by hydration of $\gamma\text{-Fe}_2\text{O}_3$ to $\gamma\text{-FeOOH}$. This hydration continues until all $\gamma\text{-Fe}_2\text{O}_3$ is consumed because $\gamma\text{-FeOOH}$ disappears by irreversible transition.

“The fact that intermediate $\gamma\text{-Fe}_2\text{O}_3$ does not appear in the transformation of $\gamma\text{-FeOOH}$ by the wet process shows, it seems to us, that the transformation paths in the wet and the dry processes must be entirely different. The additional fact that $\gamma\text{-Fe}_2\text{O}_3$ transforms by the wet process at the same temperature and at the same rate as the γ -hydrate from which it was derived, clearly indicates that $\gamma\text{-Fe}_2\text{O}_3$ must revert to $\gamma\text{-FeOOH}$, and that the rest of the transformation proceeds as if we had started with the original hydrate.”

As a particularization of a more general transformation scheme this statement is consistent with the behaviour shown in fig. 1. There all of the concentrations of $\gamma\text{-Fe}_2\text{O}_3$ are linear functions of time, not exponential of the form

$$C = ae^{-bt}.$$

The reactions or transformations are, therefore, of zero order and require a transformation scheme which will provide for the existence of intermediates that remain of constant concentration. In the present case the intermediates must be hydrates. But fig. 1 also shows that the simple scheme,



must be extended to provide other hydration paths, other irreversible transitions between isomeric hydrates, and possibly other end products.

* L. A. Welo and O. Baudisch, *Phil. Mag.* [7] xxiv. p. 80 (1937).

A single transformation rate at a given temperature is seen to be the exception rather than the rule. Only curves A and B run to completion at one rate. In curves C, F, G, L, and M two rates appear in each, and in each, and in curves D and E three different rates are clearly perceptible.

Of the twenty rates that appear in fig. 1, excluding N and O and the second part of M, those that are to be associated with the same combination of hydration, irreversible transition, and dehydration can be identified by considering that they are all exponential functions of absolute temperature,

$$\frac{dC}{dt} = Ae^{BT}.$$

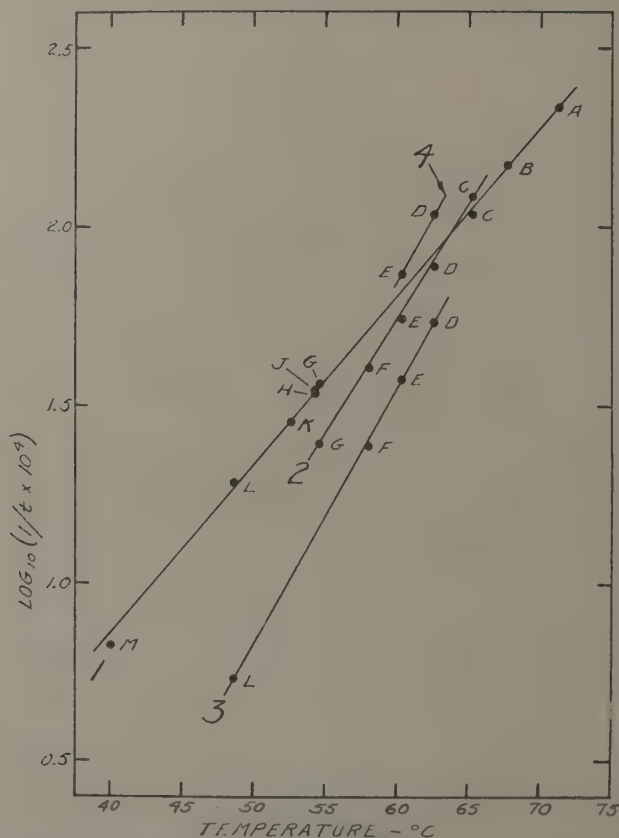
Those associated with a given combination should be found on the same straight line when their logarithms are plotted against temperature. This is the case, and quite accurately so, as fig. 2 shows. All but two of the twenty rates, computed as fractional parts of $\gamma\text{-Fe}_2\text{O}_3$ transformed per day and plotted logarithmically, lie along the three straight lines expected. The two rates left over, D_4 and E_4 , apparently belong to the third of a system of three parallel lines, 2, 3, and 4. In any case, they belong to a fourth curve, and we infer that, within the range of temperature used in this study, at least four combinations of hydration, irreversible transitions, and dehydration are possible.

A further inference from fig. 2 is that the concentration of the hydrate which is formed by hydration of $\gamma\text{-Fe}_2\text{O}_3$ and which undergoes transition to a more stable isomer, is practically independent of the temperature within its range of existence. The possibility of the existence, however, of a given combination of hydration, transition, and dehydration is determined by both the temperature and the concentration of $\gamma\text{-Fe}_2\text{O}_3$. The curves of fig. 1 show that as many as three different combinations may exist at certain temperatures at successive stages of a transformation.

The concentration of hydrate formed by $\gamma\text{-Fe}_2\text{O}_3$ hydration does not, however, remain constant to the very end of a transformation. As may be seen in fig. 1, curves A, B, C, D, and E go to near completion as exponential curves instead of straight lines. This would indicate that at low concentrations, $\gamma\text{-Fe}_2\text{O}_3$ cannot maintain a constant concentration of the hydration product which disappears by irreversible transition. We can estimate these minimum concentrations in the cases of the five transformations mentioned. As fractions of the initial $\gamma\text{-Fe}_2\text{O}_3$ concentrations they are evidently equal to the ratios of the ordinates of the points of departure from linearity to the intercepts on the deflexion axis of the extrapolated initial line segments. For the transformations corresponding to the line segments, A_1 , B_1 , C_2 , D_4 , and E_3 these concentrations are, respectively, 0.13, 0.14, 0.08, 0.09, and 0.03. While

very rough, they are significant. They form distinct groups. The rates corresponding to lines A₁ and B₁ are on the same straight line in fig. 2. Transformations A₁ and B₁ were therefore associated with the same combination of hydration, irreversible transition, and dehydration. Now we see that the concentrations of $\gamma\text{-Fe}_2\text{O}_3$ when the changes from

Fig. 2.



The groups of transformation rates derived from fig. 1. The time, t , is in days.

linear to exponential variations with time occur are also the same, within the error of the determinations. E₃ was assigned to another combination and departs from linearity at a lower concentration. C₂ and D₄ were assigned to different combinations. Their rates appear on different lines in fig. 2. But the concentrations of $\gamma\text{-Fe}_2\text{O}_3$ at departure from a linear

variation with time are practically the same. We venture to suggest that the hydration paths are identical for C_2 and D_4 , but that irreversible transitions occur to different isomers, leading, in the end, to different non-ferromagnetic oxides also.

Analysis for hydrate water after a few partially or nearly completed transformations as shown in Table I. provide additional evidence that the transformations involve hydrates as intermediates, and that shifts in their concentrations occur. Of particular significance is the fact that the oxide which was partially transformed as shown by curve M_1 in fig. 1, and which, on further heating showed a slow increase in magnetic susceptibility, had no hydrate water. Oxide N, which had been maintained at room temperature with no decrease in susceptibility, likewise had no hydrate water. Oxide L, however, while still undergoing transformation at the stage L_3 , had nearly one-half per cent. of water of hydration. Oxide H at the stage H_1 had 1.2 per cent.

All of the other hydrate values in the column for oxides in Table I. were determined after the transformations had proceeded beyond the linear portions of the curves and were changing along the final exponential portions. As we have already pointed out, the hydrate concentrations should not be expected to be constant after departure from the linear law. The concentration of hydrate would depend on how long the exponential portion of the curve had been followed. Accordingly, the hydrate concentration values for nearly completed oxide transformations can only indicate minimum values for the water present as hydrate constituents during the linear transformations immediately preceding. The value 1.4 per cent. for the nearly completed B_1 is probably the same, within error of determination, as the value 1.2 per cent. for partially completed H_1 . B_1 and H_1 are transformations of the same type, both being grouped on the same line in fig. 2.

Our definition of hydrate water was dictated by experimental convenience, but it is consistent with experience with ferric oxide monohydrates which decompose at slightly over 200°C . It is the water that is lost, expressed as per cent. of the resulting dry weight of oxide, when the material, dried to constant weight at 105°C ., is heated for one hour at 300°C . The possibility of the existence of hydrates that would decompose between room temperature and 105°C . is precluded; in no case was more than one-half of one per cent. of water lost at 105°C ., after drying to constant weight at room temperature in a desiccator with P_2O_5 for periods of a month to six weeks.

In our previous paper * on the transformation of $\gamma\text{-Fe}_2\text{O}_3$ and $\gamma\text{-FeOOH}$ to non-ferromagnetic Fe_2O_3 at low temperatures in the presence

* L. A. Welo and O. Baudisch, *Phil. Mag.* [7] xxiv. p. 80 (1937).

of water, we stated that both the oxide and its parent monohydrate converted in the same time and at approximately the same temperature. This statement was based on the fact that a sample of oxide assumed near zero susceptibility on being heated for one hour at 136° C., and that the monohydrate, similarly treated, retained only about 1.2 per cent. of hydrate water instead of the original 11.2 per cent. The data on residual hydrates

TABLE I.

Hydrate Water in Oxides and Corresponding Monohydrates after Partial or Nearly Complete Transformation.

Trans- formation, designated in fig. 1.	Temperature ° C.	Oxide Conversion, per cent.	Hydrate Water, per cent. of dry weight *.	
			Oxide.	Mono- hydrate.
A ₁	71.3	100, near	0.4	2.8
B ₁	67.7	100, near	1.4	8.0
C ₂	65.3	100, near	0.0	4.8
D ₂	62.7	43	—	12.2
D ₄	62.7	100, near	1.1	9.5
E ₄	60.4	58	—	11.8
E ₂	60.4	86	—	10.0
G ₂	54.6	100, near	0.3	6.6
H ₁	54.4	44	1.2	—
L ₃	48.7	45	0.45	11.7
M ₁	40.0	13	0.0	10.2
N	Room	0	0.0	10.7

from monohydrate, given in Table I., show that our previous result was fortuitous and not generally valid. For example, monohydrate which was heated in the same oven and for the same length of time as oxide A, was also, in large part, converted to non-ferromagnetic Fe₂O₃, since the hydrate water was reduced to 2.8 per cent. But another sample of monohydrate, which was heated at the same temperature and during the same time as the nearly completely transformed oxide D, lost only a small fraction of its hydrate water. The water content was still 9.5 per cent., or only 1.7 per cent. less than the theoretical content in FeOOH.

* After heating one hour at 300° C..

The Transformation Paths : Hydration, Irreversible Transition, and Dehydration.

With the information at hand it is not possible to specify the combinations of hydration, irreversible transition, and dehydration believed to be responsible for the four rate constants clearly indicated by the fact that all of the twenty observed rates group themselves upon four separate straight lines when their logarithms are plotted against temperature (fig. 2). But it is interesting to consider the possibilities suggested by the oxide and oxide hydrate system of aluminium. It is well known that, in so far as they have members in common, the systems of ferric iron and aluminium are analogous. Both systems are shown in Table II. Not all writers would agree with our series assignments. According to Edwards, Frary, and Jeffries*, gibbsite belongs to the α series, but Haber† assigns it to the γ series because it dehydrates to γ -alumina. Iso-gibbsite is our own designation for the aluminium oxide trihydrate described by Haber as dehydrating to γ -alumina, although its crystal structure differs from gibbsite. Haber considered it to be a member of a branched γ series.

We retain the simple hydration-irreversible transition-dehydration scheme: $\gamma\text{-Fe}_2\text{O}_3 \rightarrow \gamma\text{-FeOOH} \rightarrow \alpha\text{-FeOOH} \rightarrow \alpha\text{-Fe}_2\text{O}_3$ suggested in our previous paper as one of the possible combinations involved in the more complex transformations we have just described. We extend it to include other hydrates, and transitions to other series. The low temperatures used during this study, with consequent low hydrate dissociation pressures, may have provided just the conditions necessary for their existence as components of the system ferric oxide, ferric oxide hydrate, and water.

In considering the possible new combinations we need not limit ourselves to the members of the iron system listed in Table II. as missing. They merely denote those necessary to complete the analogy with the aluminium system as far as that is known at the present time. However, we must exclude dehydration within the γ' series. The end product of such dehydrations would be $\gamma'\text{-Fe}_2\text{O}_3$, identical, according to Haber, with the $\gamma\text{-Fe}_2\text{O}_3$ with which we start. With these things in mind we see that the hydration paths from $\gamma\text{-Fe}_2\text{O}_3$ are to γ and $\gamma'\text{-Fe}_2\text{O}_3 \cdot 3\text{H}_2\text{O}$ and to γ and $\gamma'\text{-FeOOH}$. Each of these can undergo transition to either the α series or the β series. There are, therefore, eight possible combinations of hydration and irreversible transition. The final step in each of these transformations would be dehydration to either α or $\beta\text{-Fe}_2\text{O}_3$ according to the series determined by the path of irreversible transition. In either

* Edwards, Frary, and Jeffries, 'The Aluminium Industry,' first edition, vol. i. pp. 164-168. (McGraw Hill, New York (1930).)

† F. Haber, *Naturwissenschaften*, xiii. p. 1007 (1925).

series the hydrate produced by transition decomposes to the corresponding oxide to maintain the equilibrium requirements of the system: oxide, oxide hydrate, and water.

According to this, an oxide differing from both γ and α - Fe_2O_3 , a β - Fe_2O_3 , might be present after some of the transformations shown in fig. 1. At the present time we are repeating some of the transformations shown in fig. 1 to obtain material for X-ray crystal analysis. Structure

TABLE II.

Oxide and Oxide Hydrate Systems of Aluminium and Ferric Iron.

Composi- tion.	Series.			
	γ' .	γ .	α .	β .
$\text{Al}_2\text{O}_3 \cdot 3\text{H}_2\text{O}$.	Gibbsite (iso).	Gibbsite (monoclinic).		β -trihydrate.
AlOOH .		Synthetic bauxite.	Diaspore (orthorhombic). $a : b : c =$ $\cdot 937 : 1 : 0 \cdot 604$	
Al_2O_3 .		γ -alumina (cubic).	Corundum (rhombohedral).	β -alumina (hexagonal).
$\text{Fe}_2\text{O}_3 \cdot 3\text{H}_2\text{O}$.	Missing.	Missing.		Missing.
FeOOH .		Lepidocrocite (orthorhombic) $a : b : c =$ $\cdot 308 : 1 : \cdot 296$	Goethite (orthorhombic) $a : b : c =$ $\cdot 459 : 1 : \cdot 303$	
Fe_2O_3 .		γ -oxide (cubic) (ferromagnetic).	Hematite (rhombohedral.)	Missing.

determination will identify the series to which irreversible transitions occur, because an oxide must belong to the same series as the hydrate from which it derives.

By the study of γ - Fe_2O_3 itself it does not seem possible to distinguish hydration paths to γ' or γ - FeOOH from the hydration paths to γ or γ' - $\text{Fe}_2\text{O}_3 \cdot 3\text{H}_2\text{O}$. Both of these monohydrates and both of these trihydrates are intermediates from which the transitions occur during the heating of γ - Fe_2O_3 along with water in sealed tubes. As we have seen

in fig. 1, all of these transformations are of zero order and are linear with respect to time. If, however, we should start with γ -FeOOH, instead of γ -Fe₂O₃, conversions of both first and zero orders might be found provided changes of paths occur of the types we have actually found on transforming γ -Fe₂O₃. The hydrate undergoing transition by the paths γ -FeOOH \rightarrow α -FeOOH or γ -FeOOH \rightarrow α -FeOOH already exists. No source of constant hydrate concentration is present; therefore a first order conversion should be found. By way of γ or γ' -Fe₂O₃.3H₂O, on the other hand, preliminary hydration to a higher hydrate is necessary. A zero order conversion would be expected, and it is conceivable that a complete conversion curve of γ -FeOOH, at a given temperature, would consist of a succession of straight lines and exponential curves.

Whether or not the rates obtainable from a study of γ -FeOOH could be used to identify hydration paths from γ -Fe₂O₃ would depend on whether or not any of them could be grouped upon lines similar to those of fig. 2 on plotting their logarithms against temperature. Perhaps we should not expect the concentration of a given trihydrate from γ -FeOOH to be the same as from γ -Fe₂O₃, but we should expect the same dependence of its rate of transition on temperature. We regard the rates of irreversible transition between hydrates as actually controlling during a zero order transformation, although, taken as a whole, such a transformation involves hydration and dehydration as well.

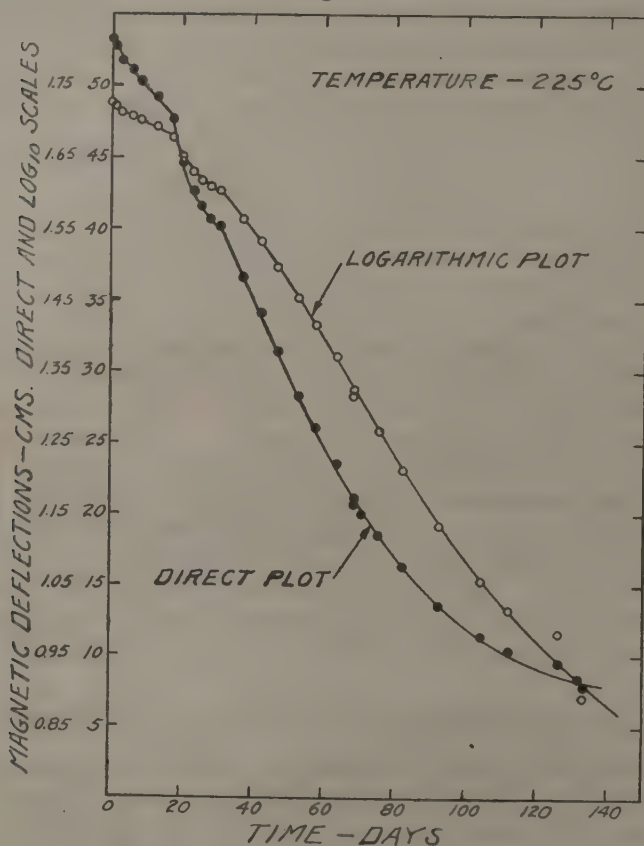
Such a study of γ -FeOOH can be made in either of two ways. We may determine the amount of unconverted γ -FeOOH at any time by analysis for residual hydrate water, or we may dehydrate the unconverted γ -FeOOH to γ -Fe₂O₃ and measure the magnetic susceptibility. Either method destroys the sample. Many sealed tubes containing γ -FeOOH and water would be placed in the same oven and removed, one at a time, during the course of the conversion for the determination of unconverted γ -FeOOH.

Transformation of γ -Fe₂O₃ in Open Tubes at Higher Temperatures.

To emphasize the contrast in behaviour of γ -Fe₂O₃ as between heating with water in sealed tubes and heating in open tubes at much higher temperatures, we present the curves of fig. 3. Both the direct and the logarithmic plots of the magnetic deflexions are shown. We are unable to offer any suggestions to account for the discontinuities; but we note that at no stage is the first order transformation, γ -Fe₂O₃ \rightarrow α -Fe₂O₃, strictly followed. We believe that transformations, such as form the subject of this paper, are superposed upon the direct transformation γ -Fe₂O₃ \rightarrow α -Fe₂O₃. Traces of water would make this possible, and its gradual elimination would account for the diminished rates observed as the transformation proceeds. Indeed, the observations recorded in fig. 3

offer ground for the suspicion that the direct transformation path $\gamma\text{-Fe}_2\text{O}_3 \rightarrow \alpha\text{-Fe}_2\text{O}_3$ is not possible, and that absolutely dry $\gamma\text{-Fe}_2\text{O}_3$ cannot be changed to non-ferromagnetic Fe_2O_3 . For this reason we are continuing magnetic observations on $\gamma\text{-Fe}_2\text{O}_3$ while it is being heated in open tubes for still longer times and at other temperatures than 225°C .

Fig. 3.

Transformation of $\gamma\text{-Fe}_2\text{O}_3$ in an open tube.

The experimental work was done in the Research Laboratory of the Consolidated Gas, Electric Light, and Power Company of Baltimore. We thank its director, Dr. S. Karrer, for the use of its facilities.

XII. *The Crystal Structures of some Heterocyclic Organic Compounds of Analogous Constitution.*—Part III. *Phenazine and Diphenylene Dioxide.*

By R. G. WOOD, M.Sc., and G. WILLIAMS, M.Sc.*

[Received March 4, 1940.]

1. *Introduction.*

THE compounds to be discussed in this paper are phenazine (I.) and diphenylene dioxide (II.). Crystallographic, optical, and X-ray measure-



ments are described and discussed in relation to the information yielded by other types of investigation. At the end of the paper will be found a table summarizing the principal data which have been obtained for the eight compounds dealt with in this series of papers.

2. *Phenazine.*

(a) *Crystallography.*

Phenazine crystallizes from acetone or from a mixture of acetone and alcohol in long yellow needles. Fig. 1 is a stereographic projection of the crystal constructed from the following interfacial angles :—

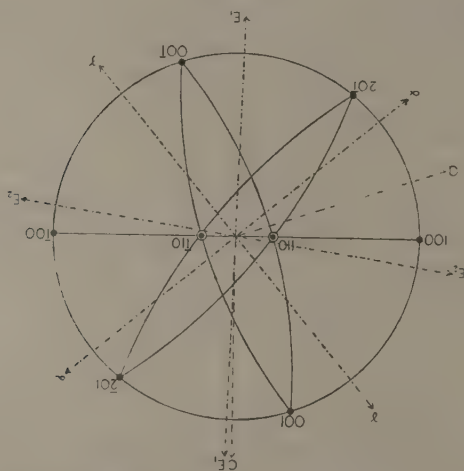
	Observed.	Calculated.
001 : 100	71° 5'*	—
100 : 20 $\bar{1}$	51° 39'	51° 43'
20 $\bar{1}$: 110	76° 32' *	—
100 : 110	67° 55' *	—

Owing to differences in the relative development of different faces there appeared to be two varieties of crystals, but they were found to be crystallographically identical. Both types are illustrated in fig. 2, and

* Communicated by Professor R. T. Dunbar.

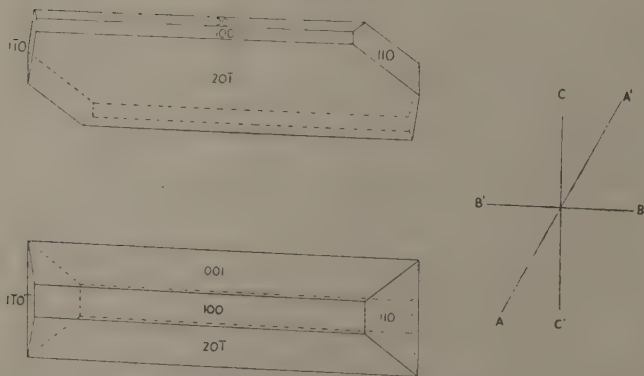
it will be observed that externally phenazine is rather similar to thianthren and selenanthren (see Part I. of this series of papers). The crystal be-

Fig. 1.



Stereographic projection of phenazine.

Fig. 2.



Typical crystals of phenazine.

longs to the monoclinic holohedral class, and the axial ratios and angle calculated from the angles marked with an asterisk are

$$a : b : c = 2.61 : 1 : 1.39, \quad \beta = 108^\circ 55'.$$

(b) *X-ray Measurements.*

Rotation photographs taken about the three axes gave the following values for the spacings :—

$$a=13.2 \text{ \AA.}, \quad b=5.07 \text{ \AA.}, \quad c=7.12 \text{ \AA.}$$

The unit cell of phenazine contains two molecules, giving a calculated density which agrees with the observed density 1.33 gm./ml.

Oscillation photographs were taken around the *a*- and *c*-axes. All general (*hkl*) spectra were present, showing that the unit cell chosen is primitive. Special indices showed the following features :—

(0*k*0) absent when *k* is odd,

(*h*0*l*) „ „ *h* „ .

The structure is therefore built up on the monoclinic lattice T_m and the space-group is $P2_1/a$ (C_{2h}^5).

(c) *Optical Measurements.*

The refractive indices of phenazine presented a difficult problem, since the lowest index α was found to be greater than that of a concentrated solution of potassium mercuric iodide, while other liquids of higher index dissolved the crystal rather rapidly. It was found possible, however, to determine α by matching with a solution of barium mercuric iodide, but the available range of refractive indices was too limited to allow the use of the graphical method which has been applied to the other crystals in this series. By using a fresh crystal for each matching operation, however, it was found possible to match β with a mixture of certain organic liquids. The optic axial angle could then be measured and the value of γ calculated. The direction of γ was found to be that of the acute bisectrix, showing the birefringence to be positive. In this way the following values of the refractive indices and optic axial angle were found :—

$$\alpha=1.73, \quad \beta=1.82, \quad \gamma=1.96, \quad 2V=83^\circ.$$

The indices are probably correct to 0.01 and the optic axial angle to $\frac{1}{2}^\circ$.

The orientation of the axes of the indicatrix relative to the crystallographic axes was determined by immersing the crystal in a mixture of liquids of refractive index β and finding the positions of the optic axes relative to the microscope stage. The positions of the normals to the faces of the crystal in the zone parallel to β (which is in the same direction as *b*) had been previously determined relative to the stage by the method described by Wood and Ayliffe ⁽¹⁾. It was thus found that γ made an angle of 40° with the *c*-axis taken towards the obtuse angle β , while one of the optic axes made an angle of about $1\frac{1}{2}^\circ$ with the *c*-axis away from the

obtuse angle β . The α - and γ -axes are shown on the stereographic projection (fig. 1), together with the optic axes.

(d) *Structure.*

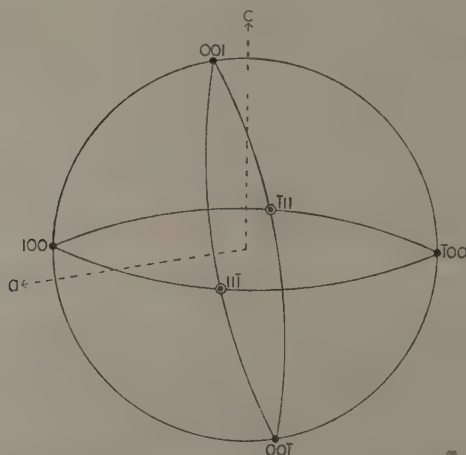
The magnetic properties of phenazine have been investigated by Dr. Kathleen Lonsdale (work unpublished so far), but there does not appear to be any correspondence between the optical and the magnetic properties. In this respect the crystal is anomalous, and without further investigation it will be safer to leave open the question of the orientation of the molecules in the unit cell. It is possible to assert, however, that since there are only two molecules in the unit cell the molecule must possess a centre of symmetry. This result is in agreement with the experiments of Bergmann, Engel, and Meyer ⁽²⁾ and Campbell, Le Fèvre, Le Fèvre and Turner ⁽³⁾, who found that the dipole moment of phenazine is zero, from which it follows that the molecule is plane.

3. Diphenylene Dioxide.

(a) *Crystallography.*

Diphenylene dioxide crystallizes from alcohol or acetone in very long colourless crystals but better specimens are obtained by crystallization

Fig. 3.



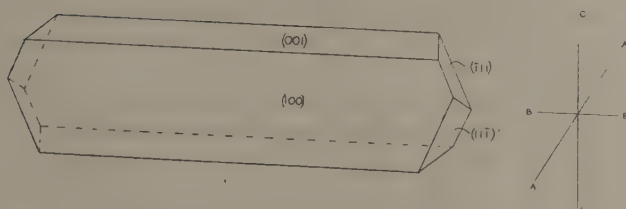
Stereographic projection of diphenylene dioxide.

from petroleum ether. It shows a strong tendency to twin formation, and on microscopic examination all specimens, including apparently single crystals, were found to be multiply twinned. The plane of twinning

is (100). The single crystal is represented in stereographic projection in fig. 3, while figs. 4 and 5 are drawings of a single crystal and of a simple twin respectively. The observed interfacial angles are as follows :—

100 : 001	79° 38',
100 : 11 $\bar{1}$	76° 32',
001 : $\bar{1}11$	70° 12'.

Fig. 4.



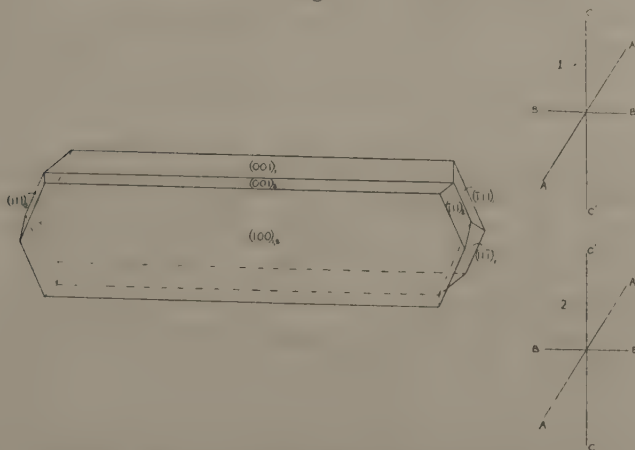
Single crystal of diphenylene dioxide.

The axial ratios and angle calculated from these are

$$a : b : c = 2.99 : 1 : 2.30, \quad \beta = 100^\circ 20'.$$

It appears from the external symmetry that the crystal belongs to the monoclinic holohedral class.

Fig. 5.



Twin crystal of diphenylene dioxide.

(b) *X-Ray Measurements.*

Rotation photographs taken about the three axes gave the following spacings :—

$$a=15.2 \text{ \AA}, \quad b=5.07 \text{ \AA}, \quad c=11.7 \text{ \AA}.$$

The observed density of the crystal is 1.36 gm./ml., corresponding to four molecules per unit cell (calculated density 1.38 gm./ml.).

Oscillation photographs were taken about the axes a and c . Those taken around the c -axis indicated, in some cases, an apparent plane of symmetry perpendicular to c . The presence of intensity differences between corresponding spots, however, showed that this was not a real plane of symmetry but that the appearance was due to the twinning already mentioned. In the multiply twinned specimens successive layers have their respective b - and c -axes pointing in opposite directions, as shown in fig. 5. The a -axes, on the other hand, all point in the same direction. It follows that in an oscillation photograph about c the c -axis is vertically upwards for one set of crystal layers and vertically downwards for the other. The resulting photograph is then built up by the superposition of spots from one set of crystal layers together with spots from the other set, which is upside down relative to the first. If the two sets gave spots of the same intensity the photograph would indicate the existence of an apparent plane of symmetry. In oscillation photographs about a there is no indication of a plane of symmetry, real or apparent.

In fig. 5 the faces of the crystal drawn with reference to the first set of axes are indexed $(\)_1$, while those drawn with reference to the second set of axes are indexed $(\)_2$.

In the oscillation photographs the following features of the indices were observed :—

(hkl) absent when $k+l$ is odd.

$(h0l)$ „ h „ .

The crystal is thus built up on the monoclinic lattice Γ'_m and the unit cell is centred in the (100) plane. The most probable space-groups are either $Aa(C_s^4)$ or $A2/a(C_{2h}^6)$. The fact that the crystals exhibit no pyroelectric effect favours the second of these.

(c) *Optical Properties.*

It was impossible to make any optical measurements on diphenylene dioxide on account of the multiple twinning.

(d) *Structure.*

As in the case of phenazine it is impossible at the present stage to say very much about the crystal structure of diphenylene dioxide. Bennett,

Summary Table giving principal observed data on all the substances discussed in the preceding three papers.

	<i>a.</i>	<i>b.</i>	<i>c.</i>	β .	Space-group.	Mols./cell.	α .	β .	γ .	2V.
Thianthren	14.4	6.11	11.9	110° 0'	P ₂ ₁ / <i>a</i>	4	1.646	1.759	1.950	82° 10'
Selenanthren	14.5	6.24	12.1	110° 20'	P ₂ ₁ / <i>a</i>	4	1.686	1.790	1.964	82° 0'
Phenthiazine	5.91	7.90	21.0	—	P ₆ <i>mm</i> ?	4	1.61	1.73	1.95	81°
Phenoxthionine	5.94	7.76	20.5	—	P ₂ ₁ ² ₁ ² ₁	4	1.62	1.72	1.86	85°
Phenoxselenine	5.93	7.85	20.5	—	P ₂ ₁ ² ₁ ² ₁	4	1.66	1.74	1.87	81°
Phenoxtellurine	5.97	8.16	20.5	—	P ₂ ₁ ² ₁ ² ₁	4	>1.73	—	—	—
Phenazine	13.2	5.07	7.12	108° 55'	P ₂ ₁ / <i>a</i>	2	1.73	1.82	1.96	83°
Diphenylene dioxide ...	15.2	5.07	11.7	100° 20'	A2/ <i>a</i> ?	4	—	—	—	—

Earp, and Glasstone⁽⁴⁾ measured the dipole moment of diphenylene dioxide and found it to be zero, a result which implies that the molecule is plane. Cullinane and Plummer⁽⁵⁾ have shown that diphenylene dioxide forms eutectics without any solid solution formation with thi-anthren and selenanthren, and Cullinane and Rees⁽⁶⁾ have made similar observations on the system diphenylene dioxide-phenoxthionine. These results would be expected if the diphenylene dioxide molecule is plane while the others are folded. The deductions to be drawn from the X-ray data so far available are unfortunately less definite than in the case of phenazine. If, however, the space-group is $A2/a$, then the molecule must possess either a centre or a twofold axis of symmetry, and in the former case the molecule would necessarily be plane. The most that can be said, therefore, is that the X-ray results are consistent with a plane molecule for diphenylene dioxide, but other possibilities cannot be excluded.

4. Summary.

An account is given of crystallographic, optical, and X-ray measurements on phenazine and diphenylene dioxide. It is shown that the results for these substances imply that the phenazine molecule is plane, and are consistent with the molecule of diphenylene dioxide being plane.

Our thanks are due to Dr. N. M. Cullinane, of the Chemistry Department of this College, who prepared the diphenylene dioxide; to Dr. E. E. Turner for specimens of phenazine; to Dr. E. G. Cox for access to some unpublished photographs of diphenylene dioxide; to Dr. Kathleen Lonsdale for unpublished magnetic measurements and for many valuable discussions; and to Professor R. T. Dunbar for his interest throughout the whole of the present work. One of us (G. W.) acknowledges the receipt of a University of Wales Postgraduate Studentship.

A table summarizing the principal measurements on the eight crystals discussed in this series of papers is given above.

References.

- (1) Wood and Ayliffe, *J. Sci. Inst.* xii, p. 299 (1935).
- (2) Bergmann, Engel, and Meyer, *Ber. dtsh. chem. Ges.* lxxv, p. 446 (1932).
- (3) Campbell, Le Fèvre, Le Fèvre and Turner, *J. Chem. Soc.* p. 404 (1938).
- (4) Bennett, Earp, and Glasstone, *J. Chem. Soc.* p. 1179 (1934).
- (5) Cullinane and Plummer, *J. Chem. Soc.* p. 63 (1938).
- (6) Cullinane and Rees, *Trans. Faraday Soc.* xxxvi, p. 507 (1940).

University College,
Cardiff.

March 2, 1940.

ERRATA.

On page 66 of this volume, six lines from the bottom of the page, for $b' \neq 6.14 \text{ \AA.}$ read $b' = 6.14 \text{ \AA.}$

Also on page 71, delete "r" in formula II.

XIII. On Lamé Functions.

By A. ERDÉLYI, Mathematical Institute of the
University, Edinburgh *.

[Received July 16, 1940.]

1. RECENTLY Ince ⁽²⁾ has introduced for periodic solutions of Lamé's differential equation a new notation which is likely not only to furnish a better and simpler representation of the present stage of the theory of Lamé functions, but also to facilitate further systematic research in this field of analysis. Not only would the results presented in the following lines, for instance, look much more involved than they are when written in one of the old notations; probably it would be more difficult to gain the insight into the matter necessary to arrive at them without the aid of a rational, simple notation. In fact, the investigations presented in this note were directly suggested to the author by a careful study of Dr. Ince's work.

Ince investigated solutions having a real period of Lamé's equation. It will be shown that in general, *i. e.*, apart from polynomial solutions, these Lamé functions are only simply-periodic and have no imaginary period. There are transcendental Lamé functions with an imaginary period as well. These again are simply-periodic, have no real period, and can be expressed by the symbols of Dr. Ince's notation.

For certain values of n (and corresponding values of h) a solution of real period and one of imaginary period coexist. They are, however, distinct in general. Only in the case of Lamé *polynomials* does the solution of imaginary period coincide with that of real period: Lamé polynomials are the only *doubly-periodic* solutions of Lamé's differential equation.

Regarding Lamé polynomials as a coincidence of two Lamé functions—one of real, the other of imaginary period—a transformation formula of Lamé polynomials connecting two polynomials belonging to complementary moduli is easily arrived at. This again involves a certain relation between the characteristic numbers of Lamé's equation belonging to complementary moduli. This relation is thought to be of some value also from the practical point of view, for it reduces the work of computing the characteristic numbers corresponding to Lamé *polynomials* to the

* Communicated by the Author.

half of its extent. In particular it explains certain regularities in Ince's tables of characteristic numbers.

As a by-product, some results on the zeros of Lamé polynomials are obtained.

Beside the transformation dealt with in this note there is another one. This second transformation, introducing an imaginary modulus, is thought to be of less practical importance, and will not be dealt with.

2. Let the modulus k be real and between 0 and 1; let k' be the complementary modulus, $K=K(k)$ the complete elliptic integral of first kind, $K'=K'(k)=K(k')$. Let u be the complex variable of the elliptic functions and

$$v=K'-iK+iu. \quad (1)$$

The following abbreviations will be used throughout:

$$\left. \begin{aligned} s &= \operatorname{sn}(u, k), & c &= \operatorname{cn}(u, k), & d &= \operatorname{dn}(u, k); \\ \hat{s} &= \operatorname{sn}(v, k'), & \hat{c} &= \operatorname{cn}(v, k'), & \hat{d} &= \operatorname{dn}(v, k'). \end{aligned} \right\} \quad (2)$$

$\hat{s}, \hat{c}, \hat{d}$ are connected with s, c, d by Jacobi's imaginary transformation:

$$ks=\hat{d}, \quad ikc=k'\hat{c}, \quad d=k'\hat{s}. \quad (3)$$

In order to prove the first of these relations we remark that $2iK'$ being a half-period of $\operatorname{dn}(u, k)$ (§ 22.34), and hence $2iK$ a half-period of $\operatorname{dn}(v, k')$,

$$\hat{d}=\operatorname{dn}(K'-iK+iu, k')=-\operatorname{dn}(K'+iK+iu, k').$$

Hence from the periodic property with respect to $K+iK'$ of $\operatorname{dn}(u, k)$ (§ 22.33) or with respect to $K'+iK$ of $\operatorname{dn}(v, k')$,

$$\hat{d}=-ik \frac{\operatorname{sn}(iu, k')}{\operatorname{cn}(iu, k')}.$$

Now from Jacobi's imaginary transformation⁽⁵⁾ (§ 22.4)

$$\operatorname{sn}(iu, k')=i \frac{\operatorname{sn}(u, k)}{\operatorname{cn}(u, k)} \quad \text{and} \quad \operatorname{cn}(iu, k')=\frac{1}{\operatorname{cn}(u, k)}.$$

Hence

$$\hat{d}=k \operatorname{sn}(u, k)=ks.$$

The proof of the other two relations (3) is similar.

3. The "Jacobian" form of Lamé's differential equation⁽⁵⁾ (Chapter XXIII.).

$$\frac{d^2y}{du^2} + \{h - n(n+1)k^2s^2\}y = 0 \quad (4)$$

will be used. In the last decades of the 19th century, when Lamé's equation was the subject of many investigations by leading analysts, the Jacobian form was mainly used by Hermite⁽¹⁾. Hence in earlier

papers (4) is frequently called Hermite's equation. We shall follow the general usage and call (4) Lamé's equation, as equivalent to the algebraic form of Lamé's equation or its "Weierstrassian" form.

Any periodic solution of Lamé's equation will be called a Lamé function. To fix ideas, n will be assumed to be real. There is no further loss of generality in supposing $n \geq -\frac{1}{2}$, for (4) does not change if n is replaced by $-n-1$.

The following theorem on Lamé functions of real period is due to Ince.

Lamé functions of periods $2K$ and $4K$ exist for every real value of n . They will be represented by the symbol $Ec_n^m(u, k^2)$ when even and by $Es_n^m(u, k^2)$ when odd functions of u , where m , which is necessarily a not negative integer, denotes the number of zeros in the interval $0 \leq u < 2K$.

Functions with even m are periodic mod. $2K$, those with odd m periodic mod. $4K$. The characteristic values associated with $Ec_n^m(u, k^2)$ and $Es_n^m(u, k^2)$ will be denoted by $a_n^m(k^2)$ and $b_n^m(k^2)$ respectively. The abbreviations

$$a_n^m = a_n^m(k^2), \quad b_n^m = b_n^m(k^2), \quad Ec_n^m = Ec_n^m(u, k^2), \quad Es_n^m = Es_n^m(u, k^2) \quad (5)$$

will be used.

The existence of Lamé functions of imaginary period can be inferred from Ince's theorem by Jacobi's imaginary transformation. By (1) and (3), (4) transforms to

$$-\frac{d^2y}{dv^2} + \{h - n(n+1)\hat{d}^2\}y = 0,$$

or, being

$$\hat{d}^2 = 1 - k'^2 \hat{s}^2,$$

$$\frac{d^2y}{dv^2} + \{\hat{h} - n(n+1)k'^2 \hat{s}^2\}y = 0, \quad \dots \dots \dots (6)$$

where

$$\hat{h} = n(n+1) - h. \quad \dots \dots \dots (7)$$

Hence Ince's theorem assures the existence of functions periodic in v mod. $2K'$ and $4K'$, i. e., periodic in u mod. $2iK'$ and $4iK'$. The characteristic values associated with $Ec_n^m(v, k'^2)$ and $Es_n^m(v, k'^2)$ are $\hat{h} = a_n^m(k'^2)$ and $b_n^m(k'^2)$, i. e., $h = n(n+1) - a_n^m(k'^2)$ and $n(n+1) - b_n^m(k'^2)$ respectively.

Hence we have the following theorem :—

Lamé functions of periods $2iK'$ (m even) and $4iK'$ (m odd) exist for every real value of n . Even and odd functions of $u - (K + iK')$ will be represented by the symbols $Ec_n^m(v, k'^2)$ and $Es_n^m(v, k'^2)$ respectively where m denotes the number of zeros in the interval $u = K + iK' + it$, $0 \leq t < 2K'$. The corresponding characteristic numbers are $h = n(n+1) - a_n^m(k'^2)$ and $h = n(n+1) - b_n^m(k'^2)$ respectively.

The abbreviations

$$\hat{a}_n^m = a_n^m(k'^2), \quad \hat{b}_n^m = b_n^m(k'^2), \quad \hat{E}c_n^m = Ec_n^m(v, k'^2), \quad \hat{E}s_n^m = Es_n^m(v, k'^2) \quad (8)$$

will be used.

4. The question arises whether there are special pairs of values n, h for which Lamé's equation has *two* periodic solutions at the same time.

The only case in which two independent solutions of *real* period $2K$ or $4K$ coexist is the case of integer n smaller than the index m . In fact

$$a_n^m = b_n^m \quad (n=0, 1, 2, \dots, m-1), \quad \dots \quad (9)$$

and hence Ec_n^m and Es_n^m ($n=0, 1, \dots, m-1$) are solutions of the same differential equation necessarily distinct, the one being even, the other odd.

From this result, which is due to Ince, the corresponding theorem on solutions of imaginary periods immediately follows.

The only case in which two independent solutions of *imaginary* period $2iK'$ or $4iK'$ coexist is the case of integer order n smaller than the index m .

In fact $\hat{a}_n^m = \hat{b}_n^m$ ($n=0, 1, \dots, m-1$), and hence $\hat{E}c_n^m$ and $\hat{E}s_n^m$ ($n=0, 1, \dots, m-1$) are solutions of the same differential equation and necessarily distinct, for one is an even function, the other an odd function, of $u-(K+iK')$.

Turning now to the question of coexistence of a solution of real period and one of imaginary period, there are two possibilities:—

(i.) If one of the equations $h=a_n^m$ or $h=b_n^m$ ($m=0, 1, \dots$) should be identical with one of the equations $h=n(n+1)-\hat{a}_n^{m'}$ or $h=n(n+1)-\hat{b}_n^{m'}$ ($m'=0, 1, \dots$), then to any pair of values (n, h) satisfying this equation there would belong a Lamé function of imaginary period as well as one of real period. This is, however, impossible, for $a_n^m, b_n^m, \hat{a}_n^{m'}, \hat{b}_n^{m'}$ are according to Ince asymptotically, for large values of n , linear functions of n . Hence an equation of the form $a_n^m = n(n+1) - \hat{a}_n^{m'}$ or a corresponding one where one or both of the a 's is replaced by a b could never be true for *every* real n .

(ii.) There is a second possibility. To a pair of values (n, h) which are the coordinates of a point of intersection of any of the curves $h=a_n^m$ or $h=b_n^m$ with any of the curves $h=n(n+1)-\hat{a}_n^{m'}$ or $h=n(n+1)-\hat{b}_n^{m'}$ of the (n, h) -plane there must belong a Lamé function of imaginary period as well as one of real period. The question is whether such intersections exist and whether the two Lamé functions of real and imaginary periods respectively are distinct or identical (and in this latter case doubly periodic).

From the asymptotic behaviour of the characteristic numbers for large n it is easily seen that such intersections do exist. More about their number and location will be said in section 6.

Corresponding to an intersection belonging to a non-integral value of n there exist two distinct Lamé functions, one of real the other of imaginary period. In case of an intersection with an integer the two solutions coincide, and we have only one, doubly periodic, Lamé function which is a polynomial in s, c, d .

5. Let us first turn to intersections belonging to integer values of n . The existence of such intersections and their location follow from the relations

$$\left. \begin{aligned} a_n^{2m} + \hat{a}_n^{n-2m} &= a_n^{2m+1} + \hat{b}_n^{n-2m} = b_n^{2m+1} + \hat{b}_n^{n-2m-1} = n(n+1) \text{ if } n \text{ even,} \\ a_n^{2m} + \hat{b}_n^{n-2m} &= a_n^{2m+1} + \hat{a}_n^{n-2m} = b_n^{2m} + \hat{b}_n^{n-2m+1} = n(n+1) \text{ if } n \text{ odd,} \end{aligned} \right\}. \quad (10)$$

which in their turn are consequences of the transformation formulæ

$$\left. \begin{aligned} Ec_n^{2m} &= \hat{E}c_n^{n-2m}, & Ec_n^{2m+1} &= \hat{E}s_n^{n-2m}, & Es_n^{2m+1} &= \hat{E}s_n^{n-2m-1} \text{ if } n \text{ even,} \\ Ec_n^{2m} &= \hat{E}s_n^{n-2m}, & Ec_n^{2m+1} &= \hat{E}c_n^{n-2m}, & Es_n^{2m} &= \hat{E}s_n^{n-2m+1} \text{ if } n \text{ odd,} \end{aligned} \right\}. \quad (11)$$

for Lamé polynomials. In these transformation formulæ constant factors have been disregarded.

Take for instance n even. Then [see Ince ⁽²⁾, (2.1)]

$$Ec_n^{2m} = \sum_{r=0}^{n/2} A_{2r} s^{2r} = \sum_{r=0}^{n/2} A_{2r} \hat{d}^{2r} / k^{2r},$$

using the transformation (1), (3). This is again a polynomial of degree n in \hat{s} , and hence, except for a constant factor, of the form $Ec_n^{2m'}$. In order to find m' the zeros of this polynomial must be considered more closely.

(i.) Ec_n^{2m} has exactly n zeros in the parallelogram $-K \leq \sigma < K$, $-K' \leq t < K'$, where $u = \sigma + it$ and σ and t are real. Also $Ec_n^{2m}(-K) \neq 0$. For Ec_n^{2m} is a polynomial of degree n in s and vanishes for n different values of s . Now in the above parallelogram s takes every value and none twice. Hence Ec_n^{2m} has n zeros there. Also if $Ec_n^{2m}(-K)$ should vanish, then Ec_n^{2m} would have a factor c , and being a polynomial in s it would have even a factor c^2 , which is impossible.

(ii.) $2m' \leq n - 2m$. For $2m'$ is the number of zeros of $\hat{E}c_n^{2m'} = Ec_n^{2m}$ in the interval $u = K + iK' + it$, $0 \leq t < 2K'$, or, in other words, in $u = -K + it$, $-K' \leq t < K'$. $2m$ of the n zeros of Ec_n^{2m} lying on the real axis and $-K$ being not a zero, there remain $n - 2m$ zeros, part or all of which may lie on the left edge of our parallelogram.

(iii.) $2m' = n - 2m$. For the number m' corresponding to $2m = n$ is ≤ 0 , and hence precisely zero; consequently $Ec_n^n = \hat{E}c_n^0$. The number m'

corresponding to $m = \frac{1}{2}n - 1$ is ≤ 1 ; since $\hat{E}c_n^0 = Ec_n^n$, it cannot be $= Ec_n^{n-2}$; hence $m' = 1$ and $Ec_n^{n-2} = \hat{E}c_n^2$. Proceeding so step by step the first relation (11) can be proved. From this proof also follows that all zeros of Ec_n^{2m} are on the boundary of our parallelogram; $Ec_n^{2m} \neq 0$ for any u in $-K < \sigma < K$, $-K' < t < K$.

Since Ec_n^{2m} belongs to $h = a_n^{2m}$ and $\hat{E}c_n^{n-2m}$ to $h = n(n+1) - \hat{a}_n^{n-2m}$, their identity implies $a_n^{2m} = n(n+1) - \hat{a}_n^{n-2m}$. This proves the first of the relations (10).

n being even as before, we have [Ince ⁽²⁾ (4.3)]

$$Ec_n^{2m+1} = cd \sum_{r=0}^{\frac{1}{2}n-1} C_{2r} s^{2r} = -ik' \hat{c} \hat{s} \sum_{r=0}^{\frac{1}{2}n-1} C_{2r} \hat{a}^{2r} / k^{2r}$$

by (3). Hence

$$Ec_n^{2m+1} = \hat{s} \hat{c} \sum_{r=0}^{\frac{1}{2}n-1} \hat{C}_{2r} \hat{s}^{2r} = \hat{E}s_n^{2m'}.$$

The proof of $2m' = n - 2m$ is similar to that in the first case. There is one difference, however: $u = -K$ is a zero of Ec_n^{2m+1} , and this zero counts both as a real zero and as a zero on the line $u = -K + it$. Therefore, $-K$ being doubly counted, we have instead of (ii.) $2m' \leq n + 1 - (2m + 1)$.

Similar is the proof of the remainder of the relations (10) and (11).

From the foregoing considerations also follows that:—

The zeros of all Lamé polynomials are situated on the lines $u = \sigma + 2ir'K'$ and $u = (2r-1)K + it$ (σ, t real, $r, r' = 0, \pm 1, \pm 2, \dots$). [See also Heine ⁽¹⁾, vol. i. p. 382.]

6. Now we may draw a diagram showing the points of intersection $a_0^0 = 0$ and for integer $n > 0$ from the Sturmian theory $0 < a_n^0 < a_n^1 < b_n^1 < b_n^2 < a_n^2 < a_n^3 < \dots < a_n^n$, or b_n^n according as n is even or odd. Also, according to Ince, $a_n^{n+1} = b_n^{n+1} < a_n^{n+2} = b_n^{n+2} < \dots$ ($n \geq 0$). This gives a complete scheme of the curves $h = a_n^m$ and $h = b_n^m$. Next we draw the curves $h = x_n^m = n(n+1) - \hat{a}_n^m$ and $h = \beta_n^m = n(n+1) - \hat{b}_n^m$. α_n^0 for instance passes through the points $a_0^0, b_1^1, a_2^2, b_3^3, a_4^4$ etc.; α_n^1 through the points $a_1^1, b_2^2, a_3^3, b_4^4, a_5^5$ etc. α_n^0 meets a^n between $n=0$ and $n=1$, meets b_n^2 between $n=1$ and $n=2$, etc.

In the diagram drawn up thus we have four types of intersections: (i.) Those characterized by (9); here two different Lamé functions of real period coexist. (ii.) Intersections characterized by the relation $\alpha_n^m = \beta_n^m$ for $n=0, 1, \dots, m-1$; here two different Lamé functions of imaginary period coexist. (iii.) Intersections corresponding to relations (10); here we have a doubly-periodic Lamé polynomial; the second solution cannot be periodic [⁽⁵⁾ §23.47]. (iv.) The intersections mentioned on the end of the last paragraph, for non-integral values of n . Now, for

non-integral values of n , $u=iK'$ and $u=2K+iK'$ are branch-points of Lamé's equation. Hence no doubly periodic solution can exist. Consequently in this case we have *two* Lamé functions coexisting, one of real the other of imaginary period. A short consideration of the diagram shows that there are exactly $2N$ intersections of this type between $n=N-1$ and $n=N$, whereas there are $2N+1$ intersections (belonging to polynomials) for $n=N$.

7. The relations (10) reveal certain connexions between the tables of characteristic values belonging to complementary moduli. These connexions may be observed in Ince's tables for $k^2=0.1$ and $k^2=0.9$. In fact, as far as characteristic values belonging to polynomials are concerned, it is sufficient to calculate the characteristic numbers for $0 \leq k^2 \leq 0.5$ from the characteristic equations; those for $0.5 < k^2 \leq 1$ follow from (10). In particular from the characteristic numbers for $k^2=0$ [$a_n^m(0)=b_n^m(0)=m^2$] the characteristic numbers for $k^2=1$ as given by Ince presently follow.

Of some interest is the table for $k^2=\frac{1}{2}$, which is complementary to itself. From (10) for $k^2=k'^2=\frac{1}{2}$ the relations

$$\left. \begin{aligned} a_n^{2m} + a_n^{n-2m} &= a_n^{2m+1} + b_n^{n-2m} = b_n^{2m+1} + b_n^{n-2m-1} = n(n+1) \text{ if } n \text{ even, } k^2=\frac{1}{2} \\ a_n^{2m} + b_n^{n-2m} &= a_n^{2m+1} + a_n^{n-2m} = b_n^{2m} + b_n^{n-2m+1} = n(n+1) \text{ if } n \text{ odd, } k^2=\frac{1}{2} \end{aligned} \right\} \quad (12)$$

and in particular

$$\left. \begin{aligned} a_n^{in} &= \frac{1}{2}n(n+1), \quad n \equiv 0(4); & b_n^{in} &= \frac{1}{2}n(n+1), \quad n \equiv 2(4), \\ a_n^{i(n+1)} &= \frac{1}{2}n(n+1), \quad n \equiv 1(4); & b_n^{i(n+1)} &= \frac{1}{2}n(n+1), \quad n \equiv 3(4), \end{aligned} \right\} k^2=\frac{1}{2}. \quad (13)$$

follow. These relations explain almost all the regularities noticed by Ince in that table.

8. A slight modification of the notation used simplifies the appearance of our formulæ still more. Denoting by \mathbf{Ec}_n^m and \mathbf{Es}_n^m Lamé functions of real period which are even or odd functions of $u-K$ (instead of u), and by a_n^m and b_n^m the corresponding characteristic numbers, we obtain

$$\left. \begin{aligned} a_n^{2m} &= a_n^{2m}, & a_n^{2m+1} &= b_n^{2m+1}, & b_n^{2m} &= b_n^{2m}, & b_n^{2m+1} &= a_n^{2m+1}, \\ \mathbf{Ec}_n^{2m} &= \mathbf{Ec}_n^{2m}, & \mathbf{Ec}_n^{2m+1} &= \mathbf{Es}_n^{2m+1}, & \mathbf{Es}_n^{2m} &= \mathbf{Es}_n^{2m}, & \mathbf{Es}_n^{2m+1} &= \mathbf{Ec}_n^{2m+1}. \end{aligned} \right\} \quad (14)$$

There are corresponding relations for Lamé functions of imaginary period.

In this altered notation equations (10) and (11) read

$$\left. \begin{aligned} a_n^m + \hat{a}_n^{n-m} &= b_n^m + \hat{b}_n^{n-m+1} = n(n+1), \text{ and} \\ \mathbf{Ec}_n^m &= \hat{\mathbf{Ec}}_n^{n-m}, \quad \mathbf{Es}_n^m = \hat{\mathbf{Es}}_n^{n-m+1}, \quad (m=0, 1, \dots, n). \end{aligned} \right\} \quad (15)$$

Likewise (12) and (13) simplify to

$$\left. \begin{aligned} a_n^m + a_n^{n-m} &= b_n^m + b_n^{n-m+1} = n(n+1) \quad (k^2=\frac{1}{2}), \text{ and} \\ a_n^{in} &= \frac{1}{2}n(n+1) \text{ if } n \text{ be even, } b_n^{i(n+1)} = \frac{1}{2}n(n+1) \text{ if } n \text{ be odd} \end{aligned} \right\} (k^2=\frac{1}{2}). \quad (16)$$

In this note I dealt only with Lamé functions of periods $2K$, $4K$, $2iK'$, and $4iK'$. There are corresponding properties of functions of other periods. So for instance the relations for functions of period $8K$ corresponding to the fifth relation (12) and the third equation (13) have been conjectured by Ince from the features of the corresponding tables of characteristic numbers. The relations between characteristic numbers always resemble closely (10). The relations between Lamé functions of periods $8K$ etc. are slightly more involved than (11) when using the notation of the first seven sections of this note, owing to the fact that in this case Lamé's equation has *two* doubly periodic solutions. The method which has been used here for Lamé functions of periods $2K$, $4K$, $2iK'$, $4iK'$ lends itself equally well to elucidating the connexions between Lamé functions of larger periods as well.

Using the notation of this section in connexion with Lamé functions of periods $8K$ etc. means a new definition of these functions. Adopting this new definition the transformation formulæ always resemble closely (15). Hence this new notation should be even more valuable in connexion with Lamé functions of periods larger than $4K$ and $4iK'$.

References.

- (1) E. Heine, 'Handbuch der Kugelfunktionen,' Berlin, 1878-1881.
- (2) E. L. Ince, Proc. Royal Soc. Edinburgh, lx. pp. 47-63 (1940).
- (3) E. L. Ince; *ibid.* pp. 83-99.
- (4) Ch. Hermite, 'Sur quelques applications des fonctions elliptiques,' Paris, 1885.
- (5) E. T. Whittaker and G. N. Watson, 'Modern Analysis,' Cambridge, 1927.

XIV. *Relationships between Lattice Types and Brillouin Zones.*

By GEOFFREY VINCENT RAYNOR *.

[Received July 29, 1940.]

IN recent years the forms of the Brillouin Zones for the simple metallic types of crystal structure have been securely established, and the results have been extended to cover such complex examples of crystal structure as the γ -brass and β -manganese types. This has led in many cases to a satisfactory interpretation of some of the physical and electrical properties of metals and alloys ⁽¹⁾.

Since a knowledge of the Brillouin Zones for the various structures which may be found in metals and intermetallic systems is becoming of increasing importance in any theoretical examination, it is of interest to discuss certain lattice relationships and the corresponding Brillouin Zone relationships. In this way it is possible to obtain at least some idea of the form of the zones for the more complex structures, if they can be related to more simple forms.

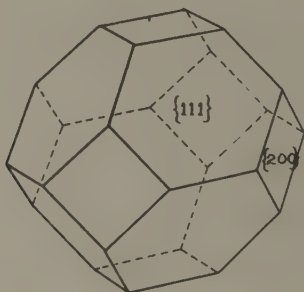
In the first place, we may consider crystal lattices which may be referred to cubic axes. The face-centred cubic structure forms a convenient basis for discussion. The appropriate Brillouin Zone for this lattice may readily be shown, by the usual methods, to be bounded by planes of the type $\{200\}$ and $\{111\}$ in k -space ⁽²⁾. These are the only planes of low indices for which the structure factor does not vanish. The form of the zone for the face-centred cubic structure is shown in fig. 1.

The face-centred cubic lattice may, however, be regarded as a body-centred tetragonal lattice with an axial ratio, c/a , equal to $\sqrt{2}$. Thus it follows that the form of the Brillouin Zone for a body-centred tetragonal lattice with parameters $a = \frac{z}{\sqrt{2}}$ and $c = \alpha$ is the same as that for a face-centred cubic lattice of parameter α . The bounding planes of the zone will, of course, have a different nomenclature when referred to the tetragonal structure. The $\{002\}$ planes of the face-centred cube remain the $\{002\}$ planes of the tetragonal structure. The $\{200\}$ and $\{020\}$ planes of the face-centred cube become the $\{110\}$ planes of the tetragon, while

* Communicated by Professor N. F. Mott, F.R.S.

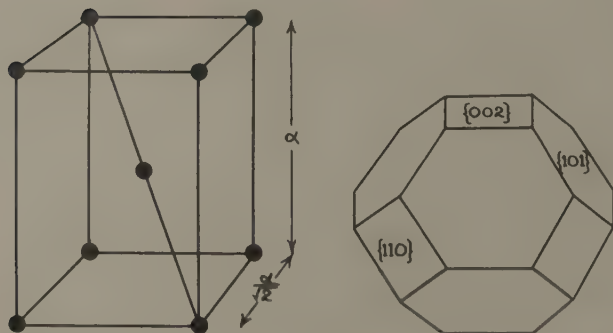
the $\{111\}$ planes of the cube become the $\{101\}$ family of tetragonal planes. The form of the zone, together with the unit cell of the body-centred tetragonal lattice equivalent to a face-centred cube, is shown in fig. 2. For this particular structure with c/a equal to $\sqrt{2}$, the slopes of the faces of the zone correspond with the slopes of equivalent planes in the face-centred cube.

Fig. 1.



Brillouin Zone for face-centred cubic lattice.

Fig. 2.

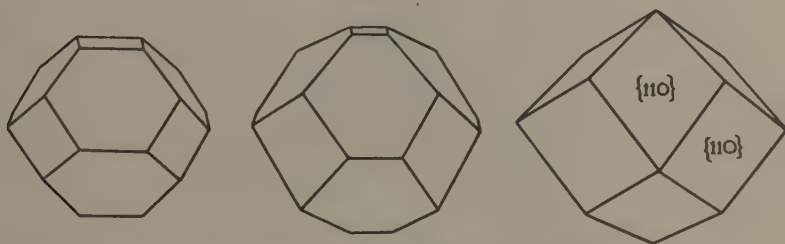
Unit cell of lattice, and Brillouin Zone for body-centred tetragonal structure of $c/a = \sqrt{2}$.

We may now consider the body-centred tetragonal structure with axial ratio $\sqrt{2}$ to be compressed along the c axis until it becomes a body-centred cube, of side $\frac{a}{\sqrt{2}}$ for instance, and may consider the corresponding changes in the form of the Brillouin Zone. As compression of the lattice takes place, the inter-planar spacing of the $\{002\}$ planes decreases, so

that the $\{002\}$ faces of the Brillouin Zone are displaced outwards from the origin of k -space. At the same time the planes of the type $\{101\}$ become more horizontal in slope, while the planes of the type $\{101\}$ and $\{110\}$ tend to become, and eventually do become, exactly equivalent. We may thus visualize the changes in the form of the Brillouin Zone as shown in fig. 3. The derived zone for the body-centred cube is the same as that established by wave-mechanical calculations ⁽³⁾.

It is therefore clear that the form of Brillouin Zone for the face-centred cube is the same as that for the body-centred tetragonal lattice of axial ratio $\sqrt{2}$, while the zone for the body-centred cube is of the same form as that for a face-centred tetragonal of axial ratio $\frac{1}{\sqrt{2}}$. There are clearly two electron states per atom in each of these zones, as in the case of the zone for the face-centred cube.

Fig. 3.



Body-centred tetragonal lattice, $c/a = \sqrt{2}$. Body-centred tetragonal lattice, $c/a < \sqrt{2}$ but > 1 . Body-centred cube.

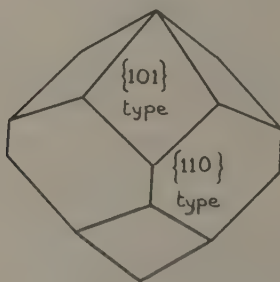
The changes in the form of the Brillouin Zone in passing from a body-centred tetragonal lattice of axial ratio $\sqrt{2}$ to a body-centred cube have been traced. We may continue the process through the stage of the body-centred cube in order to obtain the form of the zone for the body-centred tetragonal structure of axial ratio less than unity. The $\{002\}$ planes will clearly have disappeared from the zone structure; the slopes of the $\{110\}$ type of plane in the lattice and in the zone retain their character. The $\{101\}$ type of plane in the lattice, however, falls towards the horizontal, while the interplanar spacing decreases. In the zone, therefore, the $\{101\}$ type of plane becomes more horizontal and at the same time is displaced outwards from the origin. The result of these changes is shown in fig. 4.

It is evident that the Brillouin Zones for the body-centred and face-centred tetragonal lattices are intimately related in form. They may be visualized as undergoing exactly the same variations in form and shape

as the axial ratio varies, but with a lag between them. If the axial ratio for a body-centred tetragon is greater than $\sqrt{2}$ it is equivalent to a face-centred tetragon of axial ratio greater than 1, and the zones are the same in form. This conclusion is not surprising, since any face-centred tetragonal lattice, by simple rotation of the two equal axes through 45° , can be transformed into a body-centred tetragonal lattice with a unit cell of half the size.

The body-centred cubic structure is equivalent to a face-centred tetragonal lattice of axial ratio 0.707; this may be used to deduce the form of the Brillouin Zone for the white-tin structure. This structure belongs to the tetragonal system; there are four atoms in the unit cell with the basis $(0, 0, 0)$, $(\frac{1}{2}, \frac{1}{2}, \frac{1}{2})$, $(\frac{1}{2}, 0, \frac{1}{4})$, $(0, \frac{1}{2}, \frac{3}{4})$. It may be regarded as built up of two interpenetrating face-centred tetragonal lattices; if the basis of one of these lattices is $(0, 0, 0)$, $(0, \frac{1}{2}, \frac{1}{2})$, $(\frac{1}{2}, 0, \frac{1}{2})$, $(\frac{1}{2}, \frac{1}{2}, 0)$,

Fig. 4.



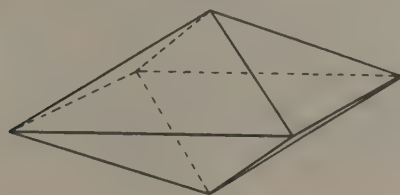
Brillouin Zone for body-centred tetragonal
structure of $c/a < 1$.

then that of the other is, relative to the first $(\frac{1}{4}, \frac{1}{4}, \frac{1}{4})$, $(\frac{1}{4}, \frac{3}{4}, \frac{3}{4})$, $(\frac{3}{4}, \frac{1}{4}, \frac{3}{4})$, $(\frac{3}{4}, \frac{3}{4}, \frac{1}{4})$. The Brillouin Zone for the white-tin structure may therefore be considered as similar to that for a face-centred tetragonal lattice of axial ratio less than $\sqrt{2}$, and therefore to that for a body-centred tetragonal lattice of axial ratio less than 1. The zone would at first sight be expected to take the form shown in fig. 4. The effect of the relative displacements of the two interpenetrating lattices, however, is to eliminate the X-ray reflexions from the $\{110\}$ planes. That is to say, the structure factor for planes of this type becomes zero; and since only planes for which the structure factor does not vanish can give rise to planes of energy-discontinuity in k -space, the $\{110\}$ type of plane must be absent from the zone. The Brillouin Zone for white-tin is therefore bounded by the planes of the type $\{101\}$, and its form is shown in fig. 5.

This zone may be shown to contain 4.24 electron states per atom. White-tin has four valency electrons per atom and is a conductor of electricity. It is probable, therefore, that there is a small overlap across each of the eight faces of the zone; this should be reflected in the properties of the metal and its solid solutions, and this will be discussed in later publications.

The diamond structure presents a problem similar to that of white-tin. The diamond lattice may be regarded as two interpenetrating face-centred cubic lattices, so that we might expect the form of the zone to be similar to that for the face-centred cube. The effect of the relative displacement of the two interpenetrating lattices, however, is to reduce the structure factor for the $\{200\}$ planes to zero. The zone bounded by the $\{111\}$ planes contains too few electron states per atom, and since the properties of diamond suggest that the structure corresponds with a completely filled zone, we have to find a system of planes enclosing a

Fig. 5.



Brillouin Zone for the white tin structure.

zone of four states per atom. Such a zone is bounded by the $\{220\}$ planes, so that the probable form of the zone for the diamond structure is the same as that for the body-centred cube.

The metal indium has a face-centred tetragonal structure of axial ratio 1.06, and the form of the corresponding zone should thus be intermediate between that for a face-centred cube and that for a body-centred cube. It will obviously be closely similar to the zone for the face-centred cube, but compressed vertically. Alternatively, it may be obtained from that of the body-centred cube by expanding the "c" axis of the lattice and compressing the "c" axis of the zone so that the $\{002\}$ planes appear as bounding planes of the zone again. The zone for the indium structure will contain two electron states per atom, so that there is a considerable overlap across all faces of the zone. The overlap across the $\{002\}$ planes will, however, exceed that across the four vertical faces owing to the shape of the zone, and this will lead to interesting solid solution effects, such as are met with in the system cadmium-indium ⁽⁴⁾.

Other and more complex metallic structures may be treated in a similar way. As an instance, we may consider the mercury structure. This metal has a simple rhombohedral lattice. At -46°C . the lattice constant is 2.999 \AA . with $\alpha=70^{\circ} 31.7'$. Although this cannot be referred directly to cubic axes, we may still obtain an idea of the form of the zone.

The face-centred cubic lattice may be considered as a simple rhombohedral lattice with $\alpha=60^{\circ}$, as shown in fig. 6. To put the basal plane of the rhombohedral lattice into the horizontal we must rotate the cube along

Fig. 6.

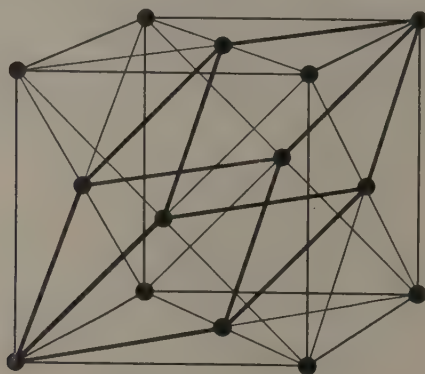
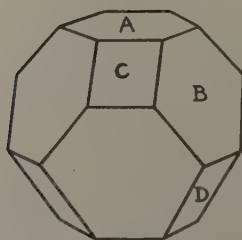


Fig. 7.

Zone for rhombohedral lattice, $\alpha=60^{\circ}$.

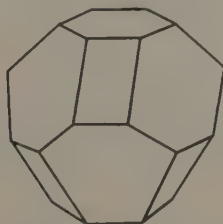
xy through an angle of 45° and then rotate the line xy about x in a vertical plane through an angle $\tan^{-1} \frac{1}{\sqrt{2}}$. Thus the Brillouin Zone for the rhombohedral lattice with $\alpha=60^{\circ}$ is the same as that for the face-centred cube, taken through the rotations described above (fig. 7). For the face-centred cube, A and B are planes of the type $\{111\}$, and C and D are planes of the type $\{200\}$. Referred to the rhombohedral lattice, A is of the type

$\{001\}$, C of the type $\{101\}$, and B of the type $\{111\}$. At the particular angle $\alpha=60^\circ$, $\{111\}_{\text{f.c.c.}} = \{001\}_{\text{rhomb.}}$ and $\{111\}_{\text{rhomb.}}$.

If now the angle α is increased, the slope of the $\{001\}$ pair of planes is unchanged, but they get farther apart in the lattice, and the zone is therefore compressed in the direction perpendicular to these planes. The $\{111\}$ and $\{101\}$ types of plane become more horizontal and the interplanar spacing in the lattice decreases. In the zone therefore these boundary planes become more horizontal and are displaced outwards from the origin of k -space. Thus the zone for mercury, with $\alpha=70^\circ 31'7''$, will take the form of fig. 8.

The number of electron states per atom in the rhombohedral zone is easily seen to be 2. The volume of the zone, when $\alpha=60^\circ$, is the same as that for the face-centred cube, since the planes and interplanar distances concerned are the same in both cases. Its value is $\frac{4}{a^3}$, where a is the cubic

Fig. 8.



Zone for the mercury structure.

lattice constant. The volume of the unit cell of the rhombohedral lattice outlined in fig. 6 is $\frac{a^3}{4}$, where a is the lattice constant of the parent face-centred cubic lattice. Since the rhombohedral cell contains one atom, the volume per atom is $\frac{a^3}{4}$, so that the number of electron states = 2 per atom.

It is suggested that, by the application of processes similar to those described above, the form or the approximate form of the Brillouin Zones for complex structures may be obtained, even in cases where rigid application of the more formal methods might lead to difficulties.

Acknowledgments.

The author expresses his gratitude to Professor C. N. Hinshelwood, F.R.S., for his kindness in providing laboratory accommodation, and to

the Department of Scientific and Industrial Research for a Senior Research Award. Grateful acknowledgment is also made to Dr. W. Hume-Rothery, F.R.S., and Professor N. F. Mott, F.R.S., for helpful comment.

References.

- (1) N. F. Mott and H. Jones, 'The Theory of the Properties of Metals and Alloys,' Oxford, 1936, chapter v.
- (2) N. F. Mott and H. Jones, *ibid.* p. 156.
- (3) N. F. Mott and H. Jones, *ibid.* p. 158.
- (4) W. Hume-Rothery and G. V. Raynor. (To be published.)

XV. *The Brillouin Zone for the Gallium Structure.*

By GEOFFREY VINCENT RAYNOR *.

[Received July 29, 1940.]

THE Brillouin Zones for the majority of the crystal structures met with in the study of metals and alloys have been satisfactorily worked out and correlated with the properties of the metals and intermetallic systems concerned.

The metals of subgroup III B of the periodic table are important from the point of view of the theory of alloy formation, particularly in the case of solid-solution formation in magnesium as solvent ⁽¹⁾. Of these metals, the Brillouin Zones for aluminium, indium and thallium have been established, but that for the more complex gallium structure has hitherto not been discussed.

The crystal structure of metallic gallium has been investigated by Laves ⁽²⁾ and by Bradley ⁽³⁾, with almost complete agreement. The later work of Bradley is to be preferred; according to this work, the gallium structure is orthorhombic, with 8 atoms in the unit cell. The dimensions of the unit cell are :—

$$a=4.5167 \text{ \AA.}$$

$$b=4.5107 \text{ \AA.}$$

$$c=7.6448 \text{ \AA.}$$

Two of the axes are therefore very nearly equal, and the structure is superficially similar to a tetragonal structure. The space group is V_h^{18} and the atomic coordinates are :

$$(m, 0, p), \quad (m+\frac{1}{2}, \frac{1}{2}, \bar{p}), \quad (\bar{m}+\frac{1}{2}, \frac{1}{2}, p), \quad (\bar{m}0\bar{p}),$$

$$(m, \frac{1}{2}, p+\frac{1}{2}), \quad (m+\frac{1}{2}, 0, \bar{p}+\frac{1}{2}), \quad (\bar{m}+\frac{1}{2}, 0, p+\frac{1}{2}), \quad (\bar{m}, \frac{1}{2}, \bar{p}+\frac{1}{2}),$$

where $m=0.0785 \pm 0.0005$ and $p=0.1525 \pm 0.0005$. Each atom has

1 neighbour at 2.437 Å.

2 neighbours at 2.706 Å.

* Communicated by Professor N. F. Mott, F.R.S.

2 neighbours at 2.736 Å.

and

2 neighbours at 2.795 Å.

The volume per atom is $\frac{abc}{8}$.

For further details of the structure reference should be made to the work of Laves and of Bradley. It will be sufficient here to indicate that the structure as a whole consists of deformed hexagonal rings, and is quite different from the more normal structures assumed by the other metals of group III B of the periodic table.

The Brillouin Zone for the gallium structure will thus be of a different character from those for aluminium, indium and thallium. This is reflected also in the physical and electrical properties of these metals. The specific resistances at 0° C. and at the characteristic temperature are shown in Table I.

TABLE I.

Metal.	Sp. res. at 0° C. (ohm-cm.).	Temp. coeff.	θ_D .	Sp. res. at θ_D (ohm-cm.).
Al.	2.41×10^{-6}	430×10^{-5}	390	3.62×10^{-6}
Ga	39.5×10^{-6}	396×10^{-5}	125	16.4×10^{-6}
In	8.2×10^{-6}	490×10^{-5}	106	1.5×10^{-6}
Tl	15.0×10^{-6}	518×10^{-5}	100	1.0×10^{-6}

It is therefore clear that, compared with aluminium, indium and thallium, gallium has an abnormally high electrical resistance. This may be interpreted as indicating that the number of effectively free electrons for gallium is less than for the other metals.

The temperature-coefficient of resistance for gallium is slightly low compared with those for the other metals.

It seems probable that these differences may be due to the differences in the electron energy distributions. The Brillouin Zones for aluminium, indium, and β -thallium contain two electron-states per atom, so that there must be a considerable overlap of electrons out of this first zone. The relatively high specific resistance of gallium would be explained by the overlap of relatively few electrons from a first Brillouin Zone containing roughly three electron states per atom. The slightly low temperature coefficient of resistance might then be attributed to the opposing effects of temperature increases in increasing thermal vibrations, but also slightly increasing the number of electrons available for conduction above the planes of energy discontinuity in k -space. Such effects

are in general more marked when the overlap of electrons is relatively small.

We are therefore interested in a Brillouin Zone containing roughly three electron states per atom for the gallium structure.

The structure-factor for the gallium structure has been given by Laves ⁽²⁾ as $S = \cos 2\pi(mh + pl) + \cos 2\pi[mh - pl + \frac{1}{2}(h+k)]$ and this expression accounts satisfactorily for the observed intensities of the lines in the X-ray diffraction patterns obtained. For the purposes of deriving the form of the Brillouin Zone, we have to consider planes of low indices which give rise to the most intense X-ray reflexions. For this particular structure, no X-ray reflexions are given by planes $(0kl)$ where k or l is odd, by planes $(hk0)$ where h or k is odd, or planes (hkl) where $(k+l)$ is odd. Of the remainder, the most intense lines in the observed diffraction pattern are derived from the planes :

- 002 line of medium intensity.
 $\left. \begin{matrix} 111 \\ 102 \end{matrix} \right\}$ composite line of high intensity.
 $\left. \begin{matrix} 200 \\ 020 \end{matrix} \right\}$ composite line of high intensity.
 113 line of highest intensity.

Planes of higher indices need not be considered, especially as they give rise to relatively much less intense lines.

In the orthorhombic structure, the interplanar spacings for a plane family with indices (h, k, l) may be written

$$d = \frac{1}{\sqrt{\frac{h^2}{a^2} + \frac{k^2}{b^2} + \frac{l^2}{c^2}}}.$$

The perpendicular distance from the origin of k -space of a plane $(n_1 n_2 n_3)$ in the Brillouin Zone may therefore be given as

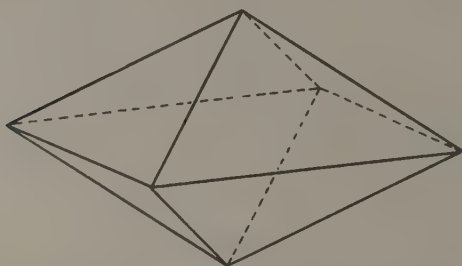
$$P n_1 n_2 n_3 = \frac{1}{2} \sqrt{\frac{n_1^2}{a^2} + \frac{n_2^2}{b^2} + \frac{n_3^2}{c^2}}.$$

Thus the zone which would be bounded by the planes of the type $\{200\}$, $\{020\}$, and $\{002\}$ would have the volume $\frac{8}{abc}$ and contain two electron states per atom. It is, in view of the electrical data, hardly to be considered as the important zone for the gallium structure, especially since the $\{002\}$ planes do not give rise to an intense reflexion,

The $\{113\}$ plane gives rise to a very strong reflexion, the line being almost as intense as the composite lines from the $\{111\}$ and $\{102\}$ planes.

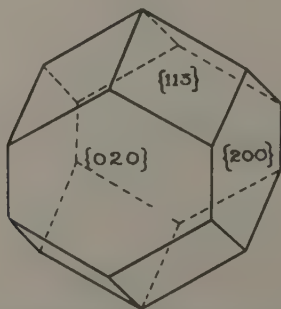
The zone bounded by $\{113\}$ type planes in k -space takes the form shown in fig. 1; the volume of this zone may be shown by the usual calculations to be such that the number of electron states per atom enclosed by the zone is 5.4. This zone may therefore be considered as a probable second Brillouin Zone for the gallium structure.

Fig. 1.

Zone bounded by planes of the type $\{113\}$.

We may now consider the zone bounded by planes of the type $\{113\}$, $\{200\}$, and $\{020\}$. All these planes give rise to intense low angle X-ray reflexions. The form of the zone bounded by these planes is shown in fig. 2.

Fig. 2.

Zone bounded by planes of the type $\{113\}$, $\{200\}$, and $\{020\}$.

Calculation of the volume of this zone shows that it can contain just three electrons per atom, and it is suggested, on the evidence of the electrical resistance data for gallium, that it constitutes the important zone for considerations of the properties of the metal.

The perpendicular distances of the planes of the zone from the origin of k -space are as follows :

$$P_{200} = \frac{1}{2} \sqrt{\frac{4}{a^2}} = \frac{1}{a} = 0.2214,$$

$$P_{020} = \frac{1}{2} \sqrt{\frac{4}{b^2}} = \frac{1}{b} = 0.2217,$$

$$P_{113} = \frac{1}{2} \sqrt{\frac{1}{a^2} + \frac{1}{b^2} + \frac{9}{c^2}} = 0.2510.$$

Since gallium is an electrical conductor, overlap of electrons must occur. We should expect this overlap to take place round the sides of the zone, that is, across the $\{020\}$ and $\{200\}$ faces, in preference to other points ; since not only does the Fermi-distribution sphere touch first at the side faces, but the energy gap should also be smallest here because the structure factor is smaller than for the $\{113\}$ planes.

It is therefore suggested that the first Brillouin Zone for the gallium structure is bounded by the planes $\{113\}$, $\{020\}$, and $\{200\}$ and can accommodate three electron states per atom. Overlap into the second zone probably occurs across the $\{020\}$ and $\{200\}$ faces of the first zone.

Acknowledgments.

The author is indebted to Professor C. N. Hinshelwood, F.R.S., for laboratory accommodation, and to Dr. W. Hume-Rothery, F.R.S., and Professor N. F. Mott, F.R.S., for helpful comment. Grateful acknowledgement is also made to the Department of Scientific and Industrial Research for a Senior Research Award.

References.

- (1) W. Hume-Rothery and G. V. Raynor, *J. Inst. Metals*, lxiii. p. 227 (1938).
- (2) F. Laves, *Zeit. Kristallographie*, lxxxiv. p. 256 (1933).
- (3) A. J. Bradley, *Zeit. Kristallographie*, xci. p. 302 (1935).

XVI. *On Turbulent Liquid Motion Outside a Circular Boundary.*—II.

By MANOHAR RAY, Lahore, India *.

[Received July 18, 1939.]

1. *Introduction.*

IN a previous paper †, the problem of turbulent motion of an otherwise uniform stream in the neighbourhood of a circular boundary has been discussed from the point of view of "vorticity transport" theory of Taylor. The starting-point was the Taylor-Goldstein Equations, which were transformed into forms suitable for treatment of motion near a circular boundary. A solution was obtained in that paper by successive approximations, and it was also pointed out that the approximation must necessarily be restricted to regions very near the boundary. Since then it has been possible to reconstruct an almost correct solution numerically even of the complicated exact differential equation describing the motion. In the previous paper only an approximate form of the complicated equation was taken. The initial values required to start the numerical integration have been supplied by the approximation solutions very close to the boundary obtained in the previous paper. The construction of the velocity field and the stream lines near the circular boundary shows some important features of the motion. The motion in the neighbourhood of the boundary is retrograde, which gradually changes into direct motion at a distance from the circular wall equal to about a third of the radius of the circular boundary. On this circle the velocity is entirely radial. The velocity perpendicular to the wall near any part possesses a maximum which is attained within a distance not exceeding about a quarter of the radius of the circular boundary. The present investigation does not extend to the region where the wake is formed. The nature of the stream lines is shown in fig. 4.

Section 2 is a recapitulation of the first part of the previous paper giving all the necessary equations of motion.

2. *Field Equations and their Applications to a Circular Boundary.*

The field equations suitable for treatment near a circular boundary have been obtained from Taylor's generalized equations of the mean

* Communicated by the Author.

† Phil. Mag. xxviii. p. 231 (1939).

motion with Goldstein's modifications. If the vector \mathbf{V} represent the mean velocity with components (u, v, w) , the vector \mathbf{V}' the eddy velocity with components (u', v', w') , $\hat{\omega}$ the mean vorticity with components (ξ, η, ζ) , $\hat{\omega}'$ the eddy vorticity with components (ξ', η', ζ') , \mathbf{F} the external force acting on the fluid per unit mass, p the mean pressure, and ρ the density of the fluid, then the vector equation of the mean motion given by Taylor is

$$\text{grad } \frac{1}{2} V^2 - \mathbf{V} \times \hat{\omega} = \mathbf{F} - \text{grad} \left(\frac{p}{\rho} + \frac{1}{2} V'^2 \right) + \mathbf{V}' \times \hat{\omega}'. \quad (1)$$

Further, we have

$$\hat{\omega} = \text{curl } \mathbf{V}, \quad \hat{\omega}' = \text{curl } \mathbf{V}', \quad (2)$$

and Goldstein has shown that

$$\hat{\omega}' = \text{curl } \mathbf{L} \times \hat{\omega}, \quad \text{div } \mathbf{L} = 0; \quad (3)$$

where \mathbf{L} is the vector mixture length with components L_1, L_2, L_3 .

The above equations can easily be transformed into equations suitable for a curved boundary. Outside the boundary motion is evidently two-dimensional and $\hat{\omega}$ has only one component ζ . If we measure x -coordinate along the arc of the cross-section of the cylinder and y -coordinate along the normal to the curve of the section and take $r(x)$ to be the radius of curvature, then the x -component of $\mathbf{V}' \times \hat{\omega}'$ or $\mathbf{V}' \times \zeta'$ in (1) becomes

$$-L_1 v' \frac{r}{(r+y)^3} u \frac{dr}{dx} + L_2 v' \left(\frac{\partial^2 u}{\partial y^2} + \frac{1}{r+y} \frac{\partial u}{\partial y} - \frac{u}{(r+y)^2} \right).$$

In arriving at the above result the usual assumption that $\frac{\partial u}{\partial x}, \frac{\partial v}{\partial x}, \frac{\partial v}{\partial y}$ are small compared with $\frac{\partial u}{\partial y}$ has been used.

Assuming, as is usual in turbulent theory, that the gradient of $\left(\frac{p}{\rho} + \frac{1}{2} V'^2 \right)$ may be neglected for first approximation and the fluid is free from body forces, then the x -equation of motion takes the following form :

$$\begin{aligned} \frac{r}{r+y} u \frac{\partial u}{\partial x} + v \frac{\partial u}{\partial y} + \frac{uv}{r+y} \\ = -L_2 v' \frac{r}{(r+y)^3} u \frac{dr}{dx} + L_2 v' \left(\frac{\partial^2 u}{\partial y^2} + \frac{1}{r+y} \frac{\partial u}{\partial y} - \frac{u}{(r+y)^2} \right). \end{aligned} \quad (4)$$

Applying this result to the case of an infinite circular cylinder of radius r , the x -equation of motion is

$$\frac{r}{r+y} u \frac{\partial u}{\partial x} + v \frac{\partial u}{\partial y} + \frac{uv}{r+y} = L_2 v' \left(\frac{\partial^2 u}{\partial h^2} + \frac{1}{r+y} \frac{\partial u}{\partial y} - \frac{u}{(r+y)^2} \right). \quad (5)$$

Further, we have the equation of continuity as

$$\frac{\partial u}{\partial x} + \frac{\partial}{\partial y} \left(\frac{r+y}{r} v \right) = 0. \quad (6)$$

We make the usual assumption of Prandtl for the mixture length and we put

$$\overline{L_2 v'} = -l^2 \frac{\partial u}{\partial y}. \quad (7)$$

Equation (5) then becomes

$$\frac{r}{r+y} u \frac{\partial u}{\partial x} + v \frac{\partial u}{\partial y} + \frac{uv}{r+y} = -l^2 \frac{\partial u}{\partial y} \left(\frac{\partial^2 u}{\partial y^2} + \frac{1}{r+y} \frac{\partial u}{\partial y} - \frac{u}{(r+y)^2} \right). \quad (8)$$

This is the final equation of motion we have to tackle. It involves, in addition to the velocity components, the mixture length l , which is a function of y .

3. *Reduction to an Ordinary Differential Equation.*

We shall now attempt to find the solution of equations (8) and (6) for the turbulent motion set up in a stream past a fixed infinite circular cylinder. First we write the equations in terms of dimensionless quantities by the substitutions,

$$x/r = \xi, \quad y/r = \eta, \quad l/r = l',$$

and

$$u = U u_1, \quad v = U v_1,$$

where U is the velocity of the undisturbed stream.

Equations (8) and (6) now become

$$\frac{1}{1+\eta} u_1 \frac{\partial u_1}{\partial \xi} + v_1 \frac{\partial u_1}{\partial \eta} + \frac{u_1 v_1}{1+\eta} = -l'^2 \frac{\partial u_1}{\partial \eta} \left[\frac{\partial u_1}{\partial \eta^2} + \frac{1}{1+\eta} \frac{\partial u_1}{\partial \eta} - \frac{u_1}{(1+\eta)^2} \right]. \quad (9)$$

and

$$\frac{\partial u_1}{\partial \xi} + \frac{\partial}{\partial \eta} \{ (1+\eta) v_1 \} = 0. \quad (10)$$

To solve these equations we introduce a function ψ_1 such that

$$u_1 = \frac{\partial \psi_1}{\partial \eta}, \quad (1+\eta) v_1 = -\frac{\partial \psi_1}{\partial \xi}. \quad (11)$$

which satisfies equation (10).

On substitution in (9) we obtain an equation for ψ_1 as follows :

$$\begin{aligned} & \left(\frac{1}{1+\eta} \right) \frac{\partial \psi_1}{\partial \eta} \cdot \frac{\partial^2 \psi_1}{\partial \xi \partial \eta} - \left(\frac{1}{1+\eta} \right) \frac{\partial \psi_1}{\partial \xi} \frac{\partial^2 \psi_1}{\partial \eta^2} - \left(\frac{1}{1+\eta} \right)^2 \frac{\partial \psi_1}{\partial \xi} \frac{\partial \psi_1}{\partial \eta} \\ & = -l'^2 \frac{\partial^2 \psi_1}{\partial \eta^2} \left[\frac{\partial^2 \psi_1}{\partial \eta^2} + \left(\frac{1}{1+\eta} \right) \frac{\partial^2 \psi_1}{\partial \eta^2} - \left(\frac{1}{1+\eta} \right)^2 \frac{\partial \psi_1}{\partial \eta} \right]. \quad (12) \end{aligned}$$

To solve this we use the substitutions

$$l'^2 = \eta^2 f_1(\eta) \cot \xi, \quad . \quad . \quad . \quad . \quad . \quad . \quad (13)$$

and
$$\psi_1 = F(\eta) \sin \xi, \quad . \quad . \quad . \quad . \quad . \quad . \quad (14)$$

so that
$$u_1 = F'(\eta) \sin \xi, \quad v_1 = -\frac{F(\eta)}{1+\eta} \cos \xi, \quad . \quad . \quad . \quad . \quad . \quad . \quad (15)$$

where a prime denotes differentiation with respect to η , and $f_1(\eta)$ is as yet an unspecified function of η . The sine and cosine functions of ξ in the above solution are to be compared with similar functions in the pure potential motion near a circular cylinder (ξ in this case is the same as the usual angular coordinate θ). Equation (12) now takes the form

$$(1+\eta)(F'^2 - FF'') - FF' = -\eta^2 f_1(\eta) F'' [(1+\eta)^2 F''' + (1+\eta)F'' - F']. \quad (16)$$

This is an ordinary differential equation in F and η . It is non-linear and of complicated structure. We note the equation still involves the function $f_1(\eta)$. Equation (16) will give us the velocity distribution within the turbulent layer.

The conditions to be satisfied at the circular boundary are

$$\frac{\partial u}{\partial y} = \infty \text{ and } v=0, \text{ i. e., } F'' = \infty \text{ and } F=0 \text{ for } \eta=0.$$

u , consequently F' , may be, however, finite or negatively infinite, as is also the case in the problem of the plate. To find a solution of the equation (16) which will give the necessary fit on the circular boundary, we have to choose the function $f_1(\eta)$ suitably, as is going to be done presently.

4. Solution of the Differential Equation.

It has not been possible to obtain an analytical solution of (16). We shall solve the equation numerically. But to start the solution we need initial values, and the initial values at the circular boundary involve infinities which are unsuitable for numerical work. We have thus to obtain at first an analytical solution which will be valid somewhere, say very near the boundary.

For $\eta \ll 1$, equation (16) takes the form

$$F'^2 - FF'' - FF' = -\eta^2 f_1(\eta) F'' (F''' + F'' - F'). \quad . \quad . \quad . \quad (17)$$

The function $f_1(\eta)$ has been chosen subject to the boundary conditions as

$$f_1(\eta) = \eta (\log \eta)^2. \quad . \quad . \quad . \quad . \quad . \quad . \quad (18)$$

Approximation solutions of the equation (17) with $f_1(\eta)$ as given in (18) have been found in the previous paper by means of successive approximations. The first approximation solution is

$$F' = A(\log \eta + 0.5), \quad . \quad . \quad . \quad . \quad . \quad . \quad (19)$$

and the second approximation solution is

$$F' = A \left(\log \eta + 0.5 - \frac{0.1875}{\log \eta} \right). \quad \dots \dots \dots (20)$$

The approximations (19) and (20) are used one after another to start the numerical integration.

In the first case for $\eta \ll 1$, taking $A=1$, we use

$$\left. \begin{aligned} F' &= \log \eta + 0.5, \\ F &= \eta (\log \eta - 0.5), \\ F'' &= \frac{1}{\eta}, \\ F''' &= -\frac{1}{\eta^2}. \end{aligned} \right\} \quad \dots \dots \dots (21)$$

If we calculate the values of these functions at $\eta=0.01$, and find the contributions of the separate terms in equation (17), we find the result quite satisfactory. For instance, at $\eta=0.01$,

$$F = -0.511, \quad F' = -4.1052, \quad F'' = 10^2, \quad F''' = -10^4, \quad \dots (22)$$

which when substituted in equation (17), namely,

$$F'^2 + \eta^3 (\log \eta)^2 F'' F''' = F F'' + F F' - \eta^3 (\log \eta)^2 F'' (F'' - F'), \quad \dots (17)$$

give $16.8 - 21.2 \simeq -5.1 + 21.22.$

The error is less than 3 per cent. of the highest term in (17).

With these initial values (22) at $\eta=0.01$, we started solution of equation (17) by means of numerical integration, applying Adam's method. There was a difficulty. F'' rapidly diminished and changed sign through zero while F''' tended to increase indefinitely for about $\eta=0.04$. The first approximation (21) was abandoned. We next started solution for a slightly higher value of η by the second approximation. As the boundary layer has been neglected too near the boundary the solutions are not of any consequence.

Next we tried the approximation (20), namely,

$$\left. \begin{aligned} F' &= \log \eta + 0.5 - \frac{0.1875}{\log \eta}, \\ F &= \eta (\log \eta - 0.5) - 0.1875 \int_0^\eta \frac{d\eta}{\log \eta}. \end{aligned} \right\} \quad \dots \dots \dots (23)$$

Calculating F, F', F'', F''' from (23) at $\eta=0.05$, we get *

$$F = -0.1723, \quad F' = -2.443, \quad F'' = 20.418, \quad F''' = -402.8, \quad (24)$$

* For the logarithmic integral 'Funktionstafeln' (Jahnke-Emde), pp. 79-86, was used.

and substituting these values in equation (17) the error is found to be of the order of about 3.5 per cent. of the highest term in (17).

Thus (23) can be used for starting a solution of our equation at $\eta=0.05$ with the initial values as given in (24). The numerical integration of (17) was carried out with these initial values, and the results up to $\eta=0.1$ are given in Table I. (a).

With the values thus obtained at $\eta=0.1$ we started solving our exact equation (16) with $f_1(\eta)$ as given in (18). The results of this calculation from $\eta=0.1$ are also given in the subsequent parts of Table I. (b).

TABLE I. (a).

$\eta=$	·05.	·06.	·07.	·08	·09.	·10.
$u/U \sin \xi = F'(\eta)$	-2.433	-2.247	-2.091	-1.936	-1.808	-1.683
$v/U \cos \xi = -F(\eta)$	0.172	0.196	0.217	0.237	0.256	0.26

5. Discussion of the Velocity Field.

The velocities in the turbulent field are given by

$$u = U \sin \xi \cdot F'(\eta), \quad v = -\frac{U}{1+\eta} \cos \xi \cdot F(\eta). \quad \dots \quad (25)$$

It may be noticed that the solution (u, v) may contain an arbitrary constant factor (which determines the scale) which can be found only by comparison with experimental results. Here the scale will be supposed to be so adjusted as to make this factor equal to one.

From Table I. it is evident that near the circular boundary the motion is retrograde, $F'(\eta)$ being negative. On any radius for about $\eta=0.3$, u vanishes. If we draw a concentric circular arc at distance from the circular boundary about 30 per cent. of the radius of the circle, u will vanish at every point of this circle and the velocity there will be radial. Beyond this circle the u -velocity will be direct and the stream-lines will bend back on the above circle $\eta=0.3$, and follow the forward direction as in the case of potential motion. The curves $u/U \sin \xi = F'(\eta)$ and $v/U \cos \xi = -\frac{F(\eta)}{1+\eta}$ have been drawn in figs. (1) and (2). The drawing of the stream-lines involves some calculations. If ψ be the stream function

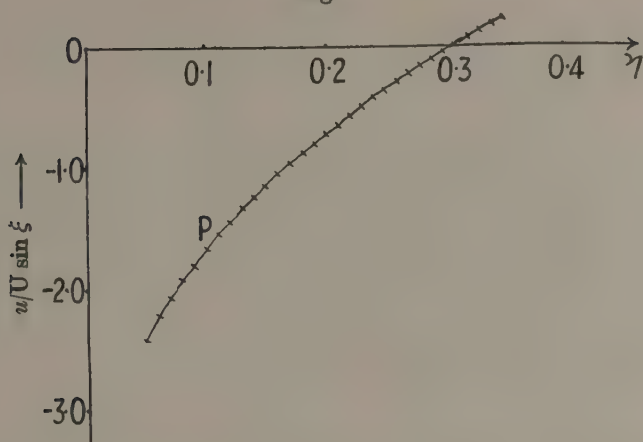
$$u_1 = \frac{\partial \psi}{\partial \eta} \quad \text{and} \quad v_1 = -\frac{\partial \psi}{\partial \xi} \quad \dots \quad (26)$$

TABLE I. (b).

$\eta =$	0.11.	0.12.	0.13.	0.14.	0.15.	0.16.	0.17.	0.18.	0.19.	0.2.	0.21.	0.22.	0.23.
$u/U \sin \xi = F'(\eta) =$	-1.568	-1.456	-1.348	-1.257	-1.16	-1.069	-0.98	-0.895	-0.815	-0.725	-0.652	-0.577	-0.504
$v/U \cos \xi = -\frac{F(\eta)}{1+\eta}$	0.262	0.273	0.283	0.292	0.3	0.307	0.313	0.318	0.323	0.327	0.329	0.332	0.333

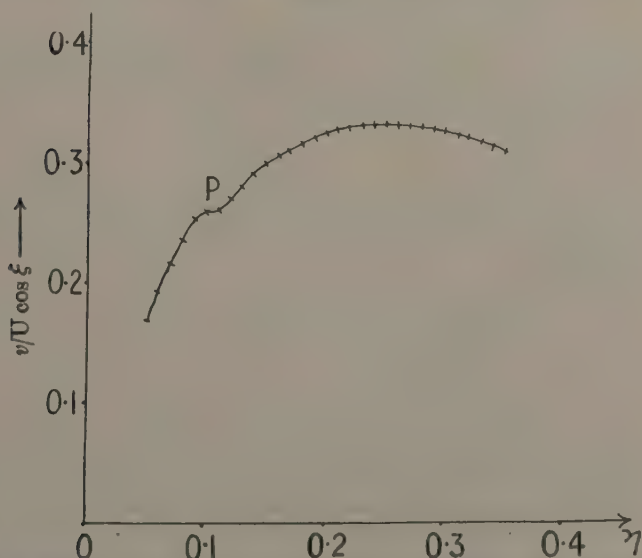
$\eta =$	0.24.	0.25.	0.26.	0.27.	0.28.	0.29.	0.3.	0.31.	0.32.	0.33.	0.34.	0.35.
$u/U \sin \xi = F'(\eta) =$	-0.432	-0.363	-0.296	-0.231	-0.166	-0.103	-0.043	+0.017	0.076	0.134	0.19	0.246
$v/U \cos \xi = -\frac{F(\eta)}{1+\eta}$	0.334	0.335	0.334	0.334	0.333	0.33	0.329	0.326	0.324	0.32	0.317	0.312

Fig. 1.



Shows the profile of the velocity parallel to the circular wall along a radius. The negative ordinates indicate a retrograde velocity which changes to direct velocity at $\eta=0.3$. The curve shows that for the larger values of η the rise is nearly straight. There is no kink in the u -curve at P here.

Fig. 2.



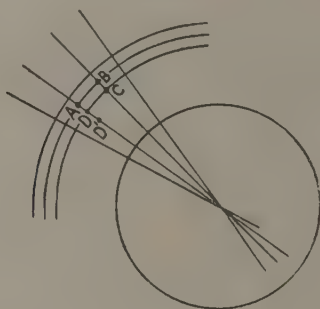
Shows the profile of the radial velocity along radius in the turbulent layer. There is a maximum for about $\eta=0.25$, η being the ratio of the distance of the point from the circular boundary to the radius of the circle. P indicates the point where the two solutions were patched up. The kink is due to rapid change of v at that region.

Hence
$$\frac{\partial \psi}{\partial \eta} = \frac{\partial \psi_1}{\partial \eta} \dots \dots \dots (27 a)$$

and
$$\frac{\partial}{\partial \xi} \{(1+\eta)\psi\} = \frac{\partial \psi_1}{\partial \xi} \dots \dots \dots (27 b)$$

To find the stream-lines we first find the ψ_1 values for each corner of the elementary rectangles formed by the lines $\xi = \text{const.}$ and circles $\eta = \text{const.}$ This can be done directly from equation (14). At each corner of an elementary rectangle the corresponding ψ_1 value is written down. Take any arbitrary corner A and assume $\psi = \psi_1$ at A. Then since $\frac{\partial \psi}{\partial \eta} = \frac{\partial \psi_1}{\partial \eta}$ and ψ and ψ_1 agree at A, they will also agree in value at all points on the radius ADD' . . . , i. e., at D, D' . . . etc.

Fig. 3.



ψ_1 value at B has been found out. But owing to (27 b) the difference in ψ_1 values at B and A = the difference between $(1+\eta)\psi$ values at these two points, so that

$$(1+\eta)[\psi(B) - \psi(A)] = \psi_1(B) - \psi_1(A).$$

This gives ψ at B. Again by (27 a)

$$\psi_1(C) - \psi_1(B) = \psi(C) - \psi(B)$$

which will give ψ at C. In this manner ψ values may be written down for every corner of the elementary rectangles. From this the approximate $\psi = \text{const.}$ curves may be drawn. The results of actual numerical calculations are recorded in the tables and figures given below. By the method described above the curves $\psi = \text{const.}$ are plotted and actually shown in fig. 4. Table II. also shows the points through which the curves $\psi = -.14, -.2, -.32$ and their reflexions pass. The two values of η for the same ξ are the two points through which the ψ -curve passes before

TABLE II.

	$\psi = -.14.$					$\psi = -.2.$					$\psi = -.32.$				
$\xi =$	20°	30°	40°	50°		30°	40°	50°	60°	70°	80°	90°			
$\eta =$.25	.11	.075	.06		.25	.14	.1	.08	.075	.07	.065	.25	.18	.155
$\eta =$.34					.35							.35		

TABLE III.

	$u/U = -.362.$					$u/U = -.841.$					$u/U = -1.22.$				
$\xi =$	10°	20°	30°	45°	60°	90°	20°	30°	45°	60°	90°	20°	30°	45°	60°
$\eta =$.07	.16	.2	.23	.24	.25	.05	.1	.14	.17	.19	.01	.05	.1	.12

and after crossing the line $u=0$. Only one such pair has been shown for each ψ -curve.

Fig. 4.

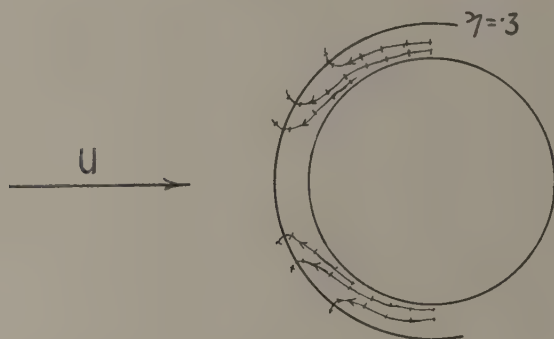


Fig. 5.

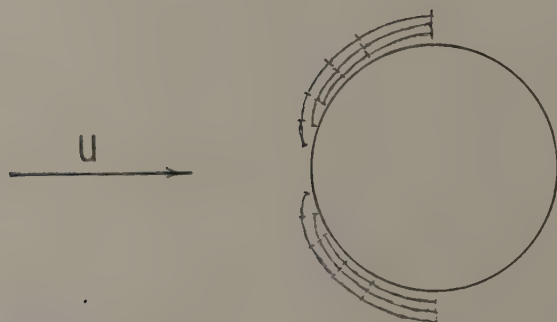


Fig. 6.



The distribution of velocity components (u, v) at points on the same radius are, in fact, shown in figs. 1 and 2. To obtain an idea how u and v

vary in the field, the curves $u=\text{const.}$ and $v=\text{const.}$ are shown in figs. 5 and 6. Tables III. and IV. also show the points through which these curves pass.

TABLE IV.

	$v/U=.086.$				$v/U=.13.$				$v/U=.284.$		
$\xi=$	20°	30°	45°	60°	20°	30°	45°	60°	10°	20°	30°
$\eta=$.02	.025	.03	.05	.03	.04	.05	.1	.14	.15	.2

In conclusion, I want to express my thanks to Prof. N. R. Sen of the Calcutta University for his kind help in this work.

Forman Christian College,
Lahore, India.

XVII. *Latent Energy and Dissociation in Flame Gases.*

By W. T. DAVID, A. S. LEAH, and B. PUGH *.

[Received May 31, 1940.]

THE gases remaining after flame has spread through an inflammable gaseous mixture are not just hot normal gases. The view has been put forward † that they contain a considerable latent energy which, in the absence of surface, persists for a long time and which varies in amount with the initial conditions of the mixture before combustion. The latent energy probably resides in a proportion of the tri-atomic molecules formed during combustion as an excess of intra-molecular energy which cannot be handed on to the translational degrees of freedom. The experimental evidence, collected over a period of years, will be briefly reviewed in Part I. of this paper—the attention being confined to mixtures of carbon monoxide and air, for our experiments have for the most part been made with these mixtures.

In Part II. experiments are described which show that there is a much larger dissociation in flame gases than in normal gases of the same composition under similar conditions of temperature and pressure. This would appear to result from the excess of intra-molecular energy in the tri-atomic molecules, and, indeed, the experiments indicate that the extent of the abnormal dissociation varies with the latent energy.

PART I.

Latent Energy in Explosion Flame Gases.

The experiments to be described were made with three spherical vessels of 3 inches, 6 inches, and 17.45 inches internal diameter. Inflammable gaseous mixtures were introduced into these vessels and were electrically ignited by means of a centrally placed spark gap. Arrangements were made to take continuous records of the pressures developed in the vessels during explosion and subsequent cooling, and at the same time continuous measurements of heat-loss to the vessel walls were made by means of bolometers mounted in various positions in the vessel walls.

* Communicated by the Authors.

† David, Phil. Mag. xxiii. p. 315 (1937), and previous papers referred to therein.

The arrangements were described by David, Brown, and El Din *, but improvements have been made in the apparatus and method of calibrating. One of the improvements made may be mentioned. Lewis and von Elbe † criticized the work of David, Brown and El Din because a small pocket was left under the indicator diaphragm in the 6-inch explosion vessel. In the present experiments this has been eliminated, but it may be stated that the pocket makes very little difference to the pressures developed, and the work of David, Brown and El Din has been confirmed in respect of carbon monoxide air explosions, to which attention is confined in this paper.

The maximum pressures developed after explosion (corrected for measured heat-loss) in the three vessels when the inflammable mixtures introduced into the vessels consisted of 50 per cent. of CO ‡ and 50 per

TABLE I.

	3-inch vessel.	6-inch vessel.	18-inch vessel.
Max. explosion pressure (lb. per sq. in. abs.), allowing for measured heat-loss.	103.1	104.8	106.7
Ideal explosion pressure (lb. per sq. in. abs.).	109.6	109.6	109.6
Combustion level (per cent. heat of combustion).	92.5	94.0	96.3
Latent energy (per cent. heat of combustion).	7.5	6.0	3.7

cent. of air at atmospheric pressure are shown in Table I. This over-rich mixture has been selected for preliminary study, for on combustion it results in flame gases in which dissociation is small §, and the experi-

* Phil. Mag. xiv. p. 764 (1932).

† J. Chem. Phys. ii. p. 659 (1934). These authors also claim (Phil. Mag. ser. 7, xxxi. p. 44 (1935)) that the measured pressures of David and Leah (Phil. Mag. ser. 7, xviii. p. 307 (1934)) are greater than the ideal pressures, but they are in error in comparing measured pressures at 3 atmospheres initial pressure with ideal pressures calculated for 1 atmosphere initial pressure.

‡ One per cent. H₂ was included in the CO in the explosion experiments.

§ It should be stated that in the calculations shown in Table I. the effects of all dissociation (which, as has been stated, are small) have been allowed for. These dissociations include $2\text{CO} + \text{O}_2 \rightleftharpoons 2\text{CO}_2$, $2\text{OH} + \text{H}_2 \rightleftharpoons 2\text{H}_2\text{O}$, $\text{CO} + \text{H}_2\text{O} \rightleftharpoons \text{CO}_2 + \text{H}_2$, $2\text{H} \rightleftharpoons \text{H}_2$, $2\text{O} \rightleftharpoons \text{O}_2$, $2\text{N} \rightleftharpoons \text{N}_2$, and $2\text{NO} \rightleftharpoons \text{N}_2 + \text{O}_2$.

mental results therefore lend themselves to fairly simple discussion. Other-mixture strengths will be dealt with later in the paper.

The ideal explosion pressures shown in Table I. have been calculated upon the basis of spectroscopic specific heats and equilibrium data and the heat of combustion of the CO-air mixtures. The observed pressures have been corrected for measured heat-loss from the flame gases. (The heat-loss from the flame gases amounts to 2·6 per cent., 2·4 per cent., and 1·8 per cent. of the heat of combustion up to the moment of attainment of maximum pressure in the 3-inch, 6-inch, and the 17·45-inch vessels respectively.)

It has been shown that equilibrium conditions have been attained at the moment of maximum pressure, for there is no further evolution of energy *. The defect of the explosion pressure (corrected for heat-loss) below the ideal therefore indicates that a long-lived latent energy resides in the flame gases after combustion—probably, as has been stated, as an excess of internal energy within a proportion of the newly formed CO₂ molecules. The amount of the latent energy expressed as a percentage of the heat of combustion of the inflammable mixture is shown in the last line of the table. The latent energy is equal to 100 *minus* the combustion level shown in the previous line, the combustion level being the energy which can be accounted for, that is, the sum of the internal energy based upon spectroscopic specific heats, the measured heat-loss and the heat of dissociation assuming the flame gases to be normal gases, expressed as a percentage of the heat of combustion.

It will be seen from Table I. that the latent energy averaged over the whole of the exploded gases increases as the size of the vessel decreases. The latent energy amounts to as much as 7·5 per cent. of the heat of combustion in the smallest vessel. Platinum thermometry measurements during the pre-pressure period † show that in the gases first burnt after the passage of the igniting spark it is still greater, being of the order of 15 per cent. To some extent this much larger latent energy in the flame gases resulting from the pre-pressure period combustion is due to the fact that the combustion during this period takes place at a much lower pressure (*viz.* 1 atmosphere) than the mean pressure (*viz.* about 4 atmospheres) at which combustion takes place during explosion, for experiment has shown that the latent energy decreases considerably as the pressure at which combustion takes place increases ‡. At a pressure of 4 atmospheres the latent energy in the flame gases during the pre-

* Phil. Mag. xxiii. p. 350 (1937).

† David and Jordan, Phil. Mag. xvii. p. 172 (1934).

‡ David and Jordan, Phil. Mag. xvii. p. 172 (1934), and David and Leah, Phil. Mag. xxii. p. 513 (1936).

pressure period combustion amounts to about 10 per cent., which is still larger than that measured in the explosions.

In order to account for these results it is necessary to postulate that the latent energy left in flame gases decreases with the distance of travel of the flame front from the igniting source, and this suggestion fits in satisfactorily with other experiments, which will now be reviewed.

Temperature Gradient in Long Tube Explosions.

Experiments of a kind similar to those just described were carried out in a long steel tube (50 feet in length) of 2 in. diameter into which an inflammable mixture was introduced. The mixture was ignited by means of an electric spark in the centre of the closed end of the tube and the temperatures attained by fine platinum-rhodium wires (0.0005 in. diameter) placed centrally in the tube at various distances from the spark were recorded.

In all cases during the major part of the 50 feet run of flame the wires recorded much the same temperature in all positions, this temperature

TABLE II.

Distance from spark, in inches	1½	8	9
Wire temperature, ° C.	1570	1750	1810

not being far removed from the ideal value. Very close to the spark, however, the temperature recorded was about the same value as found in constant-pressure explosion experiments. Within the first 9 in. or so of the spark the temperature increased considerably, as is shown in Table II.

It will be obvious that the latent energy must therefore be decreasing as the flame moves outwards from the spark, ultimately becoming small, and remaining so for the remainder of the flame travel.

Vivid demonstration of the increase of flame-gas temperature with distance of flame travel is to be found in the photographic records of flame travel in long open-ended tube explosions. One such record, taken by Bone and Frazer*, is shown in fig. 1 (a). It will be seen that the intensity of the luminosity, not only from the flame front but also from the flame gases left behind the flame front, increases with distance of flame travel.

* Phil. Trans. Roy. Soc. A, cccxxx. p. 363 (1931).

*Reasons for Variation in Latent Energy with
Distance of Flame Travel.*

It is well known that in long tube explosions the instantaneous pressure in the flame front increases with distance of flame travel, and this would appear to be the reason, or one of the reasons, why the latent energy in the flame gases left behind the flame front decreases with distance of flame travel, for, as has been previously stated, thermometry during the pre-pressure period shows an increasing temperature, and, therefore, a decreasing latent energy, in the flame gases as the pressure at which they are burnt increases. Strong support for this view may be obtained

Fig. 1.



from an examination of the Bone and Frazer flame record shown in fig. 1(b). In the experiment to which this record relates the instantaneous pressure in the flame front was artificially increased after a short distance of travel by a shock wave. It will be noted that a sudden and great increase in the intensity of the luminosity of the gases left behind the flame front results. This suggests that their temperature has greatly increased and the latent energy therefore greatly decreased.

There is also another factor which probably has a bearing upon the decrease in latent energy with distance of flame travel. Experiments with an explosion vessel in which a fan was mounted show that the rate of flame propagation during the pre-pressure period was not influenced at all by the most violent turbulence which could be produced by the

running fan, though subsequently the rate of flame propagation was greatly speeded up by turbulence *. This suggests that during the pre-pressure period the method of flame propagation is entirely by chain-reaction mechanism, and that subsequently the flame propagation was thermally assisted, owing to conduction and radiation from the high-pressure high-temperature flame front into the unburnt mixture adjacent to it. It will be clear that turbulence would produce irregularities in the thin high-pressure flame front, thus increasing the volume of heated adjacent unburnt mixture and therefore the rate of combustion.

Latent Energy in Open-flame Gases.

In open flames the propagation of the flame front against the flowing inflammable mixture is thermally assisted, and the combustion corresponds to that in long-tube explosions after some distance of flame travel. A higher temperature is therefore to be expected in the flame gases from open flames than in those resulting from pre-pressure period combustion.

Large numbers of measurements by the sodium-line reversal method of the temperatures of the flame gases from open flames of inflammable mixtures of various strengths have been made by different observers. These temperatures for weak and for over-rich mixtures are in general much too high—indeed, they are frequently greater than the ideally calculated temperatures. This is partly due, in the case of over-rich mixtures, as was pointed out by Bauer †, to the fact that the flames were totally coloured. But the temperatures are still sometimes in excess of the calculated even when the central portion only of the flames is coloured, and it would seem to us that the explanation of the high temperatures in both weak and over-rich mixtures is largely due to imperfect mixing of the inflammable gases before combustion takes place ‡. It will be clear that portions of a heterogeneous mixture would have a higher heat of reaction than that averaged over the whole, and these portions after combustion would make large, and sometimes dominating, contributions to the luminosity of the flame gases. It is hoped shortly to make sodium and platinum temperature measurements in open flame gases resulting from the combustion of inflammable mixtures previously perfectly mixed in a large tank.

In the case of combustible gas-air mixtures of strength not much greater than that of the combining proportions mixture the influence of imperfect mixing will not be great since this is the maximum tempera-

* 'The Engineer,' December 31st, p. 733 (1937).

† *Ann. de Chim. et Phys.* xxix. p. 44 (1913).

‡ 'Engineering,' March 8th, 1940, p. 241.

ture mixture, and the attention will be confined in what follows to the sodium temperatures measured in such mixtures.

The highest sodium temperatures measured in the flame gases from CO-air mixtures at a point along the axis of the flame gases a little above the inner cone, by which time equilibrium has been established, are those by Loomis and Perrot. For a 36 per cent. CO mixture the sodium temperature was 1960°C. , which is about 130°C. below the theoretically calculated temperature after making full allowance for radiation loss from the flame gases.

It seems probable to us that the sodium temperatures are higher than those corresponding to the mean molecular translational energy of the flame gases. for the excited CO_2 molecules may communicate their excess energy to the sodium atoms, but even taking them as giving a measure of the mean molecular translational energy the latent energy in the 36 per cent. CO-air flame gases is between 7 and 10 per cent. of the heat of combustion. A closer calculation of the latent energy in the flame gases is not possible because of the uncertainty of the amount of dissociation in them.

As hydrogen is added to the CO-air mixture in replacement of CO the defect of the sodium temperature below the calculated becomes less and less, and for a pure H_2 -air mixture the defect is inappreciable. The latent energy thus becomes less and less with hydrogen replacement, and in pure H_2 flames would appear to be small. An interesting correlation with flame spectra is suggested in the next section.

We suggest as a partial explanation of these results that the greater the flame propagation velocity the greater the instantaneous pressure and temperature in the inner cone and, therefore, the greater the thermal assistance to flame propagation. It is probable that shadow photographs would throw light upon this suggestion.

Spectra from Flames and Explosions.

The spectrographic examination of the after-glow of CO_2 after excitation in a vacuum tube and of the flame gases from CO-flames by Fowler and Gaydon * suggests that during combustion CO_2 molecules are formed (and remain in the flame gases) of a type similar to those responsible for the after-glow, and it seems probable that the latent energy in flame gases may be associated with excited CO_2 molecules of some kind or other.

The spectrum of the carbon monoxide-air flame consists of a continuous spectrum of considerable intensity together with the ultra-violet bands of water vapour. The continuous part of the spectrum becomes fainter with hydrogen replacements of carbon monoxide, and it is very

* Proc. Roy. Soc. A, cxlii. p. 362 (1933).

faint indeed in pure hydrogen air flames *. It would thus appear that the continuous part of the spectrum decreases in intensity as the latent energy decreases (see previous section).

An interesting correlation between latent energy and flame and explosion spectra may also be made. Bone and Weston have shown that there is a marked shortening in the ultra-violet in CO-air closed vessel explosion spectrograms when compared with those from CO-air open flames †, in spite of the fact that flame temperatures are much higher in closed vessel explosions than in open flames. It would thus seem that the greater the latent energy in the flame gases the greater is the relative intensity of the ultra-violet radiation; and this suggestion is further supported by a comparison of Bone and Weston's spectrograms * with our latent energy determinations during the constant-pressure burning of CO-mixtures at various pressures.

Duration of Latent Energy.

As has been stated, the platinum-wire temperatures during the pre-pressure period remain perfectly steady throughout that period, which in our large vessel was often of the order of 0.1 sec., and in a very large tank in which the pre-pressure period was twice as large there was no sensible variation in the temperature of the platinum wire. The latent energy therefore exists practically undiminished in amount during this time, and, indeed, from continuous records of pressure and of heat-loss to the explosion vessel walls it can be shown that the latent energy existing at the time of development of maximum pressure continues to exist in practically undiminished amount for at least 0.5 sec.

Explosion experiments have frequently been made in vessels in which transparent windows were fitted, and in a very large vessel, in which the cooling of the flame gases after explosion took place slowly, the luminous radiation emitted by them has been observed by the eye to last for at least 14 sec. after the explosion was completed. The experiments suggest that in a much larger vessel, in which the cooling would have taken place still slower, the luminous radiation would continue to be emitted for an even longer period. It would therefore appear that the excited CO₂ molecules are very long-lived.

Disappearance of Latent Energy.

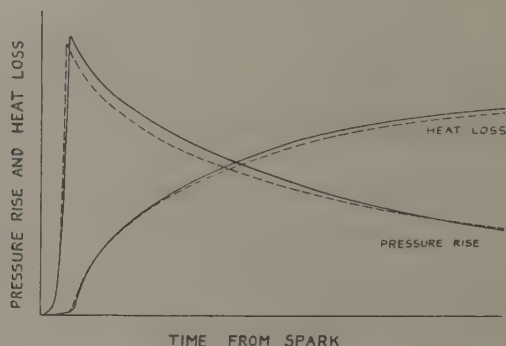
The latent energy would appear to be unloaded when the flame gases come into contact with surface. Some experiments made a few years

* 'Flame and Combustion in Gases,' Bone and Townend (Longmans), plate xxvi. (1927).

† 'Gaseous Combustion at High Pressures,' Bone, Newitt and Townend (Longmans), p. 196 (1929).

ago are of interest in this connexion. A weight of 0.67 gram of thin platinum wire (0.001 inch diameter) was loosely bunched in spherical form and suspended inside the 6-inch spherical explosion vessel. Continuous records of pressure and heat-loss to the vessel walls were made during explosion and subsequent cooling of a 91.4 per cent. CO and 8.6 per cent. O₂ mixture initially at $\frac{1}{2}$ atmosphere pressure, first with the bunched wire in position and afterwards when it was removed. The pressure and heat-loss records are shown in fig. 2. The pressures were lower when the wire was in position than when removed until .51 sec. after ignition, when they became the same. At this time, therefore, the mean gas temperatures were the same. The heat-losses to the vessel walls as shown by the bolometer records were almost exactly the same, so that the heat energy left in the flame gases in the one experiment and in the gas *plus* bunched

Fig. 2.



wire in the other was the same. It would therefore appear that at 0.51 sec. after ignition, assuming the latent energy to have been completely unloaded by the wire, the heat energy in the wire was equal to the latent energy in the flame gases in which the wire was not present. A subsidiary experiment showed that the temperature of the wire was at least equal to the mean gas temperature as inferred from the gas pressure, and calculation shows that the heat in the wire was approximately equal to 3.5 per cent. of the heat of combustion of the inflammable mixture introduced into the vessel. This compares with the latent energy of 6 per cent. of the heat of combustion estimated from the maximum explosion pressure and heat-loss in the vessel with wire removed.

PART II.

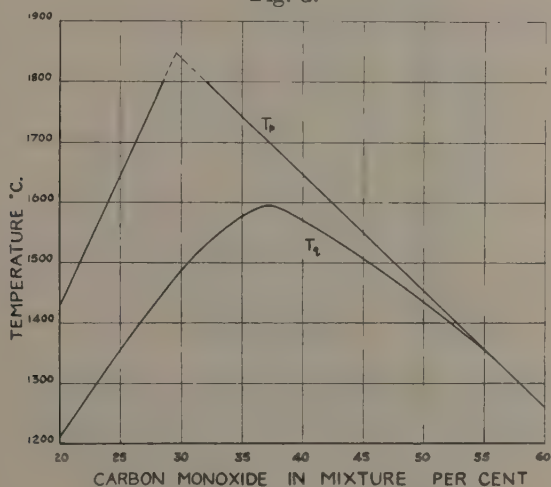
It has been shown in Part I. that there is overwhelming evidence for the view that a long-lived latent energy exists in flame gases resulting from the combustion of inflammable CO mixtures. The latent energy

probably resides in a proportion of the newly formed CO_2 molecules as excess intra-molecular energy, and experiments will now be described which show that they dissociate more rapidly than do normal CO_2 molecules under similar conditions of mixture strength, pressure, and temperature, and, indeed, that the amount of dissociation increases as the latent energy increases.

Platinum Thermometer Measurements.

In fig. 3 are given temperatures measured during the pre-pressure combustion period of mixtures of CO and air of various strengths at atmospheric pressure. Curve T_p shows the temperatures measured by a platinum-rhodium wire (0.0005 inch diameter) and curve T_q the tempera-

Fig. 3.



tures measured by a quartz-covered platinum-rhodium wire* (overall diameter 0.0005 inch).

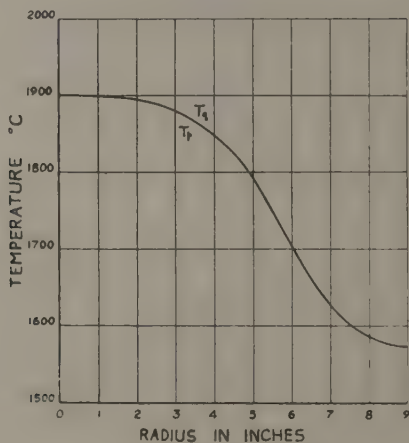
The quartz-covered wire curve is a remarkable one. It at once suggests a large dissociation in the CO_2 product, which tends to be more and more suppressed as the concentration of CO is increased. But it must be a type of dissociation which is quantitatively widely different from that which could obtain had the CO_2 been normal, for the temperatures at which it takes place are very low. The higher temperature measured by

* The wires were manufactured for us by Messrs. Baker and Co. of Newark, U.S.A., by the Taylor process. The inside core of platinum-rhodium was 0.0002 inch diameter.

the uncoated platinum wire (nearly 400°C . higher in the case of the combining proportions mixture) must be due to the combustion of the abnormally dissociated CO_2 upon its surface. For mixtures richer than about 50 per cent. CO the uncoated and the quartz-covered wire temperatures are the same, and here it is to be supposed that the concentration of CO is sufficiently great to suppress dissociation completely.

Temperature measurements were also made by means of the two types of wire along a radius of a spherical vessel of 18 inches internal diameter

Fig. 4.



after the completion of explosions within it of the following centrally ignited inflammable mixtures initially at atmospheric pressure :—

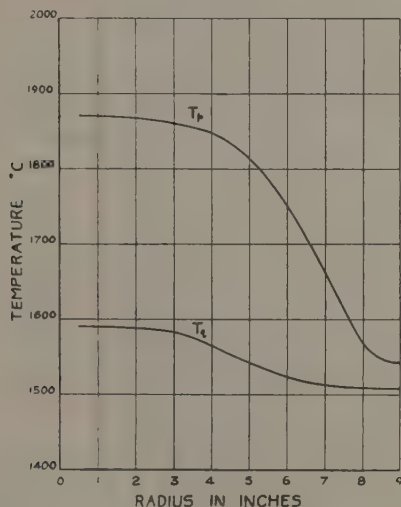
- (i.) 90.7 per cent. CO + 1 per cent. H_2 + 8.3 per cent. O_2 , and
- (ii.) 10 per cent. CO + 7 per cent. H_2 + 83 per cent. air.

The measurements for the former (over-rich) mixture are shown in fig. 4* and those for the latter (weak) mixture in fig. 5. It will be seen that the temperatures determined by the two wires are exactly the same in the case of the over-rich mixture explosion, and this was to have been expected in view of the results for over-rich mixtures shown in fig. 3. In the case of the weak mixture, however, the two wires attain widely different temperatures. The uncoated wire temperature is nearly 300°C . higher than

* The temperatures given in the curves near the centre of the vessel have been deduced from the melting-point of the platinum-rhodium wires by assuming the compression from the pressure at which the wire fused to the maximum pressure to be adiabatic.

the quartz-covered wire temperature near the centre of the explosion vessel, but the difference between the temperatures of the two wires becomes less and less with distance from the centre of the vessel, and indeed, it becomes small near the vessel walls. It would seem, therefore, that the abnormal dissociation is greatest at the centre of the vessel and, becomes less and less with distance from the centre. It will be remembered that in Part I. it was shown that latent energy decreased with distance of flame travel, and it would appear, therefore, that the extent of abnormal dissociation varies with latent energy.

Fig. 5.



Explosion Experiments.

The dependence of abnormal dissociation upon latent energy is further shown in explosion pressure and heat-loss measurements made in the 6-inch and 17.45-inch vessels. The maximum pressures developed (after correcting for measured heat-loss) during the explosion of CO and air mixtures of various strengths initially at atmospheric pressure are shown in fig. 6. By the method of Fenning and Tizard * the position of the peak of the pressure curves determines the value of the equilibrium constant for the reaction $2\text{CO} + \text{O}_2 = 2\text{CO}_2$. A small correction for the variation of measured heat-loss with mixture composition has been applied in positioning the peak. It will be seen that the peak of the pressure curves for the two vessels occurs at the same CO content (viz.

* Proc. Roy. Soc. A, cxv. p. 318 (1927).

34.8 per cent.), although the mean gas temperature in the small vessel is some 60° C. below that in the large vessel.

In Table III. are shown values for the equilibrium constant (K_p obs.) derived from the pressure curves for the two vessels together with the quantum values (K_p theor.). The latent energy expressed as a percentage of the heat of combustion is also shown. It will be seen that the

Fig. 6.

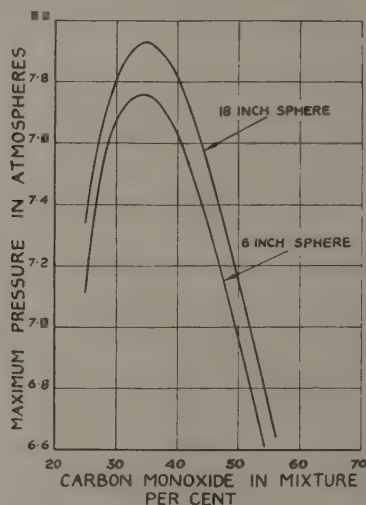


TABLE III.

Size of vessel.	T° K.	K_p obs.	K_p theor.	$\text{Log}_{10} \frac{K_p \text{ obs.}}{K_p \text{ theor.}}$	Average latent energy.
17.45 in.	2650	.0160	.00630	.40	3.5
6 in.	2590	.0156	.00335	.67	6.0

ratio K_p obs./ K_p theor. is very closely proportional to the latent energy. Experiments in which the initial pressures were varied between $\frac{1}{2}$ atmosphere and 3 atmospheres lend emphasis to this proportionality *. These will be reported in detail later. It may also be stated that further confirmation has been derived from experiments in which explosions of mixtures of CO and air are matched with explosions of over-rich mixtures of CO and O_2 .

* Leah, 'Nature,' cxlv. p. 897 (1940).

XVIII. *Circuits with Double Linkages.*

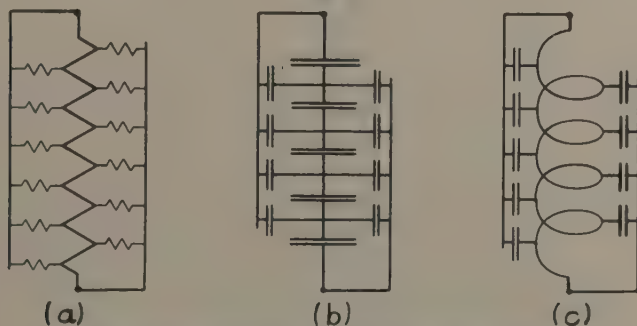
By Dr. ERIC A. WALKER *,
Tufts College, Medford, Mass., U.S.A.

[Received November 29, 1939.]

Introduction.

A PROBLEM which occasionally arises in engineering is to find the voltage distribution on a number of impedances connected in series if they have coupling to both the high voltage electrode and to the low voltage electrode. This problem is easily solved if coupling to only one electrode

Fig. 1.



Equivalent circuits of impedances with coupling
to both high and low voltage electrodes.

is present, for the problem then is only a special case of the smooth line which is treated in many textbooks^{(1), (2)}. If both couplings are present the solutions are more difficult and the results are more complex.

Specific examples of the conditions which give rise to the circuits treated in this paper are the following: A resistor, which is immersed in an electrolyte together with its electrodes, is one example. Such a condition might be represented by the circuit of fig. 1 (a). A string of suspension insulators with capacitance to ground and to the high voltage line can be represented by the circuit of fig. 1 (b). A transformer winding with

* Communicated by the Author.

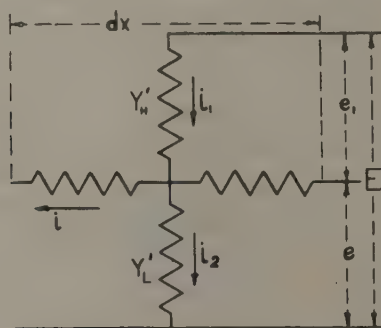
capacitance to the core and capacitance of a neighbouring high voltage winding might be represented by fig. 1 (c). Such problems as these and several others will be considered. The discussion will be limited to the cases where the impedance per unit length is constant, and also the admittances per unit length to both the high voltage and the low voltage electrodes are also constant but not necessarily equal.

The Derivation of the Differential Equation.

In fig. 2 an elemental circuit of length dx is shown. This circuit has admittance to both the high and low voltage electrodes. The change in the current i across the length of circuit is

$$di = i_2 - i_1 = eY'_L - e_1Y'_H. \quad (1)$$

Fig. 2.



The circuit for an elemental length of line with double coupling.

If the admittance per unit length to the low voltage electrode is Y_L and to the high voltage electrode is Y_H ,

$$di = eY_L dx - e_1Y_H dx = [e(Y_L + Y_H) - eY_H] dx. \quad (2)$$

Now the voltage drop across this length dx is

$$de = iZ'. \quad (3)$$

If the impedance per unit length is Z

$$de = iZ dx. \quad (4)$$

Combining (2) and (4) one has

$$\frac{d^2e}{dx^2} = Z[e(Y_L + Y_H) - eY_H]. \quad (5)$$

This is the differential equation for the voltage as measured from the low voltage electrode. If the distance x is measured from the low voltage electrode also one may define the boundary conditions as

$$\text{when } x=0, \quad e=0, \quad \dots \dots \dots (6)$$

$$\text{when } x=d, \quad e=E.$$

To solve equation (5) it is desirable to rewrite it as

$$\frac{d^2e}{dx^2} = Z(Y_L + Y_H) \left[e - E \cdot \frac{Y_H}{Y_L + Y_H} \right] \dots \dots \dots (7)$$

$$= s^2[e - Ey], \quad \dots \dots \dots (8)$$

where

$$s^2 = Z(Y_L + Y_H) \quad \text{and} \quad y = \frac{Y_H}{Y_L + Y_H}.$$

If $e - Ey$ is replaced by v one has

$$\frac{d^2v}{dx^2} = s^2v, \quad \dots \dots \dots (9)$$

$$\text{where } v = e - Ey. \quad \dots \dots \dots (10)$$

The solution of this equation is well known. It is

$$v = A\epsilon^{ax} + B\epsilon^{bx}, \quad \dots \dots \dots (11)$$

where A and B are constants determined by the boundary conditions and a and b are constants depending on the circuit constants.

The solutions will differ depending on whether a and b are real or imaginary numbers. In Table I. five possible cases are listed. In these cases the parameter γ is always a real number. Although the method shown here may readily be expanded to instances where this is not true, it will not be done in this paper. The first three cases are instances where the parameter s is a real number. The last two are instances where s is imaginary. One would then expect two types of solution for the differential equation.

The Case where s is a Real Number.

When s is a real number the arbitrary constants A and B may be evaluated. They are found to be

$$A = \frac{E[1 - \gamma + \gamma\epsilon^{-sd}]}{\epsilon^{sd} - \epsilon^{-sd}} \dots \dots \dots (12)$$

$$B = \frac{-E[1 - \gamma + \gamma\epsilon^{+sd}]}{\epsilon^{sd} - \epsilon^{-sd}} \dots \dots \dots (13)$$

If these values are replaced in equation (11) and equated to (10), one has

$$e = \frac{E\gamma}{\sinh sd} \left[\sinh (sd) - \left(1 - \frac{1}{\gamma} \right) \sinh (sx) + \sinh s(x-d) \right], \quad (14)$$

where

$$\gamma = \frac{Y_H}{Y_H + Y_L} \quad \text{and} \quad s = \sqrt{Z(Y_H + Y_L)}$$

and is real

This equation is similar to the one given by Schwaiger for the special case of a string of suspension insulators with capacitance coupling to ground and to the high voltage electrode ⁽³⁾.

TABLE I.

Case.	Z.	Y_H .	Y_L .	S.	γ .
1.....	R	G_H	G_L	$R(G_H + G_L)$	$\frac{G_H}{G_H + G_L}$
2.....	$\frac{-j}{C\omega}$	$+jC_H\omega$	$+jC_L\omega$	$\pm \sqrt{\frac{C_L + C_H}{C}}$	$\frac{C_H}{C_H + C_L}$
3.....	$+jL\omega$	$\frac{-j}{L_H\omega}$	$\frac{-j}{L_L\omega}$	$\pm \sqrt{\frac{L}{L_H + L_L}}$	$\frac{L_L}{L_H + L_L}$
4.....	$+jL\omega$	$+jC_H\omega$	$+jC_L\omega$	$\pm j\omega^2 \sqrt{L(C_H + C_L)}$	$\frac{C_H}{C_H + C_L}$
5.....	$\frac{-j}{C\omega}$	$\frac{-j}{L_H\omega}$	$\frac{-j}{L_L\omega}$	$\pm j \frac{1}{\omega^2} \sqrt{\frac{1}{C(L_H + L_L)}}$	$\frac{L_L}{L_H + L_L}$

The Case where s is an Imaginary Number.

If s is an imaginary number, one has

$$v = A\epsilon^{+jsx} + B\epsilon^{-jsx} \quad (15)$$

The arbitrary constants then become

$$A = E \frac{[1 - \gamma + \gamma^{-jsd}]}{\epsilon^{jsd} - \epsilon^{-jsd}} \quad (16)$$

$$B = -E \frac{[1 - \gamma + \gamma^{+jsd}]}{\epsilon^{jsd} - \epsilon^{-jsd}} \quad (17)$$

Then e is given by

$$e = \frac{E\gamma}{\sin sd} \left[\sin (sd) - \left(1 - \frac{1}{\gamma} \right) \sin (sx) + \sin s(x-d) \right] \quad (18)$$

where

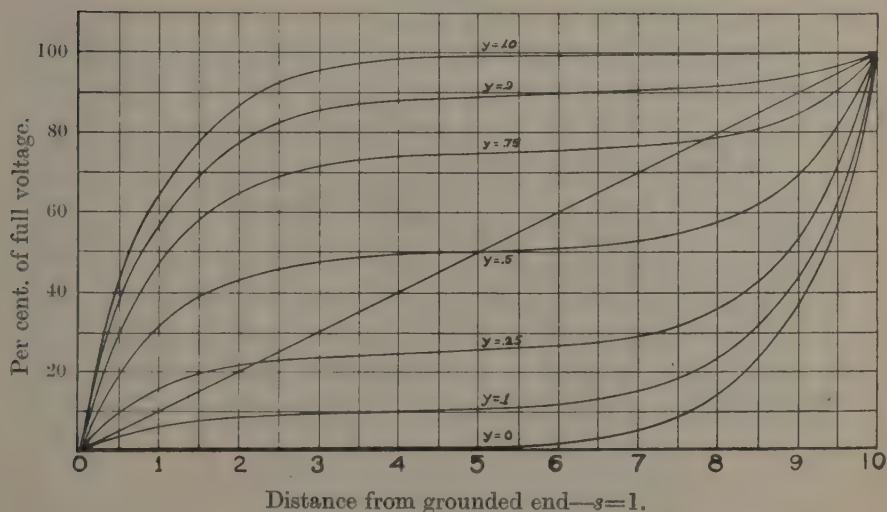
$$\gamma = \frac{Y_H}{Y_H + Y_L} \quad \text{and} \quad s = \sqrt{Z(Y_H + Y_L)}$$

and is imaginary.

Discussion of the Results.

In order to see the variation caused by change in the parameter γ equation (14) is plotted in fig. 3. Values of x from 0 to 10 are used as the abscissa and the voltage from 0 to 100 per cent. of full voltage is plotted as the ordinate. If there were no coupling to the high and to the low voltage electrodes the straight line voltage distribution shown would

Fig. 3.



Variation of voltage along the impedance if $s=1.0$ and is real. γ as is shown on the curves.

be the result. Values of γ from 0 to 1.0 are given. It is evident that the voltage gradient is always the greatest near the electrodes. Equation (14) may be differentiated to find an expression for the voltage gradient

$$\frac{de}{dx} = \frac{E}{\sinh(sd)} [(1-\gamma) \cosh(sx) + \gamma \cosh s(x-d)]. \quad (19)$$

At $x=0$ this reduces to

$$\frac{de}{dx} = \frac{E}{\sinh(sd)} [(1-\gamma) + \gamma \cosh(sd)]. \quad (20)$$

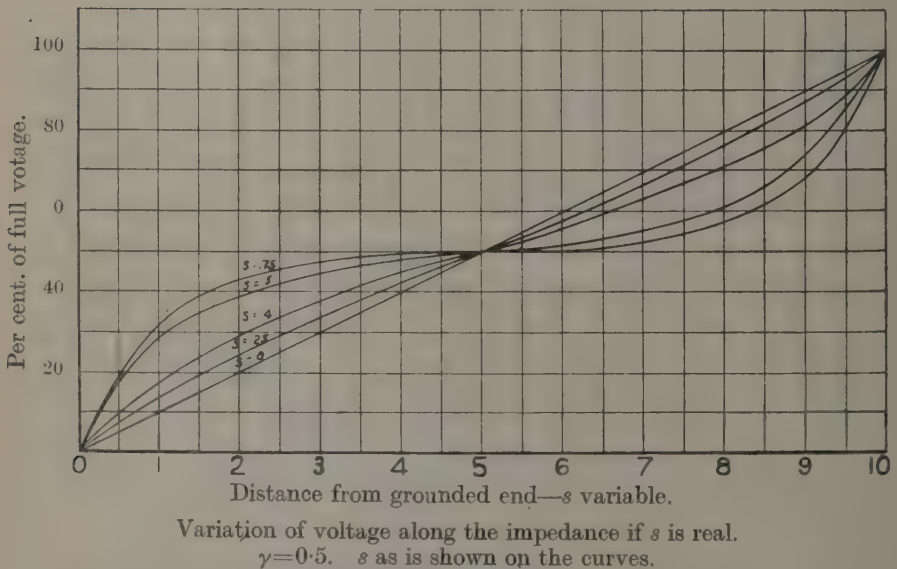
For large values of the quantity sd this equation may be simplified still further :

$$\begin{aligned} \text{at } x=0 \quad \frac{de}{dx} &= E\gamma \quad \text{approximately,} \\ \text{at } x=d \quad \frac{de}{dx} &= E(1-\gamma) \quad \text{approximately.} \end{aligned} \quad (21)$$

It is then evident that the maximum voltage gradient will be the lowest when $\gamma=0.5$ or when $Y_H=Y_L$.

In fig. 4 equation (14) is plotted with γ held constant at the optimum

Fig. 4.



value of 0.5 and s varied from 0 to 0.75. It is evident that as s becomes larger the variation from the straight line becomes greater.

In fig. 5 equation (18) is plotted for values of $\gamma=0$, 1.0, and 0.5. These are the three special cases where there is no coupling to the high voltage electrode, no coupling to the low voltage electrode, and the case where the coupling to the two electrodes are equal. In this case s is chosen as 1.0. It is again evident that the gradient is the lowest when $\gamma=0.5$. The gradient is given by

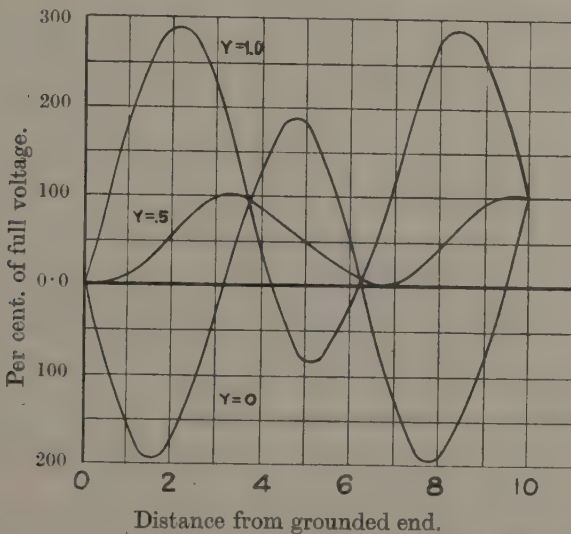
$$\frac{de}{dx} = \frac{E}{\sin sd} [(1-\gamma) \cos sx + \cos s(x-d)]. \quad (22)$$

The gradient is not the greatest at the two ends of the circuit. From this it is evident that with high frequency oscillations the maximum stress is not necessarily placed on the end turns of a transformer. At $x=0$

$$\left. \begin{aligned} \frac{de}{dx} &= \frac{E}{\sin(sd)} [1 - \gamma + \gamma \cos sd]. \\ \text{At } x=d \\ \frac{de}{dx} &= \frac{E}{\sin sd} [1 + (1 - \gamma) \cos sd]. \end{aligned} \right\} \dots \dots \dots (23)$$

Fig. 6 shows equation (18) plotted for several values of s for the particular value of $\gamma=0.5$.

Fig. 5.



Variation of voltage along the impedance s is imaginary.
 $s = \pm j1$. γ as is shown on the curves.

Conclusions.

- (1) Five types of circuit give rise to two types of equation for the voltage as a function of the distance along the impedance.
- (2) In the first type of equation the surge impedance $s = \sqrt{Z(Y_H + Y_L)}$ is real and in the second type it is imaginary.
- (3) If the surge impedance is real the voltage never exceeds the line voltage and the maximum gradient occurs at the points nearest the electrodes.

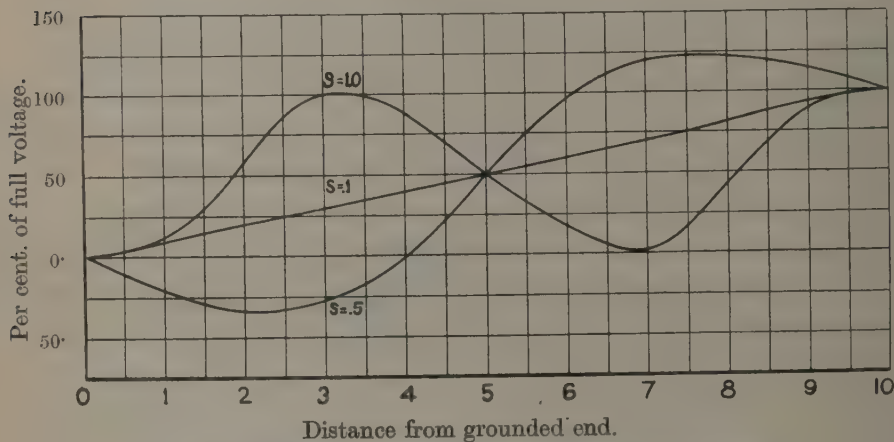
(4) If the surge impedance is real the voltage distribution is not a function of the frequency of the applied voltage.

(5) If the surge impedance is imaginary the voltage may exceed the maximum line voltage and the maximum gradient does not necessarily occur at the end of the impedance.

(6) If the surge impedance is imaginary the voltage distribution is a function of the frequency of the applied voltage.

(7) The maximum gradient is the lowest for both types of equation if $\gamma=0.5$ or if the coupling to the high side is the same as the coupling to the low side.

Fig. 6.



Variation of voltage along the impedance if s is imaginary.
 $\gamma=0.5$, s as is shown on the curves.

Bibliography.

- (1) A. E. Kennelly, 'Electric Lines and Nets' (a book). McGraw-Hill Book Co., N.Y., 1928.
- (2) L. F. Woodruff, 'Electric Power Transmission and Distribution' (a book). John Wiley & Sons, N.Y., 1928.
- (3) A. Schwaiger, 'Theory of Dielectrics' (a book). John Wiley & Sons, N.Y., 1932.

[The Editors do not hold themselves responsible for the views expressed by their correspondents.]

XIX. *Further Development of the Fabric Theory of Protein Structure.*

By DOROTHY WRINCH, Carlisle Fellow of Somerville College, Oxford *.

[Received August 16, 1940.]

SUMMARY.

Further suggestions as to possible structures for globular proteins are formulated, it being emphasized that the closed fabric cage structure explains the paradox that such proteins, though megamolecules, have definite physical and chemical properties and highly specific individualities. The structures proposed for consideration comprise closed cage structures resulting from the original cyclol fabric, the "enol" fabric, and hydrogen-bond fabrics, and have skeletal residue numbers of the forms $24n^2$, $48n^2$, $72n^2$

It has long been agreed that certain native proteins such as insulin consist of large numbers of amino and imino acid residues of the composition $(\text{NH}-\text{CHR}-\text{CO})-$, with or without units of the composition $(\text{H}_2\text{N}-\text{CHR}-\text{CO})-$ and $-(\text{HN}-\text{CHR}-\text{COOH})$. It has been the objective of the preceding series of communications ⁽³²⁾ to point out that there can be only a certain mathematically determinate set of topologically distinct structures satisfying these conditions and to formulate the problem of protein structure as the study of all geometrically permissible atomic patterns satisfying these conditions. It has been considered by the present writer of great importance to stress this point of view, since it appears unlikely that structures containing thousands of atoms will be devised without the help of geometrical techniques.

Such patterns can be of three basic kinds, line patterns, surface patterns, and volume patterns: patterns involving elements of two or more of these types cannot be excluded. Line patterns can be built on the plan of units having 2-fold functionality. These lead of course to the polypeptide chain structures



on the one hand; on the other hand, they lead to cyclo-peptides or polypeptide rings (*i. e.* polypeptides without open ends) $(\text{HN}-\text{CHR}-\text{CO})_n$. Since there appear to be no chemical data which require that such line

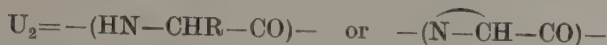
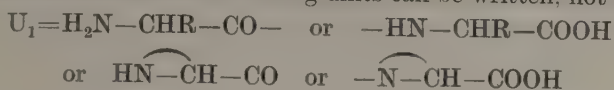
* Communicated by the Author.

patterns should have open ends, it was suggested—and the suggestion has been adopted by Bernal, Pauling and Niemann, and others—that peptide rings consisting of various numbers of residues may have to be considered.

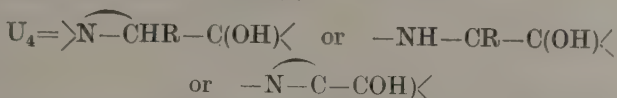
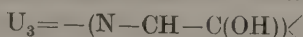
It is hardly necessary to point out the profound differences to be expected between polypeptide chains and rings, and studies on the geometrical possibilities inherent in polypeptide rings have given some preliminary indications of the implications of this idea. In view of the geometrical issues involved, attention is specially directed towards 6-, 10-, 12-, 18-residue rings etc., and it is suggested that the synthesis of such compounds, and the study of substituted diketopiperazines, preferably with residues containing asymmetric C_α atoms of *lævo* type, may mark an important step towards the understanding of protein synthesis, the many studies using glycine residues only being of limited usefulness owing to the absence of asymmetric C_α atoms. Already vast stores of information regarding polypeptide chains are available. It seems that, in all cautiousness, equal stress should be given to the information to be obtained from the synthesis and study of polypeptide rings, if a comprehensive attack on the protein problem is to be made. It is also of interest to notice that there may be compounds which lie intermediate in weight between the amino and imino acids and the globular proteins, whose polymerization leads to the formation of globular proteins: in this event the 2-, 6-, 10-, 12-, 18-residue rings etc. may be the compounds in question. A molecular weight of less than 1000 was reported for the bulk of the material from which lactalbumin is formed⁽³⁰⁾. Such compounds might be six-residue rings, which later polymerize to form the larger globular molecules. Also it has long been known that diketopiperazines are capable of polymerization: these, with one or two asymmetric C_α atoms and suitable R groups, might therefore be a suitable starting-point. In this connexion it seems likely that certain sets of amino and imino acids only may be favourable ingredients, since there is considerable evidence that the proportions of the various species do not occur at random except perhaps in the case of glycines. Diketopiperazines containing two alanine residues, one alanine and one glycine, and one leucine and one glycine have actually been isolated from proteins⁽³⁾, and polymerizations from certain proportions of these and similar molecules might prove possible. That the case of glycine may be different from that of other amino and imino acids is suggested by the figures for glycines and for arginine, histidine, and lysine in a number of keratins with different biological origins: these record a fixed 12 : 1 : 4 arginine-histidine-lysine ratio, while the glycine complement varies widely⁽⁶⁾.

Surface patterns and volume patterns of the protein building units must thus be considered. Such patterns require that some or all of the

units shall have more than 2-fold functionality. For this reason attention is drawn to the fact that the building units can be written, not only as

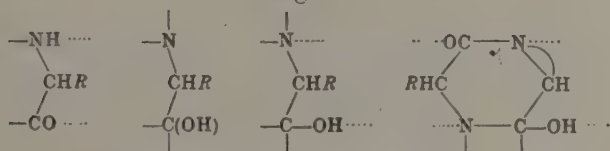


having one-fold and two-fold functionality, but also as



having three- and four-fold functionality, since it is plain that chemical analyses cannot exclude such possibilities. Following the ideas of Jordan Lloyd⁽¹⁸⁾, subsequently adopted by Huggins, Pauling and Niemann, and Bernal and others, it is also suggested that the building units may be

Fig. 1.



Building units for protein fabrics.

joined by hydrogen bonds between oxygen and nitrogen atoms or between oxygens belonging to the skeletons, leading again to units of higher functionality than 2, appropriate for the building of surface or volume patterns (fig. 1).

All these possibilities relate to interlinking of atoms N, C, O belonging to the skeletons. It appears likely that such interlinking must play a dominant part in the structure of proteins, since the protein molecules appear to require in general the regular and orderly arrangement of hundreds of building units, whose R groups take a wide variety of different forms. Many supplementary suggestions have been made as to interlinking of R groups, *e. g.*, salt linkages, S-S bridges, hydrogen bonds, etc., and I would specifically suggest that trimerization of imino groups of arginine side chains may also play a role. Such questions can only be discussed profitably when the complete chemical composition in terms of the various amino and imino acids is known.

The geometrical attack on protein structure must therefore start with a discussion of possible structures, based upon arranging the building units in various patterns. Confining attention to the crystalline globular

proteins, the problem is to devise structures which will explain their definite molecular weights, their capacity to denature, the constancy and high specificity of their patterns, and their power to crystallize in specific forms. The information regarding long chain polymers makes it unlikely that these proteins have such structures ⁽¹⁹⁾. It is then necessary to postulate that such proteins have a fine structure capable of fragmentation into certain definite numbers of polypeptide chains or rings of definite types.

There is as yet no definite indication as to the particular system of polypeptide chains or polypeptide rings which, with a fine structure superposed, give, say, the insulin molecule. And it must be emphasized that there is no reason to assume that such a molecule can yield one single polypeptide chain or ring. The fact that titration curves for proteins, at least in some cases, fit with the titratable R groups known to be present, leaving little or no scope for postulating open ends to polypeptide chains, led to the view that the molecule is made up of one chain, since if there were two or more chains, four or more extra groups should show up in the titration curve. But if chains be replaced by rings, no argument for postulating ⁽⁵⁾ one linear polymer rather than many per molecule remains. Recent studies indicate that different proteins form films whose viscosities, elasticities, etc., are characteristically different ⁽²⁹⁾. It appears likely that these parameters may permit deductions regarding the structure of these films which will throw some light upon the structure of the globular molecule, and that it will be found, for example, that, under standard conditions, pepsin and insulin, by breaking their fine structure only, can yield definite sets of polypeptide rings or chains, partially or wholly decyclized.

The general point of view which it has been the object of these publications to put forward led, in the first place, to investigations relating to the geometrical implications, of using, say, the lactim unit U_4 having 4-fold functionality to supplement the U_2 units. It was found that a series of fabrics or two-dimensional atomic patterns can be built out of definite proportions of these units. It then seemed to be of interest to investigate structures formed of lactim U_4 units alone. We found that the fabric consisting wholly of lactim U_4 units can be folded round to make a closed cage-like structure, and that these structures contain definite numbers of residues—in fact, 72, 288, etc. Here there seemed at last to be a way of understanding the existence of certain crystalline globular proteins of definite molecular weights. No attempt at solving this problem has apparently been made in terms of linear peptide structures, nor does it seem likely that any such attempt could be successful, except on the lines of the hydrogen-bonded fabrics, which essentially replace the line pattern by a surface pattern.

The polyhedral cage has its size and shape determined by the valency angles and bond lengths associated with the atoms of the $N-C_{\alpha}-C$ skeletons. It may be possible similarly to build not only closed cage-like structures, but also other closed structures after the same manner. The torus is under consideration, and all the topologically distinct types with their different degrees of connexity will be considered in turn. The important point which deserves emphasis is simply this: closed fabrics account for structures existing, whose skeletons comprise definite numbers of residues. The polyhedral cage in its simplicity was specially well adapted for purposes of exposition. The idea, however, relates to any closed surface whatever, which may be allowable from the point of view of the geometrical conditions relating to the constituent atoms. It seems of considerable interest that the complete cyclol fabric logically yields structures containing the series of residue numbers 72, 288, . . . , $72n^2$. . . Evidently any fabric whatsoever itself determines whether this or that type of closed surface can be formed, and if so the precise sets of residue numbers which will form such skeletal structures.

Any such closed surface is one of a series depending upon the natural numbers 1, 2, . . . , n , This dependence upon the natural numbers draws our attention to the very close and interesting analogy which exists between the quantum principle in atomic physics, and what may be called the quantum principle for megamolecules. The essential point about quantum mechanics can be explained simply in terms of a circular motion in which waves which go around 0, 1, 2, . . . times overlap and will, in general, destroy one another by interference. "Only in the special case where the frequency of the wave and, therefore, the energy of the corpuscle are such that an integral number of waves just circumscribe the circle do the waves which have gone around 0, 1, 2, . . . times reinforce one another so that a standing wave results" ⁽¹³⁾. "For all other energy values the waves destroy one another and, consequently, if we assume the relation between wave and corpuscle indicated by the observed diffraction phenomena, there is no motion of the corpuscle corresponding to such energy values" ⁽¹³⁾. In precisely the same way, a fabric can form a closed surface only in the special cases in which the fragment of fabric used is capable of circumscribing a portion of space, and joining up so as not to interrupt the pattern. Appropriate series of fragments of any one fabric comprise residue numbers depending upon the natural numbers, just in the same way as the series of appropriate energy values are functions of the natural numbers. There is, in fact, a direct parallelism between the reason for the restriction of the energy values to the eigen values E_1 , E_2 , . . . , E_n , . . . and the proposed restriction of skeletal residue numbers in the globular proteins to series such as 72, 288, . . . , $72n^2$, . . . In a sense the essential postulate of quantum

mechanics is fundamentally geometrical in nature. It is in this same sense that we suggest the view that many characteristics of protein structures, for example, the residue numbers appropriate for the skeletons of protein molecules, depend upon geometrical factors.

The idea of a closed surface type of structure also makes clear a number of the other important properties of the globular proteins. Particularly striking are the implications regarding the high degree of specificity of the globular proteins and their high degree of organisation.

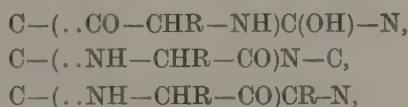
Once the technique of building closed structures from atomic fabrics is plain, it will no doubt be adaptable to all types of fabric. From the point of view of the geometer, the problem is to contrive all and every type of fabric appropriate for the protein and to study all and every type of closed surface which is geometrically permissible. In the preliminary studies of the cyclol fabric, it has been shown that there is no intrinsic impossibility in the closed type of structure, and it has been shown in detail how the atomic pattern can determine size and shape, and that these structures can be rendered highly specific by the conditions imposed upon the type of functionality of the building units. This general investigation of all possible structures is as yet in its very earliest stage only, as will be seen from the fact that the cage structures C_1 , C_2 , . . . represent what can be done with the building of structures consisting only of lactim U_4 units, under very strict metrical conditions.

The purpose of this paper is to offer suggestions as to further possible structures for globular protein molecules. These all fall into the category of closed surface structures, consisting of atomic fabrics bent round to form polyhedral skeletons, comprising in their skeletons definite numbers of residues. Since the geometrical attack on protein structure is essentially concerned with drawing attention to all the possibilities, our purpose is rather to explore, in due course, all types of structure with the composition appropriate to proteins, than to press for the adoption of this or that particular structure as the most likely type. In any case the possibility of a variety of skeletal types for different categories of globular proteins cannot be excluded *a priori*. For this reason special attention is directed, without prejudice, to the original cyclol hypothesis, to various other possibilities, namely, cages of "enol" fabrics, cages of hydrogen bond fabrics, and certain modified cyclol cages.

The original cyclol hypothesis⁽³²⁾ was built upon the idea of a fabric in which some or all of the C and N atoms in the constituent residues function as ternary rather than as binary units, giving the residue in the form $(-C(OH)-(CHR-N=))$, where these atoms are junctions of three, rather than of two, residues, as in the linear polypeptide structures in which the residue takes the form $(-CO-CHR-NH-)$. The completely cyclized fabric⁽³³⁾, which must of course be closed, yielded the

C_n cages. The modification now introduced is a closed fabric in which some, but not all N atoms are ternary, a necessary modification if imino acid residues are to be accommodated. Exactly the same idea of using some or all residues in a form in which they have more than two arms led to the "enol" fabric, in which the C_α and C atoms are, in some cases, ternary.

The result of these enquiries is to direct attention still more definitely to certain residue numbers as likely to occur in skeletons of globular proteins: the numbers $24n^2$, $48n^2$, $72n^2$ are included. But it must be emphasized that the moment skeletons containing any linear residues are under consideration there is a possibility of inserting at such points further peptides, not belonging to the skeleton. In such cases, the number of residues in the molecule will exceed the skeletal residue number. We suggest in particular such situations as the following:—



in which, in the first, an NH_2 end is inserted at a carbonyl in the skeleton by a prototropic change, and in the second and third a $COOH$ end is inserted at an NH group and at a CHR group in the skeleton with the elimination of water. Indeed, the possibility that a residue may have one only of its C, N, C_α atoms ternary, the rest being binary, should also be considered, in relation to peptides inserted into the skeleton, and also in relation to the skeleton itself.

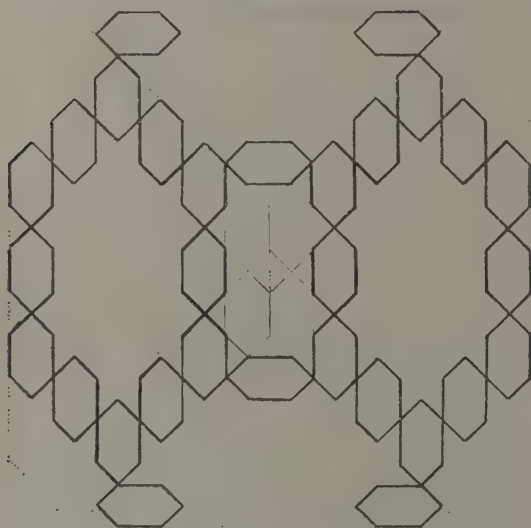
All the ways in which these various possibilities can be realized, and the consequent interrelation of the many metrical parameters of bond lengths and bond angles, can hardly be discussed in detail until precise relevant data are available which give the complete specification of the complements of the various types of amino acid and imino acid involved in individual proteins, for which crystallographic data are also forthcoming. Originally it was assumed that all the carbon and nitrogen atoms in the skeletons have valency angles which are tetrahedral. It is evident from the literature of structure analyses that such conditions are too onerous, cases being known in which these valency angles have other values. Since it is not possible to know the appropriate range of valency angles which should be considered, some of the structures suggested are to be viewed at present as suggestions regarding the topology of the molecules only.

Modified Cyclol Cages.

A study of the C_n cage skeletons shows that only one extravert and one introvert is geometrically possible in each case. For each of the C and N

atoms in the complete hexapeptides, to which the tetrapeptides are linked, lies above the median plane of the face to which it belongs, *i. e.*, outside the C_n polyhedron formed by the 8 median planes belonging to the 8 faces. This point is most easily demonstrated by means of the projection normal to a dyad axis of the fabric cage, represented by its median hexagons (shown in fig. 2), which shows plainly that the two C_α atoms at the ends of each slit lie outside the polyhedral cage. In taking account of the fact that many protein molecules contain a certain complement of imino acid residues, this becomes of special significance, for it means that suitable sites for units of this specific structure can be found at the slits of the

Fig. 2.

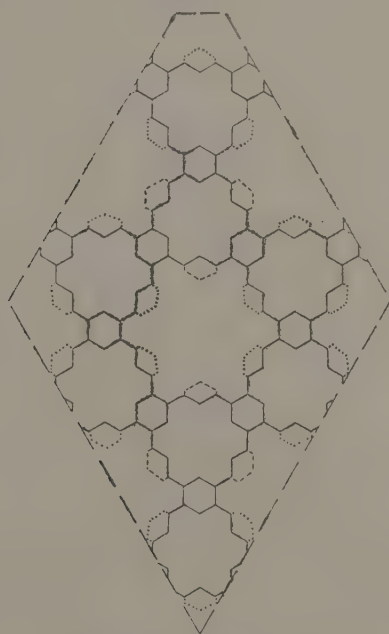
Projection of a C_n slit.

cyclol cages, whether these be introverts or extraverts. In fig. 3 it is seen that in either case and no matter whether C_1 , C_2 ... C_n ... cages be considered, any or all of the four residues bordering each slit (indicated by dotted lines) can be placed in such a way that the C—N links joining them to the residues in the adjoining hexapeptide rings are normally *outward* from the median planes of these rings, since the C and N atoms in these rings which are concerned lie above the median planes. This means that in each of the six slits of a C_n cage there are four sites capable of accommodating imino or amino acid residues giving, for C_n , twenty-four such sites in all, all twenty-four of these residues lying outside the cage. It will be seen from fig. 3 that this relieves the congestion at the

slits and that each slit can now be fringed by four $-\text{CO}-\text{C}_2\text{HR}-\text{NH}-$ units which are widely spaced from one another.

In the case of the C_1 cage, this structure with opened slits then has 24 ($-\text{CO}-\text{CHR}-\text{NH}-$) residues giving 1 in 3 as the maximum complement of imino acid residues. It has also 48 ($=\text{C}(\text{OH})-\text{CHR}-\text{N}=\text{}$) residues, which comprise 24 whose R groups leave the fabric normally and 24 whose R groups leave the fabric obliquely at an angle of 19° to the median plane.

Fig. 3.



Projection of a C_n face.

For the C_2 cages, additional sites for imino acid residues are available on the rings along the edge as shown by dashes in fig. 3, for these hexapeptide rings can be replaced by sextets of $-\text{CO}-\text{CHR}-\text{NH}-$ residues without destroying the unity of the cage fabric. Each of the 12 hexapeptide rings along the edges can then have 6 such residues capable of accommodating imino or amino acid residues, one-third lying within the polyhedron formed by the median planes of the original cage and two-thirds outside it. This gives 96 as the maximum number of imino acid sites, that is, 1 in 3, as in the C_1 case. It will be seen that this replacing of 96 ($=\text{C}(\text{OH})-\text{CHR}-\text{N}=\text{}$) residues spaces these

residues more widely, there being a possibility, by means of rotation about C—N bonds no longer imprisoned in triazine rings, of a wider spacing also of R groups in the intact hexapeptides. We notice that these 96 linear residues give to an extravert C_2 as many as 24 R groups lying *within* the polyhedron.

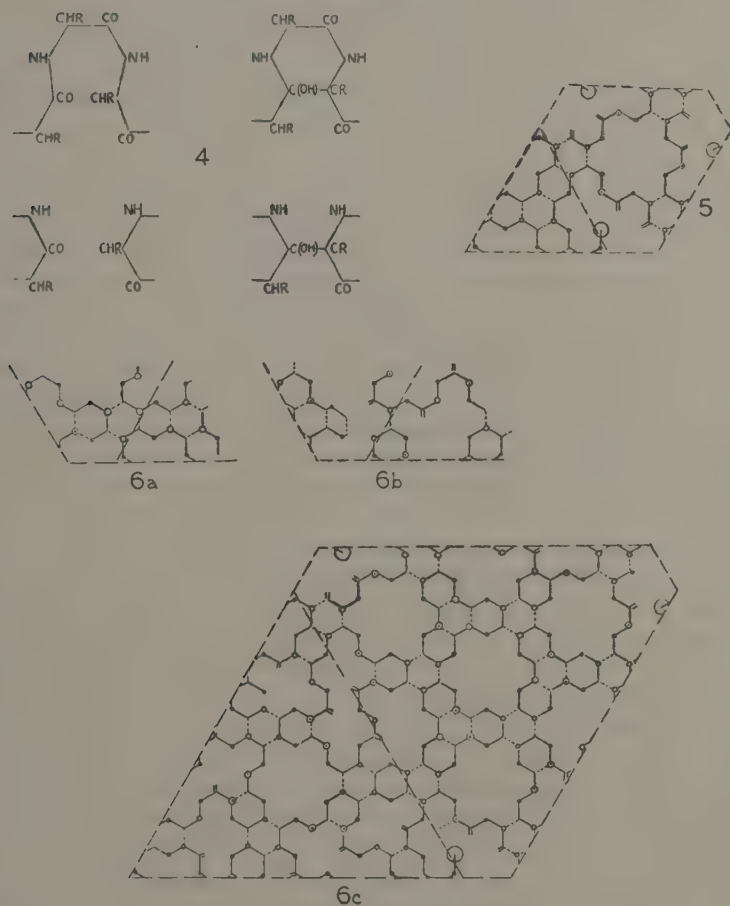
This proportion of possible imino acid sites, namely 1 in 3, is evidently in excess of what is required in all the cases for which the actual figures are known. Thus for egg albumin ⁽⁷⁾ the proportion of protein is 4 per cent., for zein ⁽¹²⁾ 9, for Bence-Jones protein ⁽¹⁴⁾ 3, for pepsin ⁽²⁵⁾ 5, for insulin ⁽¹⁶⁾ 10, for lactalbumin ⁽¹⁷⁾ 3·8, for serumalbumin ⁽²⁾ 1·0, for edestin ^{(1), (24)} 6·1, for squash seed globulin ⁽²³⁾ 3·8, and for wheat gliadin ⁽³¹⁾ 10·3 per cent.

The "Enol" Fabric.

An earlier communication has already been devoted to a second type of fabric with the composition appropriate for proteins ⁽³⁶⁾, which is put forward for consideration without prejudice to the original cyclol fabric which was built upon lactim cyclization and polymerization. This "enol" fabric, a precedent for which is provided by $\beta\beta\gamma\gamma$ tetramethyl $\alpha\delta$ diacetyl butane ⁽⁴⁾, depends upon cyclization and polymerization as shown in fig. 4. As in the original theory, the essential point about the fabric is that megamolecular structures having definite chemical individualities (such as are required by the native globular protein molecules) can be interpreted in terms of closed structures obtained by bending the fabric round to form a polyhedral skeleton, this skeleton being determined in size and shape, *i. e.*, in its skeletal residue number and symmetries, by the architecture of the fabric. We describe one specific series of enol cage structures containing $72, 288, \dots 72n^2, \dots$ residues. Figs. 5 and 6c show one-quarter of the fabrics of a 72-residue cage and of a 288-residue cage. NH groups and C_α atoms are indicated by dots and small circles, C=O groups by =. A large circle indicates an open end —CO—CHR—NH₂. As with the cyclol (lactim) cages, the median planes of the enol cages form a truncated tetrahedron. We continue to assume that all residues are of lævo type. This latter assumption leads to restricted cyclization along the edges, seen in the presence along each edge of certain residues in the linear (—CO—CHR—NH—) form, which provide more than enough sites for imino acid residues. At the slits, three alternative situations are suggested for consideration. In (a) the exact pattern along the slits is continued: since in this event —OH and —CH₂— groups come together, a condensation with the elimination of water, giving >CH—, is suggested in each case. This condensation may also occur along the edges. In (b) a modification putting two linear residues outside the polyhedron is proposed, this form being suitable only if $n > 1$. In (c) pairs of open ends each with one residue in linear form is suggested.

This structure differs from the cyclol cages in several ways, notably in the fact that the C_α atoms do not lie uniformly either within or outside the polyhedron. Actually in the 288-residue structure with (a) slits, 180 R groups emerge and 72 penetrate the cage, while 36 lie along the edges

Figs. 4-6 c.



Enol fabrics.

edges. With (b) and (c) slits, to the 180 R groups emerging are added 12 which lie right outside, and 60 R groups penetrate the cage, with 36 lying along the edges. This penetration of certain R groups within the interior seems of special interest in the case of insulin and certain other proteins,

where a considerable complement of R groups are hydrophobic in character.

It will be noticed that with (b) and (c) slits these structures have the residues near the slits very widely spaced and that there is no crowding of non-bonded atoms. With (a) slits, the condensations allow atoms to be arranged at appropriate distances. There is, further, no crowding in the lacunæ, which are fringed by two triads of NH groups. These groups have their nitrogen atoms distant about 2.7 Å. to 3.0 Å. apart, a suitable distance for the formation of NH . . . N hydrogen bridges, in view of the lengths of such bridges in structures already analysed, namely, 2.65 Å. in phthalocyanine ⁽²⁶⁾, 2.94 Å., and 2.99 Å. for ammonium azide ⁽¹¹⁾, and so on.

The possibility of OH . . . O links between the hydroxyls carried by the three way carbon hexagons also has already been pointed out, also the fact that the grouping of the C_α atoms carried by such rings is similar to that presumed (on the basis of an X-ray investigation ⁽²²⁾) in acetaldehyde ammonia, the distance in the fabric being rather greater than in that case. Small deviations of valency angles from the tetrahedral angle permit the formation of NH . . . O along the edges. In addition to these bridges, there are further possibilities of hydrogen bonding to water molecules of O . . . HO and N . . . HO types, leading to (say) two hydrogen bonds per residue, or more, for skeletal atoms only.

It may be stressed that this enol fabric, like the cyclol lactim fabric, is essentially "sticky" in the sense that it carries atoms so linked that they are able to form hydrogen bonds to many foreign molecules such as water. It is essential, in view of the facts, that any suggested fabric shall have this characteristic. This aspect of the matter is of particular significance in relation to attempts to interpret figures for the molecular weights of proteins. It was suggested several years ago—and the suggestion seems now to be generally accepted—that, in so far as the molecular weights of native proteins fall into what may reasonably be called "molecular weight classes," such classes, which are often of wide spread, are, in fact, symptomatic of definite residue numbers, and that all such results are fundamentally to be interpreted in terms of the number of residues per molecule. In this way the wide spread of a single molecular weight class can perhaps be interpreted in terms of different complements of the various types of residue, which themselves spread widely, although it must be recognized that extra residues not belonging to, but inserted into, the skeleton may also be present giving increases in residue numbers. It is also necessary to refer specifically to the possibility that considerable numbers of water molecules, being built into the structure of the molecule, may be included in the molecular weight. This matter has already been discussed in relation to the residue numbers, namely, multiples of 72,

which the cyclol theory suggested for the globular proteins and the molecular weights which have been found for them, a satisfactory correspondence being obtained. Since this discussion, Hotchkiss⁽¹⁵⁾ has suggested that the lacto globulin molecule, for which a complement of 288 residues was predicted, may contain as many as 338 residues, on the ground that it contains 115.5 grams of protein per peptide bond, and has the molecular weight 39,000. But in this calculation no account is taken of the constituent water molecules, and it seems equally legitimate to say that it may contain 288 molecules and that, since $39,000/288 = 122.5 = 115.5 + 7$, it contains a complement of (say) one water molecule to two or three residues built into its structure. On the other hand, extra residues may be inserted into the skeleton. There thus seems no reason to think that these new facts conflict with the idea of a 288-residue skeleton for the lacto globulin molecule.

The figures for the cell molecular weights for certain crystalline globular proteins are also of great interest in this connexion. It is to be expected in the case of a crystalline protein that not only the skeleton "sticks" to water molecules, but that the R groups containing oxygen and nitrogen atoms do likewise.

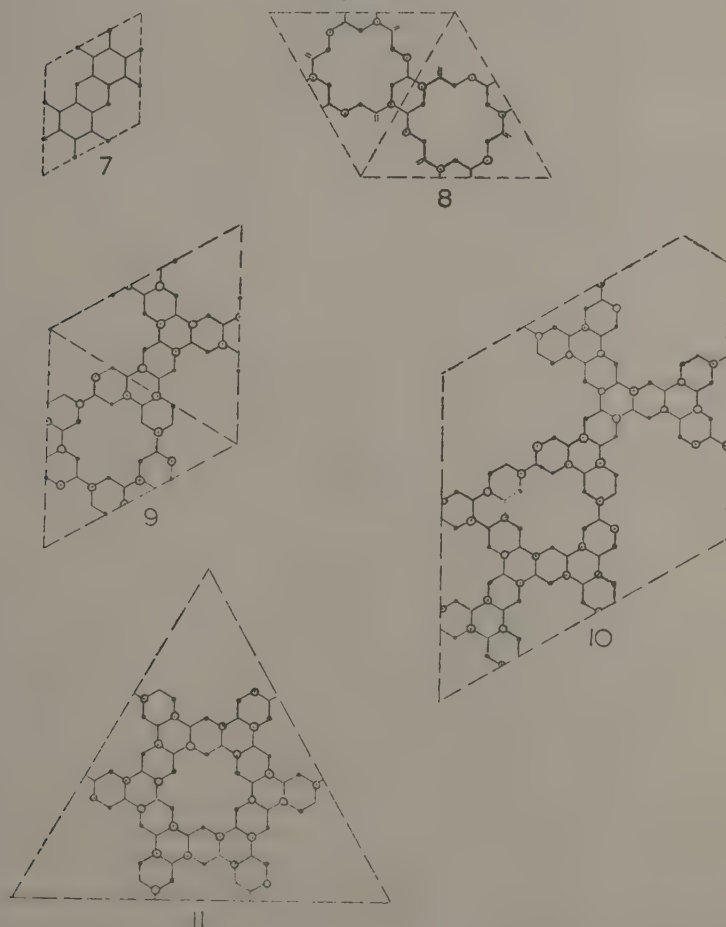
Reasonable estimates, based upon actual analyses of crystal structures containing water molecules, would allocate water molecules to the various R groups probably roughly as follows:—Arginine 4, histidine and tryptophane 1, lysine 2, aspartic and glutamic acid 2, acid amides 4, tyrosine and serine 1, and so on. In addition, the skeleton has "sticky" foci in the carbonyl or hydroxyl groups and in the imino groups or tertiary nitrogens which can account for the adherence of three or more water molecules per residue. We may compare these figures with X-ray data^{(9), (10)}. Assuming 288 residues per molecule and using tentative figures for insulin, namely, 6 lysines, 6 arginines, 18 histidines, 36 glutamic acids, 36 glutamines, and 24 tyrosines, a complement of 330 water molecules could adhere to R groups alone. Further, the skeleton could hold 576 or more water molecules. The X-ray molecular weight for "dry insulin" is 39,500 and for "wet insulin" 52,400 giving, if the average residue weight is between 120 and 125, a complement of 195–274 water molecules per molecule of insulin in the first case and 911–991 in the second. In the second case the X-ray photographs show spacings down to 2 or 3 Å., indicating a high degree of perfection in the atomic arrangement, not only of the atoms in the proteins, but also in the water molecules, effected, presumably, by their bonding to the proteins. Although the figures for wet insulin yield the huge number of 900 or more water molecules per insulin molecule, even this large number is seen from the estimate given above to be well within the capacity of the skeleton and R groups to hold in position.

The possible advantage in the enol fabric theory that some of the R groups lie embedded within the cage has been referred to. This might be regarded as particularly suitable for such a case as insulin, where about one-third of the residues are leucines, with hydrophobic side chains. To place these within the cage would certainly offer a possible explanation of the remarkable stability of this molecule. Nevertheless, it would seem that it is not yet possible, on the available facts, to decide whether a protein such as insulin, which is soluble in water (in spite of its high leucine content), must for this reason be assumed to have a structure allowing all these hydrocarbon R groups to lie within the structure. For it is to be noticed that the solubility of insulin in water is only 0.027 gm./litre, and its solubility in propylene glycol is at least fifty times as great⁽⁸⁾. This may indicate that some or even all the leucine R groups lie on the surface of the molecule, being so arranged that they form small hydrocarbon neighbourhoods, somewhat after the manner of the hydrocarbon neighbourhoods in the acetamide crystal⁽²⁸⁾. In this crystal there are neighbourhoods in which there are concentrations of methyl groups, and other neighbourhoods tenanted by nitrogen atoms bonded by hydrogen to oxygens. Were this the case with insulin, all the R groups lying outside a closed surface structure, a sufficient explanation of the solubility of insulin in water and of its superior solubility in propylene glycol might be available. A drop in solubility on surface denaturation would result if this process disturbs the compact packing together of hydrophobic groups. This question is of importance specially in relation to one of the proposed structures for insulin, namely, the C₂ cyclol (lactim) cage. This can be taken in extravert or introvert form, but the dimensions of the cage suggest that the introvert form is unlikely. Either the extravert lactim forms or the enol cage or cages with some R groups within and a majority of them outside seems a more acceptable hypothesis.

A curious feature of these new cage structures is the fact that when the 288-residue cage is broken down by complete decyclization into linear peptides consisting wholly of lævo residues, it comprises 24 hexapeptide rings, 12 decapeptide rings, and 12 dipeptide rings, for (a) and (b) slits, 12 hexapeptide rings being replaced by 12 hexapeptide chains for (c) slits. A thoroughgoing denaturation may thus lead to these products, which, however, would be quite impossible to identify, in all probability, since each type of ring may be far from homogeneous in its R groups. Less severe denaturation, and particularly denaturations which are reversible, presumably connote incomplete decyclizations, entailing characteristically different products. This theory, like the cyclol theory, can account for a variety of structurally distinct degradation products, varying with the method and severity of denaturation, such as is found experimentally, and stresses the point of view according to which there is a fundamental

difference between a native and a denatured protein, in that the structure of the first is definite and unique, the outstanding characteristic of the second being that it takes an immense variety of different forms ⁽²¹⁾. Perhaps the most unequivocal evidence regarding the variety of forms of

Figs. 7-11.



Enol cage-faces.

denatured protein is contained in the experiments of Langmuir and Schaefer on pepsin, in which pepsin was denatured by heating and shaking etc., and it was found that the monolayers formed varied in their properties according to the temperature and the time the treatment was employed,

and so on ⁽²⁹⁾. We picture the denatured monolayer as made up of the partially decyclized and partially isolated peptide rings, capable of reversible compression (owing to the breaking of the cyclol links), and in extreme cases of isolated peptide rings, moored to the surface by the hydrophilic groups and anchored by the hydrophobic groups lying in the substrate. The process of denaturation on this theory evidently releases the hydrophobic groups from the interior of the cage, the immense decrease in solubility found in protein monolayers being thereby given one possible explanation. While surface forces may be presumed to be strong enough to rip open the cages sufficiently for a suitable balance of hydrophobic and hydrophilic groups to be attained, it seems that prior denaturation may lead to increased decyclization and increased fragmentation of the fabric, which should, perhaps, prove correlatable with the gradation in properties seen in the pepsins subjected to increasingly severe denaturation.

In addition to the $72n^2$ residue skeletons, attention may be drawn to other possibilities of cage formation by "enol" fabrics, sufficiently indicated by figs. 7-10, showing one-quarter of the fabric proposed for the smallest member of each series of cages, and by fig. 11, which shows one-eighth. The skeletal residue numbers would be $24n^2$, $48n^2$, $72n^2$, $144n^2$, and $192n^2$ respectively. All these structures may require valency angles for the atoms along the edges somewhat different from the tetrahedral angle so far assumed. In all there is the possibility of $\text{NH} \dots \text{N}$ bonding in the hexa- or tetrapeptide rings.

Hydrogen Bond Fabric Cages.

At the outset of this enquiry it was seen that units with more than two arms could also be obtained by postulating hydrogen bridges between residues, and fabrics built upon this principle ⁽³⁷⁾ were put forward as early as 1936, the general idea being discussed also in 1939 ⁽³⁵⁾. In this communication specific suggestions as to the topology of surface nets which may be suitable for the purpose are made.

In accordance with this scheme, fig. 12, reproducing a fragment of a fabric proposed in 1936, exhibits two suggestions as to eight faced cage structures, one-eighth of the total fabric of the smallest cages of series comprising respectively 24, 96, . . . , $24n^2$, . . . , residues and 72, 288, . . . , $72n^2$, . . . residues being shown. The R groups lie outside the cage and suggested $\text{NH} \dots \text{O}$, hydrogen bonds are dotted. In fig. 13 a fragment of a fabric in which cyclol-6 units are hydrogen-bonded to uncyclized peptide rings is exhibited, one-eighth of the total fabric of the smallest (eight faced) cage of a series comprising $72n^2$ residues being shown. A fragment of a fabric formed by partially cyclized 18-residue rings, hydrogen-bonded internally and externally, comprising one-eighth of the material needed for the smallest cage of a series comprising $72n^2$ residues, is shown in

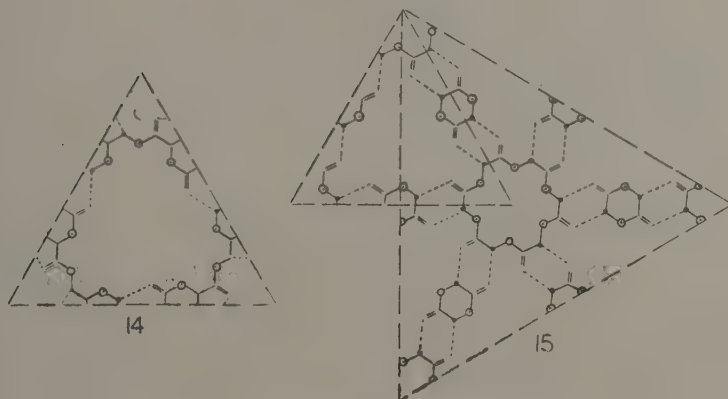
fig. 14. In these cages the corners are tenanted by partially cyclized 12-residue rings. Finally, fig. 15 provides two suggestions as to series of $48n^2$ - and $144n^2$ -residue structures. In this case 2-residue rings are hydrogen-bonded to 6-residue rings with 4-residue rings at the corners. Such examples can be multiplied, especially for cages with large complements of residues. Those detailed include only cases in which there are

Figs. 12 & 13.



Hydrogen-bond fabrics.

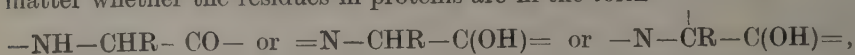
Figs. 14 & 15.



Hydrogen-bond fabrics.

such residue numbers as $24n^2$, $48n^2$, $72n^2$, $144n^2$, $192n^2$, but other series which have considerably greater numbers of residues in their first members can be constructed after the same manner. These special examples of possible nets of atoms which may be capable of folding around to form closed surface structures are recorded for two reasons. In the first place, it appears likely that the folding into cages can be so arranged as to be

consistent with the facts regarding bond lengths and bond angles in crystallographic literature, in which case they are to be considered as possible protein structures, since their composition is appropriate for protein, and they yield linear peptides when bonds are opened. Secondly, the main theme of the present attack on protein structure is the suggestion that closed surface structures provide a solution to the existence of megamolecules having definite molecular weights and other definite physical and chemical characteristics. Now an arrangement of atoms of the types shown in figs. 8–15 is as much a fabric as the original cyclol fabric and, as such, provides one special set of examples of the type of structure which, we suggest, offers a solution to the problem of the megamolecule. No matter whether the residues in proteins are in the form



no matter whether or not the whole structure is simply one or several coiled peptide chains. If with or without hydrogen bonding there is a functionality higher than 2 in a sufficient proportion of residues, a fabric structure and so, potentially, a closed fabric structure may result. In such structures many of the characteristics of the cyclol fabric cages or of the enol fabric cages may be reproduced (*e. g.*, the eight-faced polyhedra), and it may prove difficult to devise tests which would allow differentiation between the various cage types. It is, however, very desirable that the cage type of structure or, more generally, a closed fabric type of structure, should be studied with a view to discovering ways in which it would be detectable by physical or chemical techniques. This objective is, of course, distinct from the attempt to determine the nature of the atomic pattern, a question which may well be beyond the range of experiment at present. In connexion with the possibility of obtaining information on this aspect of the problem by spectroscopic studies, attention may be directed to the work of Rodebush and Buswell⁽²⁷⁾ on association through hydrogen. They refer to the striking resemblance between the absorption spectrum of gelatin and that of the associated amide $\text{C}_2\text{H}_5\text{CONH}_2\text{H}_5$. In view of the fact that there is some evidence from freezing-point data in favour of a trimeric formula for such amides, this resemblance is of special interest in relation both to the triazine ring of the original cyclol fabric (as pointed out by these authors) and to the trimeric hydrogen-bonded structures shown in fig. 12. Gelatin, though not a globular protein, appears to have retained some, at least, of their fine structure. (For a possible structure for gelatin see the fourth cyclized polypeptide shown in fig. 3, page 125. 'Cold Spring Harbor Symposium,' vi. 1938.)

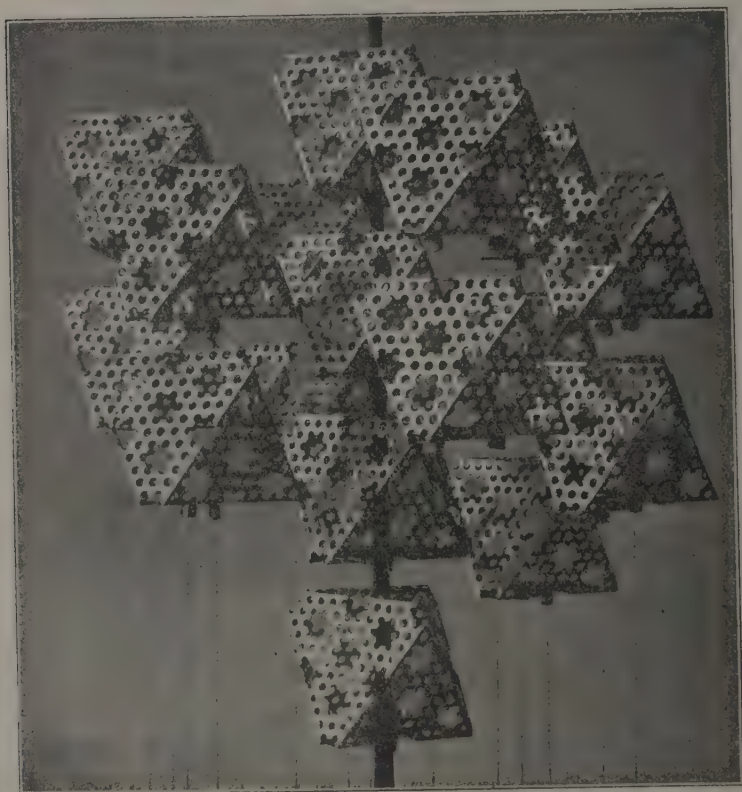
As previously suggested⁽³⁴⁾, many, perhaps most, protein molecules may consist of sets of closed fabric structures in association. Such associations would account for the capacity of certain proteins to dissociate into

aliquot parts, a characteristic which is found to be very widespread. In this event, residue numbers which are multiples of 24, with molecular weights which (roughly) are multiples of 3000, are to be expected. Such a small unit has already been suggested, but further data are required before it can be decided whether it is actually present in such a case as (*e. g.*) insulin, but it should be pointed out that 12 such units could be postulated for the insulin molecule if desired, though to date there is no evidence supporting such a suggestion, rather than the suggestion of one or four individual cages containing 288 or 4×72 residues.

The association of fabric cages brings up another point which has an importance throughout our investigations, namely, the way in which polyhedral cage skeletons are adapted for the stable association of megamolecules. It was evident from the start that the opposition of polyhedral faces allows the *simultaneous formation* of a considerable number of skeletal hydrogen-bonds or salt linkages or even of other linkages between R groups. Such linkages can bind structures together and so explain, not only the formation of protein crystals, but also the formation in the liquid state of definite polymolecular or micellar structures. It must be remembered that the strength of a hydrogen bond (say 3-8 k.cal./mole.) is by no means negligible and that, say, 10 to 20 such links can exceed a carbon-carbon bond in strength. The presence of such micelles explains many of the puzzles in protoplasmic structures, for upon the architecture and geometry of the molecule and its bond-forming groups depends the architecture of the micelles. Thus in the case of zinc-insulin the crystal structure (fig. 16) shows columns in which the structures are placed squarely one upon another. Each column is surrounded by six other parallel columns, giving the rhombohedral lattice with one 36,000-unit per cell. It seems likely that the columns are held in their relative positions by zincs, but the units are apparently adapted to form columnar fibrils by means of hydrogen bridges or other bonds. A more general case can also be visualized in which the units are capable of forming fibrils in two, three, or four definite directions. Such associations of units could give to protoplasm just the kind of structure which is required. The polarity shown by the column-like fibrils in the insulin crystal is, in fact, very suggestive in relation to the polarity shown by the developing egg. In many cases an egg showing a single axis forms a new axis when cut into two, a situation which can be understood if we bear in mind the possibility that each such axis is a manifestation of the special characteristics of certain key molecules, probably proteins, which have their own polar axes determining the architecture of the micelles which they are capable of forming. The proteins, in many cases, have been shown capable of forming crystals which contain vastly different complements of water molecules. In protoplasm in which the complement

of water is of the order of thousands to one 36,000 unit of protein, there appears to be a skeleton network which gives it some kind of structure—a structure, in fact, whose characteristics, we suggest, are determined by the structure of the key molecules, in collaboration with the power of determining orientation possessed by water molecules.

Fig. 16.



Model of zinc-insulin crystal.

Structures which would be of the kind required would be possessed by suitable sub-classes of the molecules in (say) the insulin lattice, so chosen that the structure is connected. We might, for instance, take one molecule in the insulin lattice, adding to it its six neighbours and the neighbours of neighbours which lie along the rhombohedral axes of the original molecule, all missing molecules being replaced by water molecules. Or we might delete from the complete insulin lattice five out of every

six molecules in each column, selecting the molecules to be replaced by water in such a way that the set of molecules left is connected. The concept of growth along definite curvilinear axes introduced decades ago by D'Arcy Thompson would seem to indicate a similar situation, in which the architecture of the key molecules favours the formation of micelles of definite structure which may attain micron dimension. In this way, it may in due course be possible to interpret the gross geometry of living organisms with dimensions of the order of microns and centimetres in terms of the geometry and the chemical groups of individual key molecules with dimensions of the order of angstroms, for the interlinking of neighbouring molecules would be determined by the particular groups available on their opposed faces and would be specific for the patterns in which such groups are arranged. Although such structures, representing associations of molecules which make use of only part of the power to interlink shown in the crystal, might have considerable fluidity, the interlinking which is present puts certain restrictions on the power of rotation of individual molecules and on the packing and arrangement and numbers of water molecules, which themselves impose further restrictions. Interactions at very considerable distances can be visualized in this way, just as a wrench can be transmitted along a chain in which the individual links have structure and are interlinked in a special way. An experiment just reported demonstrates the formation of just such micelles by the globular insulin molecules. A 2 per cent. solution of insulin hydrochloride in distilled water is heated at 100° C. for 30 minutes in a water bath, forming a birefringent thixotropic cell having a pH about 2.7. This, when diluted, gives a clear, slightly viscous solution which shows strong birefringence of flow⁽²⁰⁾. The particular forces which hold the insulin molecules together in this case cannot at present be deduced: the possibility that hydrogen bonds play some part—even at this pH—cannot be excluded, since little or nothing is known as to the effect of pH on such bondings, in the case of megamolecules.

These suggestions are strictly in line with the general idea in the present work, namely, that the native globular protein molecule is the repository of pattern in the organism and the seat of its specificities, and that these patterns play a dominant role in determining the superstructure of the organism, which manifests itself in grosser phenomena.

References.

- (1) Aberhalden, *Z. physiol. Chem.* xxxvii. p. 499 (1903).
- (2) Aberhalden, *Z. physiol. Chem.* xxxvii. p. 495 (1903).
- (3) Aberhalden, *Z. physiol. Chem.* cxxxvi. p. 134 (1929).
- (4) Baker, 'Tautomerism,' p. 179 (1932).
- (5) Bergman and Niemann, *J. Biol. Chem.* cxviii. p. 301 (1937).
- (6) Block, 'Cold Spring Harbour Symposium,' vi. p. 79 (1938).

- (7) Calvery, J. Biol. Chem. xciv. p. 613 (1931).
- (8) Cohn, 'Science' (1939).
- (9) Crowfoot, Proc. Roy. Soc. cxiv. A, p. 580 (1938).
- (10) Crowfoot and Riley, 'Nature,' cxliv. p. 1011 (1939).
- (11) Frevel, Z. Krist. xciv. p. 197 (1936).
- (12) Fuerth and Minnebeck, Biochem. Z. ccl. p. 18 (1932).
- (13) Herzberg, 'Atomic Spectra and Atomic Structure,' p. 31 (1937).
- (14) Hopkins and Savory, J. Physiol. xlii. p. 189 (1911).
- (15) Hotchkiss, J. Biol. Chem. cxxxi. p. 387 (1939).
- (16) Jensen, private communication.
- (17) Johns and Johns, J. Biol. Chem. xlviii. p. 437 (1931).
- (18) Jordan Lloyd, Biol. Rev. vii. p. 254 (1932).
- (19) Langmuir, Proc. Phys. Soc. li. p. 592 (1939).
- (20) Langmuir and Waugh, J. Am. C. S. forthcoming.
- (21) Mirsky and Pauling, Proc. Nat. Ac. Sci. (1936).
- (22) Moerman, Z. Krist. A, xcvi. p. 447 (1938).
- (23) Osborne and Clapp, Am. J. Physiol. xix. p. 475 (1907).
- (24) Osborne and Liddle, Am. J. Physiol. xxvi. p. 295 (1910).
- (25) Pauling and Niemann, J. Am. C. S. lxi. p. 1860 (1939).
- (26) Robertson, J. C. S. p. 615 (1935); p. 1195 (1936).
- (27) Rodebush and Buswell, J. Phys. Chem. xliii. p. 219 (1939).
- (28) Senti and Harker, J. Am. C. S. forthcoming.
- (29) Shaefer, J. Phys. Chem. xlii. p. 1089 (1938).
- (30) Sjogren and Svedberg, J. Am. C. S. lii. p. 3650 (1930).
- (31) Town, Biochem. J. xxx. p. 1837 (1936).
- (32) Wrinch, 'Nature,' cxxxvii. p. 411 (1936); Proc. Roy. Soc. A. clx., p. 59 (1937) *et seq.*
- (33) Wrinch, 'Nature' cxxxix. p. 972 (1937); Proc. Roy. Soc. A, clxi. p. 505 (1937).
- (34) Wrinch, Phil. Mag. xxvi. p. 313 (1938).
- (35) Wrinch, International Congress of Genetics, Edinburgh (1939).
- (36) Wrinch, Phil. Mag. xxx. p. 64 (1940).
- (37) Wrinch and Jordan Lloyd, 'Nature,' cxxxviii. p. 758 (1936).

© Id Spring Harbour Biological Station,
Long Island, New York.

XX. *A Method for Measuring the Internal Area of Section of a Glass Tube.*

By D. J. BEHRENS, University of Manchester *.

[Received October 9, 1940.]

IN certain experiments, it is desired to measure the internal sectional area of a glass tube at a particular point thereof. It is not always convenient to break the tube at the point concerned; *e. g.*, if the experiment may have to be repeated, or if the apparatus be of value.

The standard method is to fill the tube with some heavy liquid, usually mercury, and to weigh the resulting column of liquid, whose length and density are known. This method clearly gives not the sectional area at any point of the tube, but a mean value along a certain length. This is not always an advantage, as, for example, in the case of experiments on capillary rise due to surface tension. Again, it may happen that the tube is so small that the mercury cannot be weighed to sufficient accuracy, or so short that the meniscus errors become appreciable.

An optical method obviating these difficulties is described by Kohlrausch †, and has been extended by Anderson ‡. This method has the advantage of being applicable to a totally enclosed tube, but is not very easy to use practically. In many cases the method here described will be found to be more convenient, and it also gives a useful method of measuring the refractive index of the material of a tube whose end is accessible.

Consider first a tube whose outer and inner sections are concentric circles. In fig. 1, R and r represent the external and internal radii of the tube. ρ is the apparent internal radius as seen in a travelling microscope.

If θ and ϕ have the meanings assigned to them in the diagram, and μ is the refractive index of the tube, then we can see that $r = R \sin \theta$, $\rho = R \sin \phi$, and $\sin \phi = \mu \sin \theta$. From these it follows that

$$r = \rho / \mu. \quad \dots \dots \dots (1)$$

It is here assumed that the refractive index is uniform, and is less than the ratio R/r . Were it to exceed this ratio, then the ray leaving

* Communicated by Prof. D. R. Hartree, F.R.S.

† *Praktische Physik*, p. 97 (1921).

‡ *Journ. Sci. Instruments*, p. 24 (1922); p. 9 (1923).

$$p \tan \alpha = r \sin \alpha = dp/d\eta. \quad (4)$$

$$\delta A = \frac{1}{2} r^2 \delta(\eta + \alpha). \quad (5)$$

From the last two equations we can obtain the relation *,

$$2A = \int_0^{2\pi} \{p^2 - (dp/d\eta)^2\} d\eta. \quad (6)$$

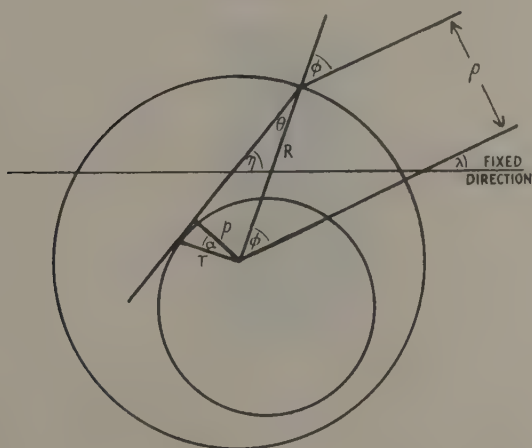
If we define β by the formula,

$$\beta = \frac{1}{\sqrt{R^2 - \rho^2}} - \frac{1}{\sqrt{k^2 R^2 - \rho^2}}, \quad (7)$$

then by differentiating equation (2) and using equations (3) we obtain the result

$$d\eta/d\lambda = 1 + \beta(dp/d\lambda).$$

Fig. 2.



Combining this last relation with formula (6), we get

$$2A = \frac{1}{k^2} \int_0^{2\pi} \left\{ \rho^2 (1 + \beta \rho') - \frac{\rho'^2}{1 + \beta \rho'} \right\} d\lambda, \quad (8)$$

where ρ' represents $dp/d\lambda$.

By the use of equations (4) and (5), it can be verified that this formula still holds good when the centre of the external section does not lie within the internal section (*e. g.*, a clinical thermometer).

Now $\beta \rho'$ is the derivative of a single-valued function of ρ , so that its integral round the whole range of λ must vanish.

* See, for example, Courant, 'Differential and Integral Calculus,' English Translation, vol. ii. pp. 213-214. The result is not given in the German original.

Formula (8) can therefore be rewritten

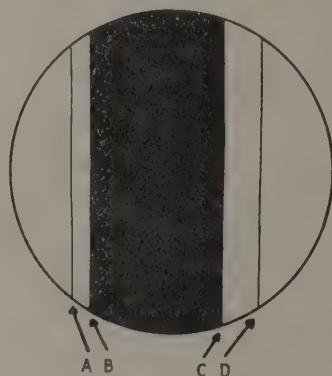
$$2k^2A = \int_0^{2\pi} (\rho^2 - \rho'^2 + \beta\rho'^3 - \beta^2\rho'^4 + \dots) d\lambda. \quad (9)$$

The expansion is justified, because when k is suitably adjusted, the value of $\beta\rho'$ —even in such a tube as a clinical thermometer—is very considerably less than unity for all λ . A numerical example is appended, which shows that the terms in this integrand do, in fact, converge very rapidly.

It has been assumed that the internal section is everywhere concave: a tube in which this was not true would not be a suitable medium for the performance of physical experiments.

Fig. 3 shows the appearance of the tube in the microscope. The central dark area in the diagram represents the internal section of the tube,

Fig. 3.



which lies between the outermost of the visible boundaries within the tube. Of the four points, A, B, C, and D, it is necessary only to measure three, say A, C, and D. If a , c , and d are the readings of the travelling microscope when these three points are observed, then R is given by $\frac{1}{2}(d-a)$, and ρ by $c - \frac{1}{2}(a+d)$. Seeing that the measurements made upon the tube are not symmetrical with respect to the two sides of the tube, it is not surprising that the sense of rotation of the tube between one observation and the next is of importance. This can also be seen from the fact that formula (9) contains odd powers of ρ' .

In an ordinary tube it is sufficient to measure ρ at 30° intervals of λ . To facilitate this, it is convenient to have two plywood dodecagons on to the middle of which are fastened corks. The tube can then be held in a horizontal position in a tank of water and the microscope mounted vertically above. To increase λ by 30° , the microscope is left undisturbed, but the tube is rotated by turning the dodecagons on to their next edges.

The sense in which the tube must be turned to increase λ is that which turns away from the microscope that side of the tube on which ρ is reckoned positive.

Diffraction effects are not usually appreciable. If chromatic effects appear, monochromatic light may be used

A set of readings for an actual tube is appended. From the readings it will be found that

$$\begin{aligned}\int_0^{2\pi} \rho^2 d\lambda &= 4.45 \text{ cm.}^2 \\ - \int_0^{2\pi} \rho'^2 \rho'^2 d\lambda &= -2.6 \times 10^{-3} \text{ cm.}^2 \\ \int \beta \rho'^3 d\lambda &= -1.75 \times 10^{-6} \text{ cm.}^2,\end{aligned}$$

and thus the values of the second and following terms of the expansion are sufficient only to affect the value of the area given by the first term to the extent of 1/10 per cent., which is far less than the experimental errors in this particular experiment.

It will very often be found sufficient to take this first term only. A rough criterion is that if the maximum deviation in ρ is less than 10 per cent. of the mean value, then it is likely that the value of the area given by the first term of the expansion will be correct to within 1 per cent.

Readings for an actual tube, nominally of 2 cm. external diameter, $1\frac{1}{2}$ cm. internal.

(1) At end :—

Max. and min. of r , 0.749 and 0.732 cm.

Max. and min. of ρ , 0.853 and 0.833 cm.

Hence $k=1.138$ and $k^2=1.297$.

(2) At particular point :—

λ .	A.	C.	D.	R.	ρ .
0°	7.263	9.115	9.291	1.014	0.838 (all lengths in cm.)
30°	7.381	9.239	9.412	1.016	0.842
60°	7.292	9.156	9.326	1.017	0.847
90°	7.423	9.289	9.457	1.017	0.849
120°	7.876	9.741	9.905	1.015	0.850
150°	7.628	9.491	9.654	1.013	0.850
180°	7.351	9.212	9.379	1.014	0.847
210°	7.489	9.348	9.521	1.016	0.843
240°	7.020	8.875	9.055	1.017	0.837
270°	7.384	9.235	9.418	1.017	0.834
300°	7.298	9.145	9.328	1.015	0.832
330°	7.404	9.252	9.430	1.013	0.835

XXI. *The Determination of Green's Function for Line Sources for the Equation of Conduction of Heat in Cylindrical Coordinates by the Laplace Transformation.*

By H. S. CARSLAW, Emeritus Professor of Mathematics,
University of Sydney,

and

J. C. JAEGER, Lecturer in Mathematics, University of Tasmania *.

[Received January 1, 1940.]

1. *Introduction.*

THE Green's Function of this paper is the temperature v at P (r, θ) at time t due to an instantaneous unit line source at P' (r', θ') at time zero, the solid being then at zero temperature, and the surface kept at zero.

The solids with which we deal fill the regions

- (i.) $0 \leq r < a$.
- (ii.) $a < r$.
- (iii.) $a < r < b$.
- (iv.) $0 < \theta < \theta_0$.
- (v.) $0 < \theta < \theta_0, \quad 0 \leq r < a$.
- (vi.) $0 < \theta < \theta_0, \quad a < r$.
- (vii.) $0 < \theta < \theta_0, \quad a < r < b$.

Let $R^2 = r^2 + r'^2 - 2rr' \cos (\theta - \theta'). \quad \dots \dots \dots (1)$

and $\dagger \quad u = \frac{1}{4\pi\kappa t} e^{-R^2/4\kappa t} \quad \dots \dots \dots (2)$

Put $v = u + w. \quad \dots \dots \dots (3)$

Then in the solid w has to satisfy

$$\frac{\partial w}{\partial t} = \kappa \left(\frac{\partial^2 w}{\partial r^2} + \frac{1}{r} \frac{\partial w}{\partial r} + \frac{1}{r^2} \frac{\partial^2 w}{\partial \theta^2} \right), \quad t > 0, \quad \dots \dots \dots (4)$$

* Communicated by the Authors.

$\dagger u$ is the temperature at time t due to an instantaneous unit line source at (r', θ') in an infinite solid. Cf. Carslaw, 'Conduction of Heat' (ed. 2), § 72.

Then from (3) and (12) we find

$$\bar{v} = \frac{1}{2\pi\kappa} \sum_{n=-\infty}^{\infty} \frac{I_n(qr')}{I_n(qa)} [I_n(qa)K_n(qr) - I_n(qr)K_n(qa)] \cos n(\theta - \theta'), \quad (14)$$

when $r > r'$, and we interchange r and r' when $r < r'$.

Using the Inversion Theorem *

$$v = \frac{1}{4i\pi^2\kappa} \sum_{n=-\infty}^{\infty} \cos n(\theta - \theta') \int_{\gamma-i\infty}^{\gamma+i\infty} e^{\lambda t} \frac{I_n(\mu r')}{I_n(\mu a)} [I_n(\mu a)K_n(\mu r) - I_n(\mu r)K_n(\mu a)] d\lambda,$$

where $\mu = \sqrt{(\lambda/\kappa)}$. This reduces to

$$v = \frac{1}{\pi a^2} \sum_{n=-\infty}^{\infty} \sum_{\alpha} e^{-\kappa \alpha^2 t} \frac{J_n(\alpha r)J_n(\alpha r')}{[J'_n(\alpha a)]^2} \cos n(\theta - \theta'), \quad (15)$$

where the α are the positive roots of $J_n(\alpha a) = 0$.

The result (15), being symmetrical in r and r' , is valid for $r \geq r'$.

3. Internal Boundary $r=a$.

$$\text{Here } \bar{w} = -\frac{1}{2\pi\kappa} \sum_{n=-\infty}^{\infty} \frac{I_n(qa)K_n(qr')K_n(qr)}{K_n(qa)} \cos n(\theta - \theta')$$

$$\text{and } \bar{v} = \frac{1}{2\pi\kappa} \sum_{n=-\infty}^{\infty} \frac{K_n(qr')}{K_n(qa)} [I_n(qr)K_n(qa) - K_n(qr)I_n(qa)] \cos n(\theta - \theta'),$$

$$a < r < r'. \quad (16)$$

Using the Inversion Theorem,

$$v = \frac{1}{4i\pi^2\kappa} \sum_{n=-\infty}^{\infty} \cos n(\theta - \theta') \int_{\gamma-i\infty}^{\gamma+i\infty} e^{\lambda t} \frac{K_n(\mu r')}{K_n(\mu a)} [I_n(\mu r)K_n(\mu a) - K_n(\mu r)I_n(\mu a)] d\lambda,$$

which gives †, for $r \geq r'$,

$$v = \frac{1}{2\pi} \sum_{n=-\infty}^{\infty} \cos n(\theta - \theta') \int_0^{\infty} e^{-\kappa x^2 t} \frac{U_n(\alpha r)U_n(\alpha r')}{J_n^2(\alpha a) + Y_n^2(\alpha a)} \alpha dx, \quad (17)$$

where

$$U_n(\alpha r) = J_n(\alpha r)Y_n(\alpha a) - J_n(\alpha a)Y_n(\alpha r). \quad (18)$$

4. The Region $a < r < b$.

$$\text{Here } \bar{v} = \frac{1}{2\pi\kappa} \sum_{n=-\infty}^{\infty} \cos n(\theta - \theta')$$

$$\times \frac{[I_n(qa)K_n(qr) - I_n(qr)K_n(qa)][I_n(qb)K_n(qr') - I_n(qr')K_n(qb)]}{I_n(qa)K_n(qb) - I_n(qb)K_n(qa)},$$

$$a < r < r', \quad (19)$$

* For the method of evaluating integrals of this type by contour integration, see Carslaw and Jaeger, *loc. cit.* The contour is fig. 1 of that paper.

† The contour is now fig. 2 of Carslaw and Jaeger, *loc. cit.*

This, from the Inversion Theorem, gives, for $r \geq r'$,

$$v = \frac{\pi}{4} \sum_{n=-\infty}^{\infty} \sum_{\alpha} \alpha^2 e^{-\kappa \alpha z} \frac{J_n^2(\alpha b) U_n(\alpha r) U_n(\alpha r')}{J_n^2(\alpha a) - J_n^2(\alpha b)} \cos n(\theta - \theta'), \quad . \quad . \quad (20)$$

where $U_n(\alpha r)$ is defined in (18), and the α are the positive roots of $U_n(\alpha b) = 0$.

5. The Region $0 < \theta < \theta_0$.

Here starting from (10) we use the result*, valid for $r > r'$, and $0 < \theta - \theta' < 2\pi$,

$$K_0(qR) = P \int_{-\infty i}^{\infty i} \frac{\cos z(\pi - \theta + \theta')}{\sin z\pi} I_z(qr') K_z(qr) i dz, \quad . \quad . \quad (21)$$

where P implies that the principal value of the integral at the origin is taken, i. e., that it is evaluated as

$$\lim_{\varepsilon \rightarrow 0} \left\{ \int_{-\infty i}^{-\varepsilon i} + \int_{\varepsilon i}^{\infty i} \right\}.$$

This gives, for $r > r'$,

$$\bar{w} = P \int_{-\infty i}^{\infty i} \frac{\cos z(\pi - \theta_0 + \theta') \sin z\theta + \cos z(\pi - \theta') \sin z(\theta_0 - \theta)}{2\pi i \kappa \sin z\theta_0 \sin z\pi} I_z(qr') K_z(qr) dz,$$

and $\bar{v} = \bar{u} + \bar{w}$

$$= \int_{-\infty i}^{\infty i} \frac{\sin z\theta' \sin z(\theta_0 - \theta)}{i\pi \kappa \sin z\theta_0} I_z(qr') K_z(qr) dz, \quad r > r', \quad \theta_0 > \theta > \theta', \quad (22)$$

where the integral is now an ordinary integral, since the integrand is finite at the origin.

The integral in (22) is evaluated by completing the contour by a large semi-circle in the right-hand half plane and summing the residues at the poles at

$$s = n\pi/\theta_0, \quad n = 1, 2, \dots \quad . \quad . \quad . \quad (23)$$

s will be used throughout in this sense, and \sum will imply a summation from $n=1$ to ∞ .

Then we find

$$\bar{v} = \frac{2}{\kappa \theta_0} \sum \sin s\theta \sin s\theta' I_s(qr') K_s(qr), \quad r > r'. \quad . \quad . \quad (24)$$

Now* for $r > r'$

$$I_s(qr') K_s(qr) = \kappa \int_0^\infty e^{-pt} dt \int_0^\infty \alpha e^{-\kappa \alpha^2 t} J_s(\alpha r) J_s(\alpha r') d\alpha.$$

* This is proved by the same method as Gray and Mathews, *loc. cit.* p. 102 (14). It is due to Dougall, Proc. Edinburgh Math. Soc. (1) xviii. pp. 33-83 (56) (1900).

† Cf. Gray and Mathews, *loc. cit.* p. 69 (18) and p. 74 (57), but note that their conditions for the latter are unnecessarily restrictive.

Thus, finally,

$$v = \frac{2}{\theta_0} \sum_s \sin s\theta \sin s\theta' \int_0^{\infty} \alpha e^{-\kappa\alpha z} J_s(\alpha r') J_s(\alpha r) d\alpha. \quad (25)$$

6. *The Region* $0 < \theta < \theta_0, \quad 0 \leq r < a$.

Here

$$\bar{v} = \frac{2}{\kappa\theta_0} \sum_s \sin s\theta \sin s\theta' \frac{I_s(qr')}{I_s(qa)} [I_s(qa)K_s(qr) - I_s(qr)K_s(qa)], \quad r > r', \quad (26)$$

and

$$v = \frac{4}{a^2\theta_0} \sum_s \sin s\theta \sin s\theta' \sum_{\alpha} e^{-\kappa\alpha z} \frac{J_s(\alpha r)J_s(\alpha r')}{[J'_s(\alpha a)]^2}, \quad (27)$$

where the α are the roots of $J_s(\alpha a) = 0$.

7. *The Region* $0 < \theta < \theta_0, \quad r > a$.

Here

$$\bar{v} = \frac{2}{\kappa\theta_0} \sum_s \sin s\theta \sin s\theta' \frac{K_s(qr')}{K_s(qa)} [(K_s(qa)I_s(qr) - K_s(qr)I_s(qa))], \quad r < r', \quad (28)$$

and

$$v = \frac{2}{\theta_0} \sum_s \sin s\theta \sin s\theta' \int_0^{\infty} \alpha e^{-\kappa\alpha z} \frac{U_s(\alpha r)U_s(\alpha r') d\alpha}{J_s^2(\alpha a) + Y_s^2(\alpha a)} \quad (29)$$

where

$$U_s(\alpha r) = J_s(\alpha r)Y_s(\alpha a) - J_s(\alpha a)Y_s(\alpha r). \quad (30)$$

8. *The Region* $0 < \theta < \theta_0, \quad a < r < b$

Here $\bar{v} = \frac{2}{\kappa\theta_0} \sum_s \sin s\theta \sin s\theta'$

$$\times \frac{[I_s(qa)K_s(qr) - I_s(qr)K_s(qa)] [I_s(qb)K_s(qr') - I_s(qr')K_s(qb)]}{I_s(qa)K_s(qb) - I_s(qb)K_s(qa)}, \quad r < r'. \quad (31)$$

This gives

$$v = \frac{\pi^2}{\theta_0} \sum_s \sum_{\alpha} \sin s\theta \sin s\theta' \alpha^2 e^{-\kappa\alpha z} \frac{J_s^2(\alpha b)U_s(\alpha r)U_s(\alpha r')}{J_s^2(\alpha a) - J_s^2(\alpha b)}, \quad (32)$$

where $U_s(\alpha r)$ is defined in (30), and the α are the positive roots of $U_s(\alpha b) = 0$.

XXII. *Measurement of Surface Tension by the Ripple Method.*

By E. TYLER, D.Sc., M.Sc., F.Inst.P., A.F.R.Ae.S., Senior Lecturer
in Physics, Science Department, South-East
Essex Technical College, Dagenham *.

[Received December 6, 1939.]

Introduction.

WHEN measuring the surface tension of a liquid by the ripple method, validity of Kelvin's equation for the velocity of propagation of surface waves under the combined influence of surface tension and gravity is assumed. This equation is expressible as

$$V^2 = \frac{2\pi\sigma}{\lambda\rho} + \frac{g\lambda}{2\pi}, \quad \dots \dots \dots (1)$$

V being the velocity of the ripples, λ the ripple wave-length, σ the coefficient of surface tension, ρ the density of the liquid, and g the acceleration due to gravity.

Since $V = N\lambda$, where N is the frequency of ripple formation, equation (1) may be rewritten as

$$\sigma = \frac{\lambda^3 N^2 \rho}{2\pi} - \frac{g\lambda^2 \rho}{4\pi^2} \dots \dots \dots (2)$$

A knowledge of λ , N , and ρ thus suffices for computation of σ .

In comparison with other surface tension methods the ripple method is more involved, and since the expression for σ contains the cube of the wave-length (and this is usually small), considerable accuracy in the measurement of λ is required. Despite this requirement, the ripple method has found favour with many workers, mainly because of its dynamic nature, independency of angle of contact, and sensitive means of detecting contamination caused by dissolved substances.

Although reliable results have been arrived at, the method of deducing σ is lacking from an instructional point of view in comparison with any graphical method that might be evolved. The following notes pertain to descriptions of graphical methods suitable for the evaluation of σ .

* Communicated by the Author.

Production and Measurement of Ripples.

The procedures adopted for such production and measurement vary considerably. General classification reveals three distinct methods :—

(a) Photographic.

Progressive waves produced by either a single or line source are photographed by spark or short time exposure. From measurements of the negative with a travelling microscope, the wave-length is obtained.

(b) Stationary Waves.

Formation of standing waves on the liquid surface is effected by the employment of two synchronous sources. Such waves are usually formed between the sources, and these may be photographed and subsequently measured. Alternately the wave-length is obtained direct with the aid of a travelling microscope or cathetometer.

(c) Stroboscopic.

Progressive waves are rendered apparently stationary by viewing them in intermittent light of same frequency as their own formation. The resulting effects are then measured in the same manner as for the stationary waves.

Methods of providing for stroboscopic illumination in synchronization with the ripple formation are numerous, and comprehensive bibliographies on ripple phenomena are to be found in the articles of W. J. Baldwin, jun.*, R. C. Brown †, and E. Tyler ‡.

THEORY.

Suggested Graphical Methods of computing σ by Measurement of N and λ .

Referring to equation (2), we may rewrite it in two ways :—

$$\lambda^3 N^2 = \frac{\lambda^2 g}{2\pi} + \frac{2\pi\sigma}{\rho}, \quad \dots \dots \dots (3)$$

or

$$\lambda N^2 = \frac{2\pi\sigma}{\rho\lambda^2} + \frac{g}{2\pi}. \quad \dots \dots \dots (4)$$

Both these expressions suggest possible methods of deducing σ by graphical treatment, provided certain conditions are fulfilled with regard to the intercepts and slopes of the graphs mentioned in the analysis.

* R. S. I. i. p. 309 (1930).

† Proc. Physical Soc. xlviii. p. 312 (1936).

‡ S. S. R. no. 63, March 1935.

METHOD 1.

Since in equation (3), $\lambda^3 N^2$ and λ^2 are the two variables, this expression is linear. A plot of $\lambda^3 N^2$ against λ^2 therefore yields a straight line graph not passing through the origin (fig. 4). From such a graph the following information is derived :—

(a) When

$$\lambda^2=0, \quad \lambda^3 N^2=OA=\frac{2\pi\sigma}{\rho}, \quad \text{whence } \sigma=\frac{OA \cdot \rho}{2\pi}, \quad . \quad . \quad . \quad (5)$$

i. e., σ is expressed in terms of OA, and density ρ .

(b) When

$$\lambda^3 N^2=0, \quad \lambda^2=\frac{-4\pi^2\sigma}{\rho g}=-OB, \quad \text{or } \sigma=\frac{OB \cdot \rho g}{4\pi^2}, \quad . \quad . \quad . \quad (6)$$

i. e., σ in terms of OB *, ρ , and g .

(c) Slope of graph $=\frac{g}{2\pi}$.

(d) The graphs for different liquids are all straight lines parallel to each other with same slope $\frac{g}{2\pi}$. Their intercepts are different, and for any pair of liquids of surface tensions σ_1 and σ_2 and densities ρ_1 and ρ_2 , we have

$$\frac{\sigma_1}{\sigma_2}=\frac{(OA_1)}{(OA_2)} \cdot \frac{\rho_1}{\rho_2}=\frac{(OB)_1}{(OB)_2} \cdot \frac{\rho_1}{\rho_2} \quad . \quad . \quad . \quad . \quad (7)$$

Reliable values of σ and σ_2 are only possible by employing equations (5) and (7), in which a knowledge of OA is required. Owing to the smallness in the percentage change of $\lambda^3 N^2$ (since gravity effects are small with such ripples over the range investigated), it is impossible to interpolate OB with reliable accuracy.

In this method, however, the cube of the wave-length is still involved. Graphical representation does, however, reduce the margin of error in the final value of σ , since we are able to draw the best line passing through the majority of the observed points, and also satisfy the condition, slope $=\frac{g}{2\pi}$.

METHOD 2.

This method depends on the validity of equation (4) and possesses distinct advantages over method 1.

* Owing to the small gradient of the graph the intercept OB cannot be shown to scale in fig. 4.

Expression 4 represents a linear relationship between the variable quantities λN^2 and $\frac{1}{\lambda^2}$, hence plotting λN^2 against $\frac{1}{\lambda^2}$ gives a straight line similar to that of fig. 5 a.

Information derived therefrom is as follows :—

(a) Slope of graph = $\frac{2\pi\sigma}{\rho}$, whence

$$\sigma = \frac{\rho}{2\pi} \cdot \text{slope}, \quad \dots \dots \dots (8)$$

i. e., σ in terms of slope of graph and density of the liquid ;

(b) when

$$\lambda N^2 = 0, \quad \frac{1}{\lambda^2} = OB = \frac{\rho g}{4\pi^2 \sigma},$$

therefore

$$\sigma = \frac{\rho g}{4\pi^2 \cdot OB}, \quad \dots \dots \dots (9)$$

Hence σ in terms of OB, ρ , and g .

(c) When

$$\frac{1}{\lambda^2} = 0, \quad \lambda \cdot N^2 = OA = \frac{g}{2\pi},$$

i. e.,

$$g = 2\pi \cdot OA. \quad \dots \dots \dots (10)$$

(d) Since intercept $OA = \frac{g}{2\pi}$, all graphs for different liquids have different slopes, but all intersect at A.

For any pair of liquids of densities ρ_1 and ρ_2 and surface tensions σ_1 and σ_2 we have

$$\frac{\sigma_1}{\sigma_2} = \frac{\rho_1 (\text{slope})_1}{\rho_2 (\text{slope})_2}. \quad \dots \dots \dots (11)$$

An advantage of this method is that only the square of the wave-length is now required. The deduction of σ from the slope of the graph, suggested by equation (8), gives the more accurate result.

Only when the intercept OB is known fairly accurately can we utilize equation (9) for computation of σ . In order to effect reliable interpolation of OB, a plot of the results for the lower frequencies below 50/sec. is only necessary, and these must be made on a convenient large scale.

Furthermore, if a source of only one frequency is available we are able to plot the observation as a point P, then insert the point A remembering $OA = \frac{g}{2\pi}$, join AP, and from a knowledge of the gradient of AP and the

density of the liquid thus evaluate σ . By this means a more accurate value of σ should be obtained than by mere substitution of λ in equation (2).

EXPERIMENTAL ARRANGEMENTS.

Three stroboscopic methods were employed, viz. :

1. A synchronous dual-reed method operating at the A.C. mains frequency (fig. 1).
2. An electrically maintained reed or rod interrupter method, suitable for frequencies between 10–50 cycles/sec. (fig. 2).
3. A synchronous photo cell rotating disk and dipper method, for use at the higher frequencies above 100/sec. (fig. 3).

In each method accurate measurement of both the ripple wave-length and frequency of formation is necessary. Furthermore, provision must be made to ensure sharp cut off in the illumination, and hence well-defined ripple images.

Concerning the measurement of the wave-length, various methods are possible.

(a) By direct measurement of the ripple spacings with a travelling microscope mounted above the ripple surface.

(b) Photograph the ripples together with a graduated glass scale placed in the ripple surface, and afterwards measure with a travelling microscope.

(c) Project the ripples upon a ground glass or translucent screen, and measure the ripple images with a travelling microscope. Calibrate by projecting upon the same screen an image of a graduated glass scale placed flat on the ripple surface. Alternately with no scale available, we can use the double lens position method, measuring the size of the ripple images in both cases, *i. e.*, if λ_1 and λ_2 be the measured wave-lengths of the ripple images for both positions of the lens, the true ripple wave-length $\lambda = \sqrt{\lambda_1 \cdot \lambda_2}$.

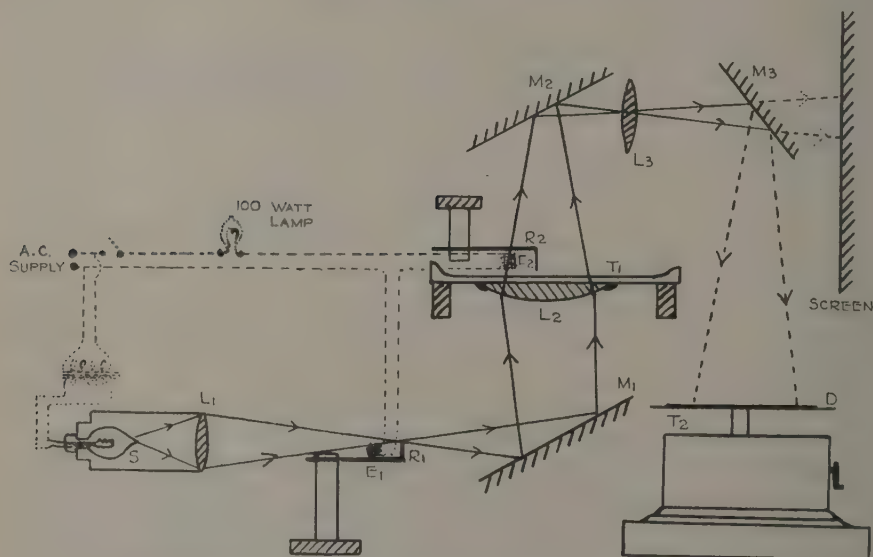
(d) Project the ripples on a distant screen at a magnification of about 10 and measure the size of the ripple image wave-length with a metre scale, afterwards calibrating as in (c). This method of calibrating with a graduated glass scale automatically eliminates any distortion introduced by the optical system.

Of the four methods cited, method *d* is most expeditious in manipulation; it gives good results despite the non-use of the travelling microscope, and for lecture demonstration it is certainly worthy of recommendation. The determination and control of either the frequency of the rippler or the intermittent illumination depend upon the method employed.

Arrangement I.

This is a modification of a dual-reed method incorporated in a "Lecture Demonstration Ripple Tank" described elsewhere*. The availability of the A.C. mains supply is essential for simultaneously energizing the electromagnetic coils E_1 and E_2 of two independent reeds R_1 and R_2 , each functioning as a light interrupter and rippler respectively. Provision is made with the aid of lens L_1 for producing an image of a straight lamp filament (36 watt), horizontally and coincident with the bent end of the maintained reed R , tuned to resonance with the A.C. mains supply. Thus,

Fig. 1.



Synchronization of ripple formation by dual-reed method.

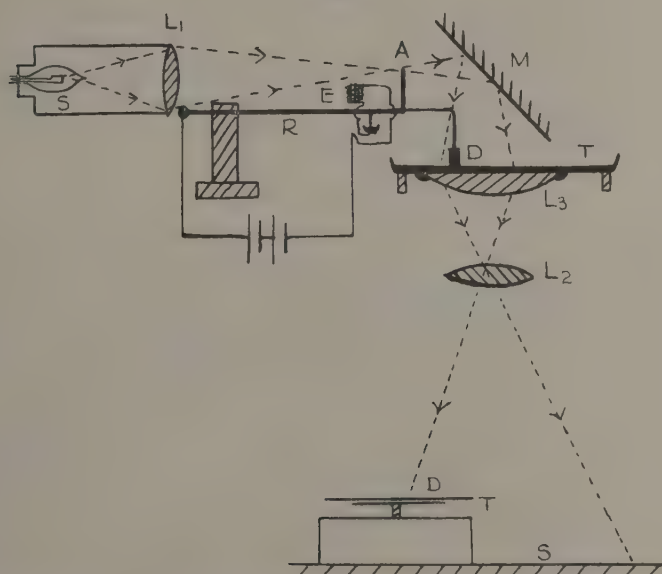
- | | |
|-------------------------------------|-----------------------------------|
| L_1 = Lamp house lens. | E_1, E_2 = Electromagnet coils. |
| L_2 = Condenser lens. | T_1 = Ripple tank. |
| L_3 = Projection lens. | T_2 = Gramophone turntable. |
| M_1, M_2, M_3 = Inclined mirrors. | D = Stroboscopic disk. |
| R_1 = Light interrupter. | S = 12 V. 36 Watt lamp |
| R_2 = Rippler. | source. |

as the reed vibrates, it causes the light passing upwards through the ripple tank *via* the mirror M_1 and condenser lens L_2 to be intermittent at a flashing frequency equal to that of the reed. If the reed is of soft iron this frequency is 100/sec. when the mains frequency is 50 cycles/sec.

* S. S. R. no. 68, June 1936.

Since R_2 is electrically driven by the same A.C. supply (not necessarily at resonance), synchronization between the ripple formation and the intermittent illumination is automatically obtained at only one frequency of 100/sec. Hence we can only apply the results to graphical method 2. The intermittent light after traversing the tank is reflected upon a distant screen by mirror M_2 and the projection of the ripple images effected by lens L_3 . For photographing we dispense with both these components and use a camera instead.

Fig. 2.



Synchronization of ripple formation by electrically maintained reed or rod method.

R=Maintained reed or rod.
E=Electromagnet coil.
A=Chopper.
D=Dipper (strip of glass).
M=Inclined mirror.
T=Ripple tank.

L_1, L_2 =Projection lenses.
 L_3 =Condenser lens.
T=Gramophone turntable.
D=Stroboscopic disk.
S=Horizontal screen.

As a check on the mains frequency a stroboscopic disk was run at a controlled but constant speed by means of a gramophone turn-table. This disk was illuminated with the same intermittent light as that thrown upon the screen by reflecting it downwards by an inclined mirror M_3 . The timing of the disk for a number of revolutions with an accurate

reading stop-watch (reading to $\cdot 01$ sec.) over a fairly long period, indicated the mains frequency could be relied upon to $50 \pm \cdot 02$ cycles/sec.

Arrangement II.

This is a device in which an electrically maintained reed or rod R at various lengths functions both as the light interrupter and rippler (fig. 2). An image of a straight lamp filament is focused upon the bent end of the reed at A. Since the reed also carries the plane dipper D, during maintained vibration, the light from the lamp is rendered intermittent in synchronization with the ripple formation; hence, by reflecting the light downwards through the tank the apparently stationary ripple images are projected upon a horizontal screen, where measurements are made. The frequency of the rippler and the intermittent illumination are determined in the same manner as in method I.

Arrangement III.

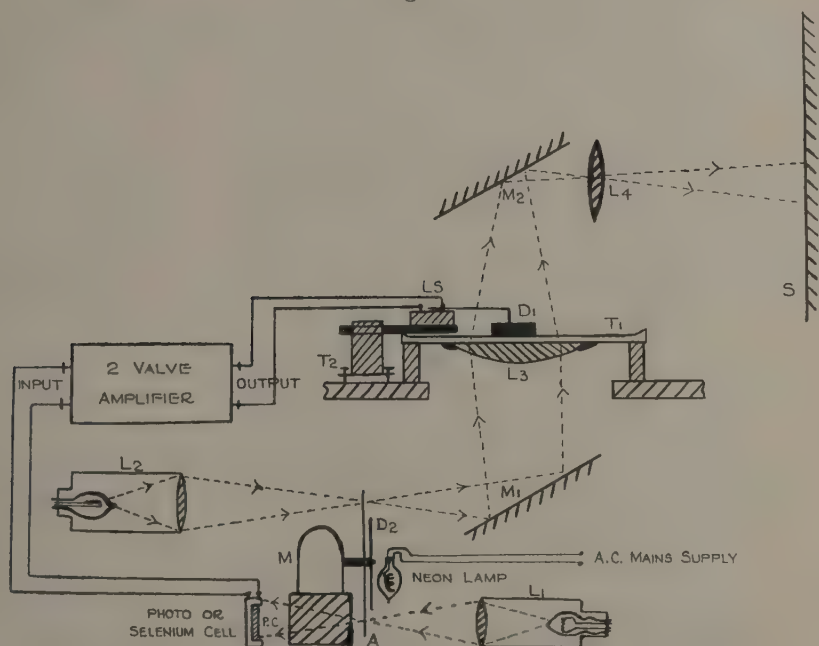
In this method we incorporate the principle of converting light into sound and utilize an electrically controlled loud-speaker unit LS with an attached plane dipper D_1 as the rippler. It is customary to operate such a source by means of either a valve oscillator or oscillating Neon tube, but in the present method this technique is dispensed with, employing instead a photo-electric cell rotating disk method. Light from an auto lamp L_1 (fig. 3) is brought to a focus at A where it is interrupted by a rotating slotted disk, driven at constant speed by either a synchronous motor M_1 or by a D.C. motor of a variable but controlled speed. The interrupted light is then allowed to fall on either a selenium or photo-electric cell, suitably coupled to a 2 stage valve amplifier. By connecting the output terminals of this amplifier to the loud-speaker unit, the latter is thus energized by the intermittent amplified photo-electric currents at a frequency equal to (revs. per sec. of the disk) \times (number of slots in the disk). Thus by using disks with varying numbers of slots in conjunction with the synchronous motor, or one slotted disk with the D.C. motor run at various controlled speeds, we can readily alter the frequency of the ripple formation.

Light from a second auto lamp L_2 is simultaneously rendered intermittent by the same rotating disk. The resultant flashing light is thus in synchronization with the ripples. This light is reflected upwards through the tank T_1 via mirror M_1 and lens L_3 , and finally projected upon a vertical screen S. Here the ripple images are viewed and measured, or alternately close up viewing is adopted and measurements of the wave-length carried out either with a microscope or camera. The mounting of the loud-speaker unit on a levelling table T_3 facilitates easy

control of the amplitude of the ripples, and since equally spaced radial slots are used, excellent definition of the ripple images is obtained.

When using the synchronous motor, the A.C. mains supply at 50 cycles/sec. is employed as a standard source of frequency. Everything becomes automatic and any personal error is eliminated, since the rated speed (in revs./sec.) of the motor and the number of slots in the disk are known.

Fig. 3.



Synchronization of ripple formation by photo-electric cell method.

- | | |
|--|--|
| M=Motor (synchronous or DC). | D ₁ =Plane dipper. |
| A=Slotted disk. | T ₁ =Ripple tank. |
| D ₂ =Stroboscopic disk. | T ₂ =Levelling table. |
| PC=Photoelectric or selenium cell. | M ₁ , M ₂ =Inclined mirrors. |
| L ₁ , L ₂ =Projection lamps. | L ₄ =Projection lens. |
| LS=Loud speaker unit. | L ₃ =Condenser lens. |
| | S =Screen. |

With the D.C. motor two methods of controlling the frequency of the ripple source and illumination may be adopted :—

(a) Resort to stroboscopic control by attaching a stroboscopic diagram D₂ with appropriate markings to the rotating slotted disk, and illuminate

it with the light of a flashing "Osglim" run from the A.C. 230 V. mains supply (*i. e.*, we again depend upon the A.C. mains frequency as our standard).

Fig. 4.

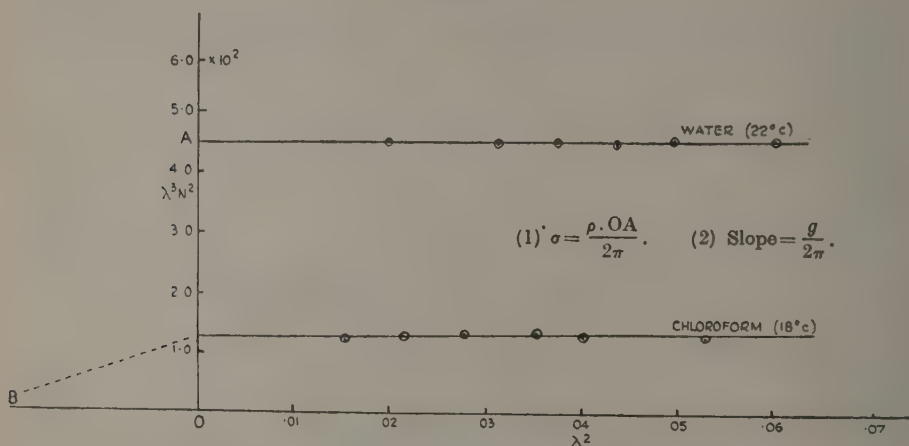
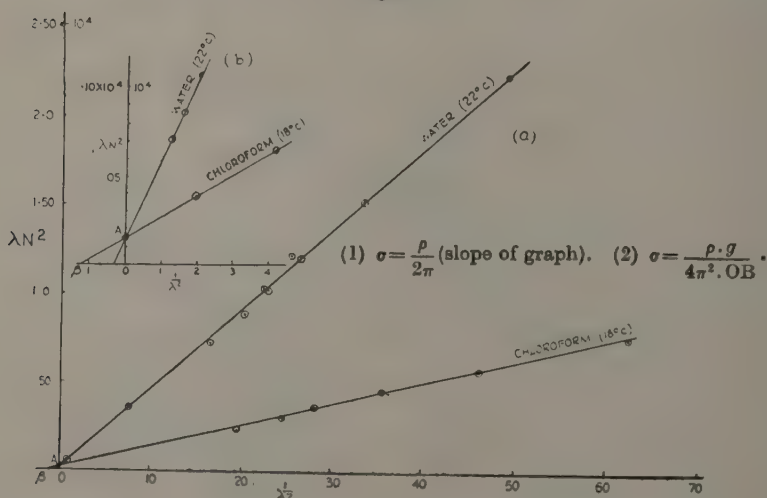


Fig. 5.



(b) Run the motor and disk at proper constant speed so that for any given speed the pitch of the note emitted by the loud-speaker unit is tuned to a similar note (by beat method) produced on a monochord, the latter being finally calibrated with a reliable fork (512). For other

TABLE I.
Specimen Results for Water and Chloroform.

Liquid.	Temperature ° C.	OA (fig. 4).	$\sigma = \frac{OA \cdot \rho}{2\pi}$. dynes/cm.	Slope (fig. 5a).	$\sigma = \frac{\rho \cdot \text{slope}}{2\pi}$. dynes/cm. (σ_1)	OB (fig. 5b).	$\sigma = \frac{\rho g}{4\pi^2 \cdot OB}$. dynes/cm.
Water. $\rho_1 = 1.00$	22.0	4.44×10^2	70.7	$.44(8) \times 10^3$	71.2 (σ_1)	0.35	71.0
Chloroform. $\rho_2 = 1.50$	18.0	1.24×10^2	29.5	$1.26(2) \times 10^3$	30.0 (σ_2)	1.25	29.9

$\frac{\sigma_1}{\sigma_2} = 2.32$ by pull on plate method.

speeds, different lengths of wire must be tuned. This method is more tedious than the synchronous motor arrangement since repeated checks on the constancy of the frequency are essential during the measurement of the wave-length. The projection method will be found the more suitable with this arrangement in view of the shorter time involved in recording the observations.

Whichever method is adopted for controlling the frequency of the rippler, the latter exhibits marked increase in amplitude of vibration as a result of resonance, and these effects may be conveniently utilized; otherwise, owing to heavy loading of the loud-speaker unit at frequencies remote from resonance, more energy will be necessary to produce sufficient amplitude of the ripples for measuring purposes, and this would mean a further stage of valve amplification.

Specimen Results.

Results for water and chloroform are shown in figs. 4 and 5 and Table I. The respective values of σ (71.2 and 30.0 dynes/cm.) for these liquids compare favourably with those obtained by other methods. The comparative merits of both methods is at once revealed by the graphs.

Whereas there is only a small change in $\lambda^3 N^2$ there is a wide range of variation of $\lambda^2 N$ and method II. becomes the obvious choice. σ is, of course, more accurately determined from the slope of the graph (fig. 5 *a*). The need for plotting the lower frequency results on a larger scale than that represented in fig. 5 *a* is also emphasized, since on the scale shown the intercept OB cannot be interpolated with sufficient reliability. Such values of OB (Table I.) were obtained by this method (fig. 5 *b*).

SUMMARY.

The surface tension σ of a liquid (water and chloroform) is computed by employing graphical methods evolved from Kelvin's equation for the velocity of surface waves under the combined influence of gravity and surface tension.

Accepting Rayleigh's and Dorsey's modified Kelvin equation, viz. :—

$$\sigma = \frac{\lambda^3 N^2 \rho}{2\pi} - \frac{g \lambda^2 \rho}{4\pi^2},$$

in which N is the frequency of ripple formation, λ the ripple wave-length, ρ the density of the liquid, and g the acceleration due to gravity, this equation is rewritten in the forms

$$\lambda^3 N^2 = \frac{\lambda^2 g}{2\pi} + \frac{2\pi\sigma}{\rho}, \quad \dots \dots \dots (a)$$

and

$$\lambda N^2 = \frac{2\pi\sigma}{\rho \lambda^2} + \frac{g}{2\pi}. \quad \dots \dots \dots (b)$$

Regarding the variables of these equations as $\lambda^2 N^2$ and λ^2 (eq. *a*), and λN^2 and $\frac{1}{\lambda^2}$ (eq. *b*), the validity of such relationships is confirmed graphically by the linearity of the graphs obtained.

σ is derived either from the intercept $\frac{2\pi\sigma}{\rho}$, (eq. *a*), or from the slope $\frac{2\pi\sigma}{\rho}$, and intercept $\frac{\rho g}{4\pi^2\sigma}$ (eq. *b*). Preference is given to the latter results utilizing equation (*b*), since only the square terms of λ are involved.

Measurement of the frequency of ripple formation and corresponding wave-length is effected over a wide range (N from 20 to 400 per sec.) by three different stroboscopic methods: (*a*) a synchronous dual-reed device operated at the A.C. mains supply frequency, (*b*) an electrically maintained reed or rod interrupter method at the lower frequencies. (*c*) a synchronous photo-cell rotating slotted disk and dipper arrangement for frequencies above 100/sec. The results show good agreement with those obtained by other methods.

XXIII. *On a Hydraulic Problem involving
Discharge into Tidal Water.*—II.

By A. G. WALKER, Ph.D., Department of Pure Mathematics,
University of Liverpool,
and

J. R. DAYMOND, M.Sc., Assoc.M.Inst.C.E., Department of Civil
Engineering, University of Liverpool †.

[Received May 8, 1940.]

1. A PREVIOUS paper ‡ dealt with the hydraulic problem of discharge from a tank into tidal water, the tank at the same time receiving a constant inflow. It was proved that the level in the tank always settled down to a periodic rise and fall, and the paper was thereafter concerned only with this settled state. In the conclusion it was mentioned that the more general problem which still remained was a study of the case when the rate of inflow to the tank was not constant but variable. The present paper, while by no means attempting to deal fully with this problem, does consider two departures from uniformity. We shall first consider what happens when the settled state (constant inflow) is disturbed by an isolated surge which abruptly raises the level in the tank. Secondly, we shall consider the effect of surges which occur periodically. Each of these problems has a significant counterpart in engineering, and it is hoped that they will indicate certain qualitative results which can be applied to the more general case mentioned above.

In the previous paper we considered a cylindrical tank of area A into which water flows at a constant rate Q . At the same time there is an outflow into tidal water, the tide, assumed to follow a sine curve, having period T and amplitude $2R$. The rate of outflow is $k\sqrt{h}$, where k is a constant determined by the outflow pipe, and h is the head of water in the tank, *i. e.*, the height of the tank level above the tide. The outflow pipe is assumed fitted with a valve to prevent backflow, so that $h=0$ when the tank level drops below that of the tide. If z is the height of the tank

† Communicated by the Authors.

‡ A. G. Walker and J. R. Daymond, *Phil. Mag.* (2) xxviii. pp. 520–531 (1939). This paper will be referred to as (I).

level above mean-tide level at time t , then the differential equation governing z is

$$\frac{dz}{dt} + \alpha h^{\frac{1}{2}} = m, \quad (1)$$

where
$$\left. \begin{aligned} h &= z - R \sin 2\pi t/T & \text{when } z > R \sin 2\pi t/T, \\ h &= 0 & \text{when } z \leq R \sin 2\pi t/T, \end{aligned} \right\} . . . (2)$$

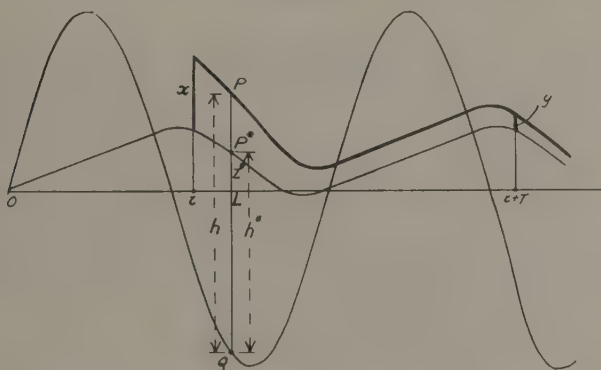
and α and m are constants given by

$$\alpha = k/A, \quad m = Q/A. \quad (3)$$

In paper (I) we referred to constants m and s , where $s = Q/k$.

The above equation has an infinity of solutions, but it was proved in paper (I) that every solution tends asymptotically to one particular

Fig. 1.



$$OL=t, \quad LP*=z^*(t), \quad LP=z(t), \quad QP*=h^*(t), \quad QP=h(t).$$

solution, which is periodic of period T . Each solution is regarded as a curve in a t - z plane, called a “ z -curve,” and the periodic solution is called the “periodic z -curve.” The latter thus describes the ultimate behaviour of the tank level whatever its initial height. We shall write $z^*(t)$ for the “periodic” value of z at time t , and h^* for the corresponding value of h from (2).

2. Consider now the case when the basic constants T, R, α, m are fixed and the resulting periodic state is disturbed, at time τ , say, by a surge which causes the level in the tank to rise suddenly by a given amount x . We know that the behaviour will settle down again to the original state, but we are now concerned with the rate at which it settles down. To measure this we shall compare x and y , where y is the height of the tank level above the periodic level z^* at time $\tau + T$, i. e., after one full period (fig. 1). For τ fixed, y evidently depends only upon x , and we can write

$y=f(x)$, where f is certainly a continuous function. This we shall call an *approach function*, and its study and application are the concern of the present paper. The curve $y=f(x)$ in an x - y plane is called an *approach curve*; it evidently passes through the origin, since $y=0$ when $x=0$ for any τ .

To find the value of y when x is given, it is necessary to find that solution of (1) which is determined by the initial condition $z=z^*(\tau)+x$ when $t=\tau$. If this solution is $z(t)$, then y is given by $z(\tau+T)-z^*(\tau+T)$. Since, however, (1) cannot be solved in finite terms, the relation between x and y can be found only by experiment, by approximate calculations, or by graphical methods. Significant information of a general nature can, on the other hand, be obtained from theoretical considerations, and we shall proceed to discuss the shape of an approach curve. We shall first consider the derivative of $f(x)$, and then the asymptotic form of the function.

3. Let us suppose that x is increased by a small amount δx with a consequent increase δy in y . Then if $z(t)$ is the solution of (1) with the initial value $z^*(\tau)+x$ when $t=\tau$, and if $z(t)+\phi(t)$ is the solution with the initial value $z^*(\tau)+x+\delta x$, we have

$$\phi(\tau)=\delta x, \quad \phi(\tau+T)=\delta y. \quad (4)$$

It can be assumed that ϕ is so small that ϕ^2 can be neglected, and substituting $z+\phi$ for z in (1), expanding $h^{\frac{1}{2}}$ in a Taylor series, and remembering that $z(t)$ also satisfies (1), we have

$$\frac{d\phi}{dt} + \frac{1}{2}\alpha h^{-\frac{1}{2}}\phi = 0, \quad (5)$$

where h is determined by $z(t)$ from (2), and $h^{-\frac{1}{2}}$ is replaced by 0 when $h=0$. This, then, is the equation for ϕ , and integrating $d\phi/\phi$ from τ to $\tau+T$, we have

$$[\log \phi]_{\tau}^{\tau+T} = -\frac{1}{2}\alpha \int_{\tau}^{\tau+T} h^{-\frac{1}{2}} dt.$$

From (4) the left-hand side of this equation is $\log \frac{\delta y}{\delta x}$, which becomes $\log f'(x)$ in the limit $\delta x \rightarrow 0$. We thus have

$$f'(x) = e^{-g}, \quad (6)$$

where

$$g = \frac{1}{2}\alpha \int_{\tau}^{\tau+T} h^{-\frac{1}{2}} dt, \quad (7)$$

$h^{-\frac{1}{2}}$ being replaced by 0 when $h=0$. Here g is a function of x , since the form of h depends upon x ; g also depends upon τ , as well, of course, as upon the basic constants R, T, α, m .

From the above argument it follows that $f'(x)$ exists for all values of x , so that the approach curve is smooth. Further, since $g > 0$ from (7), we have from (6) that, for all x ,

$$0 < f'(x) < 1.$$

It was shown in paper (I) that no two z -curves can intersect. Hence if x is increased, $z(t)$ increases, and h either increases or remains unaltered for all t . It thus appears from (7) that g decreases when x is increased, and from (6) we then have, for all x , that $f'(x)$ increases with x . The approach curve is, therefore, always concave upwards.

Finally, we see that $f'(x)$ tends to a definite limit as $x \rightarrow 0$, for then $h \rightarrow h^*$ and g can still be evaluated. We now note that, since h^* is periodic, g is, in the limit, independent of τ , and we can write

$$f'(0) = \exp \left(-\frac{1}{2}\alpha \int_0^T (h^*)^{-\frac{1}{2}} dt \right). \quad \dots \quad (8)$$

The approach curve therefore starts from the origin with a definite slope between 0 and 1, and the slope increases continuously with x without ever reaching 1.

4. Further information about the shape of the approach curve can be obtained from a study of its asymptotic behaviour as $x \rightarrow \infty$. When x is large, the tank level is high in the first tide period, and the effects of the variation in tide level and of the inflow can be neglected. This can be seen from (1), where z is now very large. We can therefore ignore m and write z for h in this equation, which thus becomes approximately $dt = -\alpha z^{-\frac{1}{2}} dz$. Integrating from τ to $\tau + T$, and writing $z(\tau) = x$, $z(\tau + T) = y$, since x and y are large compared with z^* , we have finally

$$\sqrt{x} - \sqrt{y} = \frac{1}{2}\alpha T. \quad \dots \quad (9)$$

This, then, is the asymptotic relation between x and y .

The curve given by this equation is a parabola, so that the approach curve has a parabolic asymptote. The axis of the parabola is the line $y = x$, and the curve touches the x - and y -axes at distances $(\frac{1}{2}\alpha T)^2$ from the origin, the chord joining these points being the latus rectum.

This information, together with the results of § 3, shows very clearly the shape of the approach curve. An example of such a curve, with its parabolic asymptote, is drawn in fig. 2.

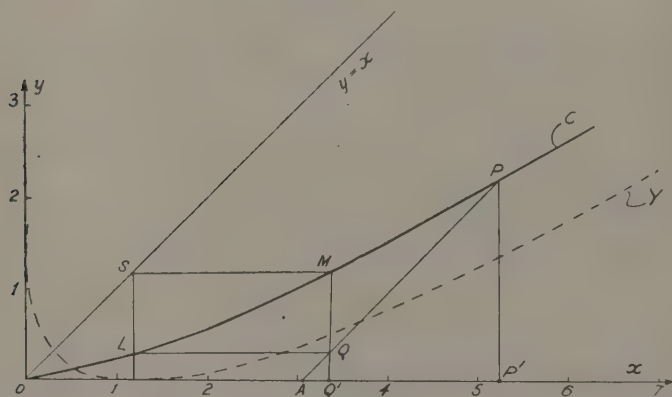
5. It appears from its definition that an approach curve depends not only upon the basic constants R , T , α , m , but also upon τ , the time of commencement of the period over which the approach to the settled state is measured. It is natural to enquire how $f(x)$ varies with τ , keeping the basic constants unaltered, and we first note that, from (8) and (9), the slope at the origin and the parabolic asymptote are both independent of τ

It thus follows from the general shape of the curve that $f(x)$ cannot vary very much with τ .

In order to make a more detailed investigation, actual results were obtained by solving (1) graphically by the method mentioned in paper (I). A series of z -curves were drawn for the values $R=1$, $T=3600$, $\alpha=6.2 \times 10^{-4}$, $m=4.13 \times 10^{-4}$ in foot-second units, and x and y were measured at the quarter-tides. These values of x and y enabled us to draw four approach curves, corresponding to the values $0, \frac{1}{4}T, \frac{1}{2}T, \frac{3}{4}T$ of τ . It was found that *the four curves were indistinguishable from each other*. In this particular case, therefore, the approach curve is approximately independent of τ . This curve is the one drawn in fig. 2.

Since the slope at the origin and the asymptote are independent of τ for all values of the basic constants, and since the whole curve is approxi-

Fig. 2.



Approach curve (C) when $R=1$, $T=3600$, $\alpha=6.2 \times 10^{-4}$, $m=4.13 \times 10^{-4}$.

Asymptote (γ) is $\sqrt{x} - \sqrt{y} = 1.12$. $OA=\xi$, $P'P=X$, $Q'Q=X'$.

mately independent of τ in one particular but typical case, we can reasonably draw the conclusion that *the approach curve is always approximately independent of τ* .

6. We have so far considered the approach curve which compares heights x and $y=f(x)$ above the periodic z -curve before and after one period of the tide. If now $f(x)$ is known, then we can at once deduce a similar curve which compares heights before and after two periods. For if x is the initial height, y_1 the height after one period, and y_2 the height after two periods, then the "one-period" approach function gives $y_1=f(x)$ and $y_2=f(y_1)$, whence the "two-period" approach curve is given by the relation

$$y_2=F(x)=f(f(x)). \quad (10)$$

It can easily be verified from (10) that the curve defined by $F(x)$ has the same general properties as the $f(x)$ -curve. Its slope at the origin has the definite value $(f'(0))^2$, the slope increases with x without reaching the value 1, and the curve has the parabolic asymptote

$$\sqrt{x} - \sqrt{y} = \alpha T. \quad \dots \dots \dots (11)$$

This equation follows at once from (9). From the conclusion of § 5 it also follows that the "two-period" approach curve is approximately independent of the time of commencement of the double period.

Similar results can be obtained for an approach curve over three or more periods. We can also consider the approach over a sub-division of the tide period, but a further analysis of the z -curves mentioned in § 5 showed clearly that the approach curve is not in this case independent of the position of the sub-division relative to the tide.

7. We can now deduce from the approach curve the way in which the tank level settles down to the periodic behaviour after an isolated surge. If at time τ the periodic level z^* is suddenly raised by an amount X , then the height above z^* is $y_1 = f(X)$ after one period, $y_2 = f(y_1)$ after two periods, $y_3 = f(y_2)$ after three periods, etc. The successive values X, y_1, y_2, \dots indicate how the level settles down; we know from the general theory that $y_n \rightarrow 0$ as $n \rightarrow \infty$.

The above sequence of heights can be illustrated by approximating to the approach curve. It is clear from the general shape that the curve closely approximates a straight line for some distance from the origin, and for other than large heights we can assume the form

$$y = \mu x, \quad 0 < \mu < 1. \quad \dots \dots \dots (12)$$

The sequence of heights after successive periods is now seen to be approximately

$$X, \mu X, \mu^2 X, \dots, \mu^n X, \dots \quad \dots \dots \dots (13)$$

where $\mu^n \rightarrow 0$ as $n \rightarrow \infty$, as expected. If λ is the height after n periods, then $\lambda = \mu^n X$. The curve obtained by plotting λ and n from this relation shows clearly how any z -curve approaches the periodic curve, or how any isolated surge is absorbed. The significant constant μ in this approximation is $f'(0)$, and is given in terms of the periodic z -curve by (8). It is certainly independent of τ , and depends only upon the basic constants.

8. The remaining problem we set out to discuss concerns the effect of a periodic surge. As before, the tank is receiving a constant inflow, and in addition there is now a surge, which abruptly raises the tank level by an amount ξ , say, at times $\tau, \tau + T, \tau + 2T, \dots$. Since the total inflow to the tank is periodic, it should be expected that the tank level will

ultimately rise and fall periodically, whatever the initial height. This will be proved to be the case, and we shall find how the new behaviour is related to the periodic state without the surges. Heights will be measured above z^* , which still refers to the periodic state with the same basic constants but without the surges. The approach curve determined by these constants is $y=f(x)$ as before, and the results obtained above can be applied here.

Let us suppose that the level in the tank at time $\tau-0$, *i. e.*, just before the surge, is at a height x_0 above $z^*(\tau)$, where $x_0 \geq 0$ without loss of generality. Then at time $\tau+0$, *i. e.*, just after the surge, the height is $x_0+\xi$, whence the height at time $\tau+T-0$ is $x_1=f(x_0+\xi)$. Similarly the height is $x_1+\xi$ at time $\tau+T+0$, and $x_2=f(x_1+\xi)$ at time $\tau+2T-0$. Continuing this process, we find that the height at time $\tau+nT-0$ is x_n , where, for all values of n ,

$$x_{n+1}=f(x_n+\xi). \quad \dots \dots \dots (14)$$

This relation enables us to watch the effect of the periodic surge.

We shall now prove that, for any value of x_0 , the sequence x_n tends to a unique limit X which is the root of the equation

$$X=f(X+\xi). \quad \dots \dots \dots (15)$$

That this equation has one, and only one, real root can be seen from a construction for X . Let OA in fig. 2 be of length ξ , and draw AP at 45° to Ox . Then from the properties of $f(x)$ proved in §§ 3, 4, we see that AP meets the approach curve at one and only one point P . If $P'P$ is the ordinate to P , and if $P'P=X$, then $OP'=X+\xi$ and $P'P=X=f(X+\xi)$. Thus X is the required root, and is unique. It can now easily be proved that if $0 < x_n < X$, then $x_n < x_{n+1} < X$, and that if $x_n > X$, then $x_n > x_{n+1} > X$. It follows that x_n always tends to a limit, and since any limit must satisfy (15), the root X of this equation is in all cases the limit of x_n .

We have thus proved that the behaviour of the tank level is ultimately periodic, the settled state being unique. After settling down to the new state, the height is $z^*(\tau)+X$ above mean-tide level just before each surge, and there is an additional ξ just after the surge. In the interval between two surges, the level steadily approaches the previous periodic (z^*) state. The general behaviour is illustrated in fig. 3.

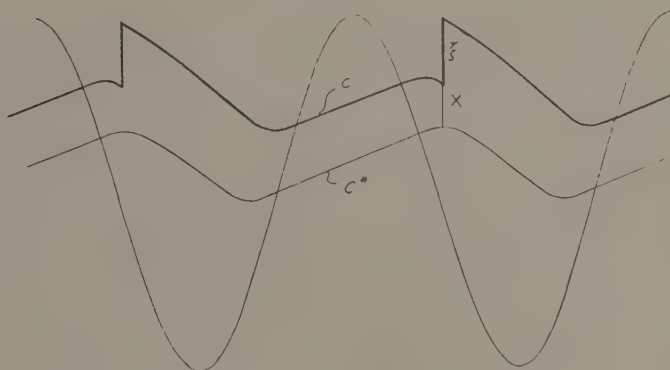
9. We have for simplicity considered the case when the surges occur during each period of the tide, but in application to engineering a more important case is when the surges occur during alternate periods. The method in this case is exactly the same as in § 8, the appropriate approach function being, from § 6, $y=f(f(x))$. Whatever the initial level in the tank, the behaviour is ultimately periodic of period $2T$. Just before

each surge (after the settled state has been reached) the height above mean-tide level is $z^*(\tau) + X'$, where X' is the root of the equation

$$X' = f(f(X' + \xi)). \quad . \quad . \quad . \quad . \quad . \quad (16)$$

The value of X' can be found, as in § 8, by a construction on the curve $y = f(f(x))$, which curve can easily be drawn when the curve $y = f(x)$ is known. To avoid drawing this second curve, X' can be obtained by a simple trial and error construction on the curve $y = f(x)$. It is required to find the point Q on the line AP (fig. 2) such that if the lines through Q parallel to the axes meet $y = f(x)$ at L and M, then the remaining vertex S of the rectangle LQMS lies on the line $y = x$. The ordinate Q'Q is then X' .

Fig. 3.



C*. Periodic z -curve without surges.

C. Periodic curve with periodic surges.

For writing $Q'Q = X'$, then $Q'M = f(X' + \xi)$, and this is equal to the abscissa of L, whence the ordinate X' of L is equal to $f(f(X' + \xi))$ as required.

If the approximation (12) for $f(x)$ is adopted, then X in § 8 and X' above can at once be calculated, and we find

$$X = \frac{\mu \xi}{1 - \mu}, \quad X' = \frac{\mu^2 \xi}{1 - \mu^2} \quad . \quad . \quad . \quad . \quad . \quad (17)$$

10. Although, from the conclusion of § 5, the values of X and X' are independent of τ , the effect of the surges in relation to mean-tide level will depend upon τ , since X (or X') must be added to $z^*(\tau)$. If H and D are the greatest and least values respectively of $z^*(t)$ (see paper I) and if ξ is fixed, then the highest level in the tank is reached when the surges occur at the maxima of $z^*(t)$, this level being $H + X + \xi$ (or $H + X' + \xi$). In the same way the lowest level is reached when the surges occur at the

minima of $z^*(t)$, this level being $D+X$ (or $D+X'$). Considerations such as these would be necessary for some applications owing to the fact that the tide period is slightly more than 12 hours. A daily surge would thus be out of phase with the double tide, and all combinations of tide and surge would occur

ERRATUM.

In our previous paper, *Phil. Mag.* xxviii. p. 530 (1939), line 14 *should read* :

$$\frac{\pi}{6} < t \leq \frac{\pi}{2}, \quad f(t) = 1 - \frac{9}{2\pi^2} \left(t - \frac{\pi}{2} \right)^2.$$

XXIV. *On the Raman Spectrum of m-Diphenyl Benzene.*

By S. K. MUKERJI, M.Sc., Ph.D., Professor of Physics,
Agra College, Agra, and S. ABDUL AZIZ, M.Sc., Agra University
Research Scholar in Physics *.

[Plate VI.]

[Received August 21, 1939.]

ABSTRACT.

The Raman Spectrum of *m*-diphenyl benzene in the molten state has been investigated for the first time. The spectrum of this substance resembles that of *o*-diphenyl benzene also studied by the authors †, and is so highly fluorescent under the total radiation of the mercury arc that no trace of Raman lines appeared. But by employing $\lambda 4358$ as the exciting line filtered through a concentrated solution of sodium nitrite, the continuous background was very much cut down and a very fair spectrum was obtained, giving 27 new lines not recorded before at frequencies, 3062 (2), 1607 (4), 1597 (10), 1566 (1), 1494 (4), 1453 ($\frac{1}{2}$), 1403 ($\frac{1}{2}$), 1345 (0), 1309 (10), 1279 (2), 1241 (4 br.), 1153 (2), 1098 ($\frac{1}{2}$), 1039 (1), 1000 (10), 964 ($\frac{1}{2}$), 901 (1), 838 (1), 801 ($\frac{1}{2}$), 766 (1), 707 (3), 611 (3), 406 (3), 275 (3 diff.), 238 (3 diff.), 151 (2 diff. & br.), and 80 (4 diff. & br.).

The most prominent frequency observed is at 1309 cm^{-1} and is the characteristic frequency due to the C—C binding of the benzene rings of this compound. This frequency is equally strong in diphenyl and *o*-diphenyl benzene but is not present in benzene. The other strong frequency is at 1597 cm^{-1} due to the benzene nucleus characteristic of the aromatic linking C=C. The third most prominent frequency observed at 1000 cm^{-1} also occurs prominently in diphenyl ‡ and *o*-diphenyl benzene, but very weakly in benzene.

The authors' results are compared with the benzene, diphenyl, and *o*-diphenyl benzene spectra and are discussed.

* Communicated by Prof. S. K. Mukerji.

† Mukerji and Aziz, 'Nature,' vol. cxlii. p. 477 (1938).

‡ Mukerji and Aziz, Ind. J. Phys. vol. xii. pt. iv. (August 1938); also Wood, vol. xxxvi. p. 1431 (1931).

INTRODUCTION.

No investigation so far appears to have been done on the Raman spectra of compounds with three benzene rings. There have been also very few complete structure determinations of such compounds. In this investigation we have studied for the first time the Raman spectra of *m*-diphenyl benzene, and in a preliminary report to 'Nature' * the Raman lines yielded by ortho- and meta-diphenyl benzene have already been submitted. We have also reported in a previous communication † a large number of Raman lines due to diphenyl, which is solid at the ordinary temperature and which consists of two benzene nuclei joined end on by (C—C bond in the para direction. *m*-diphenyl benzene is also solid at the ordinary temperature, and it consists of three benzene rings instead of two, two of these being substituted in the third in the meta position. It is therefore interesting to obtain and compare the Raman spectra of this compound with those of diphenyl and *o*-diphenyl benzene. This substance is found to be even more highly fluorescent under the total radiation of the mercury arc than *o*-diphenyl benzene previously reported by the authors. But by employing $\lambda 4358$ as the exciting line filtered through a concentrated solution of sodium nitrite, the continuous background was very much cut down and a very fair spectrum was obtained giving a large number of Raman lines not recorded before. The results are discussed in the present paper.

EXPERIMENTAL.

Pure crystallized *m*-diphenyl benzene was purchased from Messrs. Eastman Kodak Company and was further purified by repeated crystallization from pure benzene. The substance was then distilled and the middle portion of the distillate was received directly into the Wood's tube. The Wood's tube containing *m*-diphenyl benzene was then kept in a specially constructed small oven, and as the substance was studied in the molten state this oven was heated electrically to a temperature slightly above the fusion point of the substance by adjusting the current flowing in the heated coil of the oven.

This substance was found to be even more powerfully fluorescent than *o*-diphenyl benzene previously studied by the authors when scattered by mercury arc radiation, but by employing $\lambda 4358$ as the exciting line filtered through a concentrated solution of sodium nitrite the continuous background was very considerably cut down and a large number of Raman lines, though comparatively weaker than those due to *o*-diphenyl

* *Loc. cit.*† *Loc. cit.*

benzene, have been obtained. No record of these lines due to this compound by any previous investigator has been found. The spectrograms were taken on Agfa Isochrome backed plates, speed H and D. 4400, with a new Füess glass spectrograph having a dispersion of about 21 Å.U. at λ 4358. The period of exposure was about 40 hours. Measurements were made, as usual, on a fairly accurate photomeasuring micrometer. Wave-lengths were calculated using the well-known Hartmann dispersion formula.

TABLE I.

m-Diphenyl Benzene Frequencies.

(With a filter of concentrated solution of sodium nitrite.)

Number.	$\Delta\nu$ in cm^{-1} .	Intensity I.	Number.	$\Delta\nu$ in cm^{-1} .	Intensity I.
1.....	3062	2	15	1000	10
2.....	1607	4	16	964	($\frac{1}{2}$)
3.....	1597	10	17	901	1
4.....	1566	1	18	838	1
5.....	1494	4	19	801	($\frac{1}{2}$)
6.....	1453	($\frac{1}{2}$)	20	766	1
7.....	1403	($\frac{1}{2}$)	21	707	3
8.....	1345	(0)	22	611	3
9.....	1309	10	23	406	3
10.....	1279	2	24	275	3 (diff.)
11.....	1241	4 (br.)	25	238	3 (diff.)
12.....	1153	2	26	151	2 (diff. & br.)
13.....	1098	($\frac{1}{2}$)	27	80	4 (diff. & br.)
14.....	1039	1			

diff.=diffuse. br.=broad.

As noted above, the λ 4358 excitation did not give a good photograph, the Raman lines being almost completely masked by fluorescence. But with λ 4358 excitation and using a filter of concentrated solution of sodium nitrite the continuous spectrum was very much cut down, and a fairly good photograph was obtained giving 27 new lines not recorded before.

In Table I. is given the results obtained by the authors using only the λ 4358 excitation.

The Raman frequencies due to benzene, diphenyl, *o*-diphenyl benzene and *m*-diphenyl benzene have been tabled together in Table II. for a comparative study, as these substances contain one, two, and the last

TABLE II.

No.	Benzene (Ananthakrishnan).	Diphenyl (Mukerji & Aziz).	o-Diphenyl benzene (Mukerji & Aziz).	m-Diphenyl benzene (Mukerji & Aziz).
1.....	3910 (0)
2.....	3187 (0)	3192 (0)	3196 (0)	..
3.....	3164 ($\frac{1}{2}$)
4.....	3064 (8)	3062 (5)	3059 (6)	3062 (2)
5.....	3048 (4)	3047 (1)
6.....	2949 (5)	2961 (0)
7.....	2928 (0 d)
8.....	2617 ($\frac{1}{2}$)
9.....	2547 ($\frac{1}{2}$)
10.....	2457 ($\frac{1}{2}$)
11.....	2272 (0)
12.....	1605 (2)	1610 (10)	1608 (5)	1607 (4)
13.....	1584 (3)	1590 (8)	1595 (10)	1597 (10)
14.....	1577 (1)	1566 (1)
15.....	..	1506 (4)	1503 (5)	1494 (4)
16.....	1480 (0)	..	1471 ($\frac{1}{2}$)	..
17.....	1445 (0)	1452 (1)	1430 ($\frac{1}{2}$)	1453 ($\frac{1}{2}$)
18.....	1400 ($\frac{1}{2}$)	1403 ($\frac{1}{2}$)
19.....	..	1376 (0)
20.....	..	1318 ($\frac{1}{2}$)	..	1345 (0)
21.....	..	1283 (10)	1288 (10)	1309 (10)
22.....	1279 (2)
23.....	..	1241 (1)	1247 (4)	..
24.....	1175 (2)	1189 (3)	1180 (2)	..
25.....	..	1157 (4)	1158 (6)	1153 (2)
26.....	..	1090 ($\frac{1}{2}$)	..	1098 ($\frac{1}{2}$)
27.....	1059 (2)	..
28.....	1035 (0)	1032 (5)	1032 (7)	1039 (1)
29.....	1006 ($\frac{1}{2}$)
30.....	998 (1)	1003 (10)	1005 (8)	1000 (10)
31.....	992.5 (10)	..	993 (8)	..
32.....	984 (1)	980 (1)
33.....	979 ($\frac{1}{2}$)	964 (1)	..	964 ($\frac{1}{2}$)
34.....	..	898 ($\frac{1}{2}$)	..	901 (1)
35.....	874 ($\frac{1}{2}$)	..
36.....	850 (2)	838 (4 br.)	839 (4)	838 (1)
37.....	801 (0)	801 ($\frac{1}{2}$)
38.....	778 (0)	779 (4)	774 (5)	766 (1)
39.....	..	740 (5)	744 (2)	..
40.....	708 (6)	707 (3)
41.....	688 ($\frac{1}{2}$)
42.....	606 (5)	614 (4)	615 (5 br.)	611 (3)

TABLE II. (continued).

No.	Benzene (Ananthakrishnan).	Diphenyl (Mukerji & Aziz).	<i>o</i> -Diphenyl benzene (Mukerji & Aziz).	<i>m</i> -Diphenyl benzene (Mukerji & Aziz).
43.....	..	548 (1)	558 (3)	..
44.....	521 (2)	..
45.....	501 ? (1)	..
46.....	..	449 (0)
47.....	400 (1 d.)	408 (5 br.)	406 (6)	406 (3)
48.....	..	368 (0)	359 (5)	..
49.....	..	313 (4 br.)	319 (3)	..
50.....	..	267 (4 br.)	253 (1)	275 (3 diff.)
51.....	238 (6 br.)	238 (3 diff.)
52.....	..	193 (0)
53.....	..	140 (4 br.)	144 (6 br.)	{ 151 (2 diff. & br.)
54.....	112 (5 br.)	..
55.....	73 (5 br.)	{ 80 (4 diff. & br.)

diff.=diffuse. br.=broad.

TABLE III.

Exciting Lines.

Exciting line Å.	Notation.	Wave-number cm. ⁻¹ .
4358.3	A	22938
4347.5	A ₁	22995
4339.2	A ₂	23039

two, three benzene rings respectively in their compounds and have fairly strong common frequencies.

The exciting frequencies are given in Table III., and complete tables showing assignments are given in Table IV.

The shifts for benzene are taken from the paper of Ananthakrishnan *, and the values for diphenyl and *o*-diphenyl benzene are taken from the papers of the present authors.

* Ananthakrishnan, Proc. Ind. Acad. Sci. A, iv. p. 52 (1936).

TABLE IV.
m-Diphenyl Benzene Frequencies.

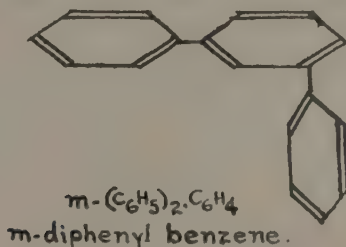
No.	Wave-number.	Assignment.	Shift.	Intensity.
1.....	19876	A	3062	2
2.....	21331	A	1607	4
3.....	21341	A	1597	10
4.....	21372	A	1566	1
5.....	21399	A ₁	1596	1
6.....	21444	{ A A }	{ 1494 1595 }	4
7.....	21485	A	1453	$\frac{1}{2}$
8.....	21535	A	1403	$\frac{1}{2}$
9.....	21593	A	1345	0
10.....	21629	A	1309	10
11.....	21687	A ₁	1308	1
12.....	21659	A	1279	2
13.....	21697	A	1241	4 br.
14.....	21785	A	1153	2
15.....	21840	A	1098	$\frac{1}{2}$
16.....	21899	A	1039	1
17.....	21938	A	1000	10
18.....	21974	A	964	$\frac{1}{2}$
19.....	21993	A ₁	1002	$\frac{1}{2}$
20.....	22037	{ A A }	{ 901 1002 }	1
21.....	22100	A	838	1
22.....	22137	A	801	$\frac{1}{2}$
23.....	22172	A	766	1
24.....	22231	A	707	3
25.....	22285	A ₁	710	0
26.....	22327	A	611	3
27.....	22532	A	406	3
28.....	22587	A ₁	408	0
29.....	2263	A	275	3 d.
30.....	22700	A	238	3 d.
31.....	22787	A	151	2 d. & br.
32.....	22858	A	80	4 d. & br.

In the above tables d. means diffuse, br. means broad.

Results and Discussion.

The spectrogram obtained with molten *m*-diphenyl benzene is reproduced in Pl. VI. It will be observed that with λ 4358 excitation and using a filter of sodium nitrite solution the continuous spectrum due to fluorescence has been very considerably cut down, giving a large number

of fairly strong Raman lines. The most prominent frequencies observed in this substance are at 1597, 1309, and 1000 cm^{-1} respectively. Table II. will show that the frequency at 1597 cm^{-1} is observed in benzene, diphenyl, and also in ortho- and *m*-diphenyl benzene. In benzene it is fairly strong; it is stronger still in diphenyl, and is strongest in both ortho- and meta-diphenyl benzene. In benzene there is a single ring with, so to say, all the carbon atoms free, in diphenyl one of the carbon atoms is loaded with a phenyl group, and in ortho- and meta-diphenyl benzenes two of the carbon atoms are loaded with phenyl groups in the ortho and meta positions respectively. This is then the characteristic frequency due to the aromatic linking ($\text{C}=\text{C}$), and is due to the benzene nucleus present in all these compounds. In fact, the lines at 1584 and 1605 cm^{-1} due to benzene form a close doublet and have been attributed by S. Bhagwantam * as due to a transverse oscillation of the hydrogen atom. It will be seen in Table II. that this doublet occurs very strongly



in diphenyl at 1590 and 1610 cm^{-1} respectively. It is also present strongly in *o*-diphenyl benzene and in *m*-diphenyl benzene, investigated here, it occurs almost equally strongly.

The most prominent frequency observed in *m*-diphenyl benzene is at 1309 cm^{-1} . It occurs most prominently in diphenyl and also in all the three compounds of the diphenyl benzene family, but is not present in benzene. In diphenyl it is observed at 1283 cm^{-1} , in *o*-diphenyl benzene at 1288 cm^{-1} , and in *m*-diphenyl benzene it is displaced to 1309 cm^{-1} . But in this latter compound alone a faint companion to the main line is also observed at 1279 cm^{-1} . It is evident that the $\text{C}-\text{C}$ binding amongst the benzene nuclei of these compounds is responsible for the origin of the strong frequency at 1309 cm^{-1} .

The line at 1000 cm^{-1} also deserves attention. It is observed as a single strong line in *m*-diphenyl benzene. In benzene and in diphenyl it is also observed as a single strong line. But in ortho- and in para-diphenyl benzene, which last has just been investigated by us, two equally strong

* S. Bhagwantam, Ind. Jour. Phys. vol. v. p. 615 (1930).

lines are observed instead of a single one. In *o*-diphenyl benzene this doublet is intensely strong, but in *p*-diphenyl benzene, which has been studied in the solid state, it is only fairly strong. The other frequency of this doublet is observed at 993 cm.^{-1} in *o*-diphenyl benzene and at 981 in *p*-diphenyl benzene. If the occurrence of this frequency is characteristic of compounds with three benzene rings it is curious no trace of it is observed in *m*-diphenyl benzene.

In addition to the lines which are characteristic of benzene and diphenyl *m*-diphenyl benzene has shown some more lines which are also found present only in *o*-diphenyl benzene, and they do not depend much upon the isomerism of the molecule. The frequency shifts of these lines are at 1566 , 707 , 238 , and 80 cm.^{-1} respectively. *m*-diphenyl benzene has also shown two more lines, but they are not observed in *o*-diphenyl benzene and are therefore characteristic of this compound. These are observed at 1403 and 1279 . The lines at 1059 , 521 , 501 , 112 cm.^{-1} in the ortho- and 1279 cm.^{-1} in the meta-compound would appear to depend upon the position of the benzene nuclei with respect to one another in the molecule.

The frequency at 1453 cm.^{-1} is found in all the four compounds and is fairly weak with very little variation in intensity from compound to compound. The line at 1035 cm.^{-1} is also observed throughout, but in benzene it is very weak, in diphenyl it is fairly strong, and it is stronger still in *o*-diphenyl benzene, but in *m*-diphenyl benzene it again grows weaker. It has also been observed by one of the authors * as a strong line in tetralin and is also present in cyclo-hexane, and, in fact, it is present in the Raman spectra of all benzene derivatives. There can be no doubt that this frequency is characteristic of benzene, and the presence of the aromatic rings in these compounds is primarily the cause of its presence in *m*-diphenyl benzene.

Similar is the case with the line at 766 cm.^{-1} . It is observed in all the four compounds, but shows marked changes of intensity and is strongest in *o*-diphenyl benzene. The frequencies at 238 and 80 cm.^{-1} present in both the ortho- and the meta-compound may probably be due to the vibrations of the three benzene rings against one another.

It may be observed here that *m*-diphenyl benzene has shown two fairly weak lines, one at 1345 cm.^{-1} and the other at 1279 cm.^{-1} , which are not found present in the other three compounds. But there are more than a dozen lines, some of them being fairly strong, as Table II. will show, which are present in *o*-diphenyl benzene but not in *m*-diphenyl benzene. It is possible that the very weak ones amongst these have been masked by the strong fluorescence shown by the *m*-diphenyl benzene

* Mukerji, Phil. Mag. ser. 7, vol. xix, p. 1079 (1935).

plate. But some of the strong ones are evidently due to the shift of one of the phenyl groups of the compound from the meta to the ortho position.

In conclusion, it may be pointed out that structural formulæ of diphenyl, *o*-diphenyl benzene, and *m*-diphenyl benzene tend to show that there should be some common strong frequencies in all these three compounds due to the two common benzene nuclei joined end on by the C—C bond in the para direction in these compounds. Table II. will show that there are a large number of such common frequencies the existence of which has already been discussed. But it will be noticed that the frequencies which are common only to the ortho- and the meta-compound are very few, which is perhaps due to their phenyl groups being present in different positions, that is, in ortho and meta positions respectively. Our results on *p*-diphenyl benzene are also nearly complete now, and it is hoped very interesting comparisons will be possible to make or some important conclusions may be drawn about the structure of compounds with three benzene rings so little work on which has been done so far.

This investigation was carried on in the Physics Laboratory, Agra College, with a new Füess glass spectrograph bought for this type of work. One of us (S. Abdul Aziz) is greatly indebted to the authorities of the Agra University for the award of a Research Scholarship which enabled him to commence the research.

XXV. *On the Space Attenuation of Impact Sounds
in a Brick Building.*

By A. E. KNOWLER, M.Sc., Physics Department,
National Physical Laboratory, Teddington, Middlesex *.

[Received October 16, 1939.]

It is well known that if a part of the fabric of a building receives a sharp blow, the sound may be transmitted through the material of the walls, partitions, and floors to remote parts of the building. With the object of assisting in the assessment of noise transmission by such means to rooms at a distance from the disturbing source, this paper presents the results of measurements of the space rate of attenuation of the equivalent loudness of impact noises on concrete floors as heard in the rooms of a brick-walled building. Measurements were first made in both horizontal and vertical directions in relation to the source of sound, and afterwards in a series of general directions.

The building on which the measurements were made was the Physics Building of the National Physical Laboratory. This is a three-storey brick-built building about 40 ft. high and 160 ft. long. The building is not steel-framed, but there are transverse steel girders on stanchions bridging the rooms every 10 ft. The disposition of the rooms is shown in fig. 1, the positions of the stanchions being shown by broken lines. The thickness of the outer walls and of the main transverse walls is $13\frac{1}{2}$ in. on the two upper floors and 18 in. on the ground floor, of the non-structural brick partitions between rooms $4\frac{1}{2}$ in., and of the brick partitions between rooms and corridors 9 in. The floors are of concrete filler-joist construction and are about 8 in. thick. A basement runs the greater part of the length of the building. The rooms are situated along the front of the building, entrance to them being made from corridors which run the length of the building at the back. The floors are partially broken at the centre of the building by a staircase and a lift shaft. The external longitudinal walls are much interrupted by windows, whereas the transverse walls are not.

The source of sound was a rapping machine † consisting essentially of a set of hammers which were raised in succession by cams and allowed

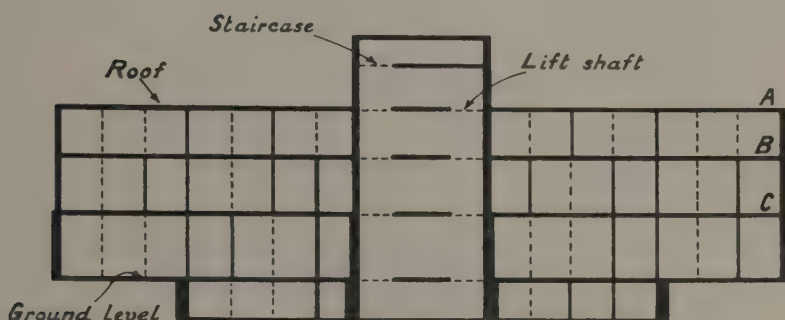
* Communicated by Dr. G. W. C. Kaye.

† See G. W. C. Kaye, *Journ. Acous. Soc. Amer.* vii. p. 167 (1936).

to fall under their own weight on to the floor. The blows approximated in energy to heavy footsteps, the energy of each blow being $\frac{1}{4}$ ft. lb. and the blows falling at the rate of four per second. One set of hammer-heads was shod with ebonite which gave a sharp blow, the other with rubber which gave a dull blow.

Measurements of the loudness of the sound were made by means of a calibrated subjective noise-meter of the Barkhausen type, in which a reference note of 800 cycles per second and of variable loudness as heard in a telephone earpiece is balanced against the test noise heard by the other ear. Measurements were made at night when the conditions were very quiet. To minimize the effect of air conduction along corridors, etc., all doors and windows were closed. Only one observer was employed.

Fig. 1.



Sectional elevation of building, showing positions of rapping machine for horizontal transmission measurements.

but as it is the rate of decay that is being measured, any systematic error is not so important as it would be if absolute values of the loudness were required. For the determination of the loudness of sound in a room, at least three observations were made in different parts of the room and the mean value taken. The space rate of attenuation was found by plotting the mean loudness in a room against the distance of the room from the source of sound, the latter being conveniently taken as the distance of the centre of the observation room. The best straight line was drawn through the points, the slope of the line giving the space rate of attenuation.

For measurements in a horizontal direction, the rapping machine was placed in the middle of the floor in positions A, B, and C in turn (position A being on the asphalt roof), and measurements were made for each position in the rooms in the storey immediately below the machine.

For both sharp and dull blows the decrease of loudness with distance was found to be roughly linear. The mean values of the space rate of attenuation are given in Table I. As will be seen, the space rate of attenuation for dull blows is substantially greater than for sharp blows.

The rooms in any one storey have in common a floor, a ceiling, an external wall and the bounding wall of the corridor, and any of these could transmit sound from room to room along the storey. It is fairly certain, however, that the chief path of sound is along the floor (or roof) in which the impact sound is generated, for it is unlikely that the vibration would find an easier path through the flanking walls, which are at least as heavy as the floor and are, therefore, no more free to vibrate.

For measurements on the transmission of sound vertically, the rapping machine was placed on the roof of the building in four positions in turn

TABLE I.
Attenuation of Sound in a Horizontal
Direction through Building.

Position of machine.	Space rate of attenuation of sound horizontally.	
	Dull blows.	Sharp blows.
	Phon per ft.	Phon per ft.
A	0.5	0.3
B	0.6	0.3
C	0.5 ₅	0.3

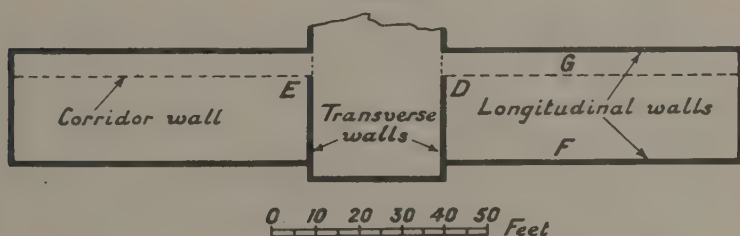
and, for each position, loudness measurements were made in the rooms vertically below the machine. The positions are indicated as D, E, F, and G in fig. 2. The value of the space rate of attenuation for both sharp and dull blows for each position of the machine was determined four times, for, owing to the limited number of storeys, determinations of the space rate of decay in a vertical direction could not be made as accurately as in a horizontal direction.

For the position D, the rooms in which measurements were made had in common the heavy transverse wall flanking the lift shaft, and it is likely that the chief path of the sound to the lower rooms was down this wall. Similarly, the chief path of sound to the lower rooms beneath E was doubtless the wall flanking the staircase, while the most probable transmission paths for positions F and G were the front and back longitudinal walls respectively. The space rates of attenuation for trans-

mission vertically are given in Table II. To illustrate the degree of consistency of the results, the four separate values of the space rate of decay for each machine position and each type of blow are given.

It will be seen that the mean space rates of decay for dull blows are greater, in general, by 50 per cent. or more than for sharp blows. Incidentally, similar qualitative results have been obtained from observations in a block of flats. As regards sharp impacts, the mean rates for the two transverse walls (D and E) are about the same (about 0.3 phon per ft.), while the average rate of decay down the front and back walls (F and G) is about half as much again (about 0.45 phon per ft.). For dull blows the mean rate of decay down the longitudinal walls is again about 50 per cent. greater than that down the transverse walls. The higher rate of attenuation down the main longitudinal walls is probably due to the numerous window spaces that they contain. Another explanation of the difference in the behaviour of the two types of wall is the greater

Fig. 2.



Plan of building, showing positions of rapping machine on roof for vertical transmission measurements.

amount of spreading of sound in the longitudinal wall which is 70 ft. long than in the transverse wall which is only about 20 ft. wide.

The results given in Tables I. and II. agree in indicating that for corresponding sound paths the attenuation of the equivalent loudness of dull blows is at least half as much again as that of sharp blows. As this effect may be bound up with frequency, measurements were made to find the influence of frequency on the loudness decay. For the purpose an analysis was made of the noise below a floor which was being struck by the rapping machine. It was found that, for the particular floor, the noise due to the sharp blows was centred about a frequency of 400 cycles per second, and for the dull blows about 100 cycles per second. Inspection of the characteristic curves given by Fletcher and Munson *

* Fletcher and Munson, Journ. Acous. Soc. Amer. v. p. 82 (1933).

for the sensitivity of the ear at these frequencies shows that, if the rate of decay of intensity can be assumed to be the same in each case, the rate

TABLE II.
Attenuation of Sound in a Vertical
Direction through the Building.

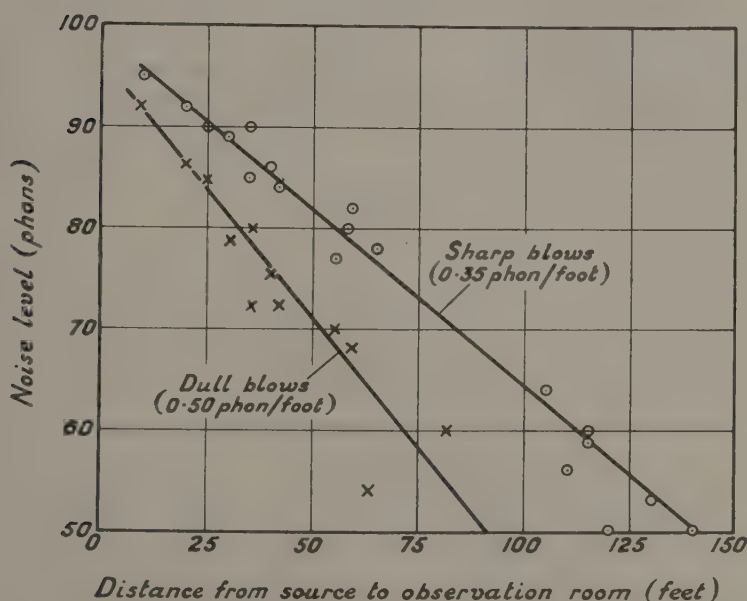
Position of machine.	Space rate of attenuation of sound vertically.	
	Dull blows.	Sharp blows.
D {	Phon per ft.	Phon per ft.
	0.5	0.3
	0.5	0.2
	0.5 ₅	0.2 ₅
	0.6	0.3
	—	—
	Mean.. 0.5 ₅	Mean.. 0.2 ₅
E {	0.6	0.3
	0.5	0.3
	0.4 ₅	0.3
	0.4 ₅	0.3 ₅
	—	—
	Mean.. 0.5	Mean.. 0.3
F {	0.7	0.4
	0.7 ₅	0.4
	0.6	0.3 ₅
	0.7 ₅	0.4
	—	—
	Mean.. 0.7	Mean.. 0.4
G {	0.7	0.5
	0.7 ₅	0.4 ₅
	0.7	0.5 ₅
	0.6 ₅	0.4
	—	—
	Mean.. 0.7	Mean.. 0.5

of decay of equivalent loudness would be half as much again for dull blows as for sharp ones. Constable, in some unpublished work, has recently found the attenuation of the intensity of impact sound in the

material of walls to be almost independent of the frequency, so that the difference now found between the loudness attenuations is to be expected.

The space rate of attenuation of noise was then measured in the building generally, *i. e.*, in a series of directions not necessarily horizontal or vertical, but rather a combination of both. The rapping machine was placed on the roof in position A (fig. 1) and measurements of the loudness were made in most of the rooms in the building.

Fig. 3.



Relation for impact noises (position A) between equivalent loudness in a room and distance from source.

The results are shown graphically in fig. 3, in which the loudness is plotted against the actual distance between the source and the centre of the measurement room. It will be seen that the results for sharp and dull blows are each fairly well distributed about a straight line, the slope being about 0.5 phons per ft. for dull blows and 0.35 phons per ft. for sharp blows. It would appear, therefore, by comparison with the earlier results, that the predominating factors in the "general" transmission are the floors and the transverse walls.

Summary.

A study of impact noises on concrete floors, as heard in the different rooms of a brick building, leads to the following conclusions :—

1. The relation between the equivalent loudness heard in a room and the distance of the room from the source of the impact noise is roughly linear.

2. The space rate of attenuation of the loudness of dull blows is substantially more than that of sharp ones, the mean values for a concrete floor or uninterrupted brickwork being about 0·3 phon per ft. for the type of sharp blows used and about 0·5 phon per ft. for the dull blows.

3. For the same type of blow, the space rate of attenuation down a longitudinal wall interrupted by windows may be 50 per cent. greater than that down an equally heavy unbroken transverse wall.

In conclusion, the author wishes to thank Dr. G. W. C. Kaye, F.R.S., Superintendent of the Physics Department, and Dr. A. H. Davis for helpful criticism and advice.

XXVI. *The Latent Heats of Fusion of some Organic Refrigerants.*

By J. H. AWBERRY, B.A., B.Sc., F.Inst.P., Physics Department,
National Physical Laboratory *.

[Received December 7, 1940.]

ABSTRACT.

The latent heats of fusion of methyl chloride, ethyl chloride, and dichloro-difluoro-methane are 31, 17, and 8.2 cal. per gm. respectively. They show no simple relationships with either the viscosities or the melting points of the substances.

Introduction.

THE well known work of Ramsay and Young ⁽¹⁾ was concerned with measuring a number of physical properties of each of a group of organic materials, largely with a view to discovering or checking relationships between the different properties, but little has been done on these lines in more recent years. The chief thermodynamic properties—total heats, entropies and specific volumes—of refrigerants are well known, and it appeared to be of interest to determine some other properties of the same materials. Results of measurements of the viscosities η of several refrigerants had already been published ⁽²⁾, and in view of the suggestion put forward by Kudar ⁽³⁾ to the effect that the constant Q of the equation $\eta = Ae^{Q/RT}$ might be the latent heat of fusion, the latter property was next selected for study. Here A is a constant, R the gas constant, and T the absolute temperature. The refrigerants on which results are reported are ethyl chloride, methyl chloride, and dichloro-difluoro-methane, known to the industry as Freon 12. They melt respectively at -140°C. , -91°C. and -155°C.

Description of Method.

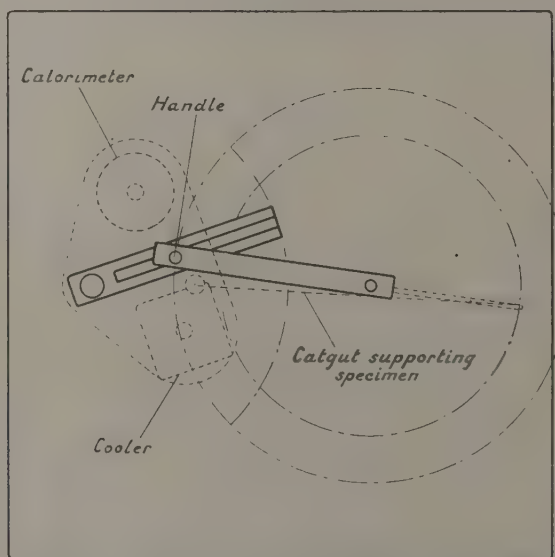
The method adopted was to measure the heat absorbed by the specimen in warming to about room temperature from various temperatures above and below the freezing point. The heat content of the solid and the liquid at the melting point could each be deduced, and the latent heat is the difference of the two. For this purpose the sample was sealed in a

* Communicated by the Author.

metal tube, cooled in a special cooler to the desired initial temperature, and rapidly transferred to an oil calorimeter. The heat corresponding to the observed cooling of the calorimeter was found by heating the calorimeter electrically through the same temperature range. The cooler and calorimeter were mounted in a chamber in which the air was kept dry by means of silica gel, the transfer being effected from outside the chamber (see fig. 1). The temperatures of the specimen and of the calorimetric fluid were measured by thermocouples.

The specimen container was constructed of thin-walled steel tubing, 14 cm. long and 1.8 cm. in diameter, to which conical ends were silver-

Fig. 1.

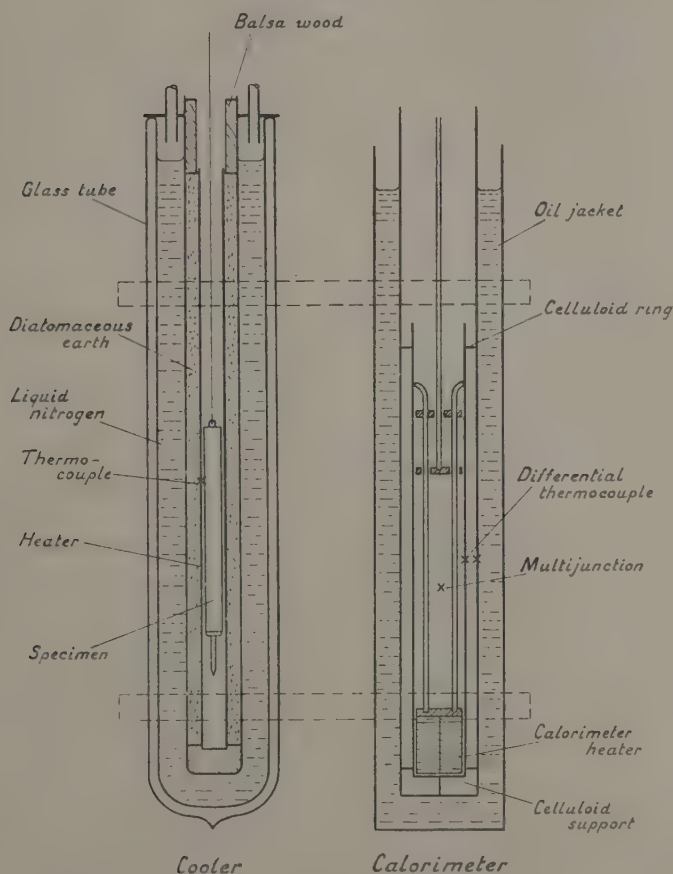


Transfer mechanism. (Movement half completed.)

soldered. The upper end was fitted with a ring from which the tube could be suspended, and the lower end was fitted with a short copper tube through which the liquid was introduced. The weight of the specimen was about 40 grams and the thermal capacity of the container was about 30 per cent. of the whole. The procedure adopted for filling the container was first to evacuate it and then to force the liquid in under pressure. The specimen was then cooled by solid carbon dioxide, the connexion to the copper tube was cut, and the end of the latter flattened and soldered. The container was tested for leaks by immersion in warm water and noting whether bubbles were formed.

The cooler (fig. 2) consisted of a vacuum flask filled with liquid nitrogen, in which was immersed a closed-ended tube, 3.5 cm. in diameter, of heat-resistant glass, within which was a copper tube of 1.9 cm. internal diameter, the interspace being packed with diatomaceous earth to serve as insulation. The copper tube, which was about twice as long as the specimen tube,

Fig. 2.



Apparatus for the determination of the latent heat of fusion of organic compounds.

was wound with a heater of silk-covered constantan wire, so that the temperature in the cooling space could be maintained at any desired value above the boiling point of nitrogen, and would be reasonably uniform over the central section. In order to ensure that the cold nitrogen

gas evaporated from the cooler should not disturb the temperature of the calorimeter, it was led away to the atmosphere outside the enclosure by means of the central supporting tube, which passed through the lid of the cooler. The liquid nitrogen was introduced into the cooler through a tube passing through its lid, and projecting through a hole in the side of the outer enclosure. It was found that a convenient means of transferring the liquid was to close the neck of the storage vessel with a bung through which passed two tubes, one dipping into the liquid and the other reaching only to the vapour space. Nitrogen from a cylinder was admitted through the latter tube, the whole arrangement acting like a wash-bottle. Tests with an empty specimen-tube to which thermocouples were attached showed that the temperature within the cooling space was very uniform. Consequently a single thermocouple, attached to the copper tube, was sufficient to measure the initial temperature of the specimen.

The calorimeter, which is also shown in fig. 2, was constructed of copper tubing approximately 4 cm. in diameter and 25 cm. high, was supported within an oil jacket of metal tube, the gap between the calorimeter and the inner wall of the jacket being about 5 mm., and the jacket extending a considerable distance above the top of the calorimeter.

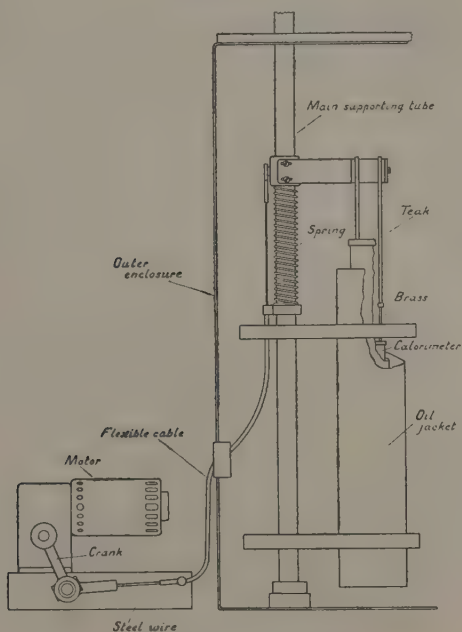
The calorimeter was fitted with a heater for the electrical calibration, thermocouples, a stirrer and suitable guides for receiving the specimen on transfer. The heater was wound on a light former of synthetic resin and was situated at the bottom of the calorimeter. Since the calorimetric fluid was oil, it was possible to use bare wire for the heater. The stirrer consisted of a horizontal brass ring supported by two vertical brass rods and was reciprocated over about three-quarters of the length of the calorimeter by an external motor, movement being transmitted by a Bowden cable as shown in fig. 3. The upper part of the support was of teak. The guides were formed of a framework of brass rod, so designed as to support the specimen out of contact with the sides, and clear of the stirrer. Two thermocouples were used, one a differential couple soldered to the outside of the calorimeter and the inside of the oil jacket so as to show the temperature excess of the calorimeter over the jacket throughout the experiment, and the other of three elements in series stretched along the length of the calorimeter with the junctions in the oil.

The cooler and calorimeter were clamped to the supporting tube, which could be rotated. By means of the mechanism shown in fig. 1, the specimen was lifted from the cooler, the vertical tube rotated and the specimen lowered again, without jarring, into the original position (now occupied by the calorimeter), the operation requiring less than one second. The transfer was thus effected rapidly in dry air, so reducing to a minimum any gain of heat or deposition of frost on the specimen tube.

The chamber containing the apparatus was of planished steel sheet welded at the corners, with a thick celluloid window occupying the whole of one side, and contained a tray of silica gel to absorb moisture from the air.

The course of the experiment was therefore as follows. The chamber having been closed and left for some time to become dry, the specimen was allowed to cool until its temperature was steady for an appreciable time, the temperature being noted from the thermocouple attached to the cooler. Meanwhile, the current in the calorimeter heater was

Fig. 3.



Stirring mechanism.

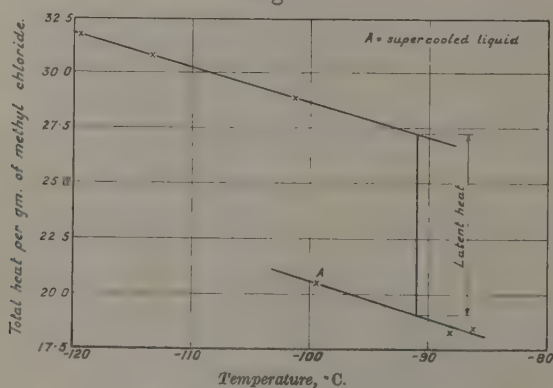
switched on in order to raise its temperature above the desired initial temperature. Throughout this period, the stirrer was operated at its standard rate. The heater was then switched off, and temperatures in the calorimeter observed periodically until the maximum had been passed, and cooling was proceeding at its standard rate. The specimen was transferred at a known instant of time, when the calorimeter temperature had reached a value such that on introduction of the specimens the final temperature would be about that of the room. The temperature of the calorimeter and its excess over the jacket temperature were read

periodically for a period of about 25 minutes. From independent experiments the rate of cooling was known as a function of the temperature excess, and hence a correction to the total fall of temperature was evaluated. The thermal capacity of the calorimeter was determined by electrical calibration. Since only the latent heat of fusion was required, it was not necessary to know the thermal capacity of the tube containing the specimen.

Results.

For each refrigerant, six to eight experiments were carried out, three or four on each side of the melting point. The total heat from room temperature (corrected to the mean as a standard temperature by means of published values for the specific heat in this range) was plotted against initial temperature. A typical curve is that for methyl chloride, shown in fig. 4.

Fig. 4



Total heat of methyl chloride.

The values are shown in the table below.

Observed Latent Heats of Fusion.

Refrigerant.	Freezing point.	Latent Heat.	
		Cal. per gm.	k-cal. per gm. mol.
Methyl chloride	- 91° C.	31	1.57
Ethyl chloride	-140	17	1.10
Freon 12 (Dichloro-difluoro-methane)	-155	8.2	0.99

The values predicted on Kudar's theory, from viscosity data obtained at the Laboratory, are 24.3, 22.7, and 11.7 cal. per gm. for the three materials, as against the observed values of 31, 17, and 8.2.

It thus appears that the theory gives values which may be in error by large amounts, and diverge in either direction from the true value. The theory must therefore be abandoned.

It is, however, of interest to compare the molecular heats of fusion with those for other materials melting at low temperatures, since this might be expected to give an alternative method of estimating the latent heat of a material for which this property has not been measured. An examination of the present results, together with a selection of other results below 0°C ., taken from the Landolt-Bornstein-Meyer tables of chemical constants, shows that there is very little correlation. This is in striking contrast to the case of evaporation, where molecular latent heats are to a first approximation functions of temperature only. Thus ethane and methane, with freezing-points differing only 1.1°C ., have latent heats of 0.224 and 0.668 *k*-cal. per mol. respectively and tri-methyl butane, freezing at -25°C ., has a lower molecular heat than hexane, which freezes at -95°C .

Acknowledgment.

Mr. V. M. Hickson set up the apparatus, and to him are due the ingenious mechanism used for transferring the specimen and the very satisfactory stirrer. He also took most of the observations and reduced them.

References.

- (1) Ramsay, W., and Young, S., *Phil. Trans. A*, clxxviii. p. 329 (1887) ; Young, S., *Sci. Proc. R. Dublin. Soc.* xii. p. 374 (1910).
- (2) Awbery, J., and Griffiths, E., *Proc. Phys. Soc.* xlviii. p. 372 (1936).
- (3) Kudar, H. C., *Zeits. Phys.* lxxx. p. 217 (1933).

XXVII. Some Formulæ for the E-function.

By T. M. MACROBERT, Professor of Mathematics,
University of Glasgow †.

[Received November 28, 1939.]

§ 1. Introductory.

THE E-function $E(p; \alpha_r; q; \rho_s; x)$ was defined (Proc. Roy. Soc. Edin. vol. lviii. p. 3 (1937)) by the formula

$$E(p; \alpha_r; q; \rho_s; x) = \frac{\Gamma(\alpha_{q+1})}{\Gamma(\rho_1 - \alpha_1) \Gamma(\rho_2 - \alpha_2) \dots \Gamma(\rho_q - \alpha_q)} \\ \times \prod_{\mu=1}^q \int_0^\infty \lambda_\mu^{\rho_\mu - \alpha_\mu - 1} (1 + \lambda_\mu)^{-\rho_\mu} d\lambda_\mu \prod_{v=2}^{p-q-1} \int_0^\infty e^{-\lambda_{q+v}} \lambda_{q+v}^{\alpha_{q+v}-1} d\lambda_{q+v} \\ \times \int_0^\infty e^{-\lambda_p} \lambda_p^{\alpha_p-1} \left\{ 1 + \frac{\lambda_{q+2} \lambda_{q+3} \dots \lambda_p}{(1 + \lambda_1)(1 + \lambda_2) \dots (1 + \lambda_q)x} \right\}^{-\alpha_{q+1}} d\lambda_p, \quad (1)$$

the constants being such that the integrals converge. It is assumed that $|\operatorname{amp} x| < \pi$ and that $p \geq q+1$. In the paper referred to the E-functions were employed to evaluate a number of integrals involving Hypergeometric and Legendre Functions.

If $p \geq q+1$,

$$E(p; \alpha_r; q; \rho_s; x) = \sum_{r=1}^p \frac{\prod_{s=1}^{p'} \Gamma(\alpha_s - \alpha_r)}{\prod_{t=1}^q \Gamma(\rho_t - \alpha_r)} \Gamma(\alpha_r) x^{\alpha_r} \\ \times {}_{q+1}F_{p-1} \left\{ \begin{matrix} \alpha_r, \alpha_r - \rho_1 + 1, \dots, \alpha_r - \rho_q + 1; (-1)^{p-q} x \\ \alpha_r - \alpha_1 + 1, \dots, \alpha_r - \alpha_p + 1 \end{matrix} \right\}, \quad (2)$$

where, when $p = q+1$, $|x| < 1$. If $p \leq q+1$ the function can be defined by the equation

$$E(p; \alpha_r; q; \rho_s; x) = \frac{\prod_{s=1}^p \Gamma(\alpha_s)}{\prod_{s=1}^{p-1} \Gamma(\rho_s)} {}_pF_q \left(\alpha_r; \rho_s; -\frac{1}{x} \right), \quad (3)$$

where $x \neq 0$ and, if $p = q+1$, $|x| > 1$. If $p > q+1$ the R.H.S. of (3) gives the asymptotic expansion of the E-function.

† Communicated by the Author.

Proofs of formulæ (2) and (3) for the case $p > q + 1$ were given in the paper referred to above. For the case $p = q + 1$ reference may be made to the Phil. Mag. (xxv. pp. 848-851 (1938)).

In section 2 of this paper a number of integrals for the *E*-function are established. Many formulæ for the Confluent Hypergeometric, Bessel, and Legendre Functions are particular cases of these formulæ. Two examples of such particular cases are given in section 3, and from them is deduced a new formula for the Associated Legendre Functions of the First Kind. A generalization of an integral formula due to Meijer is also proved; and a note is added pointing out that a formula obtained by Meijer for a product of two confluent Hypergeometric Functions is an *E*-function formula. In section 4 some recurrence formulæ for the *E*-function are established.

§ 2. Integrals for the *E*-function.

The first formula is

$$\frac{1}{2\pi i} \int_C e^{\zeta} \zeta^{-p_q+1} E(p; \alpha_r : q; \rho_s : \zeta x) d\zeta = E(p; \alpha_r : q+1; \rho_s : x), \quad (4)$$

where C is a contour starting at $-\infty$ on the real axis, passing positively round the origin and returning to $-\infty$ on the real axis, and $\text{amp } \zeta = 0$ to the right of the origin.

When $p \geq q + 2$ the formula can be proved by substituting from (2) for the *E*-function in the integrand and then integrating. When $p \leq q + 1$ formula (3) is employed.

The second formula is

$$\int_0^\infty e^{-\lambda} \lambda^{\alpha_{p+1}-1} E\left(p; \alpha_r : q; \rho_s : \frac{x}{\lambda}\right) d\lambda = E(p+1; \alpha_r : q; \rho_s : x), \quad (5)$$

where $R(\alpha_{p+1}) > 0$.

If $p \geq q + 1$, the formula can be derived from (1); if $p \leq q + 1$, formula (3) may be employed.

Next, in the integral

$$\int_C e^{\zeta} \zeta^{\alpha_{p+1}-1} {}_pF_q\left(\alpha_r; \rho_s; -\frac{\zeta}{x}\right) d\zeta,$$

where $p \leq q$, let it be assumed that $R(\alpha_{p+1}) > 0$. For simplicity it may also be assumed that x is positive. Then deform the contour into parts of the negative real axis and a circle with the origin as centre. When the radius of this circle tends to zero the integral becomes

$$2i \sin(\alpha_{p+1}\pi) \int_0^\infty e^{-\lambda} \lambda^{\alpha_{p+1}-1} {}_pF_q\left(\alpha_r; \rho_s; \frac{\lambda}{x}\right) d\lambda,$$

from which, with (3), it follows that

$$\int_C e^{\zeta} \zeta^{\alpha_{p+1}-1} E\left(p; \alpha_r: q; \rho_s: \frac{x}{\zeta}\right) d\zeta \\ = 2i \sin(\alpha_{p+1}\pi) E(p+1; \alpha_r: q; \rho_s: -x), \quad \dots \quad (6)$$

where $p \leq q$ and α_{p+1} may have any value.

If $p \geq q+2$, it follows from (2) that

$$\int_C e^{\zeta} \zeta^{\alpha_{p+1}-1} E\left(p; \alpha_r: q; \rho_s: \frac{x}{\zeta}\right) d\zeta \\ = \sum_{r=1}^{p+1} \frac{\prod_{s=1}^{p+1} \Gamma(\alpha_s - \alpha_r)}{q} \Gamma(\alpha_r) x^{\alpha_r} 2i \sin(\alpha_{p+1} - \alpha_r)\pi \\ \times {}_{q+1}F_p \left\{ \begin{matrix} \alpha_r, \alpha_r - \rho_1 + 1, \dots, \alpha_r - \rho_q + 1; (-1)^{p-q} x \\ \alpha_r - \alpha_1 + 1, \dots, \alpha_r - \alpha_{p+1} + 1 \end{matrix} \right\},$$

so that

$$\int_C e^{\zeta} \zeta^{\alpha_{p+1}-1} E\left(p; \alpha_r: q; \rho_s: \frac{x}{\zeta}\right) d\zeta = e^{i\alpha_{p+1}\pi} E(p+1; \alpha_r: q; \rho_s: xe^{-i\pi}) \\ - e^{-i\alpha_{p+1}\pi} E(p+1; \alpha_r: q; \rho_s: xe^{i\pi}). \quad \dots \quad (7)$$

If $p = q+1$, this holds provided that C encloses the point x as well as the origin.

If $p < q$, or if $p = q$ and $x > 1$, the R.H.S. of (7) is uniform in x and (7) reduces to (6). Thus (7) holds for all values of p and q .

Again, if $R(\alpha_{p+1}) > 0$, $R(\rho_{q+1} - \alpha_{p+1}) > 0$,

$$\int_0^\infty \frac{\lambda^{\rho_{q+1} - \alpha_{p+1} - 1}}{(1+\lambda)^{\rho_{q+1}}} E\{p; \alpha_r: q; \rho_s: (1+\lambda)x\} d\lambda \\ = \Gamma(\rho_{q+1} - \alpha_{p+1}) E(p+1; \alpha_r: q+1; \rho_s: x). \quad \dots \quad (8)$$

If $p \geq q+1$, this can be derived from (1); if $p \leq q+1$, formula (3) may be employed.

Finally, from (2) it follows that, if

$$p \geq q+2, \quad R(x) > 0 \quad \text{and} \quad R(k + \alpha_r) > 0 \quad \text{for} \quad r=1, 2, \dots, p,$$

$$\int_0^\infty e^{-\lambda x} \lambda^{k-1} E(p; \alpha_r: q; \rho_s: \lambda y) d\lambda \\ = \frac{1}{x^k} \sum_{r=1}^p \frac{\prod_{s=1}^p \Gamma(\alpha_s - \alpha_r)}{\prod_{t=1}^q \Gamma(\rho_t - \alpha_r)} \cdot \Gamma(\alpha_r) \Gamma(k + \alpha_r) \left(\frac{y}{x}\right)^{\alpha_r}$$

$$\times_{q+2} F_{p-1} \left\{ \begin{matrix} \alpha_r, k+\alpha_r, \alpha_r-\rho_1+1, \dots, \alpha_r-\rho_q+1; (-1)^{p-q} \frac{y}{x} \\ \alpha_r-\alpha_1+1, \dots * \dots, \alpha_r-\alpha_p+1 \end{matrix} \right\}, \quad (9)$$

provided that, if $p=q+2$, $|y/x| < 1$.

§ 3. Some Special Cases.

In particular cases the formulæ of section 2 reduce to integrals involving Bessel Functions, Legendre Functions and Confluent Hypergeometric Functions.

For example, since

$$E(\tfrac{1}{2}+n, \tfrac{1}{2}-n; 0; : 2\lambda) = \frac{\sqrt{(2\pi\lambda)}}{\cos n\pi} e^{\lambda} K_n(\lambda), \quad \dots \quad (10)$$

on putting $p=2$, $q=1$, $\alpha_1=n+1$, $\alpha_2=-n$, $\alpha_3=m+1$, $\rho_1=m+1$ in (5), and replacing x by $2x$, that formula becomes

$$K_{n+\frac{1}{2}}(x) = \sqrt{\left(\frac{\pi}{2x}\right)} \frac{e^{-x}}{\Gamma(m+1)} \int_0^\infty e^{-\lambda} \lambda^m F\left(\begin{matrix} n+1, -n; \\ m+1 \end{matrix}; \frac{-\lambda}{2x}\right) d\lambda.$$

Hence, on putting $\lambda=x(t-1)$, we find that

$$K_{n+\frac{1}{2}}(x) = \sqrt{\left(\frac{\pi}{2}\right)} x^{m+\frac{1}{2}} \int_1^\infty e^{-xt} (t^2-1)^{\frac{1}{2}m} P_n^{-m}(t) dt, \quad \dots \quad (11)$$

where $R(x) > 0$, $R(m) > -1$. [Phil. Mag. ser. 7, vol. xxi. p. 700 (1936).]

Again, in (9) put $p=2$, $q=0$, $\alpha_1=n+1$, $\alpha_2=-n$, $k=m$, $y=2$, and replace x by $x+1$; then

$$\begin{aligned} & \frac{\sqrt{(2\pi)}}{\cos(n+\frac{1}{2})\pi} \int_0^\infty e^{-\lambda x} \lambda^{m-\frac{1}{2}} K_{n+\frac{1}{2}}(\lambda) d\lambda \\ &= \Gamma(n+1) \Gamma(m+n+1) \Gamma(-n) \Gamma(m-n) (x+1)^{-m} \\ & \times \left\{ \frac{\Gamma(-2n-1)}{\Gamma(-n) \Gamma(m-n)} \left(\frac{2}{x+1}\right)^{n+1} F\left(\begin{matrix} m+n+1, n+1; \\ 2n+2 \end{matrix}; \frac{2}{x+1}\right) \right. \\ & \quad \left. + \frac{\Gamma(2n+1)}{\Gamma(n+1) \Gamma(m+n+1)} \left(\frac{2}{x+1}\right)^{-n} F\left(\begin{matrix} m-n, -n; \\ -2n \end{matrix}; \frac{2}{x+1}\right) \right\}, \end{aligned}$$

whence it follows that

$$\begin{aligned} & \int_0^\infty e^{-\lambda x} \lambda^{m-\frac{1}{2}} K_{n+\frac{1}{2}}(\lambda) d\lambda \\ &= \sqrt{\left(\frac{\pi}{2}\right)} \Gamma(m+n+1) \Gamma(m-n) (x^2-1)^{-\frac{1}{2}m} P_n^{-m}(x), \quad \dots \quad (12) \end{aligned}$$

where $R(x) > -1$, $R(m+n) > -1$, $R(m-n) > 0$. [Phil. Mag. ser. 7, xxvii. p. 704 (1939).]

On putting $l-m-1$ for m in (12), substituting for $K_{n+\frac{1}{2}}(\lambda)$ from (11), and then changing the order of integration, we find that

$$\begin{aligned} \Gamma(l) \int_1^\infty (x+t)^{-l}(t^2-1)^{\frac{1}{2}m} P_n^{-m}(t) dt \\ = \Gamma(l-m+n) \Gamma(l-m-n-1) (x^2-1)^{\frac{1}{2}(m-l+1)} P_n^{m-l+1}(x), \end{aligned} \quad (13)$$

where $R(x) > -1$, $R(l-m+n) > 0$, $R(l-m-n) > 1$, $R(m) > -1$.

The formula

$$4 \int_0^\infty \lambda^{m-1} K_n(2\lambda) E\left(p; \alpha_r: q; \rho_s: \frac{x}{\lambda^2}\right) d\lambda = E(p+2; \alpha_r: q; \rho_s: x), \quad (14)$$

where $\alpha_{p+1} = \frac{1}{2}(m+n)$, $\alpha_{p+2} = \frac{1}{2}(m-n)$, $R(m \pm n) > 0$, and, for simplicity, x may be taken to be real and positive, was given by Meijer (Proc. Lond. Math. Soc. xl. p. 2 (1934)), for the case $q=p-1$. It can be proved as follows.

By formula (5)

$$\begin{aligned} E(p+2; \alpha_r: q; \rho_s: x) \\ = \int_0^\infty e^{-\lambda} \lambda^{\alpha_{p+1}-1} d\lambda \int_0^\infty e^{-\mu} \mu^{\alpha_{p+2}-1} E\left(p; \alpha_r: q; \rho_s: \frac{x}{\lambda\mu}\right) d\mu. \end{aligned}$$

On replacing μ by $\frac{1}{2}\mu$ and λ by $2\lambda^2/\mu$, this becomes

$$2^{n+1} \int_0^\infty \lambda^{m+n-1} E\left(p; \alpha_r: q; \rho_s: \frac{x}{\lambda^2}\right) d\lambda \int_0^\infty e^{-\frac{1}{2}\left(\mu + \frac{4\lambda^2}{\mu}\right)} \mu^{-n-1} d\mu,$$

from which (14) follows.

Note.—The formula

$$\begin{aligned} 2^{\alpha+\beta-1} \Gamma(\alpha) \Gamma(\beta) E\left(4; \alpha, \beta, \frac{\alpha+\beta}{2}, \frac{\alpha+\beta+1}{2}: 1; \alpha+\beta: \frac{x^2}{4}\right) \\ = \Gamma\left(\frac{1}{2}\right) E(2; \alpha, \beta: 0; : ix) E(2; \alpha, \beta: 0; : -ix), \end{aligned} \quad (15)$$

which can also be expressed in the form

$$\begin{aligned} E\left(4; \frac{1}{2}-k+m, \frac{1}{2}-k-m, \frac{1}{2}-k, 1-k: 1; 1-2k: \frac{x^2}{4}\right) \\ = 2^{2k} \Gamma\left(\frac{1}{2}\right) \Gamma\left(\frac{1}{2}-k+m\right) \Gamma\left(\frac{1}{2}-k-m\right) x^{-2k} W_{k,m}(ix) W_{k,m}(-ix), \end{aligned} \quad (15')$$

was proved by Meijer (Proc. Lond. Math. Soc. xl. p. 21 (1934)). The E-functions on the right are expanded by (2) and multiplied. With the help of this formula many integral formulæ have been obtained by Meijer (Quart. Journ. of Math. (Oxford), vi. pp. 241-248 (1935)) and by Bailey (Quart. Journ. of Math. (Oxford), viii. pp. 51-53 (1936)).

§4. Recurrence Formulæ.

The following formulæ for the generalized Hypergeometric Functions are required :

$$\alpha_1 {}_pF_q(\alpha_r; \rho_s; x) = \alpha_1 {}_pF_q\left(\begin{matrix} \alpha_1+1, \alpha_2, \dots, \alpha_p \\ \rho_1, \rho_2, \dots, \rho_q \end{matrix}; x\right) - x \frac{\alpha_1 \alpha_2 \dots \alpha_p}{\rho_1 \rho_2 \dots \rho_q} {}_pF_q(\alpha_r+1; \rho_s+1; x), \quad (16)$$

where $q \geq p-1$;

$$(\alpha_1 - \rho_1 + 1) {}_pF_q(\alpha_r; \rho_s; x) = (1 - \rho_1) {}_pF_q\left(\begin{matrix} \alpha_1, \alpha_2, \dots, \alpha_p \\ \rho_1-1, \rho_2, \dots, \rho_q \end{matrix}; x\right) + \alpha_1 {}_pF_q\left(\begin{matrix} \alpha_1+1, \alpha_2, \dots, \alpha_p \\ \rho_1, \rho_2, \dots, \rho_q \end{matrix}; x\right), \quad (17)$$

where $q \geq p-1$.

Formula (16) may also be expressed in the forms

$$\frac{d}{dx} x^{\alpha_1} {}_pF_q(\alpha_r; \rho_s; \pm x) = \alpha_1 x^{\alpha_1-1} {}_pF_q\left(\begin{matrix} \alpha_1+1, \alpha_2, \dots, \alpha_p \\ \rho_1, \rho_2, \dots, \rho_q \end{matrix}; \pm x\right). \quad (18)$$

On interchanging α_1 and α_2 in (16), and subtracting, it is found that

$$(\alpha_1 - \alpha_2) {}_pF_q(\alpha_r; \rho_s; x) = \alpha_1 {}_pF_q\left(\begin{matrix} \alpha_1+1, \alpha_2, \dots, \alpha_p \\ \rho_1, \rho_2, \dots, \rho_q \end{matrix}; x\right) - \alpha_2 {}_pF_q\left(\begin{matrix} \alpha_1, \alpha_2+1, \dots, \alpha_p \\ \rho_1, \rho_2, \dots, \rho_q \end{matrix}; x\right). \quad (19)$$

Now apply formula (16) to the first generalized Hypergeometric Function on the right of (2) and formula (17) to the others. Then

$$\begin{aligned} E(p; \alpha_r; q; \rho_s; x) &= \frac{\Gamma(\alpha_2 - \alpha_1 - 1) \Gamma(\alpha_3 - \alpha_1) \dots \Gamma(\alpha_p - \alpha_1)}{\Gamma(\rho_1 - \alpha_1) \Gamma(\rho_2 - \alpha_1) \dots \Gamma(\rho_q - \alpha_1)} \Gamma(\alpha_1) x^{\alpha_1} \\ &\times \left[(-1)^{p-q} x \frac{(\alpha_1 - \rho_1 + 1) \dots (\alpha_1 - \rho_q + 1)}{(\alpha_1 - \alpha_3 + 1) \dots (\alpha_1 - \alpha_p + 1)} \right. \\ &\quad \times {}_{q+1}F_{p-1} \left\{ \begin{matrix} \alpha_1+1, \alpha_1 - \rho_1 + 2, \dots, \alpha_1 - \rho_q + 2 \\ \alpha_1 - \alpha_2 + 2, \dots, \alpha_1 - \alpha_p + 2 \end{matrix}; (-1)^{p-q} x \right\} \\ &\quad - (\alpha_1 - \alpha_2 + 1) \\ &\quad \times {}_{q+1}F_{p-1} \left\{ \begin{matrix} \alpha_1+1, \alpha_1 - \rho_1 + 1, \dots, \alpha_1 - \rho_q + 1 \\ \alpha_1 - \alpha_2 + 1, \dots, \alpha_1 - \alpha_p + 1 \end{matrix}; (-1)^{p-q} x \right\} \left. \right] \\ &+ \sum_{r=2}^p \frac{\prod_{s=1}^p \Gamma(\alpha_s - \alpha_r)}{\prod_{t=1}^q \Gamma(\rho_t - \alpha_r)} \frac{\Gamma(\alpha_r)}{\alpha_1} x^{\alpha_r} \\ &\times \left[(\alpha_1 - \alpha_r) {}_{q+1}F_{p-1} \left\{ \begin{matrix} \alpha_r, \alpha_r - \rho_1 + 1, \dots, \alpha_r - \rho_q + 1 \\ \alpha_r - \alpha_1, \alpha_r - \alpha_2 + 1, \dots, \alpha_r - \alpha_p + 1 \end{matrix}; (-1)^{p-q} x \right\} \right. \\ &\quad \left. + \alpha_r {}_{q+1}F_{p-1} \left\{ \begin{matrix} \alpha_r+1, \alpha_r - \rho_1 + 1, \dots, \alpha_r - \rho_q + 1 \\ \alpha_r - \alpha_1 + 1, \dots, \alpha_r - \alpha_p + 1 \end{matrix}; (-1)^{p-q} x \right\} \right], \end{aligned}$$

and, therefore,

$$\begin{aligned} E(p; \alpha_r : q; \rho_s : x) &= \frac{1}{\alpha_1} E(\alpha_1 + 1, \alpha_2, \dots, \alpha_p : q; \rho_s : x) \\ &\quad + \frac{1}{\alpha_1 x} E(p; \alpha_r + 1 : q; \rho_s + 1 : x). \quad (20) \end{aligned}$$

As the E-function is symmetrical in the α 's, formula (20) is equivalent to p different recurrence formulæ.

Again, on differentiating (2), making use of (18), it is found that

$$\frac{d}{dx} E(p; \alpha_r : q; \rho_s : x) = \frac{1}{x^2} E(p; \alpha_r + 1 : q; \rho_s + 1 : x). \quad (21)$$

This formula can also be derived directly from formula (1).

Next, on applying (19) to (2), we find that

$$\begin{aligned} E(p; \alpha_r : q; \rho_s : x) &= \frac{1}{\rho_1 - 1} E(p; \alpha_r : \rho_1 - 1, \rho_2, \dots, \rho_q : x) \\ &\quad + \frac{1}{(\rho_1 - 1)x} E(p; \alpha_r + 1 : q; \rho_s + 1 : x). \quad (22) \end{aligned}$$

This is equivalent to q recurrence formulæ.

From (20) it follows that

$$\begin{aligned} (\alpha_1 - \alpha_2) E(p; \alpha_r : q; \rho_s : x) &= E(\alpha_1 + 1, \alpha_2, \dots, \alpha_p : q; \rho_s : x) \\ &\quad - E(\alpha_1, \alpha_2 + 1, \alpha_3, \dots, \alpha_p : q; \rho_s : x), \quad (23) \end{aligned}$$

and from (22) that

$$\begin{aligned} (\rho_1 - \rho_2) E(p; \alpha_r : q; \rho_s : x) &= E(p; \alpha_r : \rho_1 - 1, \rho_2, \dots, \rho_q : x) \\ &\quad - E(p; \alpha_r : \rho_1, \rho_2 - 1, \rho_3, \dots, \rho_q : x). \quad (24) \end{aligned}$$

When $p < q + 1$, formulæ (20) to (24) may be easily derived from formula (3).

Note.—By means of the relation

$$\begin{aligned} E(\tfrac{1}{2} - k - m, \tfrac{1}{2} - k + m : 0 : x) \\ = \Gamma(\tfrac{1}{2} - k - m) \Gamma(\tfrac{1}{2} - k + m) x^{-k} e^{ix} W_{k, m}(x) \quad (25) \end{aligned}$$

it is easy to deduce known formulæ for the Confluent Hypergeometric Function from formulæ (20) and (21).

XXVIII. *Notices respecting New Books.*

Applied Aerodynamics. By L. BAIRSTOW. (Published by Longmans, Green and Co., Ltd. Pp. xviii+808+27 plates. Price 63s.)

THIS volume is based on the first edition (which was published in 1919), but the work has been enlarged, and the greater part of the material is new. The character of the book is in keeping with its title ; it makes no attempt to cover the design problems associated with aircraft, but aims at setting out in a comprehensive manner the physical and mathematical conceptions which form the aerodynamic background to aeronautics. In an endeavour to keep the practical aspect of the work clear, Professor Bairstow has, whenever possible, provided examples of the application to aircraft of the principles discussed, with the result that the volume should be valuable both to the student and to the worker in the aerodynamic laboratory.

The volume can be divided broadly into three parts. The first is concerned with the elementary principles of flight, and with the methods commonly used to provide design data. A chapter on Dynamical Similarity is interposed between this first section and the second, which deals with the theory of fluid motion. A chapter on airscrews leads to the third part, which covers aircraft performance and stability.

The first part of the book opens with a chapter on the historical background to aerodynamics ; this chapter is of necessity incomplete, but it serves to introduce the student to the train of thought and experiment which has led to modern knowledge. Chapter II. is headed "The Principles of Flight" and it covers this subject, as applied to the aeroplane, flying boat, autogyro, and lighter than air craft, in an elementary fashion. The chapter is clearly intended for the beginner, and as such is well conceived, but in places it tends to take simplicity to the point at which it becomes misleading. Chapters III. and IV. deal with methods of measurement and laboratory technique ; they cover the basic essentials comprehensively, though the reading is occasionally rendered a little difficult to the beginner because use is made of material dealt with more fully in other parts of the book, and adequate cross-references are not always provided. These chapters discuss the standard measuring instruments, wind-tunnels, and wind-tunnel tests on the components of an aircraft, and on a complete aeroplane. They include a fairly comprehensive section on wing stalling, but this might usefully have been extended to include a discussion on the stalling problem as it affects the complete aeroplane. One could also have wished for a fuller discussion on the fundamentals affecting the design of a wind tunnel, since this apparatus is so essential a part of the aerodynamic laboratory. However, the chapters form a good introduction to the practical side of aerodynamic work. The chapter on aerial manoeuvres which follows covers the elementary theory of the loop, dive, roll and spin : the chapter forms a sound basis for further study, but it is marred, as is the whole of the first part of the book, because exact definitions are often left to later sections, and cross-referencing is not so complete as might be desired.

Chapter VI. deals with Dynamical Similarity. This is a subject on which a great deal of aerodynamic work is based, and its importance to a book of this

kind cannot be overstressed. The careful consideration which Professor Bairstow gives to it is therefore fully justified. There is much in this chapter that is very sound, though there are some omissions, such, for example, as the general theorem relating the number of non-dimensional criteria which specify a condition to the number of independent variables associated with it.

The next section of the volume is devoted to the mathematical and physical theory associated with the motion of fluids. Individual chapters deal with the usual aspects of the subject: the inviscid and incompressible fluid, the aerofoil of finite span and the trailing vortex, the viscous but incompressible fluid, the compressible fluid, and turbulent flow. The treatment is standard throughout and is comprehensive from the student's viewpoint. These chapters contain enough to give a clear picture of the scope of the subject, but they are not entirely without defects. It is possibly because the subjects are kept too closely within the bounds of their own chapters that some practical points have escaped discussion: an example is the subject of the transition of the laminar boundary layer to the turbulent form on wings, with its practical repercussions. This point receives mention in the chapters on laminar and turbulent flow, but it might have been considered to be of sufficient importance to justify a more complete discussion to itself. While in many cases Professor Bairstow has backed his argument with experimental data, the impression arose occasionally, while reading this section, that the practical side of the subject had been lost behind a wealth of mathematical detail.

The chapter on compressibility is well conceived, and it is pleasing to note that this important aspect of aerodynamics is discussed fairly thoroughly, having regard to the compass of the volume. The chapter on turbulence and turbulent motion, however, calls for certain criticisms. The statistical theory of turbulence is introduced but without satisfactory definitions and examples to excite the reader's attention. One feels that this important subject deserves a better fate and might have been considered to merit a little more space, or alternately, have been omitted entirely. The impression left by this chapter is that it is the least satisfactory in the volume.

A chapter on airscrews follows the section on fluid motion. This chapter is very satisfactory: it provides a good insight into the physics of the airscrew and into the methods which may be used to evolve a good design. A section on fans might perhaps have been included; this is a subject of growing importance and would merit consideration in a volume of this kind.

The final chapters are devoted to the reduction and prediction of aeroplane performance, and to stability. The treatment is very sound, and, within the compass of the book, is complete. One might, perhaps, have expected more consideration of the control problem, but it must be recognized that in a work of this kind space is always at a premium.

This book can be recommended confidently to the student and aerodynamic worker as containing a sound exposition of the fundamentals of present day aerodynamics. That there are omissions, and sometimes important ones, cannot be denied, but to undertake to cover aerodynamics in one volume is an ambitious aim. If, however, to introduce certain of the omissions had necessitated the removal of other subject-matter the change might, in some cases, have been made with advantage. It is considered that the volume might also have been improved by more frequent cross-references and by the inclusion of a more extensive bibliography.

The presentation of the work is good; it is well printed and well illustrated, and among the plates are some excellent examples of scientific photography.

Introduction to Chemical Physics. By J. C. SLATER. [Pp. xiv+521.] (New York and London: McGraw-Hill, 1939. Price 33s.)

THE term "chemical physics," used by the author to denote a rather indefinite range of study which is common to physics and chemistry, is not entirely satisfactory. In this book, which is primarily a survey of thermodynamics and statistical mechanics, there is nothing peculiarly chemical in the physics, except perhaps the limitation of the applications to fields of chemical interest.

The book is divided into three parts. The first, "Thermodynamics, Statistical Mechanics, and Kinetic Theory" provides, in just over a hundred pages, a survey of general methods and results which will be admirable for those who already have some familiarity with the subjects. Owing to the brevity there is almost unavoidably some inequality in the treatment. The account of Bose-Einstein and Fermi-Dirac statistics, for example, seems unnecessarily involved, but the difficult topic, fluctuations, is presented with great clearness.

"Gases, Liquids, and Solids" form the theme of the second part, which deals with equations of state, specific heats, homogeneous and heterogeneous equilibria, and phase changes. The formal aspects of the various problems are well presented, but the physical or chemical significance of the formal results is not always well brought out. The formalism of the approach is perhaps unconsciously illustrated by the hasty sentence (p. 265): "But in general, the closer together the energy levels of any problem are, the lower the temperature at which its specific heat becomes approximately classical."

"Atoms, Molecules, and the Structure of Matter" are treated in the third part. This opens with a fairly elementary account of temperature radiation, ionization, and excitation, and the periodic table. Interatomic and intermolecular forces are then very fully discussed in as quantitative a way as is possible without quantum mechanical detail. The remainder of the book is in the main an interpretative description of different types of chemical substances—ionic crystals, molecular compounds, organic compounds, the silicates, and metals.

In a book of this kind there is naturally much which could be criticized. The arrangement of the parts is illogical, as is admitted by the author, but it may, as he suggests, make for easy presentation by proceeding from the more to the less familiar to many readers, and it does correspond roughly to a historical order. The actual course of historical development is, however, very much in the background throughout. There are very few dates, and, apart from a list of books on the same general themes, very few references. On the mathematical side there is little uniformity. Although there is no recondite mathematics, mathematical steps of considerable complexity are often introduced very casually, while in other places there are elaborate qualitative discussions which could be effectively replaced, with a mild use of mathematics, by shorter and more convincing statements. The difficulties of the author are obvious. With so extensive and rich a field, he cannot deal fully with any aspect, but in his enthusiasm he is loath to leave anything out. The result is a book which, as a general introduction, is long and formidable, but which frequently lacks the crowning stages in the separate sections. There are, however, few sections which are devoid of novel and illuminating methods and points of view such as are characteristic of the author. The great value of the book lies in the fact that it brings together an enormous range of well-considered material in a unified presentation. It may not replace other books, but it will be a great help towards good use being made of them, and it is in itself a most valuable addition to the literature of a field of ever growing interest and importance.

E. C. S.

Tensor Analysis of Networks. By GABRIEL KRON. [Pp. xxiv+635.] (New York: Wiley and Sons; London: Chapman and Hall, 1939. Price 37s. 6d.)

THIS book is written for engineers with the avowed intention of introducing them to a mathematical method long since familiar to physicists. The main purpose is to show that by the use of tensor analysis problems containing a large number of known and unknown quantities, and in particular electrical networks of all types, can be treated in an organized way, so that the time incurred in studying detailed difficulties can be reduced to a minimum and the main labour of calculation handed over to computers.

In the early chapters matrix algebra is introduced as an organized method of dealing with a large number of simultaneous quantities. Later on the transformation tensor is introduced as a method of treating the interconnexion of components to form a network. Engineers will not be slow to appreciate the advantages of setting out the physical constants of the branches in one matrix and the interconnexions in a second matrix, and then obtaining the final direct and transfer impedances of the various parts by simple rule-of-thumb manipulation.

I do not see how it would have been possible to improve this book for the purpose for which it is intended. The engineer is introduced to the necessary conceptions in an order which is very easy to follow, and he will immediately appreciate that the mathematics involved in the tensor analysis is easily within his comprehension. As a result I fancy that tensor analysis is likely to become a standard of engineering mathematics, and that this book is likely to be the classic exposition of the method. .

E. L. E. WHEATCROFT.

ERRATUM.—December 1940.

In fig. 3, p. 441, circles refer to platinum, oblique cross to alundum, points and vertical crosses to quartz. The author is obliged to Mr. Geo. Morris, B.Sc., for drawing this omission to his notice.

[The Editors do not hold themselves responsible for the views expressed by their correspondents.]



Raman spectrum of *m*-diphenyl benzene (with a filter of concentrated solution of NaNO_2).

XXIX. *The Hall Effect and other Physical Properties of the Copper-Tin System of Alloys.*

By G. G. ANDREWARTHA, M.Sc., and Professor E. J. EVANS, M.Sc.
(Physics Department, University College of Swansea) *.

[Received November 29, 1939.]

THE present investigation is a continuation of work previously carried out in this laboratory by Stephens ⁽¹⁾, who examined the physical properties of nine alloys belonging to the copper-tin system. This number of alloys was insufficient to give an adequate representation of the variation of the physical properties with composition, and to fix the position of the phase boundaries with accuracy. Consequently in the present investigation, 34 alloys of different compositions between that of pure copper and tin and well distributed over the various phases were prepared, and their densities, resistivities, temperature coefficients of resistance, thermoelectric powers, and Hall coefficients were determined. The alloys were prepared from pure materials, and were subjected to a process of annealing so that the alloys were in a stable reproducible state at room temperature.

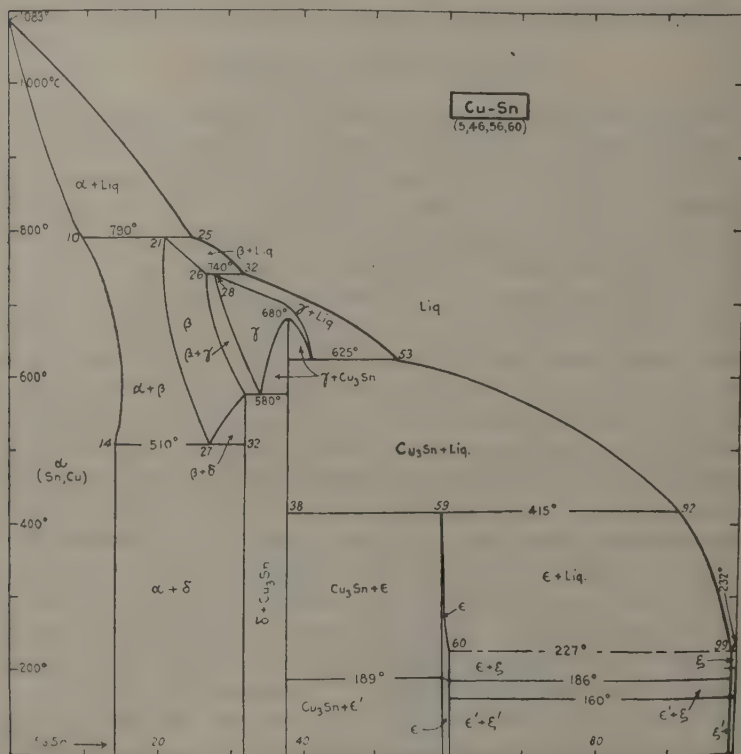
The constitution of the copper-tin system of alloys has been the subject of a large number of investigations, and here reference will be made to only some of these. Heycock and Neville ⁽²⁾ published a complete freezing point curve, which was in good agreement with that of other workers, and later ⁽³⁾ they produced the first equilibrium diagram, which laid claim to any completeness. Modifications in the diagram were suggested as the result of investigations by Shepherd and Blough ⁽⁴⁾, Haughton ⁽⁵⁾, and others. Hamasumi and Nishigori ⁽⁶⁾ examined the system over the range of composition from 15 to 41 per cent. tin, and found evidence for the existence of two intermetallic compounds $\delta(\text{Cu}_{31}\text{Sn}_8)$ and $\eta(\text{Cu}_3\text{Sn})$. The first compound contains 68.1 per cent. of copper, and has a composition approximating to Cu_4Sn .

The equilibrium diagram used as a basis in the present investigation is taken from the 'International Critical Tables' ⁽⁷⁾, and is reproduced in fig. 1. This diagram incorporates the results of the earlier workers, but slight modifications of it have been advocated as the result of more recent investigations.

* Communicated by Prof. E. J. Evans.

The α -phase has been studied by Hansen ⁽⁸⁾, who found that there was a change in the direction of the α -phase boundary at 518° C. He gave the limits of solubility of tin in copper at 500° and 400° C. as 15.3 and 14.3 per cent. respectively. This variation in the position of the α -phase boundary has also been deduced by Owen and Iball ⁽⁹⁾, as the result of their X-ray investigations. Owen and Williams ⁽¹⁰⁾ have also carried

Fig. 1.



out an X-ray analysis of the copper-tin system, paying special attention to the δ and η phases. The δ region was examined at temperatures below 550° C., and it was found to be a solid solution. The range of solution increases from zero at the eutectoid point [which occurs at a composition of 67.4 per cent. copper and a temperature of 330° C.] to 0.4 $\frac{1}{8}$ per cent. composition by weight at 550° C. The η -phase was also found to be a solid solution; the range of solution at 250° C. extending from 61.68 to 62.10 per cent. by weight of copper, and at 530° C. from 61.68 to 62.20 per cent. by weight of copper. Observations were also recorded which

indicated that the δ -phase transforms into $(\alpha+\eta)$ at a temperature of about 330°C .

According to Westgren and Phragmen ⁽¹¹⁾ Cu_4Sn has a face-centred cubic structure with 416 atoms in the unit cell, while Cu_3Sn has an hexagonal close-packed structure. Jones and Evans ⁽¹²⁾ have also examined the structure of Cu_3Sn , and their results agree very closely with those of other workers.

However, as the result of the X-ray analysis of single crystals, Bernal ⁽¹³⁾ suggests that, although the evidence shows conclusively that definite intermetallic compounds do exist, their compositions and structures are much more complex than those usually assigned to them. He brings forward evidence that the simplest formula for δ bronze (Cu_4Sn) is $\text{Cu}_{41}\text{Sn}_{11}$, and regards the retention of the formula Cu_4Sn as being due on the one hand to insufficient annealing, and on the other to the desire for a simple formula. As the result of X-ray analysis of a single crystal of η bronze, he deduced a cell containing 16 molecules of Cu_3Sn , but micrographical analysis gives results which agree better with the formula $\text{Cu}_{50}\text{Sn}_{16}$. Bernal also examined the structure of ϵ bronze (CuSn), and found that both X-ray analysis of a single crystal and also micrographical analysis indicate that the simplest formula is $50\text{Cu}_6\text{Sn}_5$. Hume-Rothery ⁽¹⁴⁾ has also investigated the structures of η bronze (Cu_3Sn), and came to the conclusion that the η -phase is a solid solution, with limits at 24.5 and 25.1 atomic per cent. tin. It is therefore seen that although the copper-tin system of alloys has been subjected to extensive analysis by metallurgical and X-ray methods, there is still uncertainty concerning many points.

The curves obtained by Stephens ⁽¹⁵⁾ for the variation of the physical properties of the alloys with composition indicate the presence of singular points at compositions corresponding to Cu_4Sn and Cu_3Sn . Similar singular points were also found by Ledoux ⁽¹⁶⁾, who investigated the electrical resistivities, temperature coefficients of resistance, and thermo-electric powers of the alloys of the system. In the present experiments, owing to the employment of a large number of alloys, the curves show far more detail than those given by Stephens, and the phase boundaries at room temperature have been fixed with reasonable accuracy.

Preparation of the Alloys.

The alloy plates were prepared from nearly pure specimens of copper and tin. The chief impurities in copper expressed as percentages by weight were :—

	Per cent.
Iron	0.005
Arsenic	0.0002

Similarly, the chief impurities in the tin were :—

	Per cent.
Lead	0.01
Iron	0.002

The copper and tin were melted together in a salamander crucible and finely divided carbon was used as a flux to prevent oxidation. The molten mixture was thoroughly stirred by a carbon rod to ensure that the alloy was homogeneous. The alloys were cast in graphite moulds in the form of rectangular plates with dimensions of approximately $9 \times 2 \times 0.3$ cm.

For alloys containing up to 40 per cent. Cu, it was found that satisfactory plates were obtained by merely heating the mould in a bunsen flame, but for alloys containing more than 40 per cent. Cu it was necessary to heat the mould to a temperature about equal to that of the melting-point of the alloy.

After casting, all plates with the exception of those containing between 48 and 75 per cent. Cu, were first planed, and then rubbed with emery cloth until their dimensions were nearly uniform. The alloys containing between 48 and 75 per cent. of copper were found to be too brittle for planing, and were rubbed down to uniform dimensions by means of emery cloth.

In all 36 plates were cast, and the compositions by weight of the alloys are given in Table I.

Analysis of the Alloys.

The copper content of the alloys was examined by the iodine-sodium thiosulphate volumetric method, and the tin content was determined by difference. This method depends upon the fact that cupric salts when treated with potassium iodide liberate iodine.

A sample of an alloy was taken from each end of a plate, and each sample was analysed separately. The results agreed to within 0.1 per cent. and showed that the plates were of uniform composition. The analyses of alloys containing less than 5 per cent. Cu were also checked by determining their tin content, and the agreement between the results obtained by the two methods was good.

The Annealing of the Alloys.

The alloy plates were annealed in a vacuum electric furnace, and the uniform temperature over a region at the centre of the furnace was measured by a thermocouple connected to a galvanometer. The latter was calibrated by determining the readings corresponding to the boiling-point of water, and to the known melting-points of the pure metals tin, zinc, and aluminium.

The resistivity of each alloy plate at 0° C. had already been determined immediately after preparation. A group of plates was then placed inside the furnace in the uniform temperature region, and annealed at a temperature which was ascertained from the equilibrium diagram. The alloys were heated up to the annealing temperature and maintained at that temperature for several days. The furnace was then allowed to cool slowly to room temperature and the resistivity of each alloy determined

TABLE I.
Composition of the Alloys.

Percentage weight of copper.	Percentage weight of tin.	Percentage weight of copper.	Percentage weight of tin.
100.00	0.00	53.40	46.60
95.40	4.60	47.98	52.02
92.20	7.80	43.60	56.40
89.77	10.23	41.02	58.98
86.86	13.14	39.60	60.40
85.85	14.15	38.70	61.30
85.20	14.80	37.10	62.90
82.21	17.79	35.30	64.70
79.51	20.49	29.97	70.03
75.48	24.52	24.85	75.15
69.70	30.30	20.44	79.56
67.64	32.36	15.28	84.72
66.74	33.26	9.88	90.12
64.60	35.40	4.79	95.21
63.66	36.34	2.70	97.30
62.25	37.75	1.03	98.97
61.23	38.77	0.34	99.66
57.40	42.60	0.00	100.00

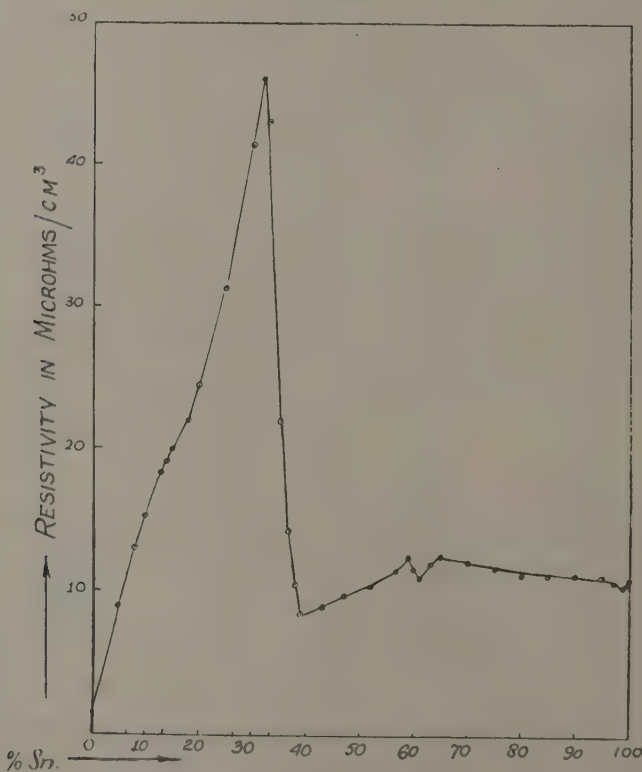
at 0° C. The plates were then replaced in the furnace, and the annealing at the previous annealing temperature was continued for a further period. After cooling to room-temperature the resistivity of each plate at 0° C. was again determined. This process of annealing was continued until no change in resistivity was obtained on further annealing. The plates should then be fully annealed. Since phase boundaries may be curved or inclined to the temperature axis, and since they are not always correctly given in equilibrium diagrams, it is difficult to be sure of the complete annealing of alloys situated at or near phase boundaries. In the present investigation the alloys were therefore annealed down to room-tempera-

ture, the temperature of annealing being reduced by steps of about 100°C. from the highest annealing temperature.

Measurements of the Physical Constants.

In a previous communication ⁽¹⁷⁾ the methods employed in the determinations of the various physical constants have been described in detail,

Graph 1.



Variation of resistivity with composition.

and here it is only necessary to give a brief account of the measurements undertaken.

Resistivity.

The resistivity of each alloy was measured at 0°C. , and the experimental results are given in Table II. and plotted in Graph 1.

TABLE II.

Resistivities of the Alloys.

Percentage composition by weight.		Resistivities before annealing in microhms per cm. ³ at 0° C.	Resistivities after annealing in microhms per cm. ³ at 0° C.
Per cent. of copper.	Per cent. of tin.		
100.00	0.00	1.62	1.59
95.40	4.60	8.12	8.99
92.20	7.80	10.91	13.02
89.77	10.23	12.48	15.23
86.86	13.14	16.43	18.35
85.85	14.15	18.03	19.13
85.20	14.80	18.90	19.90
82.21	17.79	22.41	22.07
79.51	20.49	25.05	24.57
75.48	24.52	22.95	31.52
69.70	30.30	44.25	41.30
67.64	32.36	47.53	45.94
66.74	33.26	45.34	43.02
64.60	35.40	17.67	21.97
63.66	36.34	13.83	14.32
62.25	37.75	10.54	10.64
61.23	38.77	10.90	8.60
57.40	42.60	8.86	9.07
53.40	46.60	12.76	9.73
47.98	52.02	10.63	10.39
43.60	56.40	8.95	11.57
41.02	58.98	9.52	12.44
39.60	60.40	9.57	11.68
38.70	61.30	8.45	11.00
37.10	62.90	9.20	12.10
35.30	64.70	10.70	12.47
29.97	70.03	10.46	12.18
24.85	75.15	10.74	11.67
20.44	79.56	11.37	11.24
15.28	84.72	11.10	11.31
9.88	90.12	11.90	11.32
4.79	95.21	11.49	11.10
2.70	97.30	11.60	10.78
1.03	98.97	10.62	10.52
0.34	99.66	14.93	10.63
0.00	100.00	11.10	10.90

Temperature Coefficient of Resistance.

The mean temperature coefficient of resistance of each alloy was determined over the temperature range 0° – 100° C., and the values are given in Table III. and plotted in Graph 2.

TABLE III.

Temperature Coefficients of Resistance of Alloys.

Percentage composition by weight.		Mean temperature coefficient of resistance between 0° C. and 100° C. $\times 10^4$.	Percentage composition by weight.		Mean temperature coefficient of resistance between 0° C. and 100° C. $\times 10^4$.
Copper.	Tin.		Copper.	Tin.	
100.00	0.00	40.78	53.40	46.60	33.90
95.40	4.60	9.88	47.98	52.02	33.74
92.20	7.80	7.43	43.60	56.40	34.74
89.77	10.23	6.34	41.02	58.98	35.25
86.86	13.14	5.63	39.60	60.40	34.43
85.85	14.15	5.14	38.70	61.30	33.50
85.20	14.80	5.35	37.10	62.90	33.92
82.21	17.79	5.89	35.30	64.70	34.06
79.51	20.49	6.20	29.97	70.03	35.96
75.48	24.52	6.21	24.85	75.15	37.90
69.70	30.30	6.02	20.44	79.56	39.39
67.64	32.36	5.93	15.28	84.72	40.86
66.74	33.26	7.47	9.88	90.12	42.97
64.60	35.40	13.06	4.79	95.21	44.27
63.66	36.34	16.55	2.70	97.30	45.14
62.25	37.75	22.11	1.03	98.97	45.90
61.23	38.77	35.75	0.34	99.66	45.70
57.40	42.60	34.90	0.00	100.00	45.67

Thermoelectric Power.

The mean thermoelectric power of each alloy with respect to a plate of pure electrolytic copper was determined over the range 10 – 100° C., and the results are shown in Table IV. (p. 274) and Graph 3 (p. 275).

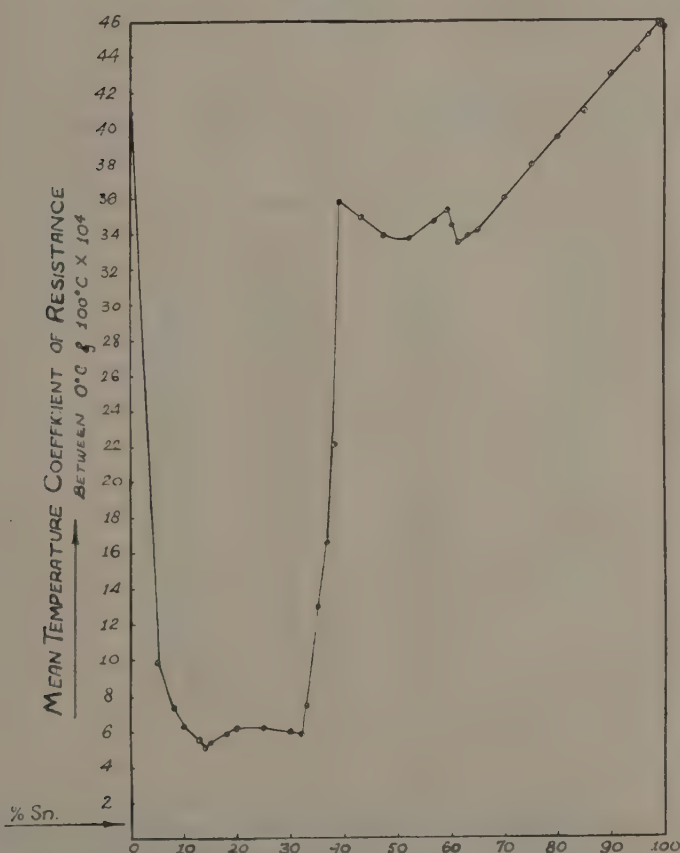
Density.

The densities of the alloys are given in Table V. (p. 276) and plotted in Graph 4 (p. 277).

Hall Effect.

The Hall coefficient of each alloy was measured for six different fields of magnitudes 3001, 4441, 5517, 6550, 7495, and 8116 gauss. The Hall coefficients of both copper and tin are negative, and the value of the

Graph 2.



Variation of mean temperature coefficient with composition.

coefficient in the case of tin is very small and consequently difficult to measure with accuracy.

The values of the Hall coefficients are given in Table VI. (p. 278) and plotted in Graph 5 (p. 279). The variation of the Hall potential difference with field intensity is shown for four alloy plates in Graph 6 (p. 280).

This graph shows that the Hall potential difference is proportional to the intensity of the magnetic field. This result, together with the values given in Table VI. (p. 278), indicates that within experimental error the Hall coefficients are independent of the magnetic field strength.

TABLE IV.

Thermoelectric Powers of Alloys with respect to pure Copper.

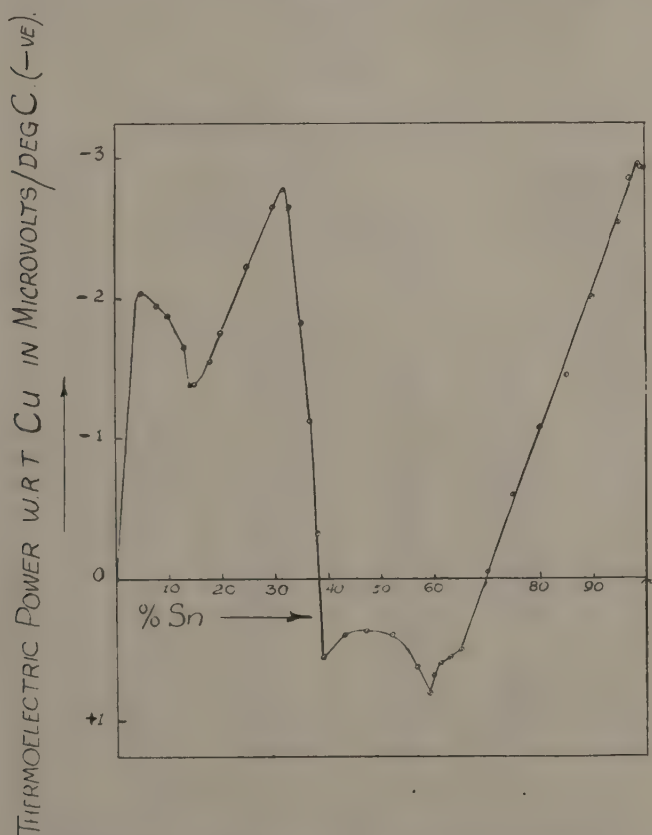
Percentage composition by weight.		Mean thermo-electric power with respect to copper in microvolts per degree C.	Percentage composition by weight.		Mean thermo-electric power with respect to copper in microvolts per degree C.
Copper.	Tin.		Copper.	Tin.	
100.00	0.00	0.00	53.40	46.60	+0.37
95.40	4.60	-2.04	47.98	52.02	+0.40
92.20	7.80	-1.94	43.60	56.40	+0.62
89.77	10.23	-1.87	41.02	58.98	+0.80
86.86	13.14	-1.65	39.60	60.40	+0.67
85.85	14.15	-1.37	38.70	61.30	+0.60
85.20	14.80	-1.38	37.10	62.90	+0.55
82.21	17.79	-1.55	35.30	64.70	+0.50
79.51	20.49	-1.76	29.97	70.03	-0.057
75.48	24.52	-2.22	24.85	75.15	-0.59
69.70	30.30	-2.64	20.44	79.56	-1.08
67.64	32.36	-2.77	15.28	84.72	-1.45
66.74	33.26	-2.66	9.88	90.12	-2.01
64.60	35.40	-1.82	4.79	95.21	-2.53
63.66	36.34	-1.12	2.70	97.30	-2.85
62.25	37.75	-0.33	1.03	98.97	-2.96
61.23	38.77	+0.54	0.34	99.66	-2.92
57.40	42.60	+0.40	0.00	100.00	-2.93

Discussion of Results.

The X-ray investigations of various workers have shown the existence in the copper-tin system of alloys of three intermetallic compounds, which have compositions in the neighbourhood of Cu_4Sn (δ), Cu_3Sn (η), and CuSn (ϵ). The equilibrium diagram indicates the existence of phase boundaries at 86 per cent. Cu, 68.1 per cent. Cu (Cu_4Sn), 61.6 per cent. Cu (Cu_3Sn), 41 per cent. Cu, 39 per cent. Cu, and approximately 1 per cent. Cu. It is well known that the physical properties of the alloys vary considerably in passing through the various phases given in the equilibrium diagram, and consequently the experimental results will be considered in relation to the position of the phase boundaries.

In the first place the results (Table II., Graph 1) showing the variation of the electrical resistivity with composition will be considered. An examination of Graph 1 shows that the addition of tin to copper is accompanied by a steady increase in the resistivity until a composition

Graph 3.



Variation of thermoelectric power with composition.

of about 14 per cent. Sn is reached. At this point approximately the slope of the resistivity-composition curve changes, but it is difficult from the graph to fix exactly the limit of the α -phase.

In the $(\alpha+\delta)$ phase the resistivity increases rapidly, reaching a maximum at the composition corresponding approximately to the intermetallic compound Cu_4Sn , which contains 68.1 per cent. Cu. This

maximum is followed by a sharp drop in the resistivity, which reaches a minimum at the composition 61.2 per cent. Cu, corresponding approximately to the compound Cu_3Sn . The resistivity of this alloy is 3.6 microhms per cm^3 , and is only about one-fifth that of Cu_4Sn .

As the $(\eta + \epsilon')$ phase is traversed there is a gradual increase in the resistivity, which reaches a maximum at the composition 41 per cent. copper corresponding to the boundary between the $(\eta + \epsilon')$ and ϵ' phases.

TABLE V.
Densities of the Alloys.

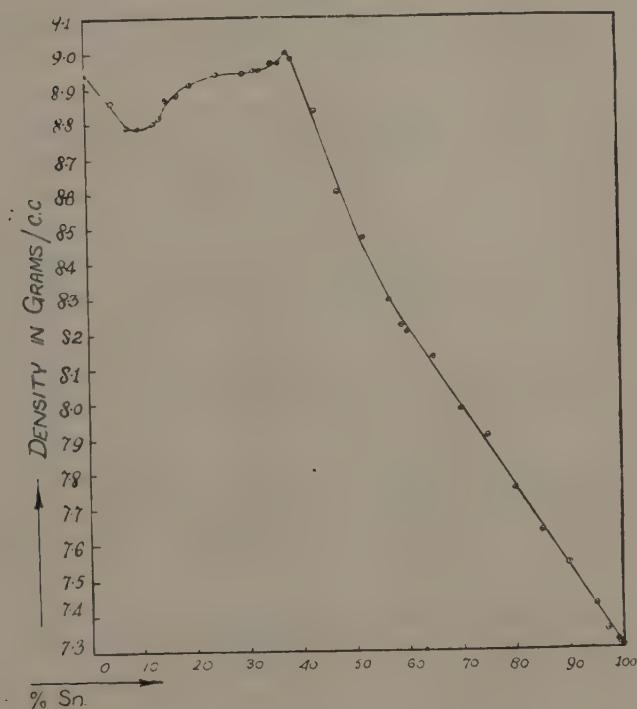
Percentage composition by weight.		Density in grams per c.c. at 12° C.	Percentage composition by weight.		Density in grams per c.c. at 12° C.
Copper.	Tin.		Copper.	Tin.	
100.00	0.00	8.94	57.40	42.60	8.83
95.40	4.60	8.87	53.40	46.60	8.60
92.20	7.80	8.80	47.98	52.02	8.47
89.77	10.23	8.79	43.60	56.40	8.29
86.86	13.14	8.82	41.02	58.90	8.22
85.85	14.15	8.83	39.60	60.40	8.20
85.20	14.80	8.87	35.30	64.70	8.13
82.21	17.79	8.88	29.97	70.03	7.98
79.51	20.49	8.91	24.85	75.15	7.90
75.48	24.52	8.94	20.44	79.56	7.75
69.70	30.30	8.94	15.28	84.72	7.63
67.64	32.36	8.95	9.88	90.12	7.54
66.74	33.26	8.95	4.79	95.21	7.42
64.60	35.40	8.97	2.70	97.30	7.35
63.66	36.34	8.97	1.03	98.97	7.32
62.25	37.75	9.00	0.34	99.66	7.31
61.23	38.77	8.98	0.00	100.00	7.30

At this point the η phase disappears, and as the percentage of copper diminishes there is a slight fall in the resistivity, which reaches a minimum at the composition 38.7 per cent. copper corresponding to the boundary of the ϵ' and $(\epsilon' + \zeta')$ phases. Entry into the $(\epsilon' + \zeta')$ phase is accompanied by an initial rise in resistivity, which continues until the composition 35.3 per cent. Cu is reached, and from this point to the end of the $(\epsilon' + \zeta')$ phase there is comparatively little variation in the resistivity. A change of slope is shown at the composition 99 per cent. Cu, which corresponds to the boundary between the $(\epsilon' + \zeta')$ and ζ' phases.

No general statement can be made concerning the effect of annealing on the resistivities of the alloys. The variation in the resistivities due to annealing is irregular in both magnitude and sign.

On examining Graph 2 showing the variation of the temperature coefficient of resistance with composition, it is again observed that changes of slope occur at compositions corresponding to all phase boundaries

Graph 4.



Variation of density with composition.

given in the equilibrium diagram. In this graph the limit of the α -phase is more clearly indicated.

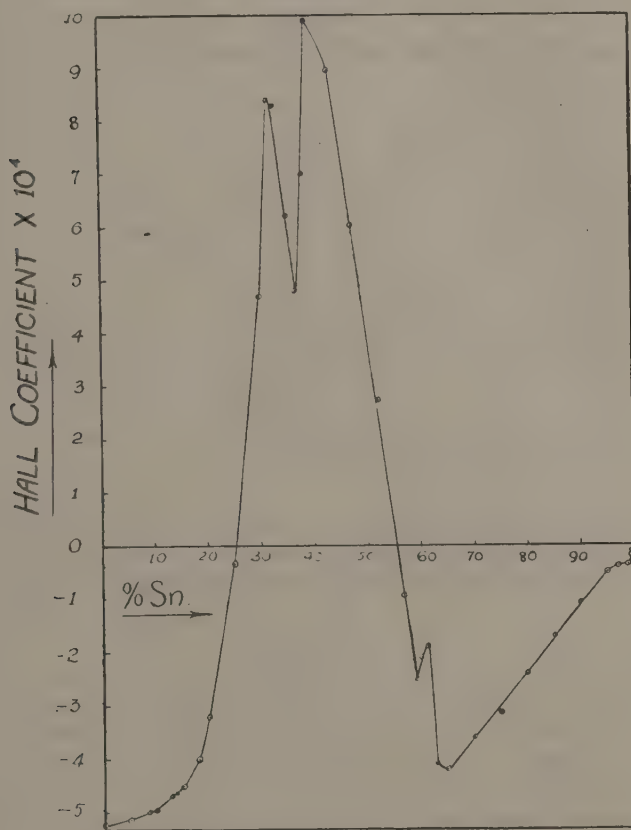
The various phase-boundaries are also clearly shown in Graph 3, which represents the variation of thermo-electric power with composition. A peculiar feature of this curve is the maximum which occurs at 95 per cent. Cu. It was at first considered that the alloys in this region had not been fully annealed, but further prolonged annealing produced very little change in the shape of the curve. It is of interest to note that this peculiarity does not appear in the other curves.

TABLE VI.—Hall Coefficients of the Alloys.

(Composition by weight of copper.	Hall coefficients in absolute units $\times 10^4$ (magnetic fields in gauss).					Mean value of coefficient $\times 10^4$.	Temperature in degrees C.
	3001.	4441.	5517.	6550.	7495.	8116.	
100.00	-5.12	5.24	5.32	-5.19	-5.23	5.32	17.0
95.40	-5.31	5.22	5.10	-5.13	-5.10	5.10	13.5
92.20	-4.91	4.91	5.09	-5.17	-4.98	5.11	13.5
89.77	-5.05	5.08	5.00	-4.90	-4.80	4.88	16.0
86.86	-4.63	4.70	4.76	-4.63	-4.64	4.73	16.0
85.85	-4.61	4.58	4.70	-4.70	-4.64	4.65	18.0
85.20	-4.40	4.48	4.52	-4.50	-4.53	4.53	17.5
82.21	-3.92	4.07	3.98	-3.87	-3.93	4.04	18.0
79.51	-3.20	3.15	3.31	-3.22	-3.08	3.29	17.5
75.48		0.40	0.37	-0.35	-0.33	0.33	13.5
69.70	+4.68	4.60	4.66	+4.90	+4.67	+4.70	17.5
67.64	+8.36	8.38	8.37	+8.39	+8.47	+8.46	17.5
66.74	+8.36	8.38	8.24	+8.30	+8.25	+8.35	18.5
64.60	+6.21	6.26	6.30	+6.20	+6.20	+6.24	19.5
63.66	+4.82	4.83	4.84	+4.89	+4.88	+5.00	20.5
62.35	+7.16	7.02	6.97	+6.98	+6.94	+7.08	20.5
61.33	+9.80	10.02	10.10	+9.70	+9.90	+10.00	20.5
57.40	+9.01	9.08	9.09	+8.82	+8.76	+8.86	14.0
53.40	+5.85	6.11	6.05	+5.90	+6.22	+6.25	15.5
47.98	+2.78	2.72	2.70	+2.85	+2.67	+2.84	18.5
43.60			0.88	-0.91	-0.92	-1.00	18.5
41.02	-2.48	2.46	2.56	-2.41	-2.52	-2.74	20.5
39.60	-2.00	2.12	2.03	-2.10	-2.10	-2.20	18.5
38.70	-1.76	1.88	1.91	-1.86	-1.96	-1.80	18.5
37.10	-3.96	4.12	4.06	-4.18	-4.15	-4.16	18.5
35.50	-4.21	4.19	4.27	-4.13	-4.20	-4.21	18.5
29.97		3.50	3.59	-3.65	-3.62	-3.64	18.7
24.85	-3.00	2.96	3.19	-3.21	-3.19	-3.27	18.5
20.44	-2.49	2.34	2.40	-2.35	-2.54	-2.44	17.5
15.28			1.71	-1.72	-1.73	-1.72	22.5
9.88			0.99	-1.10	-1.08	-1.10	22.5
4.79				-0.48	-0.50	-0.52	22.5
2.70				-0.42	-0.43	-0.43	19.0
1.03				-0.40	-0.39	-0.39	21.0
0.34				-0.18	-0.18	-0.18	21.5
0.00 (Su)				-0.18	-0.21	-0.23	21.5

It is difficult to draw definite conclusions from the density-composition curve (Graph 4), as the variation in density over the region 60–100 per cent. copper is comparatively small, and also errors in density of the order of 0.5 per cent. due to the presence of blow-holes are possible.

Graph 5.



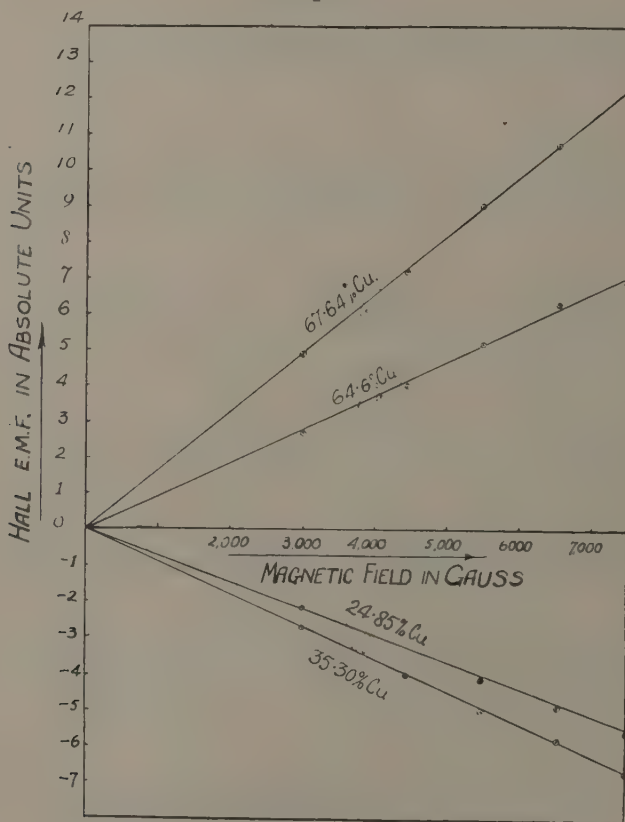
Variation of Hall coefficient with composition.

Initially, the addition of tin to copper causes a decrease in density, but the minimum in the curves is situated at 90 per cent. Cu, and not at 86 per cent. Cu, which is the limit of the α -phase. The density then increases in the $(\alpha+\delta)$ and the $(\delta+\eta)$ phases, reaching a maximum value, which is even greater than that of pure copper, at a composition in the neighbourhood of the compound Cu_3Sn . It is therefore seen that the

formation of alloys in the $(\delta + \eta)$ phase is accompanied by a measurable contraction in volume.

The variation of the Hall coefficient with percentage composition of the alloy is shown in Graph 5. This curve, like the others (1, 2, and 3), indicates changes of slope at compositions corresponding to the phase

Graph 6.



Variation of Hall E.M.F. with intensity of field.

boundaries as given in the equilibrium diagram (fig. 1). Although the Hall coefficients of both copper and tin are negative, it will be observed that in the neighbourhood of the compounds Cu_4Sn and Cu_3Sn , the coefficients have much larger positive values. It is evident from the curve that the Hall coefficient is intimately connected with the structure and composition of the alloys. The curve also crosses the axis of zero Hall

coefficient at compositions corresponding to about 44 and 74 per cent. copper.

Graph 5 shows very clearly some features which have not hitherto been considered. There is a very well-defined minimum in the neighbourhood of the composition 63.6 per cent. Cu, and the Hall coefficient rises steeply to a maximum at the composition 61.2 per cent. Cu, corresponding to the compound Cu_3Sn . In Graphs 1, 2, and 3, the discontinuity at 63.6 per cent. Cu is not obvious, but a close examination of these curves shows that the results in the $(\delta+\eta)$ phase are represented by two straight lines of slightly different slopes intersecting at the composition 63.6 per cent. Cu. The results therefore indicate that there is a narrow phase extending from 61.2 to about 63 per cent. Cu, and this conclusion is of interest in view of the fact that other investigators have suggested that the η phase consists of a solid solution. According to Owen and Williams⁽¹⁸⁾ the solid solution extends from 61.68 to 62.1 per cent. Cu; whereas Hume-Rothery's⁽¹⁹⁾ results indicate the range 61.5 to 61.8 per cent. Cu. It is difficult to estimate with accuracy the extent of the phase from the present results, as the curves are steep in the region considered, and small errors in fixing the points would make a marked difference in the extent of the solid solution.

An examination of Graphs 1, 2, and 3 indicates the presence of a slight change of slope at a composition in the neighbourhood of 35 per cent. Cu corresponding to the compound CuSn . The formation of this compound is also suggested by the well-defined minimum at the same composition in the Hall coefficient-composition curve (Graph 5). However, the results of X-ray investigations carried out by Bernal⁽²⁰⁾ indicate that the formula of the compound is more complex.

The limit of solubility of tin in copper has been the subject of a number of investigations, and the results obtained vary from 11 to 15 per cent. tin. The present results, which are in agreement with those of Isihara⁽²¹⁾ and Hansen⁽²²⁾, clearly indicate that the limit occurs at 14 per cent. Sn.

The results of the present investigation are in general agreement with those previously obtained by Stephens⁽²³⁾, and the differences can in the main be attributed to the fact that in the earlier work an insufficient number of alloys were employed to fix with accuracy the variation in the physical properties with composition.

It is difficult to draw any general conclusions connecting the relative variations of the electrical properties, although the different curves possess some features in common. They all show sudden changes in slope at points corresponding to the phase boundaries, and also the marked change in physical properties which occurs in traversing the $(\delta+\eta)$ phase from Cu_4Sn to Cu_3Sn . It is also noticeable that over certain ranges of composition there exists a linear relation between the physical property

examined and the composition. The experimental results show that the physical properties of the alloys are closely associated with their crystal structure.

References.

- (1) Stephens, *Phil. Mag.* viii. p. 273 (Sept. 1929).
- (2) Heycock and Neville, *Phil. Trans. A*, clxxxix. p. 63 (1897).
- (3) Heycock and Neville, *Phil. Trans. A*, ccii. p. 1 (1903).
- (4) Shepherd and Blough, *Journ. Phys. Chem.* x. p. 630 (Nov. 1906).
- (5) Houghton, *Journ. Inst. Metals*, xiii. p. 222 (1915).
- (6) Hamasumi and Nishigori, *Tech. Report Tohoku Imperial Univ.* (10) i. p. 131 (1931).
- (7) 'International Critical Tables,' ii. p. 433.
- (8) Hausen, *Zeits. fur. Metallkunde*, xix. p. 407 (1927).
- (9) Owen and Iball, *Journ. Inst. Metals*, lvii. p. 267 (1935).
- (10) Owen and Williams, *Journ. Inst. Metals*, lviii. p. 283 (1936).
- (11) Westgren and Phragmen, *Zeits. fur Metallkunde*, xviii. p. 279 (1926).
- (12) Jones and Evans, *Phil. Mag.* iv. p. 1302 (Dec. 1927).
- (13) Bernal, 'Nature,' cxxii. p. 54 (1928).
- (14) Hume-Rothery, *Phil. Mag.* viii. p. 114 (July 1929).
- (15) Stephens, *loc. cit.*
- (16) Ledoux, *Comptes Rendus*, clv. p. 35 (1912).
- (17) Thomas and Evans, *Phil. Mag.* xvi. p. 329 (1933).
- (18) Owen and Williams, *loc. cit.*
- (19) Hume-Rothery, *loc. cit.*
- (20) Bernal, *loc. cit.*
- (21) Isihara, *Sci. Report. Tohoku Imp. Univ.* xvii. p. 927 (1928).
- (22) Hansen, *loc. cit.*
- (23) Stephens, *loc. cit.*

XXX. *An Investigation of the Flow of a Viscous Fluid past a Flat Plate, using Elliptic Coordinates.*

By T. V. DAVIES, B.Sc.*

[Received October 24, 1939.]

CONTENTS.

	Page
1. Introduction	283
2. Relevant results obtained previously	285
3. Proof that the drag is associated with multivalued solutions of the equation $\left(\frac{\partial}{\partial \alpha} + \nu \nabla^2\right)U=0$	288
4. The determination of multivalued solutions	289
5. The contribution of these multivalued solutions to the drag, and verification of the Filon-Goldstein Theorem	292
6. Evaluation of the constants from the boundary conditions and their elimination from the expression for the drag	294
7. An approximate value for the drag for small values of the Reynolds Number, and comparison with the results of Piercy and Winny	297
8. Appendices: with results of investigations in Associated Mathieu Functions	303
8 (a). The convergence of certain series for small values of k	303
8 (b). The behaviour of the Associated Mathieu Functions in the neighbourhood of $\xi=0$	304
8 (c). The approximation to $Cek_n(0)$ suitable for small values of k	305
8 (d). The special cases $Cek_0(0)$ and $Cek_1(0)$	309
8 (e). The approximation to $Cek_n(0)$ suitable for small values of k	311
8 (f). The ratio of the Associated Mathieu Function to its derivate at $\xi=0$	313

1. *Introduction.*

The present work is concerned with the motion of a viscous liquid past a flat plate of infinite length along the z -axis, of finite breadth in the plane $y=0$, and of vanishingly small width in the direction of the y -axis.

* Communicated by T. Lewis.

the motion of the liquid being the same in all planes parallel to $z=0$, and parallel to the x -axis at infinity. I deal with the construction of the stream function for the motion, the expression for the drag on the flat plate, and, as the analytical basis of the whole work, the theory of the Mathieu and Associated Mathieu Functions.

The general theory and the method of attack are derived from a paper by T. Lewis ⁽¹⁾, and the results which are relevant to this problem are included for convenience in Section 2 of this work. Elliptic coordinates in the plane $z=0$ form the basis of the treatment. The third section includes a proof that the drag is associated with multivalued solutions of the partial differential equation

$$\left(\frac{\partial}{\partial \alpha} + \nu \nabla^2\right) U = 0.$$

The idea for the construction of such multivalued functions arose from a paper by Filon ⁽²⁾, but in place of the trigonometric and Bessel Functions which he uses, we here utilize Mathieu and Associated Mathieu Functions. Section 5 then contains the exact contribution to the drag of these multivalued solutions, together with an interesting verification of our result by the Filon-Goldstein Theorem ⁽³⁾, which expresses the drag in terms of the inflow at the wake. Section 6 is concerned with the boundary conditions at the plate and the derivation of linear equations to determine the constants in the stream function. These equations are of such a form that we are able to eliminate the constants in the expression for the drag and express it as the ratio of two infinite determinants. This result is valid for all values of the Reynolds number for which the determinants converge. As yet, however, only an approximate expression for the drag for small values of the Reynolds number has been derived from this general result. To a first approximation this result for the drag is the same as that obtained by Piercy and Winny ⁽⁴⁾, but to a second approximation the results differ slightly.

In the course of the work a convenient Second Solution of the Associated Mathieu Equation is introduced, and the Appendix contains several important results concerning the behaviour of the Associated Mathieu Functions in the neighbourhood of $\xi=0$ (ξ being the argument or independent variable), together with approximate expressions for some of these functions at $\xi=0$ suitable for small values of the Reynolds number. In particular it is found that as ξ tends to zero, the Associated Function $\text{Sek}_n(\xi)$ tends, not to zero as Meksyn ⁽⁵⁾ suggests in his numerical work, but to a finite non-zero limit which is its greatest value in the range concerned.

One very important feature concerning the stream function is worthy of special mention. In the stream function ψ constructed in this work

the terms S_n defined in (2.16), though solutions of the differential equation, do not occur at all. It is shown, however, that the terms $\sum_n S_n$ can be added to ψ without affecting the value of the drag and that they can be made to satisfy the boundary conditions independently. This indicates that there is necessarily a great degree of arbitrariness in the solutions of all problems involving the flow of a viscous fluid past solids.

2. Relevant Results obtained previously.

Using Oseen's approximation, the equations of motion of a viscous fluid can be written in the form (Lewis, 1938) :

$$\left. \begin{aligned} \nu \frac{\partial \omega}{\partial \beta} &= -\frac{\partial P}{\partial \alpha}, \\ -\omega - \nu \frac{\partial \omega}{\partial \alpha} &= -\frac{\partial P}{\partial \beta}, \end{aligned} \right\} \dots \dots \dots (2.1)$$

where ω and P are defined by the relations

$$\omega = \frac{\partial v}{\partial x} - \frac{\partial u}{\partial y} = \nabla^2 \psi, \quad P = \frac{p}{\rho} + \frac{1}{2}(u^2 + v^2), \dots \dots \dots (2.2)$$

ψ being the stream function, ν the kinematic viscosity, and

$$\alpha + i\beta = -V(x + iy). \dots \dots \dots (2.3)$$

It is easily verified from the equations (2.1) that both ω and P satisfy the equation

$$\frac{\partial U}{\partial \alpha} + \nu \left(\frac{\partial^2 U}{\partial \alpha^2} + \frac{\partial^2 U}{\partial \beta^2} \right) = 0. \dots \dots \dots (2.4)$$

If one of them is known the other can be found by quadrature; for example,

$$P = \int \left\{ -\nu \frac{\partial \omega}{\partial \beta} dx + \left(\omega + \nu \frac{\partial \omega}{\partial \alpha} \right) d\beta \right\}, \dots \dots \dots (2.5)$$

or alternatively both can be derived from a single function U satisfying (2.4) by means of the relations

$$\omega = \frac{\partial U}{\partial \alpha}, \quad P = -\nu \frac{\partial U}{\partial \beta}. \dots \dots \dots (2.6)$$

From (2.6) and (2.3) we obtain

$$\left. \begin{aligned} P &= \frac{\nu}{V} \frac{\partial U}{\partial y}, \\ \omega &= -\frac{1}{V} \frac{\partial U}{\partial x} = -\frac{\nu}{V^2} \nabla^2 U = \nabla^2 \psi, \end{aligned} \right\} \dots \dots \dots (2.6)'$$

where in the second relation we have used the differential equation (2.4). It follows that

$$\psi = (\text{a harmonic function}) - \frac{\nu}{V^2} U. \dots \dots \dots (2.7)$$

In order to solve the partial differential equation (2.4) we write $U = U' e^{-\alpha/2\nu}$, so that U' satisfies the equation

$$\frac{\partial^2 U'}{\partial \alpha^2} + \frac{\partial^2 U'}{\partial \beta^2} = \frac{U'}{4\nu^2} \quad (2.8)$$

Making the transformation

$$\alpha + i\beta = -Vc \cosh (\xi + i\eta) \quad (2.9)$$

we find that U' satisfies the equation

$$\frac{\partial^2 U'}{\partial \xi^2} + \frac{\partial^2 U'}{\partial \eta^2} = k^2 (\cosh^2 \xi - \cos^2 \eta) U', \quad (2.10)$$

where

$$k = \frac{Vc}{2\nu} \quad (2.11)$$

Solving equation (2.10) by substituting $U' = f(\xi)g(\eta)$ and separating the variables, we are led to the Mathieu Equation and the Associated Mathieu Equation :

$$\left. \begin{aligned} \frac{d^2 g}{d\eta^2} + (E + k^2 \cos^2 \eta) g &= 0, & (a) \\ \frac{d^2 f}{d\xi^2} - (E + k^2 \cosh^2 \xi) f &= 0. & (b) \end{aligned} \right\} \quad (2.12)$$

Solutions periodic in η are obtained for a discrete set of characteristic values of E . They fall into the four groups :—

$$\left. \begin{aligned} ce_{2n}(\eta) &= \sum_{r=0}^{\infty} A_{2r}^{2n} \cos 2r\eta, & (a) \\ ce_{2n+1}(\eta) &= \sum_{r=0}^{\infty} A_{2r+1}^{2n+1} \cos (2r+1)\eta, & (b) \\ se_{2n}(\eta) &= \sum_{r=0}^{\infty} B_{2r}^{2n} \sin 2r\eta, & (c) \\ se_{2n+1}(\eta) &= \sum_{r=0}^{\infty} B_{2r+1}^{2n+1} \sin (2r+1)\eta, & (d) \end{aligned} \right\} \quad (2.13)$$

The corresponding pairs of solutions of (2.12 b) are

$$\left. \begin{aligned} Cek_{2n}(\xi) &= \sum_{r=0}^{\infty} A_{2r}^{2n} K_{2r}(k \cosh \xi), \\ Cekh_{2n}(\xi) &= \sum_{r=0}^{\infty} A_{2r}^{2n} I_{2r}(k \cosh \xi), \\ Cek_{2n+1}(\xi) &= \sum_{r=0}^{\infty} A_{2r+1}^{2n+1} K_{2r+1}(k \cosh \xi), \\ Cekh_{2n+1}(\xi) &= \sum_{r=0}^{\infty} A_{2r+1}^{2n+1} I_{2r+1}(k \cosh \xi), \end{aligned} \right\} \quad (2.14)$$

$$\left. \begin{aligned}
 \text{Sek}_{2n}(\xi) &= \tanh \xi \sum_{r=0}^{\infty} 2r B_{2r}^{2n} K_{2r}(k \cosh \xi), \\
 \text{Sekh}_{2n}(\xi) &= \tanh \xi \sum_{r=0}^{\infty} 2r B_{2r}^{2n} I_{2r}(k \cosh \xi), \\
 \text{Sek}_{2n+1}(\xi) &= \tanh \xi \sum_{r=0}^{\infty} (2r+1) B_{2r+1}^{2n+1} K_{2r+1}(k \cosh \xi), \\
 \text{Sekh}_{2n+1}(\xi) &= \tanh \xi \sum_{r=0}^{\infty} (2r+1) B_{2r+1}^{2n+1} I_{2r+1}(k \cosh \xi),
 \end{aligned} \right\} \begin{array}{l} (c) \\ (d) \end{array} \quad (2.14)$$

(cont.).

where the functions $\text{Cek}_n(\xi)$ and $\text{Sek}_n(\xi)$ tend to zero as ξ tends to infinity, and the functions $\text{Cekh}_n(\xi)$ and $\text{Sekh}_n(\xi)$ tend to infinity as ξ tends to infinity. For small values of k the characteristic values of E corresponding to the $\text{ce}_n(\eta)$ solutions are

$$\left. \begin{aligned}
 E_0 &= -16q - 32q^2 + 224q^4 + \dots \\
 E_1 &= 1 - 24q - 8q^2 + 8q^3 - \frac{8}{3}q^4 + \dots \\
 E_2 &= 4 - 16q + \frac{80}{3}q^2 - \frac{6104}{27}q^4 + \dots \\
 E_3 &= 9 - 16q + 4q^2 - 8q^3 + \dots \\
 E_4 &= 16 - 16q + \frac{32}{15}q^2 + \frac{6928}{3375}q^4 + \dots \\
 E_5 &= 25 - 16q + \frac{4}{3}q^2 + \frac{11}{189}q^4 + \dots
 \end{aligned} \right\} \quad (2.15)$$

and

$$E_n = n^2 - 16q + \frac{32}{n^2-1}q^2 + \frac{128(5n^2+7)}{(n^2-1)^3(n^2-4)}q^4 + \dots,$$

where

$$k^2 = 32q.$$

The general value E_n is valid up to order q^2 for $n \geq 3$, and to order q^4 for $n \geq 5$.

For small values of k the characteristic values of E corresponding to the $\text{se}^n(\eta)$ solutions are

$$\left. \begin{aligned}
 E'_1 &= 1 - 8q - 8q^2 - 8q^3 - \frac{8}{3}q^4 + \dots \\
 E'_2 &= 4 - 16q - \frac{16}{3}q^2 + \frac{40}{27}q^4 + \dots \\
 E'_3 &= 9 - 16q + 4q^2 + 8q^3 + \dots \\
 E'_4 &= 16 - 16q + \frac{32}{15}q^2 - \frac{5072}{3375}q^4 + \dots \\
 E'_5 &= 25 - 16q + \frac{4}{3}q^2 + \frac{11}{189}q^4 + \dots
 \end{aligned} \right\} \quad (2.16)$$

and

$$E'_n = n^2 - 16q + \frac{32}{n^2-1}q^2 + \frac{128(5n^2+7)}{(n^2-1)^3(n^2-4)}q^4 + \dots$$

As before, the general value E'_n is valid up to order q^2 for $n \geq 3$, and to order q^4 for $n \geq 5$. For large values of n the differences between the characteristic values corresponding to $ce_n(\eta)$ and $se_n(\eta)$ occur in the higher powers of q .

For future reference we include here the functions which satisfy (2.4), namely,

$$\left. \begin{aligned} C_n &= e^{k \cosh \xi \cos \eta} \text{Cek}_n(\xi) ce_n(\eta), \\ S_n &= e^{k \cosh \xi \cos \eta} \text{Sek}_n(\xi) se_n(\eta). \end{aligned} \right\} \quad \dots \quad (2.17)$$

The solutions involving $\text{Cekh}_n(\xi)$ and $\text{Sekh}_n(\xi)$ are omitted because they tend to infinity when ξ tends to infinity, except when $\eta = \pi$.

3. Proof that the Drag is associated with Multivalued Solutions

$$\text{of } \left(\frac{\partial}{\partial \alpha} + v \nabla^2 \right) U = 0.$$

If we transform the coordinates (α, β) to (x, y) by the transformation (2.3), the first of the Oseen Equations (2.1) may be written

$$\frac{\partial P}{\partial x} + v \frac{\partial \omega}{\partial y} = 0.$$

Let us now integrate the left-hand side over the region D bounded internally by a cylinder C and externally by any contour Γ contained in the liquid. Then applying Green's Theorem to this double integral it becomes

$$\oint_C (P dy - v\omega dx) = \oint_\Gamma (P dy - v\omega dx), \quad \dots \quad (3.1)$$

where the integrals along the contours are taken in the anticlockwise sense. But on the cylinder C we have $u=0$ and $v=0$, and hence from (2.2)

$$P = \frac{p}{\rho} \text{ on } C,$$

so that

$$\oint_C (p dy - \mu\omega dx) = \rho \oint_\Gamma (P dy - v\omega dx). \quad (\mu = \rho v). \quad \dots \quad (3.2)$$

We recognise the left-hand side of (3.2) as being identical with the resultant force exerted by the cylinder on the liquid in the direction of the stream. It is therefore equal and opposite to the drag, hence

$$\text{Drag} = -\rho \oint_\Gamma (P dy - v\omega dx). \quad \dots \quad (3.3)$$

In the integral taken around Γ we can replace P and ω by the expressions (2.6)', giving

$$\begin{aligned}\text{Drag} &= -\rho \oint_{\Gamma} \left(\frac{\nu}{V} \frac{\partial U}{\partial y} dy + \frac{\nu}{V} \frac{\partial U}{\partial x} dx \right), \\ &= -\frac{\mu}{V} [U]_{\Gamma} \\ &= -\frac{\mu}{V} (\text{change in } U \text{ when taken once round } \Gamma). \quad (3.4)\end{aligned}$$

Hence we can state in general that the only contributions to the drag will arise from multivalued solutions of the equation (2.4).

In particular the terms S_n in the function U , which are single-valued functions of η , will not contribute towards the drag. This assertion has been verified independently of the above theorem, but the length of the analysis does not permit us to include it here. It is easily verified also that the series $\sum \sigma_n S_n$ can be included in the stream function and made to satisfy the boundary conditions. This leads to the great degree of arbitrariness in the form of the stream function, a fact which has been mentioned earlier.

4. The Determination of Multivalued Solutions.

We start from the integral expression (2.5) for P which is a solution of the differential equation (2.4). Transforming the integrand to elliptic coordinates (ξ, η) this becomes

$$P = -\nu \int e^{2k \cosh \xi \cos \eta} \left\{ \frac{\partial}{\partial \eta} (\omega e^{-2k \cosh \xi \cos \eta}) d\xi - \frac{\partial}{\partial \xi} (\omega e^{-2k \cosh \xi \cos \eta}) d\eta \right\}. \quad (4.1)$$

We first show that each integral in this expression for P satisfies the differential equation (2.4) when $\omega = C_n$. For let

$$\begin{aligned}U_n &= \nu \int_{\eta}^{\eta} \frac{\partial}{\partial \xi} (\omega e^{-2k \cosh \xi \cos \eta}) e^{2k \cosh \xi \cos \eta} d\eta \\ &= \nu \int_{\eta}^{\eta} \left\{ \frac{\partial \omega}{\partial \xi} - 2k \sinh \xi \cos \eta \cdot \omega \right\} d\eta, \quad (4.2)\end{aligned}$$

then

$$\frac{\partial U_n}{\partial \xi} = \nu \int_{\eta}^{\eta} \left\{ \frac{\partial^2 \omega}{\partial \xi^2} - 2k \cosh \xi \cos \eta \cdot \omega - 2k \sinh \xi \cos \eta \frac{\partial \omega}{\partial \xi} \right\} d\eta. \quad (4.3)$$

Making use of the fact that ω satisfies the equation

$$\frac{\partial^2 \omega}{\partial \xi^2} + \frac{\partial^2 \omega}{\partial \eta^2} = 2k \left\{ \sinh \xi \cos \eta \frac{\partial \omega}{\partial \xi} - \cosh \xi \sin \eta \frac{\partial \omega}{\partial \eta} \right\},$$

we find, on substituting for $\frac{\partial^2 \omega}{\partial \xi^2}$, that the right-hand side of (4.3) is immediately integrable, giving

$$\frac{\partial U_n}{\partial \xi} = -\nu \left[\frac{\partial \omega}{\partial \eta} + 2k \cosh \xi \sin \eta \cdot \omega \right]^\eta.$$

Taking $\omega = C_n$, and choosing the lower limit to be zero, we easily obtain

$$\frac{\partial \omega}{\partial \eta} n = 0, \quad \eta = 0; \quad \omega \sin \eta = 0, \quad \eta = 0,$$

and hence

$$\frac{\partial U_n}{\partial \xi} = -\nu \left[\frac{\partial C_n}{\partial \eta} + 2k \cosh \xi \sin \eta \cdot C_n \right]. \quad (4.4)$$

It follows immediately from (4.2) that

$$\frac{\partial U_n}{\partial \eta} = \nu \left[\frac{\partial C_n}{\partial \xi} - 2k \cosh \xi \sin \eta \cdot C_n \right], \quad (4.5)$$

and hence that

$$\frac{\partial^2 U_n}{\partial \xi^2} + \frac{\partial^2 U_n}{\partial \eta^2} = 2k \left\{ \sinh \xi \cos \eta \frac{\partial U_n}{\partial \xi} - \cosh \xi \sin \eta \frac{\partial U_n}{\partial \eta} \right\}.$$

Therefore the integral

$$U_n = \int_0^\eta \left\{ \frac{\partial C_n}{\partial \xi} - 2k \sinh \xi \cos \eta \cdot C_n \right\} d\eta \quad (4.6)$$

satisfies (2.4): and so also does the remaining integral of (4.1) when taken between certain definite limits.

If now we take the integral U_0 and substitute in it for C_0 we obtain

$$U_0 = \frac{d \text{Cek}_0(\xi)}{d\xi} \int_0^\eta e^{k \cosh \xi \cos \eta} \text{ce}_0(\eta) d\eta \\ - k \sinh \xi \text{Cek}_0(\xi) \int_0^\eta e^{k \cosh \xi \cos \eta} \cos \eta \text{ce}_0(\eta) d\eta. \quad (4.7)$$

Substituting the expansions for the Mathieu function $\text{ce}_0(\eta)$ from (2.14 a) and using the Sonine expansion

$$e^{k \cosh \xi \cos \eta} = I_0(k \cosh \xi) + 2 \sum_{n=1}^{\infty} I_n(k \cosh \xi) \cos n\eta. \quad (4.8)$$

we find that the integral U_0 gives rise to periodic terms $\sin n\eta + a$ term in η whose coefficient reduces to

$$\left\{ A_0^0 I_0(k \cosh \xi) + A_2^0 I_2(k \cosh \xi) + A_4^0 I_4 + \dots \right\} \frac{d}{d\xi} \text{Cek}_0(\xi) \\ - \left\{ A_0^0 \frac{d}{d\xi} I_0(k \cosh \xi) + A_2^0 \frac{d}{d\xi} I_2 + A_4^0 \frac{d}{d\xi} I_4 + \dots \right\} \text{Cek}_0(\xi). \quad (4.9)$$

In (2.14 a) we define a function

$$\text{Cek}_0(\xi) = \sum_{r=0}^{\infty} A_{2r}^0 I_{2r}(k \cosh \xi), \quad (4.10)$$

so that now (4.9) can be written in the form

$$\text{Cek}_0(\xi) \frac{d}{d\xi} \text{Cek}_0(\xi) - \text{Cek}_0(\xi) \frac{d}{d\xi} \text{Cek}_0(\xi) = \chi \text{ (say)}. \quad . (4.11)$$

In the theory leading up to the solutions of the Associated Mathieu Equation, Meksyn (1937) uses Gray and Mathews' (Bessel Functions) definition of the $K_n(z)$ functions which is such that I_n and K_n obey the same recurrence relations. It follows, therefore, from the definition of the functions (2.14 a) that $\text{Cek}_0(\xi)$ satisfies the same differential equation as $\text{Cek}_0(\xi)$ with the same characteristic value; and we can write

$$\begin{aligned} \frac{d^2}{d\xi^2} \text{Cek}_0(\xi) - (E_0 + k^2 \cosh^2 \xi) \text{Cek}_0(\xi) &= 0, \\ \frac{d^2}{d\xi^2} \text{Cek}_0(\xi) - (E_0 + k^2 \cosh^2 \xi) \text{Cek}_0(\xi) &= 0. \end{aligned} \quad (4.12)$$

We easily derive from (4.12) the relation

$$\text{Cek}_0(\xi) \frac{d}{d\xi} \text{Cek}_0(\xi) - \text{Cek}_0(\xi) \frac{d}{d\xi} \text{Cek}_0(\xi) = \text{constant}. \quad . (4.13)$$

The constant on the right-hand side of (4.13) can easily be evaluated by taking a large value of ξ and replacing the functions on the left-hand side by their asymptotic expansions, namely,

$$\begin{aligned} \text{Cek}_0(\xi) &\sim \sqrt{\left(\frac{\pi}{2k \cosh \xi}\right)} e^{-k \cosh \xi} \sum_{r=0}^{\infty} A_{2r}^0 \left(1 + \frac{16r^2 - 1}{8k \cosh \xi} + \dots\right), \\ \text{Cek}_0(\xi) &\sim \sqrt{\left(\frac{1}{2\pi k \cosh \xi}\right)} e^{k \cosh \xi} \sum_{r=0}^{\infty} A_{2r}^0 \left(1 - \frac{16r^2 - 1}{8k \cosh \xi} + \dots\right). \end{aligned} \quad (4.14)$$

(These asymptotic expansions have been derived from (2.14 a) by substituting in them the asymptotic expansions of the $K_n(z)$ and $I_n(z)$ functions.)

The constant reduces to $-(\sum_0^{\infty} A_{2r}^0)^2$, and so the multivalued term occurring in the integral U_0 is

$$-\gamma \left(\sum_0^{\infty} A_{2r}^0\right)^2. \quad (4.15)$$

From the form of the left-hand side of (4.13) it would appear that this result would cease to be true for $\xi=0$. But this apparent breakdown in the formula is easily explained when the behaviour of the functions at $\xi=0$ is known (Appendix 8 b).

Similar analysis holds good for all the even C_n 's, but a change of sign occurs with the odd C_n 's due to the $\cos n\pi$ in the definition of the K_n functions, and we find that we can state in general that the integral

$$U_n = \int_0^\eta \left\{ \frac{\partial C_n}{\partial \xi} - 2k \sinh \xi \cos \eta \cdot C_n \right\} d\eta \quad \dots \quad (4.16)$$

satisfies the differential equation (2.4) and possesses a multivalued term

$$\eta(-1)^{n+1}(\sum A_r^n)^2 \quad \dots \quad (4.17)$$

(where we now adopt the convention that the summation includes all positive values of r differing from n by an even number). It is these functions U_n that we utilize in the construction of the stream function, which we can now form.

Using the result (2.7), which gives the form of the stream function, we take

$$\psi = -Vc \sinh \xi \sin \eta + \sum_0^\infty \alpha_n U_n + \sum_1^\infty \beta_n e^{-n\xi} \sin n\eta + A\eta, \quad \dots \quad (4.18)$$

where A , α_n , and β_n are constants which must be determined from the boundary conditions, etc., and U_n is defined by the integral (4.16).

5. The Contribution of these Multivalued Solutions to the Drag, and Verification of the Filon-Goldstein Theorem.

From the stream function (4.18) it follows that the function U of (2.7) is defined by

$$U = -\frac{V^2}{\nu} \sum_0^\infty \alpha_n U_n \quad \dots \quad (5.1)$$

We have found that the multivalued term of U_n is given by (4.17), hence the whole multivalued term in U is

$$-\eta \cdot \frac{V^2}{\nu} \sum_{n=0}^\infty \alpha_n (-1)^{n+1} (\sum_r A_r^n)^2 \quad \dots \quad (5.2)$$

Hence using the result (3.4) we obtain a formula for the drag in the form

$$\begin{aligned} \text{Drag} &= \frac{2\pi\mu}{V} \cdot \frac{V^2}{\nu} \sum_{n=0}^\infty \alpha_n (-1)^{n+1} (\sum_r A_r^n)^2, \\ &= 2\pi\rho V \sum_{n=0}^\infty (-1)^{n+1} \alpha_n (\sum_r A_r^n)^2. \quad \dots \quad (5.3) \end{aligned}$$

We can verify the result (5.3) by applying a theorem due, in the first place to Filon (1926) and extended by Goldstein (1929). It states that:—

“The drag is associated exclusively with a particular term in the solution (at infinity) which corresponds to an inward flow along the tail and a compensating outward flow across a large contour, excluding the portion where it crosses the tail; denoting this outward flow by E , the drag is ρVE .”

Our method of proof, however, does not follow the same lines as that used in these two papers but utilizes the physical interpretation of ψ as the flow across a curve PQ in unit time, reckoned positive when this flow is from right to left.

We obtain immediately on referring to (4.18) that the outward flow across a large contour surrounding the flat plate is

$$-2\pi A. \quad (5.4)$$

Owing to the single-valuedness of the stream function this outward flow is compensated by some inward flow, and to determine this we shall investigate the change in ψ in the wake of the flat plate, which here corresponds to small values of η for large ξ . To make the analysis lighter we shall take just one term $\alpha_0 U_0$ of the series $\sum_0^{\infty} \alpha_n U_n$.

For small values of η the only relevant contribution to the inward flow arising from the term $\alpha_0 U_0$ of ψ is

$$-\alpha_0 \int_{-\eta_1}^{\eta_1} e^{k \cosh \xi \cos \eta} \left\{ \frac{d \operatorname{Ce} k_0(\xi)}{d\xi} \operatorname{ce}_0(\eta) - k \sinh \xi \cos \eta \operatorname{ce}_0(\eta) \operatorname{Ce} k_0(\xi) \right\} d\eta, \quad (5.5)$$

where η_1 is small. For large values of ξ we can replace the Associated Mathieu Function $\operatorname{Ce} k_0(\xi)$ and its derivate by their asymptotic expansions (see (4.14)), and (5.5) then becomes

$$-\alpha_0 \int_{-\eta_1}^{\eta_1} e^{-k \cosh \xi (1 - \cos \eta)} \sqrt{\left(\frac{\pi}{2k \cosh \xi} \right)} \{ -k \sinh \xi (1 + \cos \eta) \} \times \operatorname{ce}_0(\eta) (\Sigma A_{2r}^0) d\eta, \quad (5.6)$$

where only the first terms of the asymptotic expansions have been retained. Writing

$$F(\eta) = \operatorname{ce}_0(\eta) (1 + \cos \eta) (\Sigma A_{2r}^0), \quad (5.7)$$

and making η small in the integrand, (5.6) becomes

$$\alpha_0 \int_{-\eta_1}^{\eta_1} e^{-\frac{1}{2} k \cosh \xi \eta^2} \sqrt{\left(\frac{\pi}{2k \cosh \xi} \right)} k \sinh \xi F(\eta) d\eta. \quad (5.8)$$

Writing

$$R^2 \eta^2 = \frac{1}{2} k \cosh \xi, \quad \eta^2 = \theta^2, \quad R d\eta = d\theta,$$

(5.8) becomes

$$\alpha_0 \int_{-R\eta_1}^{R\eta_1} e^{-\theta^2} \sqrt{\frac{\pi}{2}} \cdot \frac{1}{\sqrt{2R}} \cdot 2R^2 \cdot F\left(\frac{\theta}{R}\right) \frac{d\theta}{R}.$$

The quantity η_1 is small, but $R\eta_1$ can be made as large as we please,

and thus the limits for this integral can be taken as $-\infty$ and $+\infty$ as R tends to infinity. Hence we obtain for the inward flow the expression

$$\alpha_0 \sqrt{\pi} F(0) \int_{-\infty}^{\infty} e^{-\theta^2} d\theta \\ = \pi \alpha_0 F(0).$$

Equating the outward flow to this inward flow in the wake we obtain

$$A = -\frac{1}{2} \alpha_0 F(0).$$

But by (5.7)

$$F(0) = 2 \left(\sum_0^{\infty} A_{2r}^0 \right)^2,$$

therefore

$$A = -\alpha_0 \left(\sum_0^{\infty} A_{2r}^0 \right)^2.$$

Using the Filon-Goldstein Theorem, the contribution to the drag of the term $\alpha_0 U_0$ is

$$-2\pi\rho V \alpha_0 \left(\sum_0^{\infty} A_{2r}^0 \right)^2,$$

which is identical with the previous result.

6. Evaluation of the Constants from the Boundary Conditions and their Elimination from the Expression for the Drag.

We take the stream function defined in (4.18), namely,

$$\psi = -Vc \sinh \xi \sin \eta + \sum_0^{\infty} \alpha_n U_n + \sum_1^{\infty} \beta_n e^{-n\xi} \sin n\eta + A\eta, \quad (6.1)$$

where A , α_n , and β_n are constants and U_n is defined by the integral (4.16). The stream function is necessarily a single valued function, therefore we choose A so as to cancel with the non-periodic term of $\sum_0^{\infty} \alpha_n U_n$, and by using (4.17) we obtain

$$A = - \sum_{n=0}^{\infty} (-1)^{n+1} \alpha_n \left(\sum_r A_r^n \right), \quad (6.2)$$

with the usual convention regarding $\sum_r A_r^n$. The boundary conditions that have to be satisfied are $u=0$, $v=0$ at the plate, or in terms of the stream function

$$-h \frac{\partial \psi}{\partial \eta} = 0, \quad h \frac{\partial \psi}{\partial \xi} = 0, \quad \text{for } \xi=0, \quad (6.3)$$

where

$$h^{-2} = c^2 (\cosh^2 \xi - \cos^2 \eta).$$

From (4.3) and (4.4) we obtain

$$\left. \frac{\partial U_r}{\partial \xi} \right|_{\xi=0} = -e^{k \cos \eta} \text{Cek}_r(0) \left\{ \frac{d \text{ce}_r(\eta)}{d\eta} + k \sin \eta \text{ce}_r(\eta) \right\},$$

$$\left. \frac{\partial U_r}{\partial \eta} \right|_{\xi=0} = e^{k \cos \eta} \text{Cek}'_r(0) \text{ce}_r(\eta),$$

and using these expressions the boundary conditions (6.3) become

$$\begin{aligned} 0 &= -Vc \sin \eta - \sum_1^{\infty} n \beta_n \sin n\eta - \sum_{r=0}^{\infty} \alpha_r e^{k \cos \eta} \left\{ \frac{d \text{ce}_r(\eta)}{d\eta} + k \sin \eta \text{ce}_r(\eta) \right\} \text{Cek}_r(0), \\ 0 &= A + \sum_1^{\infty} n \beta_n \cos n\eta + \sum_{r=0}^{\infty} \alpha_r e^{k \cos \eta} \text{Cek}'_r(0) \text{ce}_r(\eta). \end{aligned} \quad (6.4)$$

Using Fourier expansions for

$$e^{k \cos \eta} \text{ce}_r(\eta) = \sum_{s=0}^{\infty} g_s^r \cos s\eta. \quad (6.5)$$

$$\text{and} \quad e^{k \cos \eta} \left\{ \frac{d \text{ce}_r(\eta)}{d\eta} + k \sin \eta \text{ce}_r(\eta) \right\} = \sum_{s=0}^{\infty} f_s^r \sin s\eta, \quad (6.6)$$

these conditions can be written

$$0 = -Vc \sin \eta - \sum_1^{\infty} n \beta_n \sin n\eta - \sum_{s=1}^{\infty} \sin s\eta \left\{ \sum_{r=0}^{\infty} f_s^r \alpha_r \text{Cek}_r(0) \right\}. \quad (6.7)$$

$$0 = A + \sum_1^{\infty} n \beta_n \cos n\eta + \sum_{s=0}^{\infty} \cos s\eta \left\{ \sum_{r=0}^{\infty} g_s^r \alpha_r \text{Cek}'_r(0) \right\}. \quad (6.8)$$

Equating to zero the coefficients of $\sin s\eta$ and of $\cos s\eta$ in (6.7) and (6.8) respectively, we derive the following relations between the constants

$$\left. \begin{aligned} n \beta_n + \sum_{r=0}^{\infty} f_n^r \alpha_r \text{Cek}_r(0) &= -Vc \text{ for } n=1, \\ &= 0 \text{ for } n \geq 2, \end{aligned} \right\} \quad (6.9)$$

$$\left. \begin{aligned} n \beta_n + \sum_{r=0}^{\infty} g_n^r \alpha_r \text{Cek}'_r(0) &= 0 \text{ for } n \geq 1, \\ A + \sum_{r=0}^{\infty} g_0^r \alpha_r \text{Cek}'_r(0) &= 0. \end{aligned} \right\} \quad (6.10)$$

The last of these conditions is easily shown to be identical with the relation (6.2) obtained by making ψ a single valued function. For we can show from the identity (6.5) that

$$g_0 = \text{Cek}_r(0),$$

then by using the relation (Appendix 8 b)

$$\text{Cek}'_r(0) \text{Cek}_r(0) = (-1)^{r+1} (\sum_n A_n^r)^2 \quad (6.11)$$

the identity of the relations follows immediately.

We can write the remaining boundary conditions in the form

$$\left. \begin{aligned} n\beta_n + \sum_{r=0}^{\infty} f_n^r \alpha_r \text{Cek}_r(0) &= -\delta_1^n \cdot \text{Vc}, \\ n\beta_n + \sum_{r=0}^{\infty} g_n^r \alpha_r \text{Cek}'_r(0) &= 0, \end{aligned} \right\} n \geq 1, \quad \dots \dots (6.12)$$

$$\dots \dots (6.13)$$

where

$$\delta_\beta^\alpha = \begin{cases} 1, & \alpha = \beta, \\ 0, & \alpha \neq \beta. \end{cases}$$

By subtracting these two sets of equations we get rid of the β 's and so obtain

$$\sum_{r=0}^{\infty} \alpha_r \{f_n^r \text{Cek}_r(0) - g_n^r \text{Cek}'_r(0)\} = -\delta_1^n \cdot \text{Vc} \quad (n \geq 1). \quad \dots \dots (6.14)$$

The system of linear equations (6.14) can be solved for the α 's and the β 's will follow from either of (6.12) or (6.13). We are more concerned, however, with evaluating an expression for the drag. From (5.3), by writing

$$\left. \begin{aligned} k_0 &= - \left(\sum_0^{\infty} A_{2r}^0 \right)^2, \\ k_1 &= + \left(\sum_0^{\infty} A_{2r+1}^1 \right)^2 \end{aligned} \right\} \dots \dots \dots (6.15)$$

and so on, we can write the expression for the drag in the form

$$D \times \frac{1}{2\pi\rho V} = \{k_0\alpha_0 + k_1\alpha_1 + k_2\alpha_2 + \dots\}. \quad \dots \dots (6.16)$$

Suppose now in the set of equations (6.14) we write

$$\alpha'_n = f_n^r \text{Cek}_r(0) - g_n^r \text{Cek}'_r(0).$$

Then the set of equations takes the form

$$\left. \begin{aligned} \alpha_0 a_1^0 + \alpha_1 a_1^1 + \alpha_2 a_1^2 + \dots &= -\text{Vc}, \\ \alpha_0 a_2^0 + \alpha_1 a_2^1 + \alpha_2 a_2^2 + \dots &= 0, \\ \alpha_0 a_3^0 + \alpha_1 a_3^1 + \alpha_2 a_3^2 + \dots &= 0, \\ \dots \dots \dots &\dots \end{aligned} \right\} \dots \dots (6.17)$$

We multiply the first equation of this set by λ_1 , the second by λ_2 , the third by λ_3 and so on, choosing the λ 's so that

$$\left. \begin{aligned} a_1^0 \lambda_1 + a_2^0 \lambda_2 + a_3^0 \lambda_3 + \dots &= k_0, \\ a_1^1 \lambda_1 + a_2^1 \lambda_2 + a_3^1 \lambda_3 + \dots &= k_1, \\ a_1^2 \lambda_1 + a_2^2 \lambda_2 + a_3^2 \lambda_3 + \dots &= k_2, \\ \dots \dots \dots &\dots \end{aligned} \right\} \dots \dots (6.18)$$

Then by adding the equations (6.17) multiplied in this manner we obtain

$$k_0\alpha_0 + k_1\alpha_1 + k_2\alpha_2 + \dots = -\text{Vc} \cdot \lambda_1. \quad \dots \dots (6.19)$$

But λ_1 is given from the set (6.18) by the determinant ratio

$$\lambda_1 \begin{vmatrix} a_1^0 & a_2^0 & a_3^0 & \dots \\ a_1^1 & a_2^1 & a_3^1 & \dots \\ a_1^2 & a_2^2 & a_3^2 & \dots \\ \dots & \dots & \dots & \dots \end{vmatrix} = \begin{vmatrix} k_0 & a_2^0 & a_3^0 & \dots \\ k_1 & a_2^1 & a_3^1 & \dots \\ k_2 & a_2^2 & a_3^2 & \dots \\ \dots & \dots & \dots & \dots \end{vmatrix} \quad (6.20)$$

Hence from (6.16) and (6.19) the drag is given by

$$D = 2\pi\rho V(-Vc \cdot \lambda_1) = -2\pi\rho V^2 c \lambda_1, \quad (6.21)$$

where

$$\lambda_1 \begin{vmatrix} f_1^0 \text{Cek}_0 - g_1^0 \text{Cek}'_0 & f_2^0 \text{Cek}_0 - g_2^0 \text{Cek}'_0 & f_3^0 \text{Cek}_0 - g_3^0 \text{Cek}'_0 & \dots \\ f_1^1 \text{Cek}_1 - g_1^1 \text{Cek}'_1 & f_2^1 \text{Cek}_1 - g_2^1 \text{Cek}'_1 & f_3^1 \text{Cek}_1 - g_3^1 \text{Cek}'_1 & \dots \\ f_1^2 \text{Cek}_2 - g_1^2 \text{Cek}'_2 & f_2^2 \text{Cek}_2 - g_2^2 \text{Cek}'_2 & f_3^2 \text{Cek}_2 - g_3^2 \text{Cek}'_2 & \dots \\ \dots & \dots & \dots & \dots \end{vmatrix} = \begin{vmatrix} k_0 & f_2^0 \text{Cek}_0 - g_2^0 \text{Cek}'_0 & f_3^0 \text{Cek}_0 - g_3^0 \text{Cek}'_0 & \dots \\ k_1 & f_2^1 \text{Cek}_1 - g_2^1 \text{Cek}'_1 & f_3^1 \text{Cek}_1 - g_3^1 \text{Cek}'_1 & \dots \\ k_2 & f_2^2 \text{Cek}_2 - g_2^2 \text{Cek}'_2 & f_3^2 \text{Cek}_2 - g_3^2 \text{Cek}'_2 & \dots \\ \dots & \dots & \dots & \dots \end{vmatrix} \quad (6.22)$$

The investigation of the convergence of these infinite determinants in the general case has not been attempted, but for small values of k we show in the next paragraph that the ratio is finite. This is left until the next Section.

7. An Approximate Value of the Drag for Small Values of k , and Comparison with the Results of Piercy and Winny.

In the determinant ratio (6.22) we replace k_2, k_3, \dots by their explicit expressions $\text{Cek}'_2(0) \text{Cek}h_2(0), \text{Cek}'_3(0) \text{Cek}h_3(0), \dots$ (see (6.11) and (6.15)) leaving the first and second rows as before. We now divide the third rows on either side by $\text{Cek}_2(0)$, the fourth rows on either side by $\text{Cek}_3(0)$, and so on, giving

$$\lambda_1 \begin{vmatrix} f_1^0 \text{Cek}_0 - g_1^0 \text{Cek}'_0 & f_2^0 \text{Cek}_0 - g_2^0 \text{Cek}'_0 & f_3^0 \text{Cek}_0 - g_3^0 \text{Cek}'_0 & \dots \\ f_1^1 \text{Cek}_1 - g_1^1 \text{Cek}'_1 & f_2^1 \text{Cek}_1 - g_2^1 \text{Cek}'_1 & f_3^1 \text{Cek}_1 - g_3^1 \text{Cek}'_1 & \dots \\ f_1^2 \text{Cek}_2 - g_1^2 \text{Cek}'_2 & f_2^2 \text{Cek}_2 - g_2^2 \text{Cek}'_2 & f_3^2 \text{Cek}_2 - g_3^2 \text{Cek}'_2 & \dots \\ f_1^3 \text{Cek}_3 - g_1^3 \text{Cek}'_3 & f_2^3 \text{Cek}_3 - g_2^3 \text{Cek}'_3 & f_3^3 \text{Cek}_3 - g_3^3 \text{Cek}'_3 & \dots \\ \dots & \dots & \dots & \dots \end{vmatrix} = \begin{vmatrix} k_0 & f_2^0 \text{Cek}_0 - g_2^0 \text{Cek}'_0 & f_3^0 \text{Cek}_0 - g_3^0 \text{Cek}'_0 & \dots \\ k_1 & f_2^1 \text{Cek}_1 - g_2^1 \text{Cek}'_1 & f_3^1 \text{Cek}_1 - g_3^1 \text{Cek}'_1 & \dots \\ -\mu_2 \text{Cek}h_2 & f_2^2 - \mu_2 g_2^2 & f_3^2 - \mu_2 g_3^2 & \dots \\ -\mu_3 \text{Cek}h_3 & f_2^3 - \mu_3 g_2^3 & f_3^3 - \mu_3 g_3^3 & \dots \\ \dots & \dots & \dots & \dots \end{vmatrix}, \quad (7.1)$$

where
$$\mu_n = \frac{\text{Cek}'_n(0)}{\text{Cek}_n(0)} \dots \dots \dots (7.2)$$

If we neglect all powers of k greater than k^3 we can find without undue labour the Fourier coefficients g^n_r . To derive the f^n_r coefficients we may utilize the equations (which follow simply from (6.5) and (6.6) by differentiation of the former)

$$\left. \begin{aligned} f^n_1 &= -g^n_1 + k(2g^n_0 - g^n_2), \\ f^n_n &= -ng^n_n + k(g^n_{n-1} - g^n_{n+1}), \quad n > 1. \end{aligned} \right\} \dots \dots \dots (7.3)$$

We find that, of the terms g^n_r , only those corresponding to $r=n-3$, $n-2$ $n+2$, $n+3$, are of order k^3 or less; the same is true of the terms f^n_r . In this general case we find that

$$\left. \begin{aligned} g^n_{n-3} &= \left(\frac{2}{3} - \frac{1}{n-1} \right) kq + \dots, \\ f^n_{n-3} &= -kq \left\{ 4 - \frac{2}{n-1} + (n-3) \left(\frac{2}{3} - \frac{1}{n-1} \right) \right\} + \dots, \\ g^n_{n-2} &= \left(4 - \frac{2}{n-1} \right) q + \dots, \\ f^n_{n-2} &= -q \left\{ 16 + (n-2) \left(4 - \frac{2}{n-1} \right) \right\} + \dots, \\ g^n_{n-1} &= \frac{1}{2}k + \left(2 - \frac{1}{n-1} \right) kq + \dots, \\ f^n_{n-1} &= -\frac{n+1}{2}k - kq \left\{ 2n+1 + \frac{2}{n-1} \right\} + \dots, \\ g^n_n &= 1 + 8q + \dots, \\ f^n_n &= -n(1+8q) + \dots, \\ g^n_{n+1} &= \frac{1}{2}k + \left(2 + \frac{1}{n+1} \right) kq + \dots, \\ f^n_{n+1} &= -\frac{n-1}{2}k - kq \left\{ 2n-1 + \frac{2}{n+1} \right\} + \dots, \\ g^n_{n+2} &= \left(4 + \frac{2}{n+1} \right) q + \dots, \\ f^n_{n+2} &= q \left\{ 16 - (n+2) \left(4 + \frac{2}{n+1} \right) \right\} + \dots, \\ g^n_{n+3} &= \left(\frac{2}{3} + \frac{1}{n+1} \right) kq + \dots, \\ f^n_{n+3} &= kq \left\{ 4 + \frac{2}{n+1} - (n+3) \left(\frac{2}{3} + \frac{1}{n+1} \right) \right\} + \dots, \end{aligned} \right\} \dots \dots \dots (7.4)$$

where
$$32q = k^2. \dots \dots \dots (7.5)$$

The ratio μ_n is derived in the Appendix (8f) and we have the result

$$\mu_n = -n \left\{ 1 + \frac{8q}{n^2-1} + \dots \right\}, \quad n \geq 2. \quad (7.6)$$

For the first and second rows of the determinants we can use the results (Appendix 8d)

$$\begin{aligned} \text{Cek}_0(0) &= - \left(\gamma + \log \frac{k}{4} \right) (1 + 8q) + \text{terms of order } q^2 \text{ and higher,} \\ \text{Cek}_1(0) &= - \frac{2}{k} - \frac{1}{2} k \left(\gamma + \log \frac{k}{4} \right) + \text{terms of order } kq \text{ and higher.} \\ \text{Cek}_0(0) &= -1 + \text{terms of order } q^2 \text{ and higher,} \\ \text{Cek}_1(0) &= \frac{2}{k} (1 - 2q) + \text{terms of order } kq \text{ and higher.} \end{aligned} \quad (7.7)$$

The terms of the four rowed determinants in the top left-hand corners of (7.1) are easily evaluated making use of these results and neglecting all quantities of order greater than k^3 . For the general elements we obtain the formulæ

$$\begin{aligned} b_{n-3}^n &= f_{n-3}^n - \mu_n g_{n-3}^n = -kq \left\{ 2 + \frac{1}{n-1} \right\} + \dots, \\ b_{n-2}^n &= f_{n-2}^n - \mu_n g_{n-2}^n = -q \left\{ 8 + \frac{4}{n-1} \right\} + \dots, \\ b_{n-1}^n &= f_{n-1}^n - \mu_n g_{n-1}^n = -\frac{1}{2} k - kq \left\{ 2 + \frac{3}{n-1} - \frac{4n}{n^2-1} \right\} + \dots, \\ b_n^n &= f_n^n - \mu_n g_n^n = \frac{8nq}{n^2-1} + \dots, \\ b_{n+1}^n &= f_{n+1}^n - \mu_n g_{n+1}^n = \frac{1}{2} k + kq \left\{ 2 - \frac{3}{n+1} + \frac{4n}{n^2-1} \right\} + \dots, \\ b_{n+2}^n &= f_{n+2}^n - \mu_n g_{n+2}^n = q \left\{ 8 - \frac{4}{n-1} \right\} + \dots, \\ b_{n+3}^n &= f_{n+3}^n - \mu_n g_{n+3}^n = kq \left\{ 2 - \frac{1}{n+1} \right\} + \dots \end{aligned} \quad (7.8)$$

We are going to consider all the b_r^n outside this set to be zero, for they are of order greater than k^3 . The ratio giving λ_1 can then be written down it is possible, however to simplify the determinant ratio still further by dividing each row after the second by a $\frac{1}{2}k$. We then obtain

λ_1	$k(1-\alpha)+kq(5-10\alpha),$	$\frac{k^2}{8}(3-2\alpha),$	$kq\left(\frac{10}{3}-2\alpha\right),$	0,	0,	0,	0,	...
	$\frac{1}{8}k(7-4\alpha),$	$1+\frac{17}{3}q,$	$\frac{3k}{8},$	$3q,$	0,	0,	0,	...
	$-1-\frac{4q}{3},$	$\frac{k}{3},$	$1+\frac{22}{3}q,$	$\frac{5k}{12},$	$\frac{10}{3}q,$	0,	0,	...
	$-\frac{5k}{8},$	$-1-4q,$	$\frac{3k}{16},$	$1+\frac{11}{2}q,$	$\frac{7k}{16},$	$\frac{7q}{2},$
	$-\frac{14q}{3},$	$-\frac{7k}{12},$	$-1-\frac{58}{15}q,$	$\frac{2k}{15},$	$1+\frac{74}{15}q,$	$\frac{3k}{20},$
	0,	$-\frac{9}{2}q,$	$-\frac{9k}{16},$	$-1-\frac{23}{6}q,$	$\frac{5k}{48},$	$1+\frac{14}{3}q,$
	0,	0,

	0,	...
	0,	...
	$2q\left[2-\frac{1}{n-1}\right],$...
	$\frac{k}{16}\left[8-\frac{4}{n}\right],$...
	0,	0,	$-\frac{k}{16}\left[8+\frac{4}{n-1}\right],$	$-1-2q\left[2+\frac{3}{n-1}-\frac{4n}{n^2-1}\right],$	$\frac{nk}{2(n^2-1)},$	$1+2q\left[2-\frac{3}{n+1}+\frac{4n}{n^2-1}\right],$

[illegible]

where we have written

$$\alpha = \gamma + \log \frac{k}{4} \dots \dots \dots (7.10)$$

To derive the first approximation we neglect all terms of the two determinants which are of order k or higher, with the exception of the first term of the leading diagonal. We obtain the result

$$\lambda_1 = \frac{1}{k} \frac{1}{1-\alpha} \dots \dots \dots (7.11)$$

To derive the second approximation we proceed as follows: we first evaluate λ_1 when the order of the determinants on either side is four; this leads to the result

$$(\lambda_1)_4 = \frac{1}{k} \cdot \frac{1 + q(8\alpha + 6) + \dots}{1 - \alpha + q(-4\alpha^2 - 6\alpha + 4\frac{1}{3}) + \dots}, \dots \dots (7.12)$$

$$= \frac{1}{k} \cdot \frac{A_4}{D_4} \dots \dots \dots (7.13)$$

(say).

Now on considering the determinants of order $(n+1)$ on the left-hand side of (7.9), we find, on expanding D_{n+1} by the $(n+1)$ th column and neglecting all powers higher than q , that we ultimately obtain a recurrence formula

$$D_{n+1} = D_n + q(1-\alpha) \left[-\frac{8}{n+1} + \frac{6}{n} + \frac{2}{n-1} \right].$$

This formula holds for all n greater than 3, and replacing n in turn by 4, 5, 6, ..., we can write

$$D_5 = D_4 + q(1-\alpha) \left[-\frac{\overset{x}{8}}{5} + \frac{6}{4} + \frac{2}{\overset{x}{3}} \right],$$

$$D_6 = D_5 + q(1-\alpha) \left[-\frac{\overset{v}{8}}{6} + \frac{\overset{x}{6}}{5} + \frac{2}{4} \right],$$

$$D_7 = D_6 + q(1-\alpha) \left[-\frac{8}{7} + \frac{\overset{v}{6}}{6} + \frac{\overset{x}{2}}{5} \right],$$

$$D_8 = D_7 + q(1-\alpha) \left[-\frac{8}{8} + \frac{6}{7} + \frac{\overset{v}{2}}{6} \right],$$

etc.

... (7.14)

By addition of the equations (7.14) and suitable cancelling on the right-hand side we obtain

$$D_\infty = D_4 + q(1-\alpha) \left[\frac{6}{4} + \frac{2}{4} + \frac{2}{3} \right] \dots \dots (7.15)$$

Similarly, we can show that for the determinant on the right-hand side

$$\Delta_{\infty} = \Delta_4 + q \left[\frac{6}{4} + \frac{2}{4} + \frac{2}{3} \right].$$

Hence the exact expression for λ_1 to order q is

$$(\lambda_1)_{\infty} = \frac{1}{k} \frac{1 + q(8\alpha + 8\frac{2}{3}) + \dots}{1 - \alpha + q(-4\alpha^2 - 8\frac{2}{3}\alpha + 7) + \dots} \quad (7.17)$$

Using the result (6.21), the first approximation (7.11) leads to the formula

$$\text{Drag} = 4\pi\mu V \frac{1}{1 - \alpha}, \quad (7.18)$$

which is identical with the first approximation obtained by Piercy and Winny (1933).

The second approximation (7.17) leads to the formula

$$\text{Drag} = 4\pi\mu V \frac{1 + q(8\alpha + 8\frac{2}{3}) + \dots}{1 - \alpha + q(-4\alpha^2 - 8\frac{2}{3}\alpha + 7) + \dots} \quad (7.19)$$

The second approximation obtained by Piercy and Winny is

$$\text{Drag} = 4\pi\mu V \frac{1 + 4q(\frac{7}{6} + \alpha) + \dots}{1 - \alpha + q(3 - \frac{14}{3}\alpha) + \dots} \quad (7.20)$$

To compare the results (7.19) and (7.20) we expand the denominators in each case in ascending powers of q , collect the terms in q and neglect terms of order q^2 . By this process (7.19) and (7.20) become

$$4\pi\mu V \cdot \frac{1}{1 - \alpha} \left\{ 1 + \frac{q}{1 - \alpha} \left(\frac{5}{3} + 8\alpha - 4\alpha^2 \right) + \dots \right\},$$

$$4\pi\mu V \cdot \frac{1}{1 - \alpha} \left\{ 1 + \frac{q}{1 - \alpha} \left(\frac{5}{3} + 4\alpha - 4\alpha^2 \right) + \dots \right\},$$

and we note that the results differ slightly.

8. Appendices.

8 (a). The Convergence of certain Series for Small Values of k .

I have investigated the convergence of the following series which enter in the text, the results being obtained for small values of k .

$$\sum_0^{\infty} A_{2r}^0 K_{2r}(k) \text{ is convergent.} \quad (8.1)$$

$$\sum_0^{\infty} A_{2r}^0 I_{2r}(k) \text{ is convergent.} \quad (8.2)$$

$$\sum_1^{\infty} A_{2r}^0 I_{2r-1}(k) \text{ is convergent (arises by differentiation of } \text{Cek}h_0(\xi)). \quad (8.3)$$

$\sum_0^{\infty} A_{2r}^0 K_{2r+1}(k)$ is divergent (arises by differentiation of $Cek_0(\xi)$). . . (8.4)

$\sum_n^{\infty} (2r+1) B_{2r+1}^1 K_{2r+1}(k)$ is divergent. (8.5)

$\sum_0^{\infty} (2r+1) B_{2r+1}^1 I_{2r+1}(k)$ is convergent. (8.6)

Similar results will hold when other Mathieu Coefficients are substituted for those used above. These facts concerning convergence or divergence will be utilized in the next Section to determine the form of $Cek_0(\xi)$, $Cek_{h_0}(\xi)$, $Sek_1(\xi)$, and $Sekh_1(\xi)$ in the neighbourhood of $\xi=0$.

8 (b). *The Behaviour of the Associated Mathieu Functions in the Neighbourhood of $\xi=0$.*

If we transform the Associated Mathieu Equation (2.12 b) by introducing a new independent variable

$$z = k \cosh \xi$$

the equation becomes

$$(z^2 - k^2) \frac{d^2 f}{dz^2} + z \frac{df}{dz} - (E + z^2) f = 0.$$

In the neighbourhood of the apparent singularity $z=k$ the solutions of this equation are

$$\phi_1(z-k) \quad \text{and} \quad (z-k)^{\frac{1}{2}} \phi_2(z-k), \quad (8.7)$$

where $\phi_1(w)$ and $\phi_2(w)$ are regular functions of w not vanishing when $w=0$. Hence we can write, for the time being,

$$\left. \begin{aligned} Cek_0(\xi) &= A\phi_1 + B(z-k)^{\frac{1}{2}}\phi_2, & Cek_{h_0}(\xi) &= C\phi_1 + D(z-k)^{\frac{1}{2}}\phi_2, \\ Sek_1(\xi) &= \alpha\phi_1 + \beta(z-k)^{\frac{1}{2}}\phi_2, & Sek_{h_1}(\xi) &= \gamma\phi_1 + \delta(z-k)^{\frac{1}{2}}\phi_2. \end{aligned} \right\} \quad (8.8)$$

From the result (8.2) it follows that $Cekh_0(\xi)$ is finite and non-zero at $\xi=0$, and from the result (8.3) it follows that $\frac{d}{d\xi} Cek_{h_0}(\xi)$ tends to zero as ξ tends to zero on account of the factor $\sinh \xi$. Thus in the above expression for $Cekh_0(\xi)$ we must have $D=0$, $C \neq 0$. From the result (8.1) it follows that $Cek_0(\xi)$ tends to a finite non-zero limit as ξ tends to zero, therefore $A \neq 0$. But since $Cekh_0(\xi)$ and $Cek_0(\xi)$ are two independent solutions of the Associated Mathieu Equation, the term $(z-k)^{\frac{1}{2}}\phi_2$ must occur in one or other of them, therefore $B \neq 0$.

By definition

$$Sekh_1(\xi) = \tanh \xi \sum_{r=0}^{\infty} (2r+1) B_{2r+1}^1 I_{2r+1}(k \cosh \xi),$$

hence using the result (8.6) it follows that $Sekh_1(\xi)$ tends to zero as ξ tends to zero. Therefore in (8.8) we must have $\gamma=0$ and $\delta \neq 0$. Now

since $\text{Sek}_1(\xi)$ and $\text{Sekh}_1(\xi)$ are two independent solutions of the Associated Mathieu Equation, the term ϕ_1 must occur in one or other of them, therefore $\alpha \neq 0$. Thus for small values of k we have the results

$$\left. \begin{aligned} \text{Cek}_0(\xi) &= A\phi_1 + B(z-k)^{\frac{1}{2}}\phi_2, & \text{Cekh}_0(\xi) &= C\phi_1 \\ \text{Sek}_1(\xi) &= \alpha\phi_1 + \beta(z-k)^{\frac{1}{2}}\phi_2, & \text{Sekh}_1(\xi) &= \delta(z-k)^{\frac{1}{2}}\phi_2 \end{aligned} \right\} \quad (8.9)$$

From the formulæ (8.9) we can deduce some important consequences. It follows immediately from the form of $\text{Sek}_1(\xi)$ in the neighbourhood of $\xi=0$ that $\text{Sek}_1(\xi)$ tends to a finite non-zero limit as ξ tends to zero.

The seeming breakdown of the formulæ (4.13), namely,

$$\text{Cekh}_0(\xi) \frac{d}{d\xi} \text{Cek}_0(\xi) - \text{Cek}_0(\xi) \frac{d}{d\xi} \text{Cekh}_0(\xi) = \text{constant},$$

at $\xi=0$ is now easily explained. For

$$\frac{d}{d\xi} = \sqrt{z^2 - k^2} \frac{d}{dz},$$

and therefore, using the results (8.9) the left-hand side of the expression becomes

$$\begin{aligned} \sqrt{z^2 - k^2} \left\{ C\phi_1 \left[A \frac{d\phi_1}{dz} + B(z-k)^{\frac{1}{2}} \frac{d\phi_2}{dz} + \frac{1}{2} B(z-k)^{-\frac{1}{2}} \phi_2 \right] \right. \\ \left. - [A\phi_1 + B(z-k)^{\frac{1}{2}}\phi_2] \left[C \frac{d\phi_1}{dz} \right] \right\}. \end{aligned}$$

As z tends to k this expression tends to the limit

$$\frac{1}{2} \sqrt{2k} BC. \quad (\phi_1(0)=1, \quad \phi_2(0)=1.)$$

This then gives us the important result

$$\text{Cekh}_0(\xi) \frac{d}{d\xi} \text{Cek}_0(\xi) \Big|_{\xi=0} = - \left(\sum_0^{\infty} A_{2r}^0 \right)^2 = k_0. \quad (8.10)$$

8 (c) *The Approximation for $\text{Cek}_n(0)$ suitable for Small Values of k .*

By definition

$$\text{Cek}_n(0) = \dots + A_{n-2}^n K_{n-2}(k) + A_n^n K_n(k) + A_{n+2}^n K_{n+2}(k) + \dots \quad (8.11)$$

We are going to normalize the Mathieu Coefficients so that $A_n^n = 1$, this being permissible for small values of k , and from Mathieu's original paper (6) we then have the formulæ

$$\left. \begin{aligned} A_{n_1}^n &= 1, \\ A_{n+2r}^n &= \frac{2^r n!}{r! (n+r)!} q^r + O(q^{r+2}), \\ A_{n-2r}^n &= \frac{(-1)^r 2^r (n-r-1)!}{r! (n-1)!} q^r + O(q^{r+2}). \end{aligned} \right\} \quad (8.12)$$

The last set of coefficients is finite in number. $n/2$ if n is even and $(n-1)/2$ if n is odd.

Using the definition of $K_n(k)$ given in Whittaker and Watson's Modern Analysis, we obtain

$$K_n(k) = -(\log \frac{1}{2}k + \gamma)I_n(k) + \text{positive powers of } k \text{ of order } k^n \text{ and higher} \\ + \frac{1}{2} \left\{ \left(\frac{1}{2}k \right)^{-n} \frac{(-1)^n (n-1)!}{1!} + \left(\frac{1}{2}k \right)^{-n+2} \frac{(-1)^{n-1} (n-2)!}{1!} \dots \right\}. \quad (8.13)$$

In evaluating the leading terms in $Cek_n(0)$ we note that $A_n^n K_n(k)$ will contribute terms of the form a/k^n and b/k^{n-2} ; $A_{n+2r}^n K_{n+2r}(k)$ will also contribute terms of this order, but $A_{n-2r}^n K_{n-2r}(k)$ will not make any contributions to terms of these orders in k . We find that the coefficient of $1/k^n$ in $Cek_n(0)$ is

$$(-1)^n 2^{n-1} n! \sum_{r=0}^{\infty} \frac{(n+2r-1)!}{r! (n+r)! 2^{2r}}, \quad \dots \dots \dots (8.14)$$

and the coefficient of $1/k^{n-2}$ in $Cek_n(0)$ is

$$(-1)^{n-1} 2^{n-3} n! \sum_{r=0}^{\infty} \frac{(n+2r-2)!}{r! (n+r)! 2^{2r}}, \quad \dots \dots \dots (8.15)$$

The evaluation of these series entails heavy analysis, and only the broad outline of the method of summation will be included here. We take the case of n even and replace the n of (8.14) by $2n$. The $(r+1)$ th term of (8.14) can then be written in the form

$$2^{2n-1} \cdot \frac{1.3.5\dots(2n+2r-1)}{2.4.6\dots(2n+2r)} \cdot \frac{(n+r-1)(n+r-2)\dots(r+1)}{(2n+r)(2n+r-1)\dots(n+r+1)}.$$

We now consider the Binomial Expansion of $(1-x)^{-\frac{1}{2}}$, namely,

$$(1-x)^{-\frac{1}{2}} = 1 + \frac{1}{2}x + \frac{1.3}{2.4}x^2 + \dots \dots + \frac{1.3.5\dots(2n+2r-1)}{2.4.6\dots(2n+2r)}x^{n+r} + \dots$$

If we integrate both sides of this expression n times between the limits 0 and x (<1) we obtain

$$\int_0^x \dots \int_0^x (1-x)^{-\frac{1}{2}} dx_1 \dots dx_n = \frac{x^n}{n!} + \frac{1}{2} \frac{x^{n+1}}{(n+1)\dots 2} + \dots \\ + \frac{1.3\dots(2n+2r-1)}{2.4\dots(2n+2r)} \frac{x^{2n+r}}{(2n+r)(2n+r-1)\dots(n+r+1)} + \dots$$

We now divide through by x^{n+1} , then differentiate both sides $(n-1)$ times with respect to x , obtaining thereby

$$\frac{d^{n-1}}{dx^{n-1}} \left\{ \frac{1}{x^{n+1}} \frac{1}{D^n} u \right\} = \frac{d^{n-1}}{dx^{n-1}} \left\{ \frac{1}{n! x} \right\} \\ + \sum_{r=0}^{\infty} \frac{1.3\dots(2n+2r-1)}{2.4\dots(2n+2r)} \frac{(n+r-1)(n+r-2)\dots(r+1)}{(2n+r)(2n+r-1)\dots(n+r+1)} x^r,$$

where

$$\frac{1}{D^m} u = \int_0^x \int_0^x \dots \int_0^x (1-x)^{-\frac{1}{2}} dx_1 \dots dx_m.$$

Hence

$$\begin{aligned} s &= \sum_{r=0}^{\infty} \frac{1.3\dots(2n+2r-1)}{2.4\dots(2n+2r)} \frac{(n+r-1)(n+r-2)\dots(r+1)}{2(n+r)(2n+r-1)\dots(n+r+1)} \\ &= \frac{d^{n-1}}{dx^{n-1}} \left\{ \frac{1}{x^{n+1}} \frac{1}{D^n} u \right\}_{x=1} - \frac{d^{n-1}}{dx^{n-1}} \left\{ \frac{1}{n! x} \right\}_{x=1}. \end{aligned}$$

To evaluate the right-hand side we replace $\frac{d}{dx}$ by D and expand the $(n-1)$ th differential by Leibniz's Theorem, making use of the fact that

$$D^r \frac{1}{x^{n+1}} = (-1)^r \frac{(n+1)(n+2)\dots(n+r)}{x^{n+r+1}}.$$

We derive the result

$$\begin{aligned} s &= \frac{1}{D} u - \binom{n-1}{1} (n+1) \frac{1}{D^2} u + \binom{n-1}{2} (n+1)(n+2) \frac{1}{D^3} u + \dots \\ &\quad + (-1)^{n-1} (n+1)\dots(2n-1) \frac{1}{D^n} u + \frac{(-1)^n}{n}, \end{aligned}$$

where by $\frac{1}{D^m}$ we now mean

$$\frac{1}{D^m} u \equiv \int_0^1 \int_0^x \dots \int_0^x (1-x)^{-\frac{1}{2}} dx_1 \dots dx_m.$$

We find that

$$\begin{aligned} \frac{1}{D^m} u &= 2 \cdot \frac{1}{(m-1)!} - \frac{2^2}{1.3} \frac{1}{(m-2)!} + \frac{2^3}{1.3.5} \frac{1}{(m-3)!} \dots \\ &\quad + (-1)^{m+1} \frac{2^m}{1.3.5\dots(2m-1)}, \end{aligned}$$

and thus the $(r+1)$ th term in s is

$$\begin{aligned} a_{r+1} &= (-1)^r \binom{n-1}{r} (n+1)\dots(n+r) \left\{ \frac{2}{r!} - \frac{2^2}{1.3} \frac{1}{(r-1)!} \right. \\ &\quad \left. + \frac{2^3}{1.3.5} \frac{1}{(r-2)!} \dots + (-1)^r \frac{2^{r+1}}{1.3.5\dots(2r+1)} \right\}. \end{aligned}$$

(Collecting the terms in $\sum_{r=0}^{n-1} a_{r+1}$ which have $(-1)^r \frac{2^{r+1}}{1.3.5\dots(2r+1)}$ for

factor, we find that they reduce to

$$(-1)^{n-1} 2^{2r+2} \binom{n+r}{2r+2} \frac{1}{n-r-1} = (-1)^{n-r} 2^{2r+2} \binom{n+r}{2r+1} \frac{1}{2r+2},$$

and that s can now be expressed by the sum

$$s = \frac{(-1)^{n-1}}{n} \left\{ 2^2 \cdot \frac{n^2}{2!} - 2^4 \frac{n^2(n^2-1^2)}{4!} + 2^6 \frac{n^2(n^2-1^2)(n^2-2^2)}{6!} \dots n \text{ terms} \right\} + \frac{(-1)^n}{n}.$$

Using an identity given in Chrystal's Algebra, Part 2, namely,

$$\{x + \sqrt{(x^2 + y^2)}\}^{2m} + \{x - \sqrt{(x^2 + y^2)}\}^{2m} \\ \equiv 2 \left\{ y^{2m} + 2^2 \frac{m^2}{2!} x^2 y^{2m-2} + 2^4 \frac{m^2(m^2-1^2)}{4!} x^4 y^{2m-4} \dots \right\},$$

we find on replacing y by unity and x by i that

$$\frac{2^2 n^2}{2!} - \frac{2^4 n^2(n^2-1^2)}{4!} + \frac{2^6 n^2(n^2-1^2)(n^2-2^2)}{6!} + \dots = 1 - (-1)^n.$$

Thus

$$s = \frac{(-1)^{n-1}}{n} \{1 - (-1)^n\} + \frac{(-1)^n}{n}, \\ = \frac{1}{n}.$$

We have thus shown that

$$\sum_{r=0}^{\infty} \frac{1.3.5\dots(2n+2r-1)}{2.4.6\dots(2n+2r)} \cdot \frac{(n+r-1)(n+r-2)\dots r+1}{(2n+r)(2n+r-1)\dots(n+r+1)} = \frac{1}{n},$$

and it follows that the coefficient of $\frac{1}{k^{2n}}$ in $\text{Cek}_{2n}(0)$ is

$$2^{4n-2} \frac{(2n)!}{n} = 2^{4n-1} (2n-1)!$$

By a similar method we find that the coefficient of $\frac{1}{k^{2n-2}}$ in $\text{Cek}_{2n}(0)$ reduces to

$$- \frac{2^{4n-4} (2n)!}{n(4n^2-1)},$$

and an approximate expression for $\text{Cek}_{2n}(0)$ suitable for small values of k is thus

$$\text{Cek}_{2n}(0) = \frac{1}{k^{2n}} \{2^{4n-1} (2n-1)!\} - \frac{1}{k^{2n-2}} \left\{ \frac{2^{4n-4} (2n)!}{n(4n^2-1)} \right\} + \dots \quad (8.16)$$

Similarly, it is possible to show that in the case of $\text{Cek}_{2n+1}(0)$ the corresponding approximation is

$$\text{Cek}_{2n+1}(0) = - \frac{1}{k^{2n+1}} \{2^{4n+1} (2n)!\} + \frac{1}{k^{2n-1}} \left\{ \frac{2^{4n-1} (2n)!}{(2n)(2n+2)} \right\} + \dots, \quad (8.17)$$

so that for $\text{Cek}_n(0)$ we can use the formula

$$\text{Cek}_n(0) = \frac{(-1)^n}{k^n} \{2^{2n-1}(n-1)!\} + \frac{(-1)^{n-1}}{k^{n-2}} \left\{ \frac{2^{2n-3}n!}{n(n^2-1)} \right\} + \dots \quad (8.18)$$

It is evident that $\text{Cek}_0(0)$ and $\text{Cek}_1(0)$ are special cases. We shall investigate their behaviour in the next Section.

8 (d). The Special Cases $\text{Cek}_0(0)$ and $\text{Cek}_1(0)$.

By definition

$$\text{Cek}_0(0) = A_0^0 K_0(k) + A_2^0 K_2(k) + \dots + A_{2r}^0 K_{2r}(k) + \dots$$

Whittaker's formulæ (Modern Analysis) for the Mathieu Coefficients in this case are

$$\begin{aligned} A_0^0 &= 1, \\ A_{2r}^0 &= \frac{2^{r+1}q^r}{r! r!} - \frac{2^{r+3}r(3r+4)}{(r+1)!(r+1)!} q^{r+2} + \dots \end{aligned}$$

We also have the results

$$K_0(k) = -(\log \tfrac{1}{2}k + \gamma)(1 + 8q + 16q^2 + \dots) + 8q + 24q^2 + \dots,$$

$$K_2(k) = -(\log \tfrac{1}{2}k + \gamma)(4q + \dots) + (3q + \dots) + \frac{1}{2} \left(\frac{1}{8q} - 1 \right).$$

$$\begin{aligned} K_{2r}(k) &= -(\log \tfrac{1}{2}k + \gamma)(0(q^r) \dots) + \dots \\ &+ \frac{1}{2} \left\{ \frac{(2r-1)!}{2^{3r+1}q^r} - \frac{(2r-2)!}{2^{3r-2}q^{r-1}} + \frac{(2r-3)!}{2^{3r-5} \cdot 2! q^{r-2}} + \dots \right\}. \end{aligned}$$

Using these two sets of formulæ we obtain the result

$$\begin{aligned} \text{Cek}_0(0) &= \left\{ -(\log \tfrac{1}{2}k + \gamma) + \sum_1^{\infty} \frac{(2r-1)!}{r! r! 2^{2r}} \right\} \\ &+ q \left\{ -8(\log \tfrac{1}{2}k + \gamma) + 6 - 8 \sum_2^{\infty} \frac{(2r-2)!}{r! r! 2^{2r}} \right\} \\ &+ q^2 \left\{ -32(\log \tfrac{1}{2}k + \gamma) + 36 - \frac{7}{4} + \sum_2^{\infty} \frac{(2r-3)!}{r! r! 2^{2r-6}} \right. \\ &\quad \left. - \sum_2^{\infty} \frac{r(3r+4)(2r-1)!}{(r+1)!(r+1)! 2^{2r-2}} \right\} + \dots \end{aligned}$$

The infinite series occurring in this expression are easily summed by making use of the same Binomial Expansion as in 8 (c); we find

$$\begin{aligned} \sum_1^{\infty} \frac{(2r-1)!}{r! r! 2^{2r}} &= \log 2. \\ 6 - 8 \sum_2^{\infty} \frac{(2r-2)!}{r! r! 2^{2r}} &= 8 \log 2. \\ \sum_2^{\infty} \frac{(2r-3)!}{r! r! 2^{2r-6}} - \sum_2^{\infty} \frac{r(3r+4)(2r-1)!}{(r+1)!(r+1)! 2^{2r-2}} &= 32 \log 2 - 16 - \frac{41}{4}. \end{aligned}$$

It follows, therefore, that $\text{Cek}_0(0)$ can be represented approximately by the expression

$$\begin{aligned} \text{Cek}_0(0) = & - \left(\gamma + \log \frac{k}{4} \right) (1 + 8q + 32q^2 + \dots) \\ & + 8q^2 + \text{terms of higher order in } q. \quad (8.19) \end{aligned}$$

The function $\text{Cek}_1(0)$ is defined by

$$\text{Cek}_1(0) = A_1^1 K_1(k) + A_3^1 K_3(k) + \dots \dots + A_{2r+1}^1 K_{2r+1}(k) + \dots$$

In this case the Mathieu Coefficients are

$$A_1^1 = 1,$$

$$A_{2r+1}^1 = \frac{2^r q^r}{(r+1)! r!} - \frac{2^{r+1} \cdot r q^{r+1}}{(r+1)! (r+2)!} + \frac{2^r q^{r+2}}{(r-1)! (r+2)!} + \dots$$

and it should be particularly noted that they are power series in q and not q^2 as in all the other functions. The odd $K_n(k)$ functions are

$$K_1(k) = -\frac{1}{2} k (1 + 4q + \dots) \left(\gamma + \log \frac{k}{2} \right) + \frac{1}{4} k + \frac{5}{2} k q + \dots,$$

$$K_3(k) = -\frac{2}{3} k q (1 + \dots) \left(\gamma + \log \frac{k}{2} \right) + \frac{11}{3} k q + \dots + \frac{1}{2} \left\{ -\frac{16}{k^3} + \frac{2}{k} - \frac{k}{4} \right\}.$$

$$\begin{aligned} K_{2r+1}(k) = & - \left(\gamma + \log \frac{k}{2} \right) (o(k^{2r+1}) \dots) + \dots \\ & + \frac{1}{2} \left\{ -\frac{(2r)!}{k q^r 2^{3r-1}} + \frac{(2r-1)!}{k q^{r-1} 2^{3r-4}} - \frac{(2r-2)!}{k q^{r-2} 2^{3r-6}} \dots \right\}. \end{aligned}$$

Working to the order kq we find that $\text{Cek}_1(0)$ can be represented by

$$\begin{aligned} \text{Cek}_1(0) = & -\frac{1}{k} \left\{ \sum_{r=0}^{\infty} \frac{(2r)!}{(r+1)! r! 2^{2r}} \right\} + \frac{1}{2} k \left\{ - \left(\log \frac{1}{2} k + \gamma \right) \right. \\ & \left. + \sum_1^{\infty} \frac{(2r-1)!}{r! r! 2^{2r+2}} + \sum_1^{\infty} \frac{(2r-1)!}{(r+1)! (r+1)! 2^{2r+2}} \right\} \\ & + k q \left\{ -2 \left(\gamma + \log \frac{k}{2} \right) + \frac{5}{2} - \frac{1}{64} \left[\sum_{r=1}^{\infty} \frac{(2r-2)!}{(r+1)! r! 2^{2r-6}} \right. \right. \\ & \left. \left. + \frac{r(2r-1)!}{(r+1)! (r+1)! 2^{2r-5}} + \frac{(2r)!}{(r-1)! (r+2)! 2^{2r-1}} \right] \right\} + \dots \end{aligned}$$

For the infinite series we obtain the results

$$\sum_{r=0}^{\infty} \frac{(2r)!}{(r+1)! r! 2^{2r}} = 2,$$

$$\sum_1^{\infty} \frac{(2r-1)!}{r! r! 2^{2r+2}} + \sum_1^{\infty} \frac{(2r-1)!}{(r+1)! (r+1)! 2^{2r+2}} = \log 2,$$

$$\sum_{r=1}^{\infty} \left[\frac{(2r-2)!}{(r+1)! r! 2^{2r-6}} + \frac{r(2r-1)!}{(r+1)! (r+1)! 2^{2r-5}} + \frac{(2r)!}{(r-1)! (r+2)! 2^{2r-1}} \right] \\ = \frac{308}{3} - 128 \log 2.$$

and thus $\text{Cek}_1(0)$ is represented approximately by

$$\text{Cek}_1(0) = -\frac{2}{k} - \frac{1}{2}k(1+4q) \left(\gamma + \log \frac{k}{4} \right) + \frac{43}{48}kq \\ + \text{terms of higher order in } k. \quad (8.20)$$

8 (e). *The Approximation to $\text{Cekh}_n(0)$ suitable for Small Values of k .*

By definition

$$\text{Cekh}_n(0) = \dots A_{n-2}^n I_{n-2}(k) + A_n^n I_n(k) + A_{n+2}^n I_{n+2}(k) + \dots$$

Referring to the Mathieu Coefficients already defined in (8.12) and bearing in mind that

$$I_m(k) = \left(\frac{1}{2}k \right)^m \left\{ \frac{1}{m!} + \frac{(\frac{1}{2}k)^2}{1! (m+1)!} + \dots \right\},$$

it is evident that the leading terms in $\text{Cekh}_n(0)$ for small k are derived only from the terms $A_n^n I_n(k)$, $A_{n-2}^n I_{n-2}(k)$ and so on. We find that the coefficient of k^n is given by the finite sum

$$\frac{1}{(n-1)! 2^n} \left\{ \frac{(n-1)!}{n!} - \frac{(n-2)!}{1! (n-2)! 2^2} + \frac{(n-3)!}{2! (n-4)! 2^4} + \dots \right\} \quad (a)$$

and the coefficient of k^{n+2} is the finite sum

$$\frac{1}{(n-1)! 2^n} \left\{ \frac{(n-1)!}{(n+1)! 2^2} - \frac{(n-2)!}{1! (n-1)! 2^4} + \frac{(n-3)!}{2! (n-3)! 2^6} \dots \right\} \quad (b)$$

the number of terms in the summation being $(n/2+1)$ if n is even and $(n+1)/2$ if n is odd.

We will only evaluate here the sum (a) in the case of n even for all the others are summed by the same method. The required sum is then

$$S = \frac{1}{(2n-1)! 2^{2n}} \left\{ \frac{1}{2n} - \frac{1}{2^2} + \frac{(2n-3)}{2! 2^4} \right. \\ \left. - \frac{(2n-4)(2n-5)}{3! 2^6} \dots (-1)^r \frac{(2n-r-1) \dots (2n-2r+1)}{r! 2^{2r}} \dots \right\}, \\ = \frac{1}{(2n)! 2^{2n}} \left\{ 1 - \frac{2n}{2^2} + \frac{2n(2n-3)}{2! 2^4} - \frac{2n(2n-4)(2n-5)}{3! 2^6} \dots \right. \\ \left. (-1)^r \frac{2n(2n-r-1) \dots (2n-2r+1)}{r! 2^{2r}} \dots \right\}.$$

Consider now the identity (Chrystal's Algebra, Part 2)

$$\alpha^{2n} + \beta^{2n} \equiv p^{2n} - \frac{2n}{1!} p^{2n-2} q + \frac{2n(2n-3)}{2!} p^{2n-4} q^2 + \dots$$

$$(-1)^r \frac{2n(2n-r-1) \dots (2n-2r+1)}{r!} p^{n-2r} q^r \dots$$

where

$$p = \alpha + \beta, \quad q = \alpha\beta.$$

If we take $p=1$ and $q = \left(\frac{1}{2^2}\right)$, then $\alpha = \frac{1}{2}$ and $\beta = \frac{1}{2}$, and hence

$$1 - \frac{2n}{1!} \frac{1}{2^2} + \frac{2n(2n-3)}{2!} \frac{1}{2^4} - \frac{2n(2n-4)(2n-5)}{3!} \frac{1}{2^6} \dots = \frac{1}{2^{2n-1}}.$$

Therefore the coefficient of k^{2n} in $\text{Cek}_{2n}(0)$ is

$$S = \frac{1}{(2n)! 2^{4n-1}}.$$

Similarly, we can show that the coefficient of k^{2n+2} in $\text{Cek}_{2n}(0)$ is

$$S_1 = -\frac{1}{(2n+1)! (2n-1) 2^{4n+1}}.$$

and thus

$$\text{Cek}_{2n}(0) = k^{2n} \left\{ \frac{1}{(2n)! 2^{4n-1}} \right\} - k^{2n+2} \left\{ \frac{1}{(2n+1)! (2n-1) 2^{4n+1}} \right\} \dots \quad (8.21)$$

The case of the odd $\text{Cek}_n(0)$ does not involve any further difficulty and we find that in general we can write

$$\text{Cek}_n(0) = k^n \left\{ \frac{1}{2^{2n-1} n!} \right\} - k^{n+2} \left\{ \frac{1}{(n+1)! (n-1) 2^{2n+1}} \right\} \dots \quad (8.22)$$

Although the cases $n=0$ and $n=1$ again require special treatment, they can now be written down immediately, since they only involve a few terms; we obtain the results

$$\text{Cek}_0(0) = 1 + 8q + 32q^2 + \dots \quad (8.23)$$

$$\text{Cek}_1(0) = \frac{1}{2}k(1 + 4q + \dots). \quad (8.24)$$

We may note that the coefficients of $\left(\gamma + \log \frac{k}{4}\right)$ in $\text{Cek}_0(0)$ and $\text{Cek}_1(0)$ to order q^2 and kq respectively are identical with $\text{Cek}_0(0)$ and $\text{Cek}_1(0)$ respectively.

8 (f). *The Ratio of the Associated Mathieu Function to its Derivate at $\xi=0$.*

Using a generalization of the result (8.10) we find that the ratio μ_n of $\text{Cek}'_n(0)$ to $\text{Cek}_n(0)$ can be expressed in the form

$$\mu_n = (-1)^{n+1} \frac{(\sum A_r^n)^2}{\text{Cek}_{h_n}(0) \text{Cek}_n(0)}.$$

By substitution of the approximations to $\text{Cek}_{h_n}(0)$ and $\text{Cek}_n(0)$ from (8.22) and 8.18) respectively and of the Mathieu Coefficients from (8.12), we can derive quite simply the formula

$$\mu_n = -n \left\{ 1 + \frac{8q}{n^2 - 1} + \dots \right\}, \quad . \quad . \quad . \quad . \quad . \quad (8.25)$$

which is valid for small values of k and for $n \geq 2$.

Conclusion.

The problem of the flow of a viscous fluid past a flat plate for large values of the Reynolds number remains to be solved making use of this mode of attack. The asymptotic result obtained by Piercy and Winny (1933) working to Oseen's Approximation is identical in form with the result obtained by Blasius using "boundary layer" methods, although the numerical value obtained by them is 70 per cent. in excess of that of Blasius. It is of great interest therefore, to find the asymptotic result in this case.

In conclusion I wish to thank Mr. T. Lewis, University College of Wales, Aberystwyth, for his most helpful criticisms and suggestions.

References.

- (1) T. Lewis, *Quart. Journ. Math.*, Oxford Series, vol. ix. no. 33, p. 21 (1938).
- (2) L. N. G. Filon, *Proc. Roy. Soc. A*, vol. cxiii. p. 7 (1926).
- (3) S. Goldstein, *Proc. Roy. Soc. A*, vol. cxiii. (1929).
- (4) Piercy and Winny, *Proc. Roy. Soc. A*, vol. cxl. p. 543 (1933).
- (5) D. Meksyn, *Proc. Roy. Soc. A*, vol. clxii. p. 232 (1937).
- (6) P. Humbert, *Memorial des Sciences Mathematiques*, fasc. x. (1926).
- (7) Whittaker and Watson, 'Modern Analysis,' chs. xvii., xix.
- (8) Knopp, 'Theory and Application of Infinite Series,' ch. 8.
- (9) E. Mathieu, *Journal de Mathematiques*, Deuxième Serie, t. xiii. p. 137 (1868).

XXXI. *On the Migration of Atoms in Iron-Nickel Alloys.*

By Professor E. A. OWEN, M.A., Sc.D., and A. H. SULLY, Ph.D.,
University College of North Wales, Bangor*.

[Received December 2, 1940.]

[Plate VII.]

1. *Introduction.*

THE equilibrium diagram of iron-nickel alloys at temperatures below 1000°C. , referred to in a recent paper ⁽¹⁾, was deduced from a survey of lines appearing in X-ray spectra obtained with alloys which had been subjected to different heat treatments; no particular reference was made to parameter measurements carried out on the alloys. In the present paper it is proposed to put these measurements on record and to use them for the further study of the iron-nickel alloy system, in particular, the study of the migration of atoms between the α - and γ -phases.

A certain amount of data concerning the parameters of iron-nickel alloys has already been published ⁽²⁾; these data will be amplified here. Factors that are important in the study of these alloys, namely, rigorous heat treatments and quenching processes, were employed, so as to ensure definite and reproducible results.

2. *Pure γ -phase Alloys quenched from Temperatures between 500°C. and 800°C.*

From the survey of the X-ray spectra it had been found that at temperatures not lower than 500°C. , alloys containing more than about 25 atomic per cent. nickel were all in the pure γ -phase, but that on quenching from these temperatures the γ -structure in some alloys suffered a partial conversion into the distorted α_2 -lattice (metakamacite). In alloys quenched from 800°C. this partial conversion into metakamacite extends over compositions from about 25 to 32 atomic per cent. nickel, but in alloys containing between about 2 and 25 atomic per cent. nickel and quenched from this temperature, the conversion of the γ into α_2 is complete.

Lattice parameters of the pure γ -phase alloys have been the subject of accurate measurement by Phragmen ⁽³⁾, Jette and Foote ⁽⁴⁾, Bradley, Jay and Taylor ⁽⁵⁾, in addition to the work carried out in this laboratory ⁽²⁾:

* Communicated by Professor E. A. Owen.

all these investigators found that on adding iron to nickel, the parameter increases to a maximum value at about 39 atomic per cent. nickel. As the iron content is further increased the parameter decreases almost linearly with atomic composition.

The first measurements in the present investigation were made on alloys which had been quenched from temperatures ranging between 500° C. and 800° C., with a view to examining the effect, on the γ -parameter, of the rate of cooling through the temperature of magnetic transformation, and also of the presence of the α_2 -structure when this was present with the γ -structure in the same alloy.

For this purpose alloys were prepared ranging in composition from 32.48 to 46.74 atomic per cent. nickel; these alloys were annealed for different periods at 500°, 600° C., 700° C., and 800° C. respectively, and then quenched in iced water. Each specimen in the form of filings was held in an evacuated silica tube and supported in the middle of a long furnace which was mounted vertically so that the tubes could be dropped into the quenching medium. About a hundred parameter measurements were made, the period of annealing ranging at some of the temperatures between 48 and 260 hours. Particular attention was directed to the quenching operation; a special technique was adopted to ensure that it was carried out effectively and in the same manner on each occasion. A description of the method and the design of furnace employed will be given in another paper. With this method of quenching the following values of the parameters of the γ -phase at 15° C. were obtained after the various heat treatments (Table I.).

The values of the parameter of any one alloy agree with each other within experimental accuracy of measurement, and they agree with those published previously ⁽²⁾ except for alloys 37.24 and 39.46, which have compositions in the neighbourhood of the maximum of the parameter-composition curve. The more accurate value of the parameter now found at the maximum, which occurs at 38.6 atomic per cent. nickel, is 3.5889 A. at 15° C.; previously it was found to be 3.5895 A.

The alloys were all given an initial heat treatment when in ingot form—some were maintained at 1150° C. for 20 hrs. in a nitrogen atmosphere, and others at the same temperature for 8 hours *in vacuo*.

The present results show that the lattice parameter values determined by the examination of samples quenched from temperatures between 500° C. and 800° C., are independent of the temperature at which the annealing is conducted. If, however, the quenching operation is not rigorous, discrepancies arise in the measured lattice parameters and the observed values may differ from the true values by as much as ± 0.001 A. Rapid and efficient quenching removes this effect and leads to uniformity in the results.

TABLE I.

Composition of alloy (atomic per cent. nickel).	Parameter (A.) at 15° C. of γ -phase in alloys quenched after			
	1 hr. at 800° C.	7 hrs. at 700° C.	14 hrs. at 600° C.	48 hrs. at 500° C.
32.48	3.5833 ₄	3.5832 ₈	3.5832 ₀	
33.97	3.5860 ₈	3.5857 ₁	3.5859 ₇	
36.01	3.5883 ₂	3.5882 ₄	3.5882 ₇	3.5881 ₁
37.24	3.5884 ₈	3.5887 ₄	3.5886 ₇	3.5886 ₀
39.46	3.5885 ₈	3.5888 ₂	3.5885 ₆	3.5887 ₈
41.50	3.5880 ₆	3.5879 ₂	3.5882 ₈	
44.26	3.5858 ₀	3.5858 ₂	3.5858 ₇	3.5857 ₄
46.74	3.5829 ₉	3.5828 ₁	3.5826 ₇	

TABLE II.

Lattice Parameters of γ -phase Iron-nickel Alloys at 15° C.

Nickel content of alloy.		Lattice parameter of γ -phase at 15° C.	Nickel content of alloy.		Lattice parameter of γ -phase at 15° C.
Weight per cent.	Atomic per cent.		Weight per cent.	Atomic per cent.	
100	100	3.5171 ₃	40.66	39.46	3.5886 ₈
96.75	96.58	3.5206 ₆	38.42	37.24	3.5886 ₂
93.95	93.65	3.5241	37.17	36.01	3.5883 ₂
91.04	90.63	3.5278	35.10	33.97	3.5858 ₉
82.86	82.13	3.5378	34.46	33.34	3.5847 ₀
74.00	73.03	3.5494	34.18	33.07	3.5841 ₇
63.82	62.66	3.5626	33.59	32.48	3.5833 ₁
58.41	57.19	3.5691	33.40	32.29	3.5829 ₂
52.15	50.91	3.5779	32.20	31.13	3.5808 ₀
48.00	46.74	3.5828 ₄	31.67	30.60	3.5798 ₂
45.50	44.26	3.5858 ₆	30.30	29.25	3.5769 ₃
42.71	41.50	3.5881 ₈	28.12	27.12	3.5742 ₈

The figures given in Table II. for the mean parameters of the γ lattice in alloys which are in the pure γ -phase region at or above 500° C., and

which are quenched in iced-water, are taken as standard. They agree closely with the figures previously published ⁽²⁾.

To summarize the results obtained with specimens ranging in composition from pure nickel to 27 atomic per cent. nickel and quenched in iced water from temperatures between 500° C. and 800° C.: (1) When iron is added to nickel, the nickel lattice expands almost linearly with atomic composition. (2) The lattice parameter reaches a maximum value of 3.5889 Å. at 15° C. for an alloy containing 38.6 atomic per cent. nickel. (3) On further addition of iron, the lattice contracts, again almost linearly with composition, down to about 27 atomic per cent. nickel. (4) The alloy containing 38.6 atomic per cent. nickel at the maximum of the parameter-composition curve, is able to take into solution either nickel or iron, and in each case the lattice parameter decreases. (5) The maximum occurs at a composition close to that of the intersection of the magnetic-transformation curve and the $\gamma-(\gamma+\alpha)$ boundary ⁽¹⁾; this suggests that the shape of the parameter-composition curve is influenced by both the phase boundary and the position of the magnetic transformation curve. (6) Since the parameter values are the same from whatever temperature between 500° C. and 800° C. they are quenched, they are independent of the rate at which the alloys are cooled through the magnetic transformation point. (7) The partial conversion of some alloys, within the range of composition investigated, into the distorted body-centred α_2 -structure, does not affect the parameter of the γ -phase, which is the same as that of the γ -phase when it occurs alone in the same alloy quenched from a different temperature. Thus the γ -structure is not affected by the α_2 -material which is present with it. (8) The time of annealing before quenching has no effect on the parameter if it exceeds a certain minimum period which rapidly increases as the temperature is lowered. (9) The quenching operation must be efficiently performed else the parameter of the γ -lattice in the quenched specimen shows variation. (10) The spectral lines are well defined, and are capable of accurate measurement, except in those alloys which have been annealed for too long a period, resulting in the formation of large crystals in the specimen and spectral lines which are "spotty," and therefore badly defined. In such cases the annealing period was shortened until the texture of the lines was satisfactory.

3. Experimental.

Little success has hitherto attended attempts to measure lattice parameters of alloys in the two-phase region. This is due to one or both of two reasons, namely, (1) the unsuitability of the heat treatment adopted, and (2) the use of radiation of unsuitable wave-length.

(i.) *The Heat Treatment of the Alloys.*

From the results of the previous survey ⁽¹⁾ it is known that in alloys containing not more than about 25 atomic per cent. nickel, quenching from temperatures higher than about 580° C. results in the complete conversion of the γ into a distorted α_2 -lattice, the latter being so distorted that it yields no visible spectral lines with the focusing camera, and even if spectral lines could be obtained measurements upon them would be valueless, since the results would not refer to the condition of the alloy before being quenched.

In addition, it was found that if the two-phase alloys were raised to a temperature at which complete conversion to the γ -lattice occurs and the alloys were then cooled, say, to 500° C. and quenched, the distorted α_2 -structure is again produced. If, however, alloys containing below about 25 atomic per cent. nickel were raised to a temperature not exceeding about 580° C. and annealed at this temperature before quenching, the α - and γ -structures appear together. Hence if parameter measurements of alloys in the two-phase region are to be successful, the temperature of the alloys during the annealing process must be raised to the annealing temperature and not lowered to that value from a higher temperature before quenching, and, further, an annealing temperature above about 580° C. must be avoided.

(ii.) *Choice of Radiation.*

Some investigators have used copper radiation for the measurement of the γ -parameters. At high nickel content this radiation gives spectra which are satisfactory for parameter measurement, but for high iron content, the strong absorption of copper radiation by iron results in poor contrast between spectral line and background and so makes accurate measurement somewhat difficult. Further, in those two-phase alloys in which the proportion of the γ constituent is small, the weakness of the γ -lines militates against accurate measurement.

For these reasons manganese radiation was used exclusively in this investigation to determine γ -phase parameters. This radiation gives good contrast between line and background and thus considerably assists the measurement of the lines. For the α -structure, cobalt radiation was used. This yields well-defined spectral lines at small arcs where the accuracy of measurement is greatest.

4. *Lattice Parameters of Alloys in the Two-phase region.*

Parameter measurements were made on alloys which had been heat-treated at 500° C., 400° C., and 350° C., and all the values of lattice parameter were obtained by the aid of the focusing camera, the constants

of which were accurately known. Lattice parameters could be determined with this camera to an accuracy not less than ± 1 in 20,000 with spectral lines of normal definition; the accuracy is lower than this for lines which are not well defined, as frequently occurs with the alloys under investigation after certain heat treatments.

Three types of heat treatment at 500° C. will be investigated.

(a) *Alloys quenched after various Periods of Annealing at 500° C.*

Four periods of annealing, namely, 48, 112, 132, and 260 hrs., were employed before quenching the specimens. Table III. contains the results obtained with an alloy containing 39.46 atomic per cent. nickel; these show that the value of the parameter is the same after each annealing treatment.

TABLE III.

Annealing period (hours).	Parameter (A.) at 15° C. after quenching from 500° C. in iced water (A.).
48	3.5888 ₈
112	3.5887 ₂
132	3.5888 ₂
260	3.5887 ₀
Mean value.... 3.5887 ₈	

Two sets of alloys, one set annealed for 48 hrs. and the other for 132 hrs. before quenching, yielded the mean values of α - and γ -parameters given in Table IV.

From the graph in fig. 1, it will be seen that the α -curve consists of a straight portion through the pure α -region and the parameter reaches a maximum value of 2.8634₂ A. at about 7.5 atomic per cent. nickel; then as the nickel content of the alloy increases, it falls off rapidly to the value 2.8615₆ A. at 25 atomic per cent. nickel.

The γ -curve reaches a minimum value of 3.5742 A. at 25 atomic per cent. nickel and then, as the nickel content decreases, it rises to a maximum value of 3.5779 A. at about 17 atomic per cent. nickel. The curve in the region of this maximum is difficult to determine with accuracy; little importance is therefore attached to the exact form given to it in fig. 1.

The curves in fig. 1 are the general forms for alloys in the two-phase region which have been quenched after a period of annealing. Their exact shape may vary according to the efficiency of the quench. The results show that the period of annealing at 500° C. before the quenching operation has no effect on the value of the lattice parameters if this period exceeds 48 hours. Shorter periods were not investigated.

(b) *Alloys annealed for different Periods at 500° C. and cooled at the same Rate to Room-temperature.*

Alloys over the same range of composition as above, were annealed at 500° C. for 48 hours, 132 hours, and 36 days respectively, and after these

TABLE IV.

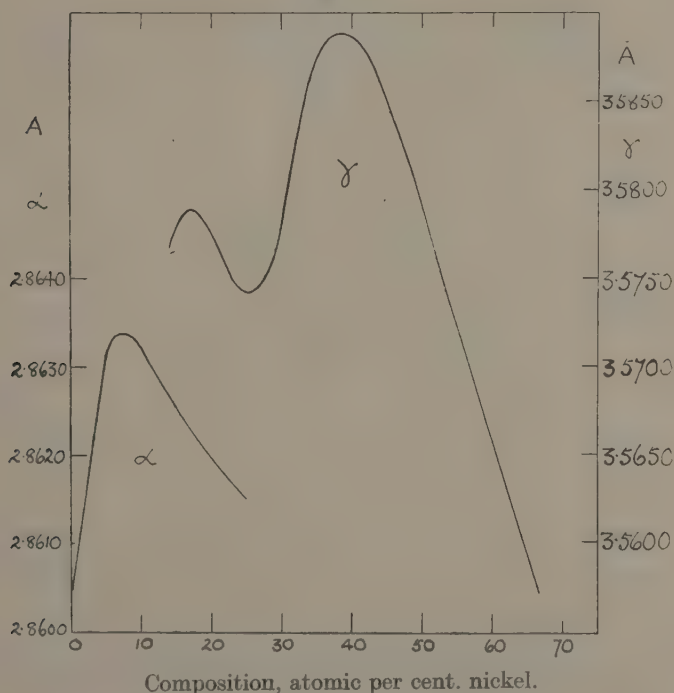
Nickel content (atomic per cent.).	Parameter (A.) at 15° C.	
	α -phase.	γ -phase.
2.96	2.8623 ₈	—
5.73	2.8632 ₉	—
8.56	2.8633 ₈	—
12.16	2.8627 ₁	—
14.01	2.8626 ₂	3.5772 ₉
15.05	—	3.5767 ₅
15.98	2.8623 ₃	3.5787 ₇
20.32	2.8619 ₅	3.5769 ₁
23.32	2.8616 ₈	3.5751 ₇
27.12	—	3.5745 ₃
29.25	—	3.5768 ₈
30.60	—	3.5794 ₅
31.13	—	3.5806 ₂
32.48	—	3.5832 ₉
33.97	—	3.5859 ₀

heat treatments, cooled over a period of 12 days to room-temperature. Thirty-three parameter measurements on the α -phase and thirty-one on the γ -phase resulted in the curves that are shown in fig. 2. Curves A, B, and C represent respectively the results obtained after 48 hours, 132 hours, and 36 days annealing before the cooling was started. The α -curves are all of the same type, they reach approximately the same maximum parameter, and the rise to the maximum through the pure α -phase as the nickel content is increased, is the same as in the previous case considered; but the rate of fall of parameter with increase of nickel

content beyond that corresponding to the maximum, *i. e.*, about 7 atomic per cent. nickel, becomes greater as the initial period of annealing is increased.

The γ -curves also show differences according to the period of annealing. The effect here is that as the nickel content is decreased the parameter follows the standard parameter-composition curve in each case until the composition of the alloy reaches between 28 and 31 atomic per cent.

Fig. 1.



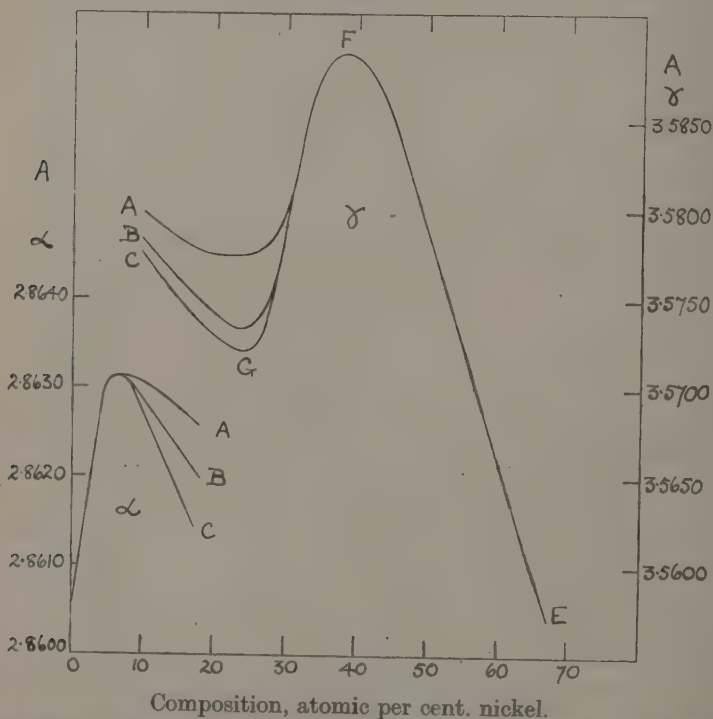
Relations between parameter and composition for α - and γ -phases in alloys quenched from 500° C.

nickel, but the form of the curves remains the same. After departing from the standard curve, a minimum value of the parameter is reached and then the parameter increases again as the nickel content is still lowered. Whereas the minimum for each curve occurs at about 25 atomic per cent. nickel, the value of the parameter at the minimum decreases as the initial period of annealing increases. It would appear from a graph of the minimum parameter against period of annealing,

that the parameter tends to reach its final minimum value exponentially with time.

An instability evidently exists in the two-phase region; the parameters of both the α - and the γ -components vary according to the length of time the alloy is initially annealed. As the period of annealing is increased there is associated with the decrease in α -parameter a marked change in the quality of the spectral lines. The lines recorded after 132 hours' annealing are considerably less well defined than those after 48 hours'

Fig. 2.



Relations between parameter and composition for α - and γ -phases in alloys annealed for different periods at 500° C. and cooled at the same rate to room-temperature.

annealing, and after 864 hours' annealing the lines are so badly defined that they cannot be measured at compositions greater than about 16 atomic per cent. nickel.

It is of interest to consider certain points concerning these curves at this stage. Take first the α -curves. After the maximum is reached the

lattice parameter decreases with increase in nickel content, the decrease for a given alloy being greater, the longer is the initial annealing. If the decrease of parameter may be taken to signify that nickel is being precipitated out of the α -solution in accordance with the pure phase parameter-composition curve, then the longer the time of annealing the more nickel is removed if the rate of cooling is kept constant. The nickel that is precipitated is not free as no lines characteristic of pure nickel appear in the spectra.

Considering now the γ -lattice, the curves (fig. 2) show that over the range of composition where the α -parameter decreases, the γ -parameter also decreases, and if this decrease in γ -parameter indicates solution of nickel in accordance with the limb FE of the standard parameter-composition curve, then the nickel deposited from the α -phase may be

TABLE V.

Time of annealing (hrs.).	Nickel content after slow cooling.	
	α -phase.	γ -phase.
	per cent.	per cent.
48	4.4	50.5
132	3.6	52.2
864	2.5	52.7

accommodated in the γ -phase, the cooling being slow enough for this process to take place.

Table V. contains data obtained from the actual curves for an alloy containing 15 atomic per cent. nickel, from which it will be seen that, on the above assumptions, the decrease in nickel content of the α -component is accompanied by an increase in the nickel content of the γ -component.

As the amount of nickel migrating from the α to the γ increases with increase of the initial annealing period when the rate of cooling is kept constant, a progressive increase in the distortion might be expected which would explain the rather unexpected result that the definition of the lines deteriorate as the time of annealing is prolonged.

That the composition along the limb FE of the standard parameter-composition curve and not that along the limb FG is followed by the γ -phase as the composition changes from 10 to 20 atomic per cent. nickel, is supported by the fact that no free nickel was detected in the alloy at the end of the heat treatment.

(c) *Alloys annealed at 500° C. for 48 Hours and cooled at different Rates to Room-temperature.*

Sets of samples of twenty-three alloys in the range from 0 to 47 atomic per cent. nickel were annealed for 48 hours at 500° C., then the first set was cooled to room-temperature in 1 day, the second set in 12 days, and the third set in 25 days. The effect of the slow cooling operation was to improve the definition of the spectral lines; the lower the rate of cooling, the better is the definition of the lines and the more accurate, therefore, the determination of the parameters. The samples in the second set were cooled from 500° C. to 200° C. in 12 days, and were afterwards allowed to cool to room-temperature in the furnace, after having switched off the current. A different procedure was adopted with the third set. The current through the furnace was supplied by a large capacity storage battery, and by this means the temperature could be accurately controlled. After the initial annealing treatment, the alloys were slowly cooled to room-temperature at the rate of about 20° C. per day, the whole cooling process occupying 25 days.

The values of the lattice parameters of the α - and the γ -phases, as calculated from measurements made on precision films, are collected in Table VI. Values of the parameters of quenched specimens are also included in the table for reference.

From the data supplied in this table it will be observed that as the rate of cooling is lowered, the parameters show a tendency to reach a constant value. What actually occurs can be seen more clearly from the graph shown in fig. 3.

Consider first the γ -phase curves. The curve for quenched specimens has already been shown in fig. 1, and is therefore omitted from the present graph. It need only be mentioned in relation to the quenched specimens, that the γ -parameter values in the two-phase region showed marked fluctuations, far more than the fluctuation shown after the other treatments. Curve ABC of fig. 3 refers to 1 day's, curve ADC to 12 days', and curve EFC to 25 days' cooling. These curves show the progressive flattening out that occurs, eventually reaching steady values for alloys containing between 15 and 30 atomic per cent. nickel. The values of the parameters are practically constant for curve ADC between the compositions 20 and 25 atomic per cent. nickel: there is no indication of a level portion in curve ABC which refers to alloys cooled in 1 day.

Examining now the α -parameter curves, it is observed that these show the same characteristics as the γ -curves. Here the α -curve HOR refers to the 1 day cooling; the parameter drops in value continuously over the whole range from about 8 to 25 atomic per cent. nickel and the curve is similar in form to those shown in fig. 2, the difference now being that the range of composition has been extended. The α -curves HOP and HMN

TABLE VI.

Parameters of α - and γ -phases in Alloys cooled over varying Periods after Annealing Treatment at 500° C. for 48 hours.

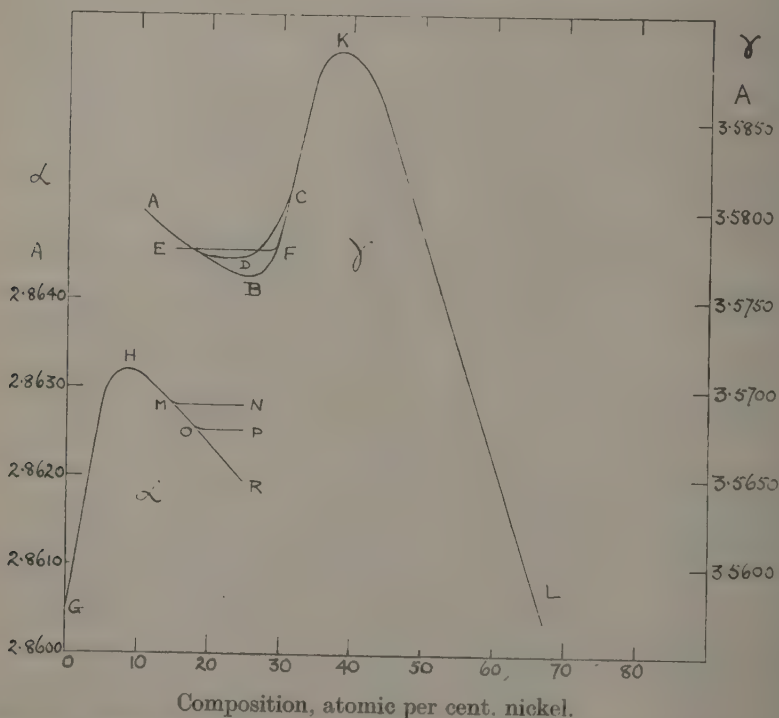
Composition of alloy (atomic per cent. nickel).	Parameter (A.) at 15° C.			
	Quenched.	Cooled in 1 day.	Cooled in 12 days.	Cooled in 25 days.
α -phase.	—	—	—	—
0.91	—	—	2.8611 ₀	—
2.12	—	—	2.8617 ₂	—
2.96	2.8623 ₅	—	2.8619 ₂	2.8620 ₃
5.73	2.8632 ₂	—	2.8629 ₅	2.8629 ₀
8.56	2.8634 ₃	2.8632 ₀	2.8631 ₄	2.8632 ₂
9.55	2.8632 ₄	2.8631 ₉	2.8630 ₅	—
12.16	2.8628 ₂	2.8631 ₄	—	—
12.83	—	2.8631 ₄	—	—
14.01	2.8625 ₅	2.8629 ₈	2.8629 ₀	2.8627 ₉
15.05	2.8625 ₁	2.8628 ₈	—	—
15.98	2.8624 ₅	2.8628 ₈	2.8627 ₇	2.8627 ₆
20.32	2.8621 ₆	2.8625 ₈	2.8624 ₇	2.8628 ₉
23.32	2.8618 ₄	2.8621 ₆	2.8625 ₈	2.8628 ₁
γ -phase.	—	—	—	—
12.16	—	—	3.5794 ₀	—
12.83	—	3.5790 ₀	—	—
14.01	3.5776 ₈	3.5787 ₁	3.5784 ₄	—
15.05	3.5767 ₅	3.5776 ₀	—	—
15.98	3.5788 ₁	3.5779 ₂	3.5780 ₆	3.5775 ₈
20.32	3.5777 ₀	3.5780 ₁	3.5774 ₅	3.5777 ₀
23.32	3.5751 ₆	3.5768 ₉	3.5775 ₆	3.5778 ₂
27.12	3.5745 ₃	3.5756 ₀	3.5781 ₈	3.5776 ₄
29.25	3.5768 ₈	3.5774 ₃	3.5788 ₆	3.5778 ₂
30.60	3.5794 ₅	3.5797 ₀	3.5797 ₀	—
31.13	3.5812 ₇	—	—	—
32.48	3.5832 ₉	—	—	3.5833 ₆
33.97	3.5858 ₂	—	3.5856 ₅	—
36.01	—	—	3.5880 ₃	—
41.50	—	—	3.5881 ₃	—
44.26	—	—	3.5850 ₉	—
46.74	—	—	3.5825 ₀	—

are of different form; these show a horizontal portion corresponding to the horizontal portions of the γ -curves which refer to the same rate of cooling. As the rate of cooling is lowered, the constant parameter

values occur over a longer range of composition and at a higher α -parameter value; the horizontal part moves upwards with the one end running along the curve HOR.

It is interesting to note that the form of the α -curve GHMN is similar to the form of the γ -curve LKFE. Also the nickel contents corresponding to the horizontal parts MN and OP, as estimated from the pure α -parameter-composition curve, are 5.0 and 4.4 atomic per cent. nickel, so that as the cooling treatment is lengthened, more nickel goes into the α -phase. This

Fig. 3.



Relations between parameter and composition for α - and γ -phases in alloys annealed at 500° C. for 48 hours and cooled at various rates to room-temperature.

nickel must come out of the γ -phase, and this should accordingly show a decrease of nickel content of approximately the same amount. Taking the nickel content corresponding to the horizontal parts of γ -curves EFC and ADC from the portion KL of the standard curve, it is found that the nickel content does show about the required decrease, the composition

corresponding to the parameters being respectively 50.7 and 51.2 atomic per cent. nickel. It would appear, therefore, that the effect of the longer cooling is to allow nickel to migrate from the γ - to the α -phase. Whether the final state of equilibrium has been reached cannot be definitely stated until a still slower rate of cooling has been tried. This needs special technique, and will have to be recorded later.

According to the views expressed in this section on material heat-treated at 500° C., alloys falling within the two-phase region of the iron-nickel system will consist of an α -component richer and a γ -component poorer in nickel the lower the rate of cooling from the annealing temperature after a given initial period of annealing. They will consist of an α -component poorer and a γ -component richer in nickel, the longer the initial period of annealing followed by a constant rate of cooling to room-temperature; in other words, nickel atoms migrate in increasing numbers from the γ - to the α -phase as the rate of cooling from the annealing temperature is increasingly retarded, but for a given rate of cooling the nickel atoms migrate in increasing numbers from the α - to the γ -phase as the initial period of annealing is increased.

5. *Measurement of Parameters after Heat Treatment at Temperatures below 500° C.*

Measurements of parameters were made after annealing the alloys at 400° C. and 350° C. They are of a preliminary nature, but are of sufficient interest and well enough established to be included in the present survey. The composition of the alloys examined extended from 0 to about 60 atomic per cent. nickel. This wide range of composition was chosen in order to include the pure γ -alloys beyond the $(\alpha+\gamma)-\gamma$ boundary, so that parameter values at the lower temperatures could be compared with those above 500° C. in the region of the pure γ -phase. The investigation is of a preliminary character, because it is necessary to submit the alloys to heat treatments extending over much longer periods than was possible up to this stage. However, it was found that alloys annealed at 400° C. yielded good spectral lines even after short periods of annealing; for example, a heat treatment at 400° C. for 66 hours with subsequent air-cooling, resulted in satisfactory lines. The resolution of the lines at high angles of reflexion was always better for the α - than for the γ -structure. It was also noticed that the lines in the spectrum of the α -phase were free from the "fuzziness" associated with the breakdown of the γ -phase on rapid cooling.

(i.) *Heat Treatments at 400° C.*

Twenty-eight alloys covering a range of composition from 0 to about 60 atomic per cent. nickel were annealed at 400° C., (a) for 132 hours and

quenched in iced water, (b) for 260 hours * and quenched, (c) for 132 hours * and cooled to room-temperature in 96 hours. The measured parameters of the α - and γ -structures found in these alloys are collected in Table VII.

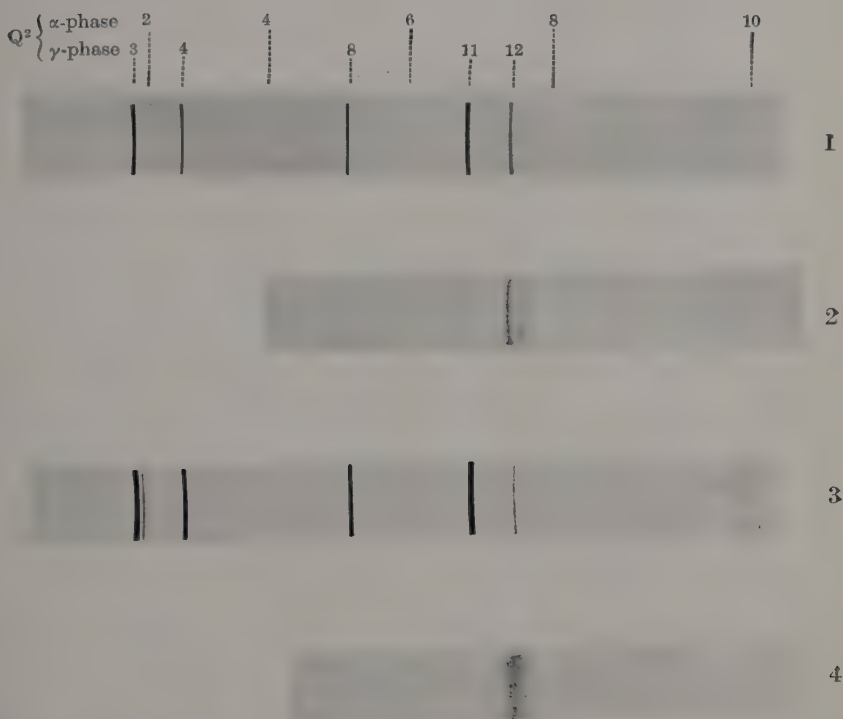
The figures in this Table appear at first glance to be somewhat erratic, but when they are plotted (see fig. 4) it is found that they fall on curves which in some respects resemble those in figs. 1, 2, and 3, but they possess certain features which are different from these curves. For example, all the γ -phase curves show that between the compositions 35 and 42 atomic per cent. nickel, the parameter of the γ -phase is approximately constant, whereas over the same range of composition after heat treatment at temperatures between 500° C. and 800° C., the γ -parameter values show continuous change on either side of the maximum which occurs at 38.6 atomic per cent. nickel. For alloys with nickel content lower than 35 atomic per cent. all the parameters follow the descending limb of the standard composition-parameter curve for the γ -phase, but the curves corresponding to the different heat treatments part with the standard curve at various points and for still lower nickel content, follow diverse courses. The curve DCBA refers to the first heat treatment of 132 hours at 400° C. followed by rapid quenching. This curve is similar in form to the curve over this range of composition, obtained with alloys quenched from 500° C. and over, but the actual parameter values are, of course, different.

The α -curve PQR after the same heat treatment is also similar to the curve obtained after quenching from the higher temperatures, but the fall from the maximum is not so pronounced as with alloys annealed at the higher temperatures. In fact, the values of the α -parameters are nearly constant for alloys in the range of composition from about 10 to 30 atomic per cent. nickel.

When the alloys are cooled comparatively slowly from 400° C. to room-temperature after annealing at this temperature for 132 hours, the γ -parameter-composition curve is much modified. It now follows the course DHG; the parameter values do not show the wide variation shown after the previous treatment. The α -curve is only slightly modified, and the parameter values are not far removed from those previously obtained—the α -curve PST replaces the α -curve PQR. The slower rate of cooling has thus had the effect of flattening out the γ -curve and has had but little effect on the α -curve. The variation in the α -parameter over the range of composition from about 10 to 30 atomic per cent. nickel is almost within the error of measurement.

* Not all the alloys were given these treatments.

FIG. 6.



Spectra obtained with alloy, containing 41.5 atomic per cent. nickel, after annealing at 350° C. 1 and 2 are fibre and focusing camera films after 89 days' annealing; 3 and 4 after 186 days' annealing.

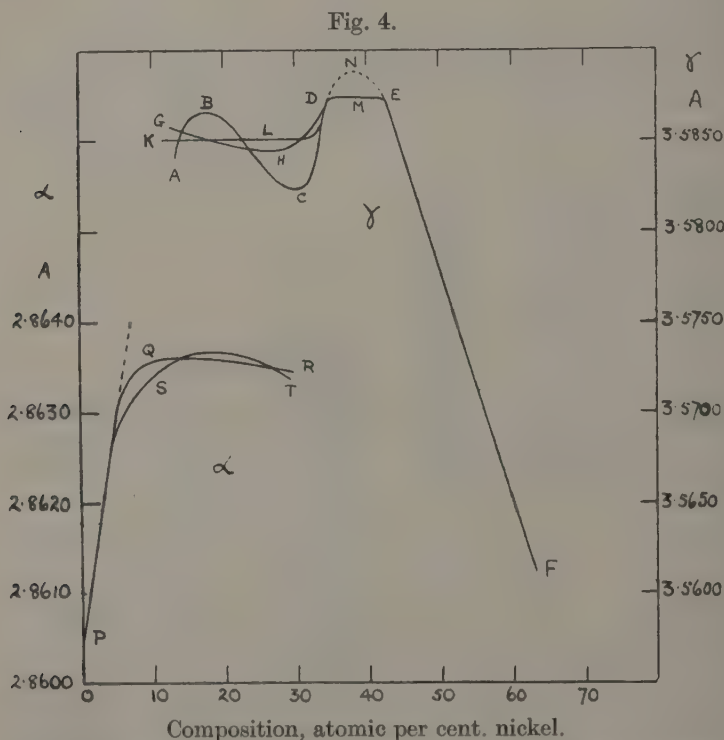
TABLE VII.

Parameters of α - and γ -phases in Alloys after Heat Treatment at 400° C.

Composition of alloy (atomic per cent. nickel).	Parameter (A.) at 15° C.				
	α -phase.		γ -phase.		
	132 hrs. at 400° C. and quenched.	132 hrs. at 400° C., cooled over 96 hrs.	132 hrs. at 400° C. and quenched.	132 hrs. at 400° C. cooled over 96 hrs.	260 hrs. at 400° C. and quenched.
2.12	2.8615 ₉	—	—	—	—
2.96	2.8622 ₁	2.8620 ₆	—	—	—
5.73	2.8630 ₇	2.8630 ₉	—	—	—
8.56	2.8634 ₈	2.8632 ₈	—	—	—
9.55	2.8636 ₀	2.8632 ₉	—	—	—
12.16	2.8635 ₈	2.8633 ₅	—	—	—
12.84	2.8636 ₂	2.8634 ₇	3.5841 ₄	—	—
14.01	2.8634 ₃	2.8636 ₂	3.5851 ₁	—	—
15.05	2.8635 ₀	2.8636 ₂	3.5840 ₂	—	—
15.98	2.8636 ₀	2.8635 ₆	3.5865 ₁	3.5852 ₈	3.5850 ₀
20.32	2.8637 ₃	2.8637 ₂	3.5857 ₂	3.5848 ₈	3.5848 ₃
23.32	2.8633 ₉	2.8636 ₃	3.5853 ₈	3.5849 ₇	3.5854 ₀
27.12	2.8634 ₂	2.8634 ₇	3.5831 ₃	3.5843 ₈	—
29.25	—	—	3.5821 ₉	3.5847 ₇	—
30.60	—	—	3.5823 ₄	5.5846 ₂	3.5848 ₁
31.13	—	—	3.5820 ₈	—	—
32.29	—	—	3.5829 ₂	—	—
32.48	—	—	3.5832 ₀	3.5855 ₂	3.5864 ₃
33.07	—	—	3.5841 ₇	—	—
33.34	—	—	3.5865 ₇	—	—
33.97	—	—	3.5859 ₂	3.5863 ₄	3.5868 ₉
36.01	—	—	3.5873 ₃	3.5879 ₀	3.5864 ₃
37.24	—	—	3.5873 ₅	3.5875 ₈	3.5871 ₅
39.46	—	—	3.5873 ₉	—	3.5873 ₉
41.50	—	—	3.5873 ₀	3.5878 ₁	3.5873 ₀
44.26	—	—	3.5858 ₇	3.5852 ₆	3.5848 ₁
50.90	—	—	3.5775 ₂	—	3.5769 ₉
57.19	—	—	3.5690 ₀	3.5691 ₀	—

The effect of a longer initial period of annealing before quenching—260 hrs. instead of 132 hrs.—is to produce greater constancy in the values

of the γ -parameter. In fact, the values are constant within error of measurement and are represented by the curve KLD in fig. 4. The corresponding α -curve was not determined, but on comparison with the curves obtained at 500° C., the α -parameter will also have a constant value over this range of composition, the estimated value being 2.8635₆ A. This value places the α -boundary at about 6.5 atomic per cent. nickel. The parameter-composition curve is linear in the pure α -phase. This has been found to be so after all the heat treatments to which the pure α -alloys were subjected.



Relations between parameter and composition for α - and γ -phases in alloys after heat treatment at 400° C.

The γ -precision lines for the alloys were rather diffuse and in consequence difficult to measure, particularly for alloys containing less than 25 atomic per cent. nickel. The limit of accuracy in these parameter measurements is about ± 0.0005 A. In some spectra the lines were sharp and well resolved, and these yielded more accurate values; this occurred in spectra of those alloys whose parameter values followed the

standard parameter-composition curve for pure γ -phase alloys, namely, those alloys between 33 and 35 and beyond about 42 atomic per cent. nickel.

The two-phase region at this temperature (400°C.) was found in the previous investigation to extend to about 42 atomic per cent. nickel. Beyond this boundary the alloys are in the pure γ -phase, and their parameter values follow the pure γ -phase parameter-composition curve. This is so beyond about 42 atomic per cent. nickel at 400°C. , and the fact that the present curve joins up with the pure phase curve at this composition lends support to the previous determination of the boundary of the two-phase region at this temperature.

Since the γ -parameters of alloys between 33 and 35 atomic per cent. nickel follow the pure γ -phase parameter-composition curve, the γ -parameter assumes the same value in the presence of the α -constituent as it had when the alloy consisted of γ -phase alone.

As with alloys heat treated at 500°C. , there is an interchange between the two constituents α and γ also at 400°C. , although, perhaps, this is not so obvious as it is at the higher annealing temperature.

The alloys submitted to these treatments at 400°C. are probably not in the equilibrium state; they should be annealed for longer periods and submitted to a slower rate of cooling to room-temperature.

One definite result that has emerged from the work already done on alloys annealed at 400°C. , is that the γ -lattice has a constant parameter value of 3.5874 Å. for alloys containing between about 35 and 42 atomic per cent. nickel, that is, between the limbs of the pure γ -parameter-composition curve at this parameter value; also 42 atomic per cent. nickel agrees with the position of the $(\alpha+\gamma)-\gamma$ boundary at 400°C. as previously determined. The parameter values for nickel content higher than 42 atomic per cent. obtained with alloys annealed at 400°C. , agree with the values obtained for the same alloys quenched after annealing at temperatures between 500°C. and 800°C. This is so both for the quenched and the slowly cooled alloys. Thus the slow cooling process has not resulted in a state of equilibrium corresponding to a temperature lower than 400°C. ; from this it is concluded that in the two-phase region the transfer of atoms between the α - and γ -structure is small during the time of cooling allowed.

(ii.) *Heat Treatments at 350°C.*

A set of samples was annealed in a thermostatically controlled furnace for 89 days at 350°C. and quenched. A few samples were also annealed for 186 days at the same temperature and quenched. The α - and γ -parameters are given in Table VIII.

The definition of the α -lines in the focusing camera was good for pure

phase alloys, but in the two-phase region the doublets, although resolved, were rather diffuse. For alloys with nickel content greater than 30 atomic per cent., the α -lines were faint, and for this reason the accuracy of

TABLE VIII.

Parameters of α - and γ -phases in Alloys after Heat Treatment at 350° C.

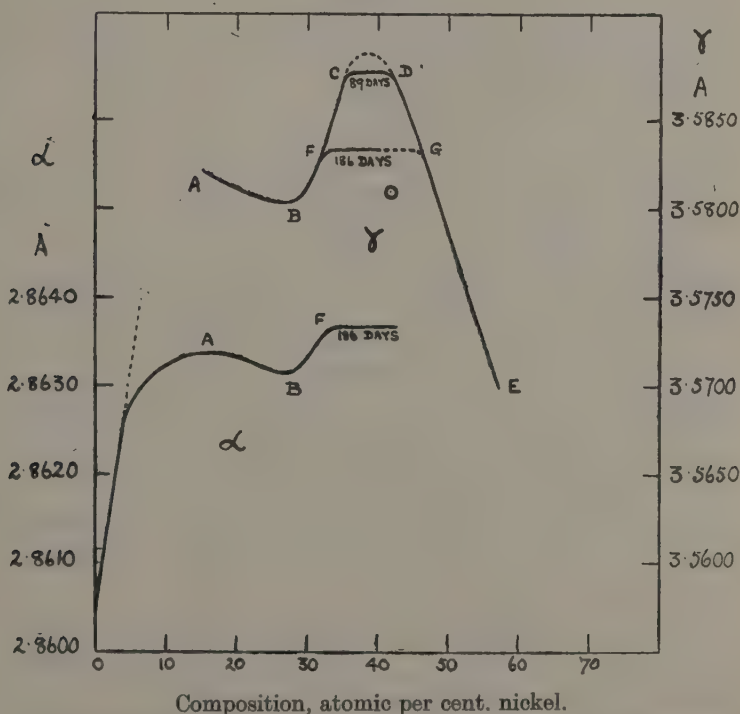
Composition of alloy (atomic per cent. nickel).	Parameter (A.) at 15° C.			
	α -phase.		γ -phase.	
	89 days at 350° and quenched.	186 days at 350° and quenched.	89 days at 350° and quenched.	186 days at 350° C. and quenched.
2.96	—	2.8621 ₄	—	—
5.73	—	2.8630 ₉	—	—
8.56	2.8631 ₆	—	—	—
12.16	2.8632 ₃	—	—	—
14.01	2.8633 ₄	—	—	—
15.98	2.8633 ₇	—	3.5819 ₆	—
20.32	2.8632 ₅	—	3.5810 ₄	—
23.32	2.8632 ₈	—	3.5806 ₂	—
27.12	2.8631 ₃	—	3.5805 ₀	—
30.60	2.8633 ₈	—	3.5820 ₀	—
32.48	—	2.8636 ₀	—	—
33.97	2.8637 ₄	—	{ 3.5852 ₅ 3.5832 ₂	—
36.01	—	—	3.5877 ₈	3.5835 ₇
37.24	—	—	3.5878 ₂	3.5835 ₂
39.46	—	—	—	3.5832 ₂
41.50	—	2.8635 ₉	3.5875 ₄	3.5810 ₈
44.26	—	—	3.5832 ₃	—
46.74	—	—	{ 3.5823 ₆ 3.5822 ₃	—
50.90	—	—	3.5777 ₃	—

parameter measurement for these alloys is less than for alloys with lower nickel content. The run of the parameter values is seen clearly in the graph in fig. 5. The α -parameter increases approximately linearly with atomic composition for low nickel content; at about 4 atomic per cent. nickel it departs from the linear course and reaches a maximum at about 15 atomic per cent., falling to a minimum value at

about 27 atomic per cent. before rising again to a higher value at about 33 atomic per cent., afterwards remaining steady at a value of about 2.8636, for alloys annealed for 186 days. Before discussing the shape of this part of the α -curve, the γ -parameters will be considered.

After 89 days' annealing, the γ -phase parameters followed the curve ABCDE. As the nickel content increases beyond 15 atomic per cent. the γ -parameter decreases, reaching a minimum value at about 27 atomic

Fig. 5.



Relations between parameter and composition for α and γ -phases in alloys after heat treatment at 350° C.

per cent. nickel; it then increases and follows the curve for quenched pure γ -alloys, but the parameter value does not reach the maximum of the standard curve. Between C and D its value is about 3.5877 A., and it remains constant between about 35 and 42 atomic per cent. nickel; beyond the latter nickel content, the parameter follows the curve for pure γ -alloys. The lines in the precision spectra were badly defined for alloys with nickel content less than about 35 atomic per cent. nickel,

but for alloys with higher nickel content they were better defined and well resolved.

Alloys containing 36.01, 37.24, and 39.46 atomic per cent. nickel which yielded good spectral lines after 89 days' annealing followed by quenching, gave poor lines and much lower γ -parameter values after 186 days' annealing and quenching; the γ -phase therefore contains more nickel after this treatment than it did after the first treatment. Another alloy containing 41.50 atomic per cent. nickel yielded a still lower parameter value. It was noticed that the proportion of the α -constituent present in these alloys was much greater after the longer period of annealing. This was marked in the case of the 41.50 per cent. alloy, which also showed the biggest parameter change.

After 89 days' annealing the α -constituent could only be detected by the line from the (110) plane, the other reflexions being too faint to observe. After 186 days, however, all the reflexions were clearly visible. The α -structure, judged by the sharpness of the spectral lines, was in every case in good equilibrium, but not so the γ -structure.

The above effects are clearly seen in the spectra of alloy 41.50 per cent. nickel shown in Pl. VII. fig. 6. Here no. 1 shows the full spectrum of the phases in the alloy after annealing for 89 days at 350° C. and quenching. The γ -lines are intense and well defined, but the α -lines are weak, only line 2 being visible. No. 3 shows the spectrum of the same alloy after 186 days at 350° C. and quenching. The γ -lines are still prominent, but the intensity of the α -lines has greatly increased. Now all the α -lines are visible and the 10 doublet is sharp and well defined. A closer examination of the 12 doublet of the γ -spectrum with the focusing camera shows that whereas the doublet is well defined after the first heat treatment (Pl. VII. fig. 6, no. 2), it is very indefinite after the 186 days' treatment Pl. VII. fig. 6, no. 4).

It is to be noted that the process of phase formation is different for alloys with nickel content less than about 25 atomic per cent. nickel from what it is for alloys with higher nickel content. It will be recalled that the initial treatment of the alloys in ingot form was to quench them from high temperatures. After this treatment alloys with less than 25 atomic per cent. nickel will be in the distorted α_2 -state; between 25 and about 35 atomic per cent. they consist of a mixture of the distorted α_2 - and γ -structures, and at higher nickel content they consist entirely of the γ -structure. The alloy to which the spectra in fig. 6 refer, falls in the pure γ -range, so that during prolonged annealing the α -structure is being gradually developed. After 89 days very little of the α -constituent has been formed and the γ is practically free from distortion, but not as free as the original specimen before annealing. As the period of annealing is lengthened more α -structure is produced, and from the sharpness of the

lines in its spectrum it is undistorted, even the 10 doublet being well resolved. The γ -component, however, has now become distorted and, from, the value of its parameter, it has become richer in nickel; this transfer of iron makes possible the formation of the α -phase, which is rich in iron. Hence as more α -structure is formed, the distortion in the γ -structure becomes more pronounced whilst the α -structure is free from distortion. This is true for quenched specimens. It is necessary to carry the investigation further with specimens which have received the same annealing treatments, but which have been slowly cooled from 350° C. to atmospheric temperature. The work up to this stage shows definitely that at these high nickel contents α -structure is formed at comparatively low temperatures, so that the $(\alpha+\gamma)-\gamma$ boundary moves towards the nickel end of the equilibrium diagram as indicated in our previous communication⁽¹⁾.

Reference was made to the low value of the γ -parameter in alloy 41.50; it differed from the other alloys in that the decrease in parameter was greater than in the other alloys after the same annealing treatment. It is likely that this anomalous behaviour is to be attributed to the fact that the phase boundary crosses the magnetic transformation curve at a composition very near to that of the alloy. There is no doubt that the magnetic properties of these alloys play an important part in their behaviour under different heat treatments.

Another point to mention concerning the curves in fig. 5 is the parallel behaviour of the two phases; the variation of the parameter of the α -phase with composition is reflected in that of the parameter of the γ -phase, and is similar to that observed with alloys quenched after annealing at other temperatures. The correspondence is more clearly shown at 350° C. than at the higher temperatures, because the parameter of the α -phase can be measured over a greater range of composition.

It is also obvious from the spectra that the alloys have not reached their final state of equilibrium and that they will have to be submitted to further heat treatment.

(iii.) *Consideration of Parameter Measurements at 400° C. and 350° C.*

The α -phase parameter yielded values which increased linearly with composition in the pure phase region. The precision lines were easily measured, although they were never quite sharp; the definition was observed to deteriorate as the nickel content increased. The γ -phase alloys never appeared to be in a true state of equilibrium even after the longest annealing periods. A tendency for the parameter values to become constant at different compositions was, however, noticed as the period of annealing was increased.

Judging by the quality of the spectral lines, the α -structure is more easily brought to a state of equilibrium than the γ -structure. This is due in part to the difference in the slopes of the α - and γ -boundaries over this range of temperature.

When alloys with nickel content greater than about 35 atomic per cent., which initially consisted of the pure γ -phase, are annealed at temperatures at which they are in the two-phase region, iron atoms are removed from regions or nuclei throughout the material leaving a γ -structure which is nearer to the equilibrium composition at the chosen annealing temperature than that of the original pure γ -structure. The iron unites with nickel to form α -structure of the equilibrium composition for the temperature of annealing; it readily finds enough nickel atoms to form the appropriate equilibrium α -composition, and after a short period of annealing the α -structure appears to have reached its final state of equilibrium. As the annealing proceeds more iron is liberated, and more α -structure is formed. The α -structure always appears to be in a state of equilibrium, and it may be inferred from this that fresh regions are continuously being produced which readily reach the required equilibrium composition. Thus the material consists of a large number of nuclei of α -structure, the nuclei consisting of fine grains which scatter the incident radiation yielding lines which show a slightly diffuse outline, even though the α -structure may be in a state of equilibrium judged by the complete resolution of the doublets at large angles of reflexion.

The γ -structure, on the other hand, is in the initial stage practically free from distortion, but as the annealing proceeds it becomes more distorted, the amount of distortion increasing as the time of annealing is prolonged. The γ -structure adjusts itself with difficulty to the equilibrium composition; the spectral lines become diffuse, so that either the γ -structure is in a continuous state of transition—a condition that would exist if the material had not reached its final state of equilibrium,—or the nuclei of the γ -phase are even smaller than those of the α -component, thus giving rise to more pronounced particle scattering.

These results are well illustrated by the results obtained after annealing at 350° C. The α -lattice was present in alloy 37.24 after 28 days' annealing, but the γ -lattice had not appreciably changed its dimensions. After 89 days' annealing the α -lines had slightly increased in intensity, but were still weak, and the γ -lattice yielded approximately the same parameter as it had when the alloy was in the pure γ -state after quenching, but the lines were not so well defined, although the 12 doublet was well resolved. After 186 days' annealing, more α -structure had been formed, the spectral lines from which were well resolved at large glancing angles, but now show a certain amount of diffuseness. Accompanying the formation of the α -structure was a change in the γ -lattice; a doublet

that was initially well resolved, appeared after the last annealing treatment as a wide badly defined band, which yielded a parameter value much lower than that observed after the other shorter annealing periods.

For compositions below 25 atomic per cent. nickel the alloys are initially in the distorted α_2 -condition; the structure is homogeneous throughout, being a supersaturated solid solution of nickel in iron. When annealed, nickel is precipitated, leaving regions or nuclei in the material which are less rich in nickel and of the proper composition to produce α -structure in equilibrium at the temperature of annealing. The nickel dissolves the amount of iron required to produce the γ -structure of the equilibrium composition at the temperature of annealing. It again appears that the α -structure reaches its state of equilibrium much more readily than the γ -structure. In fact, the γ -structure formed in this transformation from the distorted α_2 -condition, was never found in a state in which doublets at high angles yielded sharp and well-resolved lines.

The α -structure probably reaches its equilibrium state rather readily, because only a small amount of nickel is required to produce the saturated alloy and the maximum solubility of nickel in iron, at these low temperatures, does not vary much with change in temperature. The γ -structure, on the other hand, requires high percentages of both iron and nickel to produce saturation, and the concentrations necessary are, at low temperatures, difficult to obtain because of the sluggish migration of atoms from one region to another. Also the saturation composition varies rapidly with change of temperature so that it is necessary to keep the temperature of annealing constant and to effect a rapid quench.

6. Summary.

A summary of the results obtained with alloys quenched from temperatures between 500° C. and 800° C. is contained at the end of Section 2 of the paper.

Measurements were made to determine the lattice parameters of the constituents of alloys in the two-phase region. The alloys were subjected to different heat treatments after annealing at 500° C., 400° C., and 350° C. respectively. The curves showing the relation between composition and parameter of both α - and γ -components are of different shapes according to the manner in which the heat treatments are carried out. On the interpretation of these curves suggested in the paper, it is possible to so vary the heat treatment as to make nickel atoms to migrate either from the α - to the γ -structure or from the γ - to the α -structure, and the measurements enable this migration of atoms to be studied in some detail for an annealing temperature of 500° C. Useful information in this connexion is also supplied by the alloys annealed at 400° C. and 350° C. The results point to the formation of nuclei of α -phase alloy

which are small enough in the initial stages to cause particle scattering of the incident radiation, but this component of the two-phase alloy appears to be in a state of equilibrium corresponding to the temperature of annealing. The γ -phase, on the other hand, either does not reach its final state of equilibrium during the heat treatments to which the alloys were subjected, or it exists in the form of nuclei which are even smaller than the α -nuclei. The investigation is of a preliminary nature.

References.

- (1) E. A. Owen and A. H. Sully, *Phil. Mag.* ser. 7, xxvii. p. 614 (1939).
- (2) E. A. Owen, E. L. Yates, and A. H. Sully, *Proc. Phys. Soc.* xlix. p. 315 (1937).
- (3) G. Phragmen, *J. Iron Steel Inst.* cxxiii. p. 465 (1931).
- (4) E. R. Jette and F. Foote, 'Metals Technology,' iii. (1936), *Tech. Publ.* no. 670.
- (5) A. J. Bradley, A. H. Jay, and A. Taylor, *Phil. Mag.* ser. 7, xxiii. p. 545 (1937).

XXXII. On the Measurement of Particle Size by the X-Ray Method.

By A. TAYLOR, Ph.D., F.Inst.P.*

[Received August 16, 1940.]

The Diffraction Broadening.

IT was shown by P. Scherrer ⁽¹⁾ that when monochromatic X-rays of wave-length λ fall on a randomly oriented mass of crystals, the diffraction maxima become broadened when the particle size is very small. The angular broadening β at the half-peak value was given by the expression

$$\beta = \frac{K\lambda}{\epsilon \cos \theta} \dots \dots \dots (1)$$

ϵ is the linear dimension of the particle normal to the diffracting planes, θ is the Bragg angle, and K is a constant. Different methods of obtaining equation (1) lead to different values of the constant K . This has been fully discussed in a recent set of papers by A. L. Patterson ⁽²⁾. The effect of particle shape on K is also considered. The half-peak width β can be

defined as an integral breadth $\frac{\int I dx^{(3)}}{I_{max}}$, or as a direct measure in radians

(Scherrer, *loc. cit.*). A suitable value of K must be chosen to conform with the choice of definition; it is, however, of the order of unity.

Unfortunately, equation (1) cannot be used directly because it is true only for the idealised case of diffraction broadening by a point specimen. The geometry of the X-ray camera, the size and absorption factor of the specimen, and the divergence of the X-ray beam all influence the width of the spectrum line to produce a halo of width B from which β has to be derived. Probably far greater errors have arisen from the derivation of β than from an incorrect value of K . Scherrer gives the following simple definition of the broadening

$$\beta_{Scherrer} = B - b, \dots \dots \dots (2)$$

b being the diameter of the specimen. This would only be true for a perfectly transparent specimen irradiated by parallel monochromatic radiation. In actual practice b is not assumed to be constant but is measured for a line corresponding to infinite particle size in the exact

* Communicated by the Author.

position of the broadened diffraction maximum. Because the base of a broadened line receives its main contribution from the smallest crystallites in the aggregate, a direct measurement of the half-width diminishes their contribution to the line. For this reason the Laue definition of line width is to be preferred.

B. E. Warren and J. Biscoe ⁽⁴⁾ state that the Scherrer definition of β is wrong and propose, without proof, the alternative relation

$$\beta_{\text{Warren}} = \sqrt{B^2 - b^2} \quad \dots \dots \dots (3)$$

Since B is greater than b it would seem that this relationship would put undue emphasis on B and thus tend to give a low result for the mean particle size.

F. W. Jones ⁽⁵⁾ has developed a most interesting manner of approach in which a mixture method is used. Lines whose breadth depend on the particle size to be measured as well as the experimental conditions are termed m -lines. The calibration lines from particles greater than 1000 Å whose finite breadths depend entirely on the experimental conditions are termed s -lines. The integral definition of line width is used throughout.

The s -line is expressed by the function $I_s(x) = I_{s(\text{max})} f(x)$. Each element of area of width dx of the s -line is broadened by diffraction into a line of equal area but with a shape function $I_d = I_{d(\text{max})} F(kx)$. These new broadened elements build up the shape of the broad diffraction maximum produced by the small crystallites. One can then obtain the following expressions:—

$$\frac{\text{True diffraction breadth}}{\text{Observed breadth of } m\text{-line}} = \frac{\beta}{B} = \frac{\int F(kx)f(x) dx}{\int f(x) dx} \quad \dots \dots (4)$$

$$\frac{\text{Breadth of } s\text{-line}}{\text{Observed breadth of } m\text{-line}} = \frac{b}{B} = \frac{\int F(kx)f(x) dx}{\int F(kx) dx} \quad \dots \dots (5)$$

The parameter k is a function of the particle size. $f(x)$ is determined experimentally, but intensity distributions have to be assumed to obtain $F(kx)$.

Laue assumes

$$F(kx) = e^{-k^2 x^2} \quad \dots \dots \dots (6)$$

and

$$F(kx) = \frac{1}{1 + k^2 x^2} \quad \dots \dots \dots (7)$$

The function of Bragg ⁽⁶⁾

$$F(kx) = \frac{\sin^2 kx}{(kx)^2} \quad \dots \dots \dots (8)$$

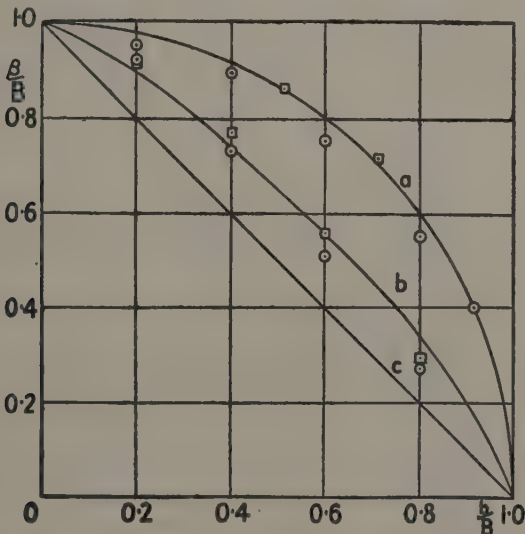
gives almost exactly the same result as (6).

Equations (4), (5), and (6) lead to curve (a) in fig. 1, whilst (4), (5), and (7) yield curve (b). The Scherrer definition, equation (2), yields the straight line (c). In order to use the Jones curves the ratio $\frac{b}{B}$ is first calculated and the graph used to find $\frac{\beta}{B}$. Then the value of β is easily

obtained as

$$\beta = \left(\frac{\beta}{B} \right) \times B.$$

Fig. 1.



Jones's type of correction curve for experimental conditions, but derived theoretically. The circles are points taken at convenient intervals from Jones's actual curves, the squares are calculated from data obtained from Ceylon graphite.

○ Jones's molybdenum.

□ Graphite.

a. Warren circle $\beta = \sqrt{B^2 - b^2}$.

b. Arbitrary curve $\frac{\beta}{B} = \sqrt{\frac{\beta_{\text{Scherrer}}}{B} \cdot \frac{\beta_{\text{Warren}}}{B}}$.

c. Scherrer line $\beta = B - b$.

Derivation of the Warren Expression of β .

We can rewrite equation (3) in the form

$$\left(\frac{\beta_{\text{Warren}}}{B} \right)^2 + \left(\frac{b}{B} \right)^2 = 1. \quad \dots \dots \dots (8)$$

This is clearly the equation of a circle using the coordinates $\left(\frac{\beta}{B}, \frac{b}{B}\right)$.

Now when a diffraction peak corresponding to particles of infinite size is microphotometered, the shape obtained can be closely matched by a curve

$$I_s(x) = I_{s(\max)} e^{-a^2 x^2}, \quad \dots \dots \dots (9)$$

i. e.,

$$f(x) = e^{-a^2 x^2}. \quad \dots \dots \dots (9a)$$

Using equation (9a) in equations (4) and (5) with the function (6) we obtain

$$\frac{\beta}{B} = \frac{\int e^{-(a^2 + k^2)x^2} dx}{\int e^{-a^2 x^2} dx} = \frac{\sqrt{\frac{\pi}{a^2 + k^2}}}{\sqrt{\frac{\pi}{a^2}}} = \sqrt{\frac{a^2}{a^2 + k^2}},$$

$$\frac{b}{B} = \frac{\int e^{-(a^2 + k^2)x^2} dx}{\int e^{-k^2 x^2} dx} = \sqrt{\frac{k^2}{a^2 + k^2}},$$

whence on squaring and adding

$$\left(\frac{\beta}{B}\right)^2 + \left(\frac{b}{B}\right)^2 = 1.$$

Thus, by the use of a reasonable expression (9) for the shape of an *s*-line, we can obtain the Warren expression for β given in equation (3). A careful examination of the curve obtained by Jones, who used molybdenum as a standard in his work on colloidal gold, shows it to be almost identical with the Warren circle. The author has made similar calculations on the spectra of Ceylon graphite using the function (6), and also obtains close agreement with the Warren circle. Using equation (7) the graphite results agree closely with those from molybdenum, which yield curve (b). This agreement is all the more remarkable when one considers the great difference in the absorption factors of the specimens and the different experimental conditions generally.

It seems from the above that the Warren definition of β , which we now see to be based on equation (6), is to be preferred to the quite arbitrary definition given originally by Scherrer. Jones, however, was able to demonstrate that equation (7) leading to curve (b) gave the best results for colloidal gold, and the reason is probably connected with the rôle played by the size distribution function which has not been considered in the above discussion.

If we let

$$\frac{\beta}{B} = \sqrt{\frac{\beta_{\text{Warren}}}{B} \cdot \frac{\beta_{\text{Scherrer}}}{B}}, \quad \dots \dots \dots (10)$$

a curve can be obtained which is not very different from (b) using the function (7). This arbitrary mean between the two extreme functions seems to take into account the size distribution factor to some extent. The accuracy of determining a particle shape and size is such that it does not warrant the elaborate calculation involved in the Jones method. It is quite good enough to use for the integral half-peak width,

$$\beta = \sqrt{\beta_{\text{Warren}} \cdot \beta_{\text{Scherrer}}}$$

$$= \{\sqrt{B^2 - b^2} \cdot (B - b)\}^{\frac{1}{2}} \quad . \quad . \quad . \quad . \quad . \quad (11)$$

The mixture method or the method advocated by the author⁽⁷⁾ for the measurement of b can be used. The value of β can then be obtained from the simplified Jones curve described above, namely, the curve which gives $\frac{\beta}{B}$ as the root mean between the Scherrer straight line and the Warren circle.

The Effect of Nuclear Growth.

The X-ray measurements give some idea of the average crystallite size, but usually give no information whatever of the particle size distribution. Under normal conditions the size of Debye-Scherrer camera should in no way influence the size computation, cameras of large radii merely leading to excessive exposure times. A 9 cm. diameter Debye-Scherrer camera is a convenient size to use with a specimen diameter up to 0.5 mm. Special circumstances may arise in which a much larger camera (*i. e.*, 19 cm. diameter) has to be employed. As a rule, the smaller size is to be preferred for measurements below 30 Å., while above this the larger camera is preferable.

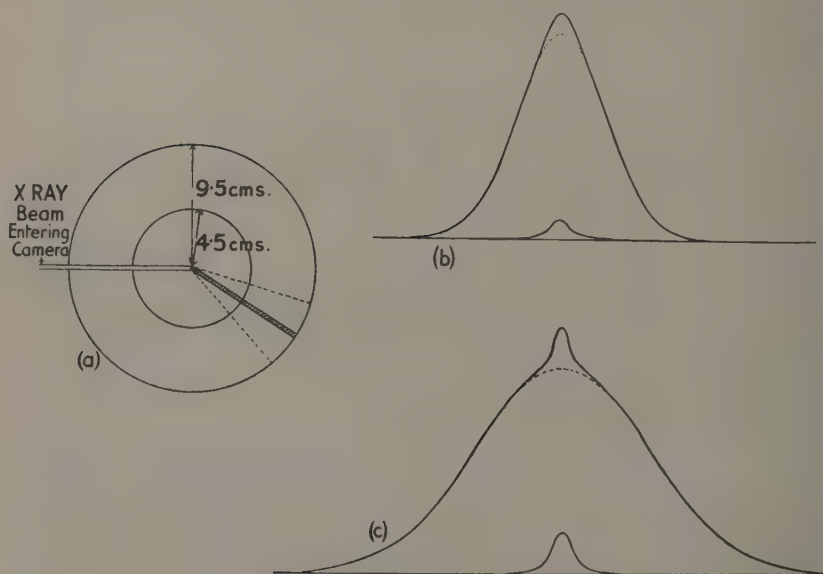
A very special circumstance is described below in which the anomalous growth of the crystallites lead to an abnormal distribution of particle sizes and make necessary the use of the larger camera. It is well known that a crystal which is below a critical size will not grow below a certain temperature. We can imagine an aggregate of crystallites of very small particle sizes heated to a given temperature. Let us suppose that a very small fraction have a magnitude greater than the critical size so that they can grow partly by diffusion and partly by capture of molecules from the vapour. After a certain time the aggregate may consist of two discrete groups of sizes, the first being very little different from the original distribution, the second being composed of particles bigger than 1000 Å., these latter being considered as of infinite size.

If now a Debye-Scherrer photograph of the material were taken, the result would be that of a broad spectrum line of breadth B and a sharp line corresponding to particles of infinite size of breadth b . No allowance is being made for a possible variation of lattice parameter with crystallite

size. If the camera is small, B and b may not be very different and the two peaks will blend together. On the other hand, if a large camera is used, b in mm. remains almost unchanged because the slit system is designed to keep the s -lines sharp, but the spread of B in mm. is increased just over two-fold (fig. 2). Moreover, the ratio of the integrated intensities of the s - and m -lines must be constant, and so there is an actual gain in contrast of the s -lines.

The result is that whereas nothing abnormal is detected in the small camera picture, the larger camera immediately shows up the presence of infinite particles and reveals the true nature of the growth of the crystallites. Since with the small camera the undetected s -line adds

Fig. 2.



- (a) Illustrative of how the line width of an s -line is little affected by increasing the size of X-ray camera from 9 cm. to 19 cm. diameter. The m -line is, however, more than doubled in linear dimension on the film wrapped round the periphery of the camera. This increase in resolving power shows the dual nature of the peak resulting from a mixture of particles ≈ 15 A., and $\gg 1000$ A. Note the increase in peak height of s -line in (c) in order to maintain correct ratio of line intensities, but the linear half-peak width is the same as in (b).
- (b) Line contour from small Debye Scherrer camera. Dotted line gives true peak of m -line. Effect of the superimposed s -line not observed.
- (c) Line contour from large camera. Dotted line gives true peak of m -line. The effect of the superimposed s -line now easily observed.

height to the composite peak but very little to the area, the value of $\int I dx / I_{\max}$ can become absurdly low, and the resulting high value of the crystallite size would give a totally erroneous idea of the true state of affairs.

Calculation of the Error for a Mixed Specimen.

We wish to find the order of error involved if the small camera is used and a fraction x of the total sample is bigger than 1000 Å., the remainder being almost entirely unchanged.

Let there be n_i particles of size ϵ_i among the aggregate, each scattering a portion I_i of the total intensity. The group ϵ_i thus contributes $n_i I_i$ to the line, so that the total intensity

$$I = \sum_0^{\infty} n_i I_i. \quad (12)$$

If this group of sizes ϵ_i is a fraction x of the total amount of scattering material, then they will also contribute a fraction x of the total intensity, i. e.,

$$xI = n_i I_i. \quad (13)$$

Each group of particles ϵ_i give a line of height h_i and a total half-peak width

$$B_i = \frac{\int I_x dx}{I_{\max}} = \frac{I_i}{h_i}. \quad (14)$$

The mean half-peak width when all the groups scatter is

$$\bar{B} = \frac{\sum n_i I_i}{\sum n_i h_i} = \frac{\sum x I}{\sum n_i h_i} = \frac{I}{\sum n_i h_i}. \quad (15)$$

From (13), (14), and (15) we get

$$\bar{B} = \frac{I}{\sum \frac{n_i I_i}{B_i}} = \frac{I}{\sum \frac{x I}{B_i}} = \frac{1}{\sum \frac{x}{B_i}}. \quad (16)$$

or

$$\frac{1}{\bar{B}} = \sum \frac{x}{B_i}.$$

If now a fraction x of the whole is bigger than 1000 Å. in size and gives a line of width b and $(1-x)$ give a line of width B , then, if the peaks overlap exactly, (16) becomes

$$\frac{1}{\bar{B}} = \frac{x}{b} + \frac{1-x}{B}, \quad (17)$$

\bar{B} corresponds to the erroneous particle size $\bar{\epsilon}$ which we calculate. For

A simple relationship is shown to exist between the Jones method of determining the line broadening and the definition of Warren, which is $\beta_{\text{Warren}} = \sqrt{B^2 - b^2}$, the latter replacing the Scherrer definition $\beta_{\text{Scherrer}} = B - b$, which Warren asserts is incorrect. The intermediate value $\beta = \sqrt{\beta_{\text{Scherrer}} \beta_{\text{Warren}}}$ is not very different from that using the Jones curve from a molybdenum calibration specimen for the particle size of colloidal gold, nor from that of the author for graphite. Thus the need for carrying out a lengthy series of graphical integrations to obtain a Jones curve no longer seems to be required.

It is also shown how a sudden onset of growth in a small fraction of the crystallites in the specimen leads to extremely high values of the particle size. In order to interpret the result correctly as a real growth of the entire specimen or as merely the increase in percentage of the portion greater than 1000 Å. in size, the use of a large (19 cm. diameter) Debye-Scherrer camera is shown to be essential. An approximate relationship between the apparent fractional increase in particle size and the weight fraction of the specimen greater than 1000 Å. is given. An anomaly in the growth of carbon crystallites from heat-treated cellulose is cited as a specific example.

References.

- (1) Scherrer, P., Zsigmondy, 'Kolloidchemie,' 3rd ed., p. 387 (1920).
- (2) Patterson, A. L., Phys. Rev. lvi. p. 972 (1939) ; lvi. p. 978 (1939).
- (3) von Laue, M., Zeits. Krist. A, xcix. p. 448 (1926).
- (4) Warren, B. E., & Biscoe, J., Journ. Am. Ceramic. Soc. xxi. p. 49 (1938).
- (5) Jones, F. W., Proc. Roy. Soc. A, clxvi. p. 16 (1938).
- (6) Bragg, W. L., 'The Crystalline State,' i. p. 189 (1933).
- (7) Blayden, H. E., Riley, H. L., and Taylor, A., J. Chem. Soc. p. 67 (1939).
- (8) Blayden, H. E., Riley, H. L., and Taylor, A., Journ. Am. Chem. Soc. lxii. p. 180 (1940).

XXXIII. *Notices respecting New Books.*

Physical Chemistry. An Introduction. By Dr. E. A. MOELWYN-HUGHES.
[Pp. viii + 660.] (Cambridge University Press, 1940. Price 45s. net.)

THE scope and content of physical chemistry have changed in one generation out of all recognition, and the boundaries between the subjects of physics and chemistry are rapidly becoming obliterated.

Dr. Moelwyn-Hughes's massive and masterly treatise admirably demonstrates this changed aspect of physical chemistry. Its pages are grouped into two sections—Part I. dealing with general principles, Part II. with applications. The first part is concerned with the experimental and mathematical foundations of the kinetic-molecular theory and of the quantum theory, with the chemical elements and with the principles of thermodynamics as applied to chemistry. The second part is devoted to applications of the principles to various simple systems—to monatomic, diatomic and triatomic molecules, to equilibria and kinetics in the homogeneous gas phase and to crystal chemistry;

Throughout the treatment the author rightly lays stress on experiment: "facts come first," and facts are found in the laboratory. A very refreshing feature of the book is the appearance, on almost every page—certainly on every third or fourth page—of very full tables of experimental data which are, for the most part, carefully and critically selected from original sources. and theoretical deductions are always viewed and reviewed in the light of the facts which these figures supply.

The author is to be congratulated also on his selection of subjects for discussion—the day is long past when a detailed survey of the field of physical chemistry could be compressed within the covers of one volume—on his admirably clear treatment of the topics chosen, and above all on his emphatic insistence that physical chemistry is, first of all, an experimental science.

The book is a very welcome addition to the literature of the subject. A. F.

An Introduction to the Theory of Newtonian Attraction. By A. S. RAMSEY.
[Pp. ix + 184.] (Cambridge University Press, 1940. Price 10s. 6d. net.)

MR. RAMSEY has rounded off his very valuable series of text-books on Dynamics, Statics, Hydrostatics, and Electricity and Magnetism by this treatise on Newtonian Attraction. The book covers familiar ground with the clarity and thoroughness which were to be expected from a teacher of Mr. Ramsey's experience and reputation.

The mathematical knowledge expected of a student who is taking the subject to the standard of an honours degree is carefully summarized and explained; indeed, the reader who desires a rapid and very competent survey of, say, the elements of the subject of harmonic functions could not do better than peruse the sixth chapter of Mr. Ramsey's book.

As has been said, the book covers familiar ground—first dealing with the fundamental concepts and simple applications of potential theory, then proceeding to a study of attraction and potential at internal points, the theorems of Laplace, Poisson, Gauss, and Green, harmonic functions and the attraction of ellipsoids. Very useful sets of examples, of graded degrees of difficulty, are appended to each chapter.

A. F.

[The Editors do not hold themselves responsible for the views expressed by their correspondents.]

XXXIV. *The Excitation of the Hydrogen Molecule by Electron Impact.*

By R. ROSCOE, Ph.D., Physics Department,
King's College, Newcastle-upon-Tyne *.

[Received January 15, 1940.]

THE various methods available for making calculations on the scattering of electrons by gases have been worked out in some detail ⁽¹⁾. Of these, the simplest consists in the use of the Born approximation ⁽²⁾, which should yield correct results with electrons of high velocity. More complicated methods are necessary for slow electrons.

Calculations have been made on the elastic scattering in molecular hydrogen by Fiske ⁽³⁾ using a method suitable for very slow electrons, and by Massey and Mohr ⁽⁴⁾, and the author ⁽⁵⁾, using the Born approximation. There are, however, no calculated results on the inelastic scattering by this molecule, beyond those of Massey and Mohr ⁽⁴⁾, who considered only the excitation of the $2s\sigma^3\Sigma$ and $2p\sigma^1\Sigma$ states. In the present work calculations are made to cover the excitation of all the more important states by fast electrons, using the Born approximation. This method gives zero probability of excitation for the triplet states, but it is known from experimental evidence that these are not excited by fast electrons.

The Born Formula.

The differential cross-section $I(\delta)$ for the excitation of a particular electronic state of the molecule is defined so that $2\pi I(\delta) \cdot \sin \delta \cdot d\delta$ is the fraction of the incident electrons scattered through the small solid angle contained between the angles δ and $\delta + d\delta$, with excitation of that state, in passing through unit length of gas containing one molecule per unit volume. With this definition the Born approximation gives

$$I(\delta) = \frac{4\pi^2 m^2}{h^4} \frac{k'}{k} A \left| \iiint V \psi_0 \bar{\psi}_1 e^{i\mathbf{K} \cdot \mathbf{R}_1} d\tau_1 d\tau_2 d\tau_3 \right|^2, \quad \dots (1)$$

where

A denotes averaging over all orientations of the molecular axis ;

$\frac{kh}{2\pi m}$ is the velocity of the incident electrons ;

$\frac{k'h}{2\pi m}$ is the velocity of the scattered electrons ;

* Communicated by Professor R. Whiddington, F.R.S.

\mathbf{K} is the vector difference between k and k' ;

V is the scattering potential ;

ψ_0 and ψ_1 are the normalised electronic wave functions of the unexcited and excited states of the molecule respectively ;

R is the radius vector from the centre of the molecule, and the suffix 1 denotes the coordinates of the scattered electron, whereas 2 and 3 refer to the bound electrons

The scattering potential is given by

$$V = -e^2 \left(\frac{1}{r_1} + \frac{1}{p_1} - \frac{1}{r_{12}} - \frac{1}{r_{13}} \right),$$

where r_1 denotes the distance of electron 1 from one nucleus, p_1 its distance from the other, and r_{12} stands for the distance between electrons 1 and 2. By making use of the orthogonal properties of the wave functions and the relation

$$\int \left(\frac{1}{r_1} - \frac{1}{r_{12}} \right) e^{i\mathbf{K} \cdot \mathbf{r}_1} d\tau_1 = \frac{4\pi}{K^2} (1 - e^{i\mathbf{K} \cdot \mathbf{r}_2})$$

together with the two vector equations involving the nuclear separation c

$$\mathbf{R} = \mathbf{r} + \frac{1}{2}\mathbf{c} = \mathbf{p} - \frac{1}{2}\mathbf{c} \quad . \quad . \quad . \quad . \quad . \quad . \quad (2)$$

equation (1) may be reduced to the form

$$I(\delta) = \frac{16}{(Ka_0)^4} \frac{k'}{k} A \left| \iiint \psi_0 \bar{\psi}_1 e^{i\mathbf{K} \cdot \mathbf{R}_2} d\tau_2 d\tau_3 \right|^2 \quad . \quad . \quad . \quad (3)$$

for singlet states, while the cross-section vanishes for triplet states. In this equation $I(\delta)$ is measured in units of a_0 , where

$$a_0 = \frac{\hbar^2}{4\pi^2 e^2 m}.$$

The wave functions appearing in (1) and (3) should, correctly speaking, be products of functions of the electronic and nuclear coordinates, and the integration should include the nuclear coordinates. However, it will be shown later that the nuclear parts may be neglected in calculating the cross-section corresponding to excitation of all the vibrational levels of a particular electronic state, provided the molecules are initially in the lowest vibrational level of the ground state. It will also be shown that the appropriate value of c is the mean nuclear separation in the lowest level of the ground state ($1.417 a_0$).

The Electronic Wave Functions.

In order to evaluate the integral occurring in (3), it is necessary to use fairly simple expressions for the wave functions such as those obtained

by variational methods. For the ground state, Wang's formula ⁽⁶⁾ is suitable :

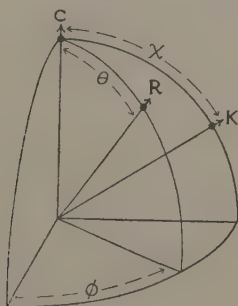
$$\psi_0 = N_0 (e^{-Z(r_a + p_s)} + e^{-Z(p_a + r_s)}). \quad (4)$$

Wave functions for the excited states have been obtained by Guillemin and Zener ⁽⁷⁾ (for the $2p\sigma^1\Sigma$ or B state) and by MacDonald ⁽⁸⁾. The latter has constructed wave functions for all the more important states, out of the wave function for the ground state of the hydrogen molecule ion and the wave functions for the excited states of the hydrogen atom, of the type

$$\psi_{lmn} = N_1 \{ \psi_+(2) \psi(nlm|3) \pm \psi_+(3) \psi(nlm|2) \}, \quad (5)$$

where the positive sign corresponds to singlet states and the negative sign to triplet states. Here ψ_+ denotes the wave function of the molecular ion, for which Guillemin and Zener's function in spheroidal coordinates ⁽⁹⁾

Fig. 1.



is used, while $\psi(nlm)$ denotes the wave function of an excited state of the hydrogen atom in polar coordinates with the centre of the molecule as origin, and N_1 is a normalizing factor.

Excitation of the $2p\pi^1\Pi$ or C State.

The calculation of the cross-section corresponding to excitation of this state is fairly simple and serves to illustrate the methods employed for the other states. Spherical coordinates (R, θ, ϕ) are used, θ being measured from the nuclear axis, ϕ from the plane at right angles to that containing the axis and the vector K , and R from the centre of the axis (fig. 1). Spheroidal coordinates (ρ, μ, ϕ) are also employed, ρ and μ being defined by the relations

$$\rho = \frac{r+p}{c}, \quad \mu = \frac{r-p}{c}.$$

For the C state, MacDonald's wave function may be written

$$\psi_{211} = N_1 \{ \psi_+(2) e^{-R_3/2a_0} R_3 \sin \theta_3 e^{i\phi_3} + \psi_+(3) e^{-R_2/2a_0} R_2 \sin \theta_2 e^{i\phi_2} \},$$

where

$$\psi_+(2) = c^{-a\mu_2} (e^{-b\mu_2} + e^{b\mu_2})$$

and the constants a and b have the values 1.045 and 0.673 respectively for the separation of the ground state of the molecule. The Wang formula (4) is used for ψ_0 (with $Za_0 = 1.166$), and after performing the integration over the 3-coordinates the cross-section is obtained in the form

$$I(\delta) = \frac{16}{(Ka_0)^4} \frac{k'}{k} (N_0 N_1 B)^2 A |T|^2,$$

where

$$B = \int \psi_+(3) e^{-Zr_3} d\tau_3 = \int \psi_+(3) e^{-Zp_3} d\tau_3,$$

$$T = \int (e^{-Zr_3} + e^{-Zp_3}) e^{-R_2/2a_0} e^{iK \cdot R_2} R_2 \sin \theta_2 e^{i\phi_2} d\tau_2.$$

A further simplification may be introduced by expressing the scalar product $K \cdot R$ in terms of the coordinates and the angle χ between K and the nuclear axis:

$$K \cdot R = KR (\cos \theta \cos \chi + \sin \theta \sin \chi \sin \phi),$$

which gives

$$T = - \int (e^{-Zr} + e^{-Zp}) e^{-R/2a_0} e^{iKR \cos \theta \cos \chi} J_1(KR \sin \theta \sin \chi) R \sin \theta \cdot d\tau.$$

The evaluation of the integral B presents no difficulties, but a simple expression for T can only be obtained for very large and very small values of K . For intermediate values, special methods must be adopted. Numerical computation is not suitable, as the integral is a function of both K and χ , and the process of averaging over all orientations of the nuclear axis involves dividing by 2 and integrating the square of the modulus of T with respect to $\sin \chi d\chi$ from 0 to π . Expansion in powers of K is suitable only for small values of K , because the series converges very slowly and the higher terms are tedious to compute. Massey and Mohr, in their calculation for the B state ⁽⁴⁾ employed another type of expansion, but this is also difficult to use for moderately large values of K . The method found most suitable in the present work for giving values of $I(\delta)$ for values of Ka_0 between 0 and 2, consists in replacing the exponential terms involving the distances r and p by an expression which is a simple function of R and θ , and represents a good approximation to the original expression. The whole integral now involves only polar coordinates having the centre of the molecule as origin, and may consequently be evaluated without difficulty and used to calculate an approximate value for $I(\delta)$. For moderate values of K , the error in this value can be made small by a careful choice of the approximate expression

used in the integral, and the calculation of an upper bound to this error is a simple matter.

Before this approximation is introduced, the integral is expanded as a series of associated Legendre polynomials :

$$T = - \sum_{n=1}^{\infty} \frac{2n+1}{2} \frac{(n-1)!}{(n+1)!} \alpha_n P_n^1(\cos \chi),$$

where

$$\alpha_n = \int_0^{\pi} T P_n^1(\cos \chi) \sin \chi d\chi.$$

After performing the averaging operation denoted by A , the cross-section is obtained as a series :

$$I(\delta) = \frac{16}{(Ka_0)^4} \frac{k'}{k} (N_0 N_1 B)^2 \sum_{n=1}^{\infty} \frac{2n+1}{4} \frac{(n-1)!}{(n+1)!} |\alpha_n|^2.$$

The expression for α_n may be simplified by means of the theorem ⁽¹⁰⁾ that

$$\begin{aligned} \int_0^{\pi} e^{iKR \cos \theta \cos \chi} J_m(KR \sin \theta \sin \chi) P_n^m(\cos \chi) \sin \chi d\chi \\ = \left(\frac{2\pi}{KR} \right)^{\frac{1}{2}} i^{n-m} P_n^m(\cos \theta) J_{n+\frac{1}{2}}(KR), \end{aligned}$$

which gives

$$\alpha_n = i^{n-1} \int (e^{-Zr} + e^{-Zp}) e^{-R/2a} \left(\frac{2\pi}{KR} \right)^{\frac{1}{2}} J_{n+\frac{1}{2}}(KR) P_n^1(\cos \theta) R \sin \theta d\tau.$$

It is clear from this that α_n vanishes when n is even, and it is found that α_3 and succeeding odd terms are negligible compared to α_1 when Ka_0 is less than 2. The calculation of α_1 is performed by replacing

$$e^{-Zr} + e^{-Zp}$$

by

$$2e^{-ZR} \cosh \left(\frac{Zc}{2} \cos \theta \right) \cdot \left(1 - \frac{Zc^2}{8R} \sin^2 \theta \right).$$

This gives α_1 in the form of an algebraic function of K , involving the constants of the wave functions and the nuclear separation c in a rather complicated way. Values of $I(\delta)$ calculated from this, with c set equal to $1.417a_0$, are shown in Table I. This calculation gives fairly accurate results when K is moderately small, because in such cases the contribution to the integral arising from small values of R is negligible, and for large values of R the foregoing approximation is very good. An upper bound for the error in the value of α_1 derived in this way has been computed, and it is found that when Ka_0 has the values 0, 1, and 2 the error cannot exceed 1.4, 3.5, and 20 per cent. respectively, and must actually be less than these figures.

The exact expression for T when K is very small is

$$T = -\pi K \sin \chi \int \int (e^{-Zr} + e^{-Zp}) e^{-R/2a_0} R^4 dR \sin^3 \theta d\theta.$$

This provides a check on the approximate calculation, and shows that for very small values of K the cross-section falls off as K^{-2} . It cannot be used to obtain accurate results, however, if Ka_0 is greater than 0.005. When K is very large the exact expression is

$$T = -\frac{64\pi Z}{K^5} \sin \chi \left\{ e^{-c/4a_0} \cos \left(\frac{Kc}{2} \cos \chi \right) + \frac{1}{2Za_0} e^{-Zc/2} \right\},$$

from which it follows that the cross-section falls off as K^{-14} for large values of K.

The cross-section corresponding to the excitation of the $3p\pi^1\Pi$ or D state is obtained in an exactly similar way. The results are also shown in Table I.

Excitation of the $2p\sigma^1\Sigma$ or B State.

For this state the calculation is performed in much the same way as for the C state, MacDonald's wave function (5) being used :

$$\psi_{210} = N_1 \{ \psi_+(2) e^{-R_3/2a_0} R_3 \cos \theta_3 + \psi_+(3) e^{-R_2/2a_0} R_2 \cos \theta_2 \}.$$

The integral occurring in (3) may be simplified, but in this case it reduces to the sum of two integrals. Of these, one is similar to the integral T for the C state and is treated in much the same way, while the other is of the form

$$\int \psi_+(2) (e^{-Zr_2} - e^{-Zp_2}) e^{i\mathbf{K} \cdot \mathbf{R}_2} d\tau_2.$$

Although the integrand may be expressed fairly simply in terms of spheroidal coordinates alone, the integral is difficult to evaluate. The easiest method in this case consists in expanding the last exponential term in powers of K and integrating term by term. This is tedious, but fortunately a high degree of accuracy is not required because for moderate values of K the contribution of this integral to the value of $I(\delta)$ is small.

The calculated results for the cross-section are shown in the table. For very small values of K, it falls off as K^{-2} and is greater than the C state cross-section. At $Ka_0 = 0.9$ it becomes less than the C state cross-section, but rises above it again for very large K since in this region it falls off as K^{-12} .

It is also possible to calculate the cross-section for this state using Guillemin and Zener's wave function :

$$\psi_{210} = N \{ e^{-a\rho_1 - b\rho_2} \sinh c\mu_3 + e^{-a\rho_2 - b\rho_1} \sinh c\mu_2 \}.$$

This function was employed by Massey and Mohr in their calculations for the B state, and leads to an expression for the cross-section which involves three integrals of the type

$$\int e^{-\alpha\rho} \sinh \beta\mu e^{i\mathbf{K}\cdot\mathbf{R}} d\tau,$$

with different values for the constants α and β . When these integrals are expanded as a series of powers of K , it is found that the even terms vanish, so that for very small K the cross-section is inversely proportional to K^2 —the same result as is obtained by using MacDonald's function. This point is emphasized because Massey and Mohr, who performed the calculation in a somewhat different way, obtained a small cross-section at low voltages and angles and a maximum at somewhat higher values. This maximum they attribute to a "diffraction factor" which occurs in their results :

$$\left(1 - \frac{\sin Kc}{Kc}\right).$$

However, such a factor could not produce a maximum at low values of K , since it is multiplied by a term which varies as K^{-4} in this region. The averaged term of equation (3) perhaps shows minor oscillations, but these are rendered insignificant by the rapid decrease of the whole expression. A calculation made on a more accurate basis than the Born approximation might give significant maxima and minima, similar to those which have been proved to exist in the case of atomic systems, but these could not be ascribed to a diffraction effect arising from the presence of the two nuclei.

It is interesting to compare the cross-sections calculated from the two different types of wave function. As the constants for the Guillemin and Zener function are given only for the normal separation of the B state ($c=2.5 a_0$), the comparison is made by calculating the cross-section for this separation in the two cases. For very small K the results are

$$I(\delta) = 2.12 \frac{k'}{k} (Ka_0)^{-2} \quad (\text{Guillemin function}),$$

$$I(\delta) = 1.92 \frac{k'}{k} (Ka_0)^{-2} \quad (\text{MacDonald function}).$$

The agreement is quite satisfactory, considering the difference in the two wave functions.

Excitation of the $2s\sigma^1\Sigma$ or 1X State.

In all states of this type, which derive from the S states of the helium atom, wave functions of the type (5) are not orthogonal to the ground state function (4). Since it is essential to use orthogonal functions, some

alteration must be made. The simplest method is one used by Massey and Mohr ⁽¹¹⁾ in their consideration of the scattering by helium, which consists in making a very slight alteration in the constants of the function for the excited state so as to make it orthogonal to the ground state function. So in this case the wave function is written

$$\psi_{200} = N_1 \{ \psi_+(2) e^{-\alpha R_{3/a_0}} (2 - \alpha R_{3/a_0}) + \psi_+(3) e^{-\alpha R_{2/a_0}} (2 - \alpha R_{2/a_0}),$$

where α is given the value 1.066 instead of unity. This procedure is justified by the fact that a similar alteration in the constants for the B and C states leads to a change of only a few per cent. in the values for the cross-section, the change of the integral being largely counterbalanced by that of the normalizing factor, provided K is not very large.

TABLE I.

Showing $\frac{k}{k'} I(\delta)$ (in units of a_0^2) for various excited states.

Ka_0 .	$2s\sigma^1\Sigma$ or 1X state.	$2p\sigma^1\Sigma$ or B state.	$2p\pi^1\Pi$ or C state.	$3p\pi^1\Pi$ or D state.
.1	1.00	99	84	13.7
.2	.94	23	20	3.3
.4	.74	4.4	3.8	.68
.6	.51	1.25	1.14	.22
.8	.31	.39	.38	.08
1.0	.17	.12	.13	.03
1.2	.09	.04	.05	.01
1.4	.05	.01	.02	.00

Results for the Differential Cross-sections.

The calculated results for the different states are collected together in Table I., and are accurate to the number of figures shown. The angular scattering curves for any voltage of the incident electrons may be calculated from these figures, since the angle of scattering δ is related to K by the equation

$$K^2 = k^2 + k'^2 - 2kk' \cos \delta, \quad . \quad . \quad . \quad . \quad . \quad (6)$$

and if V_0 represents the voltage of the incident electrons and V_1 that of the scattered electrons

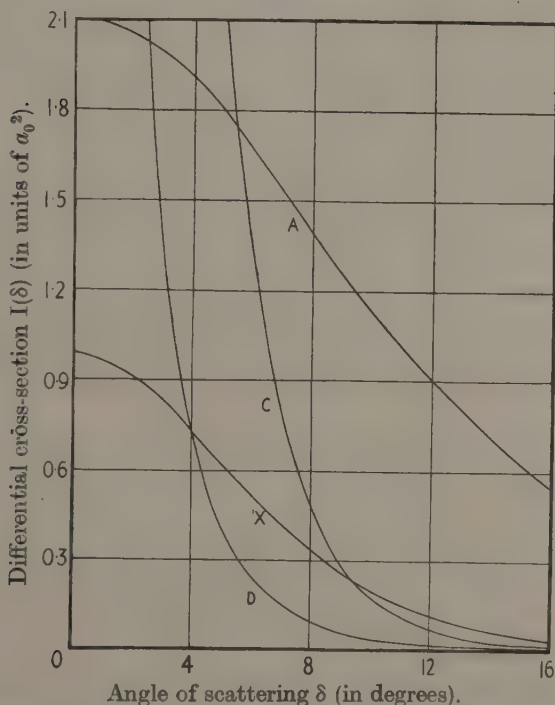
$$ka_0 = .2718 V_0^{\frac{1}{2}} \quad \text{and} \quad k'a_0 = .2718 V_1^{\frac{1}{2}}.$$

The voltage losses of electrons which have excited these states are in the neighbourhood of 12 volts, so for high voltage electrons k' is very close to k .

The angular scattering curves for 400 volt electrons are shown in fig. 2 together with the curve for elastic scattering. The curve for the B state is omitted since it lies too close to the curve for the C state to be shown clearly.

The scattering for all these singlet states falls off continuously with increasing voltage and angle, without showing appreciable maxima or minima. With small values of K the cross-section for s -states is constant, whereas for p -states it falls off as K^{-2} . For very large K , it is proportional

Fig. 2.



Angular distribution curves for 400-volt electrons. The curve marked A corresponds to elastic scattering. The curve for the B state is not shown because it lies very close to the C state curve.

to K^{-12} for s -states, to K^{-12} for $p\sigma^1\Sigma$ states, and to K^{-14} for $p\pi^1\Pi$ states. Thus the scattering is very similar to the scattering by helium⁽¹⁾, the curve for each state resembling that for the state of the helium atom from which it derives. The only point of difference is in the case of $p\sigma^1\Sigma$ states which have scattering proportional to K^{-12} for large K , as opposed to K^{-14} for the 1P states of helium. It should be noted that the MacDonald type

of wave function used in most of this work is not satisfactory for positions of the electrons near to the centre of the molecule, and may therefore lead to inaccuracies in the magnitude of the cross-sections calculated for very large values of K , but this does not affect the general considerations just given.

From fig. 2 it is apparent that the small angle scattering of electrons which have excited the 1X state is very much less than that of electrons which have excited the B and C states, while at moderately large angles the reverse is the case. From the Frank-Condon Principle it would appear that the mean energy loss of electrons which have excited the 1X state should be about half a volt greater than the loss of those which have excited the other two states. Thus the mean energy loss of electrons scattered inelastically at small angles should be appreciably less than the mean loss of those scattered at large angles. This point has been investigated experimentally by Prof. R. Whiddington in some unpublished work. It was found, however, that the most careful measurements of the energy loss failed to reveal the slightest variation with angle, although the apparatus employed was capable of detecting a very much smaller change than that which was to be expected. This conflict between the theory and experimental results may be due either to a failure of the Born approximation at angles and voltages as low as those used in the experimental work (about 600 volts), or to the failure of the Frank-Condon Principle which is discussed in a later section of this work.

The Aggregate of Inelastically Scattered Electrons.

The differential cross-section $I_A(\delta)$ corresponding to the aggregate of inelastically scattered electrons, including those which have produced ionization, is calculated by a method similar to that employed for simple atomic systems which is described by Mott and Massey ⁽¹⁾. Thus

$$2\pi I_A(\delta) \sin \delta d\delta = \sum_{n \neq 0} 2\pi I_n(\delta) \sin \delta d\delta,$$

where the summation extends over all the excited states including the continuum. The values of $I_n(\delta)$ are given for each state by equation (1), but the magnitude and direction of K , as well as the value of k' are different in each case. For the discrete states the magnitude of K is given by (6) and k' can be set equal to k provided that the initial energy of the electrons is large compared to the excitation energy of the highest discrete levels. On the other hand, for ionization collisions

$$K = k \sin \delta, \quad k' = k \cos \delta.$$

It is legitimate to use these last two relations for all the states in calculating the aggregate scattering, because they reduce to the same as the

first two when δ is small, and it is only then that the number of electrons which have caused excitation of the discrete levels is comparable with the number which have produced ionization. The difference in the directions of \mathbf{K} is immaterial on account of the process of averaging over all orientations of the molecular axis. So the expression for the aggregate scattering can be written

$$I_A(\delta) = \frac{4 \cos \delta}{(\mathbf{K}a_0)^4} \sum_{n \neq 0} \left| \int \psi_0 \bar{\psi}_n (e^{i\mathbf{K} \cdot \mathbf{R}_1} + e^{i\mathbf{K} \cdot \mathbf{R}_2}) d\tau_2 d\tau_3 \right|^2$$

with \mathbf{K} set equal to $k \sin \delta$ in each term. But

$$\sum_{n=0}^{\infty} \left| \int \psi_0 \bar{\psi}_n (e^{i\mathbf{K} \cdot \mathbf{R}_1} + e^{i\mathbf{K} \cdot \mathbf{R}_2}) d\tau_2 d\tau_3 \right|^2 = 2 + 2 \int \psi_0^2 e^{i(\mathbf{K} \cdot \mathbf{R}_1 - \mathbf{K} \cdot \mathbf{R}_2)} d\tau_2 d\tau_3.$$

TABLE II.

Comparison of the Inelastic Scattering by Molecular and Atomic Hydrogen.

The Table shows the Ratio of $I_A(\delta)$ for Molecular Hydrogen to $2I_A(\delta)$ for Atomic Hydrogen.

$ka_0 \sin \delta$	0	0.5	1	2	4
Ratio $\text{H}_2 : 2\text{H}$..	.79	.81	.87	.97	1.00

Therefore

$$I_A(\delta) = \frac{4 \cos \delta}{(\mathbf{K}a_0)^4} \left\{ 2 + 2 \int \psi_0^2 e^{i(\mathbf{K} \cdot \mathbf{R}_1 - \mathbf{K} \cdot \mathbf{R}_2)} d\tau_2 d\tau_3 - \left| \int \psi_0^2 (e^{i\mathbf{K} \cdot \mathbf{R}_1} + e^{i\mathbf{K} \cdot \mathbf{R}_2}) d\tau_2 d\tau_3 \right|^2 \right\}.$$

These integrals only contain the wave function of the ground state and can be evaluated by the same methods as are used in calculating the elastic scattering ⁽⁵⁾.

The value of $I_A(\delta)$ for two completely separated hydrogen atoms is given by

$$\frac{8 \cos \delta}{(\mathbf{K}a_0)^4} \{1 - (1 + \mathbf{K}^2 a_0^2/4)^{-4}\}$$

and the ratio of the aggregate inelastic scattering by a hydrogen molecule and by two hydrogen atoms is shown in Table II. In deriving both these expressions for the aggregate cross-section no account has been taken of the interference of the scattered and ejected electrons. A correction must be introduced to take account for this effect, but it is only of importance at large angles, and in such cases it is the same for the molecule and the separated atoms, so the value of the ratio is unaffected.

Thus the inelastic scattering in molecular hydrogen is almost the same as that in atomic hydrogen when the total number of atoms present is the same. At small voltages and angles the molecular scattering is slightly lower than the atomic, and the ratio exhibits no appreciable maxima or minima such as appear in the elastic scattering.

The Frank-Condon Principle.

In the preceding calculations of the scattering no account has been taken of the fact that each electronic level is divided into a number of vibrational levels and that these are subdivided into rotational levels. The rotational levels are so closely spaced that their existence can be neglected, but the vibrational levels require consideration. Thus correctly the cross-section $I(\delta)$ for a particular electronic state should not be calculated from equations (1) or (3), but should be obtained by summing the cross-sections $I_m(\delta)$ for each vibrational level belonging to this electronic state. The expressions for $I_m(\delta)$ are exactly similar to (1) and (3) except that the integration includes the nuclear coordinates, and the wave functions now involve the nuclear separation, each being expressible as the product of an "electronic" and a "nuclear" wave function ⁽¹²⁾ :

$$\psi_0(r_2, r_3, c) \frac{R_{0m}(c)}{c}, \quad \psi_1(r_2, r_3, c) \frac{R_{1m}(c)}{c}.$$

The first factor in each of these terms contains the electronic coordinates and the nuclear separation, but does not depend on the nuclear quantum number m , while the second depends only on the nuclear separation and m . Thus if it is assumed that the molecules are initially in the lowest level of the ground state

$$I_m(\delta) = \frac{16}{(Ka_0)^4} \frac{k'}{k} A \left| 4\pi \int M(c) R_{00}(c) R_{1m}(c) dc \right|^2,$$

where

$$M(c) = \iint \psi_0 \psi_1 e^{i\mathbf{K} \cdot \mathbf{R}_2} d\tau_2 d\tau_3.$$

The differential cross-section for the whole electronic state is the sum of all such terms as these, and since the nuclear functions are orthogonal and normalized

$$\begin{aligned} I(\delta) &= \sum_{m=0}^{\infty} I_m(\delta) = \frac{16}{(Ka_0)^4} \frac{k'}{k} A 4\pi \int |M(c)|^2 R_{00}^2(c) dc \\ &= 4\pi \int I(\delta, c) R_{00}^2(c) dc, \end{aligned}$$

where $I(\delta, c)$ is given by equation (3) for each value of c .

The true values for $I(\delta)$ have been calculated from this result, using the Morse formula for $R_{00}(c)$, but it is found that although the variation

of $I(\delta, c)$ with c is considerable, the wave function possesses such a considerable maximum in the neighbourhood of the mean nuclear separation that $I(\delta)$ is within one per cent. of the value given directly by (3) with c set equal to its mean value. So the use of equation (3) in calculating the differential cross-sections is fully justified if c is set equal to the mean nuclear separation of the ground state.

In order to obtain the integral form of the Frank-Condon Principle⁽¹³⁾ (which gives the relative probabilities of excitation of the vibrational levels of a particular electronic state) it is necessary to assume that $M(c)$ is practically constant over the range for which $R_{00}(c) R_{1m}(c)$ is large, so that

$$I_m(\delta) = I(\delta) \left| 4\pi \int R_{00}(c) R_{1m}(c) dc \right|^2.$$

This implies that the excitation probabilities of the various vibrational levels are in the ratio of the squares of the integrals

$$\int R_{00}(c) R_{1m}(c) dc.$$

However, it is found that on account of the strong dependence of $M(c)$ on c and the wide spread of the product $R_{00}(c) R_{1m}(c)$, this procedure is by no means correct and results deduced from the Frank-Condon Principle are consequently in error.

It is interesting to note that while this conclusion refers only to the excitation of the singlet states of the hydrogen molecule by electron impact, Coolidge, James, and Present⁽¹⁴⁾ have concluded from a consideration of the experimental data that the same applies to certain triplet states.

The greater part of these calculations were carried out in the Physics Department of Leeds University, at the suggestion of Prof. R. Whiddington, in connexion with his experimental work which has been referred to above. The author wishes to thank him for the interest that he has shown in this work.

Summary.

Calculations have been made on the inelastic scattering of electrons in molecular hydrogen, using the Born approximation. The differential cross-section for the aggregate of inelastically scattered electrons and also the cross-sections corresponding to the excitation of individual states are found to decrease steadily with increasing angle and voltage, showing no evidence of diffraction maxima or minima. The B and C states give very similar scattering curves, and a finite cross-section is obtained for the 1X state even at high voltages, indicating that the optically forbidden $A \rightarrow ^1X$ transition can occur under electron excitation. The scattering

curves for the different states strongly resemble the curves for the corresponding states of helium. It is found that the use of two different types of wave function for the B state leads to two very similar results for the scattering. The Frank-Condon Principle fails to give correct values for the relative probabilities of excitation of the vibrational levels.

References.

- (1) N. F. Mott and H. S. W. Massey, 'The Theory of Atomic Collisions,' Oxford, 1933.
- (2) M. Born, *Z. f. Physik*, xxxviii. p. 803 (1926).
- (3) J. B. Fiske, *Phys. Rev.* xlix. p. 167 (1936).
- (4) H. S. W. Massey and C. B. O. Mohr, *Proc. Roy. Soc. A*, cxxxv. p. 258 (1932).
- (5) R. Roscoe, *Phil. Mag.* xxvi. p. 32 (1938).
- (6) S. C. Wang, *Phys. Rev.* xxxi. p. 579 (1928).
- (7) V. Guillemin and C. Zener, *Phys. Rev.* xxxiv. p. 999 (1929).
- (8) J. K. L. MacDonald, *Proc. Roy. Soc. A*, cxxxvi. p. 528 (1932).
- (9) V. Guillemin and C. Zener, *Proc. Nat. Acad. Sci.* xv. p. 314 (1929).
- (10) G. N. Watson, 'Bessel Functions,' Cambridge (1922).
- (11) H. S. W. Massey and C. B. O. Mohr, *Proc. Roy. Soc. A*, cxxxii. p. 619 (1931).
- (12) E. U. Condon and P. M. Morse, 'Quantum Mechanics,' McGraw-Hill, 1929.
- (13) E. U. Condon, *Phys. Rev.* xxxii. p. 858 (1928).
- (14) A. S. Coolidge, H. M. James, and R. D. Present, *Journ. Chem. Phys.* iv. p. 193 (1936).

XXXV. *The Effective Separation of Points
Discharging Atmospheric Electricity.*

By J. ALAN CHALMERS, M.A., Ph.D.,
Lecturer in Physics in the Durham Colleges of the
University of Durham *.

[Received April 17, 1940.]

1. *Introduction.*

THERE are a number of phenomena in atmospheric electricity which require for their discussion the conversion of the point discharge current through a single point into a vertical current density, needing, therefore, the number of points in a given area which give as much point discharge as the one on which measurements were made.

There are various ways in which this conversion can be expressed, and it is most convenient to use the separation of points similar to the one used, which would give the actual vertical current density. Clearly an increase in the separation of points means a decrease in the vertical current density corresponding to a given current through one point, and hence a greater efficiency of the one point in supplying point discharge current to cover an area.

It is the purpose of the present paper to bring together the various phenomena that can supply evidence in regard to the effective separation of discharge points, to review the different possibilities, and to suggest further observations which may be able to settle the problem.

It must be realized that it is some distance above the earth that the ionic streams above the points, and coming from the points, can be considered to form a current of anything like uniform density, and when we discuss a current density it is only an average, not a uniform, current.

2. *Point Discharge Measurements.*

Measurements of point discharge currents have been made by Wormell ⁽¹⁾ Schonland ⁽²⁾, Whipple and Scrase ⁽³⁾, Immelman ⁽⁴⁾, and Chalmers and Little ⁽⁵⁾. Attempts to convert the point discharge current into a vertical current density have been made, by direct estimate of the number of trees judged similar to the point, by Wormell and Schonland, and also,

* Communicated by the Author.

in a less definite way, by Whipple and Scrase. Chalmers and Little have discussed the consequences of assuming various separations of discharging points.

Schonland ⁽²⁾ was particularly well able to make such an estimate, for he used an actual tree mounted on insulators as his discharging point, and he was fortunate in having a fairly regular arrangement of similar trees, so there can be little question as to the acceptance of his separation of 5 metres in his case. But Schonland only made measurements in a few thunderstorms, and conditions in South Africa, where his measurements were made, differ so widely from those in England that it is difficult to transfer the results from one place to the other.

Wormell ⁽¹⁾ counted the number of trees within a given area higher than his point and made the assumption that each of these trees gave the same point discharge as the point; this gave an effective separation of about 37 metres. Whipple and Scrase made a rough estimate of a separation of about 25 metres, while Chalmers and Little were unable to give any similar estimate.

In Wormell's estimate, it would seem that trees higher than the point might be expected to give more discharge than the point, whereas it might also be expected that trees very close together would interfere with each other's share of the total vertical current. It is not easy to estimate which is the more important factor of these altering Wormell's estimate.

3. *Vertical Currents.*

An important general principle in the discussions to be given is that, when conditions remain steady, the total vertical current due to different processes, *i. e.*, ionic current, precipitation current, and convection current, must be the same at different heights in the atmosphere, for otherwise there would be an accumulation of charge at certain levels, and conditions would not be steady. Even when conditions are not steady, *e. g.*, in a thunderstorm between flashes, the same type of reasoning can be applied.

In some cases there is evidence which can give the sign, if no more, of the total vertical current at some height and, applying the above principle, we get the same sign of current at other levels, and we can hence deduce some information as to that part of the total vertical current which is due to point discharge, if the other factors are known.

4. *The Earth's Electrical Balance Sheet.*

Wormell ⁽¹⁾ has discussed the various processes bringing charges of either sign to 1 km.² of the earth at Cambridge, and in so doing had to make the assumption quoted above as to the efficiency of his discharging point. He found a small balance of negative charge reaching the earth,

but this could be reduced to zero by altering his conversion of point discharge currents to current densities ; by reducing Wormell's estimate of 100 coulombs/km.²/year to a value of 60, a complete balance is obtained, and this reduction is obtained by assuming a rather greater spacing of discharging points, about 48 metres ; to obtain a similar result for Kew the spacing would be over 30 metres.

Over a period of time, the quantity of charge reaching the earth by means of point discharge at Durham is rather greater than that at Kew, so that, if the quantity per km.² per annum is taken as 100 coulombs, the separation at Durham must be about 30–35 metres. Reducing the quantity to 60 coulombs increases the required separation to 40–48 metres.

Any increase of spacing beyond such a value would mean that point discharge and lightning could no longer balance the fine-weather current and the precipitation current over the same area. But, for a complete balancing over the whole of the earth's surface, it is not necessary that there should be balancing over any small area, and it is quite possible that a positive excess of charge received at such places as Kew and Cambridge might be balanced by a negative excess received at other places ; in particular, point discharge and lightning are likely to be more important on mountain peaks than elsewhere. Another factor which may be very variable is the precipitation current ; most of the measurements of precipitation current have been carried out at comparatively flat places and have given a positive excess of current downwards ; but observations in mountainous districts might give the reverse, and, in fact, the observations of Chalmers and Little ⁽⁶⁾ on soft hail have shown that extremely large negative currents do occur on occasion, so much so that a few hours of such precipitation might overshadow the remainder of a year's precipitation. In localities where soft hail, and other similarly highly charged precipitation, is common, the precipitation charge over a year might be widely different from that assumed by Wormall.

Although, at first sight, the consideration of the earth's electrical balance sheet tends to confirm approximately the assumed separation of points, the above discussion shows that a much larger separation of points is not precluded by the evidence.

5. Effects in Thunderstorms and Showers.

Schonland ⁽²⁾ has shown that, in South African thunderstorms, point discharge current, bringing negative charge to the earth's surface, is of much more importance than rain current, bringing positive charge. This means that the total vertical current downwards is negative below the cloud ; and the process of separation within the cloud must be such as to bring negative charge downwards also.

If there should exist conditions similar to those in a thunderstorm, but without actual lightning discharges, then there may be a separation within the cloud supplying a vertical current the same as below the cloud, giving a steady state, with a current negative downwards.

If the results for rain under such conditions show a positive excess, it could be deduced that the negative point discharge current density should be greater than the positive rain current, thus giving some information in regard to the spacing of points. But the results of Scrase ⁽⁷⁾ and others show that, in "showers," the rain current is more frequently negative than positive, so that no further evidence is available in regard to the separation of points.

6. *Space Charge below Thunder-clouds.*

Assuming the base of the thunder-cloud to be a widespread sheet of charge, with vertical lines of force, and assuming that the vertical current is the same at all heights, Wilson ⁽⁸⁾ has calculated the effects of the space charge in the atmosphere due to a current of ions of one sign, produced by point discharge, and moving upwards; the theory gives an increase of potential gradient on rising from the ground, and the magnitude of the increase depends on the point discharge current density, *i. e.*, on the separation of discharge points if the current through one point is known.

Schonland's ⁽²⁾ results for the point discharge current density agree with the sparking potential being reached at the base of the cloud, but to obtain the same results for the observations of Wormell or Whipple and Scrase it would be necessary to have separations less than those assumed. In the case of Whipple and Scrase the separation would have to be reduced to 7 metres; but there is no evidence that the sparking potential is, in England, reached at the base of the cloud; in fact, the evidence of the alti-electrograph (see next section) is that fields below the cloud are small.

Whipple and Scrase ⁽³⁾ have pointed out that the large space charge assumed on Wilson's theory is able to account for the otherwise puzzling observation that lightning flashes frequently not only reduce the existing field but reverse it, sometimes to a larger value than previously; this can occur if there is a fairly large space charge and, therefore, a fairly large current density. These observations of field reversal may be taken as evidence that there is a current density of about the order assumed by Wormall and by Whipple and Scrase, although other explanations, such as the "unmasking" of a large upper charge, are also possible.

7. *Alti-electrograph Results.*

The alti-electrograph (Simpson and Scrase ⁽⁹⁾ and Simpson and Robinson ⁽¹⁰⁾) has been used to find the signs of the electric fields in, above, and

below thunderclouds; the actual widths of the records have been used to give estimates (admittedly only rough) of the electric fields, and the results suggest that the increase in field from the earth's surface up to the base of the cloud is always much less than would be expected from the theory of Wilson if the point discharge current density is that assumed from the estimated spacing of the points.

Discussing the one of the alti-electrograph results which shows the greatest apparent increase of field with height, Chalmers ⁽¹¹⁾ has shown that agreement with Wilson's theory requires a spacing of 140 metres at Kew as compared with the estimate of 25 metres due to Whipple and Serase. A modification of Wilson's theory to include the possibility of small negative ions moving downwards from the cloud can only, under the most favourable conditions, reduce the necessary spacing to 75 metres.

Therefore we are left with the choice that Wilson's theory is inapplicable, that the interpretation of the alti-electrograph results is wrong, or that the separation of discharging points at Kew is much larger than had been estimated.

It is difficult to see in what respect Wilson's theory is wrong, for the one unjustifiable assumption—that of a horizontal cloud sheet—cannot account for the discrepancy; if the theory were applied to a concentration of charge, it would give greater fields at some places and lower at others, and it is difficult to believe that, by chance, the alti-electrograph measurements have only been made in the cases where the fields are lower than those given by the simple Wilson theory.

Accurate measurements by a method other than the alti-electrograph could determine whether or not the quantitative interpretation of full strengths given to the alti-electrograph results is correct or not, and thus could settle the problem discussed in this section. Measurements of this type have been projected by workers at Kew Observatory, but results have not yet been obtained.

8. *Continuous Rain.*

Measurements of rain currents and point discharge currents during a long period of continuous rain in advance of a warm front have been discussed by Chalmers and Little ⁽⁵⁾. The discussion shows that the general features of the measurements can be accounted for, either by a bipolar type of cloud, with a separation of discharging points at Durham less than 120 metres, or by a cloud which is negatively charged, with a separation of discharging points greater than 120 metres; the bipolar cloud requires a point discharge current density which is greater than the rain current, and hence a current which is always negative downwards, whereas the negative cloud requires the reverse. Various factors appear to

point to each of the hypotheses being correct, and no definite conclusion has been possible.

Measurements with an alti-electrograph or similar instrument above a continuous rain cloud would be able to solve the problem, for the sign of the potential gradient above the cloud will determine the sign of the vertical current there, and hence, since conditions are steady, will determine the sign of the vertical current at other points.

Also, measurements of the charge existing in the top of the cloud would distinguish between the two types of cloud and so give evidence as to the effective separation of discharging points.

Unfortunately, the alti-electrograph used by Simpson and Scrase⁽⁹⁾ and Simpson and Robinson⁽¹⁰⁾ was not sufficiently sensitive to give records in the cases of continuous rain clouds.

9. *Eiffel Tower Observations.*

Chauveau⁽¹²⁾ gives an account of important observations undertaken at the Eiffel Tower; of particular interest is the result that there are often occasions during continuous rain when the potential gradient at the top of the Eiffel Tower remains of normal sign, while at the foot of the Tower there is a reversal of sign. The only possible interpretation of this result is that there must be a negative space charge existing in the atmosphere between the heights of the foot and top of the Tower; this can readily be seen by drawing lines of force, for, at the top of the Tower there must be negative ends of lines, while at the foot there are positive ends, and since the Tower itself is a conductor, lines cannot have both ends on the Tower.

There have not been any measurements of rain charges either at the top or foot of the Eiffel Tower, but it would seem safe to assume that, at the foot of the Tower, the rain charge would be more often positive, as it is at other places, *e. g.*, Kew and Durham.

Chauveau's results give a diminution of the normal positive potential gradient at the top of the Tower, and this might be accounted for by the assumption that the presence of the cloud increases the resistance of a cross-section of the atmosphere or by the presence of a negative space charge in the air above the level of the top of the Tower. At any rate, there must be a conduction current of positive charge coming downwards from the cloud to the top of the Tower, and at the same time a conduction current of positive charge upwards from the ground into the lower atmosphere. Thus, unless there is some process for its replenishment, the negative space charge in the lower atmosphere would quickly be dissipated; the only means by which the negative space charge in the lower atmosphere could be replenished would be by the agency of the rain, and we can therefore postulate some sort of process by which the rain acquires

a positive charge and the air in the neighbourhood is left with negative charge; the process of the breaking of drops (Simpson ⁽¹³⁾) would meet the requirements.

At the level of the top of the Tower the conduction current is positive downwards, and it is only if the rain carries a negative charge that the total vertical current is negative downwards; this would require some process within the cloud to give the rain a negative charge. for the negative current the rain could obtain by absorption of ions (process suggested by Wilson ⁽¹⁴⁾) could only be greater than the ionic current if there were a vertical air current, and it seems unlikely that there can be a sufficient vertical air current in conditions of steady rain.

Considering conditions below the level of the top of the Tower, the negative charge produced in the lower atmosphere partly rises and partly falls in conduction currents, whereas the corresponding positive charge on the rain falls only; it is only if there is an original negative charge on the rain that it is possible for the total vertical current downwards to be negative.

More probable is it that the total vertical current downwards is positive, for otherwise there must be a positive charge in the top of the cloud to give a positive current upwards to the ionosphere.

It may be considered that the conditions at the Eiffel Tower are by no means peculiar and that similar results hold in other places; transferring the results to Durham, we must consider a negative charge in the lower regions of the atmosphere giving rise to negative point discharge below it. If the total vertical current is positive downwards, then the conclusion must be drawn that the effective separation of discharging points at Durham is over 120 metres.

Measurements of rain charges at the level of the top of the Eiffel Tower would determine whether there could be a sufficient negative charge on the rain to give a total negative current, and hence, after all, agreement with a separation of less than 120 metres.

Measurements of the potential gradient at various heights during rain would give an estimate of the magnitude of the negative space charge, and hence it would be possible to get some idea of the conduction currents dissipating it.

10. Balloon Measurements of Conductivity.

Wigand ⁽¹⁵⁾ has made balloon measurements of conductivity and has given some results in which the measurements were made above and below a stratiform cloud, presumably of similar type to those giving rise to continuous rain.

The conductivity below the cloud is predominantly due to positive

ions, as would be expected from the positive space charge produced by point discharge at the earth's surface.

Above the cloud, the conductivity was found to be mainly due to negative ions; now, ions will be drawn into the region above the cloud both from the cloud itself and from the ionosphere, but the conductivity will be largely due to small ions, whose origin is more likely to be the ionosphere than the cloud. The observed effect would therefore be expected to occur only if there is a negative field above the cloud, giving a negative current downwards; this requires, at Durham (assuming the results can be transferred to Durham), a separation of less than 120 metres and a bipolar cloud.

A repetition of such measurements, simultaneously with measurements of rain currents and point discharge currents, would determine whether the above argument is valid.

11. *Non-raining Clouds.*

Wilson ⁽¹⁶⁾ has pointed out that a non-raining cloud has very little effect upon the potential gradient at the earth's surface, but that, when rain commences, there is a considerable effect. This would suggest that the rain is intimately connected with the separation of charge, and from this it seems that the rain charge, being the primary effect, should be more important than the point discharge current, which is due to the potential gradient below the cloud, a secondary effect; or we can say that if the separation process is that between positive rain and negative cloud particles, then there is a positive current downwards. This, if applicable to the measurements of Chalmers and Little, must mean a separation of points of more than 120 metres at Durham.

12. *Lightning Strokes.*

To a certain extent, at any rate, it might be expected that lightning flashes and point discharge currents follow similar tracks, and hence the efficiency of a point discharger may be related to its probability of being struck by lightning. Now it is known that isolated trees are in more danger of lightning strokes than trees of the same height in a wood or clump, so that it might be expected that Wormell's estimate of the separation of points is rather low.

On the other hand, it is known that lightning conductors can protect an area of radius about three times their height, and so it might be assumed that a point supplies point discharge current to an area of radius at most three times its height, *i. e.*, that the effective separation of points is at most six times the height of the point. According to this, the separation of points at Kew is at most 50 metres, in S. Africa 24 metres

at Cambridge 25 metres, and at Durham 40 metres. If the protected areas of different points overlap, the separation would be less than that given by the above figures.

13. *The Processes of Separation.*

Some information is obtainable by considering the process of separation of charge, for this indicates the sign of the vertical current at the place where the separation occurs.

If the process of separation is that of the breaking of drops, as originally suggested by Simpson ⁽¹³⁾ in connection with thunder-clouds, and as would account satisfactorily for the Eiffel Tower observations, then, at the point of separation, positive rain falls relative to negative air and the total vertical current downwards must be positive, corresponding to a separation at Durham of over 120 metres.

If, on the other hand, the process of separation is the same as occurs in thunder-clouds, namely, giving an upper positive charge and lower negative charge, the downward current is negative within the cloud, and so the separation at Durham must be less than 120 metres.

If both processes occur, as must be the case if the Eiffel Tower results are to be brought into agreement with a negative downward current, then it is the upper process which determines the sign of the total current, for the lower process has little effect at the higher level, whereas rain from the higher level reaches the lower, and at the higher level we can apply the principle discussed in section 3.

14. *Conclusions.*

It is not possible to draw any quite definite conclusions from the evidence as to the separation of points; it is not even possible to say whether the separation of points at Durham is over or under 120 metres. On the balance, the evidence appears to support the view that the separation is under 120 metres, and so that continuous rain-clouds are bipolar, that the alti-electrograph estimates of potential gradients are incorrect, and that the Eiffel Tower observations require two separate processes of separation, one within the cloud and the other below the level of the top of the Tower; the negative space charge brought about by this last process might account for the absence of the large potential gradients which might be expected below thunder-clouds.

Observations of the magnitudes, or even the signs, of the potential gradients above continuous rain-clouds would confirm or contradict this conclusion.

Observations of the variation of potential gradient with height below clouds would give evidence as to the correctness of Wilson's theory

and as to the current densities, and also as to the negative space charge needed to account for the Eiffel Tower observations.

Observations of charges on rain at the top of the Eiffel Tower, or in a similar situation, would decide whether there is a downward negative rain current to balance the separation of charge below this level.

Observations under conditions similar to Schonland's, but during periods of continuous rain, would determine the sign of the downward current; this could be carried out by using a single tree in a plantation such as those of Forestry Commission.

References.

- (1) Wormell, T. W., *Proc. Roy. Soc. A*, cxv. p. 443 (1927); cxvii. p. 567 (1929).
- (2) Schonland, B. F. J., *Proc. Roy. Soc. A*, cxviii. p. 252 (1928).
- (3) Whipple, F. J. W., and Scrase, F. J., *Geophys. Mem.* no. 68 (1936).
- (4) Immelman, M. N. S., *Phil. Mag.* xxv. p. 159 (1938).
- (5) Chalmers, J. A., and Little, E. W. R., *Terr. Mag.* xlv. p. 451 (1940).
- (6) Chalmers, J. A., and Little, E. W. R., '*Nature*,' cxliii. p. 244 (1939).
- (7) Scrase, F. J., *Geophys. Mem.* no. 75 (1938).
- (8) Wilson, C. T. R., *Proc. Phys. Soc.* xxxvii. p. 320 (1925).
- (9) Simpson, Sir G. C., and Scrase, F. J., *Proc. Roy. Soc. A*, clxi. p. 309 (1939).
- (10) Simpson, Sir G. C., and Robinson, G. D., *Proc. Roy. Soc. A*, clxxvii. p. 281 (1941).
- (11) Chalmers, J. A., *Quart. Journ. Roy. Met. Soc.* lxv. p. 237 (1939).
- (12) Chauveau, A. B., '*Electricité Atmosphérique*,' ii. p. 6 (1925).
- (13) Simpson, G. C., *Phil. Trans.* ccix. p. 379 (1909).
- (14) Wilson, C. T. R., *J. Frank. Inst.* ccviii. p. 1 (1929).
- (15) Wigand, A., *Ann. d. Phys.* lxvi. p. 81 (1921).
- (16) Wilson, C. T. R., *Dict. of App. Phys.* iii. p. 84 (1923).

XXXVI. *On the Problem of Wave-motion for the Wedge of an Angle.*

By Dr. ARNOLD N. LOWAN †.

[Received July 21, 1939.]

IN two previous papers ‡, the author investigated the problem of wave-motion in certain sub-infinite domains (bounded in certain directions but extending to infinity in certain other directions), under the assumption that the displacement was prescribed over the boundary of the given domains.

In the present paper we shall obtain the solution for the wedge of the angle bounded by the intersecting half planes $\theta=0$ and $\theta=\theta_0$. For the sake of simplicity, we shall assume that the term $b \frac{\partial U}{\partial t}$ is absent from the differential equation of wave-motion §.

In Part I. we shall assume that the displacement is prescribed over both boundary planes. In Part II. we shall assume that the displacement is prescribed over one of the boundary planes, while the gradient of the displacement is prescribed over the other boundary plane.

Finally, in Part III. we shall assume that the gradient of the displacement is prescribed over both boundary planes.

PART I.

The displacement $u(r, \theta; t)$ must satisfy the system

$$\left(\nabla^2 - \frac{1}{a^2} \frac{\partial^2}{\partial t^2} \right) u(r, \theta; t) = \Omega(r, \theta; t). \quad . \quad . \quad . \quad (1)$$

$$\lim_{t \rightarrow 0} u(r, \theta; t) = f(r, \theta). \quad . \quad . \quad . \quad (2)$$

$$A \quad \lim_{t \rightarrow 0} \frac{\partial}{\partial t} u(r, \theta; t) = g(r, \theta). \quad . \quad . \quad . \quad (3)$$

$$u(r, \theta; t) = \phi_1(r, t) \text{ for } \theta = 0. \quad . \quad . \quad . \quad (4)$$

$$u(r, \theta; t) = \phi_2(r, t) \text{ for } \theta = \theta_0, \quad . \quad . \quad . \quad (5)$$

† Communicated by the Author.

‡ "On the Problem of Wave-motion in Sub-Infinite Domains," *Phil. Mag.* (Feb. 1939). "On Wave Motion in an Infinite Solid bounded Internally by a Cylinder of a Sphere," *Bulletin, Amer. Math. Society*, April 1939.

§ If this is not the case, the substitution $u = \frac{1}{2} e^{ba^2 t} v$ has the effect of eliminating the first derivative.

where

$$\nabla^2 = \frac{\partial^2}{\partial r^2} + \frac{1}{r} \frac{\partial}{\partial r} + \frac{1}{r^2} \frac{\partial^2}{\partial \theta^2}.$$

The Laplace Transform

$$u^*(r, \theta; p) = \int_0^\infty e^{-pt} u(r, \theta; t) dt$$

must then satisfy the system

$$\left(\nabla^2 - \frac{p^2}{a^2} \right) u^*(r, \theta; p) = \Omega^*(r, \theta; p) - \frac{1}{a^2} [pf(r, \theta) + g(r, \theta)]. \quad (6)$$

A^*

$$= -H^*(r, \theta; p) \text{ (say)}$$

$$u^*(r, \theta; p) = \phi_1^*(r, p) \text{ for } \theta = 0 \quad . \quad . \quad . \quad (7)$$

$$u^*(r, \theta; p) = \phi_2^*(r, p) \text{ for } \theta = \theta_0, \quad . \quad . \quad . \quad (8)$$

where $\phi_1^*(r, p)$ and $\phi_2^*(r, p)$ are the Laplace Transforms of $\phi_1(r, t)$ and $\phi_2(r, t)$ respectively.

Let $G(r, \theta; r', \theta'; p)$ be the "Green's Function" corresponding to the operator $\nabla^2 - \frac{p^2}{a^2}$, the function being required to vanish over the given boundary planes.

For the two-dimensional case under consideration, $G(r, \theta; r', \theta'; p)$ considered as a function of r, θ is known to be the solution of the differential equation

$$\left(\nabla^2 - \frac{p^2}{a^2} \right) G(r, \theta; r', \theta'; p) = -\epsilon(r, \theta), \quad . \quad . \quad . \quad (9)$$

where $\epsilon(r, \theta)$ vanishes everywhere within the given domain, with the exception of the region ω inside a small circle of radius ρ , where $\epsilon(r, \theta)$ is infinite in such a manner that

$$\lim_{\rho \rightarrow 0} \iint_{\omega} \epsilon(r, \theta) d\sigma = 1. \quad . \quad . \quad . \quad (10)$$

From the above definition, it can be shown that the Green's Function is singular at (r', θ') in such a manner that

$$\lim_{\rho \rightarrow 0} \int_{\bar{\omega}} \frac{\partial G}{\partial n} ds = -1 \quad . \quad . \quad . \quad (11)$$

and

$$\lim_{\rho \rightarrow 0} \int_{\bar{\omega}} G ds = 0, \quad . \quad . \quad . \quad (12)$$

where $\bar{\omega}$ is the contour of ω .

In Green's Theorem

$$\iint_R (U \nabla^2 V - V \nabla^2 U) d\sigma = \int_{\bar{R}} \left(U \frac{\partial V}{\partial n} - V \frac{\partial U}{\partial n} \right) ds$$

(where \bar{R} is the contour of R), let U and V be replaced by u^* as defined by the system A^* and the Green's Function above defined. Further, let R consist of the given domain with the exclusion of the region inside the circle ω surrounding the singular point (r', θ') .

In view of (11) and (12) Green's Theorem ultimately yields

$$\begin{aligned} u^*(r, \theta; p) = & \int_0^{\theta_0} \int_0^\infty r' H^*(r', \theta'; p) G(r, \theta; r', \theta'; p) d\theta' dr' \\ & + \int_0^\infty \frac{\phi_1^*(r', p)}{r'} \left\{ \frac{\partial}{\partial \theta'} G(r, \theta; r', \theta'; p) \right\}_{\theta'=0} dr' \\ & - \int_0^\infty \frac{\phi_2^*(r', p)}{r'} \left\{ \frac{\partial}{\partial \theta'} G(r, \theta; r', \theta'; p) \right\}_{\theta'=\theta_0} dr'. \quad (13) \end{aligned}$$

In (13) we have the formal solution of the system A^* . The problem reduces to the determination of the Green's Function.

Making use of the known expression for the Green's Function in the Theory of Heat Conduction corresponding to the wedge of an angle whose bounding planes are kept at 0° , and of the appropriate integral representation of arbitrary functions in terms of the latter Green's Function \dagger , we are led to the identity

$$\epsilon(r, \theta) = \frac{2}{\theta_0} \sum_{n=1}^\infty \sin \frac{n\pi\theta}{\theta_0} \int_0^\infty r' dr' \int_0^{\theta_0} \epsilon(r', \theta') \sin \frac{n\pi\theta'}{\theta_0} d\theta' \int_0^\infty \alpha J_{\frac{n\pi}{\theta_0}}(\alpha r) J_{\frac{n\pi}{\theta_0}}(\alpha r') d\alpha. \quad (14)$$

In view of (14) it may be easily verified that the expression

$$\frac{2\alpha^2}{\theta_0} \sum_{n=1}^\infty \sin \frac{n\pi\theta}{\theta_0} \int_0^\infty r' dr' \int_0^{\theta_0} \sin \frac{n\pi\theta'}{\theta_0} d\theta' \int_0^\infty \frac{\epsilon(r', \theta')}{p^2 + \alpha^2 \alpha'^2} J_{\frac{n\pi}{\theta_0}}(\alpha r) J_{\frac{n\pi}{\theta_0}}(\alpha r') \alpha d\alpha$$

is a solution of (9). If the function $\epsilon(r, \theta)$ vanishes everywhere except at the point (r', θ') , where it becomes infinite in such a way that (10) is satisfied, then the above expression reduces in the limit ($\rho \rightarrow 0$) to the desired Green's Function. Thus, we ultimately have

$$G(r, \theta; r', \theta'; p) = \frac{2\alpha^2}{\theta_0} \sum_{n=1}^\infty \sin \frac{n\pi\theta}{\theta_0} \sin \frac{n\pi\theta'}{\theta_0} \int_0^\infty \frac{\alpha}{p^2 + \alpha^2 \alpha'^2} J_{\frac{n\pi}{\theta_0}}(\alpha r) J_{\frac{n\pi}{\theta_0}}(\alpha r') d\alpha. \quad (15)$$

Substituting (15) in (13) and remembering the significance of the function $H^*(r, \theta; p)$, from (6) we ultimately get

$$u^*(r, \theta; p) = u_1^* + u_2^* + u_3^*, \quad (16)$$

\dagger See Carslaw's 'Mathematical Theory of Heat Conduction,' Articles 80 & 90.

where

$$\begin{aligned}
 u_1^* = & -\frac{2a^2}{\theta_0} \sum_{n=1}^{\infty} \sin \frac{n\pi\theta}{\theta_0} \int_0^{\theta_0} \sin \frac{n\pi\theta'}{\theta_0} d\theta' \int_0^{\infty} r' dr' \\
 & \times \int_0^{\infty} \frac{\Omega^*(r', \theta', p)}{p^2 + a^2\alpha^2} J_{\frac{n\pi}{\theta_0}}(\alpha r) J_{\frac{n\pi}{\theta_0}}(\alpha r') \alpha d\alpha \\
 & + \frac{2}{\theta_0} \sum_{n=1}^{\infty} \sin \frac{n\pi\theta}{\theta_0} \int_0^{\theta_0} \sin \frac{n\pi\theta'}{\theta_0} d\theta' \int_0^{\infty} r' f(r', \theta') dr' \\
 & \times \int_0^{\infty} \frac{p}{p^2 + a^2\alpha^2} J_{\frac{n\pi}{\theta_0}}(\alpha r) J_{\frac{n\pi}{\theta_0}}(\alpha r') \alpha d\alpha \\
 & + \frac{2}{\theta_0} \sum_{n=1}^{\infty} \sin \frac{n\pi\theta}{\theta_0} \int_0^{\theta_0} \sin \frac{n\pi\theta'}{\theta_0} d\theta' \int_0^{\infty} r' g(r', \theta') dr' \\
 & \times \int_0^{\infty} \frac{1}{p^2 + a^2\alpha^2} J_{\frac{n\pi}{\theta_0}}(\alpha r) J_{\frac{n\pi}{\theta_0}}(\alpha r') \alpha d\alpha. \quad (17)
 \end{aligned}$$

$$u_2^* = \frac{2a^2\pi}{\theta_0^2} \sum_{n=1}^{\infty} n \sin \frac{n\pi\theta}{\theta_0} \int_0^{\infty} \frac{dr'}{r'} \int_0^{\infty} \frac{\phi_1^*(p, r')}{p^2 + a^2\alpha^2} J_{\frac{n\pi}{\theta_0}}(\alpha r) J_{\frac{n\pi}{\theta_0}}(\alpha r') \alpha d\alpha. \quad (18)$$

$$u_{3i}^* = \frac{2a^2\pi}{\theta_0^2} \sum_{n=1}^{\infty} (-1)^{n+1} n \sin \frac{n\pi\theta}{\theta_0} \int_0^{\infty} \frac{dr'}{r'} \int_0^{\infty} \frac{\phi_2^*(p, r')}{p^2 + a^2\alpha^2} J_{\frac{n\pi}{\theta_0}}(\alpha r) J_{\frac{n\pi}{\theta_0}}(\alpha r') \alpha d\alpha. \quad (19)$$

Making use of the identities

$$\begin{aligned}
 \int_0^{\infty} e^{-pt} \sin \alpha t dt &= \frac{a\alpha}{p^2 + a^2\alpha^2}, \\
 \int_0^{\infty} e^{-pt} \cos \alpha t dt &= \frac{p}{p^2 + a^2\alpha^2},
 \end{aligned}$$

and of Borel's Theorem, the inverse Laplace Transforms of the u^* 's are as follows:—

$$\begin{aligned}
 u_1(r, \theta; t) = & -\frac{2a}{\theta_0} \sum_{n=1}^{\infty} \sin \frac{n\pi\theta}{\theta_0} \int_0^{\theta_0} \sin \frac{n\pi\theta'}{\theta_0} d\theta' \int_0^{\infty} r' dr' \\
 & \times \int_0^{\infty} J_{\frac{n\pi}{\theta_0}}(\alpha r) J_{\frac{n\pi}{\theta_0}}(\alpha r') d\alpha \int_0^t \sin \alpha \alpha(t-\tau) \Omega(r', \theta', \tau) d\tau \\
 & + \frac{2}{\theta_0} \sum_{n=1}^{\infty} \sin \frac{n\pi\theta}{\theta_0} \int_0^{\theta_0} \sin \frac{n\pi\theta'}{\theta_0} d\theta' \int_0^{\infty} r' f(r', \theta') dr' \\
 & \times \int_0^{\infty} \cos \alpha t J_{\frac{n\pi}{\theta_0}}(\alpha r) J_{\frac{n\pi}{\theta_0}}(\alpha r') \alpha d\alpha \\
 & + \frac{2}{a\theta_0} \sum_{n=1}^{\infty} \sin \frac{n\pi\theta}{\theta_0} \int_0^{\theta_0} \sin \frac{n\pi\theta'}{\theta_0} d\theta' \int_0^{\infty} r' g(r', \theta') dr' \\
 & \times \int_0^{\infty} \sin \alpha t J_{\frac{n\pi}{\theta_0}}(\alpha r) J_{\frac{n\pi}{\theta_0}}(\alpha r') d\alpha. \quad (20)
 \end{aligned}$$

$$u_2(r, \theta; t) = \frac{2a\pi}{\theta_0^2} \sum_{n=1}^{\infty} n \sin \frac{n\pi\theta}{\theta_0} \int_0^{\infty} \frac{dr'}{r'} \int_0^{\infty} J_{\frac{n\pi}{\theta_0}}(\alpha r) J_{\frac{n\pi}{\theta_0}}(\alpha r') d\alpha \\ \times \int_0^t \sin \alpha(t-\tau) \phi_1(r', \tau) d\tau. \quad (21)$$

$$u_3(r, \theta; t) = \frac{2a\pi}{\theta_0^2} \sum_{n=1}^{\infty} (-1)^{n+1} n \sin \frac{n\pi\theta}{\theta_0} \int_0^{\infty} \frac{dr'}{r'} \int_0^{\infty} J_{\frac{n\pi}{\theta_0}}(\alpha r) J_{\frac{n\pi}{\theta_0}}(\alpha r') d\alpha \\ \times \int_0^t \sin \alpha(t-\tau) \phi_2(r', \tau) d\tau. \quad (22)$$

The final solution of the system A is therefore

$$u = u_1 + u_2 + u_3, \quad (23)$$

where u_1 , u_2 , and u_3 are given by (20), (21), and (22).

PART II.

In this case we shall assume that the displacement satisfies the mixed boundary conditions

$$u(r, \theta; t) = \phi_1(r, t) \text{ for } \theta = 0. \quad (1)$$

$$\frac{\partial}{\partial \theta} u(r, \theta; t) = \phi_2(r, t) \text{ for } \theta = \theta_0. \quad (2)$$

The Laplace Transform therefore must satisfy the boundary conditions

$$u^*(r, \theta; p) = \phi_1^*(r, p) \text{ for } \theta = 0. \quad (3)$$

$$\frac{\partial}{\partial \theta} u^*(r, \theta; p) = \phi_2^*(r, p) \text{ for } \theta = \theta_0. \quad (4)$$

If now the Green's function is required to satisfy the boundary conditions

$$G(r, \theta; r', \theta'; p) = 0 \text{ for } \theta = 0. \quad (5)$$

$$\frac{\partial}{\partial \theta} G(r, \theta; r', \theta'; p) = 0 \text{ for } \theta = \theta_0. \quad (6)$$

the application of Green's Theorem ultimately yields

$$u^*(r, \theta; p) = \int_0^{\theta} d\theta' \int_0^{\infty} r' H^*(r', \theta'; p) G(r, \theta; r', \theta'; p) dr' \\ + \int_0^{\infty} \frac{\phi_1^*(r', p)}{r'} \left\{ \frac{\partial}{\partial \theta} G(r, \theta; r', \theta'; p) \right\}_{\theta' = 0} dr' \\ + \int_0^{\infty} \frac{\phi_2^*(r', p)}{r'} \left\{ G(r, \theta; r', \theta'; p) \right\}_{\theta' = \theta_0} dr' \\ = u_1 + u_2 + u_3 \text{ (say),} \quad (7)$$

and the problem reduces to the determination of the Green's Function.

In the special case where ϕ_1 and ϕ_2 are equal to zero, u^* reduces to u_1^* . In this case, an independent solution may be obtained as follows:

We extend the domain of definition of the function u_1^* from $\theta = \theta_0$ to $\theta = 2\theta_0$ and assume that the functions f , g , and Ω are symmetrical with respect to $\theta = \theta_0$. It is then clear that the boundary condition (4) is automatically satisfied.

The desired solution may be obtained from Part I. by replacing θ_0 by $2\theta_0$. This yields

$$u_1^*(r, \theta; p) = \frac{a^2}{\theta_0} \sum_{n=1}^{\infty} \sin \frac{n\pi\theta}{2\theta_0} \int_0^{\infty} r' dr' \int_0^{\infty} \frac{\alpha d\alpha}{p^2 + a^2\alpha^2} \frac{J_{\frac{n\pi}{2\theta_0}}(\alpha r) J_{\frac{n\pi}{2\theta_0}}(\alpha r')}{2\theta_0} \\ \times \int_0^{2\theta_0} \sin \frac{n\pi\theta'}{2\theta_0} H^*(r', \theta'; p) d\theta'. \quad (8)$$

Since $H^*(r, \theta; p)$ is symmetrical with respect to θ_0 , it may be easily shown

$$\int_0^{2\theta_0} \sin \frac{n\pi\theta'}{2\theta_0} H^*(r, \theta; p) d\theta' = \begin{cases} 0 & \text{if } n \text{ is even,} \\ 2 \int_0^{\theta_0} \sin \frac{(2p+1)\pi\theta'}{2\theta_0} H^*(r, \theta; p) d\theta, & \\ \text{if } n \text{ is odd.} \end{cases} \quad (9)$$

In view of (9), (8) becomes

$$u_1^*(r, \theta; p) = \frac{2a^2}{\theta_0} \sum_{n=0}^{\infty} \sin \frac{(2n+1)\pi\theta}{2\theta_0} \int_0^{\infty} r' dr' \\ \times \int_0^{\infty} \frac{\alpha d\alpha}{p^2 + a^2\alpha^2} \frac{J_{\frac{(2n+1)\pi}{2\theta_0}}(\alpha r) J_{\frac{(2n+1)\pi}{2\theta_0}}(\alpha r')}{2\theta_0} \\ \times \int_0^{\theta_0} \sin \frac{(2n+1)\pi\theta'}{2\theta_0} H^*(r', \theta'; p) d\theta'. \quad (10)$$

In (10) we have the explicit expression of the first term of (7).

From (10) the Green's Function is at once obtained in the form

$$G(r, \theta; r', \theta'; p) = \frac{2a^2}{\theta_0} \sum_{n=0}^{\infty} \sin \frac{(2n+1)\pi\theta}{2\theta_0} \sin \frac{(2n+1)\pi\theta'}{2\theta_0} \\ \int_0^{\infty} \frac{\alpha d\alpha}{p^2 + a^2\alpha^2} \frac{J_{\frac{(2n+1)\pi}{2\theta_0}}(\alpha r) J_{\frac{(2n+1)\pi}{2\theta_0}}(\alpha r')}{2\theta_0}. \quad (11)$$

Comparison between (11) and (15) shows clearly that the former may be obtained from the latter by replacing n by $\frac{2n+1}{2}$ and replacing the symbol $\sum_{n=1}^{\infty}$ by the symbol $\sum_{n=0}^{\infty}$. This leads to the solution

$$u = u_1 + u_2 + u_3, \quad (12)$$

where

$$\begin{aligned}
 u_1(r, \theta; t) = & -\frac{2a}{\theta_0} \sum_{n=0}^{\infty} \sin \frac{(2n+1)\pi\theta}{2\theta_0} \int_0^{\theta_0} \sin \frac{(2n+1)\pi\theta'}{2\theta_0} d\theta' \int_0^{\infty} r' dr' \\
 & \times \int_0^{\infty} \frac{J_{\frac{(2n+1)\pi}{2\theta_0}}(\alpha r) J_{\frac{(2n+1)\pi}{2\theta_0}}(\alpha r')}{\frac{(2n+1)\pi}{2\theta_0}} d\alpha \int_0^t \sin \alpha(t-\tau) \Omega(r', \theta'; \tau) d\tau \\
 & + \frac{2}{\theta_0} \sum_{n=0}^{\infty} \sin \frac{(2n+1)\pi\theta}{2\theta_0} \int_0^{\theta_0} \sin \frac{(2n+1)\pi\theta'}{2\theta_0} d\theta' \int_0^{\infty} r' f(r', \theta') dr' \\
 & \times \int_0^{\infty} \cos \alpha t \frac{J_{\frac{(2n+1)\pi}{2\theta_0}}(\alpha r) J_{\frac{(2n+1)\pi}{2\theta_0}}(\alpha r')}{\frac{(2n+1)\pi}{2\theta_0}} d\alpha \\
 & + \frac{2}{a\theta_0} \sum_{n=0}^{\infty} \sin \frac{(2n+1)\pi\theta}{2\theta_0} \int_0^{\theta_0} \sin \frac{(2n+1)\pi\theta'}{2\theta_0} d\theta' \int_0^{\infty} r' g(r', \theta') dr' \\
 & \times \int_0^{\infty} \sin \alpha t \frac{J_{\frac{(2n+1)\pi}{2\theta_0}}(\alpha r) J_{\frac{(2n+1)\pi}{2\theta_0}}(\alpha r')}{\frac{(2n+1)\pi}{2\theta_0}} d\alpha. \quad \dots \dots \dots (13)
 \end{aligned}$$

$$\begin{aligned}
 u_2(r, \theta; t) = & \frac{a\pi}{\theta_0^2} \sum_{n=0}^{\infty} (2n+1) \sin \frac{(2n+1)\pi\theta}{2\theta_0} \int_0^{\infty} \frac{dr'}{r'} \\
 & \times \int_0^{\infty} \frac{J_{\frac{(2n+1)\pi}{2\theta_0}}(\alpha r) J_{\frac{(2n+1)\pi}{2\theta_0}}(\alpha r')}{\frac{(2n+1)\pi}{2\theta_0}} d\alpha \int_0^t \sin \alpha(t-\tau) \phi_1(r', \tau) d\tau. \quad \dots (14)
 \end{aligned}$$

$$\begin{aligned}
 u_3(r, \theta; t) = & \frac{2a\pi}{\theta_0^2} \sum_{n=0}^{\infty} (-1)^n \sin \frac{(2n+1)\pi\theta}{2\theta_0} \int_0^{\infty} \frac{dr'}{r'} \\
 & \times \int_0^{\infty} \frac{J_{\frac{(2n+1)\pi}{2\theta_0}}(\alpha r) J_{\frac{(2n+1)\pi}{2\theta_0}}(\alpha r')}{\frac{(2n+1)\pi}{2\theta_0}} d\alpha \int_0^t \sin \alpha(t-\tau) \phi_2(r', \tau) d\tau. \quad (15)
 \end{aligned}$$

PART III.

In this case we shall assume that the displacement satisfies the boundary conditions

$$\frac{\partial u}{\partial \theta} = \phi_1(r, t) \text{ for } \theta=0. \quad \dots \dots \dots (1)$$

$$\frac{\partial u}{\partial \theta} = \phi_2(r, t) \text{ for } \theta=\theta_0. \quad \dots \dots \dots (2)$$

The Laplace Transform must then satisfy the boundary conditions

$$\frac{\partial u^*}{\partial \theta} = \phi_1^*(r, p) \text{ for } \theta=0. \quad \dots \dots \dots (3)$$

$$\frac{\partial u^*}{\partial \theta} = \phi_2^*(r, p) \text{ for } \theta=\theta_0. \quad \dots \dots \dots (4)$$

If the Green's Function is required to satisfy the boundary condition

$$\frac{\partial G}{\partial \theta} = 0 \text{ for } \theta=0 \text{ and } \theta=\theta_0, \quad \dots \dots \dots (5)$$

the application of Green's Theorem ultimately yields

$$\begin{aligned}
 u^* = & \int_0^{\theta_0} \int_0^\infty H^*(r', \theta'; p) G(r, \theta; r', \theta'; p) r' dr' d\theta' \\
 & - \int_0^\infty \frac{\phi_1^*(r', p)}{r'} \{G(r, \theta; r', \theta'; p)\}_{\theta=0} dr' \\
 & + \int_0^\infty \frac{\phi_2^*(r', p)}{r'} \{G(r, \theta; r', \theta'; p)\}_{\theta=\theta_0} dr'. \quad (6)
 \end{aligned}$$

The problem thus reduces to the determination of the Green's Function. From the known expression for the Green's Function in the problem of heat conduction, when the boundary planes are impervious to heat, and from the appropriate integral representation of arbitrary functions in terms of the Green's Function, we are led to the identity

$$\begin{aligned}
 \epsilon(r, \theta) = & \frac{2}{\theta_0} \sum_{n=1}^\infty \cos \frac{n\pi\theta}{\theta_0} \int_0^\infty r' dr' \int_0^{\theta_0} \epsilon(r', \theta') \cos \frac{n\pi\theta'}{\theta_0} d\theta' \\
 & \times \int_0^\infty \frac{J_{\frac{n\pi}{\theta_0}}(\alpha r) J_{\frac{n\pi}{\theta_0}}(\alpha r')}{\alpha} d\alpha. \quad \dots \dots (7)
 \end{aligned}$$

It can be easily verified that the expression

$$\begin{aligned}
 & \frac{2a^2}{\theta_0} \sum_{n=1}^\infty \cos \frac{n\pi\theta}{\theta_0} \int_0^\infty r' dr' \int_0^{\theta_0} \cos \frac{n\pi\theta'}{\theta_0} d\theta' \\
 & \times \int_0^\infty \frac{\epsilon(r', \theta')}{p^2 + a^2\alpha^2} \frac{J_{\frac{n\pi}{\theta_0}}(\alpha r) J_{\frac{n\pi}{\theta_0}}(\alpha r')}{\alpha} d\alpha
 \end{aligned}$$

is a solution of I. (9). If the function $\epsilon(r, \theta)$ vanishes everywhere except at the point (r', θ') , where it becomes infinite in such a way that I. (10) is satisfied, then the above expression reduces in the limit ($\rho \rightarrow 0$) to the desired Green's Function, and we have

$$\begin{aligned}
 G(r, \theta; r', \theta'; p) = & \frac{2a^2}{\theta_0} \sum_{n=1}^\infty \cos \frac{n\pi\theta}{\theta_0} \cos \frac{n\pi\theta'}{\theta_0} \\
 & \times \int_0^\infty \frac{\alpha}{p^2 + a^2\alpha^2} \frac{J_{\frac{n\pi}{\theta_0}}(\alpha r) J_{\frac{n\pi}{\theta_0}}(\alpha r')}{\alpha} d\alpha. \quad \dots (8)
 \end{aligned}$$

Comparing (6) with I. (13) and taking into account the new expression for the Green's Function, we are led to the conclusion that the expression for u_1 in the present case may be obtained from the corresponding expression in Part I. by replacing $\sin \frac{n\pi\theta}{\theta_0}$ and $\frac{n\pi\theta'}{\theta_0}$ by $\cos \frac{n\pi\theta}{\theta_0}$ and $\cos \frac{n\pi\theta'}{\theta_0}$ respectively. Similarly, the expression u_2 and u_3 in the present case may be obtained from the corresponding expressions in Part I. by re-

placing $\sin \frac{n\pi\theta}{\theta_0}$ by $\cos \frac{n\pi\theta}{\theta_0}$ and by dividing by $-\frac{n\pi\theta}{\theta_0}$. Thus we ultimately get

$$u = u_1 + u_2 + u_3, \quad . \quad . \quad . \quad . \quad . \quad . \quad . \quad . \quad (9)$$

where

$$\begin{aligned} u_1(r, \theta; t) = & -\frac{2a}{\theta_0} \sum_{n=1}^{\infty} \cos \frac{n\pi\theta}{\theta_0} \int_0^{\theta_0} \cos \frac{n\pi\theta'}{\theta_0} d\theta' \int_0^{\infty} r' dr' \\ & \times \int_0^t J_{\frac{n\pi}{\theta_0}}(\alpha r) J_{\frac{n\pi}{\theta_0}}(\alpha r') d\alpha \int_0^t \sin \alpha(t-\tau) \Omega(r', \theta', \tau) d\tau \\ & + \frac{2}{\theta_0} \sum_{n=1}^{\infty} \cos \frac{n\pi\theta}{\theta_0} \int_0^{\theta_0} \cos \frac{n\pi\theta'}{\theta_0} d\theta' \int_0^{\infty} r' f(r', \theta') dr' \\ & \times \int_0^{\infty} \cos \alpha t J_{\frac{n\pi}{\theta_0}}(\alpha r) J_{\frac{n\pi}{\theta_0}}(\alpha r') \alpha d\alpha \\ & + \frac{2}{a\theta_0} \sum_{n=1}^{\infty} \cos \frac{n\pi\theta}{\theta_0} \int_0^{\theta_0} \cos \frac{n\pi\theta'}{\theta_0} d\theta' \int_0^{\infty} r' g(r', \theta') dr' \\ & \times \int_0^{\infty} \sin \alpha t J_{\frac{n\pi}{\theta_0}}(\alpha r) J_{\frac{n\pi}{\theta_0}}(\alpha r') d\alpha \quad . \quad . \quad . \quad . \quad . \quad . \quad . \quad . \quad (10) \end{aligned}$$

$$\begin{aligned} u_2(r, \theta; t) = & -\frac{2a}{\theta_0} \sum_{n=1}^{\infty} \cos \frac{n\pi\theta}{\theta_0} \int_0^{\infty} \frac{dr'}{r'} \int_0^{\infty} J_{\frac{n\pi}{\theta_0}}(\alpha r) J_{\frac{n\pi}{\theta_0}}(\alpha r') d\alpha \\ & \times \int_0^t \sin \alpha(t-\tau) \phi_1(r', \tau) d\tau \quad . \quad . \quad . \quad . \quad . \quad . \quad . \quad . \quad (11) \end{aligned}$$

$$\begin{aligned} u_3(r, \theta; t) = & \frac{2a}{\theta_0} \sum_{n=1}^{\infty} (-1)^n \cos \frac{n\pi\theta}{\theta_0} \int_0^{\infty} \frac{dr'}{r'} \int_0^{\infty} J_{\frac{n\pi}{\theta_0}}(\alpha r) J_{\frac{n\pi}{\theta_0}}(\alpha r') d\alpha \\ & \times \int_0^t \sin \alpha(t-\tau) \phi_2(r', \tau) d\tau \quad . \quad . \quad . \quad . \quad . \quad . \quad . \quad . \quad (12) \end{aligned}$$

Brooklyn College and Yeshiva College.

XXXVII. *The Emission of Secondary Electrons from Nickel.*

By RAFI MOHAMMAD CHAUDHRI, Ph.D.(Cantab.), M.Sc.,
 Reader in Physics, and
 ABDUL WAHEED KHAN, M.Sc., Department of Physics,
 Muslim University, Aligarh *.

[Received December 2, 1940.]

Introduction.

THE emission of secondary electrons from metals by primary electrons has been studied by a number of investigators, but the results are not consistent. For instance, the experiments of Copeland (1935) and of Warnecke (1936) reveal that the electro-positive metals, having low work function, give greater secondary emission than metals like Ni, W, and other elements possessing higher work function. On the other hand, the work of Farnsworth (1935) and of De-Boer and Bruining (1938) show contrary results. All the experimenters, however, agree that :—

(a) The coefficient of secondary electron emission (*i. e.*, the number of secondary electrons emitted per primary electron) increases with increase of energy of the primary electrons for all metals (it being less than unity for low primary energies, rising to unity and becoming greater at higher energies).

(b) It rises to a maximum, the exact value depending upon the metal, for a certain primary energy, say, V_0 , which lies between 300–700 volts for all clean metals, and diminishes at primary energies higher than V_0 .

In previous experiments the decrease in the secondary emission with increase of energies of the primary electrons higher than V_0 has never been examined in detail. In some, the energy of the primaries is confined to a range which does not permit an investigation of this variation, as the upper primary energy limit is either below (Howarth, 1935) or not much above V_0 (Petry, 1926 ; Kreft, 1928 ; Rao, 1930 ; and Coomes, 1939) ; in others (Petry, 1925) the point has been overlooked. Moreover, very few reliable data are available for the secondary emission at oblique angles of incidence of the primary beam on metal surfaces except those

* Communicated by Professor M. L. Oliphant, F.R.S.

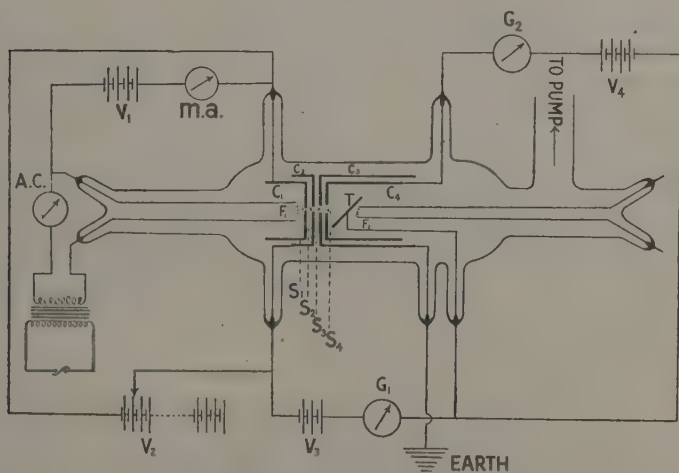
of Bruining (1938), and even in these experiments the primary energy did not exceed 1000 volts.

The present work has been carried out with primary energies lying within a suitable range of 100–4000 volts, where the upper limit is high enough for the decrease in the emission to be followed systematically as the energy exceeds V_0 . The angle of incidence of the electron beam on the nickel target was kept at $45\text{--}50^\circ$ in these experiments.

Description of the Apparatus.

The apparatus and the electrical connexions are shown in fig. 1. The main body of the apparatus consists of a cylindrical pyrex glass tube,

Fig. 1.



Apparatus and electrical connexions.

15 cm. long and 4 cm. in diameter. C_1 is a nickel cylinder, open at one end and is 3.0 cm. long and 2.5 cm. wide. The filament F_1 is placed close and opposite to the circular aperture S_1 , $\frac{3}{4}$ mm. in diameter, which is at the centre of the closed end of C_1 . C_2 is another nickel cylinder, with one end open, and is 3.0 cm. wide and 1.0 cm. deep. It encloses the top of C_1 and carries a circular aperture S_2 , 1.5 mm. in diameter, at the centre of its closed end. T is a nickel target, 1.0 cm. in diameter and 0.1 mm. thick, and is enclosed in the nickel cylinder C_4 , 2.8 cm. long and 2.5 cm. wide. It is open on one end and has a circular hole, S_4 , at the centre of the other. C_4 is enclosed in the nickel cylinder C_3 , 3.5 cm. long and 3.0 cm. wide. It is also open at one end and has a

circular hole S_3 , 2.5 mm. in diameter, at the centre of the other. The aperture S_4 is slightly bigger in diameter than S_3 . All the nickel cylinders were cut out from the same nickel sheet, 0.1 mm. thick. The slits S_1 , S_2 , S_3 , and S_4 are close and opposite to each other with their centres lying on the common axis of C_1 , C_2 , C_3 , and C_4 . The target T has its centre on the axis of the cylinders and is inclined to it at an angle of $40-45^\circ$. F_2 is another tungsten filament placed just behind T. It was heated with a low tension transformer and an electron current of 5–10 milliamps, at 5000 volts, was taken from it to bombard and degass the target when desired.

All the metal joints were made by spot-welding the parts together. The electrodes were well insulated from each other and were held firm in position in the tube with pyrex-tungsten seals.

The apparatus was connected to a Metropolitan Vicker's "02" oil condensation pump backed by a Hyvac. It was air tight and could stand a high vacuum for several days. Before any readings were taken the apparatus was well baked under a high vacuum at $400-500^\circ\text{C}$. for five to six hours with pumps on throughout. The pumps were also kept continuously running during any set of observations taken.

The thermionic electrons from F_1 , which was heated by a highlyinsulated secondary of a low tension transformer, were accelerated to C_1 through a potential V_1 , varying from 2–10 volts. The current from F_1 was regulated by controlling its temperature with a rheostat placed in the secondary circuit. The cylinder, C_1 , served to capture the electrons from F_1 , except those which escaped through the hole, S_1 , and formed the incident beam. The main accelerating potential, V_2 , which varied from 50–4000 volts, was applied to the electron beam between C_1 and C_2 . A constant potential, $V_3=10$ volts, was applied to the beam between C_2 and the target T. Some of the electrons from F_1 hit the edges of the slit S_1 and liberated from there secondary electrons. The electron beam issuing out of S_1 was thus a mixture of the secondaries from S_1 and the thermionic electrons from F_1 . The potential, V_1 , was kept low to reduce to a minimum the number of these secondaries. The geometry of the slits S_2 , S_3 , and S_4 , their diameters being in the ascending order, prevented the electron beam, issuing out of S_1 , from striking and producing secondary electrons from their edges. Moreover, since the main accelerating potential, V_2 , was applied between C_1 and C_2 , and V_1 was always small compared to V_2 , the electron beam reaching the target was almost homogeneous. The primary current going to the target was measured with a mirror galvanometer G_1 . The secondary electrons, emitted from T on bombarding it with the primary beam, were collected by C_4 by making it positive with respect to the target. The collecting potential, V_4 , on the collector C_4 , varied between 60–80 volts. The cylinder C_3 , which

was permanently earthed, acted as a shield both to the collector and the target and prevented the stray charges from reaching either. The secondary current from T to C_4 was measured with a mirror galvanometer G_2 . The sensitivity of both the galvanometers, G_1 and G_2 , was about 10^{-8} amps., but for actual measurements their readings were carefully compared by passing a constant current through them when joined in series. For determining the coefficient of secondary emission, the primary current, I_1 , going to the target, T, and the secondary current, I_2 , going to the collector C_4 , were read on the two galvanometers simultaneously. The primary current, which was of the order of micro-amperes, was found to be reasonably steady, and for eliminating error in the absolute values of the coefficient, I_2/I_1 , due to any uncertainty in the sensitivity of the two galvanometers, the primary and the secondary currents both, were also read alternately with the same galvanometer, and each reading was repeated three or four times to allow for any fluctuations in the currents. This procedure was adopted throughout the experiment.

The potentials V_1 , V_2 , V_3 , and V_4 were obtained from dry batteries, but voltages higher than 500 volts were taken from an Evershed high tension direct current motor generator set which could give up to a maximum of 5500 volts. Voltages from 0 to 500 volts were read on a D.C. voltmeter, from 500 to 3000 volts on a Dwarf's electrostatic voltmeter made by W. G. Pye, Cambridge, and from 3000 volts onwards on a Stark-Shroeder type high voltage voltmeter which could read from 1000 to 20,000 volts.

The Results.

Curves were obtained by plotting the absolute values of the ratios, I_2/I_1 , where I_2 is the total secondary current to the collector, C_4 , and I_1 the primary current to the target T, as a function of the primary electrons energy, V , which varied from 100 to 4000 volts. These give the number of secondary electrons emitted from nickel surface per primary electron of different energies. To make certain that all the secondary electrons emitted from T were collected by C_4 , readings were checked with different collecting potentials, V_4 , on the collector. It was found that the $I_2/I_1 - V$ curves remained unaltered, if V_4 was maintained above 60 volts and no change in the secondary current to the collector was noticeable by raising it up to 80 volts. If, however, its value was kept below 60 volts, some of the secondary electrons were found to escape the collector at all primary energies. Moreover, it was also observed that if C_4 was made negative by 60 volts with respect to the target, no appreciable current flowed to the collector.

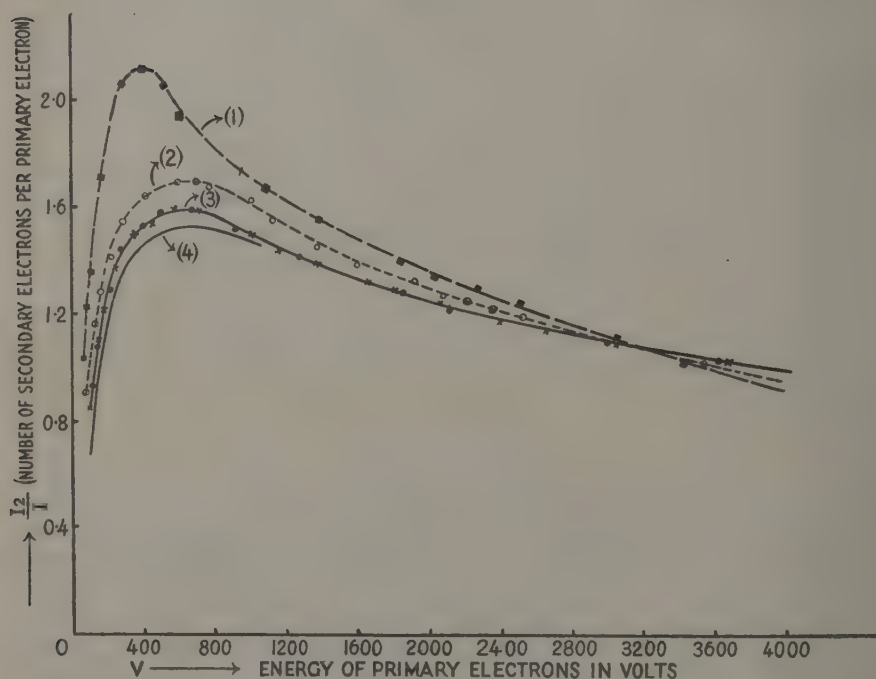
The results for dirty nickel surface which was given no heat-treatment

beyond the baking of the apparatus as a whole at 400–500° C. are given in curve (1), fig. 2, from which it is clear that

(a) The value of the secondary emission coefficient, I_2/I_1 , is less than unity for low energies, but rises to the maximum value of 2.1 at primary energy of 300–400 volts.

(b) It diminishes as the energy of the primaries exceeds 400 volts. The fall in its value, immediately beyond the maximum, is sharp, but afterwards it is gradual, and continues up to the highest energy used.

Fig. 2.



Secondary electron emission curves for nickel.

- Curve (1) Undegassed target.
 „ (2) Target heated for 15 minutes.
 „ (3) Target heated for 3 hours.
 „ (4) De-Boer and Bruining's.

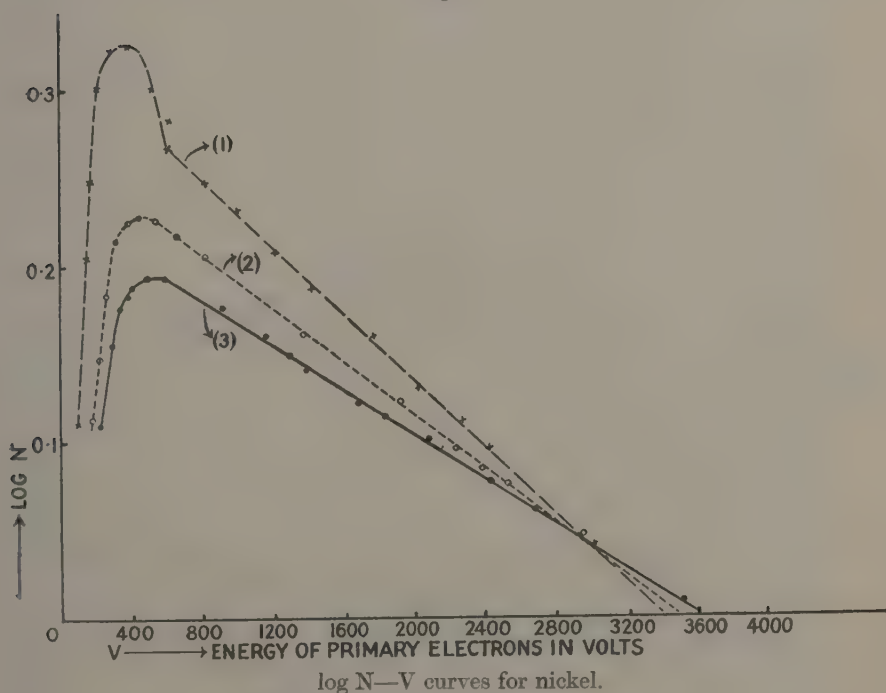
The results with partially degassed nickel surface heated for about fifteen minutes with an electron current of 5–10 milliamperes at 5000 volts are given in curve (2), fig. 2. Curve (3), fig. 2, shows results for well degassed clean surface heated at bright heat for about three hours.

No change in the secondary emission was observed on further degassing the target, as shown by circles, on curve (3), fig. 2.

It is at once evident from the curves in fig. 2, that the general character of the curves does not alter on degassing the surface. The following changes are, however, quite prominent :—

(a) The ratio, I_2/I_1 , for well-degassed surface at any particular energy of primary electrons, is smaller than for a dirty one, and for a clean nickel target its maximum value falls to 1.58.

Fig. 3.



Curve (1) Undegassed target.

„ (2) Target heated for 15 minutes.

„ (3) Target heated for 3 hours.

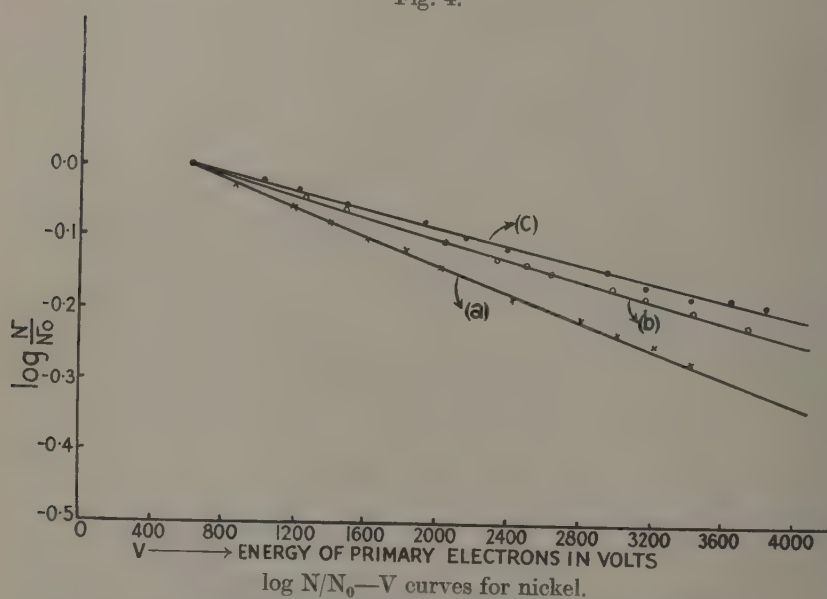
(b) The position of the maximum shifts towards higher energy and for well out-gassed nickel surface it occurs at about 600 volts energy of the primaries.

The sharp decrease in the secondary emission immediately beyond the maximum does not appear in curves for a degassed target. Moreover,

the general fall of the curves throughout beyond the maximum is less rapid for degassed than for dirty surfaces. These points become more pronounced by plotting $\log N - V$ curves, as shown in fig. 3, where N is the value of I_2/I_1 for primary energy of V volts. The corresponding values of N and V are taken from the curves given in fig. 2.

There is a kink beyond the maximum in curve (1), fig. 3, for undegassed targets, while curves (2 and 3), fig. 3, for partially and well-degassed surfaces, respectively, do not exhibit any such discontinuity. The kink in curve (1) and the maxima in curves (2 and 3) appear almost at the same energy of the primary electrons, viz., 600 volts. The portions of all the curves

Fig. 4.



- Curve (a) Undegassed target.
 „ (b) Target heated for 15 minutes.
 „ (c) Target heated for 3 hours.

in fig. 3, beyond 600 volts energy, are straight lines which intersect each other at a point lying near about 3200 volts energy of the incident beam.

From curves in fig. 2, the ratios N/N_0 , where N and N_0 are the values of the secondary emission coefficients, I_2/I_1 , at energy V and 600 volts respectively, are calculated at different primary energies all taken higher than 600 volts, and the values obtained are used in drawing curves, *a*, *b*, and *c*, fig. 4, connecting $\log N/N_0$ and V , for undegassed, partially degassed, and well-degassed nickel surfaces, respectively. These are all straight

lines, and are inclined to the energy axis at different angles. They all meet at a point lying at about 600 volts energy of the primary beam.

For the sake of comparison, Bruining and De-Boer's results (1938) for the secondary emission from a clean nickel surface, with the primary beam incident on the target at an angle of 48° , are given in curve (4), fig. 2. The highest energy of the primary electrons in their experiment was 1000 volts. The authors' results for a well out-gassed Ni target, curve (3), fig. 2, are in good agreement with those of the Dutch workers up to this energy: slightly higher values of the secondary emission in curve (3), fig. 2, throughout, are probably due to greater angle of incidence of the primary beam on the nickel target in our experiments than in Bruining's.

The values of the secondary emission coefficients were also determined with varying primary currents for any particular energy of the incident electrons. It was observed that within the limits of the experimental error the ratio, I_2/I_1 , was independent of the current strength, but was a function of the primary energy only, while the I_2/I_1 -V curves for a clean well out-gassed nickel target were reproducible.

Interpretation of the Results.

Metals usually contain adsorbed gases, and it is generally believed that the presence of films of impurities on metallic surfaces reduces their work function and increases their capacity for emitting electrons. The greater emission of secondary electrons from dirty metal surfaces than from a clean one by the action of positive ions on them has been ascribed to this factor by Oliphant (1930). The lowering of the cathode fall of potential in a gaseous discharge when the negative electrode is contaminated has been accounted for in a similar way (J. J. Thomson & G. P. Thomson, 1933).

The comparatively high values of the secondary emission coefficients for a dirty nickel target in our experiments, curve (1), fig. 2, are, probably, also due to the existence of foreign films on its surface. By heating the target the adsorbed gases are removed and the surface becomes clean and free from films of impurities if appropriate heat treatment is given to the metal for a prolonged period. The values of the coefficients of secondary emission in curve (2), fig. 2, are lower throughout than in the previous case, but are higher than those given in curve (3), fig. 2. It is because the contaminations were still present on the target, but in an amount smaller than on the dirty surface. The complete absence of surface films and adsorbed gases from the target is responsible for the lowest secondary emission from its surface as shown in curve (3), fig. 2. This corresponds to a steady state of the target when no more gases and impurities could be expelled out of it by further degassing. This

is probably why no additional decrease was observed in the secondary emission, as shown by circles, curve (3), fig. 2, on heat treating the target any longer.

The work-function of a metal is affected when a foreign film, only a few atoms deep, gets deposited on it. With addition of more layers the work-function of the metal is hardly expected to change further. In presence of films, several atoms deep, the variation of the secondary emission with the energy of the incident beam is dominated by the characteristics of the upper surface films for relatively low energies of the primaries, but when the incident electrons have energies high enough to penetrate the surface films and reach the metal proper, the phenomenon is mainly governed by the metal, and the variation of the emission with further increase of energy of the primaries depends upon the characteristics of the metal (Copeland, 1935).

We believe that the film on the dirty nickel surface in our experiment was several atoms deep and that its characteristics controlled the secondary emission up to a few hundred volts energy of the primary beam. At higher energies the incident electrons were fast enough to pierce through the film and reach the nickel surface and cause its characteristic emission. The kink in curve (1), fig. 3, at about 600 volts energy of the primaries, and the sudden change of slope of the curve beyond that, which corresponds to a sudden change in the variation of the secondary emission with energy of the primaries, are in favour of our assumption.

The curves (1, 2, and 3), fig. 3, are all straight lines beyond 600 volts energy of the incident electrons. This leads us to the conclusion that the secondary emission from nickel decreases exponentially with increase of energy of the primaries above 600 volts. It is also apparent from fig. 3, that the difference, in the secondary emission coefficients for dirty, partially, and well-degassed surfaces of nickel, at any particular energy, lying above 500–600 volts of the primary beam, becomes smaller and smaller as the energy of the incident electrons becomes greater. It appears that at high energies the secondary emission from a dirty surface is primarily the characteristic emission of clean nickel, and this is probably why the variation of the secondary emission with primary energies, higher than 600 volts, is similar in all the three cases of nickel surface.

Since the decline in the secondary emission above 600 volts primary energy is exponential, the curves (1, 2, and 3), fig. 2, beyond this energy, can be represented by an equation of the form :

$$N = N_0 e^{-\alpha(V-600)}$$

Here N and N_0 are the values of the secondary emission coefficients at primary energy of V and 600 volts, respectively, in all the three cases of nickel surface, e is the base of the Napierian Logarithms and L a con-

stant depending upon the surface condition of the metal. The slopes of the log curves in fig. 4 give the values of L for the three different conditions of the nickel target. Substituting the values of L in the above equation, we find that the values of V , where N reduces to $N_0/2$, come out to be about 3691, 4648, and 5253 volts for dirty, partially, and well-degassed nickel surface, respectively. This anticipates that the decline in the secondary emission from nickel would continue up to fairly high energies. Recent work of Rakov and Antonov (1939) shows, in any case, that the secondary emission from metals decreases continuously with increase of energy of the primaries over a wide range, from 5000 volts onwards, of the energy of the incident electrons.

In earlier investigations no simple relation has been established between the energy of the primary electrons and the secondary emission coefficient, nor any satisfactory theory has yet been put forward to explain the phenomenon of the secondary emission from metals. The present work appears, however, to offer some helpful suggestion regarding the mechanism of the secondary emission.

The secondary electrons have to overcome, in emerging from the metal, the potential field that exists over its surface. They must, therefore, possess some initial energy to start with. It is probable that the secondaries receive this energy direct from the primary electrons by a process analogous to that of ionization of gases by electrons. In gaseous ionization, electrons of a particular energy, whose value lies between 100–200 volts for all gases, are the most efficient ionizers. Their efficiency falls on either side of this energy. Let us assume that in a metal, too, incident electrons of a certain energy, E , whose magnitude depends upon the nature of the metal, are most energetic and somehow produce in all, say, n_0 secondary electrons per primary electron inside the metal, and unlike the case of gaseous ionization, become dead after having released them and, further, that their efficiency of liberating secondaries drops sharply if the energy exceeds E volts. The depth which a primary can penetrate in the metal would naturally depend upon its incident energy. We may assume a linear relation, to exist between $(E' - E)$ and x , where E' is the energy of the primaries greater than E and x is the thickness of the metal traversed in losing the amount of energy $(E' - E)$. Accordingly, an incident electron with energy E' , would penetrate the metal without producing appreciable number of secondaries in its path, unless its energy reduces to E , when it releases n_0 secondaries near the end of its range inside the metal. The depth at which the secondaries n_0 will be produced will be greater as the primary energies become higher.

The secondaries possess low energies, and in the absence of any reliable data regarding the absorption of slow electrons in metals, we assume that it increases exponentially with the thickness of the metal they travel.

If the intensity of the secondary beam at a point is I_0 , then after emerging out of depth x of the metal, it will be reduced to I , given by the relation

$$I = I_0 e^{-\mu x},$$

where e is the base of the Napierian Logarithms and μ a constant. (The case is similar to the absorption of X-rays in a metal.) Since x is proportional to $(E' - E)$, the above relation can be put as

$$I = I_0 e^{-K(E' - E)},$$

where K is another constant depending upon the surface condition and nature of the metal. If the secondaries, produced by an incident electron along its path inside the metal before its energy falls down to E , be taken very small in number as compared to those produced at the end of its range, it follows that the secondary emission should decrease exponentially with increase of energy of primary electrons beyond E volts. Thus for a clean metal the emission should be a maximum for a particular energy, should fall exponentially beyond that, and should have smaller values at lower primary energies. In any case our experimental curves represent these features of the secondary emission.

Summary.

The secondary electron emission from nickel produced by primary electrons of energy varying from 100–4000 volts, has been studied with the primary beam incident on the target at an angle of 45–50°. For a well-degassed surface the maximum value of the secondary emission coefficient has been found to be 1.58, the corresponding primary electron energy being about 60 volts. It is also observed that the secondary emission coefficient decreases exponentially as the energy of the primary electrons exceeds this value for degassed as well as un-degassed surfaces.

It is a pleasure to record our sincere thanks to Professor M. L. Oliphant for his interest in this work.

References.

- Copeland, *Phys. Rev.* **xlvi**, p. 96 (1935).
 Warnecke, *J. Physique Radium*, **vii**, p. 270 (1936).
 Farnsworth, *Phys. Rev.* **xxv**, p. 41 (1925).
 De-Boer and Bruining, *Physica*, **v**, p. 17 (1938).
 Howarth, *Phys. Rev.* **xlvi**, p. 89 (1935).
 Petry, *Phys. Rev.* **xxviii**, p. 362 (1926).
 Kreft, *Phys. Rev.* **xxxi**, p. 199 (1928).
 Rao, *Proc. Roy. Soc. A*, **cxxviii**, p. 41 (1930).
 Coomes, *Phys. Rev.* **lv**, p. 519 (1939).

Petry, Phys. Rev. xxvi. p. 346 (1925).

Bruining and De-Boer, *Physica*, x. p. 901 (1938).

Bruining and De-Boer, *loc. cit.*

Oliphant, Proc. Roy. Soc. A, cxxvii. p. 373 (1930).

Sir J. J. and G. P. Thomson, 'Conduction of Electricity through Gases,' 3rd
2nd ed. vol. p. 324 (1933).

Copeland, *loc. cit.*

Rakov and Antonov, J. Tech. Physics, U.S.S.R. ix., x. p. 870 (1939).

XXXVIII. *The Reflexion and Refraction of Photons*

By E. TAYLOR JONES, D.Sc., Professor of Natural Philosophy
in the University of Glasgow *.

[Received January 3, 1941.]

Now that the light-particle, or photon, is generally accepted as one of the essential particles of Physics, it is desirable that the theories of all optical phenomena should be re-examined, and stated, if possible, in terms of this particle. The form which such revised theories will take must depend upon the particular type of photon postulated in each case as the basis of the theory, but all photon theories must have some features in common, since there are certain general conditions which must be satisfied by all types. Among these conditions may be mentioned :

- (1) that the photon must have finite mass and energy, although it is travelling with the velocity of light ;
- (2) its frequency must be equal to that of the source by which it was emitted ;
- (3) it must have wave-length λ related to the velocity and the frequency ν by the equation $\lambda\nu=c$;
- (4) it must carry no electric charge, but it must have a transverse electrical axis in order to account for polarization and electro-optical effects.

All these properties, and others which must also be taken into account in theories of the nature of light, are possessed by a type of photon suggested by the present writer (III. p. 465) †. It is based upon a theory in which electrostatic and magnetic energy are represented by the frequency and energy changes experienced by systems of electrons regarded as vibrators coupled with each other (I., II., IV.). The mutual energy of two electrons cannot become infinite however short the distance between them, since the coupling has a natural finite limiting value. In this theory the photon is regarded as a pair of electrons, of opposite

* Communicated by the Author.

† The former papers on the vibratory electron and its applications appeared in the 'Philosophical Magazine' as follows :—I., xxi. p. 337, Suppl. (Feb. 1936) ; II., xxii. p. 921, Suppl. (Nov. 1936) ; III., xxiv. p. 458 (Sept. 1937) ; IV., xxv. p. 682 (April 1938) ; V., xxvii. p. 565 (May 1939).

sign, coupled so closely that the frequency of each is reduced to zero. It is therefore a vibratory doublet of zero energy when free and at rest or moving with any velocity less than that of light, but of finite energy when travelling with the speed of light.

In the present paper we shall consider the theory of the reflexion and refraction of vibratory doublet photons at the surface of a transparent isotropic medium.

The Laws of Reflexion and Refraction.

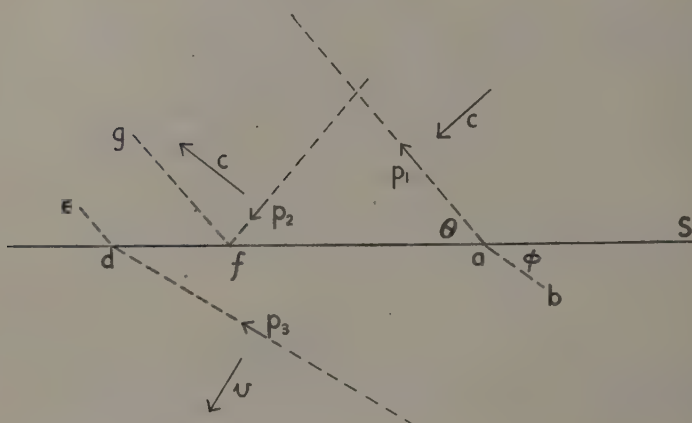
When a photon falls normally upon the plane surface of an isotropic transparent medium it becomes coupled electrically with some of the particles of the medium, its frequency becomes changed, and its velocity in the medium is changed in accordance with the dispersion formula which has been derived for photons of this type (V. p. 572). The dispersion of photons is therefore determined by the laws of vibration of coupled systems, not by those of forced oscillation and resonance upon which the classical theory is based. The new dispersion formula also differs from the classical one, particularly in reference to the imaginary values of the refractive index (defined as the ratio of the velocity of light *in vacuo* to that in the medium) which appear in the classical theory within a certain range of frequencies of the incident light. Such imaginary values do not occur in the photon theory of dispersion.

At first sight it would appear that a photon incident upon the refracting surface can, owing to the smallness of its size, insert itself between the surface particles of the medium and be deflected in almost any direction, or not deflected at all, so that no *regular* reflexion or refraction is to be expected. This would be the case if the photon were *only* a particle, and had no appendage of considerable extent to guide it in its movement relative to the surface of the medium. In fact, however, a photon moving in free space has a plane electron wave-sheet attached to it which enables it to become coupled with other electrons situated in the plane through the photon transverse to the direction of motion. It should be remarked that the vibrations of a photon which determine the frequency of the light do not consist of interchanges of position of its two electrons, or reversals of its axis, but they are the vibrations in the wave-sheet associated with the photon. Their frequency has been shown (III., p. 465) to conform with the relation $\lambda\nu=c$.

The familiar relations between the angles of incidence, refraction, and reflexion follow from the necessary condition that the wave-sheet attached to an incident photon must be unbroken at the interface separating the two media. In fig. 1 the short arrow p_1 represents the electrical axis of an incident photon approaching the surface S with velocity c in a direction

inclined at θ to the normal, the broken-line extensions of p_1 its accompanying wave-sheet. The photon is coupled with particles of the second medium near ab , this portion of the sheet travelling with velocity v in a direction inclined at ϕ to the normal. The velocity along the surface of the line of intersection of the sheet and the surface being the same in the two media, we have $c/\sin \theta = v/\sin \phi$, and, therefore, $\sin \theta = \mu \sin \phi$. The same condition holds at d in the wave-sheet of a photon p_3 which has entered the second medium, the portion de of the incident sheet not having yet reached the refracting surface. The short arrow p_2 represents a photon which has been reflected, the portion fg of its wave-sheet still travelling in the incident direction. The condition that the portions fg

Fig. 1.



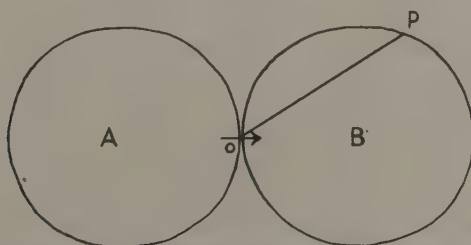
Showing incident, reflected, and refracted photons, and their accompanying wave-sheets.

and p_2f remain attached to each other leads at once to the law of the equality of the angles of incidence and reflexion. The law of reflexion also expresses the condition that the momentum of a reflected photon, resolved parallel to the surface S , is the same before and after incidence. In fig. 1 the photon is shown with its axis in the plane of incidence, but the same argument applies when the axis is perpendicular to this plane, though the wave-sheet falls off in strength with increasing distance more rapidly in the lateral than in the longitudinal direction (see fig. 2).

The other part of the laws of reflexion and refraction, viz., that the reflected and refracted rays are in the same normal plane as the incident ray, is accounted for by the symmetry of the wave-sheet with respect to the electrical axis of the photon. If the axis is either in or at right

angles to the plane of incidence, the sheet is also symmetrical with respect to this plane, and its guiding action prevents any deflexion of the photon to one side or to the other. But if the axis is neither parallel nor at right angles to the plane of incidence, the sheet is not symmetrical with regard to this plane. An idea of the form of the wave-sheet may be obtained from fig. 2, which shows how the coupling of a photon with an electron placed at a given distance from its centre varies with the angle between the axis of the photon and the line joining its centre to the electron. This line having the direction of OP, the coupling, represented by the length OP, is equal to $k/r_1 - k/r_2$, k being the coupling of two electrons at unit distance apart, and r_1, r_2 the distances of the electron from the two electrons composing the photon. The curve is drawn for the case in which the distance of the electron from the centre of the photon is 2.5 times the distance between the two components of the photon. At much

Fig. 2.



The coupling of a photon at O with an electron at a given distance on the line OP is proportional to the length OP.

greater distances from the photon the figure takes the form of two circles in contact.

If the axis of an incident photon is neither parallel nor perpendicular to the plane of incidence, the portion A (or B) reaches the refracting surface first, and, being on one side of the plane of incidence, might give rise to a lateral force on the photon deflecting it out of this plane. Such lateral force, if it exists, can be appreciable only at very minute distances, that is, when the photon itself reaches the surface, and then the other part of the sheet B (or A) comes into play with a force equal and opposite to the first, so that on the whole there is no lateral force on the photon, which, therefore, continues to move in the plane of incidence.

It will be noticed that the portion of the incident wave-sheet *ab* (fig. 1) is represented as having entered the second medium, that is, that the incident photon has become coupled with particles of the second medium just below the surface near *ab*. This appears to be the natural course of events in all cases of oblique incidence, there being, at this early stage

in the process, before the photon itself has reached the surface, apparently nothing to determine whether the photon is going to be reflected or transmitted.

The Probability of Reflexion and Refraction.

The intensities of the reflected and refracted pencils relative to that of the incident pencil are to be determined from the probability of reflexion or refraction of a photon incident upon the surface of the second medium. The expression for the probability depends in the first place upon the change of direction of motion of a photon when it becomes reflected or refracted. The smaller the change of direction of either path the greater the probability of the photon taking that path, and it is assumed that the probability of either path is proportional to the square of the component along its direction of the original propagation vector. If the only two possible directions of motion, Ox and Oy , after incidence are at right angles to each other, and if the direction of the original vector lies between them, making angles α and β with Ox and Oy , the probability of the path Ox is $\cos^2 \alpha$, and that of Oy is $\cos^2 \beta$. This method is sufficient when the probability of any path depends only upon its direction relative to the original path, but in most cases other considerations are involved, such as change of magnitude of the velocity or the momentum, which require the introduction of other factors into the expressions for the probability. There may also be other vectors, besides the velocity or momentum, associated with the photon which change in direction at incidence. In some cases it may be known that all the photons take the path Oy , none the path Ox , after incidence. This may be represented by introducing the weight factor $1/\cos^2 \beta$ for Oy , and zero for Ox . These factors in the expressions for the probability serve to maintain the total probability of both paths at the value unity, a necessary condition in the absence of absorption. Other facts which affect the probability of reflexion and refraction are that the reflected and refracted rays are not generally at right angles to each other, and that the refracted ray is travelling in a medium different from that traversed by the incident and reflected rays.

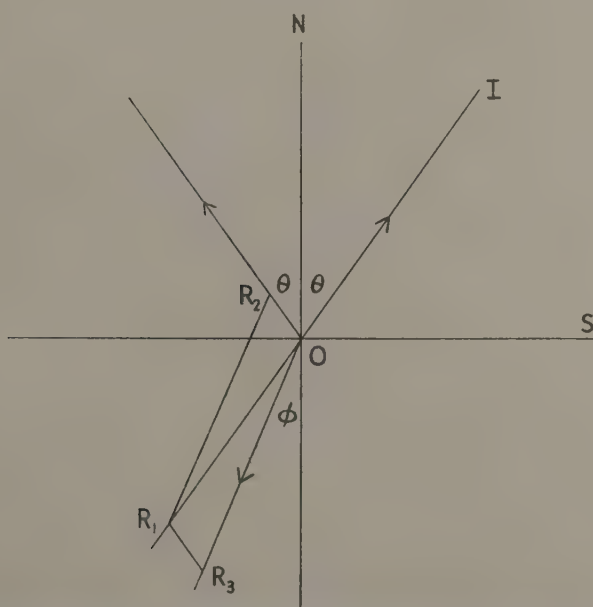
Beginning with the simplest case, in which the electrical axis of the photon is at right angles to the plane of incidence, so that no change of direction of this axis occurs at incidence, we represent by IO (fig. 3) the direction of a pencil consisting of a large number of photons, all of the same frequency incident at angle θ with the normal on a refracting surface S , by OR_1 the prolongation of IO , and by OR_2 , OR_3 , the directions of the reflected and refracted pencils. The parallelogram for these directions is $OR_2R_1R_3$. The angle of refraction being ϕ , the angles R_1OR_3 and OR_3R_1 are respectively $\theta - \phi$ and $\theta + \phi$. The number of photons conveyed in the

incident pencil per second per unit area of the cross-section of this pencil being represented by OR_1^2 , the fraction of this number which are reflected is

$$\frac{OR_2^2}{OR_1^2} = \frac{\sin^2(\theta - \phi)}{\sin^2(\theta + \phi)}, \quad \dots \dots \dots (1)$$

which therefore represents the probability of reflexion. This fraction also represents the relative intensity of the reflected and incident pencils, since the velocity of propagation, the area of the cross-section, and the energy per photon are the same in these two pencils.

Fig. 3.



The parallelogram for the directions of propagation of incident, reflected, and refracted photons. The probability of reflexion is OR_2^2/OR_1^2 .

The expression (1) is identical with Fresnel's formula for the relative intensity of reflected and incident pencils in which the vibrations are at right angles to the plane of incidence, and with that given by the classical electromagnetic theory for the case in which the electrical vector is perpendicular to that plane. It also agrees, within 1 or 2 per cent., with photometric measurements of the intensity of light polarized in this way and reflected at various angles from recently polished glass surfaces.

It may be concluded that the parallelogram law applied to probabilities gives satisfactorily the intensity of a derived pencil when it is travelling in the same medium as the incident pencil. It is to be remembered, however, that the expression (1), here derived by considerations of probability, is not to be regarded as a precise, but only as an average, measure of the intensity of the reflected light. At any moment the number of photons in the reflected pencil may differ from that indicated by (1), the relative proportions in the reflected and refracted pencils passing through rapid changes; but in the long run this expression represents satisfactorily the average intensity of the reflected beam, which is all that can be measured in photometric experiments.

With regard to the refracted pencil, the parallelogram $OR_2R_1R_3$ (fig. 3) gives for its probability

$$\frac{OR_3^2}{OR_1^2} = \frac{\sin^2 2\theta}{\sin^2 (\theta + \phi)} \quad * \quad \dots \quad (2)$$

but since a refracted photon is travelling in a medium in which its velocity, its frequency, and its energy are different from those of the photon before incidence (V. p. 569), this expression requires multiplication by other factors in order correctly to represent the probability of refraction. The correct expression is not easy to determine directly, but it may be found by subtracting (1) from unity. The probability of refraction is, therefore,

$$1 - \frac{\sin^2 (\theta - \phi)}{\sin^2 (\theta + \phi)} = \frac{\sin 2\theta \cdot \sin 2\phi}{\sin^2 (\theta + \phi)} \quad \dots \quad (3)$$

so that the weight factor required with (2) is $\sin 2\phi / \sin 2\theta$.

The expression (3) gives the probability of an incident photon finding its way into the refracted pencil, but it does not give correctly the relative intensities of the refracted and incident pencils. The principle of energy determines that the energy of the photons in a certain length of the incident pencil is equal to the sum of the energies of those in corresponding lengths of the reflected and refracted pencils. The intensity of the refracted pencil however, defined as the energy conveyed in it per second per square centimetre, is expressed by the fraction (3) multiplied by $\cos \theta / \cos \phi$, this factor being the inverse ratio in which the area of the cross-section is increased at entry into the second medium.

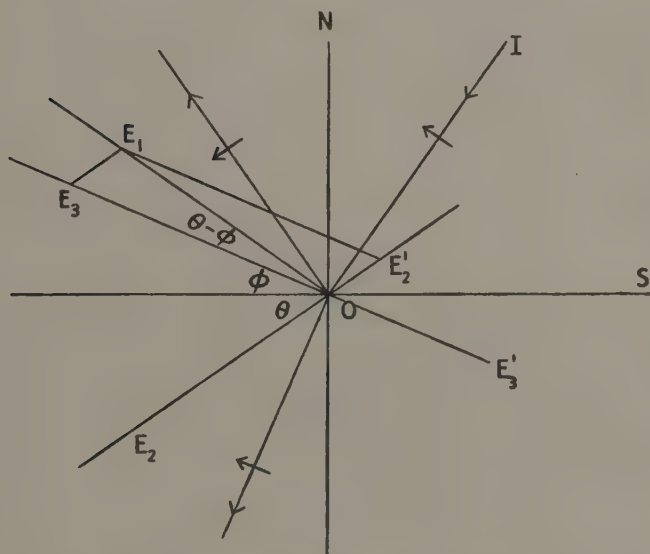
Passing to the case in which the electrical axes of the incident photons are parallel to the plane of incidence, we note in the first place that the expressions (1) and (3), representing probabilities dependent only on change of direction and of medium, must hold in this case, since the

* It may be noted that the expression (2), when multiplied by $1/\mu^2$, i. e., $\sin^2 \phi / \sin^2 \theta$, gives the relative values of the square of the amplitude of the refracted and incident waves in the classical theory.

directions of the incident, reflected, and refracted rays are in isotropic media independent of the plane of polarization of the light. In the present case, however, the probabilities are affected by changes of direction of the photon axes at incidence.

In fig. 4 the short arrows again represent the positive directions of the electrical axes of incident, reflected, and refracted photons. The lines OE_1 , OE_2 , and OE_3 are drawn from the point of incidence parallel to these directions. It appears from fig. 4 that an incident photon having its axis parallel to OE_1 has one of four directions which the axis may take

Fig. 4.



OE_1 and OE_3 are the positive directions of the electrical axes of incident and refracted photons. OE_2 and OE_2' are possible directions of the axes after reflexion.

consistently with the laws of reflexion and refraction, viz., OE_2 and OE_3 , and their opposite directions, OE_2' and OE_3' . The "incident" direction OE_1 lies between OE_3 and OE_2' , and the photon can turn into either of these directions without passing through either of the other two. If OE_3 and OE_2' were the only possible directions of the axis after incidence, the probabilities for them would be given by the parallelogram $OE_3E_1E_2'$, which is similar to the figure $OR_3R_1R_2$ in fig. 3, and would be represented by (1) for reflexion and, with allowance for the change of medium, by (3) for refraction.

glass or other transparent substance at the Brewster angle $\tan^{-1}\mu$, as it should be according to (5). Nor is the intensity of the reflected light always a minimum at this angle. If the incident pencil is polarized so that the electrical axes of its photons are inclined at 45° to the plane of incidence, a state equivalent to two pencils each of half the number of photons, the axes in one being parallel, in the other perpendicular to the plane of incidence, then at the Brewster angle the former pencil is, according to (5), not reflected at all, and the reflected light is plane polarized in the plane of incidence. In fact, however, the suppression of the former pencil is not complete, and the reflected light appears to be elliptically polarized, with its minor electrical axis in the plane of incidence.

The divergence from the Fresnel formulæ has been attributed to surface films * and to strains in the refracting medium †, and each of these suggestions has the support of some experimental evidence showing that it accounts for at least a portion of the discrepancy.

Another explanation of the failure of the tangent formula (5) to agree very closely with experimental observations of the intensity of reflected light polarized at right angles to the plane of incidence is, however, suggested by the above theory of the probability of reflexion and refraction, and it is one which does not involve surface films, or strains, or other modifications of the refracting surface. In arriving at the expression (5) we have assumed that the axes of all the incident photons turn first to the direction OE_3 (fig. 4), none directly to OE_2' . We now abandon this assumption and suppose that a small fraction f of the incident photons turn directly to OE_2' and are reflected with their axes in this direction. As already stated, this is more likely to occur at large than at small angles of incidence. The remainder $1-f$ turn directly to OE_3 , and the axes of a fraction of these, represented by (4), remain in this direction, and these are refracted. The rest, represented by the fraction (5), have their axes turned from OE_3 to OE_2 or OE_2' and are reflected. The total probability of reflexion is, therefore,

$$f + (1-f) \frac{\tan^2(\theta - \phi)}{\tan^2(\theta + \phi)} \quad \dots \dots \dots (6)$$

The value of the fraction f depends upon the angle of incidence. At normal incidence f is zero, since the expressions (1) and (6) must be identical at this angle. In some recent unpublished experiments, made with a Hilger-Nutting spectrophotometer adapted for reflexion measure-

* Drude, 'Theory of Optics,' p. 287 (1925). The influence of surface films on reflexion by liquid surfaces was investigated by Rayleigh (Phil. Mag. xxxiii. p. 1 (Jan. 1892)).

† Lummer and Sorge, *Ann. d. Phys.* xxxi. p. 325 (1910).

ments, the present writer found that when light of wave-length 5852 Å. is incident at the angle $\tan^{-1} \mu$ upon the surface of a dense flint-glass prism of refractive index 1.632, the intensity of the reflected light polarized at right angles to the plane of incidence is about 1/1000 of that of the component of the incident light polarized in the same way. This makes f equal to about 0.001 at the polarizing angle, on the assumption that this is the only cause of the divergence from the Brewster law. Whether this is the case or not, it is clear that the probability theory offers a reasonable explanation of the divergence, without the assumption of modifications in the state or nature of the surface of the refracting substance, though such modifications would doubtless affect the value of the fraction f . At grazing incidence the expression (6) has the value unity independently of the value of f .

A feature of the above method of dealing with the theory of reflexion and refraction is the important part played in it by the wave-sheet associated with a photon. The guiding effect of the wave-sheet must depend upon the distance to which it extends from the photon without serious diminution of its strength, and this depends upon the distance between the two electrons of which the photon is composed. The greatest possible distance between them is the critical distance of electron coupling *i. e.*, $2.8 \cdot 10^{-13}$ cm. If the distance between the electrons is a small fraction of this, the effective extent of the sheet is much diminished, so that no regular reflexion or refraction is to be expected, and the photons can traverse a solid medium without being much influenced by its particles. It is possible that the great penetrating power of very high-frequency radiation, such as hard X-rays or γ -rays, is to be accounted for in this way.

XXXIX. *The Electrical Conductivity of Plastic Dielectrics.*

By ANDREW GEMANT,

Department of Electrical Engineering, University of Wisconsin,
Madison, Wisconsin *.

[Received August 22, 1939.]

IN liquids, ionic mobility is controlled by the viscosity of the medium, and the viscosity of the medium with respect to motion of the ions is that obtained from large scale measurements. There is no doubt that this rule is valid for liquids of very high viscosity as well. In dealing with elasto-viscous liquids, however, the rule is likely to fail, its failure becoming quite evident, if plastic solids are being considered. Two important alterations have been introduced into the original rule valid for liquids. *First*, there is no *a priori* justification to suppose that the viscosity the ions have to overcome should have the same numerical value as that obtained from large scale measurements. *Second*, it is certain that the elastic properties of the solid will have to be taken into consideration, just as for any other deformation of the plastic. The first alteration mentioned is certainly important, but unfortunately scarcely anything definite is known on this point. This paper will therefore be concerned chiefly with the second alteration proposed.

The author has published some work on the rotation of dipolar molecules ⁽¹⁾ in vitreous solids, and has mentioned in those papers that it is possible to extend those ideas to the motion of ions as well. The fundamental conception is that generally used in connexion with deformation of plastics ⁽²⁾, namely, that each deformation is a superposition of an elastic displacement and a viscous flow. The displacement may be different for both of these components and will depend upon special experimental conditions, and since the stress for both the elastic displacement and the viscous flow is the same, they can be considered to be mechanically connected in series. The assumed elastic displacement is not ideal, but is coupled with a loss mechanism, known as solid friction. Being an integral part of the elastic displacement, as known from experiments on mechanical vibrations below the yield point, the solid friction

* Communicated by the Author. This paper was presented at the Annual Meeting of the Society of Rheology in Pittsburgh, U.S.A., December 1938.

must be considered as connected mechanically parallel to the elastic element.

The next step is to specify these three fundamental units of resistance, assumed to oppose the motion of ions, in accordance with existing experimental data.

It has just been stated that no experimental method for determination of the *viscous component* exists up to now. The electrical conductivity of the material in question, determined by means of d.c. and at low field strength, allows the ratio of the ionic concentration to the viscosity to be computed. In other words each value assumed for the viscosity will fix the value of the concentration of ions as well. We then have to choose a coupled pair of these values such that both should appear as much in accord with experimental evidence as possible. In this way we can estimate in a two-fold manner the viscosity value, thus restricting the plausible range considerably. How this has to be carried out will be shown below. Another possibility would be the application of a method recently developed by the author (Phys. Rev. lviii, p. 904 (1940),

As to the *elastic component*, we assume an elastic modulus for the surroundings of the ion, equal to that known from large scale experiments, although again it is possible that the true value differs somewhat from the assumed one. The *solid friction component* also can be estimated from numerical⁽³⁾ data available on several vitreous materials with ionic conductivity (glass, ebonite, polystyrene, etc.). The most striking feature of these data is that the frictional term, expressed as logarithmic decrement of vibrations, or as specific loss per cycle, is fairly independent of the frequency from the lowest up to around 10^5 cycles per second. We can therefore hardly speak of a dissipative term, like the viscous resistance, but rather of a resistance the value of which varies inversely with the impressed frequency.

The final equations depend on whether the impressed voltage is direct or alternating. The details of the above are published elsewhere⁽⁴⁾. The purpose of the present paper is to give some numerical computations based on our equations, and to compare the result with some experimental data of the literature. Let us first consider the case of a *d.c. voltage*. The application of our combined resistance shows that for small field strengths the viscous component prevails, but that for larger fields the elastic component comes into action. The elastic displacements of the ion, are, however, even for the highest fields applicable, small as compared with the viscous ones. In consequence of this the solid friction element will have practically no importance in this connexion. The increase of the ionic mobility, due to elastic shifts, also appears to be negligibly small. However, a rather plausible assumption seems to be that the amounts of kinetic energy collected by the ion during its transitions

from elastic to viscous displacements will, to a certain extent at least, accumulate as vibratory energy. The ionization number α , number of successful impacts during a path of 1 cm., can be shown to be

$$\alpha = \frac{e^2 E^2}{L_i \mu \lambda^2}, \quad \dots \quad (1)$$

where e is the charge of a monovalent ion, E applied electric field, L_i the ionization energy, μ the shear modulus of elasticity, and λ the molecular diameter with a numerical factor left open. Eq. 1 gives maximum figures, the true ones are probably smaller. For numerical calculations let us take paraffin wax with the following constants, in absolute units: $L_i = 10^{-11}$ (corresponding to an ionization voltage of 6 volts), $\mu = 0.5 \times 10^{10}$, $\lambda = 7 \times 10^{-8}$ cm. Then if E is in absolute units,

$$\alpha = 10^{-3} E^2. \quad \dots \quad (2)$$

The current-voltage characteristic of this material should now be calculated.

If two electrodes of 1 cm.² surface are placed at a distance of 1 cm., and the original concentration of the ions is n , then, in case internal ionization occurs, the final concentration n_E becomes ⁽⁵⁾,

$$n_E = \frac{n}{\log 2. \alpha a} (2^{\alpha a} - 1), \quad \dots \quad (3)$$

and the ratio of conductivities σ for a field E and for small fields

$$\frac{\sigma_E}{\sigma_0} = \frac{1.4}{\alpha a} (2^{\alpha a} - 1). \quad \dots \quad (4)$$

Taking for σ_0 the experimental value of 1.8×10^{-8} (2×10^{-20} mhos per cm.) we have for the current density at field E

$$i = \frac{2.5 \times 10^{-8} E}{\alpha a} (2^{\alpha a} - 1) \quad \dots \quad (5)$$

and, substituting Eq. 2. with $a = 0.025$ cm. (see below)

$$i = \frac{10^{-3}}{E} (2^{2.5 \times 10^{-5} E^2} - 1). \quad \dots \quad (6)$$

Evaluating Eq. 6 up to 150 kv./cm., fig. 1, curve A, is obtained.

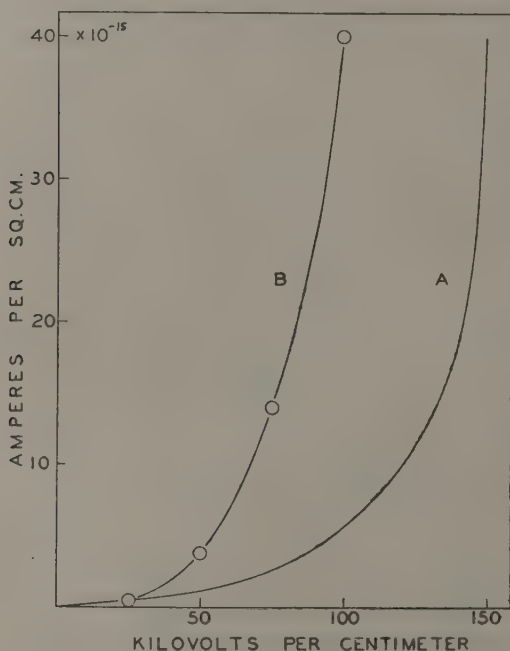
The literature contains quite a number of such current-voltage characteristics, showing a similar behaviour to fig. 1. We quote here as an example data of W. Scislowski on paraffin wax ⁽⁶⁾, and those of S. Whitehead on cellulose acetate and varnish paper board ⁽⁷⁾, solids with finite plasticity. As a comparison to our curve A, an experimental curve on paraffin wax taken by Scislowski is plotted (curve B). The above values for a and σ_0 are taken from his data. The two functions A and B are very

similar, indeed, the differences might easily be accounted for by the uncertainties in L_i and λ .

The essential features of the behaviour of the conductivity are as follows. Deviation from Ohm's law generally starts between 20 and 100 kv./cm., according to the thickness of the sample, the initial field strength increasing with decreasing thickness. Near the initial field strength our Eq. 4, in conjunction with Eq. 2, indicates that the conductivity follows an equation of the kind

$$\sigma_E = \sigma_0 + \beta E^2 + \gamma E^4,$$

Fig. 1.



Current density vs. field strength for paraffin wax.

A. Calculated after Eq. (6).

B. Experimental data of Scislowski.

in which β and γ are constants, as found empirically by L. Hartshorn for varnished cloth ⁽⁸⁾. For higher fields the increase of current is of an exponential nature. For fields between 200 and 1000 kv./cm. (again increasing with decreasing thickness) the current density becomes the order of several microamperes, and instability generally follows.

We now turn to the effect on ionic conductivity of the frequency

of the impressed voltage. For *a.c. voltages* the conductivity is separated into a real and imaginary term, the latter standing for the dielectric constant. The ratio of the two terms is then the loss angle, as usually measured. In the following, calculations of the loss angle will be carried out.

The theory as outlined above indicates that the ionic mobility, controlled by the viscosity for d.c., will be determined by the viscosity, elasticity, and solid friction together, when the frequency increases. Above a certain frequency range, which is lower the larger the viscosity, the resistance will be determined by the elasticity and solid friction alone. For temperatures considerably below the softening point the viscosity constant of solids is so large that the frequency range just mentioned will be below 1 cycle per second. This means that for the whole practical frequency range the loss angle is only a function of the elasticity and solid friction.

We are further restricted to frequencies below say 10^5 cycles, as we do not possess any data on the solid friction coefficients for higher frequencies. To be sure, the general theory is assumed to be valid for higher frequencies, but no numerical evaluation is possible at the present. In drawing comparisons with experimental data one has to bear in mind that apart from ionic motion there are other specific mechanisms leading to dielectric losses. Our formulæ will, therefore, yield only a certain fraction of the total loss, which fraction will be the higher, the less pronounced these specific mechanisms are in any special case. The other mechanisms just referred to are due to inhomogeneities of the material (Maxwell-Wagner), and to dipolar molecules (Debye). Looked upon from this angle, glass with its high ionic content appears to be best for comparison.

The final result of the corresponding deductions is that for sufficiently low temperatures the loss angle, $\tan \delta$, is

$$\tan \delta = \frac{2ne^2\theta}{\lambda\epsilon\mu}, \quad . \quad . \quad . \quad . \quad . \quad . \quad (7)$$

where n =ionic concentration, θ =specific loss of solid friction, and ϵ =dielectric constant.

Let us evaluate Equation 7 for soda glass at different frequencies. Take $\lambda=7 \times 10^{-8}$, $\epsilon=5$, $\mu=2.5 \times 10^{11}$. In glass, especially soda glass, it is safe to assume that the order of magnitude of n is of the order of magnitude of the number of molecules, n_m , namely 10^{22} . This estimate can be strengthened somewhat in connecting it with an estimate of η_0 , the ionic viscosity. We have for the d.c. conductivity at small fields the general formula

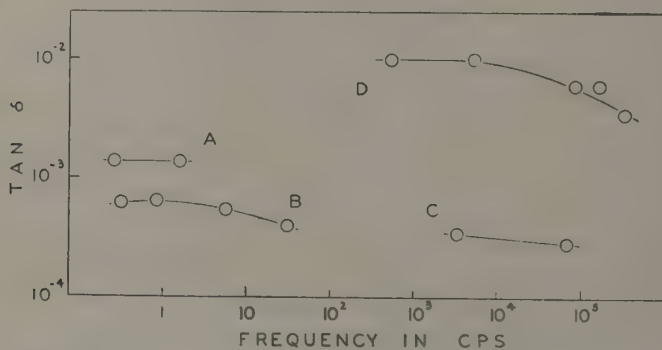
$$\sigma_0 = K \frac{n}{\eta_0}, \quad . \quad . \quad . \quad . \quad . \quad . \quad (8)$$

where K is to a first approximation independent of the material chosen since the molecular radii which enter Stokes's equation are always of the same order. K can be estimated from oils to be about 10^{-12} abs. Thus for glass with $\sigma_0 \sim 10^{-3}$,

$$\frac{n}{\eta_0} \sim 10^9.$$

With $n \sim 10^{22}$, η_0 becomes 10^{13} . The extrapolated value from large scale measurements is 10^{18} for η_0 . In a recent paper on the slow changes in physical properties of glasses E. Seddon⁽⁹⁾ also comes to the conclusion that η_0 must be high but finite. In assuming lesser orders for n , η_0 had to be decreased proportionally which, however, seems unlikely, considering the extrapolated value. Thus the pair $n \sim 10^{22}$, $\eta_0 \sim 10^{13}$ seems the most probable.

Fig. 2.



Dielectric loss angle vs. frequency at room temperature
for soda glass.

A, B, C. Calculated after Eq. (7) from solid friction data of

A. Gemant and Jackson.

B. Bennewitz and Rötger.

C. Wegel and Walther.

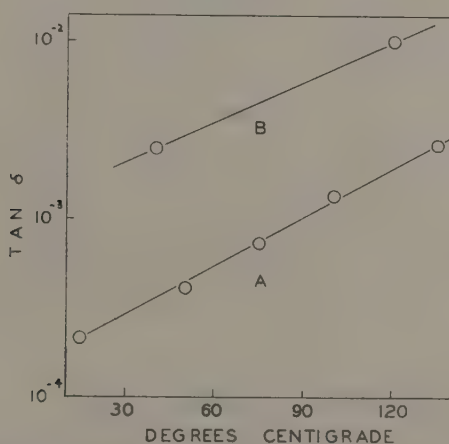
D. Experimental data of Strutt.

It has already been stated that θ is fairly independent of frequency. This independence also becomes evident by a recent paper by Krüger and Rohloff on the internal friction of wood⁽¹⁰⁾ in a frequency range of from 10 to 10^4 cycles per second. Using then for glass the data as obtained by Gemant and Jackson, we have the curve A of fig. 2. Using, on the other hand, data obtained by Bennewitz and Rötger⁽¹¹⁾, a slight variation with the frequency is noticeable (curve B of fig. 2), with a flat maximum of around 0.7 cycles. Fig. 2 C is obtained from data of Wegel

and Walther on glass ⁽¹²⁾ at a frequency range 10^3 to 10^5 . It appears that there is a slight decrease of θ , and, according to Eq. 7, of the loss angle when the frequency increases.

These conclusions may be compared with the data given by M. J. O. Strutt ⁽¹³⁾. The loss angle of glasses for any given temperature varies but slightly with frequency according to his data, becoming generally less with increasing frequency. This is the same result as seen on the calculated data of fig. 2. The absolute value of $\tan \delta$ is between 10^{-3} and 10^{-2} for room temperature, somewhat higher than the calculated values indicated in fig. 2, which is to be expected on account of additional dipole losses. Curve D in fig. 2 refers to one of his sets on a soda glass.

Fig. 3.



Loss angle vs. temperature at low frequencies for lead glass

- A. Calculated after Eq. (7) from solid friction data of Gemant and Jackson.
- B. Experimental data of Strutt.

Although Eq. (7) is not valid for elevated temperatures, a temperature curve of $\tan \delta$ for lead glass, based on solid friction data of Gemant and Jackson, and on Eq. (7) is shown in curve A of fig. 3. Until the ionic viscosity η_0 , is more definitely known, the use of the more general equations, as supplied by the theory, would offer but little advantage. Recent papers by Naunton and Waring ⁽¹⁴⁾ on the damping of vibrations in rubber indicate that by extending such measurements over a wide frequency range both θ and η_0 could be determined experimentally.

Curve B of fig. 3 is based on direct measurements by Strutt of $\tan \delta$ of a lead glass. The increase with temperature of $\tan \delta$ is, as can be seen, of an exponential nature, the factor in the exponent being usually smaller

than the corresponding factor for the d.c. conductivity, the a.c. and d.c. curves submerging asymptotically towards higher temperatures.

Summary.

1. The paper is concerned with ionic mobility in vitreous dielectrics, which generally exhibit a finite plasticity. The fundamental idea is to deal with the deformation as caused by the motion of an ion in the same way as macroscopic deformations of plastics are dealt with. This latter can be described by means of three constants of the material, namely, plasticity, elasticity, and solid friction, and the same should hold for the molecular deformation around a moving ion. The equations for the ionic mobility, as deduced by the author in another paper, are given here for numerical computation and comparison with some experimental data.

2. In the case of d.c. the current-voltage characteristic can be calculated. This is done for paraffin wax up to a field of 150 kv./cm. The curve shows the same features as measurements on paraffin by Scislowski.

3. For an a.c. voltage the dielectric loss angle can be calculated from the theory. This is done for soda glass, based on solid friction data of Gemant and Jackson, Bennewitz and Rötger, and Wegel and Walther in a frequency range between 10^{-1} and 10^5 cycles per second. Another calculated curve shows the loss angle of lead glass, dependent on temperature between 20 and 140°C . The results are consistent with experimental data on the dielectric loss of glasses obtained by Strutt.

References.

- (1) A. Gemant, *Journ. Appl. Phys.* ix. p. 730 (1938).
- (2) J. M. Burgers, *First Report on Viscosity and Plasticity*, Amsterdam, 1939.
- (3) A. L. Kimball, 'Vibration Prevention in Engineering,' New York, p. 133 (1932).
- A. Gemant and W. Jackson, *Phil. Mag.* xxiii. p. 960 (1937).
- (4) A. Gemant, *Journ. Appl. Phys.* x. p. 508 (1939).
- (5) N. Semenoff and A. Walther, *Festigkeitslehre*, Berlin, p. 150 (1928).
- (6) W. Scislowski, *Acta Phys. Polonica*, iv. p. 123 (1935).
- (7) S. Whitehead, 'World Power,' xxvi. p. 72 (1936).
- (8) S. Whitehead, *Proc. Phys. Soc.* xlvii. p. 974 (1935).
- (9) E. Seddon, *J. Soc. Glass Technol.* xxii. p. 268 (1938).
- (10) F. Krüger and E. Rohloff, *Zeits. f. Phys.* cx. p. 58 (1938).
- (11) K. Bennewitz and H. Rötger, *Physik, Zeits.* xxxvii. p. 578 (1936).
- (12) R. L. Wegel and H. Walther, *Physics*, vi. p. 141 (1935).
- (13) M. J. O. Strutt, *Arch. f. Elektrotechnik*, xxv. p. 715 (1931).
- (14) W. J. S. Naunton and J. R. S. Waring, *Trans. Inst. Rubber Ind.* xiv. p. 340 (1939).

XL. *Asymptotic Solution of Southwell and Squire ;
Modification to Oseen's Equations.*

By J. H. PRESTON, B.Sc., Ph.D., A.F.R.Ae.S., of the
Aerodynamics Department, National Physical Laboratory*.

[Received April 2, 1940.]

Introduction.

SOUTHWELL and Squire ⁽¹⁾ in 1933 suggested an interesting modification of Oseen's approximation to the equations of motion.

Instead of linearizing the equations of motion by replacing u, v when these occur explicitly with their values at infinity, *i. e.*, $U, 0$, Southwell and Squire replaced them by u', v' where u', v' are the velocities of irrotational inviscid flow past the cylinder under consideration.

They then applied Boussinesq's transformation, *i. e.*, they replaced the rectangular co-ordinates x, y by the orthogonal co-ordinates α, β , where α, β are the velocity potential and stream function for the irrotational flow past the cylinder in question. The equation governing the vorticity is similar to the equation governing the heat transfer from a hot cylinder to an inviscid fluid.

Adopting a suggestion from the method of solution for this problem, they obtained an integral equation for the vorticity. Combining certain simple distributions of this on the boundary, they were able by graphical methods to integrate the equation for ψ and satisfy the boundary condition of no slip at a finite number of points. By this means they obtained solutions for the tangential flat plate and circular cylinder at a small Reynolds number which were in satisfactory agreement with the known Oseen solutions.

It is, however, at high Reynolds numbers that Southwell and Squire's equations show a marked improvement over the Oseen equations, and it is to this end that an approximate method of solution is developed below for large Reynolds numbers. It is found in two simple cases that this leads to results already obtained by other investigators using similar approximations to the equations of motion. As the literature dealing with this is somewhat scattered, for the sake of completeness it was deemed desirable to derive solutions applicable to any cylinder directly from Southwell and Squire's equation.

* Communicated by E. F. Relf, F.R.S.

1. *Asymptotic Solution of the Equations.*

It is convenient now to define u, v, u', v' as

$$\left. \begin{aligned} u &= \frac{\partial \psi}{\partial y}, & v &= -\frac{\partial \psi}{\partial x}, \\ u' &= \frac{\partial \beta}{\partial y}, & v' &= \frac{\partial \beta}{\partial x}, \end{aligned} \right\} \dots \dots \dots (1.1)$$

The equations governing the flow are then

$$\left. \begin{aligned} (a) \quad & \frac{\partial \zeta}{\partial \alpha} - \nu_{\alpha} \nabla_{\beta}^2 \zeta = 0, \\ (b) \quad & \zeta = -H^2_{\alpha} \nabla_{\beta}^2 \psi, \\ \text{where} \quad & \alpha \nabla_{\beta}^2 \equiv \frac{\partial^2}{\partial \alpha^2} + \frac{\partial^2}{\partial \beta^2}, \\ \text{where} \quad (c) \quad & H^2 = \left| \frac{dW}{dz} \right|^2, \quad W = \alpha + i\beta, \quad z = x + iy. \end{aligned} \right\} \dots \dots \dots (1.2)$$

The corresponding equation (Boussinesq's) for the transfer of heat from a hot cylinder to an inviscid fluid is

$$\frac{\partial \theta}{\partial \alpha} - \frac{k}{c} \alpha \nabla_{\beta}^2 \theta = 0. \dots \dots \dots (1.3)$$

This has already been dealt with by Piercy and Winny⁽²⁾ and will not be considered further. We adopt their method of solution for (1.2 (a)) for the flow at large Reynolds numbers and consider only cases of symmetry.

Change the form of (1.2 (a)) as is usual by the substitution

$$\zeta = \zeta_1 e^{\alpha/2\nu}, \dots \dots \dots (1.4)$$

$$\left. \begin{aligned} \text{giving} \quad (a) \quad & n^2 \zeta_1 = \alpha \nabla_{\beta}^2 \zeta_1, \\ \text{where} \quad (b) \quad & n = 1/2\nu. \end{aligned} \right\} \dots \dots \dots (1.5)$$

Southwell and Squire's solution of (1.5 (a)) appropriate to a doublet of vorticity at the origin is

$$\left. \begin{aligned} \zeta_1 &= \frac{\beta}{r} K_1(nr), \\ \text{where} \quad & r = \alpha^2 + \beta^2. \end{aligned} \right\} \dots \dots \dots (1.6)$$

It is odd in β , as is required by symmetry, and has the property that on the axis $\beta=0$, it is zero everywhere except at $\alpha=0$.

Assuming then a distribution $\sigma(\alpha')$ of line doublets along that part of the α -axis which represents the solid boundary,

$$\left. \begin{aligned} \zeta &= \int_0^{\alpha_r} \sigma(\alpha') e^{-n(\alpha-\alpha')} \frac{\beta}{r'} K_1(nr') d\alpha', \\ (r')^2 &= (\alpha-\alpha')^2 + \beta^2, \end{aligned} \right\} \dots \dots \dots (1.7)$$

where the origin is at the leading edge and α_r corresponds to the trailing edge.

The asymptotic expansion of $K_n(x)$ is

$$K_n(x) = \sqrt{\frac{\pi}{2x}} e^{-x} (1 + \dots) \quad (1.8)$$

for sufficiently large values of x .

We now apply the argument of Piercy and Winny⁽²⁾ to (1.7). From the asymptotic expansion of $K_1(x)$, the kernel of (1.7) is seen to be negligible when $n(\alpha - \alpha')$ is large and negative. The contribution to the integral through the interval of α' near α where (1.8) ceases to apply tends to become negligible as $n\alpha_r$ increases. Thus for large values of $n(\alpha_r)$ it is nearly true that

$$\zeta = \int_0^\alpha \sigma(\alpha') e^{-n\{r' - (\alpha - \alpha')\}} \frac{\beta}{r'} \sqrt{\frac{\pi}{2nr'}} d\alpha' \quad (1.9)$$

Following Piercy and Winny

$$-n\{r' - (\alpha - \alpha')\} = n \left\{ (\alpha - \alpha') \left[1 + \frac{\beta^2}{(\alpha - \alpha')^2} \right]^{\frac{1}{2}} - (\alpha - \alpha') \right\}$$

and, expanding by the binomial theorem and taking only the first term,

$$= -n \left\{ \frac{\beta^2}{2(\alpha - \alpha')^2} \dots \right\} \quad (1.10)$$

Also, assuming that the effects of viscosity (*i. e.*, the vorticity ζ) is confined to a thin layer enveloping the cylinder, so that $\beta/(\alpha - \alpha')$ is small, and r' may be replaced by $(\alpha - \alpha')$, we obtain finally for large Reynolds numbers

$$\zeta = \sqrt{\frac{\pi}{2n}} \int_0^\alpha \sigma(\alpha') \frac{\beta}{(\alpha - \alpha')^{3/2}} e^{-\frac{n\beta^2}{2(\alpha - \alpha')}} d\alpha' \quad (1.11)$$

We come now to equation (1.2 (b)). Assuming the existence of a "boundary layer," so that $\partial^2\psi/\partial\alpha'^2$ is small compared with $\partial^2\psi/\partial\beta^2$, we have, instead of (1.2 (b)),

$$\zeta = -H^2 \frac{\partial^2\psi}{\partial\beta^2} \quad (1.12)$$

If q, w are the components of velocity along the α, β lines respectively.

$$\left. \begin{aligned} (a) \quad q &= H \frac{\partial\psi}{\partial\beta}, \\ (b) \quad w &= -H \frac{\partial\psi}{\partial\alpha}. \end{aligned} \right\} \quad (1.13)$$

One solution of (1.12) corresponding to $\zeta = 0$ is

$$\psi = \beta \quad (1.14)$$

Assume $\psi = \psi_1 + \beta; \quad (1.15)$

then $\zeta = -H^2 \frac{\partial^2 \psi_1}{\partial \beta^2}, \quad (1.16)$

and
$$\left. \begin{array}{ll} (a) & q = H \frac{\partial \psi_1}{\partial \beta} + 1, \\ (b) & w = -H \frac{\partial \psi_1}{\partial \alpha}. \end{array} \right\} (1.17)$$

Integrating (1.16),

$$\frac{q}{H} - 1 = \frac{\partial \psi_1}{\partial \beta} = \int_{\beta}^{\infty} -\frac{\zeta}{H^2} d\beta, \quad (1.18)$$

$$\psi_1 = \int_0^{\beta} d\beta \int_{\beta}^{\infty} -\frac{\zeta}{H^2} d\beta, \quad (1.19)$$

where the limits are chosen to ensure that $\psi = 0, \beta = 0; w = 0, \beta = 0; w = 0, \beta = \infty$; and $q = H, \beta = \infty$.

It remains to satisfy the condition at the boundary $q = 0, \beta = 0$. Actually, as we have assumed the existence of a boundary layer, $q \rightarrow H$ and $\beta \rightarrow \delta$, the edge of the boundary layer, where δ is small, so that through the effective part of the integration, variation of H^2 with β can be neglected, and so (1.18) gives

$$\frac{q}{H} - 1 = -\frac{1}{H_{\beta=0}^2} \int_{\beta}^{\infty} \zeta d\beta, \quad (1.20)$$

where ∞ is taken as a convenient limit which should in reality be δ ; but this gives a close approximation since between δ and ∞ ζ is zero, and so nothing is added to the integral.

Substituting for ζ from (1.11) in (1.20)

$$\frac{q}{H} - 1 = -\sqrt{\frac{\pi}{2n}} \frac{1}{H_{\beta=0}^2} \int_{\beta}^{\infty} d\beta \int_0^{\alpha} \sigma(\alpha') \frac{\beta}{(\alpha - \alpha')^{3/2}} e^{-\frac{n\beta^2}{2(\alpha - \alpha')}} d\alpha'. \quad (1.21)$$

Integrate with respect to β

$$\begin{aligned} \frac{q}{H} - 1 &= -\sqrt{\frac{\pi}{2n}} \frac{1}{H_{\beta=0}^2} \int_0^{\alpha} \sigma(\alpha') \left[-\frac{1}{n} \frac{e^{-\frac{n\beta^2}{2(\alpha - \alpha')}}}{n(\alpha - \alpha')^{1/2}} \right]_{\beta}^{\infty} d\alpha' \\ &= -\sqrt{\frac{\pi}{2}} n^{-3/2} \frac{1}{H_{\beta=0}^2} \int_0^{\alpha} \sigma(\alpha') \frac{e^{-\frac{n\beta^2}{2(\alpha - \alpha')}}}{(\alpha - \alpha')^{1/2}} d\alpha'; \end{aligned}$$

but

$$n = \frac{1}{2\nu},$$

so that

$$\frac{q}{H} - 1 = -\frac{2\sqrt{\pi} \nu^{3/2}}{H_{\beta=0}^2} \int_0^{\alpha} \sigma(\alpha') \frac{e^{-\frac{\beta^2}{4\nu(\alpha - \alpha')}}}{(\alpha - \alpha')^{1/2}} d\alpha'. \quad . . . (1.22)$$

Now, when $\beta=0$, $q/H=0$; hence

$$\frac{H_{\beta=0}^2}{2\sqrt{\pi}\nu^{3/2}} = \int_0^\alpha \frac{\sigma(\alpha')}{(\alpha-\alpha')^{\frac{1}{2}}} d\alpha', \quad (1.23)$$

which is an integral equation (Abel's) for determining $\sigma(\alpha')$, and the solution is known.

If

$$f(\alpha) = \int_0^\alpha \frac{\sigma(\alpha')}{(\alpha-\alpha')^\mu} d\alpha'$$

is the integral equation, the solution is

$$\sigma(\alpha') = \frac{\sin \mu\pi}{\pi} \frac{d}{d\alpha'} \int_0^{\alpha'} \frac{f(\alpha)}{(\alpha'-\alpha)^{1-\mu}} d\alpha,$$

so that from (1.23) we obtain

$$\sigma(\alpha') = \frac{1}{2(\pi\nu)^{3/2}} \frac{d}{d\alpha'} \int_0^{\alpha'} \frac{H_{\beta=0}^2}{(\alpha'-\alpha)^{\frac{1}{2}}} d\alpha, \quad (1.24)$$

whence the velocity can be calculated using (1.24) and (1.22).

Consider the vorticity. From (1.11), putting $n=1/2\nu$,

$$\zeta = \sqrt{\pi}\nu^{\frac{1}{2}} \int_0^\alpha \sigma(\alpha') \frac{\beta}{(\alpha-\alpha')^{3/2}} e^{-\frac{\beta^2}{4\nu(\alpha-\alpha')}} d\alpha';$$

put

$$t = \frac{\beta}{\sqrt{4\nu(\alpha-\alpha')}},$$

$$\zeta = 4\nu\sqrt{\pi} \int_{\beta/\sqrt{4\nu\alpha}}^\infty \sigma\left(\alpha - \frac{\beta^2}{4\nu t^2}\right) e^{-t^2} dt, \quad (1.25)$$

The boundary value of the vorticity ζ_0 is got by putting $\beta=0$ in (1.25), giving

$$\zeta_0 = \pm 4\sqrt{\pi}\nu\sigma(\alpha) \int_0^\infty e^{-t^2} dt,$$

i. e.,

$$\xi_0 = \pm 2\pi\nu\sigma(\alpha), \quad (1.26)$$

\pm according to whether $\beta=0$ is approached from the negative or positive side of the α -axis.

Thus the boundary value of the vorticity is proportional to the doublet intensity, as is to be expected from (1.6). Substituting from (1.24),

$$\zeta_0 = \pm \frac{1}{\pi^{\frac{1}{2}}\nu^{\frac{1}{2}}} \frac{d}{d\alpha} \int_0^\alpha \frac{H_{\beta=0}^2}{(\alpha-\alpha')^{\frac{1}{2}}} d\alpha', \quad (1.27)$$

which, by differentiating and then integrating by parts, can be shown to be equivalent to

$$\zeta_0 = \pm \frac{1}{\pi^{\frac{1}{2}}\nu^{\frac{1}{2}}} \left\{ \frac{H_{\beta=0}^2}{\alpha^{\frac{1}{2}}} + \int_0^\alpha \frac{d}{d\alpha'} \frac{(H_{\beta=0}^2)}{(\alpha-\alpha')^{\frac{1}{2}}} d\alpha' \right\}.$$

Now except in the case of the tangential flat plate $H_{\beta=0}^2=0$, since $\alpha'=0$ is at the front stagnation point. Hence for any cylinder with a blunt leading edge

$$\zeta_0 = \pm \frac{1}{\pi^{\frac{1}{2}} \nu^{\frac{1}{2}}} \int_0^\alpha \frac{d}{d\alpha'} (H_{\beta=0}^2) \frac{d\alpha'}{(\alpha-\alpha')^{\frac{1}{2}}} \quad (1.28)$$

Now this result was obtained by Burgers using a different method, and was used by Squire ⁽⁴⁾ for the case of the circular cylinder. Burgers' method is as follows:—

If the Reynolds number is large, and in effect a boundary layer exists, then in (1.2 (a)) we may neglect $\partial^2 \zeta / \partial \alpha^2$ in comparison with $\partial^2 \zeta / \partial \beta^2$ and the equation becomes

$$\frac{\partial \zeta}{\partial \alpha} = \nu \frac{\partial^2 \zeta}{\partial \beta^2}, \quad (1.29)$$

a form familiar in the non-steady conduction of heat in one-dimension.

A solution appropriate to a source at the origin is

$$\zeta = \frac{e^{-\frac{\beta^2}{4\nu\alpha}}}{\alpha^{\frac{1}{2}}}.$$

This forms the basis of the solution obtained by Burgers, who, since it is even in β , considered only the positive half of the α, β plane. It is the correct solution for the analogous temperature equation, *i. e.*, θ written for ζ in (1.29).

A solution appropriate to a doublet at the origin can be obtained from the source solution by differentiation with respect to β . It is, ignoring the constants,

$$\zeta = \frac{\beta}{\alpha^{\frac{3}{2}}} e^{-\frac{\beta^2}{4\nu\alpha}},$$

and is odd in β , as is required. For a distribution of doublets along the α -axis we have

$$\zeta = \int_0^\alpha \sigma(\alpha') \frac{\beta}{(\alpha-\alpha')^{\frac{3}{2}}} e^{-\frac{\beta^2}{4\nu(\alpha-\alpha')}} d\alpha',$$

which is identical with (1.11) except for the constant.

2. Application to the Skin Friction of Elliptic Cylinders.

Piercy and Winny ⁽⁵⁾, and also Burgers ⁽⁶⁾, have carried out detailed calculations for the velocity and drag of a tangential flat plate to Oseen's approximation, and it can be verified that our results reduce to these.

Burgers ⁽³⁾ has given the solution for the circular cylinder, of which an account is given by Squire ⁽⁴⁾. There is some interest in carrying out

$$= \frac{(1-\bar{\alpha})(1+\bar{\alpha})^{\frac{1}{2}}}{\cosh^2 \xi_0 - \bar{\alpha}^2} - \frac{\sinh^2 \xi_0}{2 \cosh \xi_0} \left(\frac{\tan^{-1} \left(\frac{\alpha+1}{\cosh \xi - \bar{\alpha}} \right)^{\frac{1}{2}}}{(\cosh \xi_0 - \bar{\alpha})^{3/2}} - \frac{\tanh^{-1} \left(\frac{\alpha+1}{\cosh \xi_0 + \bar{\alpha}} \right)^{\frac{1}{2}}}{(\cosh \xi_0 + \bar{\alpha})^{3/2}} \right). \quad (2.5)$$

The equation to the ellipse is

$$\begin{aligned} x &= 2b \cosh \xi_0 \cos \eta, \\ y &= 2b \sinh \xi_0 \sin \eta, \end{aligned}$$

whence

$$\text{chord} = c = 4b \cosh \xi_0 = 4ae^{-\xi_0} \cosh \xi_0,$$

$$\text{thickness} = t = 4b \sinh \xi_0,$$

so that

$$\frac{t}{c} = \tanh \xi_0 = \text{thickness ratio},$$

$$\frac{x}{c} = \frac{\cos \eta}{2} = \frac{\bar{\alpha}}{2},$$

$$a = \frac{c}{4} \frac{e^{\xi_0}}{\cosh \xi_0}.$$

Substituting for a in terms of the chord c in the left-hand side of (2.5), and dividing by $\frac{1}{2}\rho U^2$, we obtain

$$\begin{aligned} \frac{fR^{\frac{1}{2}}}{\frac{1}{2}\rho U^2} &= 2 \sqrt{\frac{2}{\pi}} \left(\frac{\cosh \xi}{e^{\xi_0}} \right)^{\frac{1}{2}} e^{2\xi_0} \left\{ \frac{(1-\bar{\alpha})(1+\bar{\alpha})^{\frac{1}{2}}}{\cosh^2 \xi_0 - \bar{\alpha}^2} - \frac{\sinh^2 \xi_0}{2 \cosh \xi_0} \right. \\ &\quad \times \left. \left(\frac{\tan^{-1} \left(\frac{\bar{\alpha}+1}{\cosh \xi_0 - \bar{\alpha}} \right)^{\frac{1}{2}}}{(\cosh \xi_0 - \bar{\alpha})^{3/2}} - \frac{\tanh^{-1} \left(\frac{\bar{\alpha}+1}{\cosh \xi_0 + \bar{\alpha}} \right)^{\frac{1}{2}}}{(\cosh \xi_0 + \bar{\alpha})^{3/2}} \right) \right\}, \quad (2.6) \end{aligned}$$

where $R = \text{Reynolds number} = Uc/\nu$.

For the purposes of calculation

$$\tanh^{-1} \left(\frac{\bar{\alpha}+1}{\cosh \xi + \bar{\alpha}} \right)^{\frac{1}{2}} = \frac{1}{2} \log_e \frac{1 + \left(\frac{\bar{\alpha}+1}{\cosh \xi + \bar{\alpha}} \right)^{\frac{1}{2}}}{1 - \left(\frac{\bar{\alpha}+1}{\cosh \xi + \bar{\alpha}} \right)^{\frac{1}{2}}}.$$

In the case of the flat plate $\xi_0 = 0$, and

$$\frac{fR}{\frac{1}{2}\rho U^2} = 2 \sqrt{\frac{2}{\pi}} \frac{1}{(\bar{\alpha}+1)^{\frac{1}{2}}}, \quad \dots \dots \dots (2.7)$$

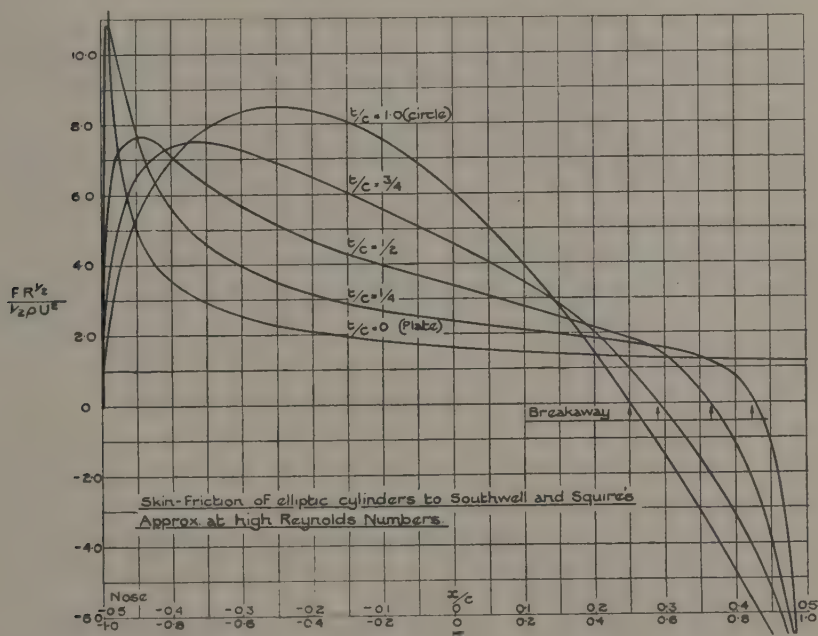
which reduces to Piercy and Winny's result ⁽⁵⁾.

In the case of the circle $\xi_0 \rightarrow \infty$, and

$$\frac{fR^{\frac{1}{2}}}{\frac{1}{2}\rho U^2} = \frac{32}{3\sqrt{\pi}}((1+\alpha)^{\frac{1}{2}}(1-2\alpha)), \quad \dots \dots \dots (2.8)$$

agreeing with Burgers' result quoted by Squire ⁽⁴⁾.

Equation (2.6) has been plotted (see figure) for various values of the thickness ratio t/c against x/c along the chord. It is seen that there is considerable variation in the curves, as the ellipse varies from a circle to



a flat plate. For thin ellipses the skin friction reaches high values at the nose. It is also seen that the skin friction becomes negative after a certain value of x/c . This is an indication of reversal of flow known as the "breakaway"; experiment confirms this phenomenon, and after the breakaway point the flow no longer remains even approximately steady, eddies are formed which constitute a wake which is no longer thin, and the theory no longer applies.

The breakaway moves progressively back from $x/c=0.75$, $\theta=120^\circ$ for the circle until it is finally non-existent in the case of the plate. Experiment shows that the breakaway in the case of the circle lies between 80° and 100° , depending on the Reynolds number. As regards the values of

$f/\frac{1}{2}\rho U^2$, the present theory considerably over-estimates them. For instance, in the case of the circle the theoretical value is some 60 per cent. greater than the experimental value. In the case of the plate the present theory gives for the drag coefficient

$$c_D = 4.514R^{-\frac{1}{2}},$$

whereas the Blasius solution, which is in close agreement with experiment, gives

$$c_D = 2.656R^{-\frac{1}{2}}.$$

We may note here that at very small Reynolds numbers there is no breakaway, so that at some intermediate Reynolds number the inception of the breakaway occurs. For the circle this occurs experimentally between $R=20$ and $R=100$, and may be expected to occur progressively later as the cylinder becomes finer until, in the limiting case of the plate, there is no breakaway, however high the Reynolds number. It is in this region that accurate solutions of (1.2) might be of considerable service, as boundary layer conditions will not then apply.

It is also interesting that the condition for breakaway, namely, the vanishing of the boundary value of the vorticity as given by equations (1.27) or (1.28), is identical with that given by Kármán and Millikan⁽¹⁾ in their first approximation, "outer" solution of the boundary layer equations.

Other Cylinders.

The possibility of dealing with actual aerofoils depends on the integration of equation (2.2). It could be carried out graphically, if so desired, in any particular case, failing the usual methods: which failure is likely, as $H_{\beta=0}^2$ for a simple aerofoil with a sharp trailing edge is considerably more complex than that for the ellipse.

There is little interest at present, as elliptic cylinders approximate to aerofoils and no new feature in the skin friction curves is to be expected, while the theory is too approximate for practical use.

The Pressure.

Examination of the expressions for the velocity or the vorticity, or those in Piercy and Winny's paper, shows that the assumption of a boundary layer when the Reynolds number is large was a correct one; so that at a comparatively short distance out from the surface the fluid attains a velocity closely equal to that of the inviscid irrotational motion and so also the pressures. Prandtl has shown that if a boundary layer exists then the pressures are transmitted through it to the surface without change, and this has been verified experimentally.

Hence the drag at high Reynolds numbers is due mainly to skin friction, and this is experimentally true for thin aerofoils and the pressures are those of irrotational flow. In the case of bluff bodies a wake of considerable width exists when the fluid is in eddying motion, and the above assumptions no longer hold.

Extension to Asymmetrical Flow.

Since the flow is (apart from the "boundary layer") identical with the ordinary irrotational flow past the cylinder, and it divides at the front stagnation point: it would also appear legitimate to apply the above solution to this case also, provided that the origin for α is still taken at the front stagnation point. There is nothing to exclude the possibility of circulation except how to determine its value. For aerofoils with sharp trailing edges and for small angles of incidence we can take the usual Kutta-Joukowski value, but for larger incidences or for aerofoils with rounded trailing edges this fails. There are other difficulties since, except in the case of the tangential flat plate, the flow reverses along the surface at high Reynolds numbers, and behind this point our assumptions no longer hold and turbulence sets in. It would seem that the lift is connected with the history of the motion from its start from rest to the Reynolds number under consideration. An approximate and somewhat artificial method of calculating the lift in cases of boundary layer flow has recently been given by Piercy, Whitehead, and the present author ⁽⁸⁾. This takes some account of the finite width of the wake.

Conclusion.

The asymptotic solution of Southwell and Squire's equations has been obtained directly from their original integral equation. This is found to lead to the same results as a simplified boundary layer theory developed by Burgers and to give the same position for breakaway as the "outer solution" first approximation of an entirely different method developed by Kármán and Millikan for the solution of the boundary layer equations. The results are in qualitative agreement with experiment, thus bearing out the remark of Southwell and Squire—that their modification to Oseen's equation should give an indication of the changes of flow pattern with Reynolds number, differing but little from Oseen's approximation at low Reynolds numbers. The solutions have been applied to the calculation of skin friction of elliptic cylinders. In the limiting cases of the plate and circle the results agree with those already obtained by Piercy and Winny and by Burgers.

The solution here obtained can be regarded as a first approximation to the solution of the boundary layer equations. In the case of the flat

Plate Piercy and the present author ⁽⁹⁾ have calculated successive approximations until Blasius's result was closely approached. In the case of the general cylinder, Piercy, Whitehead, and the present author ⁽⁸⁾ have very recently obtained an approximate solution of the boundary layer equations by the same method, but the first approximation differs from that given here owing to a different method being used. In fact no breakaway occurs. It is suggested that, starting with the solution given here, and using a method of successive approximations, these might be more rapidly convergent than those in the paper cited and preferable to the more usual method of solution in series *.

Finally, I wish to thank Mr. C. N. H. Lock for his interest and advice and Professor W. G. Bickley for valuable criticism and suggestions.

List of References.

- (1) Southwell and Squire, "A Modification of Oseen's Approximate Equation for the Motion in Two Dimensions of a Viscous Incompressible Fluid." *Phil. Trans. Roy. Soc. A*, cccxxii. p. 27 (1933).
- (2) Piercy and Winny, "On the Convection of Heat from Isolated Plates and Cylinders in an Inviscid Stream," *Phil. Mag.* (7) xvi. p. 390 (1933).
- (3) Burgers, "Stationary Streaming caused by a Body in a Fluid with Friction." *Kon. Ak. Wet. Amst.* xiii. p. 1082 (1922).
- (4) Squire, "On the Laminar Flow of a Viscous Fluid with Vanishing Viscosity," *Phil. Mag.* xvii. p. 1150 (1934).
- (5) Piercy and Winny, "The Skin Friction of Flat Plates to Oseen's Approximation," *Proc. Roy. Soc. A*, cxi. p. 543 (1933).
- (6) Burgers, "On the Application of Oseen's Theory to the Determination of the Friction experienced by an Infinitely Thin Flat Plate." *Kon. Ak. Wet. Amst.* xxxiii. p. 605 (1930).
- (7) Kármán and Millikan, "On the Theory of Laminar Boundary Layers involving Separation." N.A.C.A. Report No. 504.
- (8) Piercy, Preston, and Whitehead, "On the Approximate Prediction of Skin Friction and Lift." *Phil. Mag.* (7) p. 791 (November 1938).
- (9) Piercy and Preston, "On a Simple Solution of the Flat Plate Problem of Skin Friction and Heat Transfer." *Phil. Mag.* (7) xxi. p. 995 (May 1936).

* In a companion paper, the present author has shown that the method of successive approximations developed in the paper by Piercy, Preston, and Whitehead (ref. (8)), whilst satisfactory in the accelerated region of the boundary layer, becomes more and more slowly convergent as the breakaway is approached.

XLI. *Crystal Lattice Orientation of Rolled Magnesium.*

By D. E. THOMAS, M.A., B.Sc., F.Inst.P.*,
Research Department, Woolwich.

[Received December 27, 1940.]

[Plate VIII.]

THE crystal lattice orientation of rolled magnesium has been described as a fibre structure with the hexagonal axis perpendicular to the rolling plane. If it were a perfect fibre structure the two diffraction patterns obtained from transmitted radiation incident in the plane of the sheet and firstly, parallel, and secondly, perpendicular, to the rolling direction should be the same.

Fig. 1 (Pl. VIII.) N, P, T shows the three patterns obtained from heavily rolled magnesium with transmitted radiation :

- N, with radiation incident normal to the rolling plane ;
- P, with radiation incident parallel to the direction of rolling and to the rolling plane ;
- T, with radiation incident perpendicular to the direction of rolling and parallel to the rolling plane.

These diffraction patterns were taken with unfiltered radiation from a tungsten anode, the exciting voltage being about 130 k.v. (peak). This radiation was mainly white, but has a strong characteristic tungsten K component.

The rolled metal was in sheets of 0.06 inch thickness, and had been cold rolled to an extension of 100 per cent. No change in the pattern was to be seen between the 50 per cent. and 100 per cent. extensions.

The specimen to be examined was fixed over the end of a long " pinhole " of diameter 1 mm. and length 38 mm., and the diffracted radiation received on a film 10 cm. from the specimen.

The P and T patterns in fig. 1 (Pl. VIII.) show a distinct difference which indicates some departure from the true fibre structure.

Debye-Scherrer photographs were also taken from the faces normal to each of the above directions N, P, and T, and from magnesium powder. Cobalt K-radiation was used and the specimens were set for an angle of incidence of 20° . The specimens were made up for examination by

* Communicated by the Author.

screwing together three thicknesses of plate so that one side of the little block so made was composed of three P-faces and one end of three T-faces.

Fig. 2 (Pl. VIII.) shows the diffraction photographs so obtained. The planes producing reflexion at the smallest angles are :

100 at $18^{\circ} 45'$,

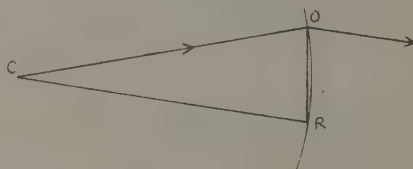
002 at $20^{\circ} 0'$,

101 at $21^{\circ} 20'$.

Comparing the photographs from the rolled face and the magnesium powder, it will be evident that there is a very strong orientation of the 002 planes in the plane of rolling.

The P- and T-faces show practically no reflexion from the 002 planes and stronger reflexions from the 100 and 110 planes than in the case of magnesium powder. The 101 reflexions always appear stronger in the P-face than in the T-face, and the 100 and 110 reflexions appear stronger in the T-face than in the P-face. These differences, too, indicate some departure from true fibre structure.

Fig. 3.



These transmission patterns are produced by radiations whose Bragg angles are of the order of 2° or 3° , so that the sphere of reflexion in reciprocal lattice theory is practically a plane. If O (fig. 3) is the origin of the reciprocal lattice, CO the incident ray, and R a point on the reciprocal lattice which is on the sphere of reflexion whose centre is C, the angle COR is of the order of 87° and CR is parallel to the reflected ray. So that the pattern of the reflexions on a film perpendicular to CO will be the same as the pattern of the intersections of the reciprocal lattice points with the plane of reflexion.

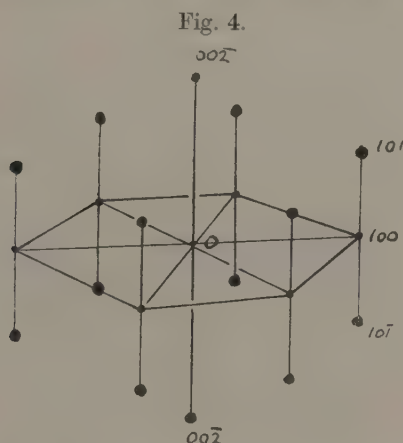
If we construct the reciprocal lattice for the above three sets of reflecting planes the 100, 002, 101, we get that shown in fig. 4.

If the reciprocal lattice is oriented with the hexagonal axis parallel to the incident ray the only planes producing reflexions are those lying in the plane through O perpendicular to the incident ray. *i. e.* the 100 planes. If the structure is a fibre structure on this hexagonal axis we may imagine the lattice to be rotated about the hexagonal axis. The 100 points of the reciprocal lattice will mark out a circle of uniform intensity. The

radiation used is white so that the circle will be broad and diffuse. The Debye-Scherrer photographs from magnesium powder show that the 100 planes are of low reflecting power, so that the normal transmission pattern from a crystal lattice oriented with the hexagonal axis perpendicular to the plane of rolling may be expected to be a broad diffuse circle of low intensity. This is, in fact, found to be the case.

The P and T patterns each shows a set of equally spaced brushes, the P brushes being narrower than the T brushes. The two brushes in the normal direction are much stronger than the others in each case.

To use the reciprocal lattice to determine the conditions for these reflexions we must now consider the hexagonal axis to lie in the plane of reflexion. In any azimuth of the lattice round this axis there will be a



reflexion from the 002 planes, at 12 and 6 o'clock in P and T, fig. 1 (P. VIII.). But there will be reflexions from the 101 planes only when these hexagon edges lie in the plane of reflexion.

The angle subtended at the origin between the 002 and 101 points of the reciprocal lattice is $\tan^{-1} \frac{2}{\sqrt{3}} \cdot \frac{c}{a}$; c/a for magnesium is 1.623. So this angle is $\tan^{-1} 1.87$ or 62° .

But the brushes are, as nearly as can be measured, 60° apart. This difference is more than the error of measurement and can be accounted for, together with the difference between the P and T patterns, as follows:—

The orientation of the hexagonal lattice is assumed to be such that

(i.) the mean position of the hexagonal axis is perpendicular to the plane of rolling with rotation of the lattice in all azimuths about this axis; combined with

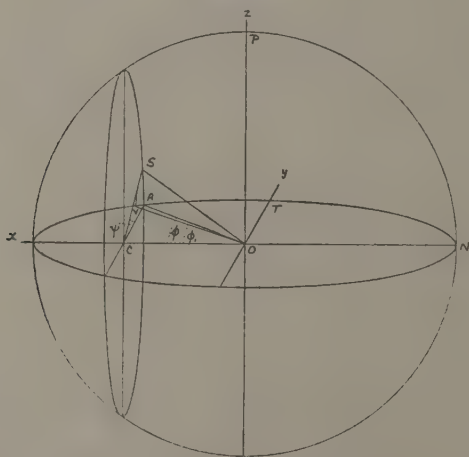
(ii.) a deviation from this mean position of about 20° on each side, about an axis parallel to the direction of rolling; and

(iii.) a larger deviation, about 25° , on each side, about an axis in the plane of rolling and perpendicular to the direction of rolling, *i. e.*, about the T direction.

The extent of these deviations of the hexagonal axis is shown by the width of the 002 brushes, those in the N direction in the P and T patterns.

When the hexagonal axis is perpendicular to the plane of rolling there will be no reflexion from the 101 planes except when they are in the position described above, *i. e.*, with the edges of the reciprocal lattice in the plane of reflexion. But by making use of the deviations postulated above we

Fig. 5.



can bring certain of these reciprocal lattice points into the plane of reflexion. This is readily seen from the following considerations:—

About centre O (fig. 5), the origin of the reciprocal lattice, describe a sphere whose radius is equal to the distance of one of these 101 lattice points from O. The plane NOT is the plane of reflexion of the reciprocal lattice, ON and OT being the normal and transverse directions.

In the rotation about the fibre axis, ON, the reciprocal lattice point moves on a small circle through an angle ψ from A to S, so that the reciprocal lattice point leaves the plane of reflexion. It can be returned to it by a rotation about the T axis. It will again move on a small circle on the sphere and will meet the plane of reflexion at V, say. The reflexion now takes place on a radius at an angle ϕ_1 from the N direction, slightly different from the original angle ϕ .

Let axes of coordinates Ox , Oy , Oz be taken in the N , T , and P directions as shown in fig. 5. The coordinates of S are

$\rho \cdot \cos \phi$; $\rho \cdot \sin \phi \cdot \cos \psi$; $\rho \cdot \sin \phi \cdot \sin \psi$: ρ being the radius of the sphere.

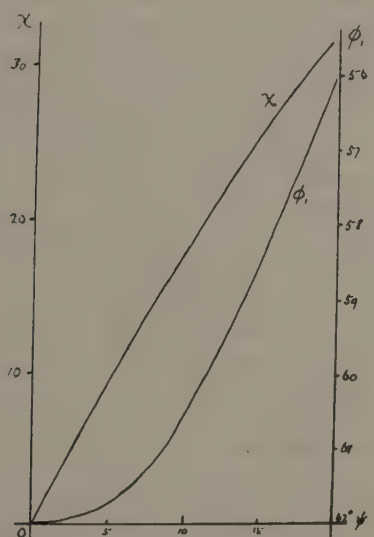
S is rotated about Oy to meet the plane xOy : the angle through which it must be rotated is χ , where

$$\tan \chi = \frac{z_s}{x_s} = \tan \phi \cdot \sin \psi.$$

V is on the circle $x^2 + y^2 = \rho^2$ at a point whose y coordinate is y_s , i. e., $\rho \cdot \sin \phi \cdot \cos \psi$, and the x coordinate of V is

$$\rho \sqrt{1 - \sin^2 \phi \cdot \cos^2 \psi}.$$

Fig. 6.



The angle ϕ_1 is given by

$$\tan \phi_1 = \frac{\sin \phi \cdot \cos \psi}{\sqrt{1 - \sin^2 \phi \cdot \cos^2 \psi}}.$$

$$\therefore \sin \phi_1 = \sin \phi \cdot \cos \psi.$$

The graph shown in fig. 6 shows the relation between χ , ϕ_1 , and ψ for the case where ϕ is 62° .

It will be seen from the graphs that if ψ is 15° a rotation of 26° about the T direction as axis will bring the 101 plane back to the reflecting position, and that the angle between the reflexion in this case and the

002 reflexion is $58\frac{1}{2}^\circ$. So that if the deviation round the T direction is more or less uniformly distributed over the range of $\pm 26^\circ$ the brush will spread from $58\frac{1}{2}^\circ$ to 62° and so will have a mean value of nearly 60° . The deviation round the P axis will widen the 101 brushes and the 002 brushes to the same extent.

This explanation is quite consistent with the dimensions of these patterns. The deviation about the T axis is about $\pm 25^\circ$ as shown by the angular width of the brushes in the T pattern. The 101 brushes in the T pattern should be about 4° wider than the 002 brushes. They do, perhaps, appear a little wider, but owing to the want of a sharp edge for measurement it is difficult to be sure of this. Any excess of width of the 101 over the 002 brushes will tend to be masked by the greater intensity of the 002 brushes.

A similar explanation accounts for the T pattern. In this case the deviation of the hexagonal axis in the reflecting plane is assumed to be greater than in the P pattern. The brushes are consequently wider.

The smaller deviation to be invoked in this case to bring the reciprocal lattice points back to the reflecting plane will tend to make the angle between the 002 and 101 brushes a little greater than in the P pattern. Owing to the greater diffuseness of these brushes it is difficult to measure them sufficiently accurately to verify this.

These considerations have dealt entirely with the reflexions from the 002 and 101 planes in the P and T patterns.

The 100 planes can only produce reflexion when the hexagon edge of the reciprocal lattice lies in the reflecting plane. If the rotation round the fibre axis takes the lattice point out of this plane the deviation of the hexagonal axis required to restore reflexion is 90° , for since $\phi = 90^\circ$, χ must be 90° , whatever the value of ψ . We thus expect a weak reflexion at 90° from the 002 brushes. This can be seen in the P pattern.

This interpretation of the transmission patterns is in agreement with the differences between the Debye-Scherrer photographs from the P- and T-faces. The Debye-Scherrer photographs were all taken with the plane of incidence parallel to the plane of rolling so that a 100 or 110 plane could only come into reflecting position when the hexagonal axis was normal to the rolling plane. If the deviation is large the number of crystals satisfying this condition of reflexion will be smaller than when the deviation is small. The 100 and 110 reflexions are stronger from the T-faces than from the P-faces, so that the deviation of the hexagonal axis from the T-faces should be the smaller.

It requires a deviation of 28° to bring the 101 plane into the P- or T-face. As the 101 reflexions are always stronger from the P-faces there must be more crystals with this large deviation from the mean position. This again agrees with the interpretation of the transmission patterns.

A still further confirmation of this difference of deviation in the P- and T-faces was obtained by taking Debye-Scherrer photographs from these faces with the plane of incidence at right angles to the plane of rolling. Photographs were taken with angles of incidence of 19° and 34° , the Bragg angles for the 100 and 110 planes. In each case the T-face gave the stronger reflexion.

Summary.

The crystal lattice orientation of rolled magnesium has been studied from evidence given by transmitted and reflected X-ray diffraction patterns. A departure from true fibre structure is indicated by the photographs and an interpretation of it is offered. The interpretation offered also explains the difference between the angular separation of the radial reflexions in the transmitted patterns and that of the planes producing them.

The author takes this opportunity of thanking Professor W. R. D. Jones, D.Sc., of the University College, Cardiff, for supplying the specimens used for the above work.

XLII. *Note on a Problem in the Conduction of Heat.**To the Editors of the Philosophical Magazine.*

GENTLEMEN,—

IN the January number of this Journal (pp. 81–87) Mr. R. V. Churchill gives the solution to one of the problems treated by me in *Phil. Mag.* vol. xxviii. November 1939, and points out that part of his solution does not agree with that given by me. He goes on to say that the first object of his paper is to give the correct solution. I should like to point out, however, that Mr. Churchill's result is in agreement with the one I originally gave.

The explanation of the difference is that the brackets have been misplaced in the transcription of the final result of my paper. The correct solution is obtained by writing $2(n+1)a$ for $(2n+1)a$ in my expressions for v_2 .

The above error was pointed out to me by Prof. H. S. Carslaw in February 1940, and I welcome this opportunity of correcting my paper and securing agreement between my result and those given subsequently by Prof. Carslaw and Mr. Churchill.

Yours faithfully,
C. J. TRANTER.

XLIII. *Notices respecting New Books.*

A Mathematician's Apology. By G. H. HARDY. (Cambridge University Press, 1940.) Price 3s. 6d.

MATHEMATICS, according to Professor Hardy, is "real" or "trivial," and the "apology" is, perhaps intentionally, the "trivial" part of his book—a peg on which to hang the many quite good things or, shall we say, the "real" things which the book contains. There are few subjects, as the author says, more generally recognized as profitable and praiseworthy, and a mathematician therefore need not consider himself on the defensive; but Professor Hardy is not quite happy about accepting this comforting justification. He is a "real" mathematician—the present reviewer firmly believes this, and is not being ironical—and there is nothing useful in "real" mathematics. But Hardy is surely wrong in maintaining that "real" mathematics has no utility. Even the theorems of Eudoxus and Pythagoras—given by the author as illustrations of "real" mathematics—have a genuine practical value, though it is rather remote and indirect, and apart from this, is it not an ample apology for these theorems that they have given pleasure to the mathematicians who discovered them, and thousands of students who have studied them since?

The examples or illustrations of "real" mathematics given in the book are very simple and within the competence of those whose mathematical training has been neglected, and they include the imposing theorems just mentioned.

The author scarcely disguises his contempt for the "trivial" mathematics whose *raison d'être* lies in its practical function, which is to "plan the rational society in which there will be leisure for all and poverty for none."

The book is full of good phrases and sayings: "conscientious imbecility"; "chess problems are the hymn tunes of mathematics"; "mathematical sophistication"; "Euclidean geometry is useful in so far as it is dull." The author is right in distinguishing between mathematical reality and physical reality. The distinction appears to the present reviewer—and possibly the author does not agree with this—to be related to the different senses of the word "true" in the following sentences:—"It is 'true' that $(a+b)^2 = a^2 + 2ab + b^2$," and "It is 'true' that Professor Hardy has written a provoking book." Mathematical reality and physical reality (which is just the same as work-a-day reality) are very different, and it is questionable whether a meaning can be assigned to the assertion that mathematical reality lies outside us and that we observe it.

There are, then, as Hardy repeats towards the end of his little book, two mathematics—the "real" and the "trivial." The former, according to Hardy, must be justified as an art, the latter by its utility. It would have been better to make the distinction which is attempted in this book somewhat as follows:—Mathematics, like the University, has an aspect which is "trivial." It is of immense utility, and most of those who come into contact with it only have in mind and only appreciate its utility. Their outlook is that of Mephistopheles:

"Grau, teurer Freund, ist alle Theorie,
Und grün des Lebens goldner Baum."

W. W.

Spectra of Long-Period Variable Stars. By PAUL W. MERRILL. [Pp. x+107; 6 plates, 13 figs.] (U.S.A. : University of Chicago Press; Great Britain and Ireland : Cambridge University Press, 1940. Price 15s. nett.)

STELLAR variability is not the unusual phenomenon it was believed to be only half a century ago. It is merely chance, of course, that the rise of spectroscopy coincided with the gradual recognition that perhaps one star in twenty is variable in brightness; but this chance has proved of the utmost importance to astrophysics. The spectra of variable stars have provided and are now providing many of the clues which will eventually lead to a solution of the many complex problems presented by these objects. It is not too much to say, however, that at present the causes of stellar variation are still obscure or even unknown. In these circumstances such a book as this will be welcomed by spectroscopists and astronomers alike. It deals with the spectra of those variables which are easily the most common; and it deals with them empirically, without paying much attention to theories except where they seem firmly established or where they can point to profitable further lines of inquiry. The spectra at maximum light are described in detail, both as to the general energy-distribution and the bands and lines, these latter both in absorption and in emission. Variations during the decline to minimum are less well known, since the visual brightness of a variable of this type may fall by a factor of 1000 or more during this period; but a short chapter gives an admirable summary of the changes exhibited. Not the least valuable features of the book are the excellent plates which illustrate it; and the volume as a whole is a worthy addition to the series of *Astrophysical Monographs*.
A. H.

Culture, Vol. V. No. 2. [Pp. 144+viii+29.] (L'Association de Recherches sur les sciences religieuses et profanes au Canada, 33 Rue de l'Alverne, Québec, Qué. Canada. Subscription \$2 per annum.)

THE issue of this quarterly magazine for June 1940 could be the starting-point for essays on many a subject. The absence of reference to the events then taking place in France may be a reminder of how blind we all were, or possibly of how remote Canada then felt herself from the War.

In itself, the very existence of the magazine is a reminder of the many peoples included in the British Empire—not only big communities like the Hindus and Moslems in India, but the small compact groups, like the Celts in Wales, the Gaels in Ireland and Scotland, and the French in Canada, each with complete freedom to use its own language and retain its own customs and outlook. These French-Canadians, as we learn from this magazine, are still intensely ardent Catholics, and much of their general culture obviously centres around their religious life.

As befits a magazine of general culture, a good deal of space (29 pages) is devoted to reviews of books, and, in addition, there are no fewer than 37 pages in which recent publications are given in classified lists.

The Half-Yearly Journal of the Mysore University, New Series, Vol. 1, No. 1 (Section B—Science). [Pp. 91.] (Bangalore Press, Mysore. Annual Subscription, 4 rupees.)

THE publication of a journal in which contributions from the members of a single University are collected together, even though they have been published elsewhere, doubtless tends to foster a co-operative spirit, which is probably

of especial value in the East, where our conception of a University is still relatively new. Thus, the University of Mysore has found it desirable to resume publication of its journal, after an interval of several years, and this, the first number of a new series, suggests that the journal will adopt a wide outlook. Besides four biological papers and one purely chemical (on the iodides of sulphur), it contains a paper on higher dynamics, one on the theory of equations and an original treatment of the three-dimensional "equation of telegraphy" ($\nabla^2 u = u + \partial^2 u / \partial t^2$). We wish the journal every success.

Table of Powers (British Association Mathematical Tables, Vol. ix.). By the British Association Committee for the Calculation of Mathematical Tables. [Pp. xii+132.] (Cambridge University Press, 1940. Price 15s. net.)

QUITE fifty years ago, the British Association began to take an interest in the calculation of mathematical tables, and various Bessel functions were printed in their reports. More recently, a newly constituted Committee set to work, and has published, in separate volumes, tables of a number of fundamental functions, many of them of interest in the theory of numbers, and others dealing with special functions.

The present volume, giving powers of integers, was initiated by J. W. L. Glaisher, a single copy of whose results fortunately came into the hands of the Committee. It has been extended by W. G. Bickley, C. E. Gwyther, J. C. P. Miller, and Miss E. J. Ternouth. As extended, it gives powers up to the 50th for numbers from 1 to 120, up to the 20th for the integers to 299, and up to the 12th for the integers to 1099.

Powers up to the 27th are in all cases printed in full, as are the powers up to the 30th of numbers not exceeding 100, and also the 40th and 50th powers. It is pointed out that if these curtailed numbers are insufficient, the provision of the 30th, 40th, and 50th powers in full enables others to be obtained by multiplication or division by a number of not more than 11 digits. The curtailed number serves as a useful check, to which may be added a test by casting out the nines. Thus if the digits of x add up to X (the summation being repeated till $X \leq 9$), then the corresponding sum for x^n must equal that for X^n . For example, the 50 digits of 103^{23} add up to 232, of which the digits add to 7, whilst the 14 digits of 4^{23} add up to 70, giving the same total.

In addition to these main tables, the volume contains a table for evaluating sums of powers and another of binomial coefficients.

As we have come to expect in these volumes, the preface (by J. C. P. Miller) is a valuable essay on the whole subject, with a bibliography of other similar tables, and corrigenda to many of these.

Both in theory of numbers and in the calculation of functions by means of power-series, these tables will be of great value, though for the latter purposes, tables of the negative powers are even more useful. J. H. A.

Electrical Contacts. By G. WINDRED. [Pp. xii+403.] (Macmillan & Co., Ltd., 1940. Price 16s. 0d.)

THE object of this book, which is written from the engineering rather than the academic aspect, is to collect together all that has been published on the properties of electrical contacts. This phrase has been interpreted very widely, so that, for example, there are sections on contact resistance, surface films, and coherer action: also a chapter on arcs and discharges, in which the relation

between length, potential difference, and pressure is discussed both for sparks and for arcs. The fact that A.C. circuits present special problems is held to justify a complete chapter of nearly fifty pages on currents in A.C. circuits.

The book is thus self-contained, in the sense that all information ancillary to the main topic is to be found between the same pair of covers. In its own specialized field, the subjects treated are the forms, strength, and efficiency of various joints (for example, bolted, welded, and plug-and-socket), switch contacts, the materials used for contacts (over 40 are tabulated in the contents list) and, finally, sliding contacts.

Each of the eight chapters is provided with a bibliography, and there are many photographs, of varying quality, either to illustrate design methods or to show the effects of wear, erosion, and other agencies.

Relaxation Methods in Engineering Science. By R. V. SOUTHWELL. [Pp. vii+252.] (Sir Humphrey Milford, at the Clarendon Press, Oxford, 1940. Price 17s. 6d.)

THE relaxation methods which have been developed in recent years by Professor Southwell take their name from the problem of the stress distribution in a framework; in this problem in its simplest form, the method consists in imagining the framework to be initially constrained at every joint, and the constraints to be *relaxed* in turn. In fact, at each stage the joint with the greatest load is relieved, so that the maximum outstanding force becomes less at each stage, and ultimately all are reduced effectively to zero, and the framework is free.

The method has already been described in papers (published mainly by the Royal Society), and the present book gives a collected treatment in an order dictated rather by logic than by the historical development which must govern the presentation in original memoirs.

As experience was gained, it was found that the relaxation method was not only a device with a physical meaning, suitable for stress calculation, but is also a purely mathematical device for solving simultaneous linear equations. It can thus be applied to the adjustment of observations, to current flow in electrical networks, and many other physical phenomena. It is even possible to generalize it so as approximately to solve problems characterized by an infinite number of degrees of freedom, and in particular to the one, of engineering importance, concerned with the modes and frequencies of vibration of mechanical systems. In this sense, it provides an extension of Rayleigh's principle.

Finally, the most striking generalization is to problems in which the governing differential equation is non-linear, as when stress and strain are not proportional.

All these matters are very clearly dealt with in the book, generally with numerical examples, and the result of a first reading is a feeling that here is a treatment which is going to be useful in many of one's own problems, and that time will have to be found for a more thorough study. The price is commendably low.

J. H. A.

[The Editors do not hold themselves responsible for the views expressed by their correspondents.]

FIG. 1.

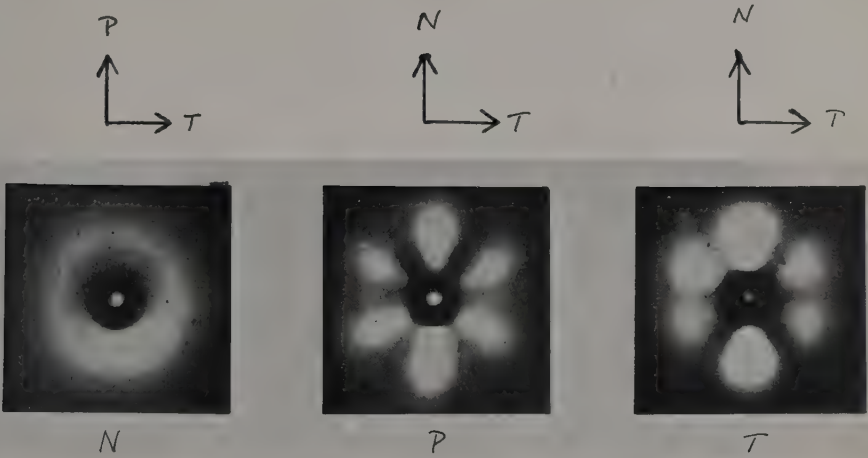
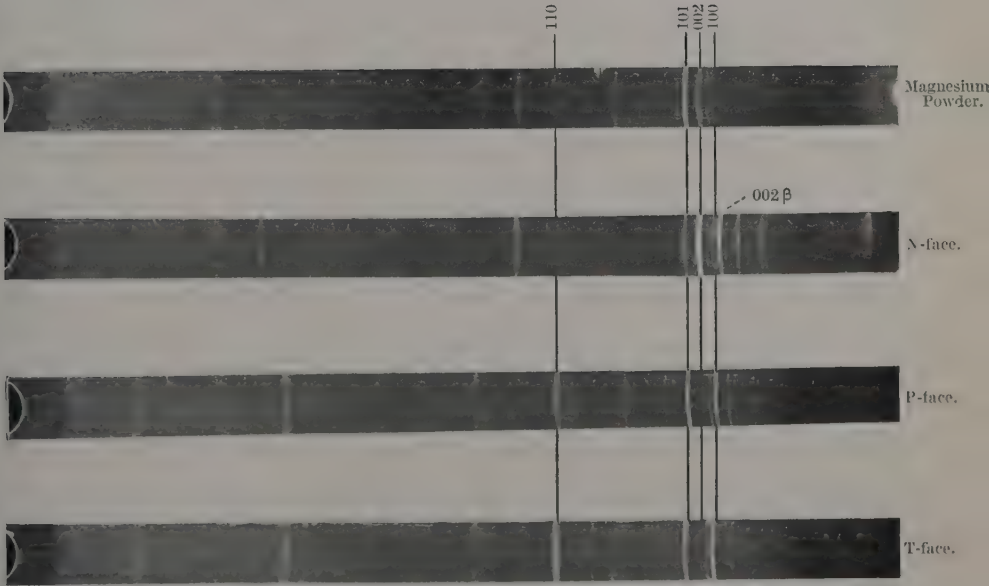


FIG. 2.



XLIV. *The Measurement by Ionization Methods of Real Energy Absorption from an X-ray Beam.*

By J. R. CLARKSON, Ph.D.*

[Received February 28, 1941.]

[Plate IX.]

Introduction.

A COMMON method of measuring absorption from a beam of radiant energy consists in observing the temperature rise of an absorber. In the case of X- or gamma-radiation this method is subject to serious uncertainty for four reasons: (a) the amounts of energy radiated by even the strongest sources are small; (b) the high penetrating power of the radiation makes it necessary to use large thicknesses of absorbing material with consequent small temperature changes; (c) where chemical compounds are used as absorbers there is the possibility of chemical processes being started. These may evolve relatively large amounts of heat and mask the small temperature changes sought; (d) corrections are necessary for scattered and fluorescent X-rays as well as for secondary electrons from the calorimetric material.

The direct heating method can be used in experiments designed to measure the total energy flux in a beam by absorbing it in lead or mercury. It is difficult to adapt the method to that class of problem in which the absorber is of light material and small extent, or in which it is required to know the variation from point to point of the rate of energy absorption.

It may be possible to use the ionization current produced in a gas contained in a small ionization chamber as an indication of the rate of absorption of energy. At ordinary pressures the absorption will take place partly in the material surrounding the gas and partly directly in the gas itself. The direct absorption in the gas may be eliminated in practice by working at very low gas pressures, and the experimental procedure consists of obtaining a curve connecting ionization current and gas pressure for a small chamber made of the material to be investigated. The slope of this curve at the origin is held to give a measure of the true energy absorption in the material. In the present work ionization-pressure curves have been obtained for a number of materials,

* Communicated by Professor W. V. Mayneord, D.Sc., F.Inst.P.

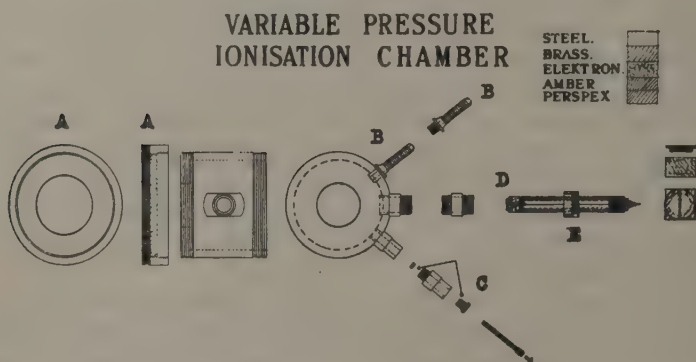
gases, and different effective wave-lengths of radiation, and the results compared with those deduced from theoretical considerations.

*Experiments with a Variable-pressure Type of
Ionization Chamber.*

(i.) *Apparatus.*

In order to vary the gas pressure, the ionization chamber was mounted inside a cylindrical pressure chamber, shown in fig. 1*a* (Pl. IX.) and fig. 1*b*. The pressure chamber was of internal dimensions 3" diameter, 3" length, and of $\frac{1}{4}$ " wall-thickness, and was turned from a solid piece of bright mild steel. The ends were threaded to carry annular end-pieces (A) of 4" external diameter turned from solid steel. The end-pieces retained

Fig. 1*b*.



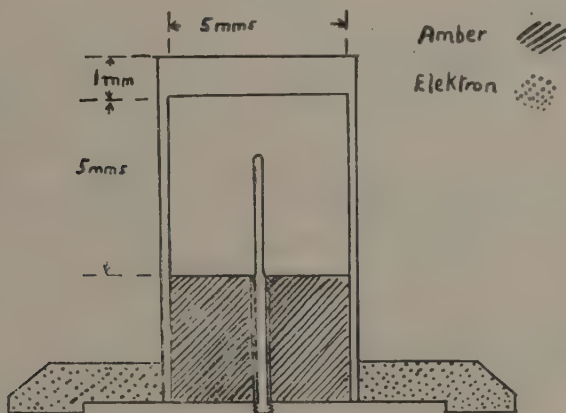
the disks, $\frac{1}{4}$ " thick, which closed the ends of the chamber and which were of "Perspex," a transparent plastic product containing only light elements. Three holes were drilled in the side of the pressure chamber to take respectively (1) a screwed-in tube (B) for connexion to the vacuum or pressure system; (2) a tube (C) through which passed a wire carried on tapered amber insulators for charging the outside wall of the chamber; and (3) the evacuated tube (D) on which the chamber was mounted. The connexion to the central electrode of the ionization chamber was carried on amber bushes in an evacuated earthed lead ⁽¹⁾ which passed through a sleeve to the interior of the pressure chamber until stopped by a flange, being then secured by a hexagonal nut (E). In this manner the evacuated tube surrounding the connexion to the electrode was carried into the pressure chamber and separated by only a few millimetres of amber from the ionizable volume. After the chamber had been placed in position and the ends screwed on, all joints were sealed with picein wax. Compressed

air for measurements at pressures above atmospheric, as well as gases other than air, were introduced through a needle valve remote from the chamber. Pressures up to more than two atmospheres were read on an open mercury manometer. A slow stream of gas was passed through for a short time before stopping the pump and allowing the pressure to rise.

Ionization currents were measured by the Townsend compensation method ⁽¹⁾.

The ionization chambers used for the measurements with tungsten K radiation were of the type shown in fig. 2. The internal diameter was 5 mm. and internal length 8 mm., but an amber bush filling one end of the chamber left an ionizable volume only 5 mm. in length. The end

Fig. 2.



of each chamber was 1 mm. thick and the side wall as thin as could conveniently be obtained. The materials used were carbon (Acheson graphite), magnesium, "Elektron," aluminium, iron, copper, zinc, and lead. The chambers, of graphite, "Elektron," and aluminium, had wall-thickness 0.5 mm., and the others walls of thickness 0.25 mm. Other sizes of chamber were used in preliminary work.

(ii.) Measurements with Tin Fluorescent Radiation.

(a) Apparatus.

A test of the variation of real absorption can only be satisfactorily made with homogeneous radiation of known wave-length. In a first series of measurements SnK radiation was used, but, owing to the small intensity available, the results can only be regarded as preliminary. They

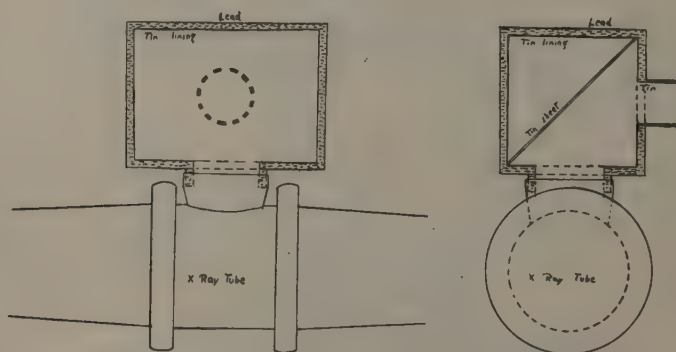
do, however, quite clearly show the general shape of the ionization-pressure curve for pressures up to two atmospheres.

The SnK radiation emerged at right angles to the incident beam from a radiator similar in design to that of Bragg and Porter ⁽²⁾. A wooden box, $4\frac{3}{4}'' \times 4\frac{3}{4}'' \times 6\frac{1}{2}''$, was lined with 1 mm. of pure tin and had a pure tin plate, 0.54 mm. thick, placed diagonally inside it (fig. 3).

(b) *Results and Discussion.*

Results of measurements on chambers of 2 cm. internal diameter and 2 cm. length made from magnesium, graphited celluloid, and graphite are shown in fig. 4. Corrections have been applied for absorption in the chamber walls.

Fig. 3.



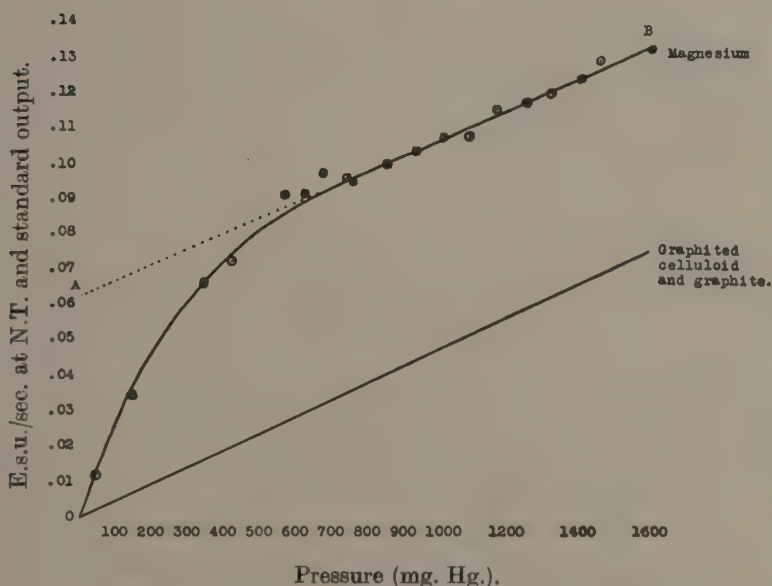
The magnesium curve consists of three portions: (a) a linear portion at low pressures merging into (b) a curved section extending up to about 600 mm., and (c) a straight line at higher pressures. For the other chambers straight lines were obtained throughout the pressure range.

The ionization in the chamber consists of two portions: (a) the ionization produced directly in the gas, which is proportional to the pressure, and (b) that due to secondary electrons from the wall material. At relatively high pressures these wall electrons will not cross the chamber, but will produce dense ionization in a layer of gas round the boundaries. It is sometimes stated ⁽¹⁶⁾ that the linear portion of the ionization-pressure curve represents the ionization due to direct absorption by the gas, and, on extrapolating it to cut the ionization axis at A (fig. 4), an ordinate OA is obtained which is said to represent the ionization due to the electrons from the walls.

The experimental results do not, however, support this explanation. The curves for the graphited celluloid and the graphite chambers are

linear throughout. Such curves will be obtained when the atomic number Z of the material composing the chamber wall is approximately the same as that of the gas enclosed. When this gas is air, such material is called "air-equivalent." It is to be observed that the linear part of the magnesium curve is parallel to the air-equivalent chamber curves, and hence the ordinate OA represents the excess ionization obtained by replacing the walls of air-equivalent material by ones of magnesium. An equation obtained by Bragg ⁽³⁾ (p. 170) for the ionization current in a gas enclosed by solid walls is to be interpreted in this way.

Fig. 4.



Results with SnK radiation: chamber volume 6.25 c.c.
Results corrected for wall absorption.

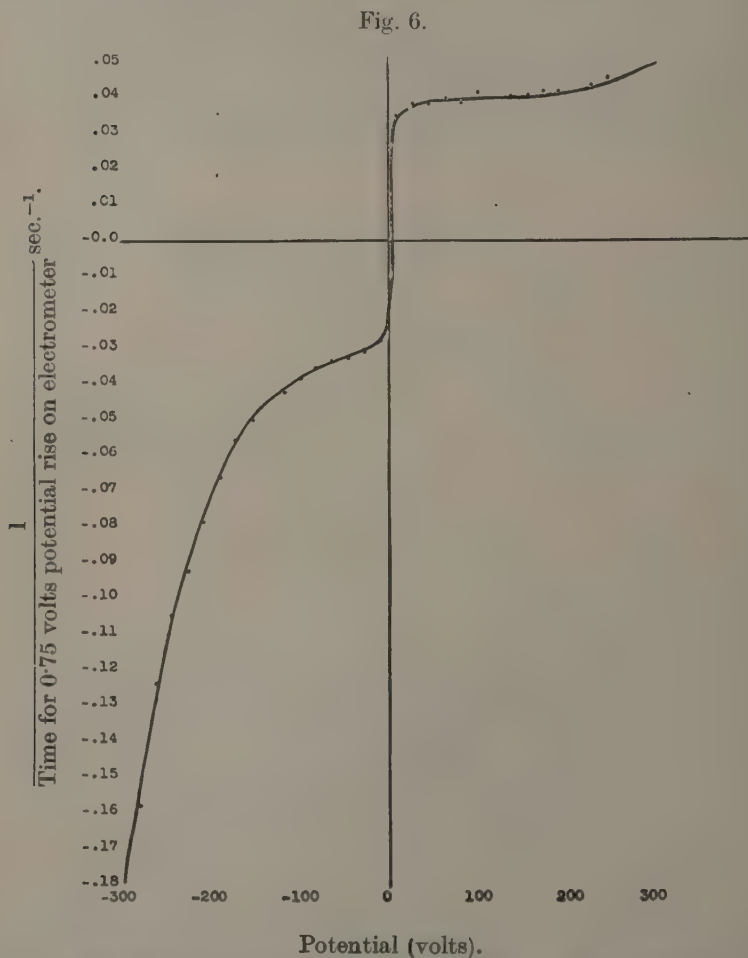
(iii.) *Measurements with Tungsten Radiation.*

(a) *Filter.*

In order to obtain a greater intensity of radiation, even with some loss of homogeneity, the X-ray tube, having a tungsten anode, was operated at 100 kv., and the radiation filtered through a layer of tungstic acid, 0.7 grammes per square centimetre, held between thin celluloid sheets, and then through 0.1 mm. copper and 1 mm. aluminium. A Seeman spectrogram (Pl. IX. fig. 5) shows that the greater part of the energy is concentrated in the tungsten K_{α} and K_{β} lines.

(b) *Saturation Curves.*

In view of the possibility that some part of the ionization current measured at low pressures might be due to collision effects, the variation of ionization current with charging potential was investigated at a gas pressure of 20 mm. Hg.



Saturation curve 19 mm. Hg. air-pressure. Lead chamber.

Fig. 6 is an example of the results obtained. As the negative charging potential is decreased from -300 volts, the ionization current rapidly decreases. There is no indication of a well-defined saturation potential.

With an earthed chamber there is a definite negative current, which is eliminated by a small positive potential. With increasing positive potential there is a rapid increase of ionization current and a well-defined saturation region extending up to about 200 volts. Above this, ionization by collision again sets in and the current rises rapidly. Curves of similar form were obtained for chambers of aluminium, iron, and lead.

These results are in agreement with preliminary ones in which it was found that at low pressures the currents measured with a negatively charged outer wall of the chamber were greater than with a positive one, and could not be shown graphically as a straight line through the origin of the ionization-pressure curve.

The general shape of these curves does not appear to depend greatly on the material of the chamber, although it must be affected by the magnitude of the contact electromotive forces present, but is probably very dependent on the air pressure, the size and shape of the chamber, and possibly on the length and diameter of the central electrode and on the wave-length of the radiation.

(c) *Variation of Ionization with Pressure in Various Gases.*

Ionization currents were measured at varying pressures for a number of chambers made of different materials, and filled with air, oxygen, carbon dioxide, nitrous oxide, and hydrogen. The results were similar to those shown in fig. 7.

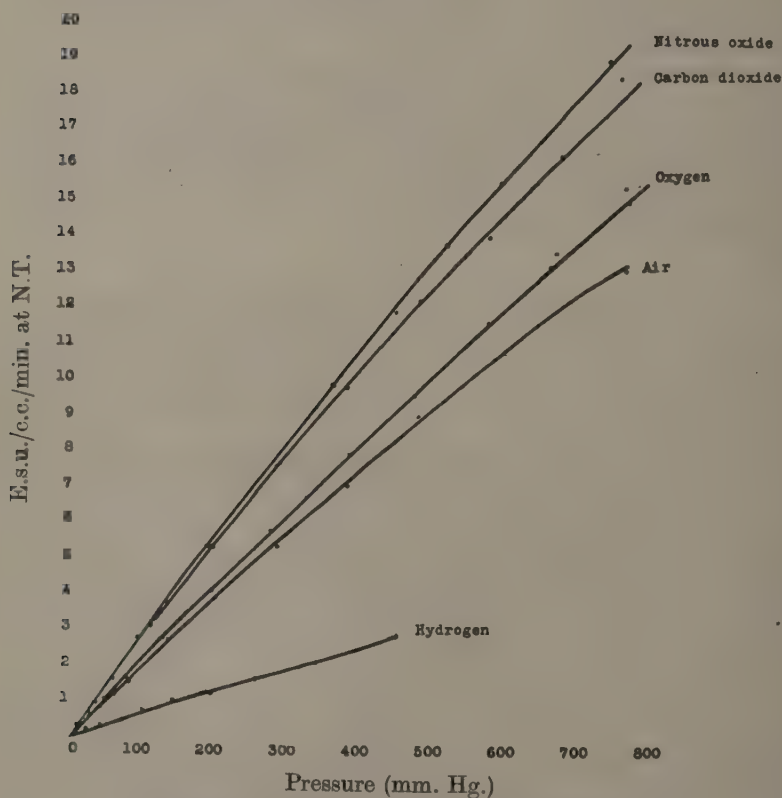
To compare results for different materials a correction has been made for the absorption of radiation in the walls of the chamber, as below. The relative intensities of the chief components of tungsten K radiation at the tube target are given ⁽⁴⁾ as $\alpha_1 : \alpha_2 : \beta_1 : \beta_2 :: 0.5 : 1 : 0.35 : 0.15$, the respective wave-lengths being 0.2135, 0.2089, 0.1844, 0.1794 Å. This distribution will be somewhat affected by filtration, but it will be sufficiently accurate to consider the radiation as having an effective wave-length of 0.20 Å.

It may be considered that the beam of radiation is a parallel one at right angles to the axis of the chamber, and the absorption in the cylindrical walls treated as an example of the interchangeability of radiating source and measuring instrument, making use of investigations due to Owen and Naylor ⁽⁵⁾. They considered the transmission of radiation in a direction parallel to a diameter of a cylindrical tube from a thin layer of radioactive material distributed uniformly over the interior surface of the tube. It may be shown that

$$\frac{I}{I_0} = \frac{2}{\pi} \int_0^{\frac{\pi}{2}} e^{-\mu a \left[\sqrt{\left(\frac{b}{a}\right)^2 - \sin^2 \theta} - \cos \theta \right]} d\theta,$$

where I_0 is the total energy emitted in the parallel beam, I the transmitted energy, a and b the internal and external radii of the tube, μ the linear absorption coefficient, and θ the angle between the radius joining the emitting element to the centre and the direction of the beam. The integral may be evaluated graphically. Using the mass absorption coefficients given by Allen ⁽⁶⁾, the percentages transmitted were, for the materials used :—Carbon 96.9, magnesium 98.2, "Elektron" 96.6,

Fig. 7.



Aluminium chamber : tungsten K radiation.

aluminium 94.2, iron 69.3, copper 56.0, zinc 59.9, lead 13.8, the wall-thicknesses being as previously stated.

Results are shown in Table I. Section 1 shows values of $\frac{di}{dp}$ taken directly from the ionization-pressure curves, of which an example is

TABLE I.

$\frac{di}{dp}$ at origin expressed in $\frac{\text{e.s.u. (quantity)/min./c.c. at N.T.}}{\text{mm. Hg.}} \times 10^3$.

(1) Measured.

Material of chamber.	Z.	Gas in chamber.				
		Hydrogen.	Air.	Oxygen.	Carbon dioxide.	Nitrous oxide.
Carbon	6	—	3.3	3.8	5.0	5.0
Magnesium	12	5.5	16.4	—	18.8	—
"Elektron" ...	12 (?)	—	14.7	17.9	23.6	23.6
Aluminium	13	7.4	20.6	22.0	29.2	29.2
Iron	26	18.0	57.0	66.0	74.0	74.0
Copper	29	—	73.0	76.0	96.0	96.0
Zinc	30	—	90.0	103.3	130.0	130.0
Lead.....	82	—	60.0	66.0	83.0	83.0

(2) Corrected for absorption in the chamber wall, electronic stopping-power and specific ionization of the gas.

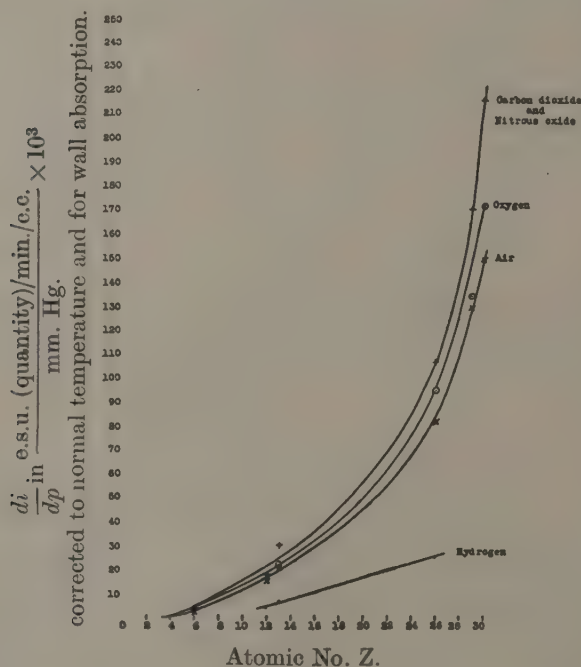
Material of chamber.	Z.	Gas in chamber.					
		Hydrogen.	Air.	Oxygen.	Carbon dioxide.	Nitrous oxide.	Theoretical.
Carbon	6	—	3.4	3.4	3.3	3.3	3.4
Magnesium	12	33.2	15.7	—	11.4	—	14.6
"Elektron" ...	12 (?)	—	14.3	15.0	14.5	15.0	—
Aluminium	13	46.3	20.6	18.9	18.4	18.9	16.9
Iron	26	143.7	72.5	72.4	59.5	60.7	126.7
Copper	29	—	111.5	100.0	92.8	95.6	194.6
Zinc	30	—	128.8	127.4	121.3	117.8	—
Lead.....	82	—	157.0	149.0	137.8	140.0	776.0

shown in fig. 7. $\frac{di}{dp}$ is expressed in $\frac{\text{e.s.u. (quantity)/c.c./minute}}{\text{mm. Hg. pressure}} \times 10^3$, and has been corrected to 0° C. and to a standard output of radiation from the tube. Fluctuations in X-ray intensity from day to day were

taken into account by measurements made with a Victoreen dosimeter in a fixed position before every set of ionization measurements.

The figures of section 1 have been corrected to 100 per cent. transmission of radiation, and the results are shown graphically in fig. 8. On multiplying by S_1 the electronic stopping power (relative to that of air) of the wall material for secondary electrons originating from the absorption of X-radiation, a measure of the real energy absorption of that material should be obtained. Values of S were taken from Gray's results ⁽¹⁰⁾.

Fig. 8.

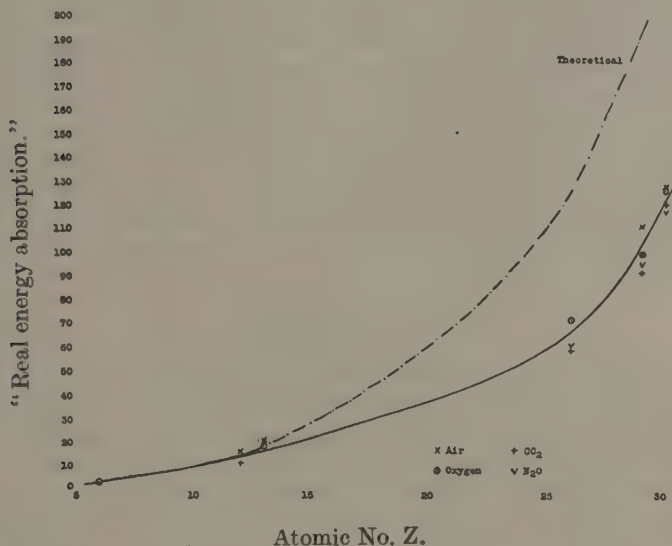


Lastly, the results have been brought to a common basis by dividing in each case by the specific ionization (relative to air) of the gas contained in the chamber (section 2). Kleeman's ⁽⁷⁾ values for specific ionization of gamma-rays have been used. On the basis of the theory to be discussed, section 2) should show the variation of real energy absorption with atomic number (fig. 9).

There is substantial agreement among the results for the various gases with the exception of those for hydrogen. It may be noted that Kleeman also calculated the specific ionization of hydrogen by assuming an additive

law and using measurements of the specific ionization in compound gases, thus obtaining a value of 0.36, his experimental one being 0.16. He comments that only to hydrogen, ammonia, and sulphur dioxide of the gases he studied could the additive law not be applied. By using this calculated value good agreement with other measurements is obtained, the hydrogen results being now for magnesium 14.75, for aluminium 20.6, and for iron 63.9.

Fig. 9.



Theory of the Method.

The first theory connecting the absorption of radiant energy of short wave-length in a material with the ionization current produced in a gas-filled cavity within it is that due to Bragg⁽³⁾. He concluded that the introduction of the cavity produces no change in the number, speed or direction of the electrons crossing that volume if the cavity be entirely empty. Even if it contains air little difference will be made unless the product of the coefficient of absorption of the radiation and the range of the secondary electrons is markedly different in the material and in the air, and there is enough air to cause appreciable absorption of the electronic energy. It was shown that if the relation between ionization and pressure be represented by a curved line at relatively high pressures, there should yet be a portion near the origin where the line is straight, and a comparison of the slopes at the origin of ionization-pressure curves

for different materials obtained under similar conditions should, when corrected by the ratio of the ranges of secondary electrons, give a ratio of the real energy absorption coefficients.

The conclusion that the existence of a cavity in an otherwise homogeneous medium in no way alters the number, speed or direction of all electrons crossing the boundaries of the cavity has been independently stated by Fricke and Glasser ⁽⁸⁾, Bruzau ⁽⁹⁾, and by Gray ⁽¹⁰⁾. Mayneord ⁽¹¹⁾ has also discussed the value of the ratio of the ionization currents in chambers of different wall material and has obtained experimental results for the case where the direct air ionization is important. He finds that for any two materials the ratio tends to unity for very short wavelengths having a maximum at some intermediate value. Gray showed that the ratio of the ionization currents in two chambers of similar dimensions irradiated under similar conditions should, if direct absorption of radiation by the gas is negligible (*i. e.* if the measurements be made at low pressures), be equal to the ratio of the real absorption coefficients per electron of the materials of the chambers, multiplied by the ratio of the ranges of the secondary electrons in the materials. This may be expressed

$$\frac{I_m}{I_n} = \frac{(\epsilon\sigma_a + \epsilon\tau)_m}{(\epsilon\sigma_a + \epsilon\tau)_n} \cdot \frac{S_n}{S_m}, \quad \dots \dots \dots (1)$$

where I_m and I_n are the ionization currents in the chambers, $\epsilon\sigma_a$ and $\epsilon\tau$ are the scattering absorption coefficients per electron and the photoelectric absorption coefficient per electron respectively, and S_m and S_n are the electronic stopping-powers of the two substances. This formula should, if valid, be in agreement with the results which have been given in section 3 of Table I., and the values of its terms are comparatively well established.

The variation of $\epsilon\sigma_a$ with wave-length has been expressed by the formula of Klein and Nishina ⁽¹²⁾. Values increase sharply to a maximum at about 0.05 Å. and then decrease slowly. They are independent of the atomic number of the elements considered.

The photoelectric absorption coefficient has been experimentally determined by a number of observers, and the empirical formulæ of Walter ⁽¹²⁾ appear to fit the data satisfactorily. They are

$$\epsilon\tau = 2.64 \times 10^{-26} Z^{2.94} \lambda^3 \text{ for } \lambda < K \text{ limit,}$$

$$\epsilon\tau = 8.52 \times 10^{-28} Z^{3.3} \lambda^3 \text{ for } \lambda_K < \lambda < \lambda_L,$$

where Z is the atomic number and λ is the wave-length.

Discussion of Results.

The experiments described have been carried out with the intention of testing the validity of equation (1) for elements of different atomic number, and it is now proposed to discuss the degree of agreement found.

Values of the real electronic absorption coefficients have been calculated in Table II.

These theoretical values of the real energy absorption have been fitted to the experimental ones of Table I., section 3, by making them coincide for carbon. They are shown in the last column of that section. In fig. 9 other elements for which no experimental data are available have also been used in obtaining a theoretical curve.

There is a satisfactory agreement between equation (1) and the experimental results for elements of atomic number less than about 12, but an increasing discrepancy for higher atomic numbers, the theoretical value for iron being about twice the measured one, whilst for lead it is over five times as great. In the latter case the tungsten radiation is longer than the K limit. In the preliminary measurements using tin characteristic

TABLE II.

Material.	Z.	$e\sigma_a \times 10^{25}$.	$e\tau \times 10^{25}$.	$e\sigma_a + e\tau \times 10^{25}$.	Electronic stopping-power (relative to air).
Carbon	6	0.43	0.40	0.83	1.01
Magnesium	12	0.43	3.14	3.57	0.94
"Elektron"	12(?)	0.43	—	—	0.94
Aluminium	13	0.43	3.7	4.13	0.94
Iron	26	0.43	30.53	30.96	0.87
Copper	29	0.43	47.0	47.43	0.855
Zinc	30	0.43	46.85	47.28	0.855
Lead.....	82	0.43	189.0	189.4	0.36

$e\sigma_a$ from Klein-Nishina formula.

$e\tau$ for carbon, magnesium, zinc, and iron from Walter's formula.

$e\tau$ for aluminium and copper from measurements by Cuykendall⁽¹⁴⁾.

$e\tau$ for lead from measurements by Hahn⁽¹⁵⁾.

radiation, and in those made with heterogeneous radiation excited at 50 and at 150 kv., a discrepancy of the same kind was noted even for the light materials such as magnesium. The present results may be tentatively taken to show that the ionization currents are those to be expected on theoretical grounds when the quantum energy of the electrons is great compared to the binding energy of the electrons removed, but discrepancies appear as the electronic energy rises relatively to that of the quantum.

Similar disagreement has been previously noted by Bragg⁽³⁾, and an explanation given is that much of the absorbed energy produces characteristic radiation in the chamber or its gas content, which radiation escapes. It scarcely appears, however, that this can be a serious source of loss of energy on account of the small quantum energy of the characteristic

radiation of the wall material in most cases and the magnitude of the Auger effect for elements of large atomic number.

It may be that the explanation is in part at least to be traced to the influence of surface conditions on the emission of photoelectrons.

The importance of surface effects in the case of photoelectric emission under the influence of ultra-violet light is well known. For X- or gamma-radiation it is usually considered that since the energy required to remove the electron is so much smaller than that of the incident quantum, all surface effects due to chemical contamination become of no importance ⁽¹⁶⁾. It would, however, appear that among the secondary electrons there must be a considerable proportion of slow-moving ones, arising from several causes.

The recoil electrons are much less energetic than the photoelectrons, and, in fact, have speeds from zero upwards. The more energetic secondary electrons will remove others from the atoms of the wall material, being themselves considerably retarded in the process. Lastly, the secondary electrons from the deeper layers of the material will emerge into the air space at very low speed. The result of these effects will be to produce a "spectrum" of secondary electrons entering the chamber, having all speeds up to that of the fastest photoelectrons, and there is a definite possibility that surface conditions may modify the speed of the slower ones. In the experiments described the surfaces of the chambers were clean and not greasy, but no rigorous chemical preparation was done on them, and no cleaning of the surface was performed when replacing one gas in the chamber by another.

Acknowledgement.

I have great pleasure in acknowledging the assistance and advice given by Professor W. V. Mayneord throughout the course of this investigation.

Summary.

Ionization currents have been measured at low pressures in various gases contained in chambers having walls of several different metals as well as of graphite and of "Elektron" alloy. The X-radiation comprised only a narrow range of wave-lengths. It is shown that the electronic real energy absorption coefficients as measured from the slopes of the ionization-pressure curves are less than those obtained from theoretical considerations, except for substances of low atomic number (<12).

References.

- (1) Mayneord, W. V., and Roberts, J. E., *Brit. Journ. Rad.* vii. p. 158 (1934).
- (2) Bragg, W. H., and Porter, H. L., *Proc. Roy. Soc. A*, lxxxv. p. 349 (1911).
- (3) Bragg, W. H., *Studies in Radioactivity*. London: Macmillan, 1912.

- (4) Duane, W., and Stenstrom, W., *Proc. Nat. Acad. Sci.* vi. p. 477 (1920).
- (5) Owen, E. A., and Naylor, B., *Proc. Phys. Soc.* xxxiv. p. 92 (1922).
- (6) Allen, S. J. M., Tables supplied for publication in 'X-rays in Theory and Experiment,' by A. H. Compton and S. K. Allison. London: Macmillan, 1935.
- (7) Kleeman, R. D., *Proc. Roy. Soc. A*, lxxix. p. 220 (1907).
- (8) Fricke, H., and Glasser, O., *Amer. Journ. Roent.* xiii. p. 453 (1925).
- (9) Bruzau, M., *Ann. d. Physique*, xi. p. 5 (1929).
- (10) Gray, L. H., *Proc. Roy. Soc. A*, cxxii. p. 647 (1929) ; and clvi. p. 578 (1936).
- (11) Mayneord, W. V., *Proc. Roy. Soc. A*, cxxx. p. 63 (1930).
- (12) Klein, O., and Nishina, Y., *Zeit. f. Physik*, lii. p. 853 (1929).
- (13) Walter, B., *Fortschritte a.d. Geb. d. Rönt.* xxxv. p. 929, p. 1308 (1927).
- (14) Cuykendall, T. R., *Phys. Rev.* l. p. 105 (1936).
- (15) Hahn, T. M., *Phys. Rev.* xlvi. p. 149 (1934).
- (16) Ledoux-Lebard, R., and Dauvillier, A., 'Physique des Rayons X.' Paris: Gauthier-Villars et Cie, 1921.

XLV. *Note on the Method of Successive Approximations for the
Solution of the Boundary Layer Equations.*

By J. H. PRESTON, B.Sc., Ph.D., A.F.R.Ae.S.,
of the Aerodynamics Department, National Physical Laboratory*.

[Received April 3, 1940.]

1. *Introduction.*

A METHOD of successive approximations was developed for the flow past a flat plate at high Reynolds numbers by Piercy and the present author⁽¹⁾. The first approximation corresponded to the asymptotic solution for Oseen's approximation, whilst the sixth was very close to the Blasius solution; thus in this case the convergence was satisfactory.

The method was generalized in a second paper by Piercy, Whitehead, and the present author⁽²⁾. Boussinesq's transformation was applied to change the ordinary rectangular co-ordinates x, y to α, β , where α, β are any conjugate functions satisfying Laplace's equation and $\beta=0$ corresponds to the boundary of the profile. In particular we took α, β to be the velocity potential and stream function of the ordinary potential flow about the profile, giving reasons for preferring these co-ordinates to the more usual s, n co-ordinates. The first approximation of this method should have corresponded to the asymptotic solution of Southwell and Squires'⁽³⁾ equation. (This has been obtained by the present author in a paper not yet published[†], and is found to be identical with a simplified boundary layer theory developed by Burgess⁽⁴⁾, and also leads to an expression for the breakaway identical with that for the first approximation "outer solution" as developed by Kármán and Millikan⁽⁵⁾.) Actually, owing to analytical and computing difficulties, a simplification had to be made leading to an inferior method of approximation. In fact the first approximation gives no breakaway; further approximations give this, and convergence was thought to be satisfactory.

In the paper quoted⁽²⁾, solutions were restricted to cases where the pressures were those of the ordinary potential flow or of a modified potential flow obtained by introducing a crude representation of the wake.

* Communicated by E. F. Relf, F.R.S.

† Now published as a companion paper, *Phil. Mag.* xxxi. p. 413 (1941).

The original purpose of the present note was to remove this restriction so that the method could be applied to cases where it was necessary to use experimental pressures.

At Mr. Falkner's suggestion comparisons were made with Professor Hartree's results for the Schubauer elliptic cylinder, and the case of retarded flow given by $v=1-\frac{1}{8}s$, also studied by Howarth, and lastly, for $v=se^{-s}$. Certain serious discrepancies were immediately apparent, suggesting that the method was not so good as examples worked in the paper ⁽²⁾ suggested.

The cause of the discrepancy has been found, and, whilst satisfactory values of the skin friction may be expected in the region of accelerated flow for a limited number of approximations, it appears that in the retarded region a large number of approximations will be required, and that even then position of the breakaway may be uncertain.

2. *Extension to Experimental Pressures.*

It is well known experimentally that at high Reynolds numbers the, flow outside the boundary layer and wake of a body is free from rotation, and in effect a potential flow exists which approximates in the case of thin cylinders to the ordinary potential flow. It is this potential flow which gives rise to the experimental pressures measured at the surface. Unfortunately it cannot be calculated with any accuracy at present—a crude attempt was made in the paper in reference ⁽²⁾ with some success. Actually we only require the details of this potential flow near the boundary, and, as shown below, this can be obtained from the measured pressures.

We suppose that the flow external to the boundary layer and wake has a potential which can be expressed in the form

$$W'=\alpha'+i\beta'=f(x+iy). \quad . \quad . \quad . \quad . \quad . \quad (1)$$

We assume the boundary layer to be so thin that $\beta'=0$ coincides with the surface of the cylinder as far as the breakaway point.

Let h_0' be the experimental velocity at the edge of the boundary layer; then we have

$$\left(\frac{\partial\alpha'}{\partial s}\right)_{\beta'=0}=h_0'=\left(\frac{\partial\beta'}{\partial n}\right)_{\beta'=0}, \quad . \quad . \quad . \quad . \quad . \quad (2)$$

where s is measured along or parallel to the surface and n is measured normal to the surface.

Just as in the paper cited ⁽²⁾, we regard α, β as a convenient set of orthogonal coordinates, so we now regard α', β' without being concerned with the actual form of

$$W'=f(x+iy),$$

since we only require α' at the surface and β' through a small distance normal to the surface of the order of the boundary layer thickness.

If s and α' are measured from the front stagnation point, then

$$\alpha'_{\beta=0} = \int_0^s h'_0 ds, \quad \dots \dots \dots (3)$$

and since the boundary layer is thin, $h' = \frac{\partial \beta'}{\partial n}$ may be supposed constant through it; hence

$$\beta' = h'_0 \cdot n. \quad \dots \dots \dots (4)$$

In the paper in reference ⁽²⁾ no restriction was placed on α, β other than that they should be conjugate functions satisfying Laplace's equation, and consequently given by a relation of the form

$$W = \alpha + i\beta = F(x + iy).$$

But

$$W' = \alpha' + i\beta' = f(x + iy)$$

is of this form, hence we can replace α, β of the paper in reference ⁽²⁾ by α', β' and the problem of boundary layer flow with experimental pressures or velocities can be dealt with, and we can drop the dashes with the understanding that

$$h_{\beta=0} = \left(\frac{\partial \alpha}{\partial s} \right)_{\beta=0} = \left(\frac{\partial \beta}{\partial n} \right)_{\beta=0}$$

refers to the experimental velocities.

The definition of the coordinates ξ, η in the paper in reference ⁽²⁾ is slightly modified for convenience.

Put

$$\left. \begin{aligned} \xi &= \left(\frac{R\bar{\beta}^2}{4\bar{\alpha}} \right)^{\frac{1}{2}}, \quad \eta = \bar{\alpha}, \\ \bar{\alpha} &= \frac{\alpha}{UL}, \quad \bar{\beta} = \frac{\beta}{UL}, \quad R = \frac{UL}{\nu}, \end{aligned} \right\} \dots \dots \dots (6)$$

where U is velocity at ∞ and L a representative length.

The function $\phi(\eta)$ defined in the paper (reference ⁽²⁾—equation (12)) becomes

$$\left. \begin{aligned} (a) \quad \phi(\eta) &= 4\bar{\alpha}_0 \frac{1}{\bar{h}_0} \frac{d\bar{h}_0}{d\bar{\alpha}_0}, \\ \text{where} \quad (b) \quad \bar{h} &= \frac{\bar{h}_0}{U} \bar{s}, \quad = \frac{s}{L}, \\ (c) \quad \bar{\alpha}_0 &= \int_0^{\bar{s}} \bar{h}_0 d\bar{s}. \end{aligned} \right\} \dots \dots \dots (7)$$

We can write $\phi(\eta)$ as

$$\phi(\eta) = 4 \int_0^{\bar{s}} \bar{h}_0 d\bar{s} \times \frac{1}{\bar{h}_0^2} \cdot \frac{d\bar{h}_0}{d\bar{s}}, \quad \dots \dots \dots (8)$$

which is readily found graphically when \bar{h}_0 is known, as a function of \bar{s} , from experiment.

The other function, $\eta \frac{d}{d\eta} \phi(\eta)$, is readily found in like manner.

Hence we can determine the constant $(A_4)_1$ or $(A_4)_2$ defined in reference ⁽²⁾, which corresponds with the third approximation to the boundary layer flow. Values are given in fig. 4 as functions of $\phi(\eta)$ neglecting $\frac{\partial \bar{q}}{\partial \eta}$.

The skin friction is given by equation (31) in reference ⁽²⁾:

$$\tau_n = \frac{\mu h_0^2}{2\nu^{\frac{1}{2}} \alpha_0^{\frac{1}{2}}} A_n,$$

or in terms of $\bar{\alpha}_0, \bar{h}_0$ by

$$\frac{\tau_n}{\frac{1}{2}\rho U^2} \cdot R^{\frac{1}{2}} = \frac{\bar{h}^2}{\bar{x}_0^{\frac{1}{2}}} \cdot A_n. \quad (9)$$

3. Application to Schubauer's Ellipse.

Application was made to the calculation of the skin friction for the elliptic cylinder which was the subject of an experiment by Schubauer⁽⁶⁾. This particular problem is regarded as in the nature of a test case for boundary layer flow.

Values of h , $\frac{d\bar{h}}{ds}$ were taken from a recent paper by Hartree ⁽⁷⁾ (who has obtained a mechanical solution which may be regarded as exact for practical purposes). Thus a possible discrepancy for purposes of comparison was removed at the start.

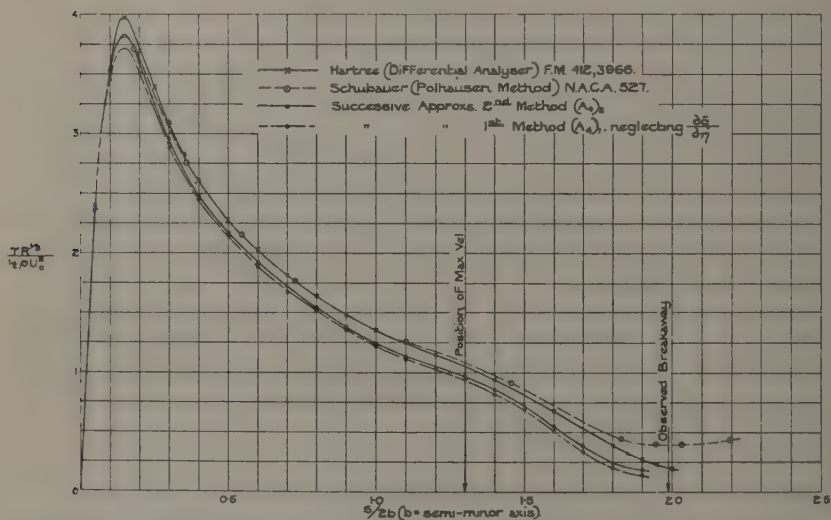
$\phi(\eta)$ was found from (8) and $\eta \frac{d}{d\eta} \phi(\eta)$ graphically; $(A_4)_2$ was found from the formula given in reference ⁽²⁾ (equation 30), and $(A_4)_1$, which neglects $\frac{\partial \bar{q}}{\partial \eta}$, from a large-scale curve from which that in the paper was drawn. These are given in fig. 4.

Finally, the skin friction was calculated from equation (9) and compared with that found by Schubauer using the Pohlhausen method and with Hartree's result. The results are shown in fig. 1.

It is seen that in so far as $(A_4)_2$ takes account of the $\frac{\partial \bar{q}}{\partial \eta}$ terms, there is little to choose between it and $(A_4)_1$, which completely neglects these terms. The iteration method gives values which are uniformly less than those of Hartree over most of the range. Hartree and Pohlhausen are in good agreement in the region where the flow is being accelerated, but in the retarded region differ considerably. The present method gives

good agreement near the nose and fair agreement as far as the position of maximum velocity. This agreement arises because the $\frac{\partial \bar{q}}{\partial \eta}$ terms are small here, and the difference from Hartree's result suggests that a sufficient number of approximations have not been carried out taking account of these terms. All three methods agree in failing to give a breakaway; but it should be noted that Polhausen's method cannot be relied upon in the retarded region. Hartree has shown that it needs but a slight modification to the pressure distribution to bring about separation at the observed

Fig. 1.



Distribution of skin friction over Schubauer's elliptic cylinder N.A.C.A. 527.

value. It would appear that the iteration method (reference (2)) with this modified distribution would give an earlier breakaway.

4. Application to $h_0 = 1 - \frac{1}{8}s$.

This is the case of flow past a flat plate in a region of increasing pressure such that the velocity at the edge of the boundary layer takes the above form. It has been treated recently by Howarth⁽⁸⁾ and by Hartree⁽⁹⁾, using a differential analyser, who has confirmed Howarth's results, which may be regarded as accurate to a high degree of approximation.

We have

$$\alpha_0 = \int_0^s \left(1 - \frac{1}{8}s\right) ds = s \left(1 - \frac{s}{16}\right), \quad \dots \quad (10)$$

$$\phi(\eta) = 4\alpha_0 \times \frac{1}{h_0^2} \frac{dh_0}{ds} = -\frac{s \left(1 - \frac{s^2}{16}\right)}{2h_0^2} \dots \dots \dots (11)$$

The calculation will be carried out for $(A_4)_1$ only as the correction for the $\left(\frac{\partial \bar{q}}{\partial \eta}\right)$ term in $(A_4)_2$ gives values differing but little from the former.

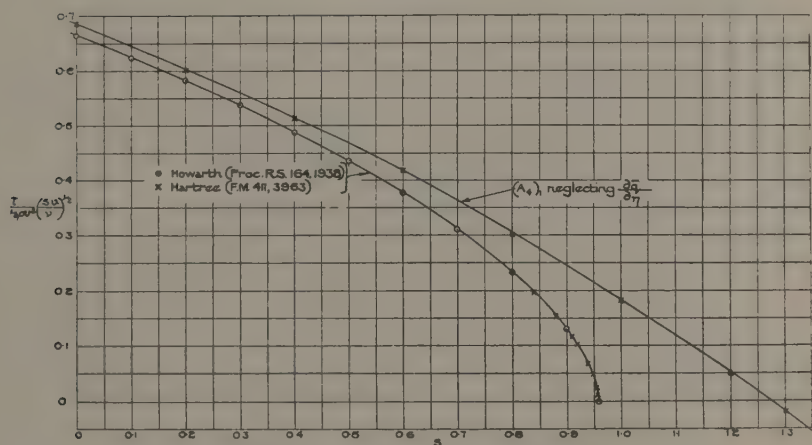
Hence from (9)

$$\tau_4 = \frac{\mu h_0^2}{2\nu^{\frac{1}{2}} \alpha_0^{\frac{1}{2}}} \cdot A_4$$

or

$$\frac{\tau_4}{\frac{1}{2} \rho h_0^2 \left(\frac{sh_0}{\nu}\right)^{\frac{1}{2}}} = \left(\frac{1 - \frac{1}{8}s}{1 - \frac{s}{16}} \right)^{\frac{1}{2}} = A_4.$$

Fig. 2.



Skin friction for retarded flow given by $h_0 = 1 - \frac{1}{8}s$.

$(A_4)_1$ is given as a function of $\phi(\eta)$ in fig. 4. The results are presented in fig. 2 for comparison with those of Howarth and Hartree.

It is seen that for moderate values of s fair agreement is obtained with Howarth's and Hartree's curve. The difference becomes serious as the breakaway is approached. Hartree and Howarth agree in giving the breakaway at $s=0.958$, whilst the iteration method $(A_4)_1$, neglecting $\frac{\partial \bar{q}}{\partial \eta}$ terms, does not give breakaway until $s=1.275$. The error is thus considerable, and points to the necessity for further iterations.

6. Application to $h_0 = se^{-s}$.

This example was suggested by Mr. Falkner, who kindly supplied his results for comparison *. It represents a variation of the type met with in the flow past cylinders other than the flat plate.

We find

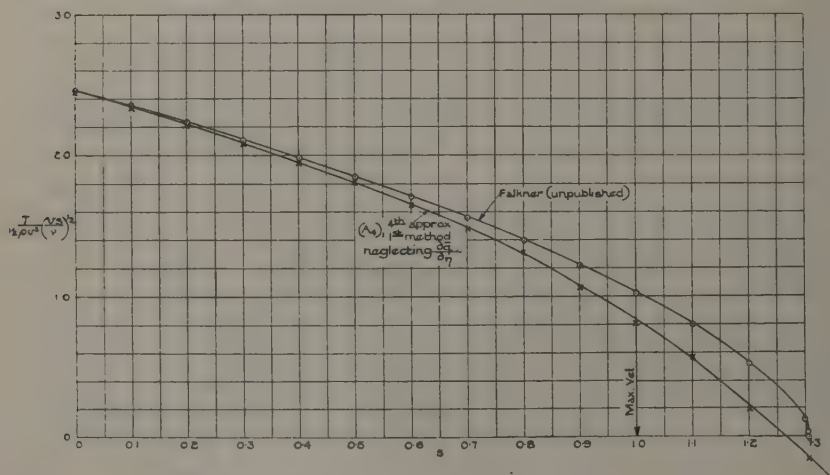
$$\alpha_0 = \int_0^s se^{-s} = 1 - e^{-s}(1+s) \quad . \quad . \quad . \quad (13)$$

and
$$\phi(\eta) = 4\alpha_0 \cdot \frac{1}{h_0^2} \cdot \frac{dh_0}{ds} = \frac{4(1-s)}{s^2}(e^s - 1 - s) \quad . \quad . \quad . \quad (14)$$

and
$$\frac{\tau_4}{\frac{1}{2}\rho h_0^2} \left(\frac{h_0^2}{\nu} \right)^{\frac{1}{2}} = s(e^s - 1 - s)^{\frac{1}{2}} \cdot A_4 \quad . \quad . \quad . \quad (15)$$

As in § 5, only $(A_4)_1$ is dealt with, and this is found from fig. 4.

Fig. 3.



Skin friction for flow given by $h_0 = se^{-s}$.

The skin friction is shown plotted in fig. 3, and compared with the result obtained by Falkner †. The difference is similar to that exhibited in fig. 1. Near $s=0$ agreement is good, but as we pass into the retarded region the differences become larger, though the positions of breakaway are close together. The steep drop of Falkner's curve near the breakaway suggests the presence of a singularity as in the case of retarded flow past a plate given in example 2. The bearing which this has on the iteration method is discussed in the next paragraph.

* "A Further Investigation of Solutions of the Boundary Layer Equations." R. & M. 1884. By V. M. Falkner.

7. Relation between the Boundary Layer Equations neglecting

$\frac{\partial \bar{q}}{\partial \eta}$ and those of Falkner and Skan, and Hartree.

The form of the boundary layer equations used in reference ⁽²⁾ equation (7) is

$$q \frac{\partial \bar{q}}{\partial \alpha} + \bar{w} \frac{\partial \bar{q}}{\partial \beta} = (1 - \bar{q}^2) \left[\frac{1}{h} \frac{dh}{d\alpha} \right]_{\beta=0} + \nu \frac{\partial^2 q}{\partial \beta^2}, \quad . \quad . \quad . \quad (16)$$

which, on transforming to ξ, η , defined by

$$\xi = \left[\frac{\beta^2}{4\nu(\alpha - \alpha_1)} \right]^{\frac{1}{2}}, \quad \eta = \frac{\alpha - \alpha_1^*}{\alpha_2 - \alpha_1} \quad . \quad . \quad . \quad (17)$$

becomes

$$\frac{\partial^2 \bar{q}}{\partial \xi^2} + 2 \frac{\partial \bar{q}}{\partial \xi} \cdot \int_0^\xi \bar{q} d\xi + (1 - \bar{q}^2) \phi(\eta) + 4\eta \left(\frac{\partial \bar{q}}{\partial \xi} \int_0^\xi \frac{\partial \bar{q}}{\partial \eta} d\xi - \bar{q} \frac{\partial \bar{q}}{\partial \eta} \right) = 0, \quad . \quad (18)$$

where

$$\phi(\eta) = \left(4(\alpha - \alpha_1) \frac{1}{h} \frac{dh}{d\alpha} \right)_{\beta=0} \quad . \quad . \quad . \quad (19)$$

$\frac{\partial}{\partial \eta}$ occurring in the last term can be replaced by $\frac{d\phi(\eta)}{d\eta} \cdot \frac{\partial}{\partial \phi(\eta)}$. If $\eta \frac{d}{d\eta} \phi(\eta)$ is small, *e. g.*, when $\eta \rightarrow 0$, or if $\frac{d}{d\eta} \phi(\eta) = 0$, *i. e.*, $\phi(\eta) = \text{const.}$, then the equation is

$$\frac{\partial^2 \bar{q}}{\partial \xi^2} + 2 \frac{\partial \bar{q}}{\partial \xi} \cdot \int_0^\xi \bar{q} d\xi + (1 - \bar{q}^2) \phi(\eta) = 0. \quad . \quad . \quad . \quad (20)$$

This is the equation which those solutions obtained in reference ⁽²⁾, by neglecting $\frac{\partial \bar{q}}{\partial \eta}$ terms, should satisfy.

Introduce $\bar{\psi}$ defined by $\bar{q} = \frac{\partial \bar{\psi}}{\partial \xi}$,

$$\frac{d^3 \bar{\psi}}{d\xi^3} + 2\bar{\psi} \cdot \frac{d^2 \bar{\psi}}{d\xi^2} + \left\{ 1 - \left(\frac{d\bar{\psi}}{d\xi} \right)^2 \right\} \phi(\eta) = 0. \quad . \quad . \quad . \quad (21)$$

This is immediately reducible to Falkner and Skan's ⁽¹⁰⁾ equation (R. & M. 1314). Put

$$\left. \begin{aligned} \bar{\psi} &= -\psi_1 \left(\frac{m+1}{4} \right)^{\frac{1}{2}}, \\ \xi &= \epsilon_1 \left(\frac{m+1}{4} \right)^{\frac{1}{2}}, \\ \phi(\eta) &= \frac{4m}{m+1}, \end{aligned} \right\} \quad . \quad . \quad . \quad (22 a)$$

* $(\alpha - \alpha_1)$ = interval of α measured from an origin at front stagnation point. $(\alpha_2 - \alpha_1)$ is interval of α between front and rear stagnation points: it could be any quantity = UL , say, where U is the velocity at infinity and L a representative length.

and we obtain

$$\frac{d^3\psi_1}{d\epsilon_1^3} - \frac{m+1}{2}\psi_1 \frac{d^2\psi_1}{d\epsilon_1^2} - m \left\{ 1 - \left(\frac{d\psi_1}{d\epsilon_1^2} \right)^2 \right\} = 0, \quad \dots \quad (22)$$

which is Falkner and Skan's equation for flows given by

$$h_0 = ks^m. \quad \dots \quad (23)$$

This corresponds to $\phi(\eta) = \text{const.}$, *i. e.*, to

$$4\alpha_0 \frac{1}{h_0} \frac{dh_0}{d\alpha_0} = \text{const.}, \quad \dots \quad (24)$$

where α_0 is measured from front stagnation point, *i. e.*, to

$$4 \int_0^s h_0 ds \times \frac{1}{h_0^2} \frac{dh_0}{ds} = \text{const.} \quad \dots \quad (25)$$

It appears that $h_0 = ks^m$ is the only relation between h_0 and s satisfying this condition. Consequently there must be a relation between $\left(A_{n \rightarrow \infty} \right)$ of the paper and Falkner and Skan's " α_2 ." In reference ⁽²⁾ the skin friction is given by

$$\tau_{n \rightarrow \infty} = \frac{\mu}{2\nu^{\frac{1}{2}}\alpha_0^{\frac{1}{2}}} h_0^2 A_{n \rightarrow \infty} = \frac{\mu\nu^2}{2\nu^{\frac{1}{2}} \left(\int_0^s h_0 ds \right)^{\frac{1}{2}}}. \quad \dots \quad (26)$$

Substituting for $h_0 = ks^m$, we find

$$\tau_{n \rightarrow \infty} = \frac{\rho\nu^2}{2} \left(\frac{\nu}{vs} \right)^{\frac{1}{2}} (m+1)^{\frac{1}{2}} A_{n \rightarrow \infty}.$$

In Falkner and Skan's paper the skin friction is given by

$$\tau = -2\alpha_2 \rho\nu^2 \left(\frac{\nu}{vs} \right)^{\frac{1}{2}}; \quad \dots \quad (27)$$

therefore, equating the two expressions, we obtain

$$A_{n \rightarrow \infty} = - \frac{4\alpha_2}{(m+1)^{\frac{1}{2}}}. \quad \dots \quad (28)$$

α_2 is given as a function of m in R. & M. 1314; hence it is possible to calculate $A_{n \rightarrow \infty}$ as a function of m , and finally, since $\phi(\eta) = \frac{4m}{m+1}$, to obtain $A_{n \rightarrow \infty}$ as a function of $\phi(\eta)$.

In fig. 4 Falkner's α_2 for a given m is transferred by this means into $A_{n \rightarrow \infty}$ for a given $\phi(\eta)$, and hence we are able to compare A_2, A_3, A_4 with this ultimate value and so form an idea of the number of iterations which would have to be carried out to obtain satisfactory agreement

with Falkner and Skan for the particular case of flow $h_0 = ks^m$ or $\phi(\eta) = \text{const.}$, i. e., neglecting $\frac{\partial \bar{q}}{\partial \eta}$.

Before discussing this we note that Hartree⁽¹¹⁾ has obtained accurate numerical solutions (Proc. Camb. Phil. Soc. 1937) of a modified form of Falkner and Skan's equation.

$$\text{Put} \quad \bar{\psi} = \frac{y}{\sqrt{2}}, \quad \xi = \frac{x}{\sqrt{2}}, \quad \phi(\eta) = 2\beta, \quad (29)$$

and we obtain

$$y''' + y y'' + (1 - y'^2)\beta = 0, \quad (30)$$

Hartree's form of Falkner and Skan's equation.

Hartree has tabulated y_0'' for various values of β , and it is easily shown that

$$A_{n \rightarrow \infty} = \sqrt{2} y_0'',$$

so that Hartree's results are readily transformed into a curve of $A_{n \rightarrow \infty}$ against β or $\frac{\phi(\eta)}{2}$.

These points are also shown plotted in fig. 4, and are seen to lie on the same curve as Falkner and Skan's results. This represents the exact solution of equations (21), (22), or (30).

On this figure are also shown $A_2, (A_3)_1, (A_3)_2, (A_4)_1, (A_4)_2$, neglecting $\frac{\partial \bar{q}}{\partial \eta}$, and also $(A_5)_2$, neglecting $\frac{\partial \bar{q}}{\partial \eta}$, which has recently been calculated by Whitehead and kindly supplied by him*.

It is seen from the figure that from $\phi(\eta) = 2.0$ or $\beta = 1$ up to $\phi(\eta) = 0$ the convergence of the A 's is satisfactory, and that $(A_5)_2$ differs but little from the results obtained by Hartree, and by Falkner and Skan. This is in the region of accelerated flow, and it accounts for the reasonably close agreement of the skin friction in this region seen in figs. 1, 2, 3, the neglect of the $\frac{\partial \bar{q}}{\partial \eta}$ terms accounting for the discrepancy. For negative values of β or $\phi(\eta)$ the convergence rapidly becomes poorer, and reasons will now be given for supposing that, however many iterations are carried out, Hartree's or Falkner and Skan's results will never be obtained.

$$\begin{aligned} * (A_6)_2 = & \frac{2}{\sqrt{\pi}} (0.5979 + 0.7143 \phi(\eta) - 0.1607 \phi(\eta)^2 \\ & + 0.0068 \phi(\eta)^3 + 0.0083 \phi(\eta)^4 - 0.00020 \phi(\eta)^5 \\ & - 0.0000086 \phi(\eta)^6 - 0.0000027 \phi(\eta)^7). \end{aligned}$$

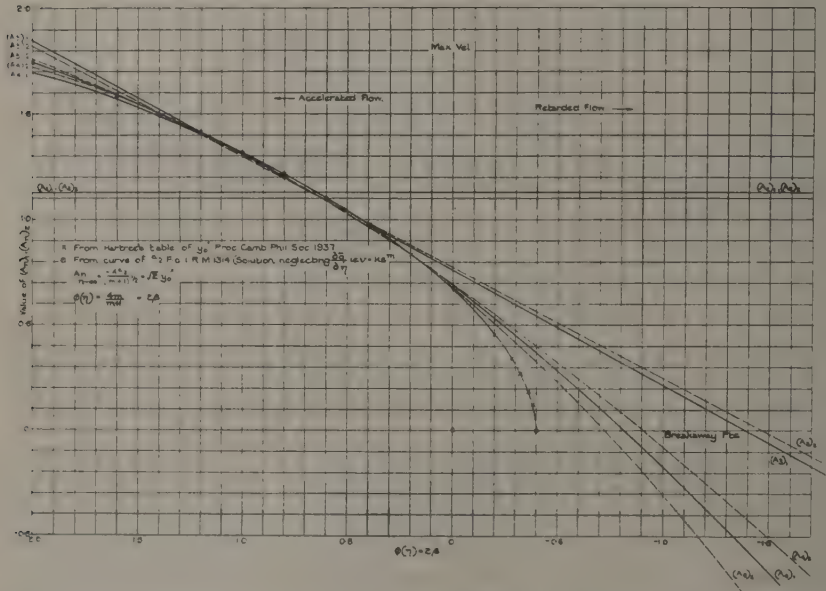
Virtually, in calculating $(A_n)_2$ by the second iteration method, we are assuming that equation (21) or (15) of the paper can be solved by assuming

$$\bar{\psi} = F_0 + F_1\phi(\eta) + F_2\phi(\eta)^2 + F_3\phi(\eta)^3 + \dots, \quad \dots \quad (31)$$

where F_0, F_1 , etc., are functions of ξ only. Substituting in this equation, and equating coefficients of the powers of $\phi(\eta)$, we obtain a series of differential equations for the F_s ; the first is

$$F_0''' + 2F_0F_0'' = 0, \quad \dots \quad (32)$$

Fig. 4.



Solution of boundary layer equations when $\frac{\partial \bar{q}}{\partial \eta} = 0$, i. e., $v = k s^m$, by successive approximations, and comparison with Falkner and Skan and Hartree.

which is Blasius's equation, giving

$$A_n \text{ at } \phi(\eta) = 0 = (F_0'')_0 = 0.664. \quad \dots \quad (33)$$

If we take Hartree's form of the equation (i. e., (30)), and assume

$$y = f_0 + f_1\beta + f_2\beta^2 + f_3\beta^3, \quad \dots \quad (34)$$

It thus appears that there are two sources of error. Firstly, that arising from a finite number of iterations being carried out, and which is present whether the $\frac{\partial \bar{q}}{\partial \eta}$ terms are included or not. For instance, the discrepancy in fig. 2 is mainly due to this cause, as can be gathered from fig. 4, since the $\frac{\partial \bar{q}}{\partial \eta}$ terms in this case are not large. Secondly, there is that arising from insufficient account being taken of the $\frac{\partial \bar{q}}{\partial \eta}$ terms in the early iterations (when these are large and an attempt is made to include them). It seems that this error to some extent cancels that arising from a limited number of iterations, and accounts for the satisfactory agreement obtained in the comparisons attempted in the paper in reference ⁽²⁾ and in figs. 1 and 3.

8. Conclusion.

The iteration method has been extended to cases of boundary layer flow with experimental pressures. The method is not so accurate as the examples worked in the original paper would suggest. Up to and for a little way behind the point of maximum velocity this should be overcome by increasing the number of iterations taking account of the $\frac{\partial \bar{q}}{\partial \eta}$ terms. The probable presence of a singularity at the breakaway point causes the method to break down if a high degree of accuracy is required. It may be that the error due to stopping after a small number of iterations is sufficiently small in the neighbourhood of the breakaway to justify its use for many practical cases or to form a starting point for more accurate methods. From the examples worked here it would seem that at least two further iterations are required, using the second method for reasonable accuracy in these cases.

It may be remarked that this failure of the iteration method to give the breakaway with accuracy in no way affects the method of approximating to the flow outside the boundary layer and the wake by the introduction of sources to give a crude representation of the effects of the wake, or the method of calculating the lift. All that is required is the position of the breakaway.

Finally, I wish to thank Mr. Falkner for suggesting the comparisons given in this note and permitting me to include the curve given in fig. 3, Professor Hartree for permitting me to use data in his unpublished papers ^{(7), (9)} on work carried out for the Aeronautical Research Committee, and Dr. Piercy, with whom the author had an opportunity of discussing this note.

List of References.

- (1) Piercy and Preston, "On a Simple Solution of the Flat Plate Problem of Skin Friction and Heat Transfer." *Phil. Mag.* (7) xxi. p. 995 (May 1936).
- (2) Piercy, Preston, and Whitehead, "On the Approximate Prediction of Skin Friction and Lift." *Phil. Mag.* (7) xxvi. p. 791 (November 1938).
- (3) Southwell and Squire, "A Modification of Oseen's Approximate Equation for the Motion in Two Dimensions of a Viscous Incompressible Fluid." *Phil. Trans. Roy. Soc. A*, ccxxxii. p. 27 (1933).
- (4) Burgers. See Squire, "On the Laminar Flow of a Viscous Fluid with Vanishing Viscosity." *Phil. Mag.* xvii. p. 1150 (1934).
- (5) Kármán and Millikan, "On the Theory of Laminar Boundary Layers involving Separation." *N. A. C. A. Report No. 504.*
- (6) Schubauer, "Air Flow in a Separating Laminar Boundary Layer." *N. A. C. A. Report No. 527.*
- (7) Hartree, "The Solution of the Equations of the Laminar Boundary Layer for Schubauer's observed Pressure Distribution for an Elliptic Cylinder." *F. M.* 412, 3966 (unpublished).
- (8) Howarth, "On the Solution of the Laminar Boundary Layer Equations." *Proc. Roy. Soc. A*, clxiv. p. 547 (February, 1938).
- (9) Hartree, "A Solution of the Laminar Boundary Layer Equation for Retarded Flow." *F. M.* 411, 3963 (unpublished).
- (10) Falkner and Skan, "Some Approximate Solutions of the Boundary Layers Equation." *R. & M.* 1314.
- (11) Hartree, "On an Equation occurring in Falkner and Skan's Approximate Treatment of the Equations of the Boundary Layer." *Proc. Camb. Phil. Soc.* 1937, p. 223.

XLVI. *Note on the Paper "A new Determination of the Viscosity of Air by the Rotating Cylinder Method"* (Phil. Mag. ser. 7, vol. xxiii. p. 313 (1937)).

By GUNNAR KELLSTRÖM, D.Sc.,
Physics Laboratory, University of Uppsala *.

[Received June 26, 1939.]

W. V. HOUSTON † has drawn attention to two corrections to the simple theory of the rotating cylinder method, which have not been considered in earlier determinations of η by this method—the end-correction to the length of the inner cylinder and the correction for the influence of the air on the effective moment of inertia of the inner cylinder. In the present paper the influence of these corrections on the writer's earlier η -value is calculated.

I. *The End-correction.*

According to Houston the effective length of the inner cylinder is obtained from the measured length l by adding a correction, which in this case, the distance between the inner cylinder and the guard cylinders being very small in comparison with the wall thickness, equals half this distance. As the distance between the guard cylinders is 100.20 mm. and the length of the inner cylinder 99.98 mm., the correction to be added to l is 0.11 mm., causing a decrease in η of 0.11/99.98, or 0.110 per cent.

II. *Correction for the Effect of the Air on the Moment of Inertia of the Inner Cylinder.*

As all determinations of the periods of oscillation were carried out in air, it is necessary to take into consideration :

(a) the influence of the air on the effective moment of inertia of the disks used for this determination ;

(b) the increase, due to the air, of the moment of inertia of the inner cylinder when freely suspended, as was the case when the moment of inertia was determined ;

(c) the somewhat smaller increase when the inner cylinder is suspended inside the outer cylinder, as was the case when determining the period T used in eq. (1), p. 315.

* Communicated by the Author.

† W. V. Houston, Phys. Rev. lii. p. 751 (1937).

(a) *The Correction for the Disks.*

Stokes * has calculated the moment of inertia of the air oscillating with both faces of a circular disk of radius R ,

$$\Delta I_1' = \frac{1}{2} R^4 \sqrt{\pi \rho \eta T}, \quad \dots \dots \dots (1)$$

where ρ is the density, η the viscosity of the air, T the period.

Further, according to Houston † the air outside the cylindrical surface of length l contributes an amount

$$\Delta I_1'' = \frac{\pi \rho l R^4}{2} \cdot \frac{G(X)}{X}, \quad \dots \dots \dots (2)$$

where $X = R \sqrt{\frac{2\pi\rho}{\eta \cdot T}}$

$$G(X) = -4 \frac{\ker'(X) \ker(X) + \operatorname{kei}'(X) \operatorname{kei}(X) \ddagger}{\ker'^2(X) + \operatorname{kei}'^2(X)}.$$

Both formulæ presume R and l to be infinite, so that edge-effects are negligible. Although this condition is not fulfilled here $\Delta I_1 = \Delta I_1' + \Delta I_1''$ is taken as an approximate value for the correction to be added. The amount of this correction is found in the fourth column of Tables II. and III., and lies between 0.078 and 0.22 per cent. of the total moment.

(b) *The Correction for the Inner Cylinder when freely suspended.*

This correction consists of two parts; one part, $\Delta I'$, is due to the air inside the cylinder, and is calculated from Houston's formula

$$\Delta I' = \frac{1}{2} \pi \rho l R_1^4 F(X_1) / X_1, \quad \dots \dots \dots (3)$$

where R is the radius of the inner surface = 2.67 cm., $X_1 = R_1 \sqrt{\frac{2\pi\rho}{\eta T}}$,

and $F(X_1) = 4\{\operatorname{ber}'(X_1)\operatorname{ber}(X_1) + \operatorname{bei}'(X_1)\operatorname{bei}(X_1)\} / \{\operatorname{bei}'^2(X_1) + \operatorname{ber}'^2(X_1)\}$;

the other part, $\Delta I''$, is due to the air outside the cylinder, and is computed from equation (2) with $R = 2.818$ cm. The total correction ΔI is obtained as $\Delta I' + \Delta I''$, and its amount for various values of T is given in Table I. End-effects are supposed to be negligible.

Using these corrections, Tables VIII. and IX. are recalculated to give the moment of inertia of the inner cylinder, reduced to vacuum. The result is given in Tables II. and III., Table II. containing the deter-

* G. G. Stokes, Math. and Phys. Papers, vol. iii. p. 21.

† W. V. Houston, *l. c.*

‡ Numerical values in Reports of the B. A. A. S. 1916, pp. 119-121.

minations made with disk I., Table III. the determinations with disk II. In Tables VIII. and IX. there was a marked increase in I with T, which is now easily explained by the fact that ΔI increases with T more rapidly

TABLE I.

T.	$\Delta I'$.	$\Delta I''$.	ΔI .
11.02	0.516	0.610	1.13
11.58	529	625	1.15
20.74	693	832	1.53
35.93	830	1.08	1.91
53.9	894	1.31	2.20
55.99	898	1.34	2.24
58.08	911	1.36	2.27
90.85	933	1.67	2.60
127.6	934	1.95	2.88

TABLE II.

I_1 (vacuum) = 401.93.

Susp. no.	T_1 .	T.	ΔI_1 .	$I_1 + \Delta I_1$.	$I + \Delta I$.	ΔI .	I.
1	11.2748	11.5613	0.32	402.25	422.95	1.15	421.80
1	11.2902	11.5799	0.32	„	423.06	1.15	1.91
2	10.7541	11.0233	0.31	402.24	422.63	1.13	1.50
2	10.7500	11.0233	0.31	„	422.95	1.13	1.82
3	35.0173	35.9379	0.56	402.49	423.93	1.91	2.02
3	34.9709	35.9086	0.56	„	424.36	1.91	2.45
4	56.5708	58.0834	0.72	402.65	424.47	2.27	2.20
5	54.5273	55.9813	0.71	402.63	424.40	2.24	2.16
6	88.4805	90.8505	0.89	402.82	424.69	2.60	2.09
7	20.2208	20.7442	0.43	402.36	423.45	1.53	1.92
7	20.2164	20.7404	0.43	„	423.48	1.53	1.95
Mean							421.98
Mean error ..							0.18

than does ΔI_1 (and ΔI_2). In Tables II. and III. this systematic variation in I has disappeared, and at the same time the mean error has decreased, in Table II. from 0.46 to 0.18 and in Table III. from 0.35 to 0.14.

As a mean value of I (vacuum) from Tables II. and III. is obtained

$$I = 422.15 \pm 0.16.$$

(c) *The Correction for the Inner Cylinder when suspended in the Outer Cylinder.*

The correction due to the air *inside* the cylinder, $\Delta I'$, is evidently the same as before, and is calculated from equation (3). $\Delta I''$, on the contrary, is smaller than before, because in this case the inner cylinder is not surrounded by an unlimited space of air, but only by the space between the inner and the outer cylinder. The theoretic computation of this case could not be carried out with the numerical tables available. The author therefore determined experimentally the change in the period, ΔT , when the outer cylinder was removed. ΔI is calculated from $\Delta T : \Delta I/I = 2\Delta T/T$.

TABLE III.
 I_2 (vacuum)=432.90.

Susp. no.	T_2 .	T.	ΔI_2 .	$I_2 + \Delta I_2$.	$I + \Delta I$.	ΔI .	I.
1	11.7175	11.5805	0.35	433.25	423.13	1.15	421.98
2	11.1529	11.0227	0.34	433.24	423.18	1.13	2.05
2	11.1527	11.0228	0.34	„	423.21	1.13	2.08
3	36.3310	35.9356	0.62	433.52	424.14	1.91	2.23
3	36.3018	35.9095	0.61	433.51	424.20	1.91	2.29
4	58.6466	58.0293	0.79	433.69	424.61	2.27	2.34
5	56.5744	55.9907	0.77	433.67	424.76	2.24	2.52
6	91.8052	90.8339	0.98	433.88	424.75	2.60	2.15
7	20.9774	20.7449	0.47	433.37	423.82	1.53	2.29
7	20.9742	20.7440	0.47	„	423.91	1.53	2.38
Mean							422.31
Mean error ..							0.14

This determination was carried out with two different suspensions: (1) a phosphor-bronze wire with $T=53.7$ sec., and (2) a phosphor-bronze strip with $T=126.9$ sec. The mean value of several determinations was

$$\begin{array}{ll}
 \text{Inner cyl. freely suspended : (1) } T=53.756 & (2) \quad T=126.917 \\
 \text{,, ,, in outer cyl.} & T=53.699 \quad T=126.755 \\
 & \Delta T = \overline{0.057} \quad \Delta T = \overline{0.162} \\
 & \Delta I = 0.90 \quad \Delta I = 1.08
 \end{array}$$

Instead of the values in Table I. corresponding to the above periods, viz. 2.20 and 2.88, the proper values to be used in this case are thus $2.20-0.90=1.30$ and $2.88-1.08=1.80$, and the corresponding values of the effective moments of inertia $422.15+1.30=423.45$ and $422.15+1.80=423.95$. In comparison with the earlier value 423.28 these values are 0.040 resp. 0.158 per cent. higher, and cause an equal increase in the

η -value. For $T=90.8$ the corresponding values with sufficient accuracy are $4.22 \cdot 15 + 2.60 - \frac{1}{2}(0.90 + 1.08) = 423.76$, and the increase 0.113 per cent. These figures are valid for outer cylinder II., but approximately they can be used also for cylinder I. (Table XX.).

III. Influence of the Corrections on the final η -value.

Considering the decrease of 0.110 per cent. in all determinations due to the end-effect, the final corrected values of η are as follows:—

Tab.	XVI.	:	increase	$0.158-0.110=0.048$	%	from	18190	to	18199	.	10^{-8}
„	XVII.	:	„	$0.113-0.110=0.003$	%	„	18205	„	18206		
„	XVIII.	:	decrease	$0.110-0.040=0.070$	%	„	18204	„	18191		
„	XIX.	:	increase	$0.158-0.110=0.048$	%	„	18200	„	18209		
„	XX.	:	„	$0.158-0.110=0.048$	%	„	18206	„	18215		
Mean value :	„			0.015	%	„	<u>18201</u>	„	<u>18204</u>	.	10^{-8}

As the two corrections act in different directions, the resulting correction is very small. Owing to the uncertainty in the calculation, however, the limit of error ought to be raised a little, and the final result may therefore be written

$$\eta_{20^\circ} = (18204 \pm 30) \cdot 10^{-8}, \text{ or}$$

$$\eta_{23^\circ} = (18352 \pm 30) \cdot 10^{-8}.$$

XLVII. *The Steady Flow of Heat from certain Objects buried under Flat Air-cooled Surfaces.*

By F. H. SCHOFIELD, B.A., D.Sc., Physics Department,
National Physical Laboratory, Teddington, Middlesex *.

[Received May 23, 1940.]

ABSTRACT.

A general method of estimating the steady flow of heat from, and the temperature distribution around, objects buried under flat air-cooled surfaces is developed for a considerable class of two-dimensional problems. By this method, an approximate solution of the problem is at once derived from the simpler solution of the corresponding problem in which the sink of heat, instead of being, as required, a surface subject to Newton's law of cooling, is an isothermal surface.

A critical examination of the method is made, with satisfactory results, in three practical cases, viz. :—

- (1) A pipe or cable buried in the ground.
- (2) The same in a wall.
- (3) A girder or ship's rib projecting into a wall.

I. *Introduction.*

THE calculation of the steady flow of heat in a solid medium is generally made in relation to an isothermal sink forming the whole or part of the boundary of the medium. There exists, however, a considerable class of case in which the sink, instead of being coincident with the boundary, is the atmosphere beyond that boundary. Examples of such cases are the heat transfer

- (1) to the air from a pipe or cable buried in the ground ;
- (2) to the air from a pipe or cable buried in a wall ;
- (3) to the air of a cold store from the ship's skin by passage through the insulating wall, into which the ribs of the ship project.

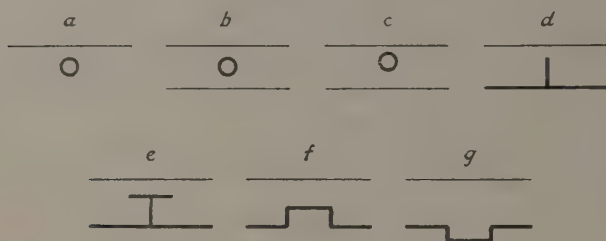
* Communicated by the Author.

Under the conditions indicated, the surface of the solid medium will not be isothermal, its temperature distribution being governed by the balance at each point of the heat conducted to the surface and that transferred from the surface by convection and radiation.

The only theoretical treatment of this class of problem appears to be that of Awbery (1929), who, in an ingenious way, has shown how to obtain a complete solution in certain cases. The method is, however, very limited in scope and difficult of application *, as indeed would be expected from the inherent complexity of the problem.

The object of the present paper is to explore the possibility of approximate calculation of heat flow in cases of the type indicated. Two-dimensional problems alone are considered, and the treatment is based almost entirely on the Christoffel-Schwarz transformation.

Fig. 1.



II. General Considerations.

The range of problems to be covered is perhaps best indicated by reference to some practical cases such as those already mentioned. Typical examples are shown in section in fig. 1, all of which, being two-dimensional, extend to infinity in a direction normal to the paper. In each case the source is assumed to have an isothermal boundary, represented by a thick line, while the air-cooled surface or surfaces appear as thin lines.

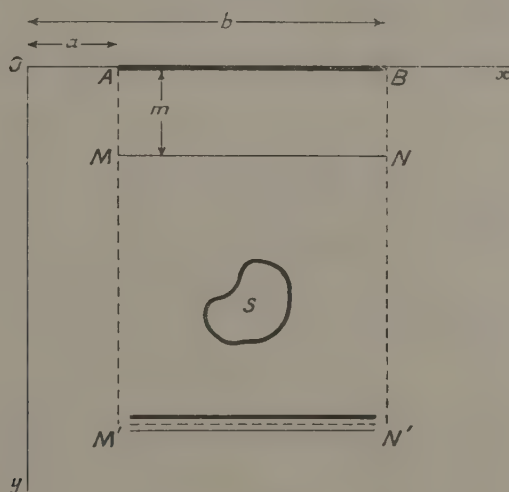
In fig. 1 the solid medium is taken as infinite in the direction parallel with the air-cooled surface. Of the individual cases, *a* represents a pipe or cable buried in the ground which is also infinite in a direction normal to the surface: *b* and *c* represent pipes or cables with their axes respectively on and off the mid-plane of a wall: *d* a rib projecting from, and isothermal with, one surface of a wall the whole of which, extending to infinity, forms the source: *e*, *f*, and *g* other modifications of the same kind of source.

* The scope of the method is touched on in Part V. below, and an example of its application given in Part IV.

All these cases have a common characteristic, the significance of which will appear later, namely, that the boundary flow lines at infinity are straight and normal to the air-cooled surface or surfaces. Incidentally, it may be remarked that this characteristic would still apply even if the sources were not themselves symmetric as shown in fig. 1.

Another set of cases to be covered is that in which symmetric sources, such as *a* to *c*, or symmetric features, such as occur in *d* to *g*, are not single, but are repeated at regular intervals. These arrangements by virtue of their symmetry would give, at the same intervals, flow lines which are straight and normal to the surface.

Fig. 2.



Though in practice dimensions cannot, of course, be infinite as assumed above, many cases of the types indicated would no doubt conform closely with the required conditions as to boundary flow lines.

The problem to be treated may now be represented generically by fig. 2, in which *S* is a source with an isothermal boundary, *MN* the air-cooled surface, *MM'* and *NN'* the boundary flow lines normal to the surface. The figure is completed by *M'N'*, parallel to *MN*, which can be either an isothermal continuous with *S*, as in fig. 1, *d* to *g*: a flow line, as in fig. 1, *a* (at infinity) or in fig. 1, *b*, when divided by the horizontal line of symmetry; an air-cooled surface similar to *MN* as in fig. 1, *b* and *c*. It may be added that in fig. 2 and subsequent diagrams, lines of flow are represented as dashed lines to distinguish them from isothermals.

The heat flow from MN to the atmosphere by radiation and convection is assumed to be subject to Newton's law, being proportional to the difference in temperature between any point on the surface and the atmosphere, and this is taken to apply whether the convection is natural or forced. Thus, if the temperature of the atmosphere is $0^\circ \text{C}.$ and that at any point on the surface MN is θ , the rate of heat transfer per sq. cm. by convection and radiation would be

$$H_n = E\theta,$$

where E is the Newton constant applicable to the particular conditions of convection and radiation. For the sake of brevity, the transfer of heat by convection and radiation from an air-cooled surface will be referred to throughout as "Newton transfer."

The expressions controlling the problem can now be set out as follows with respect to Ox and Oy as axes :—

Throughout the medium the Laplace equation for the steady state applies, viz.,

$$\frac{\partial^2 \theta}{\partial x^2} + \frac{\partial^2 \theta}{\partial y^2} = 0,$$

while the boundary conditions are as follows :—

For the isothermal boundary of the source, ds being an element of boundary

$$\partial\theta/\partial s = 0.$$

For the flow lines MM' and NN'

$$\partial\theta/\partial x = 0.$$

For $M'N'$, if a flow line $\partial\theta/\partial y = 0$, and if an isothermal $\partial\theta/\partial x = 0$.

For the air-cooled surface MN (or $M'N'$), k being the thermal conductivity of the medium

$$k(\partial\theta/\partial y) = E\theta.$$

The last condition expresses the fact that the rate at which heat is conducted to any point on MN is equal to the rate of Newton transfer from that point. The latter has already been designated H_n , and the former will be called H_c , the numerical values of either being expressed in terms of calories per sq. cm. per second.

In the method of approximation developed below the boundary conditions are exactly, or nearly exactly*, fulfilled except along the air-cooled surface MN (or $M'N'$). Here no attempt is made to realize directly the appropriate conditions; but, instead, the medium is imagined as

* In one of the three cases treated below a slight departure from the conditions applying to the source is tolerated; see Part IV.

extended by a certain thickness beyond its original surface to a fresh boundary at which simpler conditions apply, inasmuch as it is made wholly isothermal or partly isothermal and partly flow line. The object of this device is to obtain, by fairly simple means, a plausible approximation to the conditions strictly applicable to MN (or M'N'). In place of the point-to-point balance between H_n and H_c which is demanded, the following are considered as criteria for the proposed approximation :—

- (1) A balance between the rate of heat conduction to the whole of the plane MN, and the rate of the hypothetical Newton transfer from that plane, if exposed to the atmosphere, *i. e.*, a balance between the integrated values of H_c and H_n for the plane MN.
- (2) A balance between H_c and H_n at two or more important regions of the plane MN.

On investigating the possibilities of (1), it was found that if the added thickness is made equal to k/E and if the sink is the whole of the new surface which is isothermal at atmospheric temperature, then the first criterion is always obeyed by the class of case represented in fig. 2. This means that the solution of such a case for an isothermal boundary, at once gives an approximate solution of the corresponding case with a boundary subject to Newton's law.

We shall be concerned below mainly with the implications of this so-called "rule of added thickness." The possibilities of the second criterion are only briefly discussed (see Part VI.).

Rule of Added Thickness.

Referring to fig. 2, we assume that a thickness m has been added to the medium and that the new surface AB, on the x axis, is isothermal at 0°C . and, further, that throughout the extended medium the heat flow (ϕ) and temperature (θ) functions are given by

$$\phi + ik\theta = F(x + iy), \quad \dots \dots \dots (1)$$

where F is a general function.

Then, as is well known, (1) satisfies the Laplace equation, and also yields the relation

$$\frac{\partial \phi}{\partial x} = k \frac{\partial \theta}{\partial y} \quad \dots \dots \dots (2)$$

It is required to find the value of m such that the first criterion is obeyed at the plane MN.

Now the total of the hypothetical Newton transfer, ξ_y , per second

per cm. depth normal to the paper, from any plane parallel to AB is given by

$$\xi_y = E \int_a^b \theta dx, \quad \dots \dots \dots (3)$$

since the boundary flow lines are normal to the x axis, b and a are independent of y , and we may therefore treat (3) as follows:—

$$\begin{aligned} \frac{d\xi_y}{dy} &= E \int_a^b \frac{\partial \theta}{\partial y} dx \\ &= \frac{E}{k} \int_a^b \frac{\partial \phi}{\partial x} dx \quad \dots \dots \dots (4) \\ &= E\Phi/k, \end{aligned}$$

Φ being the total heat which would be conducted to the plane per second per cm. depth normal to the paper.

Integrating with respect to y between the limits m and 0, we have, since Φ is independent of y and ξ_0 is zero,

$$\xi_m = E\Phi m/k. \quad \dots \dots \dots (5)$$

Equating this to Φ we get

$$m = k/E. \quad \dots \dots \dots (6)$$

The above reasoning would also apply if two air-cooled surfaces, MN and M'N', were considered in place of one.

The relation (6) gives the rule referred to above, by which the solution of any case of the type represented in fig. 2 and having a flat isothermal boundary (or boundaries), yields an approximate solution of a corresponding case with a flat boundary (or boundaries) subject to Newton's law.

It is proposed to study critically the application of this rule to three specimen cases and employ mainly for the purpose the Christoffel-Schwarz formula. As is well known, this formula is designed to give the Laplace distribution within any polygon the boundary of which consists partly of isothermals and partly of flow lines as in our problem with its modified boundary. Provided that the necessary integrations can be performed, expressions are obtained of the type

$$x + iy = f_1(t), \quad \dots \dots \dots (7)$$

$$\phi + ik\theta = f_2(t), \quad \dots \dots \dots (8)$$

where t is an auxiliary complex variable, and hence, by elimination of t , an expression of type (1). It may be remarked that it is not apparently essential actually to perform the elimination, since we can, if desired, work in terms of the intermediate variable t , and further, that, by means of special devices, as will be seen below, it is possible to deal to some extent with curved instead of straight boundaries.

The chosen cases are those mentioned in the introduction—see *a*, *b*, and *d* of fig. 1. It will be noted that these are of two types in which, respectively, the flux density assumes a zero and a finite value at infinity.

Before considering these cases it is as well to get some idea of the order of magnitude of the added thickness *m* as given by (6). For the thermal conductivity *k* the lower limit is set by that of the best insulating materials, which is about 0.0001 c.g.s. units, while the upper limit is roughly given by the condition that the value must be small as compared with that of the material forming the source, since otherwise the latter cannot be assumed to be isothermal. If the walls of the source are restricted to metal, their lowest conductivity would be about 0.1 c.g.s. units, which applies to iron pipes and the like. Taking, quite arbitrarily, a ratio not exceeding 1/20 of the figure just mentioned as permissible for the conductivity of the medium, this would give an upper limit of 0.005 c.g.s. units. The value of *E* for still air being of the order of 0.00025 c.g.s. units*, the upper limit of *m* would thus be some 20 cm. For media of lower conductivity or for increased values of *E*, as with forced draught, *m* would be correspondingly diminished, and might in some cases become negligibly small.

III. Pipe or Cable in Ground.

The solution of the corresponding isothermal problem, *i. e.*, that of a circular cylinder buried with its axis parallel to the surface of the ground supposed to be strictly isothermal, is well known. The isothermals in the medium are a system of cylinders—in section coaxial circles—which may be considered as emanating from a line source at infinite temperature. In order to show the relation of this case with others and to indicate possible modifications of treatment, it is proposed to derive the solution independently by the Christoffel-Schwarz formula.

Turning to fig. 3 (*z* plane) *C* is the line source, *MN* the surface of the ground, and *AB* the extended surface which is isothermal at the atmospheric temperature (*0° C.*). Since, by symmetry, *BCD* is a flow line it suffices to treat half the figure, *i. e.*, the polygon *ABD*. In the *ψ* plane, we take the final rectangle *ABCC* as having a thickness of *q/2*, *q* being the total rate of heat flow from the source *C* per cm. length normal to the paper. It will be noted in fig. 3 that the boundary isothermals and flow lines are heavily drawn as full and dashed lines respectively, the whole or part of such lines at infinity being shown curved and with a small gap at each end. According to this convention the source *C* in the *z*-plane is represented by the curved line *CC* in the *ψ* plane, where it is the side of a

* The value is governed by the emissivity and orientation of the surface, among other things, see *e. g.*, Fishenden and Saunders (1932).

rectangle at infinity. The figures in brackets are the distances of the corresponding points along the real axis of the intermediate t plane measured from the origin B.

The transformations from the z and ψ planes to the t plane are

$$dz'/dt = Pt^{-\frac{1}{2}}. \quad (9)$$

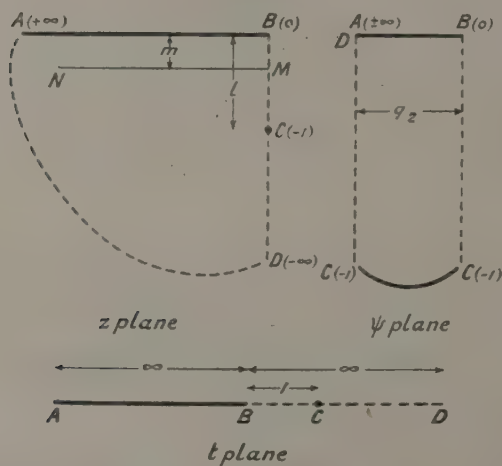
$$d\psi/dt = Qt^{-\frac{1}{2}}(t+1)^{-1}. \quad (10)$$

Integrating we get

$$z = 2P\sqrt{t} + L, \quad (11)$$

$$\psi = 2Q \tan^{-1}\sqrt{t} + M. \quad (12)$$

Fig. 3.



Taking B as origin and BA as real axis in the two planes we find on evaluation of the constants and elimination of t

$$z/l = \tan(\psi\pi/q). \quad (13)$$

In this expression the variable ψ is $(\phi + ik\theta)$. As a check we note that with $x = \infty$ and $y = 0$, ϕ has the correct value of $q/2$.

Now splitting (13) into real and imaginary parts

$$\theta = \frac{q}{4\pi k} \log \left\{ \frac{(l+y)^2 + x^2}{(l-y)^2 + x^2} \right\}, \quad (14)$$

$$\phi = \frac{q}{2\pi} \tan^{-1} \left\{ \frac{2xl}{l^2 - x^2 - y^2} \right\}. \quad (15)$$

In practice we are concerned, not with a line source, but with a pipe of finite radius (r), with its top surface buried at a certain distance (s)

below the ground-level MN. The above formulae can be applied to this case by means of the following expression for l :

$$l = [(m+s)(m+s+2r)]^{\frac{1}{2}}, \quad \dots \dots \dots (16)$$

so that, m being given by (6), we have from (14) either the total heat transfer (q) for a known temperature difference between the cylinder and the air, or the temperature rise of the cylinder for a known dissipation of energy. These two forms are appropriate to a steam pipe and electric cable respectively.

The above solution depends on the balance between the total conduction and Newton transfers of heat at the plane MN, but so far no idea has been obtained of the closeness of the resulting approximation. In the case now under consideration, this can be tested in two ways :

- (1) By a point-to-point comparison of H_n and H_c along MN.
- (2) By comparison with Awbery's solution of the problem.

For the point-to-point comparison we have the Newton transfer given by multiplying (14) by E , while the heat conducted is given by

$$k \frac{\partial \theta}{\partial y} = \frac{q}{2\pi} \left\{ \frac{(l+y)}{(l+y)^2 + x^2} + \frac{(l-y)}{(l-y)^2 + x^2} \right\} \dots \dots \dots (17)$$

Convenient places for making the comparison are the central point M, and those points at which the flux has reached $\frac{1}{4}$, $\frac{1}{2}$, and $\frac{3}{4}$ of the total (q). From (15) the x -coordinates, on the plane $y=m$, of the flow lines giving the limits of these flux values are

$$x_{\frac{1}{4}} = (2l^2 - m^2)^{\frac{1}{2}} - l, \quad \dots \dots \dots (18)$$

$$x_{\frac{1}{2}} = (l^2 - m^2)^{\frac{1}{2}}, \quad \dots \dots \dots (19)$$

$$x_{\frac{3}{4}} = (2l^2 - m^2)^{\frac{1}{2}} + l. \quad \dots \dots \dots (20)$$

Let us now apply the above-mentioned tests to the case taken by Awbery, viz., that of a line source 76 cm. below ground of conductivity 0.0045 c.g.s. units and with a heat dissipation of 1 calorie per sec. per cm. of length. Here, the Newton coefficient being 0.00025 c.g.s. units, the value of the added thickness m is 18 cm.

In Table I. are given, for the chosen points, the rate of Newton transfer H_n and of conduction transfer H_c , the percentage difference between the two (which nowhere exceeds 2.5 per cent.) and the ground temperatures. These latter are also shown corrected on the following basis :—Assuming that where H_n differs from H_c the correct value for H_n is the mean of the two, this would involve applying to the ground temperature a correction equal to one-half of the percentage difference between H_n and H_c . It

will be seen that the resulting figures are very close to those set out in the last column of Table I. which were given by Awbery's formula,

$$\theta = \frac{q}{4\pi k} \log \left[\frac{(l' + y)^2 + x^2}{(l' - y)^2 + x^2} \right] + \frac{q}{\pi} \int_0^\infty \frac{\cos \lambda x d\lambda}{(E + k\lambda)e^{\lambda(y+l')}} \quad (21)$$

When comparing this formula with (14) it must be remembered that l' , the true distance of the source below the ground, is equal to $(l - m)$.

TABLE I.

Temperature etc. of surface of ground of conductivity 0.0045 c.g.s. units ($m = 18$ cm.) due to line source buried to depth of 76 cm. and dissipating 1 cal./sec./cm. A.T.M.=added thickness method. A.M.=Awbery's method.

$2\phi/q$.	x (cm.).	A.T.M.					A.M.
		H_n $\times 10^{-3}$.	H_c $\times 10^{-3}$.	$\frac{H_n - H_c}{H_n}$ (per cent.).	θ (°C.).	θ (cor.) (°C.).	θ (°C.).
0	0	3.429	3.515	-2.5	13.72	13.89	13.94
$\frac{1}{4}$	37.71	2.930	2.957	-0.9	11.72	11.78	11.83
$\frac{1}{2}$	92.26	1.714	1.709	+0.3	6.86	6.85	6.81
$\frac{3}{4}$	225.7	0.506	0.494	+2.4	2.02	2.00	2.03

Perhaps more important than the distribution of surface temperature is the calculation of the heat loss from a finite pipe at a certain temperature above that of the air, or *vice versa*. Here our method, which yields strictly circular isothermals, gives the approximate heat flow from a truly circular pipe. Awbery's solution is no longer rigid in that his isothermals are not circular, and, moreover, the best value of l' has to be found by trial from the known radius and depth of the pipe. It should be added that the drawbacks just mentioned are quite unimportant, except for pipes very large in diameter as compared with the depth of burial.

We take below three sizes of pipe belonging to the system of circles which are coaxial with the imagined extended boundary, and of which the limit is a line source buried, as before, at 76 cm. below the true ground-level, *i. e.*, 76+18 cm. below the imagined boundary. The excess of

temperature of each pipe for a dissipation of 1 cal./sec./cm. is set out in Table II. The temperatures θ_1 and θ_2 shown under Awbery's method are respectively the values at the top and bottom of a vertical diameter of the pipe. Owing to the close agreement between these values, the calculation of the temperature elsewhere on the circumference seemed unnecessary.

The two methods of approximation are seen to agree to better than 1 part in 1000.

The very satisfactory results shown in Tables I. and II. lead us to try the method in cases probably more extreme than any likely to be encountered in practice. Accordingly data are given in Table III., in an

TABLE II.

Temperature of pipe of radius r buried to depth s in ground of conductivity 0.0045 c.g.s. units ($m=18$ cm.) and dissipating 1 cal./sec./cm. A.T.M. =added thickness method. A.M.=Awbery's method.

r (cm.).	s (cm.).	θ by A.T.M. (°C.).	By A.M. (°C.).		
			$\frac{\theta_1 + \theta_2}{2}$.	θ_1 .	θ_2 .
10	66.53	103.86	103.95	103.97	103.93
5	71.13	128.31	128.41	128.42	128.40
2.5	73.53	152.80	152.89	152.90	152.88

abridged form, for pipes of finite size based on line sources situated at 12 and 6 cm. below ground. The following points are noteworthy :—

At the central position where the biggest difference between Newton and conduction transfers occurs, ranging to over 40 per cent., the surface temperature, corrected on the basis already explained, does not depart greatly from the true temperature. No doubt at least as good results would be obtained in the same way for the whole surface. As regards the temperature of the pipe it will be seen that, in the worst case, with a pipe of radius 2 cm. and its top surface only 4 cm. below ground, the error is only of the order of 5 per cent. Consequently it seems clear that in any practical case the rule should yield a satisfactory approximation.

IV. Pipe or Cable in Wall.

In this Part is given first, a solution of the problem of a pipe symmetrically embedded in a wall with isothermal boundaries. This solu-

tion at once allows the rule of added thickness to be applied to the non-isothermal case, and it also provides a basis for the subsequent treatment of the latter by Awbery's method. Finally, some arithmetical checks are applied to the two methods.

Wall with Isothermal Boundary.

As in the preceding section, a line source is taken as generator, though it does not here yield strictly circular isothermals. Using the same

TABLE III.

Data for pipes buried near surface of ground of conductivity 0.0045 c.g.s. units ($m=18$ cm.) and dissipating 1 cal./sec./cm. A.T.M.=added thickness method. A.M.=Awbery's method.

Line source depth (cm.).	Pipe radius (cm.).	$\frac{H_n - H_c}{H_n}$ (per cent.).	Temp. over pipe (°C.).		Temp. of pipe (°C.).			
			A.T.M.	A.M.	A.T.M.	A.M.		
						$\frac{\theta_1 + \theta_2}{2}$	θ_1	θ_2
12	3	-35	57.5	54.9	106.0	108.4	108.9	107.9
6	2	-42	83.4	82.0	112.5	118.7	120.1	117.3
"	1	"	"	"	136.9	143.2	143.8	142.5

convention as before and treating one quarter of the wall section, as divided by lines of symmetry, we have in fig. 4 (z plane), C the line source, CA and CB boundary flow lines, and AB the isothermal wall surface. Omitting the intermediate t plane, the final rectangle ABCC in the ψ plane is given a thickness of $q/4$, where q is the total rate of heat flow from the source C per cm. length normal to the paper.

The transformations from the z and ψ planes are

$$dz/dt = Pt^{-\frac{1}{2}}(t+1)^{-\frac{1}{2}}, \quad \dots \dots \dots (22)$$

$$d\psi/dt = Qt^{-\frac{1}{2}}(t+1)^{-\frac{1}{2}}, \quad \dots \dots \dots (23)$$

and these yield on integration

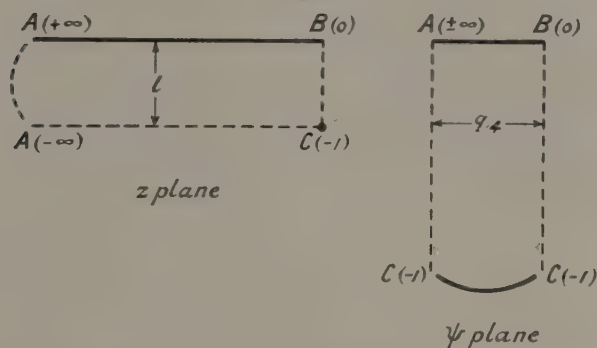
$$z = 2P \sinh^{-1} \sqrt{t} + L_2, \quad \dots \dots \dots (24)$$

$$\psi = 2Q \tan^{-1} \sqrt{t} + M. \quad \dots \dots \dots (25)$$

Taking B as origin and BA as real axis in both planes, we have, on evaluation of the constants and elimination of t ,

$$\sinh (z\pi/2l)=\tan (2\psi\pi/q). \quad . \quad . \quad . \quad (26)$$

Fig. 4.

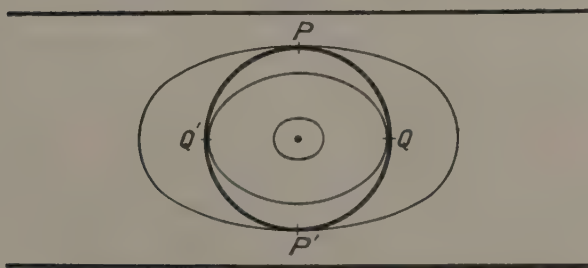


Here, as in (13), ψ is equal to $(\phi + ik\theta)$, and by splitting (26) into real and imaginary parts we obtain

$$\theta = \frac{q}{2\pi k} \tanh^{-1} \left[\frac{\sin (y\pi/2l)}{\cosh (x\pi/2l)} \right], \quad . \quad . \quad . \quad (27)$$

$$\phi = \frac{q}{2\pi} \tan^{-1} \left[\frac{\sinh (x\pi/2l)}{\cos (y\pi/2l)} \right]. \quad . \quad . \quad . \quad (28)$$

Fig. 5.



For the purpose of applying (27) to a finite pipe, we have to consider the form of the isothermals. They will obviously be ovals with diameters elongated in the x direction somewhat as in fig. 5. If a circular pipe touches the ovals as shown, and the temperature of the pipe is assumed to be that of the isothermal touching it at PP' the value of θ will be too

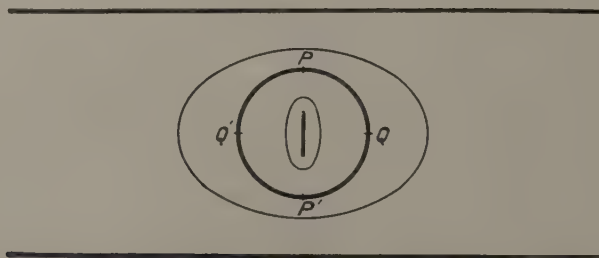
low, while the isothermal touching it at QQ' will give too high a value. These upper and lower limits for a pipe of radius r will be found from (27) to be

$$\theta_U = (q/2\pi k) \log \coth (r\pi/4l), \quad (29)$$

$$\theta_L = (q/2\pi k) \log \cot (r\pi/4l), \quad (30)$$

If, for a very large pipe, these limits should be inconveniently wide, we may then resort to a device, previously investigated by the author (Schofield, 1931), of replacing the line source * by a strip source *, as shown in fig. 6. The isothermals, as they recede from the source, will have diameters elongated in the y direction at the start and in the x direction at the finish. There will obviously be one isothermal PQP'Q' with equal diameters in the two directions, and this has been shown to give a very

Fig. 6.



close approximation to a circle. Taking this isothermal as basis, we should have for a pipe of radius r in place of (29) and (30), a single value for θ given by

$$\theta = (q/4kK')F[\operatorname{sech} (r\pi/2l), \quad (31)$$

the elliptic functions (K' and F) † having a

$$\text{modulus} = \cos (r\pi/2l) \cosh (r\pi/2l),$$

k being the conductivity and not the modulus as usual.

To apply the rule of added thickness, it suffices to replace l by $(l+m)$ in any of the above formulæ.

* The "line source" and "strip source" of the present paper were described in the former paper as they appear in section, i. e., as "point source" and "line source" respectively.

† F is the Legendre integral. In the former paper, for the reason indicated, sn^{-1} was written in place of F .

Wall with non-isothermal boundary (Awbery's method).

The principle of Awbery's method is that, if θ_1 expresses the temperature at every point for the case with an isothermal boundary, and a new equation is formed

$$\theta = \theta_1 + \theta_2, \quad (32)$$

where θ_2 is a function of x and y obeying the Laplace equation and the boundary conditions apart from those at the exposed surface; and, further, if $(\theta_1 + \theta_2)$ can be made to fit the Newton condition at this exposed surface, then (32) will give a complete solution of the problem.

For the case under consideration, if θ_2 has the harmonic form

$$\theta_2 = \int_0^\infty A \cosh \lambda(l-y) \cos \lambda x d\lambda, \quad (33)$$

the axes being as in fig. 4 (z plane) and A being independent of x and y , then the Laplace equation will be satisfied and

$$\left[\frac{\partial \theta_2}{\partial y} \right]_{y=l} = 0, \quad (34)$$

$$\left[\frac{\partial \theta_2}{\partial x} \right]_{x=0} = 0. \quad (35)$$

These two conditions would make both CB and CA flow lines as required. It also appears that the temperature rises along CB tending to induce, as desired, a hump of temperature at B. Since the temperature rises, as well, in the direction AC as C is approached, C cannot itself be a source as in fig. 4, but this would not seem to vitiate the proposed superposition, the source being without magnitude. For a correct solution a further characteristic, which is not yet apparent, must emerge, namely, that the temperature becomes zero when x is infinite.

Following Awbery, we now substitute for θ_1 and θ_2 their values from (27) and (33), so that

$$\theta = \frac{q}{2\pi k} \tanh^{-1} \left[\frac{\sin (y\pi/2l)}{\cosh (x\pi/2l)} \right] + \int_0^\infty A \cosh \lambda(l-y) \cdot \cos \lambda x \cdot d\lambda, \quad (36)$$

A being an expression which has to be determined by the remaining boundary condition. Along the surface we have

$$\theta_{y=0} = \int_0^\infty A \cosh \lambda l \cdot \cos \lambda x \cdot d\lambda, \quad (37)$$

$$\left[\frac{\partial \theta}{\partial y} \right]_{y=0} = \frac{q}{4kl \cosh (x\pi/2l)} - \int_0^\infty A \lambda \sinh \lambda l \cdot \cos \lambda x \cdot d\lambda. \quad . . . (38)$$

These expressions enable us to equate the Newton and conduction transfers at any point, thus

$$\frac{q}{4l \cosh(x\pi/2l)} - \int_0^\infty kA\lambda \sinh \lambda l \cdot \cos \lambda x \cdot d\lambda = \int_0^\infty EA \cosh \lambda l \cdot \cos \lambda x \cdot d\lambda; \quad (39)$$

whence

$$\begin{aligned} \int_0^\infty A(k\lambda \sinh \lambda l + E \cosh \lambda l) \cos \lambda x \cdot d\lambda &= \frac{q}{4l \cosh(x\pi/2l)} \\ &= \frac{q}{2l\pi} \int_2^\infty \int_0^\infty \frac{\cos \lambda x \cdot \cos \lambda y}{\cosh(\gamma\pi/2l)} d\lambda \cdot d\gamma, \end{aligned} \quad (40)$$

the last identity being obtained by the application of Fourier's integral theorem. Incidentally we observe from (40) that, for an infinite value of x the left-hand side of the equation vanishes, making θ zero for $y=0$ and also for greater values of y . Thus the characteristic, to which reference was made above, applies.

From (40) we have

$$A = \frac{q}{2l\pi(k\lambda \sinh \lambda l + E \cosh \lambda l)} \int_0^\infty \frac{\cos \lambda y}{\cosh(\gamma\pi/2l)} d\gamma. \quad (41)$$

With A substituted in (36) the expression will be unmanageable unless we can integrate (41). This can be accomplished, if only in series form, on the basis of the following :

$$\int_0^\infty \frac{\cos \lambda u \cdot d\lambda}{e^{\mu u}} = \frac{\mu}{\mu^2 + \lambda^2} = \frac{1}{\mu(1 + \lambda^2/\mu^2)}. \quad (42)$$

Thus expanding $1/\cosh(\gamma\pi/2l)$ in terms of $\exp(-\mu\gamma)$ μ being equal to $(\pi/2l)$, we have

$$\begin{aligned} \int_2^\infty \frac{\cos \lambda y \cdot d\gamma}{\cosh \mu y} &= \frac{2}{\mu} \left\{ \frac{1}{(1 + \lambda^2/\mu^2)} - \frac{1}{3(1 + \lambda^2/3^2\mu^2)} + \frac{1}{5(1 + \lambda^2/5^2\mu^2)} - \dots \right\} \\ &= \frac{4l}{\pi} f(\lambda, \pi/2l). \end{aligned} \quad (43)$$

So that, finally,

$$\theta = \frac{q}{2\pi k} \tanh^{-1} \left[\frac{\sin(y\pi/2l)}{\cosh(x\pi/2l)} \right] + \frac{2q}{\pi^2} \int_0^\infty \frac{\cosh \lambda(l-y) \cdot \cos \lambda x \cdot f(\lambda, \pi/2l) \cdot d\lambda}{(k\lambda \sinh \lambda l + E \cosh \lambda l)}. \quad (44)$$

The series $f(\lambda, \pi/2l)$ is unfortunately of a slowly converging type, but the labour of computation can be reduced by noting that with $\lambda=0$ it becomes Gregory's series for $\pi/4$. Consequently, if any term of the series becomes indistinguishable from the corresponding Gregory term, within the desired accuracy, an addition can be made for the known remainder of the Gregory series. For the calculations below, the second part of (44)

was evaluated by Simpson's rule, a single set of 20 values for the series sufficing for all temperatures.

Arithmetical Tests.

Tests similar to those in the preceding case are applied here, taking a line source 30 cm. below the surface and the same added thickness as before, namely 18 cm.

It will be noted from Table IV. that the difference between H_n and H_c ranges over about ± 12 per cent. As before, corrections equal to one half of the percentage difference between the two have been applied to

TABLE IV.

Temperature etc. of surface of wall, of thickness 60 cm. and conductivity 0.0045 c.g.s. units ($m=18$ cm.) due to line source in central plane dissipating 1 cal./sec./cm. By added thickness method.

$4\phi/q$.	x (cm.).	H_n $\times (10^{-3})$.	H_c $\times (10^{-3})$.	$\frac{H_n - H_c}{H}$ (per cent.).	θ ($^{\circ}\text{C}$.).	θ (cor.) ($^{\circ}\text{C}$.).
0	0	5.54	6.26	-13.0	22.16	23.6
$\frac{1}{4}$	10.33	5.16	5.65	- 9.5	20.64	21.6
$\frac{1}{2}$	23.13	4.04	4.07	- 0.7	16.16	16.2
$\frac{3}{4}$	44.21	2.24	1.97	+12.1	8.96	8.4

the surface temperatures, and when the corrected values are plotted, in fig. 7, the resulting curve is seen to be in good agreement with the temperatures calculated for four selected points by Awbery's method.

Table V. gives the excess of temperature, for a dissipation of 1 cal./sec./cm., calculated by the two methods for pipes up to a radius of 15 cm. θ_x and θ_y are the temperatures of the pipe at the respective points where it cuts the two axes. For the added thickness method these are calculated from (29) and (30) and are seen to be sufficiently close to render unnecessary a resort to the finer approximation of (31). Further, it will be observed that only with the largest pipe do the mean values differ from those obtained by Awbery's method by more than 1 per cent.

In view of the general similarity of the problem of a pipe in a wall, with that of a pipe in the ground, it is not proposed to take an extreme example of the former, such as we have already done of the latter, in Part III. above.

Fig. 7.

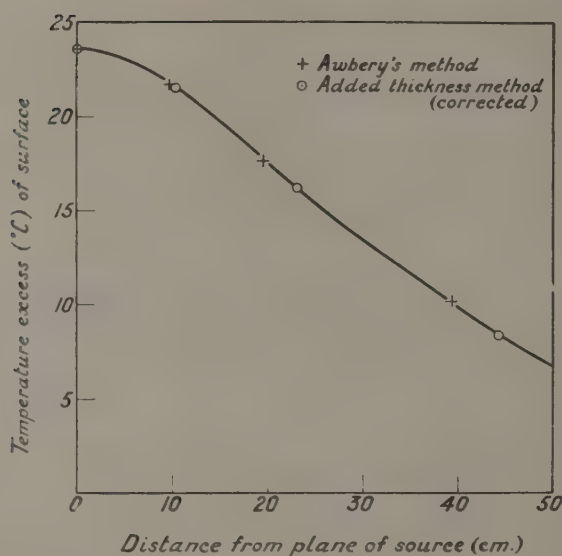


TABLE V.

Temperature of pipe of radius r and dissipating 1 cal./sec./cm. in wall of thickness 60 cm. and conductivity 0.0045 c.g.s. units ($m=18$ cm.). A.T.M.=Added method. A.M.=Awbery's method.

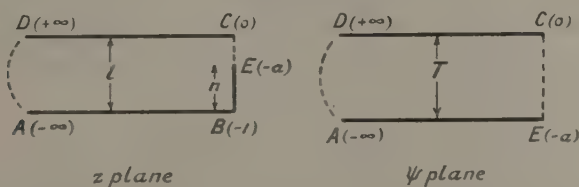
r (cm.).	A.T.M.			A.M.		
	θ_x (°C.).	θ_y (°C.).	$\frac{\theta_x + \theta_y}{2}$ (°C.).	θ_x (°C.).	θ_y (°C.).	$\frac{\theta_x + \theta_y}{2}$ (°C.).
15	50.4	49.0	49.7	51.1	49.7	50.4
10	64.4	63.7	64.1	64.9	64.2	64.6
5	88.6	88.4	88.5	89.1	89.1	89.1
2.5	113.1	113.0	113.0	113.6	113.6	113.6

V. Insulated Rib or Girder.

Awbery's Method.

This problem, illustrated in fig. 1 (*d*) and fig. 8, has been treated by Awbery, but his solution does not appear to conform with the conditions over part of the boundary, *i. e.*, the continuation of the plane of the rib (EC of fig. 8 or CP of his fig. 3). This part of the plane being, by symmetry, a flow line in section, $\partial\theta/\partial x$ must be zero, a condition which is not fulfilled. It may be added that harmonic expressions of the type employed by Awbery, involving a product of sin or cos with sinh, cosh, or exponential (see *e. g.* (33) above), require that one or both axes, or lines parallel to them, should be in themselves, complete isothermals or flow lines. Consequently, unless more complex expressions can be brought into action, the method seems to be limited to cases of the kind indicated: for example, the problem in Part III. has the complete *y* axis as a flow line

Fig. 8.



and that in Part IV. the *y* axis and a line parallel with the *x* axis, as flow lines.

Rule of added Thickness.

To apply the rule, we require a solution of the case with an outer isothermal boundary. The problems of a single rib, and of a series of ribs, in an infinite wall and isothermal with the adjacent face of the wall, have been treated respectively by Lees (1911) and the author (1928). It is convenient, however, to develop a solution on the same lines as those in the preceding cases.

The appropriate diagram is given in fig. 8. In the former cases the total flux was finite and the total temperature infinite. Here the reverse holds, and so we make the thickness of the final rectangle in the θ direction equal to T , which is the temperature difference between the isothermal boundaries.

The transformations from the *z* and ψ planes are

$$dz/dt = Pt^{-1}(t+1)^{-1}, \quad . \quad . \quad . \quad . \quad . \quad . \quad (45)$$

$$d\psi/dt = Qt^{-1}(t+\alpha)^{-1}, \quad , \quad . \quad . \quad . \quad . \quad . \quad . \quad (46)$$

Then by integration, evaluation of the constants with respect to C as origin and CD as real axis in each plane and elimination of t , we get

$$\sinh (z\pi/2l)=\cos (n\pi/2l) \sinh (\psi\pi/2T), \quad (47)$$

the constant a having been found equal to $\cos^2(n\pi/2l)$.

In (47) the variable ψ is $(\phi/k+i\theta)$ —instead of $(\phi+ik\theta)$ as in (13) and (26)—for this gives the correct value of T for the temperature of the isothermal EBA, as may easily be checked at the point E whose coordinates are $(o, l-n)$.

In problems like the present one, in which we are concerned with a plane wall having modifications of one boundary, it is usual to express the effect of the disturbing feature as being equivalent to an addition, or subtraction, from the normal flow which would occur if the feature were absent, of the normal flow from a certain width of the wall.

Along the real axes ($y=0, \theta=0$) we have, for infinite values of x and ϕ from (47),

$$(\phi\pi/2Tk)-(x\pi/2l)=\log \sec (n\pi/2l), \quad (48)$$

and if the total flux (ϕ) is equal to that from a width $(x+X)$ of the wall

$$\phi=(x+X)kT/l, \quad (49)$$

and hence the added width X due to the rib is

$$X=(2l/\pi) \log \sec (n\pi/2l). \quad (50)$$

Since we have only dealt with one-half of the figure, the added width for the complete wall is $2X$. To apply the rule of added thickness it suffices to replace l by $(l+m)$ in the above formula.

As in the preceding cases, it is proposed to check the approximation arithmetically by a point-to-point comparison of conduction and Newton transfers in a particular case. For the former $\partial\theta/\partial y$ is required and for the latter θ . These are given to a fair accuracy by Kennelly's charts of complex hyperbolic and circular functions (Kennelly, 1914). Thus θ , as the imaginary part of ψ , is readily obtainable from (47), and $\partial\theta/\partial y$ nearly as easily from

$$\frac{\partial\theta}{\partial y}=\text{real part of } \left(\frac{T}{l}\right) \frac{\cosh (z\pi, 2l)}{\cos (n\pi, 2l) \cosh (\psi\pi/2T)} \quad (51)$$

Determinations made in this way, in the case taken below, turned out to be good to about one per cent., which was not quite precise enough for the critical check required. Calculations were also made by means of the Tables of Kennelly (1914), but, with the necessity of double interpolation, somewhat more work was involved than in a direct calculation on the basis of the following formulæ and (51):

$$\cos (\theta\pi/T)=[(P+Q)^2+1+2(Q-P)]^{\frac{1}{2}}-(P+Q), \quad (52)$$

$$\cosh (\phi\pi/Tk)=[(P+Q)^2+1+2(Q-P)]^{\frac{1}{2}}+(P+Q), \quad (53)$$

where

$$P^{\frac{1}{2}} = \cosh (x\pi/2l) \sin (y\pi/2l) \sec (n\pi/2l),$$

$$Q^{\frac{1}{2}} = \sinh (x\pi/2l) \cos (y\pi/2l) \sec (n\pi/2l).$$

Table VI. gives the check data for a wall 15 cm. thick, with a rib 9 cm. deep projecting from it. It will be seen that, with an added thickness m of 5 cm., the maximum difference between H_n and H_c is 4.5 per cent.

The rule of added thickness can probably be taken, therefore, to give a good approximation in medium types of case. In the section below we develop an alternative method of treatment which enables us to test

TABLE VI.

Temperature etc. of surface of wall of thickness 15 cm. and conductivity 0.00125 ($m=5$ cm.) with a single rib 9 cm. deep, the inner boundary being maintained at 40° C. above air temperature.

Distance from rib (cm.).	$H_n \times 10^{-3}$.	$H_c \times 10^{-3}$.	$\frac{H_n - H_c}{H_n}$ (per cent.).	θ (°C.).	θ (cor.) (°C.).
0	3.36	3.51	-4.5	13.44	13.7
5	3.15	3.12	+1.0	12.60	12.5
10	2.85	2.81	+1.4	11.40	11.3
15	2.67	2.64	+1.1	10.68	10.6
∞	2.50	2.50	0	10.00	10.0

the efficacy of the rule when applied to the extreme case of a rib penetrating a wall for nearly its full thickness.

VI. Added Thickness Method—Alternative Treatment.

In this section a brief consideration is given to the second criterion of approximation mentioned in Part II. above, according to which the imagined distribution is tested by equating the conduction and Newton transfers at two or more important regions of the plane. The simple rule employed up to the present has allowed of no adjustable parameter, the added thickness being independent of the shape of the source and being governed only by the conductivity of the medium and the coefficient of Newton transfer for air, either still or moving as the case may be. If the added thickness were made adjustable there is no reason to suppose that a better, or indeed so good an, approximation would result; but

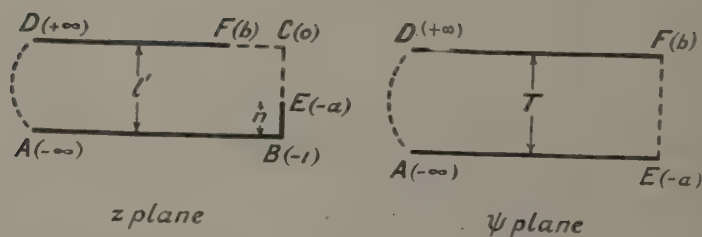
a definite possibility of improvement would lie if a second parameter were introduced, corresponding, for instance, with some modification of the boundary distribution.

An attack on these lines obviously depends on the details of the particular problem. If the insulated rib is taken as an example, we might imagine an added thickness of adjustable amount, coupled with the boundary modification indicated in *a* or *b* of fig. 9. These modifications are identical analytically, when treated by the Christoffel-Schwarz method, and one or other is adopted according as the simple rule gives an excess or deficiency of Newton transfer in the central position. As may have been observed, the central Newton transfer has been deficient

Fig. 9.



Fig. 10.



in the three cases treated above, including that of the insulated rib, and we can see on general grounds that the distribution *a* is the more appropriate.

Treating the half figure as before, we employ the scheme of transformation indicated in fig. 10. It will be observed that the *z*-plane transformation is identical with that in fig. 8. On treatment in the usual way, *i. e.*, by integration, evaluation of the constants and elimination of *t*, we obtain

$$(a+b) \cosh (\psi \pi / T)=\cosh (z \pi / l')+\alpha-(1+b), \quad . . . (54)$$

where, as before, *a* is equal to $\cos^2(n\pi/2l')$.

Instead of (50) we now have

$$X=(l'/\pi) \log [1/(a+b)], \quad (55)$$

(and for 51), (52), (53)

$$\frac{\partial \theta}{\partial y} = \text{real part of } \left(\frac{T}{l'} \right) \frac{\sinh (z\pi/l')}{(a+b) \sinh (\psi\pi/T)}, \quad \dots \quad (56)$$

$$\cos (2\theta\pi/T) = P^2 + Q^2 - [(P^2 + Q^2)^2 + 1 + 2(Q^2 - P^2)]^{\frac{1}{2}}, \quad \dots \quad (57)$$

$$\cosh (2\phi\pi/Tk) = P^2 + Q^2 + [(P^2 + Q^2)^2 + 1 + 2(Q^2 - P^2)]^{\frac{1}{2}}, \quad \dots \quad (58)$$

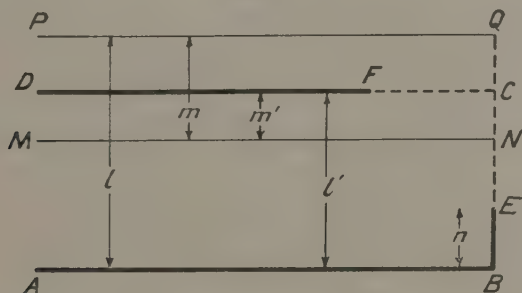
where

$$P = \frac{\cosh (x\pi/l') \cos (y\pi/l') + a - (1+b)}{(a+b)},$$

$$Q = \frac{\sinh (x\pi/l') \sin (y\pi/l')}{(a+b)}.$$

The question now arises as to what temperature is to be taken for the isothermal DF (fig. 10) in relation to the atmospheric temperature. For the simple rule, with an added thickness equal to kE , the outer boundary

Fig. 11.



has been taken as isothermal with the atmosphere. This obviously gives the correct gradient in the medium when the flow is entirely normal to the surface, as in the present case, at infinity. The temperature of DF must therefore fit into this system. Thus turning to fig. 11, if MN is the true surface of the medium, PQ the surface got by adding a thickness m equal to $k'E$ and DFC' the surface got by adding an arbitrary thickness m' , then the temperature of DF would be $(m-m')l$ of the temperature excess of ABE over PQ. This means that if we take the temperature of DF as 0°C. , we must, when computing the hypothetical Newton transfer from any point on MN, add to the temperature at this point, the temperature of DF as given above.

The two parameters are the lengths m' and FC in fig. 10. The value of the latter is $(2l'\pi) \sinh^{-1} \sqrt{b}$, but since we are not interested in this length as such, b is taken as parameter in its place. The numerical example chosen is identical with the problem in the last section, except that for a rib 9 cm. deep is substituted one 13 cm. deep, which thus falls

short of the surface by only 2 cm. Table VII. gives data calculated for this case by the added thickness method, both in its simple form and with two parameters. The values of the parameters were found by trial, some assistance being obtained from preliminary calculation by the simple rule.

TABLE VII.

Temperature etc. of surface of wall of thickness 15 cm. and conductivity 0.00125 ($m=5$ cm.) with a single rib 13 cm. deep, the inner boundary being maintained 40° C. above air temperature. A.T.M.(0)=Added thickness method with no parameter, *i. e.*, rule of added thickness. A.T.M. (2)=Added thickness method with two parameters, $m'=3.8$ cm. and $b=0.05$.

x (cm.).	A.T.M. (0).			A.T.M. (2).		
	$\frac{H_n - H_c}{H_n}$ (per cent.).	θ ($^{\circ}$ C.).	θ (cor.) ($^{\circ}$ C.).	$\frac{H_n - H_c}{H_n}$ (per cent.).	θ ($^{\circ}$ C.).	θ (cor.) ($^{\circ}$ C.).
0	-23.3	20.9	23.3	+0.4	22.5	22.5
3.25	+ 1.8	18.0	17.8	+6.9	18.6	18.0
6.5	+ 5.4	14.8	14.4	-0.3	14.6	14.6
13	+ 3.1	11.7	11.5	-1.4	11.4	11.5
∞	0.0	10.0	10.0	0.0	10.0	10.0

It will be seen that, while the second method gives a better point-to-point balance between H_n and H_c , the surface temperatures, when corrected as previously explained, are in tolerable agreement, the maximum difference being 3 per cent.

Coming to the values of X , the added width, the two methods give respectively

$$\text{From (50) } X=8.26 \text{ cm.}$$

$$\text{,, (55) } X=7.90 \text{ ,,}$$

or a difference of 4.5 per cent. It must be remembered, however, that ordinarily we are concerned, not with the value of X , but with the total heat transfer from a certain width of wall. If, for example, we were to take the total width within which the disturbance due to the rib is such

as to cause the flux density to exceed the value at infinity by more than one per cent., we should find that this limit would correspond with a value of about 32 cm. for x , and that the difference in the total heat flow, as given by the two methods, would then be less than one per cent.

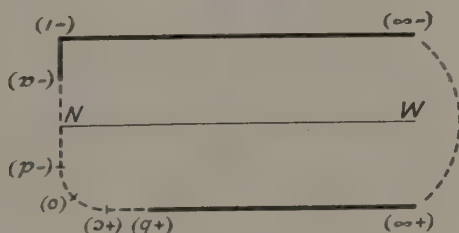
If desired, the process of boundary modification indicated in figs. 9 and 10, could be elaborated with a view to further reduction of the differences between H_n and H_c shown in Table VII. Thus curvature of the boundary could be introduced by substituting fig. 12 for fig. 10 (z plane). As Richmond (1923) has shown, the z -plane transformation would then be

$$\frac{dz}{dt} = \frac{1}{\sqrt{t+1}(\sqrt{t-c}+C\sqrt{t+d})} \quad \dots \dots \dots (59)$$

in place of

$$\frac{dz}{dt} = \frac{1}{\sqrt{t+1}\sqrt{t}} \quad \dots \dots \dots (60)$$

Fig. 12.



It will be seen that (59) contains three additional parameters, making five in all ; namely c , which can be either greater or less than b ; d , which must be such that the curvature does not extend below MN —the true surface of the medium : and C , which controls the curvature in the region from $t=c$ to $t=-d$. It will be found that if c is made equal to b and C equal to unity, so that there is only one extra parameter, then (59) gives a fairly simple integral which, however, would not readily admit of the elimination of t from the ψ plane integral given by fig. 10. In the circumstances the necessary calculations could best be made in terms of the intermediate variable t .

It is not proposed to pursue the matter here, since the immediate objective has been attained, of showing that the two methods already used, yield substantially the same result in the extreme case of a rib penetrating a wall for nearly its full thickness.

It may be added that a treatment similar to that indicated in fig. 10 could no doubt be applied to the problems dealt with in Parts III. and IV. above.

VII. *Conclusions regarding Rule of Added Thickness.*

The rule of added thickness has been submitted to detailed examination in three specimen problems. In each case the examination has covered a comparison with an alternative method of solution, as well as a point-to-point comparison of the Newton and conduction transfers over the surface. Even where the conditions have been such as to show a wide departure from the ideal of equality of the two transfers, it has been found that, by taking the mean of the two, a close approximation to the true surface temperature could be deduced, while a satisfactory estimate of overall heat flow has been obtained in all cases.

In view of these results, it would seem that the rule could be applied with some confidence to many similar problems for which the solutions of the corresponding isothermal cases are known. Such solutions by the Christoffel-Schwarz formula have been given by the author for the problems, other than those already treated, in fig. 1 under the following references, viz., *c* (Schofield, 1931) *e, f,* and *g* (Schofield, 1928). Similar applications of the formula will be found scattered in the literature, though seldom stated in terms of heat flow, which is not the most commonly treated of the phenomena covered by the Laplace equation. Thus examples occur in the work of J. J. Thomson (1893), Lees (1908), Carter (1926), and Cockcroft (1928), among others. Where it is considered necessary to submit the rule to any check, one in which the boundaries alone are concerned would probably suffice. Ordinarily this should obviate the troublesome process of splitting complex functions into real and imaginary parts, which has been necessary for the detailed analysis carried out in this paper.

Finally, it may be pointed out that the rule is applicable to solutions obtained otherwise than by the Christoffel-Schwarz transformation. This formula is generally the most useful, but it is not essential that the relation (1) should be derived in this way, nor indeed that the form of the function in this relation should be known. Consequently, solutions obtained by other mathematical methods can be used and also those by non-mathematical methods. The most important of the latter are the graphical process exploited by Lehmann (1909), and Wedmore (1923 and 1930), and the method whereby the characteristics of heat flow are deduced from measurements of electrical resistance of electrolytes of the appropriate shape (Langmuir, Adams, and Meikle, 1913) or of thin sheets of metal (Awbery and Schofield, 1928; Schofield, 1931 *). As already indicated, the only essentials are that the problem should be

* This paper gives examples of treatment by all three methods—mathematical, graphical, and electrical.

a two-dimensional one of steady heat flow in which the sink consists of the atmosphere cooling a flat surface according to Newton's law and in which the boundary flow lines are straight and normal to this surface.

References.

- Awbery, J. H., *Phil. Mag.* vii. p. 1143 (1929).
Awbery, J. H., and Schofield, F. H., *Int. Congr. Refrig.* iii. p. 59 (1928).
Carter, F. W., *J. Instn. elect. Eng.* lxiv. p. 1115 (1926).
Cockcroft, J. D., *J. Instn. elect. Eng.* lvxi. p. 385 (1928).
Fishenden, M., and Saunders, O. A., 'The Calculation of Heat Transmission' (H.M. Stationery Office), 1932.
Kennelly, A. E., 'Charts and Tables of Complex-Hyperbolic and Circular Functions,' Howard University Press, 1914. (2 vols.)
Langmuir, I., Adams, E. Q., and Meikle, G. S., *Trans. Amer. electrochem. Soc.* xxiv. p. 53 (1913).
Lees, C. H., *Phil. Mag.* xvi. p. 736 (1908).
Lees, C. H., *Proc. phys. Soc. Lond.* xxiii. p. 361 (1911).
Lehmann, T., *Elektrotech. Z.* xxx. p. 995 (1909).
Richmond, H. W., *Proc. Lond. math. Soc.* xxii. p. 389 (1923).
Schofield, F. H., *Phil. Mag.* vi. p. 567 (1928).
Schofield, F. H., *Phil. Mag.* xii. p. 329 (1931).
Thomson, J. J., 'Recent Researches in Electricity and Magnetism,' Clarendon Press, 1893, chap. 3.
Wedmore, E. B., *J. Instn. elect. Eng.* lxi. p. 568 (1923).
Wedmore, E. B., *J. Instn. elect. Eng.* lxviii. p. 1354 (1930).

XLVIII. *The Drift of the Selenium Barrier-Layer Photo-cell.*

By R. A. HOUSTOUN, D.Sc., University of Glasgow *.

[Received February 26, 1941.]

IN the book of data supplied with the Photronic Photo-cell, it is stated that the cell is subject to fatigue. When it is first exposed to a luminous source, the indications gradually diminish with time and in a few minutes reach a constant value. Curves are given for three representative cells, each at three different illumination intensities, 250, 100, and 10 foot candles, and with relatively low external resistance in the circuit. The greatest effect shown amounts to 3 per cent. of the initial value. The currents corresponding to the three illuminations were probably about 350, 140, and $14\mu\text{A}$.

In the leaflet dealing with the Tungfram barrier-layer cell it is stated that, provided the entire light sensitive area is uniformly illuminated, the cell is not subject to drift, fatigue or time-lag, but if only a small part of the light sensitive area is illuminated, an effect akin to fatigue occurs. In an article in 'Electronics and Television and Short-Wave World,' July, 1940, dealing with the E.P.L. barrier-layer cell, it is stated that barrier-layer cells are not subject to fatigue or time-lag in their response under normal conditions, though if only a small part of the light sensitive surface is brightly illuminated or the whole cell subjected to a very high illumination, a slight fatigue effect will be noticed, the current decreasing slightly to a lower and constant value during prolonged exposure.

The only recent article on the subject known to me is that of Elvegård, Lindroth and Larsson †. In summarising previous work they state that there seems hardly to exist any agreement as to the conclusions reached, but that the decrease proceeds rapidly at first and gradually slows down, the current approaching a certain final value. The time required for the current to reach its final value depends on the duration of the preceding dark period. In a few cases the current increases instead of decreasing. The drift effect is different for different wave-lengths.

The principal aim of Elvegård, Lindroth and Larsson was to investigate the dependence of the effect on wave-length and temperature. An

* Communicated by the Author.

† Journ. Optical Soc. of America, xxviii. p. 33 (1938).

E. Zierold cell, type 25 E. was placed in an electric oven and exposed through six filter combinations in succession; these had absorption minima at $650\text{ m}\mu$, $600\text{ m}\mu$, $540\text{ m}\mu$, $525\text{ m}\mu$, $490\text{ m}\mu$, and $470\text{ m}\mu$. After 10 minutes, approximately, the current became constant, the changes being -9 , -4 , $+4$, $+3$, -3 , and -8 per cent. respectively. Thus there was an increase in the middle of the spectrum and a decrease at both ends. For the temperature interval of 25 – 30°C . examined, the progress of the drift seemed practically unvarying for the different isolated regions of the spectrum. Comparative tests made with other cells showed that these behaved like the Zierold cell..

When a barrier-layer photo-cell is exposed to light or X-rays its resistance decreases. This has been investigated by A. E. Sandström*, and it is found that the change goes rapidly at first and gradually slows down, the final value being obtained in about 20 minutes. There is a gradual recovery in the dark, which takes 60 or 100 hours to complete. In a later communication† he states that there is no simple relation between the drift and the change in barrier-layer resistance.

The selenium barrier-layer cell consists of an iron base on which is deposited a thin layer of selenium. This is covered with a very thin translucent metal film. The light falls on the surface of the selenium through the translucent metal and it is here the photo-electric action takes place, the translucent metal becoming negative and the iron base positive. The efficiency is high, more than half of the light energy reappearing as energy of the electric current, and the relative spectral sensitivity is somewhat similar to the sensitivity curve of the human eye. Now the human eye is fatigued for one colour by exposure to spectral light of that colour; the visual purple is a photo-electric substance and it is natural to ask whether the barrier-layer cell behaves in the same way. If it is fatigued for green light, is it also fatigued for red? The purpose of the observations recorded here was to answer this question and obtain more information about the fatigue of these cells generally. They are widely used now and it is desirable to know as much about them as possible.

My first observations were made on a Photronic cell which was obtained seven years ago. Its sensitive area is circular, of about 3.6 cm . diameter, and it is protected by a glass window. At first the cell was merely exposed to the light of a 100 watt pearl lamp, but when coloured filters were used it had to be brought very close to the lamp, so another arrangement was substituted: the cell was put in the cone of light produced by the condenser of a projection-lantern, the source being either a 250

* *Phil. Mag.* xxviii, p. 642 (1939).

† *Phil. Mag.* xxx, p. 428 (1940).

or a 500 watt lamp. The only resistance in the circuit of the cell was that of the microammeter, 39.4 ohm. A $1\frac{3}{4}$ -inch water-filter was used to absorb heat rays. The observations recorded in this paper were made usually with the lantern, but the results were the same by both methods, and the water-filter made no difference. The voltage on the lamp was kept constant to one-tenth volt by adjusting a sensitive rheostat.

The effect was found to vary with intensity and colour. It varied roughly with the square of the current, *i. e.*, if the current was halved, the percentage change of the reading due to fatigue in a given time was reduced to one-quarter. With Chance's green tricolour filter it was much greater than with ordinary red signal-glass, and for white light it had an intermediate value. Some results are given in the following diagrams.

Fig. 1 is for Chance's tricolour green. The whole disc was illuminated, not quite uniformly, there being a brighter patch in the middle. The ordinates give the current in microamps. The scale of minutes is for the exposure, the scale of hours for the recovery. It will be seen that, when the cell was exposed to the light, the microammeter went to $103.0 \mu\text{A.}$, and that this decreased rapidly at first, and then more slowly, to $83.5 \mu\text{A.}$ The light was then shut off and the recovery curve taken: after 23 hours the current had increased almost to its initial value. It required about ten seconds to make a reading. Consequently, the first reading was taken about ten seconds after the illumination started, and during this time the current was falling rapidly. In taking a reading during recovery the cell had to be exposed for 10 seconds or thereabouts. This, of course, retarded recovery but, as these exposures did not amount altogether to more than a minute and a half in 23 hours, it was assumed they would not affect the result appreciably.

After the completion of the observations recorded in fig. 1 the cell had four hours rest. A similar set was then taken for the red signal glass; the cell had then 26 hours rest and a similar set was taken for white light. These are shown in figs. 2 and 3.

The fall for the 70 minutes recorded amounts to 18.9, 11.6, and 17.6 per cent. of the initial reading for green, red, and white respectively. The effect is always much greater for green than for red, with white occupying an intermediate position; the fall for white is unusually great in the diagram shown. There are also from time to time erratic variations of perhaps one-quarter per cent. of the total value of the current.

The electrical resistance of the cell, as has already been mentioned, falls on exposure to light. It varies of course with the direction of the current through the photo-cell and with the magnitude of the e.m.f. applied. To investigate this change of resistance a 1.50 volt cell was applied to the photo-cell through a 20,000 ohm resistance, and then

reversed and the currents noted ; this particular value of resistance was chosen in order to get the deflexion on the microammeter used for

Fig. 1.

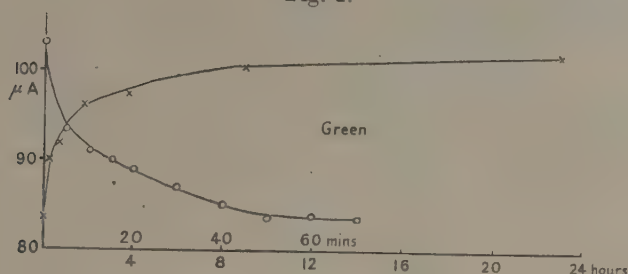


Fig. 2.

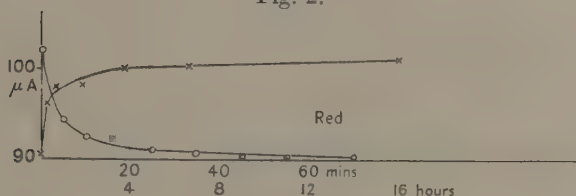
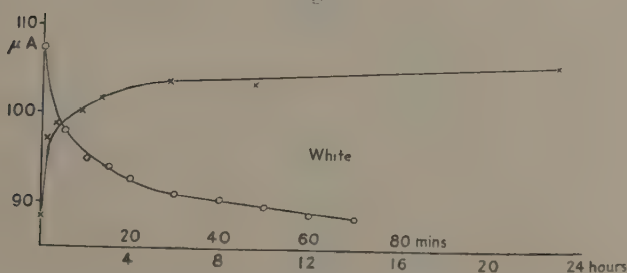


Fig. 3.



measuring the light. The following values were obtained during the experiments recorded in figs. 1, 2, and 3 :—

Resistances after long rest	9301	3080 ohm
After 70 mins. exposure to green	7130	2770 „
After 23 hours recovery	8760	2910 „
After 70 mins. exposure to red	6840	2700 „
After 18 hours recovery	8330	2830 „
After 70 mins. exposure to white	7230	2670 „
After 23 hours recovery	8330	2830 „

The cell was not exposed to light while the resistances were being measured. They are, of course, only approximate, as, once the light is shut off, recovery proceeds very rapidly and the resistance is visibly changing during measurement. I agree with Sandström that there is no simple relation between the drift and the change in barrier-layer resistance.

I was at first inclined to regard the drift as due to an exhaustion of electrons. Let x be the fraction of the whole number of electrons ineffective and I the intensity of the light in arbitrary units. Then, if we suppose that the recovery takes place according to the law of mass action, we may represent the process by the following equation :

$$\frac{dx}{dt} = I(1-x) - kx^2,$$

or

$$\frac{dx}{dt} = I(1-x),$$

since x is small. This has the solutions

$$x = \sqrt{\frac{I}{k}} \tanh \sqrt{kI}t,$$

and, for the recovery in the dark when $I=0$,

$$kx = \frac{1}{x} - \frac{1}{x_0}.$$

If we suppose that the recovery is represented by kx ,

$$\frac{dx}{dt} = I - kx,$$

and the corresponding solutions are

$$x = \frac{I}{k} (1 - e^{-kt})$$

and

$$x = x_0 e^{-kt}.$$

The kx law does not fit the data at all. The kx^2 law fits it roughly. Figs. 4 and 5, which are for the exposure and recovery already recorded in fig. 1. being typical examples. In these diagrams the ordinates represent x , so the curve ascends for exposure and descends for recovery, the reverse of fig. 1. There is, however, one very important point to note; figs. 4 and 5 are calculated with different values of k . For fig. 4 k is 0.18, and for fig. 5 k is 0.0452, using the hour as unit of time. Of course, conditions are different in the two cases; in the one case the cell is exposed to light, in the other it is in the dark. Nevertheless, I do not think the explanation can be regarded as satisfactory.

In order to investigate the effect of colour more thoroughly the cell was illuminated in succession through the Ilford infra-red filter, the Wratten and Wainwright spectrum series of filters, and Chance's ultra-violet glass filter. In this case only a part of the sensitive surface, about 1.8 cm. square, was illuminated. Only a six-minutes exposure was given

Fig. 4.

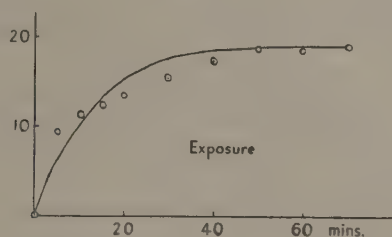
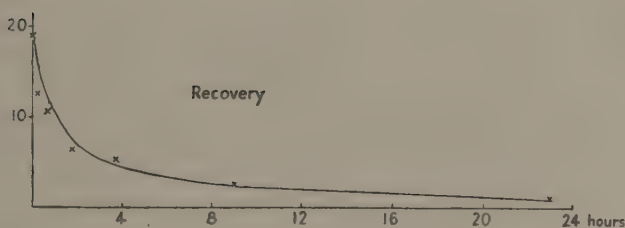


Fig. 5.



in each case, and the cell was allowed a day to recover between exposures. The following table gives the results :—

Filter.	Initial current.	Percentage change.
Infra-red.....	96.0 μ A.	0.8
α 670 m μ	100.1	6.8
β 645	105.0	6.2
γ 605	100.2	7.8
δ 575	98.0	6.0
ϵ 540	90.0	7.0
θ 490	107.6	4.5
η 450	87.2	6.5
Ultra-violet.....	73.2	4.0

The wave-length given is the point of maximum transmission of the filter. The Greek letters are the names of the filters. The number in the last column is the percentage diminution in 5 minutes. If we except the infra-red there is not much variation throughout the spectrum. The green ϵ is almost the same colour as Chance's tricolour green, very slightly bluer. There is no doubt that its fatiguing effect on the spectrum is distinctly less than that of the tricolour green; this seems remarkable. The green ϵ lets through a much narrower range of the spectrum than the tricolour green does, but I would not have expected this to make a difference.

The foregoing observations were made on a cell which has been in use for seven years. In addition to this cell I had at my disposal three other barrier-layer selenium cells, namely, a Photronic cell recently purchased, a cell made in England since the start of the war, and a cell of German origin. Fig. 6 shows fatigue experiments made with the second Photronic

Fig. 6.

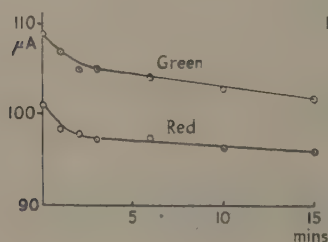
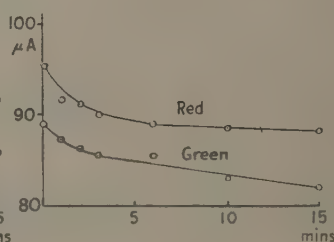


Fig. 7.



cell: the upper curve is for green light and the lower one for red light. The drop for the green is $7.4 \mu\text{A.}$ and for the red $5.0 \mu\text{A.}$; the ratio of these values is in accordance with the results for the other cell, but the values themselves are only about half as large.

Fig. 7 gives fatigue curves for the German cell. The upper curve is for red and the lower one for green; here the effects for red and green are equal. It should be stated that this cell had to be treated more severely than the Photronic cells in order to get a fatigue, *i. e.* the light had to be concentrated on about a sixth of the surface of the cell. Under uniform illumination the effect would have been much less.

The English cell showed no fatigue at all, even when the filament of the lamp was focused on its surface. It was, however, from time to time liable to erratic changes of current of perhaps one per cent. either way.

In order to see whether the cell is fatigued for red when it has been exposed to green and *vice versa*, series of observations similar to the following were made with the old Photronic cell:—

G	82.0	119.2	104.8	R	107.0	107.0
R	92.5	116.0	105.0	G	107.1	106.2
G	79.5	116.2	104.2	R	103.6	105.6
R	90.5	113.7	103.5	G	105.2	103.4
15 mins. exposure to R.				15 mins. exposure to G.		
R	86.8	108.0	100.0	G	96.6	95.0
G	72.0	104.6	96.3	R	100.2	98.8
R	87.6	109.0	101.1	G	98.0	97.1
G	72.8	106.8	96.0	R	101.0	101.2
Percentage drop in R.	5.3	6.0	3.7		4.5	5.9.
Percentage drop in G.	12.8	10.2	8.0		8.5	8.6

The cell had a day's rest before each of the five series of observations recorded above. G stands for green and R for red, the regions of the spectrum being those transmitted by Chance's tricolour green and red signal-glass; these are non-overlapping. The numbers are micro-ammeter readings. If we take the first column, we see that the cell was exposed to G, then R, then G, the readings being made as rapidly as possible; it was then exposed to R for 15 minutes, a reading being taken at the beginning and at the end of this period. It was next exposed to G, R, and G, the readings being taken as rapidly as possible. The first R and the mean of the first two G were taken as initial values, the last R and the mean of the last two G were taken as final values and the percentage diminution calculated. The results are shown in the last two rows.

It is obvious that, when the cell is exhausted for red, it is exhausted for green, and that, when it is exhausted for green, it is exhausted for red. Thus, to the main object of the investigation, it is possible to return a definite answer. It will be obvious also that, no matter whether the fifteen-minutes exposure is given to red or green, the diminution is greater for green.

The variation in the values recorded is partly due to the initial and final readings being made at a different speed in the different cases and partly due to the erratic behaviour of the cell itself. Selenium conductivity cells are usually regarded as somewhat capricious. When exposed to a gradually increasing light the resistance may remain constant and then jump suddenly, so that the cell is suitable as a relay but not for measurement. The selenium barrier-layer cell is also subject to

irregularity though in a much smaller degree; these irregularities are easily noticed when the illumination is strong and the current is read to one-tenth per cent. I do not think it would be worth while to heap up observations and get average values, unless there was a definite purpose in view, either to test a theory or examine the result of variation in the process of manufacture.

In case any reader may have been alarmed by the large variation recorded, I shall finish by emphasising the fact, that it is only for one cell and for an illumination that would rarely occur in practice.

XLIX. *Notices respecting New Books.*

A Bibliography of Orthogonal Polynomials. By J. A. SHOHAT, EINAR HILLE, and JOSEPH L. WALSH. (Bulletin No. 103 of the National Research Council of the National Academy of Sciences, Washington, D.C., 1940. Price \$3.00.)

THE enormous output of research papers and the multiplicity of research journals makes the task of keeping abreast of the latest developments of any scientific subject extremely difficult. Workers in the domain of Orthogonal Polynomials will therefore gratefully welcome this bibliography. Its main feature is an alphabetical catalogue of authors, each followed by a chronological list of his papers on the subject. Accompanying the title of each paper is a condensed abstract in code symbols. Thus the symbols

$$H : ab4-b7-c, \beta a13-a17-b14.1-b14.2,$$

when interpreted, indicate that the paper deals with the following questions :—

“ Hermite Polynomials as n th derivatives and definite integrals, the generating function of the polynomials, discussion of the expansion of functions satisfying Dirichlet conditions and of analytic functions in series of the polynomials, the uniform and absolute convergence of expansions in series of Hermite Polynomials.”

The volume contains also a list of periodicals, a bibliography of books and theses, and a topical index which includes references to papers on Hermite, Jacobi, Laguerre, and Legendre Polynomials, and on applications to statistics and interpolation. The preparation and printing of the work have been carried out with scrupulous care. It is to be hoped that the National Research Council will be able to arrange for the production of similar bibliographies on other branches of mathematics.

Algebra, a Text-Book of Determinants, Matrices and Algebraic Forms. By W. L. FERRAR. (Oxford, at the Clarendon Press, 1941. Price 12s. 6d. net.)

THIS book should be useful both to students and to teachers. The style is interesting, almost conversational, and the exposition is clear and full. There are numerous examples, with hints, where needed, as to the method of solution.

The volume is divided into three parts. The first, on Determinants, contains chapters on Elementary Properties, Minors, Products of Determinants, Jacobi's Theorem, and Symmetrical and Skew-symmetrical Determinants. The second part deals with Matrices, and includes chapters on Elementary Properties, Related Matrices, Rank of a Matrix, and Determinants associated with Matrices. The last and more advanced part is devoted to Linear and Quadratic Forms, with chapters on Algebraic Forms and Linear Transformations, the Positive-Definite Form, the Characteristic Equation and Canonical Forms, Orthogonal Transformations, and Invariants and Covariants.

The work provides an excellent introductory course on Higher Algebra. The print and format are all that is to be expected from the Oxford University Press, and the price, as mathematical books go now-a-days, is very reasonable.

La Mécanique Ondulatoire et les Quanta Électromagnétiques. By LOUIS SAUTY. [Pp. 34.] (Avignon: Ayzac Frères.)

Of the three essays in this booklet, the first sketches the history of scientific thought from pre-history to the Chaldeans, and thence from the Greeks to the present day, *via* Descartes, Voltaire, Kant, Hegel and Einstein; the second outlines modern atomic theory very briefly.

The third chapter is of a different type. It is devoted to an advocacy of the theory put forward by the Italian scientist C. L. Sagui, which claims to unify magnetic and gravitational fields. From the account given by M. Sauty, it appears that the basis of the theory is that electromagnetic quanta are the only fundamental elements, and that matter differs from energy only in the concentration of these quanta. Thus the energy-mass relation is at once obtained. Since electromagnetic quanta may be compared to an electric oscillator (the oscillations taking place in the "electromagnetic plasma"), this theory of matter is asserted to contain in itself the fundamentals of wave mechanics. Energy and matter now differ as progressive waves differ from stationary waves. (But no mention is made of the difficulty introduced by the radiation which these quanta should, on classical theory, emit.)

By postulating a constitution for light and the ether, and applying classical mechanics, a relation is obtained between the wave-length of a moving and a stationary photon which reduces for small velocities to the Lorentz formula. (In fact, with an obvious notation, $\lambda = \lambda_0 [1 - (\arctan v/c)^2]^{-\frac{1}{2}}$, which reduces to $(1 - v^2/c^2)^{-\frac{1}{2}}$ if $v \ll c$.) The formula is held to explain the zero result of the Michelson-Morley experiment to a first approximation, and also the residual effect announced by Miller. Sagui's original paper is to be found in the *Rendiconti dell' Accademia dei Lincei* for December, 1922.

Ramanujan. By G. H. HARDY. (Cambridge, 1940.)

IN this interesting book, Ramanujan's work is considered in its relation to earlier and later work by others. A surprisingly varied material is treated, including many beautiful newer results.

The introductory Chapter 1 deals with the man Ramanujan, and with Prof. Hardy's opinions about him. Chapter 2 is about Ramanujan's ideas concerning the prime number theorem. Chapter 3 contains two proofs (one by Turan) that "almost all" integers n have

$$\frac{\log n}{\log \log n} (1 + v(1))$$

prime factors. In Chapter 4 we find Ingham's proof of $\zeta(1 - it) \neq 0$ based on Ramanujan's identity

$$\sum_{n=1}^{\infty} \frac{\sigma_a(n) \sigma_b(n)}{n^s} = \frac{\zeta(s) \zeta(s-a) \zeta(s-b) \zeta(s-a-b)}{\zeta(2s-a-b)};$$

and a proof of Landau's formula for the number of integers which are a sum of two squares. Chapter 5 deals chiefly with results of Hardy, Littlewood and Ostrowski on lattice points in a right-angled triangle; Pillai's results on the Diophantine equation $2^x - 3^y = k$ are used to derive a non-trivial approximation for the number of integers of the form $2^x 3^y$. Chapter 7 concerns Ramanujan's hypergeometric identities. In the very interesting Chapters 6 and 8, arith-

metrical properties of the partition function $p(n)$ are studied, Rademacher's convergent series for $p(n)$ is proved, and some of Ramanujan's most beautiful identities are given. This work is closely connected with the theory of elliptic and modular functions, of which more is found in the Chapters 9, 10, and 12. Here, namely, we find an account of the representations of integers as sums of $2s$ squares, with a study of the singular series: and arithmetical and approximate properties of Ramanujan's function $\tau(n)$, including Mordell's proof that $\tau(n)$ is multiplicative. Some of Ramanujan's integral identities form the subject of the remaining Chapter 11.

To each chapter, notes and references are added, and the book ends with a 6-page list of books and papers connected with Ramanujan's work.

K. MAHLER (Manchester).

Gravity Anomalies and the Figure of the Earth. By B. L. GULATEE. [Pp. 116, figs. 10.] (Survey of India, Professional Paper 30. Price Rs. 3 or 5s.)

THE literature of geodesy is very scattered, and there is a need for a connected summary, with full references. This is what Mr. Gulatee has provided for the gravitational side of the subject. In places he gives two or three arguments rather too briefly, and more conviction might be produced by one expressed more fully. But the book should be useful both as an introduction and as a guide to further study.

Survey of India, Geodetic Report for 1939. (Price Rs. 3 or 5s.)

THE feature of most importance outside India recorded in the Report is the attempt by Lt.-Col. E. A. Glennie and Mr. B. C. Browne to re-determine the absolute values of gravity at the base station, Dehra Dun, by comparison of the periods of three pairs of pendulums with their periods when swung in Cambridge. The extreme pairs gave results differing by 10 milligals, whereas an accuracy of 2 or 3 mgal. is aimed at. One pair was under some suspicion, and the weighted mean was 979.054 gals. A mean with several previous determinations was 979.068 gals. In Heiskanen's recent catalogue of gravity stations it is taken as 979.063 gals. Glennie recommends that no change be made in the value adopted as the Indian standard until a further check has been obtained, but so large an area depends on Dehra Dun that its uncertainty needs to be reduced to the minimum at the earliest opportunity.

Other features of the report are new tidal data for Navlakhi and revised values for Shortt Island and Chandbali.

On Thermal Activity in Iceland and Geyser Action. By THORKELL THORKESSON. [Pp. 139.] (Reykjavik: Isafoldaprentsmidja.)

THE author provides numerous quantitative data on geysers, especially with regard to temperature and the composition of the gases emitted. He considers that there is a striking difference between them and volcanic gases, notably in their richness in nitrogen, and infers that the gases are ultimately largely derived from the air. He finds no evidence for superheating. He gives an explanation of the intermittence of some geysers, which merits further examination. It has been shown by A. L. Hales (M.N.R.A.S. Geophys. Suppl. 4, pp. 122-131) that a cylindrical column of fluid heated below will be stable unless

the temperature gradient exceeds a certain amount depending on the thermal expansion, the viscosity and thermal conductivity, and the radius. If it is deep enough to boil at the bottom, all the water will be expelled explosively, and there will be a quiet period while new water is accumulating. For larger diameters the column would be unstable and the heat can be carried steadily up by convection currents. This is satisfactory qualitatively, but the numerical results require smaller diameters than are likely to occur in geysers at the temperature gradients in question. A representative gradient given by Thorkelsson is 1.81 cm., and the radius would have to be under 0.2 cm. for intermittence, which is unlikely. Thorkelsson, who does not mention Hales's paper, has a mechanism depending on liberation of the dissolved gases under relief of pressure. This would imply that an element of fluid carried upwards would have part of its contraction under the reduced temperature neutralized by the formation of bubbles, and thus would be mechanically equivalent to reducing the thermal expansion. It would therefore favour stability at larger radii, but attention to various complications mentioned in the paper is needed.

Scattering of Light and the Raman Effect. By S. BHAGAVANTAM. [Pp. x+333.] (Waltair, India : Andhra University Press, 1940. Price 22s.)

THE interest aroused by Raman's experimental realization of the change of wave-length produced by the scattering of light by matter led, in the decade before the war, to a rapid development of the theory of the interaction of light and matter and to an enormous body of experimental tests. If this book were merely a record of achievement in this field it would be valuable, but it is a great deal more. Professor Bhagavantam possesses a double qualification for the task he has set himself. He has taken a very active part in the development and he is, as his fortunate students must know and as the reader soon delightedly discovers, a brilliant teacher. In addition, he has the gift, rare enough in experimentalists, of being able to express himself in clear, significant and flexible English. The result is a well balanced and eminently readable account of the theories of light scattering by solids, liquids, and gases, and of their experimental tests. The first seven chapters deal with what is usually called Rayleigh scattering. These are followed by two chapters on optical anisotropy. The last nine chapters are devoted to the Raman effect, and there are six mathematical appendices.

The pleasure of reading this fascinating volume is enhanced by the many clear diagrams and the really beautiful printing. The book will take its place among the classics of the literature of physical science. J. E.

Four-Figure Tables with Mathematical Formulae. By Prof. H. C. PLUMMER, M.A., F.R.S. [Pp. iv+89.] (Macmillan & Co., Ltd., 1941. Price 3s. 6d.)

A COLLECTION of formulæ in use at the Military College of Science, originally prepared by Mr. C. S. Wright, has been expanded, printed, and bound in stout covers with a collection of four-figure mathematical tables modified slightly from those published by Mr. Frank Castle. The result is a single volume, at a moderate price, which contains all that the elementary student of mathematics needs for reference. The name of the compiler, and the fact that both the tables and the formulæ have been tried out for some years, should be guarantees of the reliability and convenience of the selection.

Cambridge Physical Tracts: Surface Tension and the Spreading of Liquids.
By Dr. R. S. BURDON. [Pp. x+85.] (Cambridge University Press, 1940.
Price 7s. 6d.)

SURFACE phenomena are of great interest to the chemist inasmuch as experiments on surface films have increased his knowledge of molecular structure, and also because such highly important industrial processes as spreading, wetting, and emulsification are modified by the presence of chemical substances. For these reasons much of the research on surface problems is carried out by physical chemists, and most of the books on the subject have been written by authors belonging to this category. Physicists, therefore, are apt to be unaware of the more recent work on surfaces, and the editors of the Cambridge Physical Tracts are to be commended for having included Dr. Burdon's book in their collection.

Dr. Burdon's own researches have been concerned mainly with the experimental study of spreading, and the larger portion of the book describes his results and those of others on the spreading of liquids on water, mercury, and solid surfaces. These accounts are preceded by a chapter on the more general aspects of spreading in which the author emphasizes that although the interfacial energy relations appear to be delightfully simple, yet the mechanism of spreading requires a good deal of attention before it can be said to be perfectly understood. Experimental research in this field is difficult; for instance, the ions which are present in conductivity water probably control its behaviour on mercury, and, again, it is difficult to obtain a solid surface whose structure is uniform over an appreciable area.

The first part of the book includes a short—and not quite complete—account of the various methods of measuring surface tension, and a chapter on the problem of the surface tension of mercury which is even now by no means completely elucidated.

This little book can be thoroughly recommended to scientists in general, and Dr. Burdon is to be congratulated on having compressed so much information and apt comment into its pages.

R. C. B.

Physical Science in Art and Industry. By Dr. E. G. RICHARDSON. [Pp. xi + 293.] (London: English University Press, Ltd., 1940. Price 15s.)

DURING the past ten years or so Dr. Richardson has, from time to time, engaged upon researches which have had immediate practical application—for instance, the physical properties of clay pastes, flour doughs, gelatine solutions, and the sedimentation of particles suspended in rivers. These are in addition to the more widely known experiments in aerodynamics and acoustics. In every case Dr. Richardson has shown a flair for producing interesting results with the simplest application of physical principles and apparatus. Consequently he is familiar with many branches of applied physics and can write about them with authority.

The book he has written is unquestionably of great interest and entertainingly written. It is a mental treat for a scientist to read the book and to recognize that it was written by a fellow scientist and not, as is sometimes the case, by an author in whom the desire to make his readers wonder at "marvels" and "inventions" is far deeper than his scientific knowledge. Dr. Richardson's method of exposition makes easy reading for a physicist. What the layman will make of the book is another matter, although it is obvious that the author

frequently has this individual in mind, as, for example, when he explains the meaning of "relative humidity."

In addition to chapters on those branches of applied physics on which he has worked, such as, aeronautics, pottery, cookery, farming, river hydrology, architectural acoustics and so on, Dr. Richardson has written a chapter on musical instruments about which he is well qualified to speak, and others about locomotion, communications, fine art and archaeology, mining, textiles, and war. There are, of course, several aspects of physics in industry which are not dealt with in the book. May the second edition be "greatly enlarged." R. C. B.

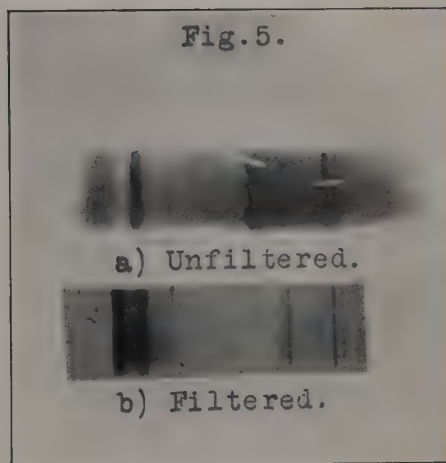
The Foundations of Geometry. By GILBERT DE B. ROBINSON. (The University of Toronto Press, 1940. Price \$2.00.)

THIS is the first of a new series of mathematical volumes, published under the auspices of the University of Toronto, and written with the object of emphasizing fundamental principles rather than of discussing subjects in detail. The purpose of the book is to examine the basic axioms of geometry. To the schoolboy there is only one geometry—that of Euclid,—just as to him there is only one algebra. It was not till the discovery, early in the 19th century, of Non-Euclidean Geometry, that mathematicians realized that it was possible to develop different geometries, based on different sets of axioms. Later it was found that the same was true of algebra, and even of logic.

What led to the discovery of the classic Non-Euclidean Geometries was, of course, the difficulty of establishing Euclid's Parallel Postulate. Different postulates about parallels led to different geometries. But in all these geometries it was assumed that length was absolute. Now-a-days even the man in the street has learned from his attempts to understand Einstein's Theory of Relativity that this is not necessarily true. It is quite possible to develop complete geometrical systems independently of the conception of length. In particular, modern expositions of Projective Geometry make no use of metrical ideas. In recent times much attention has been given to the classification of the fundamental axioms of geometry: these have been reduced to their simplest terms, with a view to determining what axioms are necessary for the building up of the various geometrical systems.

Professor Robinson gives an interesting account of these problems. The book is in two parts: the first deals with the axiomatic foundation of Projective Geometry, now regarded as the fundamental geometric system, and of Euclidean Geometry: the second with the concepts of number, order, and continuity. To all who are interested in the study of these fundamentals this volume is warmly recommended.

[The Editors do not hold themselves responsible for the views expressed by their correspondents.]



Spectrograms showing effect of filtration of X-radiation from a tungsten target through a tungstic acid filter.

closure for variable pressure ionization chamber.

INDEX TO VOL. XXXI.



AIR-JET with a velocity exceeding that of sound, 35.

Andrewartha (G. G.) and Evans (E. J.), the Hall effect and other physical properties of the copper-tin system of alloys, 265.

Asymptotic solution of Southwell and Squire; modification to Oseen's equations, 413.

Awbery (J. H.), the latent heats of fusion of some organic refrigerants, 247.

Aziz (S. A.) and Mukerji (S. K.) on the Raman spectrum of *m*-diphenyl benzene, 231.

Baudisch (O.) and Welo (L. A.), some evidence for the existence of higher hydrates of ferric oxide as transition intermediates, 103.

Behrend (D. J.), a method for measuring the internal area of section of a glass tube, 199.

Beynon (W. J. G.), formulæ for the natural dispersion of some organic liquids, 1.

Books, new :—W. R. Smythe, *Static and Dynamic Electricity*, 88; Prof. L. Bairstow, *Applied Aerodynamics*, 261; J. C. Slater, *Introduction to Chemical Physics*, 263; G. Kron, *Tensor Analysis of Networks*, 264; Dr. E. A. Moelwyn-Hughes, *Physical Chemistry. An Introduction*, 348; A. S. Ramsey, *An Introduction to the Theory of Newtonian Attraction*, 348; Prof. G. H. Hardy, *A mathematician's Apology*, 433; P. W. Merrill, *Spectra of Long-*

Period Variable Stars, 434; *Culture*, Vol. V. No. 2, 434; *The Half-Yearly Journal of the Mysore University*, 434; *Table of Powers* (British Association Mathematical Tables, Vol. IX.), 435; G. Windred, *Electrical Contacts*, 435; Prof. R. V. Southwell, *Relaxation Methods in Engineering Science*, 436; J. A. Shohat, Einar Hille, and J. L. Walsh, *A Bibliography of Orthogonal Polynomials*, 507; W. L. Ferrar, *Algebra, a Text-Book of Determinants, Matrices and Algebraic Forms*, 507; L. Sauty, *La Mécanique Ondulatoire et les Quanta Électromagnétiques*, 508; Prof. G. H. Hardy, *Ramanujan*, 508; B. L. Gulatee, *Gravity Anomalies and the Figure of the Earth*, 509; *Survey of India, Geodetic Report for 1939*, 509; T. Thorkelsson, *On Thermal Activity in Iceland and Geyser Action*, 509; Prof. S. Bhagavantam, *Scattering of Light and the Raman Effect*, 510; Prof. H. C. Plummer, *Four-Figure Tables with Mathematical Formulæ*, 510; Dr. R. S. Burdon, *Cambridge Physical Tracts: Surface Tension and the Spreading of Liquids*, 511; Dr. E. G. Richardson, *Physical Science in Art and Industry*, 511; Prof. G. de B. Robinson, *The Foundations of Geometry*, 512. *Boundary layer equations, note on the method of successive approximations for the solution of*, 452.

- Brillouin zone for the gallium structure, 139.
- Campbell (J. W.), rocket flight to the moon, 24.
- Carslaw (H. S.) and Jaeger (J. C.), the determination of Green's function for line sources for the equation of conduction of heat in cylindrical coordinates by the Laplace transformation, 204.
- Chalmers (J. A.), the effective separation of points discharging atmospheric electricity, 363.
- Chaudhri (R. M.) and Khan (A. W.), the emission of secondary electrons from nickel, 382.
- Churchill (R. V.), a heat conduction problem introduced by C. J. Tranter, 81.
- Circuits with double linkages, 169.
- Clarkson (J. R.), the measurement by ionization methods of real energy absorption from an X-ray beam, 437.
- Conduction of heat, note on a problem in the, 432.
- Crackston (J. E.) and Wood (R. G.), the crystal structures of some heterocyclic organic compounds of analogous constitution.—Part I. Thianthren and Selenanthren, 62.
- Crystal lattice orientation of rolled magnesium, 425.
- structures of some heterocyclic organic compounds of analogous constitution.—Part I. Thianthren and selenanthren, 62; Part II. Phenthiazine, phenoxthionine, phenoxselenine, and phenoxtellurine, 71; Part III. Phenazine and diphenylene dioxide, 115.
- David (W. T.), Leah (A. S.), and Pugh (B.), latent energy and dissociation in flame gases, 156.
- Davies (T. V.), an investigation of the flow of a viscous fluid past a flat plate, using elliptic coordinates, 283.
- Daymond (J. R.) and Walker (A. G.) on a hydraulic problem involving discharge into tidal water.—II., 222.
- Determination of Green's function for line sources for the equation of conduction of heat in cylindrical coordinates by the Laplace transformation, 204.
- Dispersion of some organic liquid, formulæ for the natural, 1.
- Drift of the selenium barrier-layer photo-cell, 498.
- Electrical conductivity of plastic dielectrics, 405.
- Electrolytic dissociation, factors determining.—Part II. The free energies of dissociation of salt molecules in aqueous solution, 51.
- Emission of secondary electrons from nickel, 382.
- Energy absorption from any X-ray beam, measurement by ionization methods of, 437.
- Erdelyi (A.) on Lamé functions, 123.
- Evans (E. J.) and Andrewartha (G. G.), the Hall effect and other physical properties of the copper-tin system of alloys, 265.
- Excitation of the hydrogen molecule by electron impact, 349.
- Factors determining electrolytic dissociation.—Part III. The free energies of dissociation of salt molecules in aqueous solution, 51.
- Formulæ for the natural dispersion of some organic liquids, 1.
- Further development of the fabric theory of protein structure, 177.
- Gemant (A.), the electrical conductivity of plastic dielectrics, 405.
- General interferential method, 13.
- Hall effect and other physical properties of the copper-tin system of alloys, 265.
- Hartmann (J.) and Lazarus (F.), the air-jet with a velocity exceeding that of sound, 35.
- Heat conduction problem introduced by C. J. Tranter, 81.
- Houstoun (R. A.), the drift of the selenium barrier-layer photo-cell, 498.

- Hydraulic problem involving discharge into tidal water.—II., 222.
- Investigation of the flow of a viscous fluid past a flat plate, using elliptic coordinates, 283.
- Jaeger (J. C.) and Carslaw (H. S.), the determination of Green's function for line sources for the equation of conduction of heat in cylindrical coordinates by the Laplace transformation, 204.
- Kellström (G.), note on the paper "A new determination of the viscosity of air by the rotating cylinder method," 466.
- Khan (A. W.) and Chaudhri (R. M.), the emission of secondary electrons from nickel, 382.
- Knowler (A. E.) on the space attenuation of impact sounds in a brick building, 240.
- Lamé functions, on, 123.
- Latent energy and dissociation in flame gases, 156.
- heats of fusion of some organic refrigerants, 247.
- Lattice types and Brillouin zones, relationships between, 131.
- Lazarus (F.) and Hartmann (J.), the air-jet with a velocity exceeding that of sound, 35.
- Leah (A. S.), David (W. T.), and Pugh (B.), latent energy and dissociation in flame gases, 156.
- Lowan (A. N.) on the problem of wave-motion for the wedge of an angle, 373.
- McCale (C. H.), Wood (R. G.), and Williams (G.), the crystal structures of some heterocyclic organic compounds of analogous constitution.—Part II. Phenthiazine, phenoxthionine, phenoxselenine, and phenoxtellurine, 71.
- MacRobert (T. M.), some formulæ for the E-function, 254.
- Measurement by ionization methods of real energy absorption from an X-ray beam, 437.
- of particle size by the X-ray method, on the, 339.
- Measurement of surface tension by the ripple method, 209.
- Method for measuring the internal area of section of a glass tube, 199.
- Migration of atoms in iron-nickel alloys, on the, 314.
- Mukerji (S. K.) and Aziz (S. A.) on the Raman spectrum of *m*-diphenyl benzene, 231.
- Note on a problem in the conduction of heat, 432.
- — the method of successive approximations for the solution of the boundary layer equation, 452.
- — the paper "A new determination of the viscosity of air by the rotating cylinder method," 466.
- On the problem of wave-motion for the wedge of an angle, 373.
- Orr (W. J. C.), factors determining electrolytic dissociation.—Part II. The free energies of dissociation of salt molecules in aqueous solution, 51.
- Owen (E. A.) and Sully (A. H.) on the migration of atoms in iron-nickel alloys, 314.
- Preston (J. H.), asymptotic solution of Southwell and Squire; modification to Oseen's equations, 413.
- , note on the method of successive approximations for the solution of the boundary layer equations, 452.
- Pugh (B.), David (W. T.), and Leah (A. S.), latent energy and dissociation in flame gases, 156.
- Raman spectrum of *m*-diphenyl benzene, on the, 231.
- Ramsay (B. P.) and Sturkey (L.), a general interferential method, 13.
- Ray (M.) on turbulent liquid motion outside a circular boundary.—II., 14.
- Raynor (G. V.), relationships between lattice types and Brillouin zones, 131.
- , the Brillouin zone for the gallium structure, 139.

- Reflexion and refraction of photons, 394.
- Relationships between lattice types and Brillouin zones, 131.
- Rocket flight to the moon, 24.
- Roscoe (R.), the excitation of the hydrogen molecule by electron impact, 349.
- Schofield (F. H.), the steady flow of heat from certain objects buried under flat air-cooled surfaces, 471.
- Selenium barrier-layer photo-cell, the drift of, 498.
- Simmons (N.), the wind tunnel with open working-section, 89.
- Some evidence for the existence of higher hydrates of ferric oxide as transition intermediates, 103.
- formulae for the E-function, 254.
- Space attenuation of impact sounds in a brick building, on the, 240.
- Steady flow of heat from certain objects buried under flat air-cooled surfaces, 471.
- Sturkey (L.) and Ramsay (B. P.), a general interferential method, 13.
- Sully (A. H.) and Owen (E. A.) on the migration of atoms in iron-nickel alloys, 314.
- Surface tension by the ripple method, measurement of, 209.
- Taylor (A.) on the measurement of partial size by the X-ray method, 339.
- Taylor Jones (E.), the reflexion and refraction of photons, 394.
- Thomas (D. E.), crystal lattice orientation of rolled magnesium, 425.
- Tranter (C. J.), note on a problem in the conduction of heat, 432.
- Turbulent liquid motion outside a circular boundary.—II., 144.
- Viscosity of air by the rotating cylinder method, note on the paper. A new determination of the, 466.
- Walker (A. G.) and Daymond (J. R.), on a hydraulic problem involving discharge into tidal water.—II., 222.
- Walker (E. A.), circuits with double linkages, 169.
- Wave-motion for the wedge of an angle, on the problem of, 373.
- Welo (L. A.) and Baudisch (O.), some evidence for the existence of higher hydrates of ferric oxide as transition intermediates, 103.
- Williams (G.) and Wood (R. G.), the crystal structures of some heterocyclic organic compounds of analogous constitution.—Part III. Phenazine and diphenylene dioxide 115.
- , — and McCale, the crystal structures of some heterocyclic organic compounds of analogous constitution.—Part II. Phenthiazine, phenoxthionine, phenoxselenine, and phenoxtellurine, 71.
- Wind tunnel with open working-section, 89.
- Wood (R. G.) and Crackston (J. E.), the crystal structures of some heterocyclic organic compounds of analogous constitution.—Part I. Thianthren and selenanthren, 62.
- , McCale (C. H.) and Williams (G.), the crystal structures of some heterocyclic organic compounds of analogous constitution.—Part II. Phenthiazine, phenoxthionine, phenoxselenine and phenoxtellurine, 71.
- and Williams (G.), the crystal structures of some heterocyclic organic compounds of analogous constitution.—Part III. Phenazine and diphenylene dioxide, 115.
- Wrinch (D.), further development of the fabric theory of protein structure, 177.

END OF THE THIRTY-FIRST VOLUME

